504 pages

12826

NASA Contractor Report 159251 ACEE-01-FR-3132

EVALUATION OF LAMINAR FLOW CONTROL SYSTEMS CONCEPTS FOR SUBSONIC COMMERCIAL TRANSPORT AIRCRAFT

FINAL REPORT

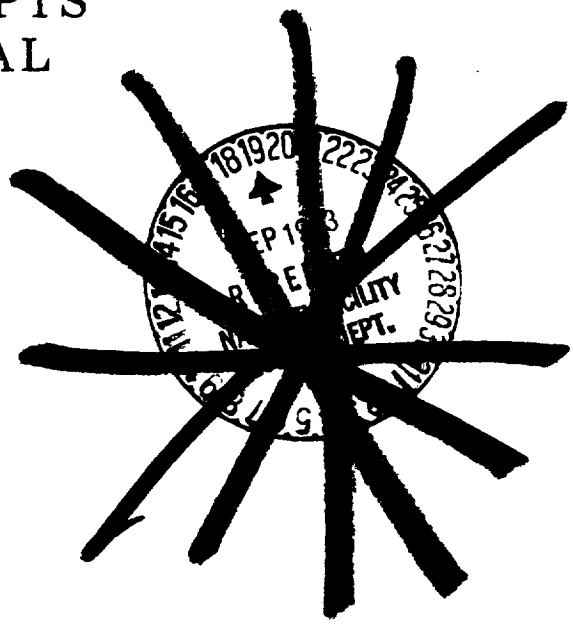

McDonnell Douglas Corporation
Douglas Aircraft Company
Long Beach, California 90846

MBM/6517

CONTRACT NAS1-14632
JUNE 1983

National Aeronautics and Space Administration

Langley Research Center
Hampton, Virginia 23665

NASA Contractor Report 159251 ACEE-01-FR-3132

EVALUATION OF LAMINAR FLOW CONTROL SYSTEMS CONCEPTS FOR SUBSONIC COMMERCIAL TRANSPORT AIRCRAFT

FINAL REPORT

McDonnell Douglas Corporation
Douglas Aircraft Company
Long Beach, California 90846

CONTRACT NAS1-14632
JUNE 1983

National Aeronautics and
Space Administration

Langley Research Center
Hampton, Virginia 23665

FOREWORD

This document covers the contract work performed by the Douglas Aircraft Company of the McDonnell Douglas Corporation, on Laminar Flow Control (LFC) under NASA Contract NAS1-14632 entitled "Evaluation of Laminar Flow Control Systems Concepts for Subsonic Commercial Transport Aircraft" and is a part of the overall Aircraft Energy Efficient (ACEE) program supported by NASA through its Langley Research Center.

Acknowledgements for their support and guidance are given to the NASA LFC Project Manager, Dr. R. Muraca, to the Project Technical Monitors Mr. R. Wagner and Mr. J. Cheely, and to the Project Chief Scientist, Mr. A. Braslow, also to Dr. W. Pfenninger and to the NASA on-site representative at Long Beach, Mr. J. Tulinius.

The Douglas personnel primarily responsible for this work were:

M. Klotzsche	ACEE Program Manager
W. Pearce	LFC Project Manager
W. Boronow	Environmental Systems
I. Goldsmith	Configuration
F. LaMar	Suction Systems
M. Platte	Economics
R. Roensch	Aerodynamics
J. Thelander	Aerodynamics
J. Welbourn	Materials & Processes
G. Wightman	Structures
W. Nelson	Structures
J. Hughes	Wind Tunnel Testing

CONTENTS

CONTENTS
(Continued)

CONTENTS
(Continued)

CONTENTS
(Continued)

CONTENTS
(Continued)

CONTENTS
(Continued)

LIST OF ILLUSTRATIONS

LIST OF ILLUSTRATIONS
(Continued)

LIST OF ILLUSTRATIONS
(Continued)

LIST OF ILLUSTRATIONS
(Continued)

LIST OF ILLUSTRATIONS
(Continued)

LIST OF ILLUSTRATIONS
(Continued)

LIST OF ILLUSTRATIONS
(Continued)

LIST OF ILLUSTRATIONS
(Continued)

LIST OF ILLUSTRATIONS
(Continued)

LIST OF TABLES

LIST OF TABLES
(Continued)

1.0 SUMMARY

This "Evaluation of Laminar Flow Control (LFC) Systems Concepts for Subsonic Commercial Transport Aircraft", considered all aspects of the application of LFC to commercial transport aircraft in operation. The problem areas were identified and tackled systematically until resolved. Program activities included configuration design and analysis, performance and economic analysis, fabrication development, environmental studies, contamination avoidance systems design and testing, structural design/analysis and testing, and wind tunnel testing. The results of LFC program activities up to December 1980 are covered in this report. For summary reports see References 1.0-1 and 1.0-2.

Laminar Flow Control was achieved by using controlled suction through the external surface to stabilize the laminar boundary layer and prevent transition to turbulent flow, thus achieving significant drag reduction.

An objective of the program was to take advantage of any new and advanced technology consistent with a mid 1990's aircraft time frame. With this in mind, it was decided to examine the possibilities of using porous materials at the surface to control suction airflow rather than use a series of very fine slots, as used previously on the Northrop X21 aircraft program. Due to the very limited data base available on the use of porous materials for achieving LFC, an extensive survey of possible porous materials and their application was undertaken. This involved design studies, fabrication development and structural and aerodynamic testing. The field was eventually narrowed down to two promising materials, a smooth finely woven stainless steel mesh manufactured under the trade name Dynapore and electron beam (EB) perforated titanium sheet material, perforated with Steigerwald equipment. The EB perforated titanium surface was finally selected, after exhibiting excellent LFC characteristics in the wind tunnel, and because of its better structural and damage resistance properties.

A number of configuration trade studies were undertaken, the most significant being a comparison of LFC on both upper and lower wing surfaces compared with LFC on the upper surface only. Using suction to 70 percent chord for LFC on

both surfaces and to 85 percent on the upper surface only, it was found that the reduction in drag coefficient and the total suction airflow required were of the same order. The advantages of having suction on the upper surface only with respect to simplicity, reduced damage vulnerability and the availability of access through the lower surface for maintenance are obvious. Not so obvious is perhaps the main advantage, the possibility of using a shield at the leading edge to avoid surface contamination. This shield can also function as a high lift device and be retracted into the lower surface after use. The trade study showed the superior performance of the upper-surface-suction-only configuration. This configuration was therefore selected for the baseline LFC aircraft to be used in subsequent studies.

Another significant trade study was a comparison of the LFC aircraft with an advanced turbulent aircraft configuration. This clearly showed the advantages of LFC with respect to reduced fuel consumption and reduced operating cost, particularly with rising fuel prices.

In examining all aspects of the practical application of LFC to commercial transport aircraft, no problem was found for which a practical solution could not be identified, as shown by analysis, design studies, and development testing undertaken in this program. The overall results indicate that the LFC aircraft configuration, suggested by Douglas in this study, could be developed into a practical design that would bring signifiant fuel saving and operating cost benefits.

SUMMARY REFERENCES

1.0-1 Pearce, W. E., Evaluation of Laminar Flow Control Systems Concepts for Subsonic Commercial Transport Aircraft - Executive Summary, NASA Contractor Report 159252.

1.0-2 Pearce, W. E., Progress at Douglas on Laminar Flow Control Applied to Commercial Transport Aircraft, Paper ICAS-82-1.5.3, Proceedings of the 13th Congress of the International Council of the Aeronautical Sciences, August 1982.

2.0 INTRODUCTION

This investigation into the possibilities of using laminar flow control (LFC) on commercial transport aircraft was initiated by NASA in response to the growing need for energy conservation.

Fuel saving results directly from the drag reduction that can be achieved by using LFC. The successful application of LFC to commercial airplane operation would result in a major reduction of fuel consumed by airline fleets throughout the world. With rising fuel costs, increasing economic benefits are also obtainable.

The airflow over the surface of an airplane is initially laminar within the boundary layer but this low drag condition is unstable and transition to turbulent flow occurs normally over a very short distance. On a swept wing this instability is aggravated by cross flow conditions in regions of steep pressure gradients. Transition can also occur due to the spanwise flow along the attachment line at the leading edge. In all of these cases, transition to turbulent flow can be avoided by the use of suction through the surface to stabilize the laminar boundary layer.

Ideally the suction airflow would be distributed over the whole area using a porous surface but when this study was undertaken a practical solution to achieving this did not exist. Very fine suction slots had been used previously to create intermittant suction at frequent intervals in order to sustain laminar flow. Although slotted systems have been tested successfully, full scale flight testing of a slotted system on the Northrop X21 airplane wing in the early 1960's demonstrated many of the difficulties of making such a system reliable and it was not considered to be commercially practical at that time.

The approach adopted by Douglas was directed towards taking full advantage of recent advances in technology to achieve a practical, reliable and economic LFC system for commercial transport aircraft, by using suction distributed through porous surfaces.

Preliminary design studies resulted in an initial LFC airplane configuration that was used as a baseline for LFC system and structural design and configuration trade studies. The baseline was updated at intervals and was compared with a turbulent design to determine relative economic and performance advantages.

Particular emphasis was placed on the design and development of suitable porous surfaces, their supporting substructure, and the use of integral ducting for the suction airflow. A variety of designs was considered. The most promising were tested to determine structural strength, airflow characteristics, and LFC performance in the Douglas wind tunnel at Long Beach. The 2.14 m (7 ft) chord swept wing LFC wind tunnel model tested was funded by Douglas in support of the LFC program.

This report is divided into sections covering the work accomplished under the principal disciplines involved. Section 5.0 describes the aircraft configuration studies and provides an overview of many of the activities covered in greater detail in the other sections. Each of these sections is virtually self contained but references are given to related activities. The conclusions and recommendations are presented in Section 12.0.

3.0 SYMBOLS AND ABBREVIATIONS

APU	=	Auxiliary power unit
AR	=	Aspect ratio
b	=	Wing span
B	=	Boron
c, C	=	Chord
C_d	=	Drag coefficient
C_F	=	Flap chord
c.g., C.G.	=	Center of gravity
C_ℓ	=	2-Dimensional lift coefficient
C_L	=	Wing lift coefficient
℄	=	Center line
C_m	=	Moment coefficient
C_{n_β}	=	Side slip force coefficient
$C_{p(N)}$	=	Pressure coefficient
CPR	=	Compressor pressure ratio
C_Q	=	Suction airflow coefficient
C_V	=	Nozzle velocity coefficient
d	=	Diameter
DOC	=	Direct operating cost
e	=	Induced drag efficiency factor
E	=	Young's modulus of elasticity
E^3	=	Energy efficient engine - NASA program
EB	=	Electron beam

EET	=	Energy Efficient Transport - NASA program
E-I	=	Electro impulse
E_p	=	Epoxy
f	=	Equivalent flat plate drag area or friction loss
f/a	=	Fuel/air ratio
F_N	=	Engine thrust
FNTO	=	Takeoff thrust
FOD	=	Foreign object damage
FPD	=	Freezing point depressant
FS	=	Front spar
g	=	Acceleration due to gravity
G	=	Shear modulus
G_r	=	Graphite (carbon)
h	=	Height
i_H	=	Horizontal stabilizer angle of incidence
i_W	=	Wing angle of incidence
$i_{Z_{LL}}$	=	Zero wing lift angle of incidence
I	=	Moment of inertia
J	=	Polar moment of inertia
K	=	Ballistic coefficient
Kev	=	Kevlar
L	=	Length
L/D	=	Lift/drag ratio
L.E.	=	Leading edge
LFC	=	Laminar Flow Control
LS	=	Lower surface

M	=	Mach number
MAC	=	Aerodynamic mean chord
MEW	=	Manufacturers empty weight
MLW	=	Maximum landing weight
MPP	=	Micro perforated plate
MTOW	=	Maximum takeoff weight
MZFW	=	Maximum zero fuel weight
N	=	Load factor
NWLO	=	Nose wheel lift-off
OASPL	=	Overall sound pressure level
OEW	=	Operator's empty weight
p, P	=	Air pressure
PGME	=	Propylene glycol methyl ether
PLM	=	Plastic laminating mold
PR	=	Pressure ratio
P_{ult}	=	Ultimate design load
q	=	Airflow dynamic pressure
Q	=	Porosity
QCSEE	=	Quiet engine - NASA program
Q_T	=	Nozzle flow rate
R	=	Fatigue stress ratio
R_c, R_e	=	Reynolds number
S	=	Distance measured along surface
SCFM	=	Standard cubic feet per minute
SFC	=	Specific fuel consumption
SLST	=	Sea level static thrust
SPF/DB	=	Super plastic formed/diffusion bonded

SPL	=	Sound pressure level
SRLT	=	Silicone rubber laminating tool
S_w	=	Wing area
t	=	Temperature or thickness
t/c, T/C	=	Thickness/chord ratio
TI, ti	=	Titanium
TKS	=	TKS Company, Cumberland, England
TOGW	=	Takeoff gross weight
T/W	=	Thrust/weight ratio
U+L	=	Suction on upper and lower surfaces
U.S.(O)	=	Upper surface (only)
V	=	Aircraft speed
V_c	=	Aircraft cruise speed
VCK	=	Variable camber Krueger flap
V_d	=	Initial droplet velocity
V_D	=	Aircraft design diving speed
V_H	=	Horizontal tail colume coefficient
V_ℓ	=	Local velocity through porous surface
V_{mcg}	=	Minimum control speed
V_N, V_W	=	Average velocity through porous surface
V_V	=	Vertical tail volume coefficient
V_∞	=	Free stream velocity
W_a	=	Suction air mass flow
W_f	=	Fuel flow or consumption
x	=	Chordwise distance from L.E.

X_W	=	Spanwise distance from aircraft C_L along wing
X_{TR}	=	Distance from L.E. to boundary layer transition
YEHUDI	=	Wing root trailing edge extension
α	=	Angle of attack
δ_F	=	Flap angle
$\delta(t)$	=	Relative pressure
θ	=	Meniscus angle of liquid against surface
$\theta(t)$	=	Relative temperature
ε	=	Height of insect deposit
η	=	Efficiency or fraction of semi-span from aircraft C_L
λ, Λ	=	Sweepback angle
μ	=	Viscosity
ν	=	Kinematic viscosity
ρ	=	Density
σ	=	Relative density of air
ϕ	=	Angle of nozzle to wing reference plane

4.0 MISSION DEFINITION

In accordance with the NASA Contract NAS1-14632, the selection of the aircraft mission and passenger sizing to be considered throughout this LFC study is the contractor's choice. The aircraft is assumed to be operational in a 1990 - 1995 time period.

The mission selection was guided by Douglas Marketing analysis based on the passenger traffic of 140 airlines and cargo traffic of 62 airlines. The airlines represent over 95 percent of the ICAO world passenger and cargo traffic, excluding USSR and China. The market analysis and prediction of the 1990-95 passenger aircraft demands included the following assumptions:

- Typical airline route structure would not change substantially over the forecast period;

- Retirement of the current fleet is considered to be after 15 years of service:

- Types of aircraft selected to fill additional needs are normally the same as those currently in service with each airline;

- Production of new aircraft types is based on -
  - Speed and utilization of aircraft replaced,
  - Assumed seating arrangements of the new aircraft,
  - Assumed increase in load factors and yields support the presumption that the airlines can raise capital to purchase equipment to meet passenger demand. Over the long term, the commercial aircraft industry is assumed to maintain its ability to meet the world demand for aircraft.

The anticipated seat/distance demand by aircraft types, as a function of time, (Figure 4-1), shows the major demand in the 1990 time period to be for long-range jet and the short/medium range jet types. Required seating capacities are estimated at 250-425 and 180-380, respectively. For purposes of this study, a 300-passenger/9260 km (5000 n. mile) range aircraft was selected.

The rationale for this selection as a design point for the LFC base case aircraft is exemplified in the aircraft development trend lines summarized in Figure 4-2. In the time period of 1990-95, it is shown that an LFC aircraft of the 300-350 passenger size class could replace a large group of current aircraft such as the B747SP, DC-10, DC-10 Stetch, L-1011, DC-8 Stretch, DC-8, B-707, B-727-200, and the A-300. The estimated time periods required for development of the aircraft are indicated by heavy horizontal lines which span a 7-9 year period.

The aircraft sizing and mission ground rules for this study are given in Table 4-1 below.

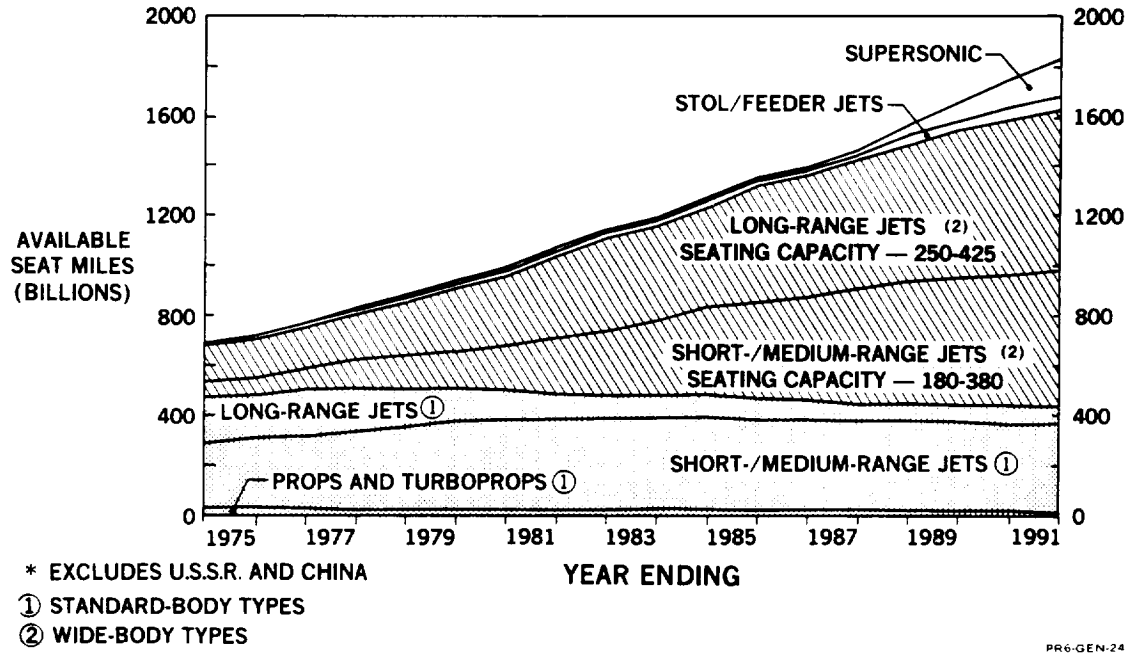

FIGURE 4-1. SEAT-MILE DEMAND BY AIRCRAFT TYPES

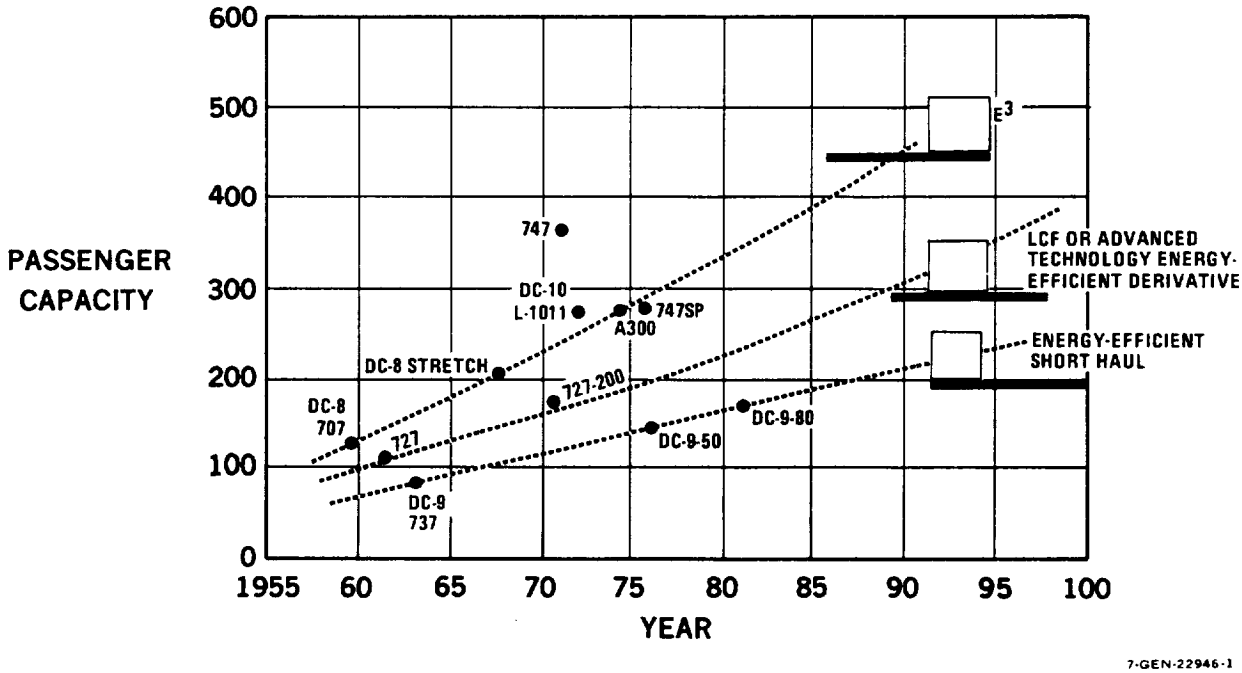

FIGURE 4-2. AIRCRAFT DEVELOPMENT TREND LINES

Table 4-1

Aircraft Sizing and Mission Ground Rules

Takeoff distance	3,050 m (10,000 Ft) Max.
Approach speed	67 m/s (130 Knot) Max.
Cruise Speed	$M_{cruise} = 0.8$
Initial cruise altitude (LFC off)	10,670 m (35,000 FT)
Step climb cruise altitude increments (Standard practice)	1,220 m (4,000 Ft)
Reserves (LFC off)	International Standard

The takeoff distance restriction of 3,050 m (10,000 Ft) feet is consistent with available airport runways from which long-range aircraft are expected to operate.

The 67 m/s (130 Knot) approach speed ensures growth capability with acceptable landing characteristics.

The cruise Mach number of 0.8 and the step climb cruise procedure are consistent with current commercial aircraft operating practice.

The selection of 10,670 m (35,000 ft) as the initial cruise altitude is to reduce the probability of encountering ice crystals in the atmosphere that can cause loss of laminar flow. Ice crystals are encountered more frequently at lower altitudes. The initial cruise altitude and the international reserves are calculated assuming LFC off. This is definitely conservative but would minimize the impact of losing LFC on aircraft operation.

5.0 CONFIGURATION DEVELOPMENT

5.1 CONFIGURATION STUDY GROUND RULES

In order to make a logical and meaningful evaluation of the laminar flow control aircraft, a side-by-side comparison with a comparable turbulent aircraft is necessary. Therefore, throughout the study, weight, performance, and economics data are generated for both laminar flow control and turbulent aircraft. The laminar flow and turbulent aircraft are configured to the same ground rules, see Table 5-1, and to the same level of technologies except for laminar flow control. The turbulent aircraft provides a basis for evaluation of the benefits and performance gains associated with the LFC.

The interior arrangement of the basic 300-passenger fuselage, shown in Figure 5-1, is the same for both the turbulent and the laminar flow cases. DC-10 loftlines are used with a fuselage extension of 2.03 m (80 in). The cabin is actually identical to a Japan Air Lines International mixed class interior, with the exception of the replacement of one lavatory by two seats, and the addition of two rows of seats for the lengthened fuselage.

As on the DC-10 commercial transport, cargo is carried under the floor with cargo containers aft of the wing and pallets forward. In the design weight of the aircraft these cargo-carrying provisions are considered to be onboard but empty, except for passenger baggage. The aircraft structural weight is compatible with carrying a full cargo load. Fuselage under-the-floor volume is sufficient to carry four extra cargo containers if desired.

24 FIRST CLASS — 965- and 990-mm (38 AND 39 IN.) SEAT PITCH

275 ECONOMY — 864-mm (34 IN.) SEAT PITCH

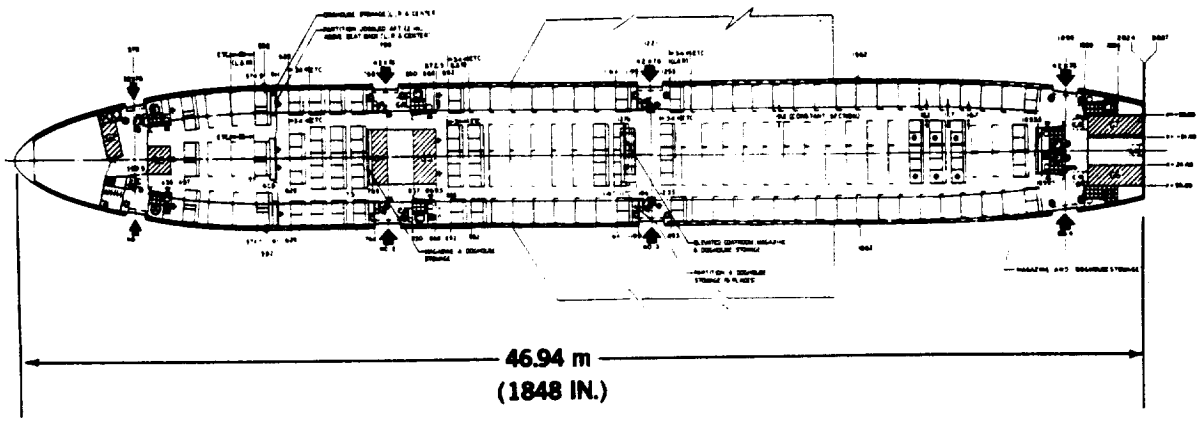

FIGURE 5-1. INTERIOR ARRANGEMENT – MIXED CLASS

Table 5-1

BASIC STUDY GROUND RULES

- o PERFORMANCE CHARACTERISTICS
  - Payload — 31,300 Kg (69,000 LB) (300 Passengers + 10% Cargo)
  - Range — 9,620 km (5,000 N MI)
  - Cruise Mach No. — 0.8
  - Field Length — 3050 m (10,000 Ft) MAX
  - Approach Speed — 66.9 m/s (130 KN) EAS MAX
- o LFC - Porous Suction Surface
- o ADVANCED TECHNOLOGY - Consistent with 1995 operation
  - Advanced Airfoils
  - Advanced Composites
  - Advanced Engines
  - Active Controls
- o COMPARE LAMINAR & TURBULENT ADVANCED AIRCRAFT

For the initial base case LFC aircraft, the first 70 percent of both surfaces of the wing is assumed to be laminarized. This is compatible with the use of a conventional trailing edge high lift system. The initial LFC surface is a porous glove concept composed of a sandwich of 50 x 250 Dynapore stainless steel outer surface supported by honeycomb and Kevlar epoxy stiffener materials. No laminarization is assumed for the fuselage and tail surfaces.

5.2 CONFIGURATION INTEGRATION STUDIES

Four major trade studies were made in the development of the final LFC aircraft configuration, as summarized below:

Study I

- Initial preliminary design of 1990-95 laminar flow control (LFC) and turbulent aircraft configurations, feasibility and performance comparisons -
  - Model No. 3128 (Laminar Flow)
  - Model No. 3127 (Turbulent Flow)
  - 4-engine arrangement
  - Suction over 70 percent chord on both wing surfaces for LFC. See Section 5.3.

Study II

- Trade study of four-engine vs three-engine configurations resulting in selection of the three-engine arrangement. See Sections 5.4 and 7.2.2.

Study III

- Trade study of four vs two wing mounted suction engines resulting in the selection of two suction engines. See Sections 5.5, 7.2.3 and 10.6.

Study IV

- Comparison of effects of extent of laminarization
  - upper and lower airfoil surface suction to 70 percent chord compared with upper airfoil surface only to 85 percent chord
- comparable turbulent aircraft
- all 3-engine arrangements

Three-views of the above-mentioned configurations, the associated performance characteristics, and the weight comparisons are presented in Section 5.6.

Discussion of these studies and pertinent subsystem descriptions for the LFC and turbulent aircraft follows. The detail substantiation of subsystem design may be found in the other sections of this report dealing with particular disciplines. However, discussions concerned with the integration of the subsystem into the aircraft configuration are included in this section. The economic evaluation of the laminar flow control versus turbulent aircraft should be based on the final configurations only, as presented in Section 6.0.

Douglas consulted with United Airlines (passenger) and with The Flying Tigers (freight/cargo) airlines during the course of these studies. Their comments are included under operational aspects, Section 5.7.

5.3 STUDY I - INITIAL BASELINE PRELIMINARY DESIGN OF LAMINAR FLOW CONTROL (LFC) and TURBULENT AIRCRAFT CONFIGURATIONS

5.3.1 General

The initial baseline laminar flow aircraft serves as a configuration into which "first-go-round" feasible LFC subsystems may be integrated. Trade studies are then performed to evaluate the merits of the LFC subsystem designs.

Updating the base case LFC configuration, as the study progresses, assures that the recommended subsystems such as the airfoil section, LFC structure, LFC suction and manifolding systems, suction compressor drives, sizing, and locations are all compatible and capable of integration into an efficient practical aircraft. For the initial baseline laminar flow aircraft, only the first 70 percent of the wing chord on both surfaces is assumed to be laminarized; there is then sufficient room for a conventional trailing edge high lift system to be installed. A porous suction surface concept is used for laminarization. All fuel tankage is in the wings. Three-views of the aircraft and the initial study ground rules are given in Figures 5-2 a & b and Table 5-2 respectively.

Discussions of configuration characteristics, rationale for selection, and the effects of technology assumptions on aircraft sizing and performance characteristics are included in subsequent paragraphs.

5.3.2 Aerodynamics

a) Wing Planform - The wing planform characteristics selected for the base case aircraft are as follows:

	Laminar	Turbulent
Sweep angle @ 1/4 chord	30°	30°
Taper ratio	.3	.3
Aspect ratio	12	12

	WING	HORIZ	VERT
AREA m^2 (FT^2)	381 (4100)	64 (693)	63 (679)
ASPECT RATIO	12	5	1
TAPER RATIO	0.3	0.4	0.8
SWEEP	30°	30°	40°
THICKNESS RATIO	0.113 AVG	0.11	0.11
DIHEDRAL	4°	-3°	—
TAIL VOLUME	—	0.75	0.051

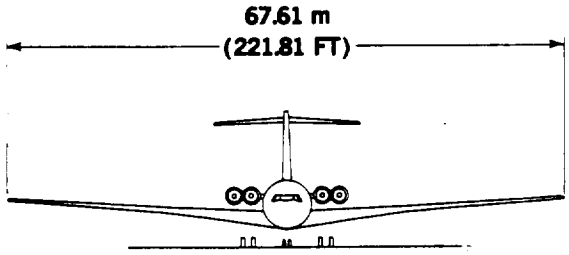

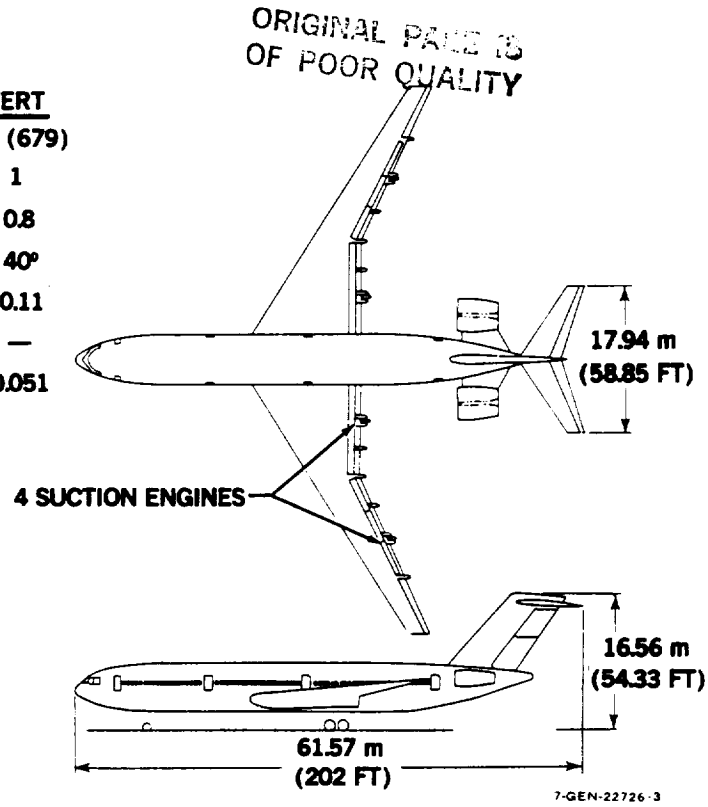

FIGURE 5-2a. INITIAL LFC BASE CASE AIRPLANE

	WING	HORIZ	VERT
AREA m^2 (FT^2)	267 (2870)	89 (960)	46 (495)
ASPECT RATIO	12	4	1.6
TAPER RATIO	0.3	0.35	0.35
SWEEP	30°	30°	35°
THICKNESS RATIO	0.132 AVG	0.10	0.10
DIHEDRAL	4°	7°	—
TAIL VOLUME	—	1.52	0.078

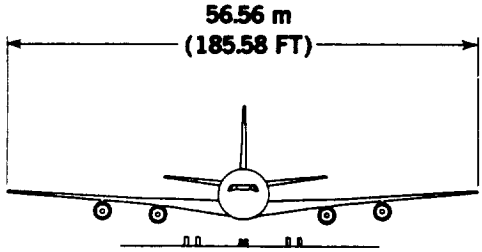

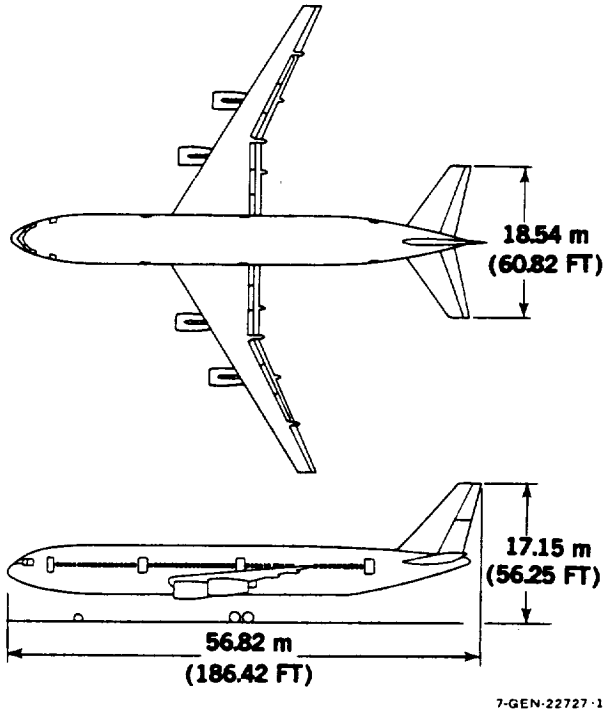

FIGURE 5-2b. INITIAL TURBULENT BASE CASE AIRPLANE

Table 5-2
INITIAL BASELINE STUDY GROUND RULES

GENERAL	
Design N	- 2.5 maneuver load factor - limit
Design Sink Speed	- 10 FPS at design landing weight
Active Controls	- Gust and maneuver load alleviation
	- Relaxed static stability
WING	
Airfoil Section	- Turbulent-Supercritical; Laminar-Shock-Free
L.E. Devices	- Turbulent-VCK; Laminar-None
T. E. Devices	- Flaps, Ailerons, Spoilers
FUSELAGE	
Cross Section	- Circular
Pressurization	- 60kPa (8.7 PSI)
LANDING GEAR	
Field	- Hard Surface
Advanced Materials	- Carbon Brakes
POWER PLANT	
Engines	- Advanced Technology Turbofan (4)
Engine T/W	- 7.0
Fan Duct Length	- Long
Thrust Reversers	- Fan, primary
By Pass Ratio	- 6
FUEL SYSTEM	
Fuel Tanks	- 4 Main tanks plus center wing all integral
Fuel Density	- 778.9 kg/m^3 (6.5 lb/gal)
FLIGHT CONTROLS & HYDRAULICS	
Actuators	- Integral servo pumps
Plumbing	- Titanium
Controls	- Fly-by-wire
Pressure	- 27.6 MPa (4,000 psi)
AUXILIARY POWER PLANT	
Unit	- Advanced technology
APU Location	- Aft fuselage
INSTRUMENTS	
Advanced Technology	- Fiber optics
ELECTRICAL SYSTEM	
Primary Power	- VSCF Generators
Supplemental Power	- VSCF Generators on APU
Circuitry	- E-Mux
AVIONICS	
Circuitry	- Mini-comp, A-Mux
Cooling	- DC-10 type
ICE PROTECTION	
Protection	- Engine inlet, wing L.E., windshield

The wing sweepback of 30^{o} is consistent with current Douglas turbulent advanced transport studies and is selected on the basis of compatibility of the wing thickness permissible for an operational C_L of .5 to .6 considering the internal volume available for landing gear stowage and the suction manifolding installation. Preliminary checks with a sweep angle of 25^{o} and the associated thinner airfoil sections indicated that volume limitations may exist.

As shown later under item 5.3.7, preliminary aspect ratio trade study results show that, for both the turbulent and laminar flow cases, aspect ratios of 12 and 14 gave essentially the same minimum takeoff gross weight. Consequently, the lower aspect ratio of 12 which gave more space for suction ducting, was selected.

The planform trailing edge fairing or "yehudi", required to submerge the landing gear strut within the wing depth, extends from the fuselage intersection to 42.8 percent semispan. Definition of the airfoil thickness at the fuselage wing intersection is based on the extended chord including the "yehudi" rather than on the trapezoidal wing chord.

b) Airfoil Section - On the basis of the supercritical and advanced airfoil work which has been accomplished and is underway at Douglas, the following airfoil sections are selected for the base case configurations:
(See Section 7.1)

	Laminar	Turbulent
Airfoil Section	Shock-free	Supercritical
Root t/c	DSMA 679 Type/13.3%	DSMA 679 Type/15%
Aero Break t/c	DSMA 691 Type/11.1%	DSMA 684 Type/12.5%
Tip t/c	DSMA 691 Type/10.5%	DSMA 686 Type/11.8%
C_L Design	.50	.64

A comparison of the base case airfoil contours, at three spanwise locations is presented in Figure 5-3. The airfoil thickness is compatible with buffet-free operation at the design C_L. Figure 5-4, which shows the $C_{L_{buffet}}$ variation with $M/M_{divergence}$ for the turbulent aircraft, indicates that

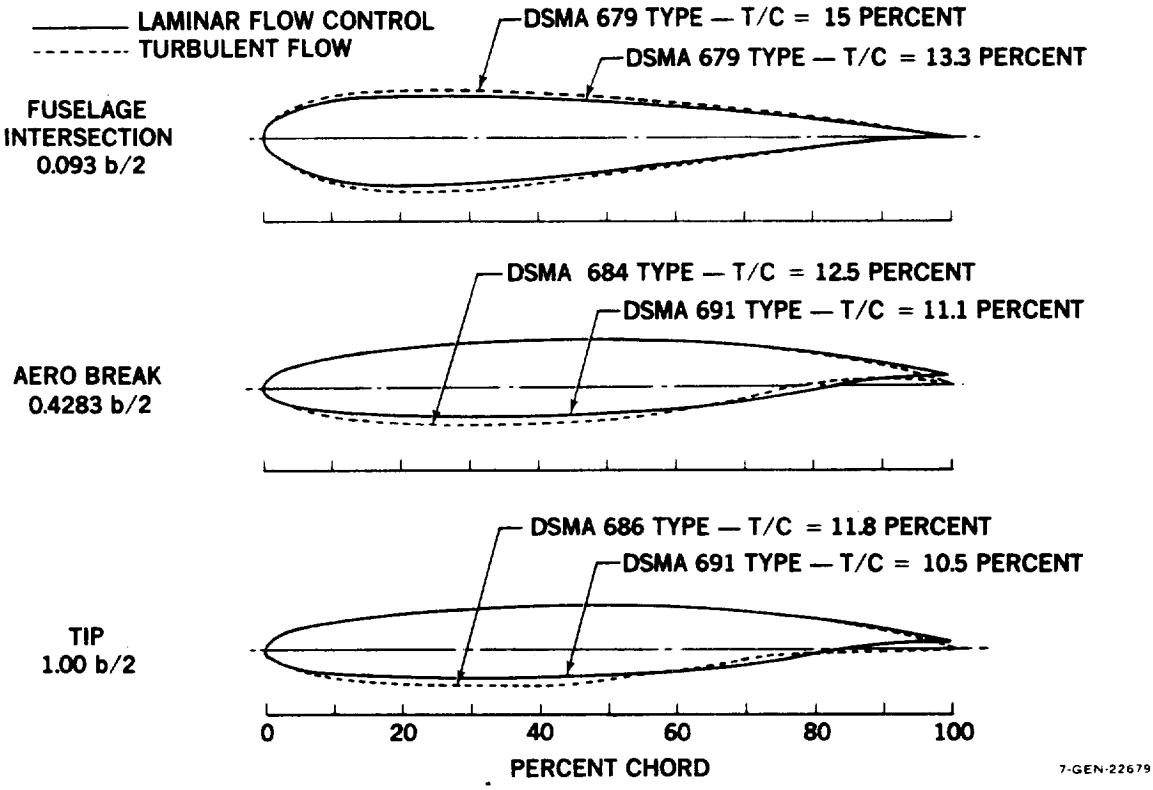

FIGURE 5-3. BASE CASE AIRFOILS ASSUMED

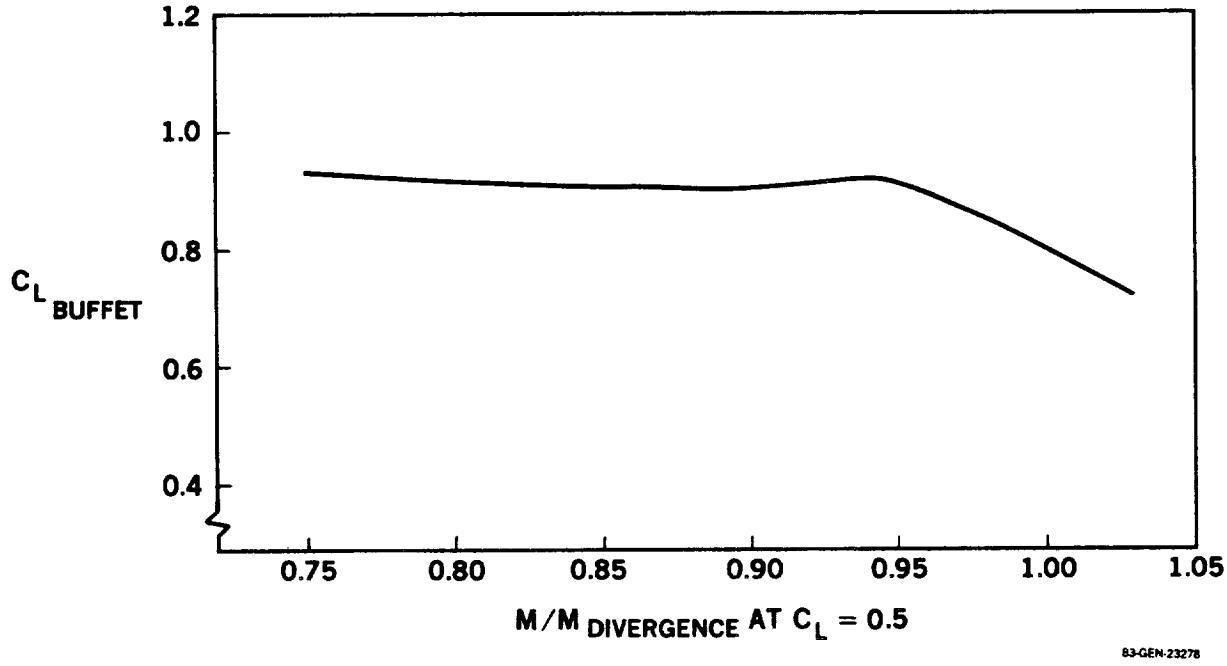

FIGURE 5-4. BUFFET BOUNDARY FOR TURBULENT BASE AIRCRAFT

$C_{L_{buffet}}$ is .9 or more in the operating regions of interest. In the case of the laminar flow aircraft, the $C_{L_{design}}$ of .5 is a more limiting condition than buffet; the corresponding $C_{L_{buffet}}$ variation for the laminar flow case is therefore not defined. The airfoils selected for the laminar aircraft are designed to be shockfree at the design C_L, with no significant amount of separation even if turbulent flow should occur on the laminarized portion of the airfoil. More than sufficient buffet margin exists with these shock-free airfoils.

The turbulent airfoils are designed to provide satisfactory compressibility drag characteristics at the cruise Mach number of 0.8 as well as an adequate margin before buffet onset. Figure 5-5 summarizes the effects of average wing thickness and airfoil design on the design cruise C_L with a wing sweep of 30^o. For the LFC wing, an operational C_L of .5 corresponds to an average wing thickness of 11.5 percent. The use of advanced supercritical airfoils for the turbulent design allows a thicker wing to be used for a given $C_{L_{operating}}$ (for example, C_L = .6 allows an average wing thickness of 14 percent). Figure 5-5 which is derived from previous Douglas aerodynamic studies, clearly illustrate the rationale for selection of a thinner wing for laminar flow aircraft than for the turbulent. The aircraft sizing work of this study shows that the design $C_{L_{cruise}}$ of .5 is essentially optimum for the base case laminar aircraft.

The maximum thickness of the wing varies spanwise, as shown in Figure 5-6. The thicknesses from the fuselage intersection to the aero break are based on the total wing chord. Relative to the trapezoidal planform chord, the root aircraft thickness would be 22 percent.

Wing Twist - The wing twist distribution, based on Douglas studies of similar wings, is as shown in Figure 5-7 for both the laminar and turbulent aircraft. For these preliminary layouts, no distinction is made between the laminar and turbulent twist distribution.

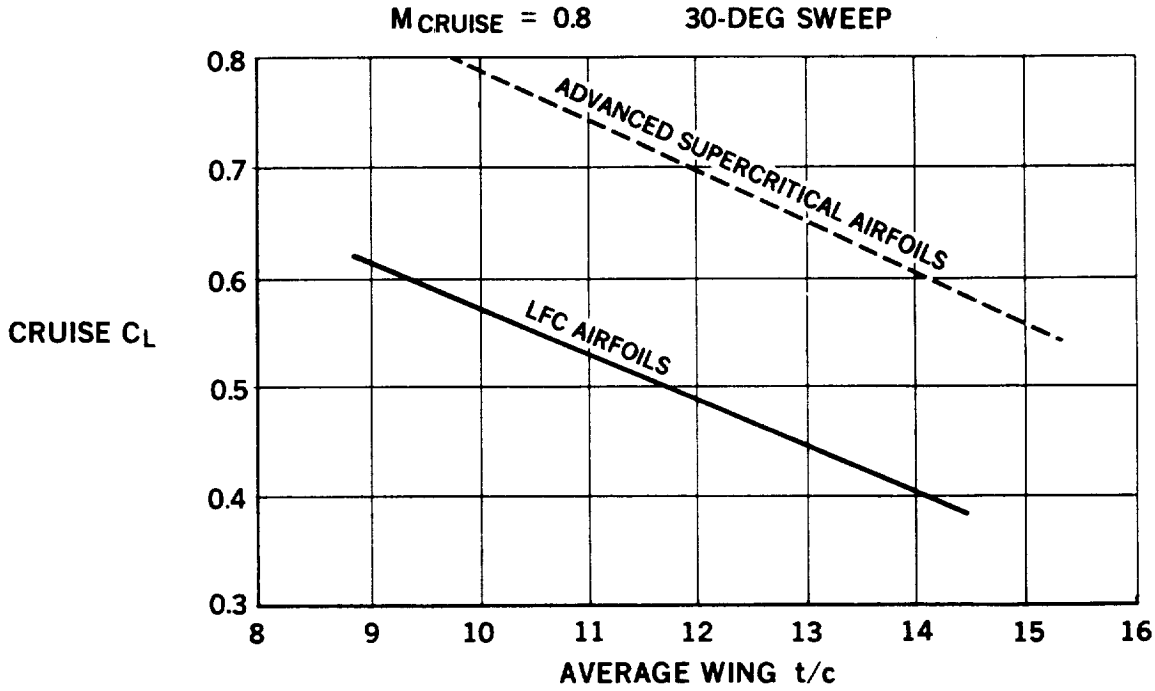

NOTES: (1) AIRFOILS DESIGNED TO HAVE LAMINAR FLOW TO 70% CHORD
(2) AIRFOILS HAVE ATTACHED TURBULENT FLOW WITH LFC OFF

FIGURE 5-5. CRUISE C_L VS WING THICKNESS/CHORD RATIO

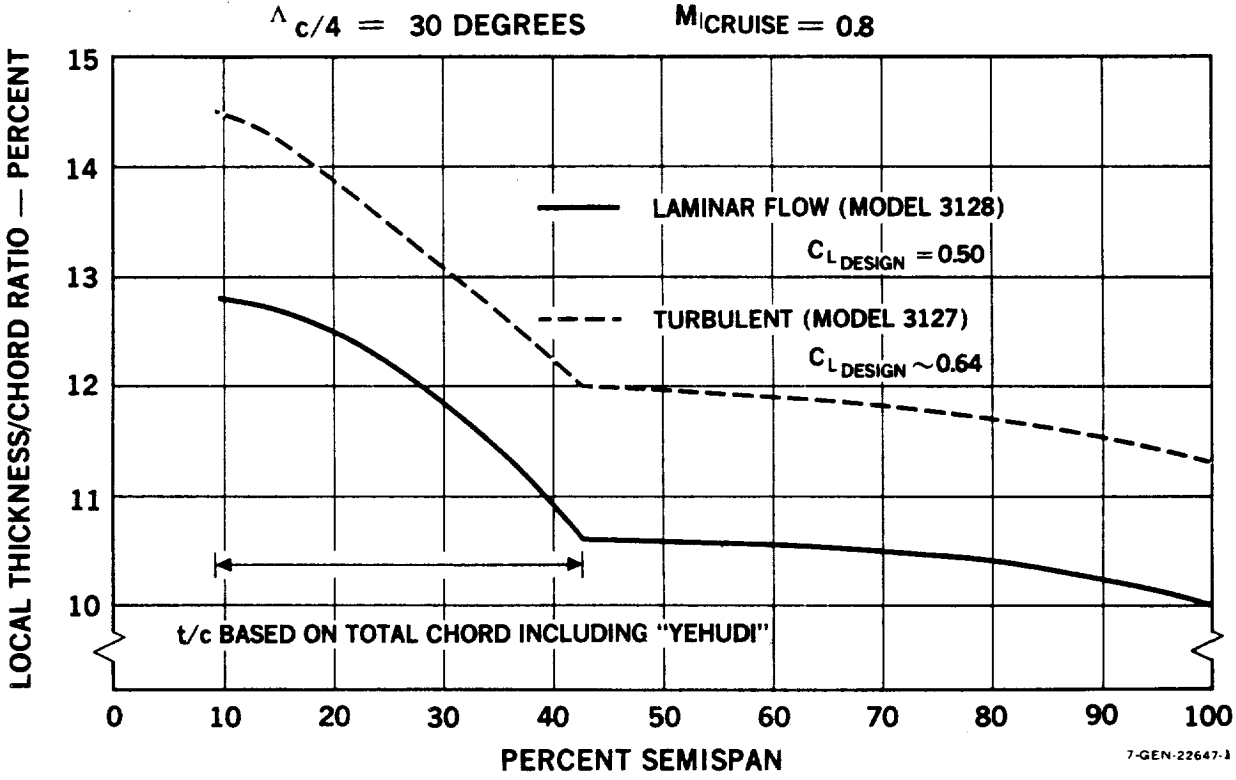

FIGURE 5-6. PRELIMINARY WING THICKNESS DEFINITION

Empennage Sizing - The size of the horizontal tails for the base case aircraft is influenced by the use of active controls compatible with a 1990-95 time period. The horizontal tails are not sized as is usual by stability considerations at the aft c.g. limit, but by the criteria given in Table 5-3 below.

Table 5-3
TAIL SIZING CRITERIA

LFC AIRCRAFT

Horizontal

Control for Nose-Wheel-Liftoff at 1.15 V_{stall} (Elevator deflected)

Vertical

Directoral Stability

TURBULENT AIRCRAFT

Horizontal

Trim at 1.4 V_{stall} in landing approach with ice on the tail

Vertical

Control, with full rudder, at 56.6 m/s (110 KN) minimum ground control speed

The stringent requirement imposed on the turbulent aircraft horizontal tail is due to its powerful high lift system and associated high pitching moments; the nose wheel lift-off criterion is less critical. For both aircraft, the amount of negative stability permissible is limited by the physical arrangement of the aircraft such that the tip-over requirements are satisfied. Tail sizing criteria and aircraft balance for each configuration are discussed separately in the following paragraphs.

a. Laminar Flow Control Aircraft - Considering the aircraft balance associated with the four rear engines, the T-tail installation and the landing gear stowage requirement in the wing, the main landing gear is located at the 60 percent wing MAC. With this arrangement, the aft c.g. is limited to 39 percent wing MAC in order to prevent the c.g. from moving aft of the main gear in the tip-over attitude (tail-on-ground).

With aft-mounted engines, the aircraft c.g. and the wing are further aft relative to the c.g. of the payload carried in the fuselage. The required c.g. travel is therefore greater than with wing mounted engines and it is estimated that a c.g. range of 28.7 percent MAC is appropriate for the LFC aircraft. This percentage MAC corresponds to a 69.6 inch c.g. travel or 3.3 percent of the fuselage length. With this c.g. range, the forward limit is at 10.3 percent wing MAC. The horizontal tail is then sized to provide sufficient longitudinal control (with elevator deflected) for nose-wheel-lift-off (NWLO) at 1.15 V_s. With this horizontal tail, neutral stability occurs at 21 percent MAC, and at the aft c.g. limit of 39 percent MAC, the aircraft has 18 percent negative stability.

The vertical tail is sized to provide adequate directional stability since the minimum ground control speed is less than 56.6 m/s (110 knots). The relatively simple high lift system assumed for the laminar flow configuration does not impose sizing requirements on the tail.

b. Turbulent Aircraft - Considering the balance of the aircraft with four wing-mounted engines, the landing gear is placed at 71 percent wing MAC. (As indicated earlier by Figure 5-3, the thicker supercritical airfoil provides adequate stowage for the landing gear strut at a more rearward % MAC than for the laminar flow aircraft.) The aft c.g. limit for this turbulent configuration is also established by the tipover limit and is at 47.5 percent wing MAC. A c.g.

travel of 20 percent MAC is judged appropriate for this aircraft, equal to 41.6 inches. This is consistent with DC-10 aircraft c.g. travel in terms of percentage of fuselage length.

Critical factors in sizing the horizontal tail are:

- Static longitudinal stability is provided at the tail-on ($dC_m/dC_L = 0$) neutral point located at 42.5 percent MAC, at a speed midway between V_C and V_D (assumed M = .77 @ 4,570 m (15,000 Ft) altitude).

- At the forward c.g. limit, the horizontal tail size must be adequate to provide longitudinal trim at 1.4 V_{stall} in the landing approach with ice on the tail. This stringent requirement is due to the powerful high lift system with associated high pitching moments. The nose wheel liftoff criterion is less critical.

With the forward c.g. limit at 22.5% MAC, the tail sized for neutral stability at the 42.5% MAC, and the aft c.g. limit allowed to go to the tip-over limit of 47.5%, the aircraft has 5 percent negative stability. It should be noted that this modest amount of negative stability is the maximum physically possible with this configuration.

Active Controls - For these base case aircraft, except for the yaw damper, active controls are not considered in the vertical tail sizing. Rationale for this decision is based on the safety consideration that with active controls on both the longitudinal and directional axes, a failure on both axes could result in the pilot not being able to control the aircraft.

A parametric tail sizing study was performed in the early stages of configuration definition. Variations of tail volume, c.g. location, and c.g. range as a function of wing area and aspect ratio as applied to the LFC and the turbulent aircraft were taken into consideration. Maneuver/gust load alleviation was not included. Douglas experience indicates that other criteria become critical before any significant advantages of maneuver or gust load alleviation can be realized. For strength-designed aircraft, gains of 1 to 2 percent are realizable in some cases. The decision not to consider maneuver/gust load alleviation on these base case aircraft was validated since the wing stiffness required to maintain aileron effectiveness was shown to be more critical than strength for the wing structure. See Section 9.1.6.

Low Speed High Lift System - With LFC limited to 70 percent wing chord, a conventional trailing edge high lift system can be used. Either a single slotted extensible flap or a double slotted flap are capable of providing the high lift characteristics that are given in Figures 5-8 and 5-9. Leading edge devices for high lift are not considered feasible for this LFC configuration. The landing flap angle is limited to that for which $1.3\ V_{min}$ occurs at zero angle of attack to avoid landing on the nosewheel first. For the base case laminar aircraft, this is a flap angle of 22.5 degrees, Figure 5-8.

The low speed high lift system assumed for the base case turbulent aircraft is an advanced system consisting of both a variable camber Krueger (VCK) leading edge device plus trailing edge flaps. Characteristics of this high lift system are shown in Figure 5-10.

5.3.3 Structural Design

With the exception of the LFC features, the structural design of the two base case aircraft is conventional but includes advanced materials and concepts appropriate to the 1990-95 operational time period. The design life, relatively crack-free, is 60,000 hours with a scatter factor of 2, or 120,000 hours for fatigue. The design load factor is 2.5 g. Section 9.1 gives details of structural concept studies.

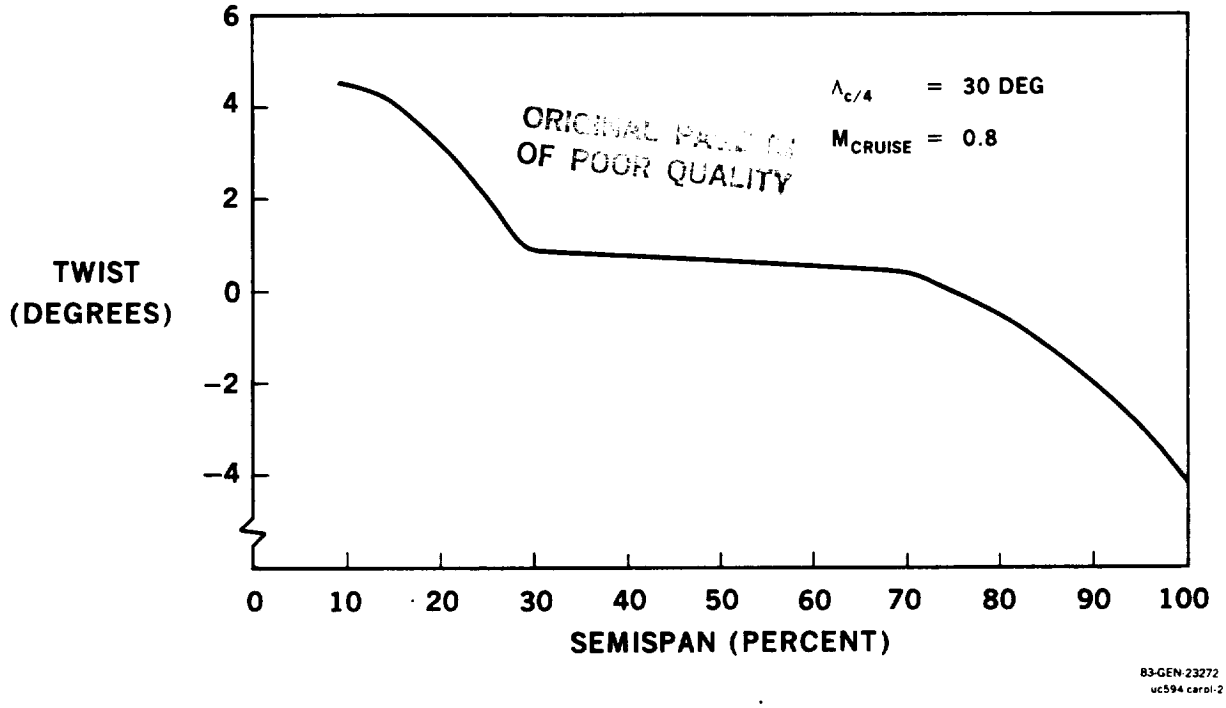

FIGURE 5-7. PRELIMINARY WING TWIST DISTRIBUTION

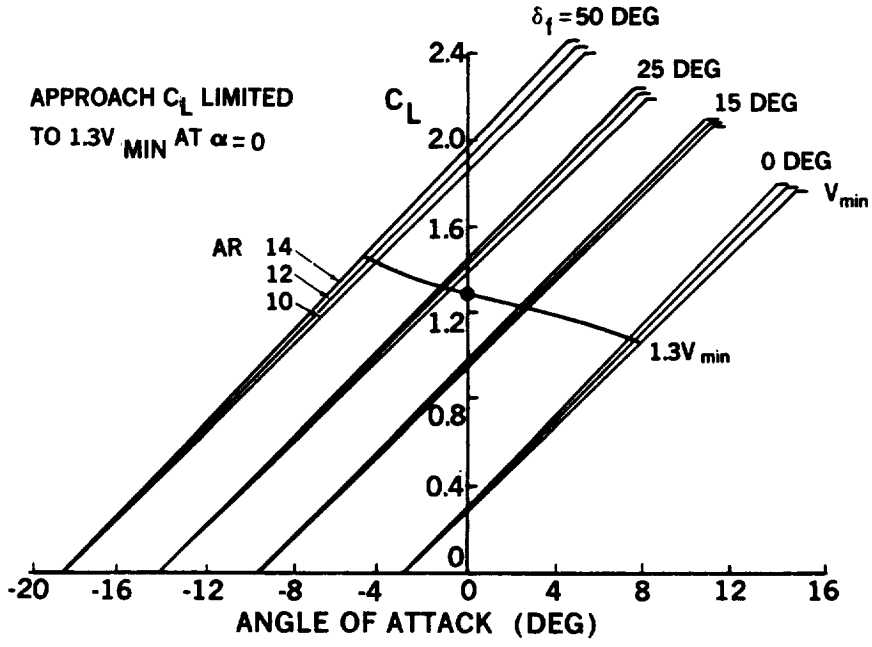

FIGURE 5-8. LIFT CURVES FOR LFC AIRCRAFT

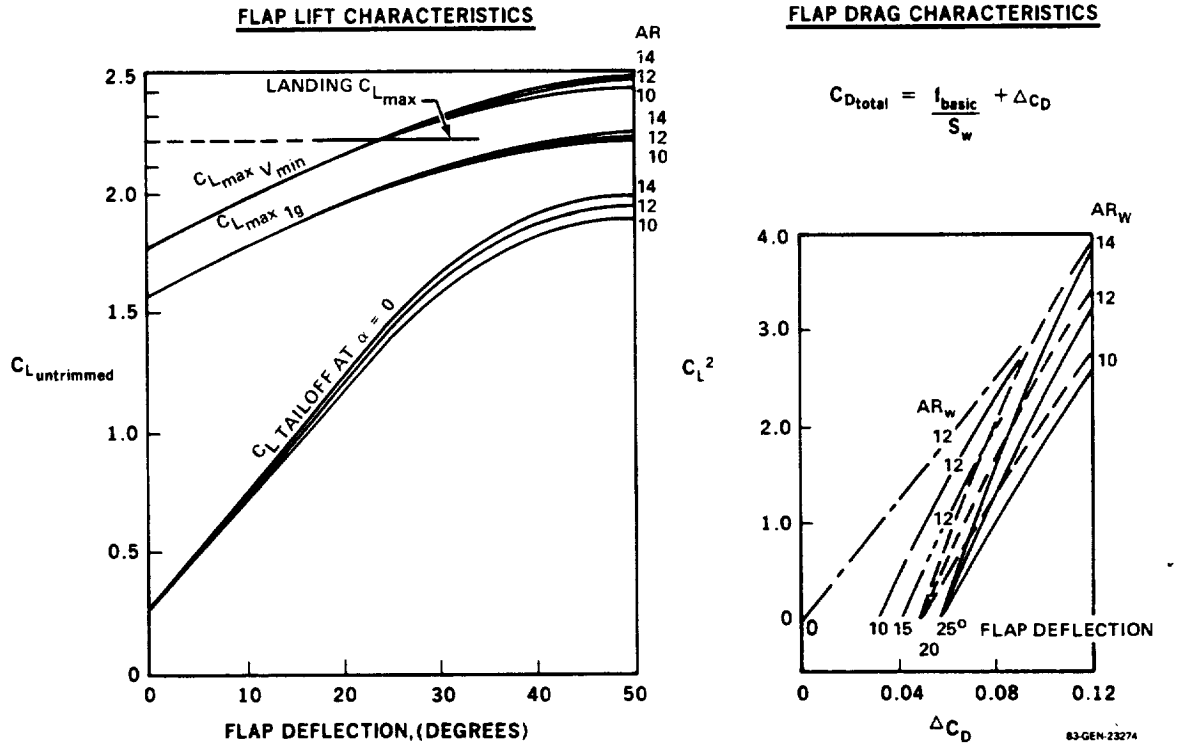

FIGURE 5-9. PRELIMINARY FLAP CHARACTERISTICS FOR LAMINAR FLOW CONTROL AIRCRAFT

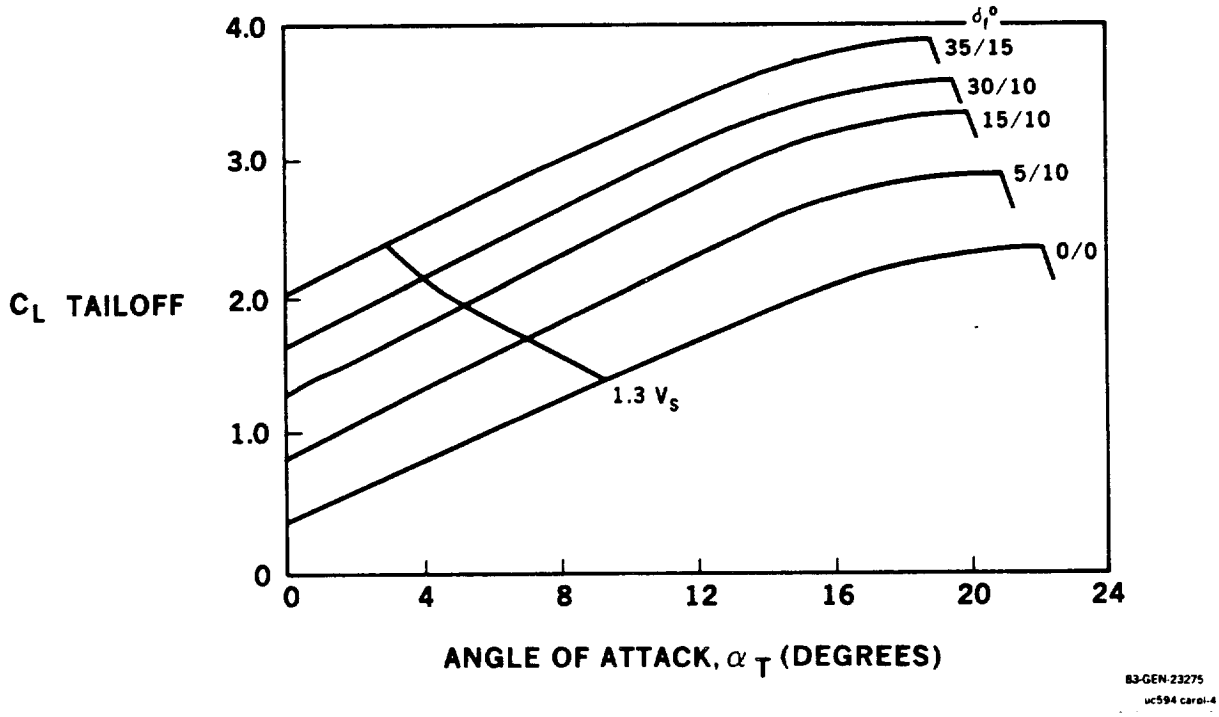

FIGURE 5-10. ESTIMATED TAILOFF LIFT CURVES FOR TURBULENT BASE AIRCRAFT

Composite Material Utilization - Advanced composite materials are used extensively as described in Tables 5-4 a and b, consistent with the current composites development programs. In the case of the wing and tail components, composite materials are used whenever practical but all attachments and fasteners are metal. The effect of this use of composite materials on component weights is shown in Table 5-4c.

In the early design study phase, composite utilization in the fuselage was subject to a trade study. Initially the optimistic assumption of 80 percent composite material was considered because NASA planning in the ACEE program originally included the development of a composite fuselage. However, it is now doubtful that the development of a full-scale fuselage will take place in time for utilization on a 1990-95 design and a much lower percentage of composite materials was therefore assumed. The effect on aircraft sizing of the more conservative assumption (15 percent composite shell panels and 0 percent composite frames) was checked and the effect on the turbulent aircraft weights, for example, is as follows:

Δ Weight empty	+2244 kg (+ 4,948 lb)
Δ Takeoff gross weight	+5806 kg (+12,800 lb)
Δ Fuselage structural weight	+14.4%

The effect of these assumptions of composite usage in the fuselage on the LFC aircraft takeoff gross weight and sizing is shown in Figure 5-11.

COMPONENT	BASIC CONSTRUCTION	MATERIAL UTILIZATION			
		COMPOSITE		METAL	
		TYPE	%	TYPE	%
WING					
Skin Panels	Skin/Stringer	Gr/Ep	100		0
Spars	Stiffened Web	Gr/Ep	80	Al	20
Ribs	Stiffened Web	Gr/Ep	90	Al	10
Leading Edge	Multi-Rib	Gr/Ep	90	Al	10
Trailing Edge	Multi-Rib	Gr/Ep	90	Al	10
Slats	Multi-Rib	Gr/Ep	70	Ti	30
Flaps	Multi-Rib	Gr/Ep Kev/Ep	40 10	Al Ti	20 30
Ailerons	Multi-Rib	Gr/Ep Kev/Ep	65 15	Al	20
Spoilers	Multi-Rib	Gr/Ep	80	Al	20
Wing Tips	Multi-Rib	Kev/Ep	80	Al	20
Fairings	Multi-Rib	Kev/Ep	100		0
Pylons	Multi-Frame	Gr/Ep	80	Ti	10
				Al	10
Nacelles	Multi-Frame	Gr/Ep	90	Al	10
MLG Doors	Multi-Beam	Gr/Ep	65	Al	20
		Kev/Ep	15		
VERTICAL TAIL					
Skin Panels	Skin/Stringer	Gr/Ep	100		0
Spars	Stiffened Web	Gr/Ep	80	Al	20
Ribs	Stiffened Web	Gr/Ep	90	Al	10
Leading Edge	Multi-Rib	Gr/Ep	90	Al	10
Trailing Edge	Multi-Rib	Gr/Ep	90	Al	10
Rudders	Multi-Rib	Gr/Ep Kev/Ep	65 15	Al	20
Tip	Multi-Rib	Kev/Ep	80	Al	20

TABLE 5-4a. Structure and Material Assumptions Compatible with 1990-95 Aircraft

(Continued).

COMPONENT	BASIC CONSTRUCTION	MATERIAL UTILIZATION			
		COMPOSITE		METAL	
		TYPE	%	TYPE	%
HORIZONTAL TAIL					
Skin Panels	Skin/Stringer	Gr/Ep	100		0
Spars	Stiffened Web	Gr/Ep	80	Al	20
Ribs	Stiffened Web	Gr/Ep	90	Al	10
Leading Edge	Multi-Rib	Gr/Ep	90	Al	10
Trailing Edge	Multi-Rib	Gr/Ep	90	Al	10
Elevators	Multi-Rib	Gr/Ep Kev/Ep	65 15	Al	20
Tip	Multi-Rib	Kev/Ep	80	Al	20
FUSELAGE					
Shell Panels	Skin/Stringer	B/Ep	15	Al	85
Frames	Stiffened Web		0	Al	100
Floor Panels	Stiffened Panel	Gr/Ep	80	Al	20
Floor Beams	Stiffened Web	Gr/Ep	90	Al	10
Keel	Stiffened Web	Gr/Ep	90	Al	10
Doors & Hatches	Multi-Beam Stiffened Panel	Gr/Ep Kev/Ep	65 15	Al	20
Radomes	Multi-Frame	Kev/Ep	100		0
LANDING GEAR					
Torque Links	Beam Fig	Gr/Ep	25	Ti	75
Drag Links	Monocoque Tube	Gr/Ep	40	Ti	60
Side Brace	Monocoque Tube	Gr/Ep	40	Ti	60

TABLE 5-4b. Structure and Material Assumptions Compatible with 1990-95 Aircraft

Table 5-4C

COMPOSITE FACTORS

	COMPOSITE WEIGHT FACTOR*
Wing	
Box	.73
Leading Edge	.73
Trailing Edge	.73
Wing/Fuselage Fairing	.70
Tips	.76
Ailerons	.76
Flaps	.85
Slats	.79
Spoilers	.76
Horizontal Tail	
Bending Material	.70
Spar Webs	.76
Ribs	.73
Leading Edge	.73
Trailing Edge	.73
Elevator	.76
Tips	.76
Fairing	.85
Vertical Tail	
Bending Material	.70
Spar Webs	.76
Ribs	.73
Leading Edge	.73
Trailing Edge	.73
Rudder	.76
Tip	.76
Fuselage	
Shell	.96
Radome	.70
Wing & Landing Gear Support	.85
Tail Support	.85
Cockpit Floor	.74
Main Cabin Floor	.74
Entrance Doors	.76
Cargo Doors	.76
Enclosure	.95
Landing Gear Doors	.76
Miscellaneous	.88
Propulsion	
Engine Cowl	.75

* Factor is a ratio of (composite and conventional material) to (all conventional material).

A comparison of the effect of the finally selected use of advanced composite in both the laminar flow and turbulent aircraft is given in Table 5-5. The result is 15 to 18 percent reduction in structural weight over that of the all-metal aircraft. In terms of manufacturer's weight empty, the weight saving due to composite usage is 9 to 10 percent.

Structural Design/Integration - LFC Wing - The wing outer surface is a porous sandwich glove concept. It is attached to the corrugated main wing box by self-sealing fasteners in press-fit bushings. The porous cover is thus removable without affecting the primary structural integrity. This simplifies maintenance activities such as cleaning, inspection and repair of the internal structure.

The design selected initially for the LFC outer glove panel is shown in Figure 5-12. The porous surface is supported by the corrugated main box panel creating an integral spanwise duct for suction air collection. The porous surface is of woven stainless steel Dynapore and the corrugations are of graphite/epoxy composite material. The diffuser is a vacuum formed thermo-plastic sheet that provides plenum compartmentation and airflow metering.

5.3.4 Suction/Manifolding System

General Arrangment - As shown in the three-view, Figure 5-2a, four compressor drive units are used on the initial baseline LFC aircraft. Final selection of the number of these compressor drive units was the subject of a separate trade study, Sections 5.6, 7.2.3, and 10.6, resulting in the selection of only two units. At this stage, however, the use of four units was based on the following design rationale:

- The design of the manifolding must maintain high efficiency throughout; therefore, the ducting must have gentle bends and the losses of momentum or velocity kept to a minimum.

Table 5-5

COMPOSITE WEIGHT REDUCTION

	LAMINAR FLOW				TURBULENT FLOW			
	ALL METAL		COMPOSITE (AS ASSUMED)		ALL METAL		COMPOSITE (AS ASSUMED)	
	kg	(lb)	kg	(lb)	kg	(lb)	kg	(lb)
WING	30,620	(67,505)	24,812	(54,700)	23,146	(51,028)	17,620	(38,846)
HORIZONTAL TAIL	1,818	(4,008)	1,328	(2,929)	2,342	(5,164)	1,715	(3,781)
VERTICAL TAIL	2,043	(4,504)	1,763	(3,886)	1,579	(3,481)	1,353	(2,983)
FUSELAGE	18,932	(41,738)	17,305	(38,152)	18,767	(41,375)	17,155	(37,820)
ENGINE COWL	1,318	(2,906)	989	(2,180)	1,387	(3,057)	1,041	(2,294)
TOTAL	54,731	(120,661)	46,197	(101,847)	47,221	(104,105)	38,884	(85,724)
REDUCTION DUE TO COMPOSITE USAGE			-8,534 kg (-18,814 lb) = 15.6%				-8,337 kg (-18,381 lb) = 17.7%	

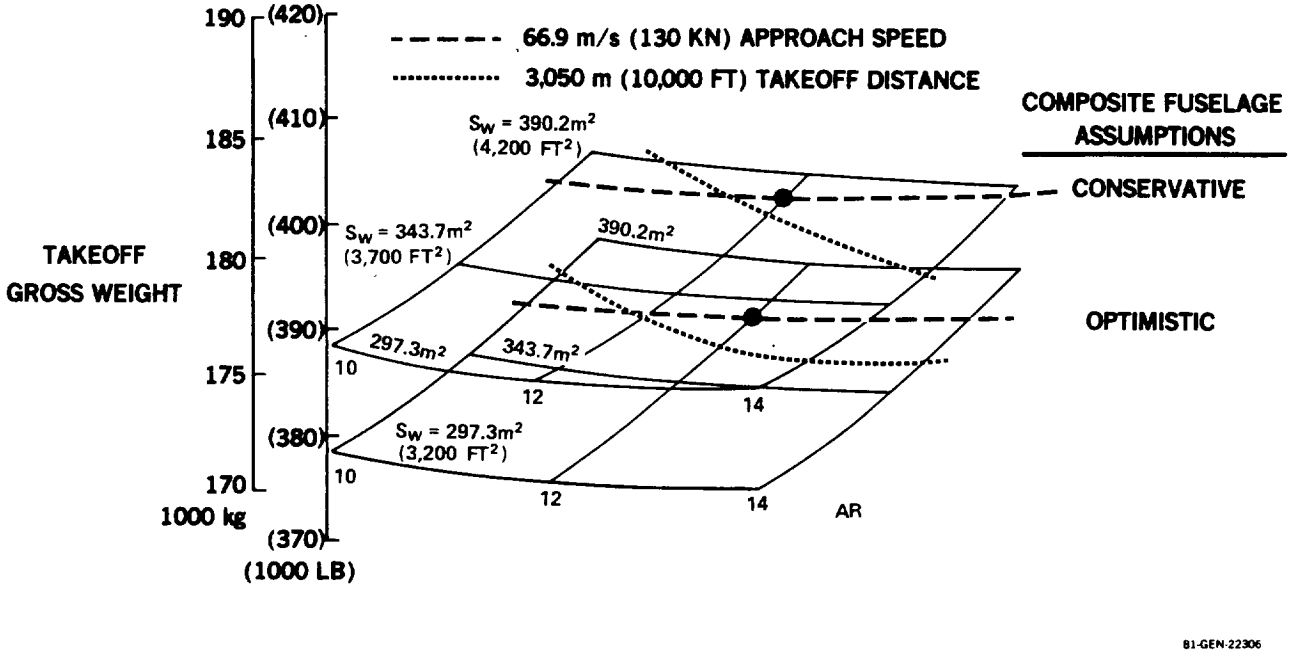

FIGURE 5-11. EFFECT OF COMPOSITE USAGE IN FUSELAGE ON LFC AIRCRAFT TAKEOFF GROSS WEIGHT

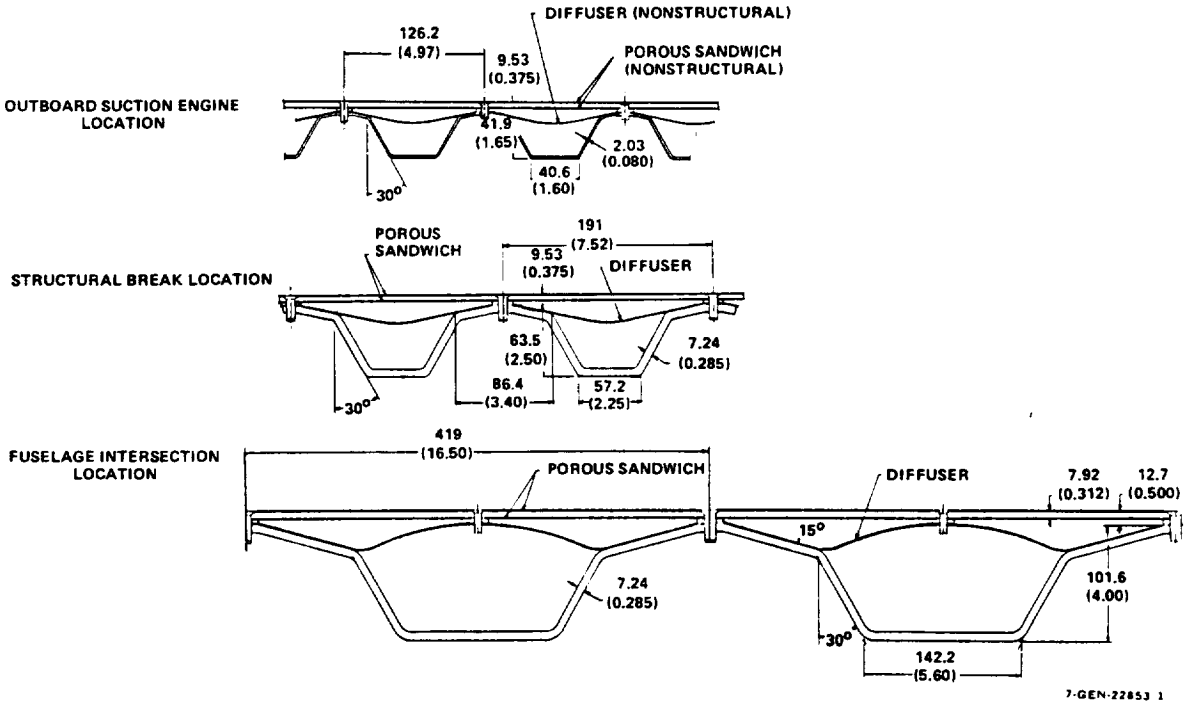

FIGURE 5-12. PSEUDO-ISOTROPIC COMPOSITE CORRUGATION

- To maintain high efficiency in the suction system, it is desirable that the air from the surface collection points be individually ducted as far as possible before being ducted to the suction pump. The individual ducting arrangement avoids large losses in momentum, or velocity, which are associated with a plenum chamber configuration.

- The internal ducting area available with corrugated stiffening is compatible with a four unit suction pump system; one suction pump per side would require larger individual ducts incompatible with the outboard wing structure.

- Four suction pumps versus two pumps reduces the effect of single pump failure. In the case of four suction pumps, the malfunction of one pump should result in loss of LFC over only one fourth of the wing surface rather than one half of the surface.

The four suction pumps are located spanwise under the wing such that the areas to be sucked are divided equally. The suction air is collected spanwise through the structural corrugations using two collector stations per side. Dry bay areas are used to provide space for the plumbing required for suction air to be ducted from the multiple spanwise corrugations (or flow channels) into mixing/collection chambers ahead of the pump inlets below the wing. Cross ducting of the suction flow between left and right wings for reliability purposes is not necessary and would incur ducting problems and weight penalties.

Integral ducting is formed by the corrugated wing structural panel and the outer surface. Sixteen spanwise corrugations run, top and bottom of the airfoil contour, tapering from the fuselage intersection to the tip of the wing. The structural/ducting integration is a critical factor in the design of the laminarized wing. In this particular case, the outboard suction engine is the critical location for ducting requirements; here the width and depth of

the corrugations as sized by structural requirements are consistent with the duct sizes required for suction manifolding. Dimensions of the structurally-designed corrugations at all other stations are in excess of those required.

Ducting requirements are based on a maximum flow velocity of M = .2, assuming 20 percent excess airflow over theoretical requirements during cruise conditions. The resulting duct areas are presented in Table 5-6 below.

Table 5-6
SUCTION SYSTEM DUCTING AREAS

Location	Flow Area	
	cm^2	(in^2)
Upper Wing Surface (X/C = .15 to .70)		
. Pump Location	322.58	(50.00)
. Minimum Flow Points	15.55	(2.41)
Lower Wing Surface (X/C = .15 to .70)		
. Pump Location	364.32	(56.47)
. Minimum Flow Points	15.35	(2.38)
Wing Leading Edge (X/C = 0 to .15		
. Pump Location	276.45	(42.85)
. Minimum Flow Points	13.81	(2.14)

Figure 5-13 presents a preliminary layout of the LFC suction air collector system for the initial base case configuration. This layout is of the dry bay area at the outboard suction pump station. For clarity, the upper and lower wing surface ducting are shown in separate drawings. The compressor drive/suction pump is mounted below the wing such that ducting may be taken through an opening in the lower wing skin.

The air collection ducting is divided into three separate manifolding systems: namely - the upper wing surface or low pressure air, the leading edge ahead of the front spar, and the lower wing surface; the latter are both higher pressure air. The lower pressure air from the upper wing surface is ducted into the low pressure ratio axial compressor where the pressure is increased to the level of that from the higher pressure areas of the wing. The two flows are then mixed and ducted into a higher pressure ratio compressor that exhausts the air at a velocity equal to the free-stream velocity. Previous studies indicate that efforts for any thrust recovery from such a system are not profitable.

Further details of the manifolding system requirements are described in Section 10.0 of this report.

Suction Pump and Drive Unit Sizing - Estimated suction requirements for laminarization, based on aerodynamic calculations, are as shown in Figure 5-14. The amount of suction air and the corresponding sizes for the suction compressors and drive units are thus determined. An axial flow compressor and a turboshaft drive were selected for the base case aircraft. The sizing ground rules are summarized in Table 5-7. See also Sections 7.1.3, 10.4 and 10.5.

Estimated fuel flow requirements are summarized in Figure 5-15. The brake specific fuel consumption is estimated to be achievable with a new technology turboshaft engine having a pressure ratio of 6 to 8.

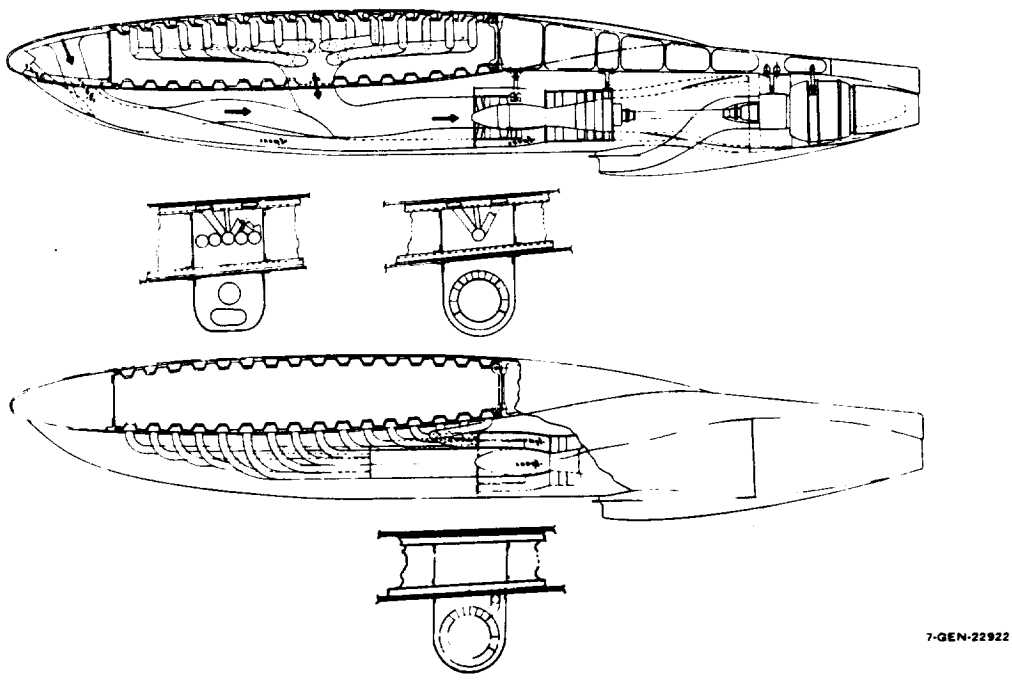

FIGURE 5-13. SUCTION PUMP/DRY BAY AREA INSTALLATION

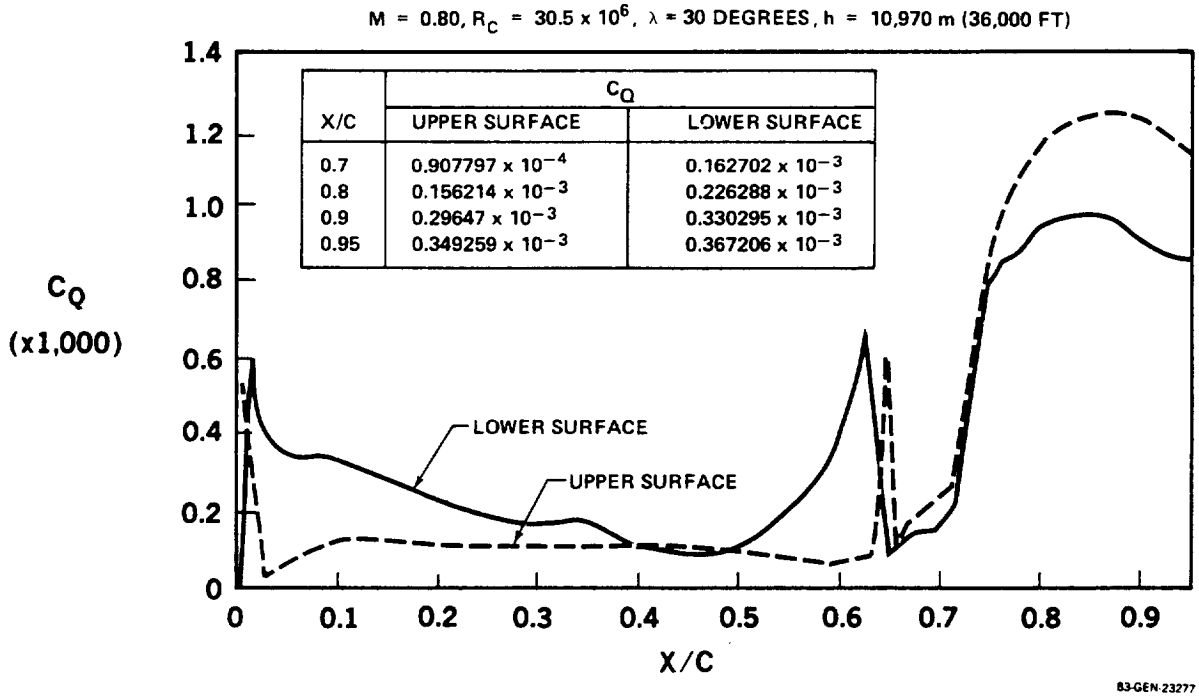

FIGURE 5-14. PREDICTED SUCTION REQUIREMENTS FOR LFC AIRFOIL

Table 5-7

SUCTION SYSTEM SIZING -- BASE CASE

SIZING CONDITION:

Altitude	=	12,190 m (40,000 Ft)
Wing Area	=	381 m^2 (4,100 Ft^2)
Aspect Ratio	=	12
Wing Sweep	=	30^o
M_o	=	0.8

SUCTION AIR QUANTITIES PER AIRPLANE Kg/s (LB/SEC)

W_{aUPPER}	=	3.04 (6.7)
W_{aLOWER}	=	5.44 (12.0)

corrected to pressure at compressor face

$\frac{W_a \sqrt{\theta_t}}{\delta_t}$ Upper = 26.22 (57.8)

$\frac{W_a \sqrt{\theta_t}}{\delta_t}$ Lower = 34.61 (76.3)

COMPRESSOR PRESSURE RATIO:

$Compressor_{Upper}$	P. R. =	1.36	
$Compressor_{Main}$	P. R. =	1.87	(for F_n = 0)

TURBOSHAFT POWER REQUIREMENTS PER AIRPLANE

At 12,190M (40,000 Ft) Altitude, 555.5 kW (745 HP)

Sea Level Equivalent = 1,566 kW (2,100 HP)

5.3.5 Propulsion System

The main propulsion units are advanced turbofan engines. Consistent with engine manufacturers' advanced technology levels, the engine is assumed to have a thrust/weight ratio of 7 and an 11 percent improvement in SFC over present day engine performance. Both of the initial laminar and turbulent flow aircraft are four engined configurations. The turbulent flow aircraft is a conventional wing installation but, the laminar flow aircraft engine installation is an aft-fuselage mounted arrangement. The aft engine mounting is necessary to avoid noise levels at the wing surface inconsistent with laminar flow. Study results of the near field noise environment due to the main propulsion engines (mixed flow CF6-50 type - E^3 concept, and a variable pitch fan - QCSEE concept) show that wing-mounted engines are not compatible with achieving LFC over the wing surface, see Section 7.2.

5.3.6 Surface Contamination Prevention/Removal

Several alternative systems were being considered at this time and reference should be made to Section 11.0.

5.3.7 Performance - Initial Baseline Aircraft

With the mission and study ground rules listed previously in Tables 5-1 and 5-2, the characteristics of the competitive LFC and turbulent aircraft that were illustrated previously in Figures 5-2a and b, are as presented in Table 5-8.

Estimated weights, based on the methods and assumptions given in Table 5-9, are as listed in Tables 5-10 a and b. Drag estimation is presented in Appendix 5A of this Section.

Geometric data for the sized aircraft are given in Table 5-11 and the resulting performance characteristics are compared in Table 5-12.

Table 5-8

AIRCRAFT CHARACTERISTICS

(STUDY I)

	LFC	TURBULENT
ENGINE	Advanced Turbofan	Advanced Turbofan
Thrust per Engine (4) kN (LB)	108.40 (24,370)	114.32 (25,700)
Installation	Aft Fuselage Mount	Pylon Mount on Wing
WING		
Area m^2 (Sq. Ft.)	381 (4,100)	267 (2,870)
Sweep Degree	30	30
Taper Ratio	0.3	0.3
Aspect Ratio	12	12
Airfoil	Shockless	Supercritical
Root T/C	13.3%	15%
Break T/C	11.1%	12.5%
Tip T/C	10.5%	11.8%
C_L Design	0.5	0.64
High-Lift System	No Leading Edge Device 25% Double Slotted Flap (or single slotted extensible flap) 80% Span	22% LE VCK 35% Two Segment Tracked Flap 80% Span
Sizing Criteria	Approach Speed 66.9 m/s (130 kN)	Takeoff Distance 3,050 m (10,000 Ft)
Configuration Selection Basis	Minimum TOGW	Minimum TOGW

Table 5-9

WEIGHT ESTIMATION METHODS & ASSUMPTIONS

COMPOSITE MATERIALS USE

As described in Tables 5-4a, b and c.

WING

Multi-station analysis based on critical gust and maneuver load conditions, Weissinger load distributions, aeroelastic effects, material allowables and weight/geometry relationships.

Gust and Maneuver Load Alleviation:

Seven percent wing weight reduction based on past studies.

Flutter:

Turbulent Flow Wing: Weight Penalty added to higher AR wings to provide stiffness equal to that of the AR = 10 wing.

Laminar Flow Wing: No penalty with fuselage mounted engines.

TAIL

Multi-component analysis based on critical gust and maneuver load conditions and weight/geometry relationships.

FUSELAGE

Shell Structure:

Multi-station analysis based on pressure, critical gust and maneuver load conditions. Pressure critical shell structure is determined by a 1P hoop tension stress allowable to prevent skin crack propagation.

Remaining Structure:

Weight/Geometry relationships.

Gust and maneuver load alleviation:

Two percent fuselage weight reduction based on past studies.

LANDING GEAR

Empirical weight relationship to takeoff gross weight based on correlation of several aircraft. Weight reduction due to carbon brakes based on Douglas, Goodyear, Goodrich, and Bendix studies.

Table 5-9 (Cont.)

POWER PLANT

Nacelle:

Empirical multi-component weight/geometry relationships.

Pylon, Thrust Reverser, and Exhaust:

Each component is based on empirical weight/geometry relationships. In addition, pylon weight considers engine position and supported weight.

Engine and Engine Systems:

Advanced technology engine weight based on T/W=7. Engine systems weight based on average of several turbofan engines.

Fuel System:

Empirical weight relationship to wing span and number of fuel tanks.

Gust and Maneuver Load Alleviation:

Pylon weight reduced 10 percent based on past studies.

FLIGHT CONTROLS AND HYDRAULICS

System Weight:

Empirical weight relationship to total control surface area based on correlation of several transport aircraft with multiple hydraulic systems.

Advanced Technology:

Total weight reduced 7 percent based on studies considering fly-by-wire, 4,000 PSI system, titanium tubing, and integral servo pump actuators.

INSTRUMENTS

Instrument weights based on DC-10 modified for four engines and advanced technology.

Fiber Optics:

Instrument wire weight reduced by 30 percent.

AVIONICS

Weight based on DC-10.

Advanced Technology:

Circuitry weight reduced by 50 percent for mini-comp wiring and 10 percent for A-Mux.

Table 5-10a

WEIGHT SUMMARY
(STUDY I)

	LAMINAR FLOW		TURBULENT FLOW	
	Kg	(LB)	Kg	(LB)
Wing	24,812	(54,700)	17,620	(38,846)
Horizontal Tail	1,329	(2,929)	1,715	(3,781)
Vertical Tail	1,763	(3,886)	1,353	(2,983)
Fuselage	17,305	(38,152)	17,155	(37,820)
Landing Gear	6,972	(15,371)	7,173	(15,814)
Nacelle	2,432	(5,361)	2,826	(6,231)
Propulsion	8,889	(19,597)	9,375	(20,668)
Fuel System	1,082	(2,386)	842	(1,857)
Flight Controls	2,530	(5,577)	2,151	(4,741)
Auxiliary Power Unit	470	(1,037)	470	(1,037)
Instruments	794	(1,751)	823	(1,815)
Hydraulics	1,047	(2,309)	890	(1,963)
Pneumatics	845	(1,862)	846	(1,864)
Electrical	1,574	(3,470)	1,574	(3,470)
Avionics	1,427	(3,146)	1,427	(3,146)
Furnishings	16,521	(36,422)	16,521	(36,422)
Air-Conditioning	1,217	(2,684)	1,225	(2,700)
Ice Protection	223	(492)	156	(344)
Handling Gear	28	(62)	28	(62)
Manufacturers Empty Weight	91,260	(201,194)	84,170	(185,564)
Operator's Items	5,596	(12,336	5,596	(12,336
Operator's Empty Weight	96,866	(213,530)	89,766	197,900
Payload	31,298	(69,000)	31,298	69,000
Fuel	54,190	(119,470	66,179	(145,900)
Takeoff Gross Weight	182,344	(402,000)	187,243	(412,800)

Table 5-10b

WING WEIGHT COMPARISON

(STUDY I)

	LAMINAR FLOW		TURBULENT FLOW	
	Kg	(LB)	Kg	(LB)
Wing Box	13,820	(30,467)	9,980	(22,002)
Wing Box Flutter Penalty	--	--	2,210	(4,873)
Leading Edge	690	(1,521)	564	(1,243)
Trailing Edge	755	(1,665)	615	(1,356)
Wing to Fuselage Fairing	572	(1,261)	457	(1,007)
Wing Tips	14	(30)	11	(25)
Ailerons	313	(689)	264	(582)
Flaps	3,137	(6,917)	2,462	(5,427)
Slats	--	--	717	(1,580)
Spoilers	455	(1,003)	341	(751)
Basic Wing Weight	19,756	(43,553)	17,621	(38,846)
Laminar Flow System:				
Leading Edge Penalty	491	(1,083)		
Laminar Flow Panels	2,633	(5,805)		
Engine/Pump Assembly	746	(1,645)		
Ducting - Wing to Pump	851	(1,876)		
Fairings	335	(738)		
Laminar Flow Penalty	5,056	(11,147)		
Total Wing Weight	24,812	(54,700)	17,621	(38,846)

Table 5-11

DESIGN DATA AND GEOMETRY SUMMARY

			LAMINAR FLOW		TURBULENT FLOW	
WING GEOMETRY						
Area - Theoretical	m^2	(ft^2)	381	(4,100)	267	(2,870)
Aspect Ratio			12		12	
Taper Ratio			0.3		0.3	
Sweep of c/4	deg		30		30	
t/c Mean			0.11		0.137	
Flap Area	m^2	(ft^2)	68	(729)	53	(572)
VCK Area	m^2	(ft^2)	0		39	(422)
Aileron	m^2	(ft^2)	15	(163)	13	(137)
Spoiler Area	m^2	(ft^2)	36	(384)	27	(287)
TAIL GEOMETRY						
Horizontal Tail Area	m^2	(ft^2)	64	(693)	89	(960)
Elevator Area	m^2	(ft^2)	16	(168)	23	(248)
Horizontal Tail Length	m	(in)	27.43	(1,080)	24.38	(960)
Horizontal Tail Volume			0.75		1.52	
Vertical Tail Area	m^2	(ft^2)	63	(679)	46	(495)
Rudder Area	m^2	(ft^2)	22	(237)	18	(191)
Vertical Tail Length	m	(in)	20.83	(820)	25.4	(1,000)
Vertical Tail Volume			0.051		1.23	
FUSELAGE GEOMETRY						
Length	m	(in)	55.65	(2,191)	55.65	(2,191)
Maximum Diameter	m	(in)	6.02	(237)	6.02	(237)
Wetted Area - Gross	m^2	(ft^2)	907	(9,767)	907	(9,767)
Main Cabin Floor Area	m^2	(ft^2)	234	(2,518)	234	(2,518)
ENGINES						
Type			Turbofan		Turbofan	
SLST/Engine	kg	(lb)	11,054	(24,370)	(11,657)	(25,700)

Table 5-12

PERFORMANCE CHARACTERISTICS
(STUDY I)

		LAMINAR FLOW	TURBULENT
WEIGHT	kg (LB)		
Takeoff		182,344 (402,000)	187,243 (412,800)
Landing		137,438 (303,000)	129,637 (285,800)
OEW		96,842 (213,500)	85,811 (198,000)
MEW		91,263 (201,200)	84,141 (185,500)
Mission Fuel		54,204 (119,500)	66,179 (145,900)
Payload		31,298 (69,000)	31,298 (69,000)
CRUISE			
Range	km (N MI)	9,620 (5,000)	(9,620) (5,000)
Altitude	m	10,670 - 11,890	9,450 - 11,890
Step/Climb	(FT)	(35,000 - 39,000)	(31,000 - 39,000)
C_L		0.40 - 0.49	0.50 - 0.60
L/D		24.0 - 25.8	16.7 - 18.2
SFC (AVG)	G/hr/N (LB/LB/HR)	60 (0.59)	59 (0.58)
$Range_{LFC\ On}/Range_{LFC\ Off}$		1.16	---
Fuel Required For Suction	kg (LB)	1,190 (2,620)	---
Takeoff Distance	m (FT)	2,800 (9,180)	3,050 (10,000)
V_2	m/s (KN)	70.5 (137)	74.1 (144)
$C_{L_{T.O.}}$		1.55	2.05
Flap Angle	Degree	25	5/10
Landing Distance	m (FT)	1,539 (5,050)	1,265 (4,150)
$V_{Approach}$	m/s (KN)	66.9 (130)	58.1 (113)
$C_{L_{Approach}}$		1.29	2.20
Flap Angle	Degree	22.5	35/15

Engine thrust is sufficient to allow an initial cruise altitude of 9,450 m (31,000 Ft) for both aircraft. This can be achieved without using LFC on the laminar flow aircraft; with LFC-on the initial cruise altitude is 10,670 m (35,000 Ft).

In accordance with commercial operational rules, a step cruise/climb mission profile and international fuel reserves are assumed. When using this commercial type flight path, the aircraft cruises at a constant altitude until enough fuel has been used to permit cruise at an altitude 1219 M (4,000 Ft) higher; the increases in cruise altitude thus are made in steps of 1219 M (4,000 Ft). Figure 5-16 presents the altitude and operating C_L profiles over the mission ranges of the two base aircraft. Climb profiles for the two aircraft are summarized in Figure 5-17.

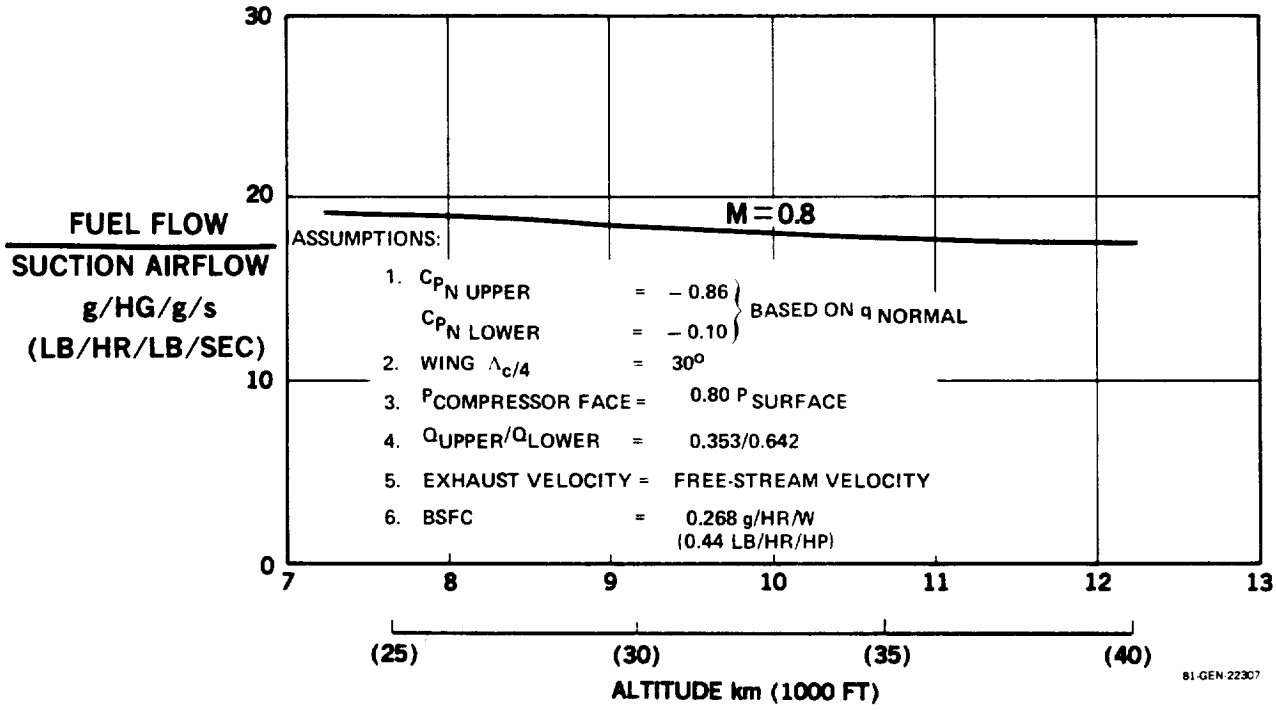

FIGURE 5-15. PRELIMINARY ESTIMATE OF FUEL FLOW FOR SUCTION SYSTEM PUMPING

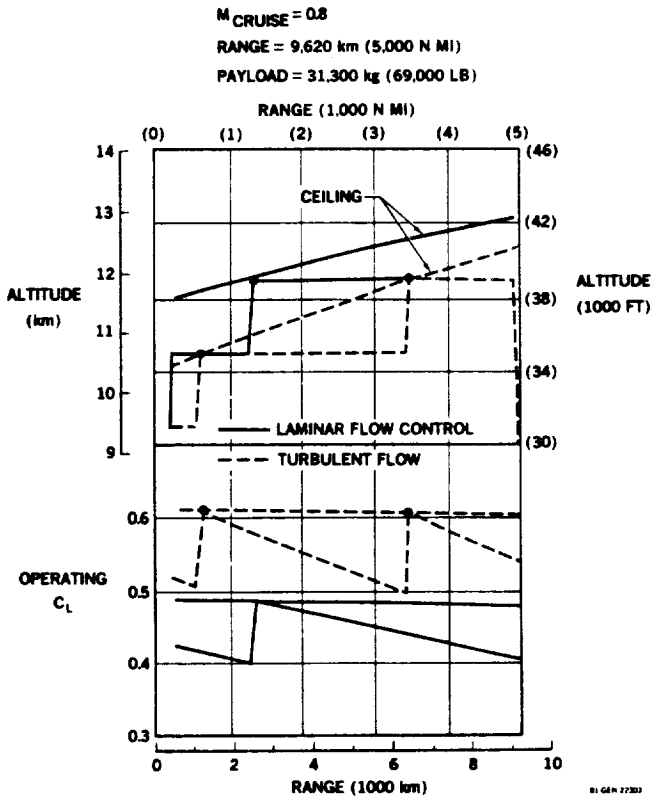

FIGURE 5-16. AIRCRAFT ALTITUDE PROFILES

The "optimization" of each aircraft configuration, as to wing area and thrust selection, is accomplished by a computer mission program (K5JA) which sizes as well as computes the performance. Typical carpet plots are shown in Figures 5-18 through 5-21. (The output is in English units and conversion to metric units in the carpet plots is impractical). See also Section 7.3.2.

Performance limitations, such as takeoff distance, minimum approach speed and thrust may be imposed on the sizing matrix. The configuration selection is made on the basis of minimum takeoff gross weight; costing and pricing of the laminar flow aircraft were not sufficiently developed at this stage to warrant using Direct Operating Costs (D.O.C.).

Results of a preliminary aspect ratio "optimization" study are presented in Figure 5-22. Aspect Ratio 12 is selected for both base cases. See also Sections 7.3.1 and 9.1.6.

5.3.8 Economics - Initial Baseline Aircraft

The results of a preliminary comparison of economic aspects of the two initial baseline aircraft is indicated in Table 5-13. This very early assessment of the probable economic trends of the two configurations, LFC and turbulent, does show the LFC to be at least competitive. A comprehensive economic analysis of the final configuration is in Section 6.0.

Table 5-13

PRELIMINARY COSTING - INITIAL BASELINE AIRCRAFT
(1976) (DOLLARS IN MILLIONS)

	LAMINAR	TURBULENT
AIRPLANE COST		
- With Engine	49.4	45.6
- Without Engines	43.1	38.5
DIRECT OPERATING COST		
$ per aircraft-km (NMI)	3.41 (6.31)	3.44 (6.38)
$ per seat-km (NMI)	.0114 (.0211)	.0115 (.0213)

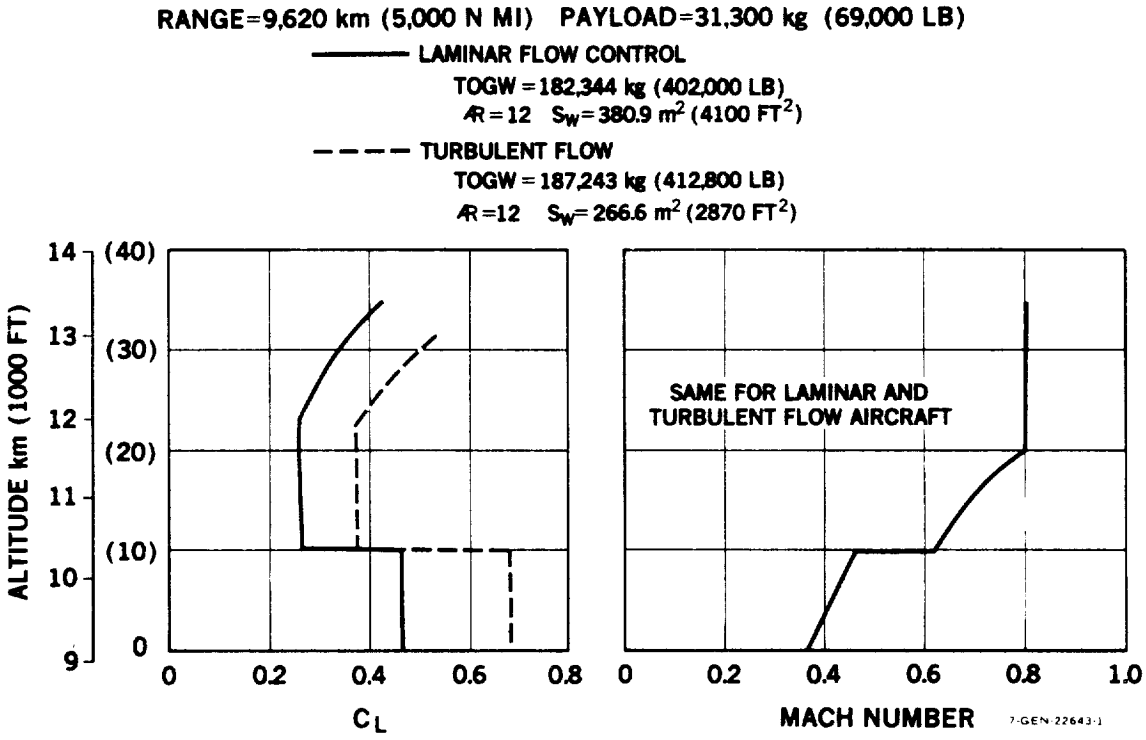

FIGURE 5-17. CLIMB PARAMETERS

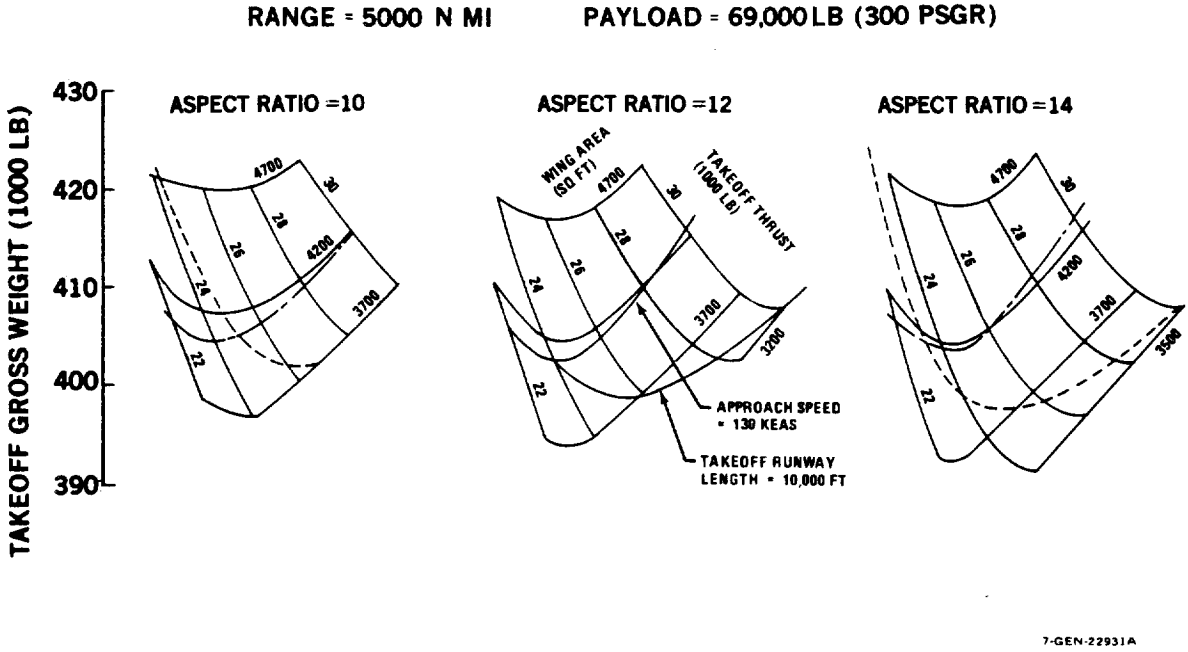

FIGURE 5-18. MISSION SIZING – LAMINAR FLOW CONTROL BASELINE

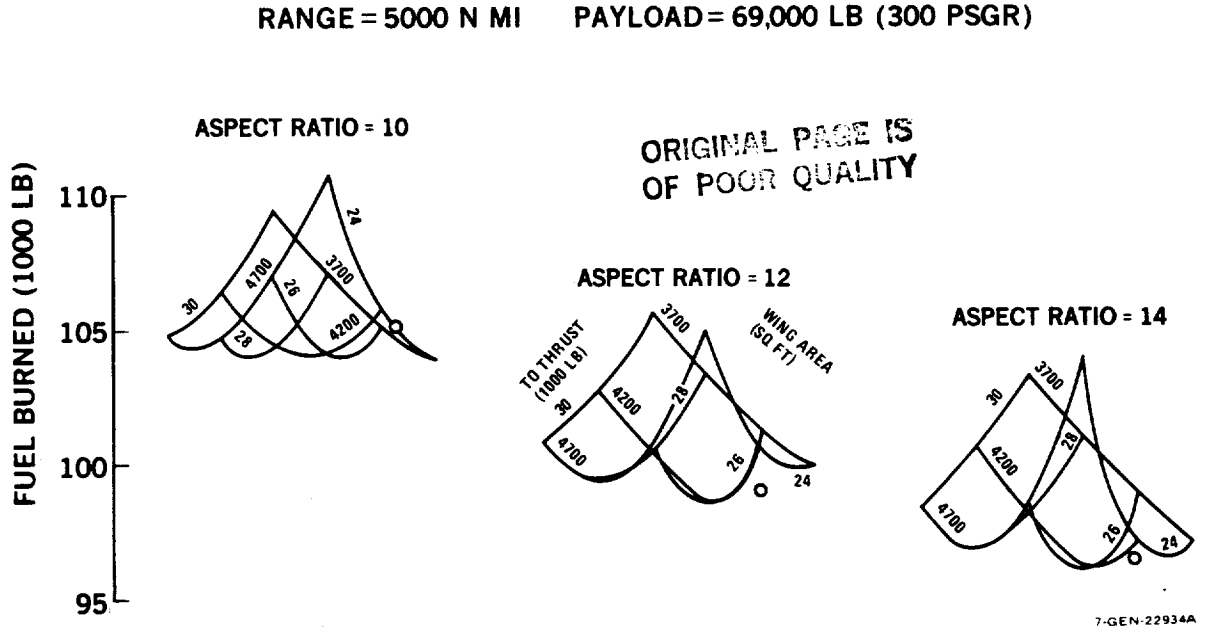

FIGURE 5-19. MISSION SIZING – LAMINAR FLOW CONTROL BASELINE – FUEL BURNED

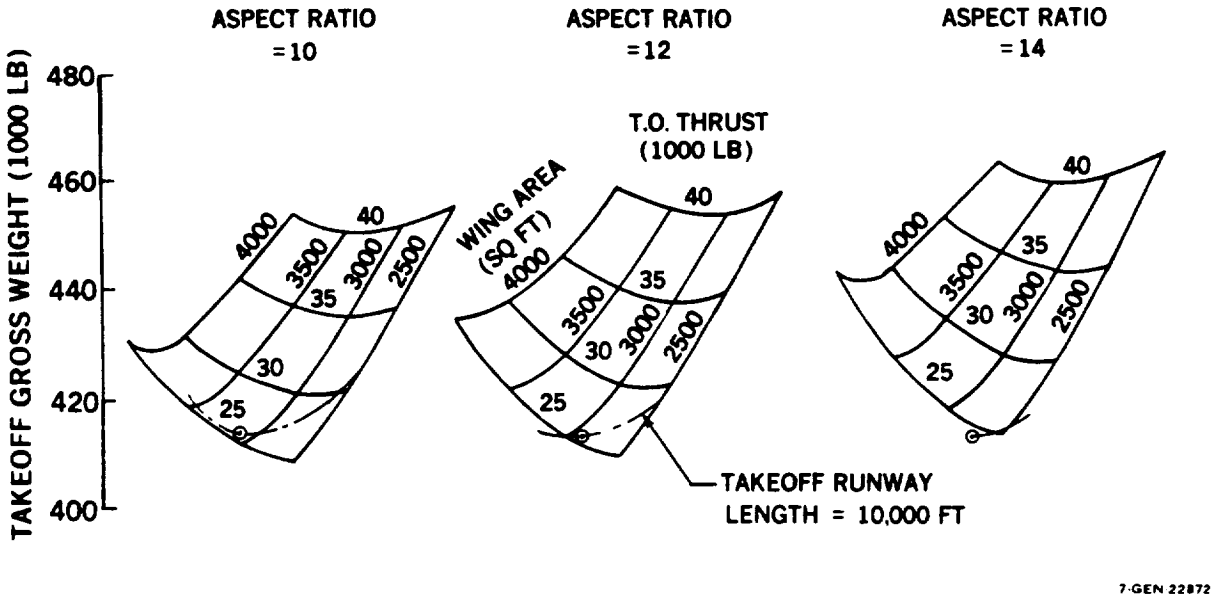

FIGURE 5-20. MISSION SIZING – TURBULENT BASELINE – TAKEOFF GROSS WEIGHT

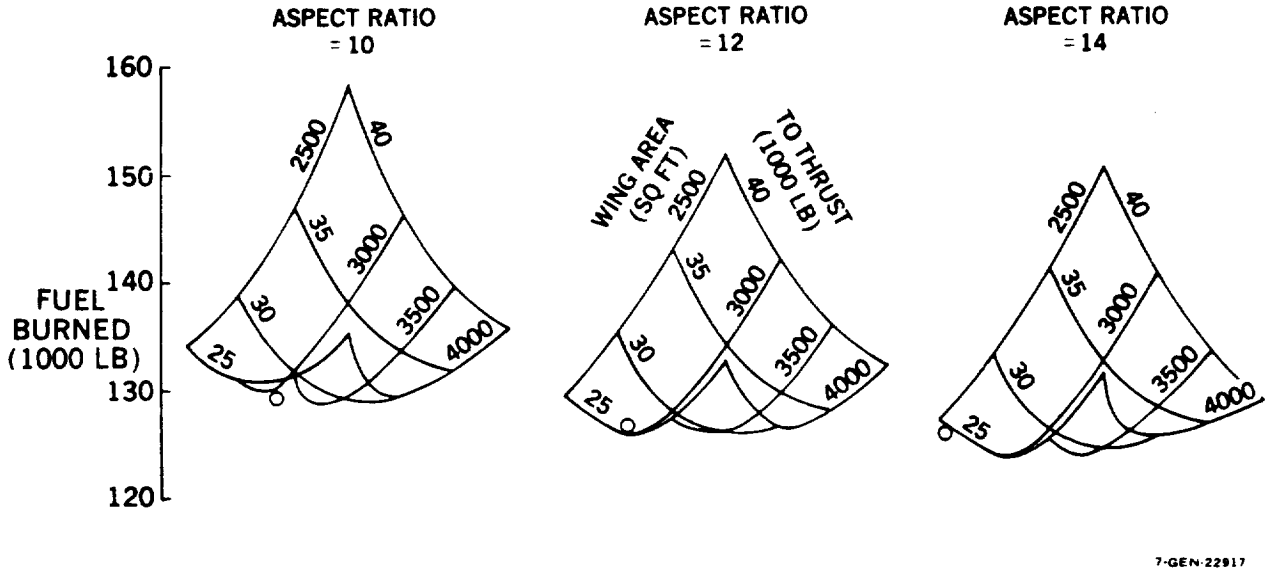

FIGURE 5-21. MISSION SIZING – TURBULENT BASELINE – FUEL BURNED

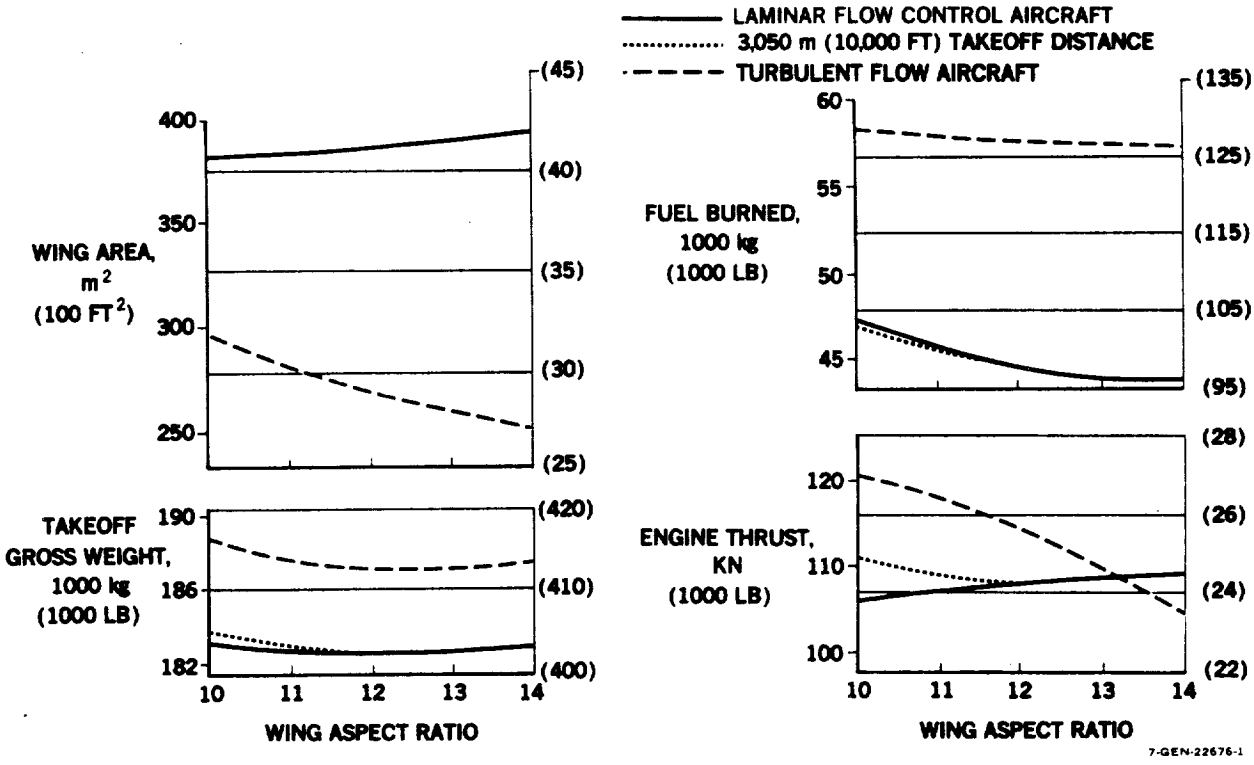

FIGURE 5-22. EFFECT OF ASPECT RATIO ON AIRCRAFT SIZING

The costing comparison shown in Table 5-13 is based on a 400 aircraft buy depreciated over 14 years. The turbulent aircraft cost estimate appears reasonable using the DC-10 prices as a comparion.

The cost of the laminar aircraft is about 8 percent higher than the turbulent. Breakdown of the cost differentials into the labor and material components shows that the major increases in the laminar flow airplane costs are due to engineering (1.2 percent), manufacturing (2.0 percent) and outside vendor costs such as materials, tooling, special engine installation parts (2.8 percent).

The DOC for the laminar flow aircraft is approximately 1 percent less but at this early stage of the economic analysis, the DOC's are essentially breaking even. It is emphasized that this preliminary costing should be considered only on a comparative basis - not on absolute values.

5.3.9 Study Conclusions - Initial Baseline Aircraft

The base case laminar flow aircraft study and the comparison with an equally advanced technology turbulent aircraft, emphasized the following areas needing special attention:

- Approach C_L - to reduce wing area
- Effective Wing Thickness-to reduce wing weight
- Optimized Structure - to reduce wing weight
- Minimum Weight LFC Panel - to reduce wing weight
- Suction System Simplification - to reduce cost and weight
- Maintenance - to reduce operating costs

The most important issue is a reduction of area for the laminar flow wing and consequent reductions in the overall airplane size and weight; the low approach C_L obtainable without a leading edge high lift device, is the critical sizing criterion. Further possible weight reductions are associated with the effective wing thickness, and minimum weight LFC panel design. Simplicity and efficient integration of the suction system into the aircraft is essential. Maintenance procedures are particularly important in making the LFC aircraft readily acceptable from an operational standpoint.

Particular attention was therefore directed to the following details for the next improved baseline configurations:

- o High Lift System
- o Wing Planform Variables
- o Extent of Laminarization
- o The Number and Location of Propulsion Engines
- o Structural Design Concept
- o LFC Surface Material
- o Structural Concept/Suction System Manifolding Integration
- o Suction System Manifolding and the Number and Location of Suction Engines
- o Integration of Leading Edge Protection

Trade studies on the number of propulsion and suction engines are summarized in the following pages. Other items are covered under the sections relating to the various disciplines involved.

5.4 STUDY II FOUR VS THREE PROPULSION ENGINES

The aircraft configurations for this study are shown in Figures 5-23a and b. The results of the trade study to determine the relative advantages of a four or a three engine main propulsion system arrangement are presented in Tables 5-14a, b and c. Sizing constraints considered in this analysis were: (1) initial cruise altitude, (2) approach speed, and (3) takeoff field length. In both cases the approach speed of 66.9 m/sec (130 KEAS) was the limiting constraint which established the aircraft size. Cost data were based upon 1976 dollars and a 45 cents per gallon fuel price. Subsequent increases in fuel prices, over and above general inflation would increase the economic difference shown between the two configurations without altering the conclusion reached. The differentials between the four engine and the three engine arrrangements favor the three engine arrangement. The three-engine configuration was estimated to be 2.54 percent lower in acquisition cost and 3.62 percent lower in direct operating cost than the four-engine configuration. Thus the three-engine configuration with engines located aft on the fuselage was selected for subsequent LFC aircraft studies.

Further detail on this trade study with respect to the influence of engine noise on engine location may be found in Section 7.2.

	WING	HORIZ	VERT
ASPECT RATIO	12	5	1
TAPER RATIO	0.3	0.4	0.8
SWEEP	30°	30°	40°

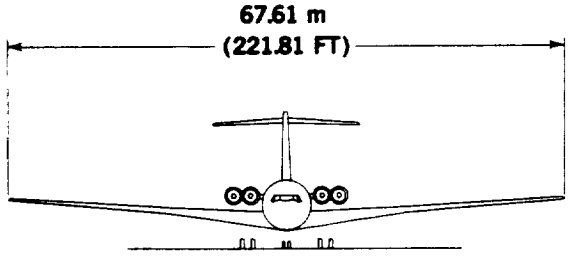

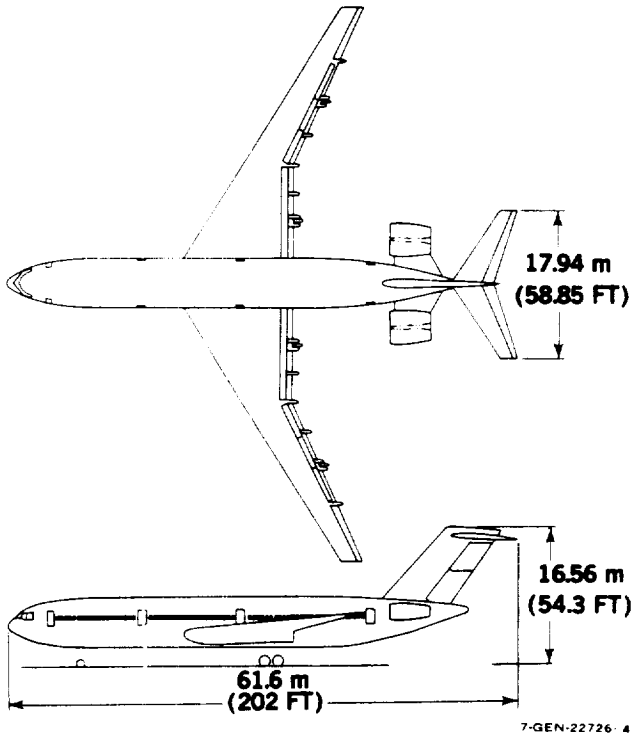

FIGURE 5-23a. STUDY II – FOUR-ENGINE CONFIGURATION

	WING	HORIZ	VERT
ASPECT RATIO	12	5	1
TAPER RATIO	0.3	0.4	0.8
SWEEP	30°	30°	40°

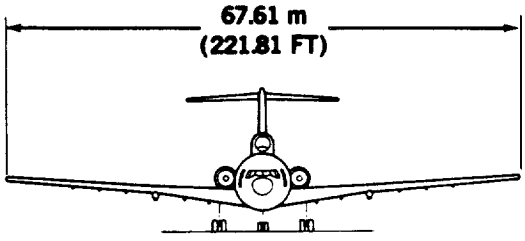

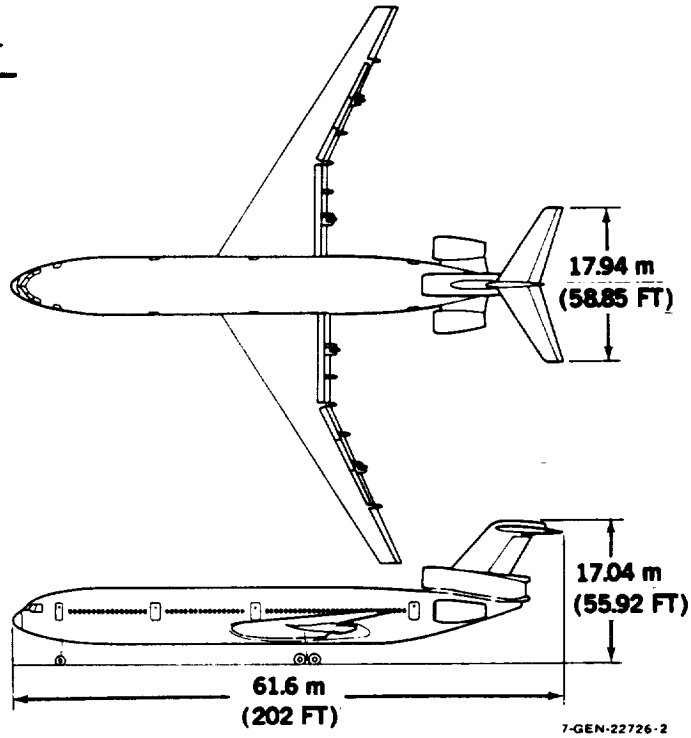

FIGURE 5-23b. STUDY II – THREE-ENGINE CONFIGURATION

Table 5-14a

FOUR VERSUS THREE PROPULSION ENGINES
DRAG & WEIGHT DIFFERENCES

	m^2	SQ. FT.
Δ D/q - 3 ENGINES		
Fuselage	0	0
Wing	0	0
Horizontal Tail	0	0
Vertical Tail	-0.0576	(-0.62)
Propulsion	+0.0102	(+0.11)
Miscellaneous	-0.0037	(-0.04)
TOTAL	-0.0511	(-0.55)
TOTAL D/q - 3 ENGINES		
LFC ON	4.312	(46.41)
LFC OFF	5.785	(62.27)
Δ OEW - 3 ENGINES	-886.3kg	(-1513 LB)

Table 5-14b

STUDY II

CHARACTERISTICS OF SIZED AIRCRAFT

RANGE = 9,260 km (5000 NMI), PAYLOAD = 31,300 kg (69,000 LB), 300 PASSENGERS

		4 - ENGINES	3 - ENGINES
TAKEOFF GROSS WEIGHT	kg (LB)	195,349 (430,670)	193,191 (425,913)
WING AREA	m^2 (SQ FT)	412.5 (4,440)	412.5 (4,440)
THRUST/ENGINE	N (LB)	112,540 (25,300)	148,593 (33,405)
FUEL BURNED	kg (LB)	46,557 (102,641)	45,900 (101,193)
TOTAL FUEL	kg (LB)	56,273 (124,061)	55,511 (122,381)
OPERATOR'S EMPTY WEIGHT	kg (LB)	107,778 (237,609)	106,382 (234,532)
LANDING WEIGHT	kg (LB)	148,791 (328,028)	147,295 (324,729)
INITIAL CRUISE ALTITUDE	m (FT)	10,670 (35,000)	10,670 (35,000)

Table 5-14c

DIRECT OPERATING COST SUMMARY

STUDY II

CONSTANT 1976 DOLLARS

ITEM	FOUR-ENGINE CONFIGURATION	THREE-ENGINE CONFIGURATION
AIRFRAME COST $ x 10^6	47.369	46.612
TOTAL ENGINE COST $ x 10^6	6.620	6.008
AIRPLANE COST $ x 10^6	53.989	52.620
LANDING FEE $/FLT CYCLE	732.14	724.05
COCKPIT CREW $/FLT CYCLE	4,434.23	4,420.39
CABIN CREW $/FLT CYCLE	3,491.17	3,491.17
DEPRECIATION/INSURANCE $/FLT-CYCLE	11,096.04	10,814.67
MAINTENANCE $/FLT-CYCLE	6,432.47	5,653.45
FUEL $/FLT CYCLE	6,893.80	6,796.54
TOTAL $/FLT CYCLE	33,079.85	31,900.27
DOLLARS/km ($/NMI)	3.57 (6.62)	3.44 (6.38)
CENTS/SEAT-km (¢/ASNMI)	1.19 (2.21)	1.15 (2.13)

5.5 STUDY III FOUR VS TWO WING-MOUNTED SUCTION ENGINES

The results of this trade study discussed in Section 10.6, indicate that two wing-mounted suction engines per airplane can provide adequate suction for the 300 passenger aircraft configuration.

The initial LFC configuration distributed suction along the wing using four suction engines. However, closer examination shows that the integral duct sizing is adequate to permit the required suction flow to be handled by two suction engines, placed at the wing break on each side.

A comparison of two versus four suction engine characteristics is presented in Table 5-15 and the advantages of two suction engines only is summarized as follows:

- o Simpler system
- o Lower weight and drag
- o More efficient units
- o Lower initial cost
- o Lower operating cost

The decision was therefore made to use two suction engines only on further LFC configurations.
Further discussion of this trade study may be found in Section 7.2.

Table 5-15

COMPARISON OF TURBOSHAFT ENGINE ARRANGEMENTS FOR SUCTION SYSTEM

CHARACTERISTIC/ENGINE	2-ENGINES	4-ENGINES
Rated (SLS) Power kW (SHP)	895 (1200)	447 (600)
Airflow kg/s (LB/SEC)	2.90 (6.4)	1.59 (3.5)
Pressure Ratio	12-14	8-10
Weight kg (LB)	115.7 (255)	95.3 (210)
Installed BSFC kg/h/N (LB/HR/SHP) at 12,190m (40,000 FT)	0.040 (0.39)	0.043 (0.42)

5.6 STUDY IV FINAL AIRCRAFT CONFIGURATIONS

In this study, two improved LFC configurations having different extents of laminar flow are considered. They are then compared with an updated turbulent configuration and the final LFC configuration is selected. The configuration ground rules are given in Table 5-16. Changes relative to the initial LFC configuration, that result from previous trade studies and analysis include:

- o Three propulsion engines instead of four.
- o Two wing mounted suction engines instead of four.
- o Updated wing structural design.
- o Wing leading edge protection system added.
- o High lift systems improved.

The resulting LFC configurations are illustrated in Figures 5-24a and b. Figure 5-24a shows the improved LFC configuration with LFC on both wing surfaces to 70 percent chord as before and Figure 5-24b shows the competitive LFC configuration with LFC extending to 85% chord on the upper wing surface only. The updated turbulent configuration is shown in Figure 5-24c.

Detail consideration leading to the selection of these final configurations are discussed in the following paragraphs.

Table 5-16

FINAL CONFIGURATIONS - GROUND RULES

PAYLOAD	299 Passengers at 75 kg (165 LB)/PAX 31,300 kg (69,000 LB) Design Mission 42,980 kg (94,755 LB) MAX 7 Pallets forward, 12 LD3 Containers Aft Cargo Density 160 kg/m^3 (10 LB/FT^3)
GALLEY SERVICE	International standard 1st Class-13 kg (28.5 LB)/PAX Tourist-6kg (13.5 LB)/PAX
PASSENGER SERVICE	1.8 kg (4 LB)/PAX
C. G. TRAVEL	-2 to 32 Percent MAC - LFC upper surface 0 to 32 Percent MAC - LFC both surfaces 14.5 to 39.5 Percent MAC - Turbulent

Items not covered are the same as for the initial baseline, Tables 5-1 and 5-2.

	WING	HORIZ	VERT
AREA m^2 (FT^2)	331 (3560)	98.8 (1064)	62.0 (667)
ASPECT RATIO	10	5	1.1
TAPER RATIO	0.25	0.4	0.7
SWEEP	30 DEG	30 DEG	40 DEG
THICKNESS RATIO	0.117 AVG	0.11	0.11
TAIL VOLUME	—	1.23	0.0646

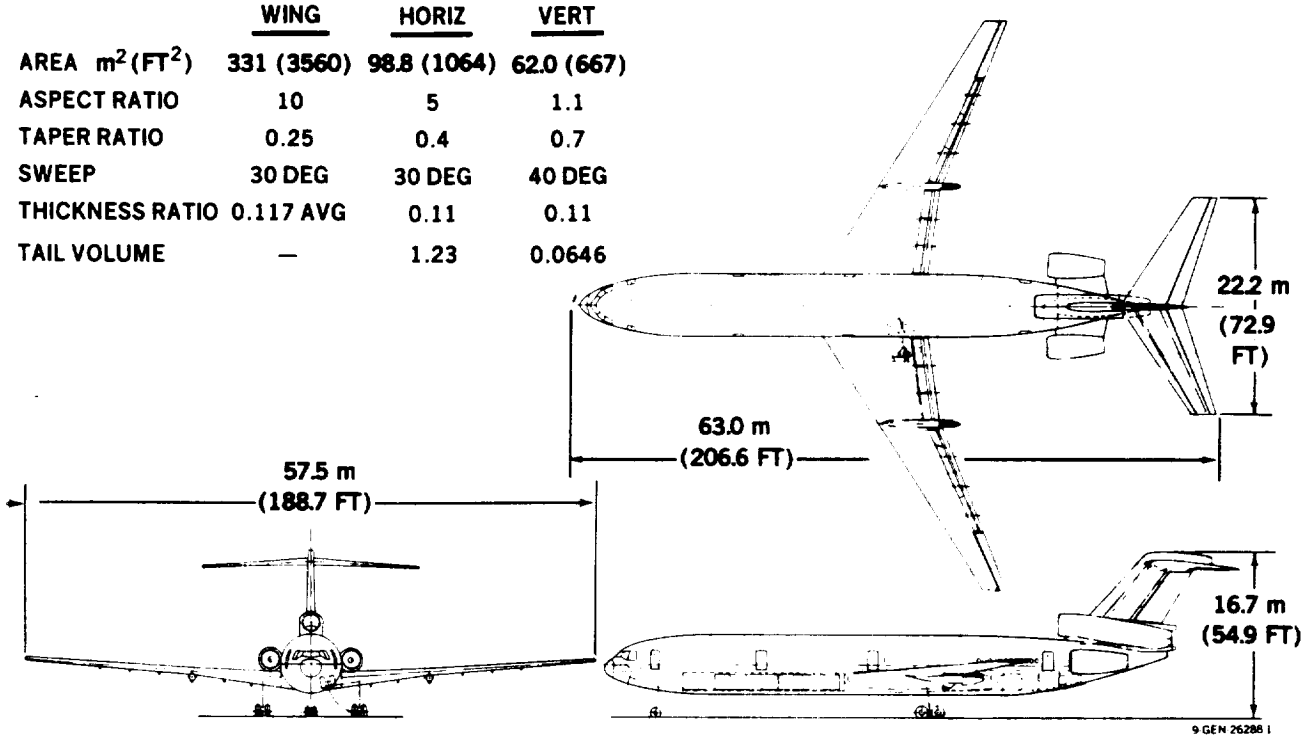

FIGURE 5-24a. LFC AIRCRAFT – UPPER AND LOWER WING SURFACE LAMINARIZED TO 70-PERCENT CHORD

	WING	HORIZ	VERT
AREA-m^2 (FT^2)	288 (3100)	80.3 (864)	52.7 (567)
ASPECT RATIO	10	5	1.1
TAPER RATIO	0.25	0.4	0.7
SWEEP	30 DEG	30 DEG	40 DEG
THICKNESS RATIO	0.108 AVG	0.11	0.11
TAIL VOLUME COEF	—	1.24	0.068

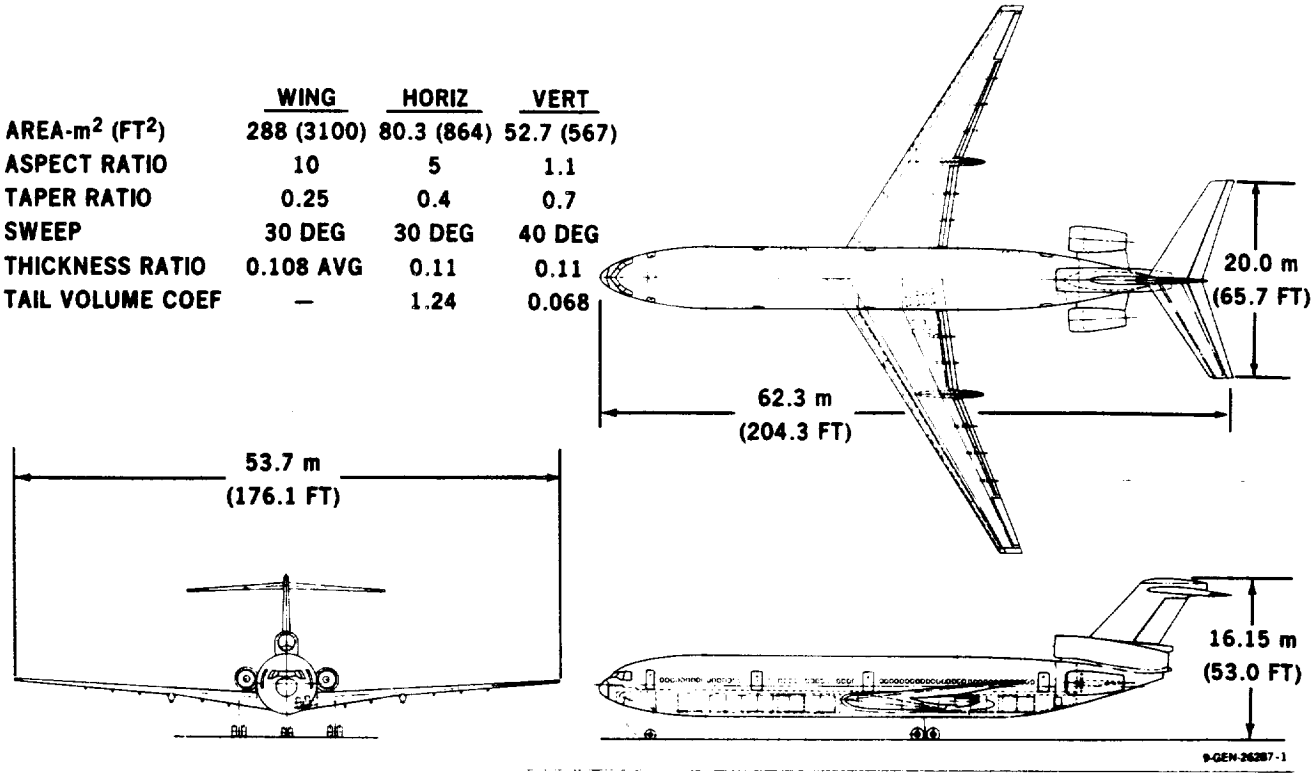

FIGURE 5-24b. LFC AIRCRAFT – WING UPPER SURFACE LAMINARIZED TO 85-PERCENT CHORD

	WING	HORIZ	VERT
AREA — m^2 (FT^2)	260 (2800)	89.6 (964)	47.2 (508)
ASPECT RATIO	10.85	3.95	1.60
TAPER RATIO	0.25	0.35	0.35
SWEEP	30 DEG	35 DEG	40 DEG
THICKNESS RATIO	0.127 AVG	10	10.5
TAIL VOLUME	—	1.38	0.079

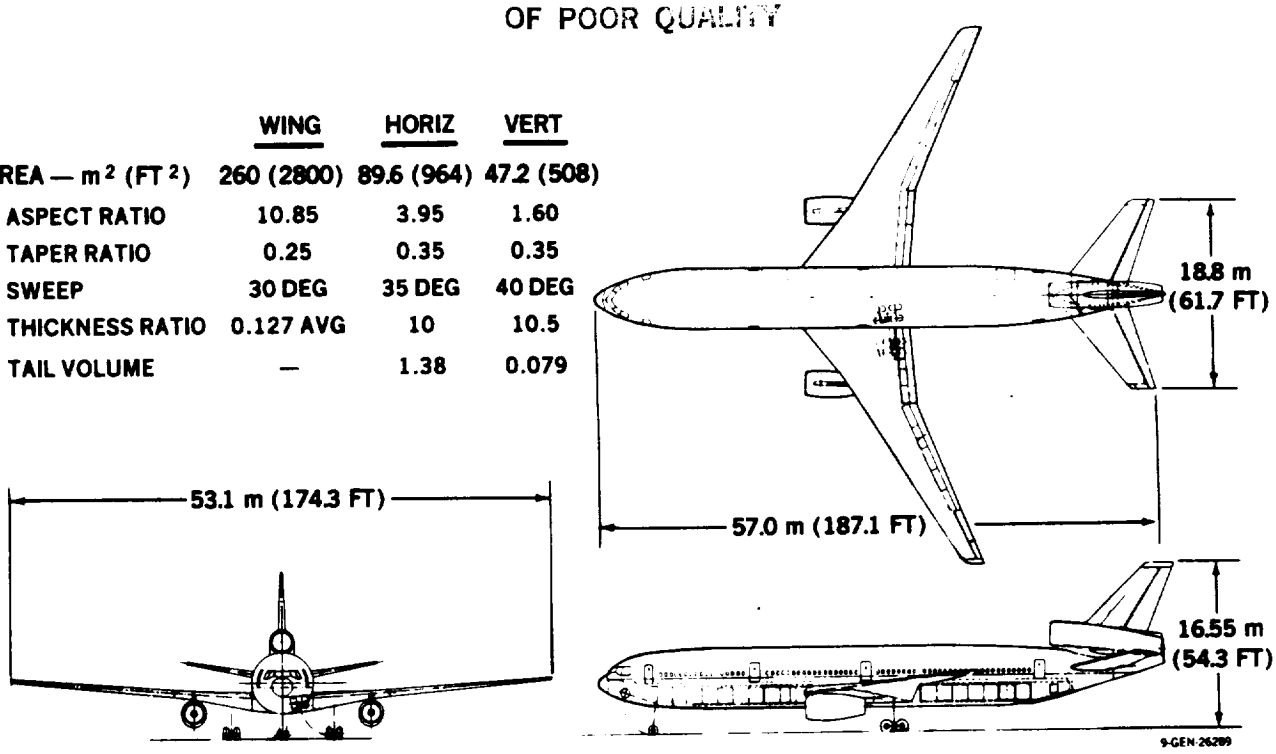

FIGURE 5-24c. ADVANCED TURBULENT AIRCRAFT

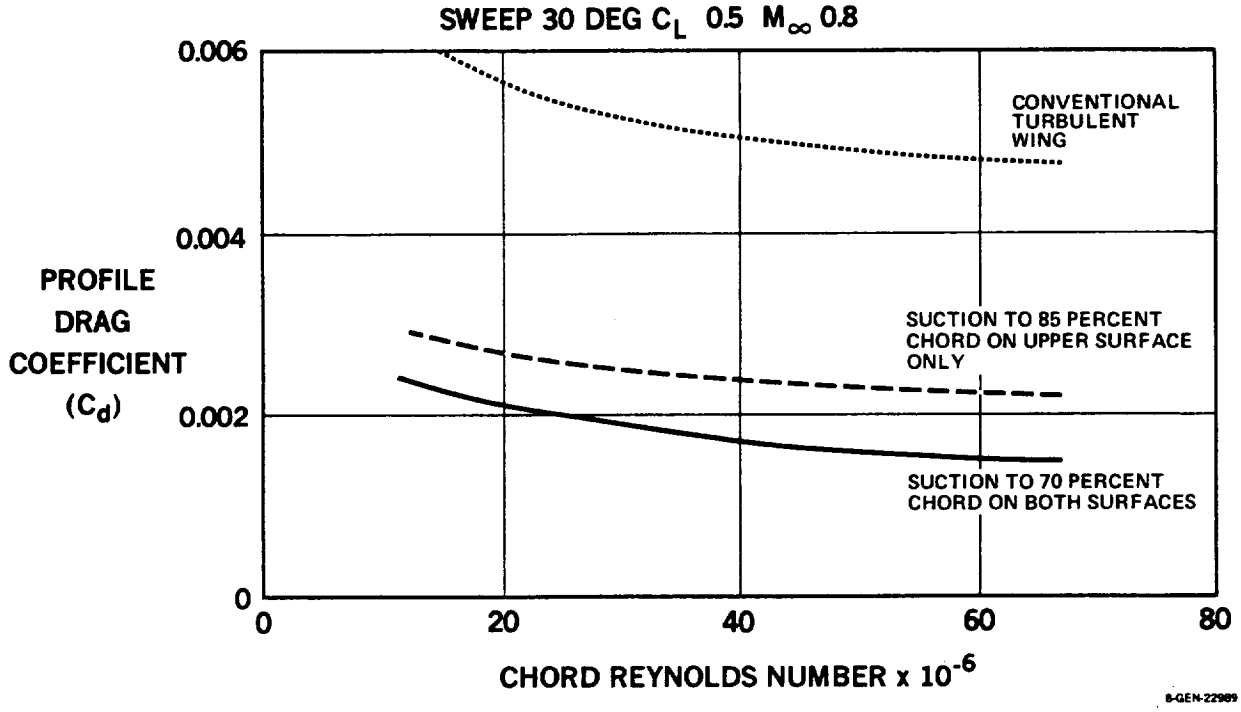

FIGURE 5-25. EFFECT OF LFC EXTENT ON PROFILE DRAG

5.6.1 LFC Aircraft

5.6.1.1 Aerodynamic Considerations -

a. Extend of Lamination

This significant trade study was prompted by the fact that the drag reduction achieved with laminar flow to 85 percent chord on the upper surface approaches that obtainable with laminar flow to 70 percent chord on both surfaces. This is shown in Figure 5-25. The study shows that the advantages gained by utilizing LFC on the upper wing surface only, more than compensate for the increase in drag coefficient. These advantages include:

1. Simplification of the LFC system.

2. LFC system weight is reduced.

3. Initial cost is less.

4. Vulnerability of the lower LFC surface to damage from foreign objects thrown up from the runway (FOD) is avoided.

5. The possibility of fuel leakage into the LFC panels and integral ducts is avoided.

6. Conventional access panels to wing leading and trailing edge systems and fuel tanks can be provided for inspection and maintenance without disturbing any LFC surface.

7. Maintenance costs are reduced.

8. A shield for contamination avoidance can be deployed forward of the wing leading edge and can be retracted into the lower surface when not required.

9. The shield can be designed geometrically to function as a high lift device. Wing area can then be reduced and wing loadings become competitive with those of advanced turbulent aircraft.

10. The use of a retractable high lift device allows the safe use of a sharper leading edge on the basic wing. This results in a reduction or possible elimination of suction requirements along the attachment line.

Both LFC configurations were investigated in depth and the results are summarized in the following paragraphs under headings of the technical disciplines involved.

b. Wing Planform - The wing planform characteristics are:

Sweep angle 30^{o}
Taper ratio .25
Aspect ratio 10

The wing sweepback of angle of 30^{o} was selected on the basis of wing thickness permissible for an operational C_L of .5 to .6 and the practical aspects of associated internal space available for landing gear stowage and suction manifolding installation. With an alternative sweep angle considered of 25^{o} and a correspondingly thinner airfoil section, gear and duct space limitations were found. The selected wing planform, sweep and taper ratio of .25 allows the use of analytical and wind tunnel test results performed during the Douglas EET-related design work on similar wings.

Aspect ratio of 10 was selected for both the upper surface only and the upper-plus-lower laminarization cases. An extensive aspect ratio study for LFC on both surfaces with wing strength, stiffness, flutter and aeroelastic effects taken into account, is discussed in Sections 7.3 and 9.1.8. Aspect ratios of 10, 12 and 14 were considered. The variation of wing weight with aspect ratio is not definitive between aspect ratios 10 and 12; the curve is essentially flat. Consequently, aspect ratio 10, which gives increased wing depth and shorter span for the ducting was selected for both LFC configurations.

c. Airfoil Section - As stated previously in Section 5.3.2.(b), the supercritical type airfoils selected for the laminar flow aircraft are designed to be shock-free at the design C_L, also no significant amount of separation should occur even with turbulent flow on the laminarized portion of the airfoil. More than sufficient buffet margin exists with these shock-free airfoils. Continued "optimization" during the LFC study resulted in the selection of the airfoil thickness as a function of the operating C_L, as shown in Figure 5-26. Wing thickness variation was considered in the aircraft sizing program. The selected airfoil thicknesses are as follows:

	Upper-Surface LFC Only	Upper-Plus-Lower-Surface LFC
Cruise C_L	0.56	0.50
Airfoil Section	Shock-free	Shock-free
Root t/c (DSMA 679 Type)	12.76	13.82
Aero Break t/c (DSMA 691 Type) (40% Span)	10.08	10.92
Tip t/c (DSMA 691 Type)	10.08	10.92
Avg t/c	10.3	11.7

d. High Lift System - Figure 5-27 illustrates the wing cross-sections for the two extents of laminarization considered. The figure shows that the extent of laminarization is a controlling factor on the ducting/structure integration and on the trailing edge flap installation. The finite thickness at the airfoil trailing edge is required to provide adequate depth for the flap structure. This increased depth is provided by rotating the lower airfoil surface contour about the 60 percent chord point without significantly affecting the airfoil characteristics. The resulting depth of the airfoil at the trailing edge is less than one percent of the chord; consequently any drag contribution is negligible.

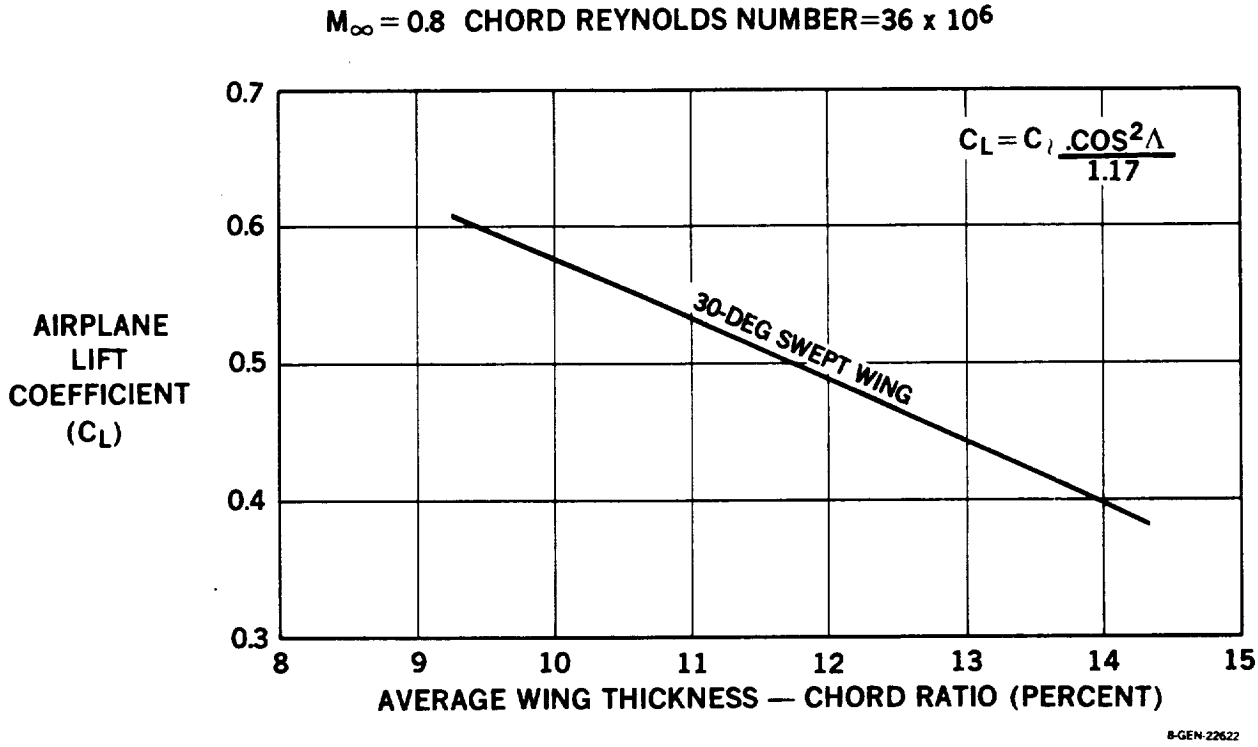

FIGURE 5-26. VARIATION OF DESIGN LIFT COEFFICIENT WITH AIRFOIL THICKNESS

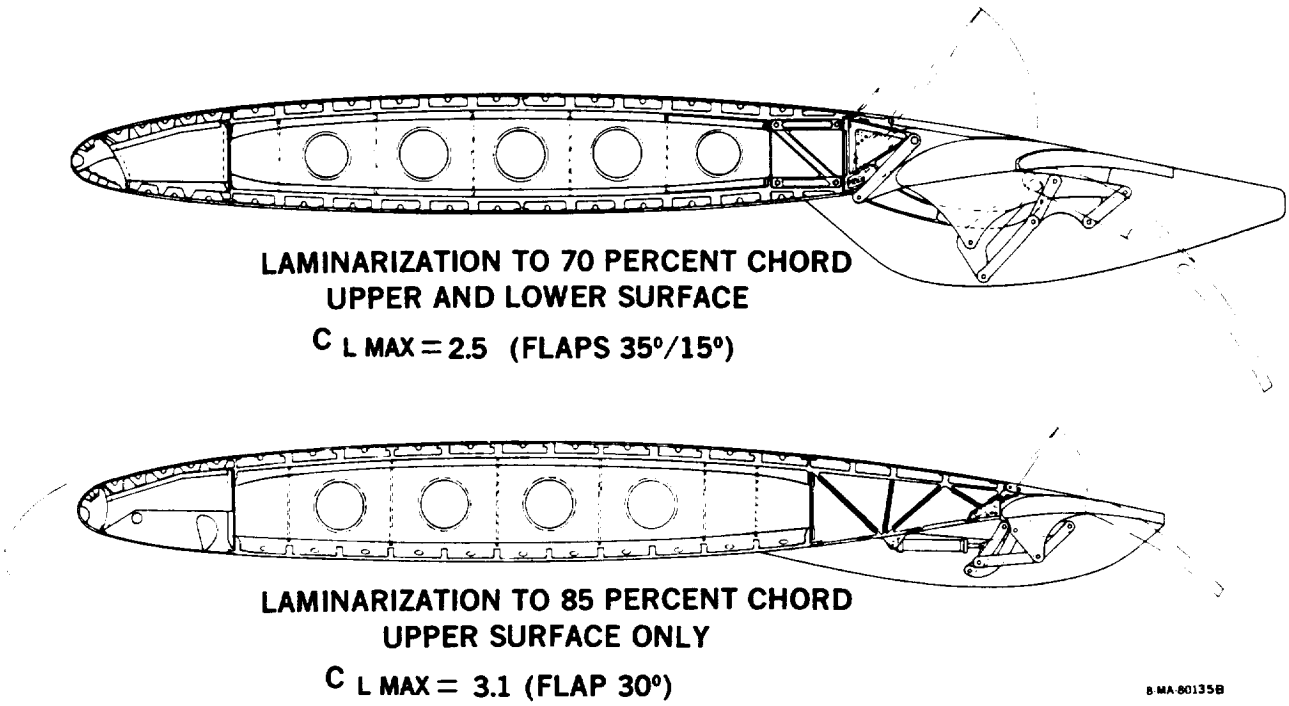

FIGURE 5-27. COMPARISON OF LFC WING SECTIONS

A highly efficient and powerful high lift system is critical to the design of a competitive LFC aircraft. Takoff distance or approach speed are usually the wing sizing criteria; both of these depend on the aircraft high lift capability. Therefore, in each laminarization case, an effort was made to install the most efficient high lift system consistent with space available and compatibility with the laminar flow installation. Note that in either case, laminar flow is not carried across the flap hinge.

For LFC on both surfaces, Figure 5-27 shows the selected 25 percent chord trailing edge double-slotted flap, with a maximum deflection of $35^{o}/15^{o}$. No leading edge device is used since such an arrangement, with its retraction requirements, is not compatible with achieving laminar flow on the lower surfaces.

With LFC on the upper surface only, and suction over a larger percent chord, the trailing edge flap is reduced to 15 percent chord with a single slot, and the maximum deflection is 30^{o}. However, with the lower wing surface not laminarized, a 10 percent chord leading edge shield is usable as both a high lift device and as protection of the leading edge from insect impingement, and can be retracted into the lower surface without affecting the extent of laminar flow.

With either extent of laminarization, the flap mechanism is designed to provide considerable chord extension before angular deflection take place, namely:

- 15 percent chord extension with the 25 percent chord double-slotted flap
- 7 percent chord extension with the 15 percent chord single-slotted flap

The low speed high lift characteristics of the two flap systems are shown in Figures 5-28 through 5-31.

e. Horizontal Tail Sizing - The horizontal tail sizing scissor plots for the two laminar configurations are presented in Figures 5-32 and 5-33. Several points of interest may be noted from these plots:

- o The critical sizing criteria for the forward c.g. limits are different for the two aircraft. For the case of laminarization of the upper-surface-only, the nose wheel liftoff is the critical sizing factor. In the case of upper-plus-lower surface laminarization, the critical condition is the trim to 1.4 V_{stall} in landing approach with ice on the horizontal tail and flaps deflected $35^{o}/15^{o}$.

- o The landing gear position at 49 percent MAC, in conjunction with the airplane static ground angle of 12^{o}, establishes the aft c.g. limit for both aircraft as 30 percent MAC, due to a tip-over limitation.

  This tip-over limit precludes effective use of negative stability or even stability limits in establishing the aft c.g. limits. The landing gear is positioned at the most aft location compatible with submerging the retracted gear strut into the airfoil contour. The combination of a supercritical airfoil, a thinner airfoil for the laminar flow requirement, and a wing planform with a minimum "yehudi" (trailing edge extension) at the wing root, imposes this restriction on landing gear placement.

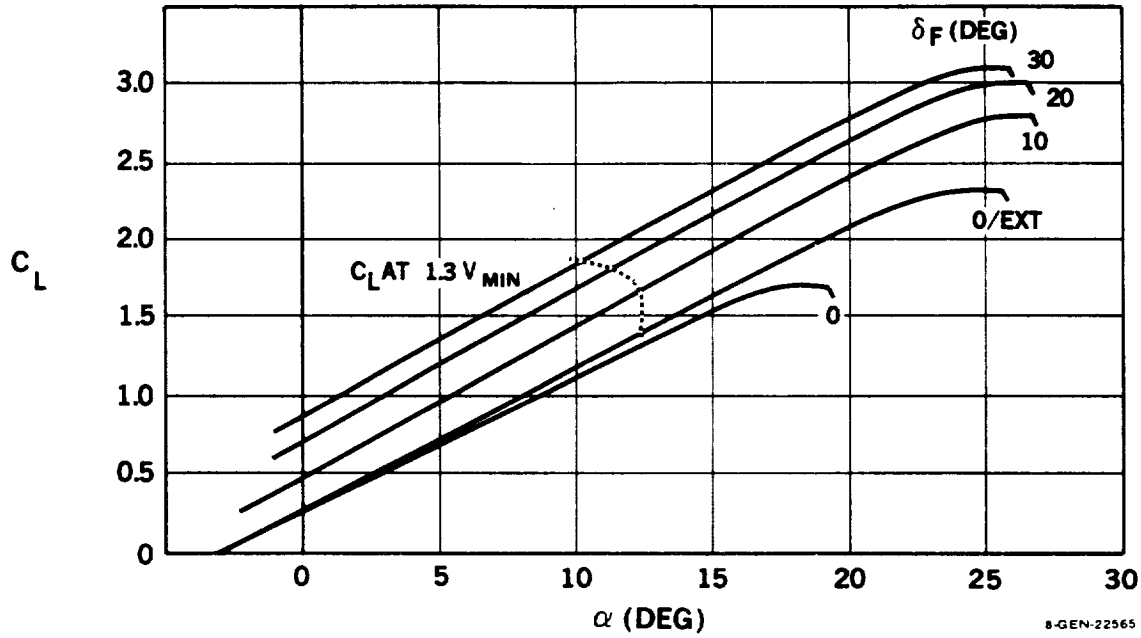

FIGURE 5-28. LOW-SPEED LIFT CURVES – UPPER SURFACE SUCTION ONLY

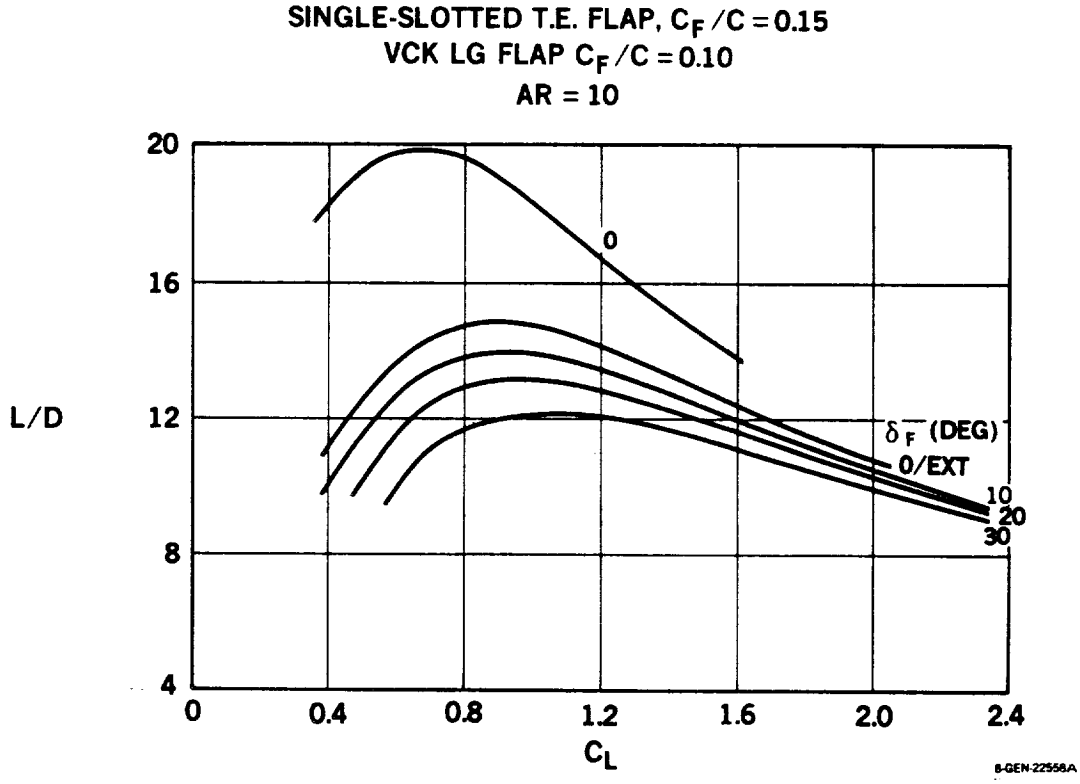

FIGURE 5-29. LOW-SPEED L/D CHARACTERISTICS – UPPER SURFACE SUCTION ONLY

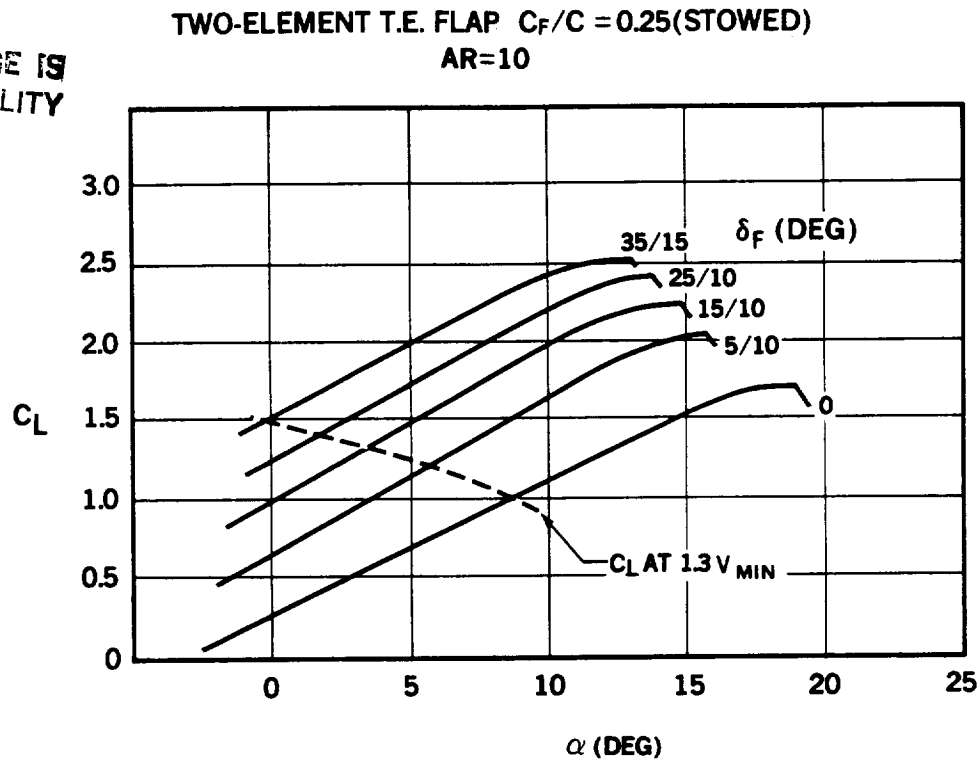

FIGURE 5-30. LOW-SPEED LIFT CURVES – BASE CASE – SUCTION ON BOTH SURFACES

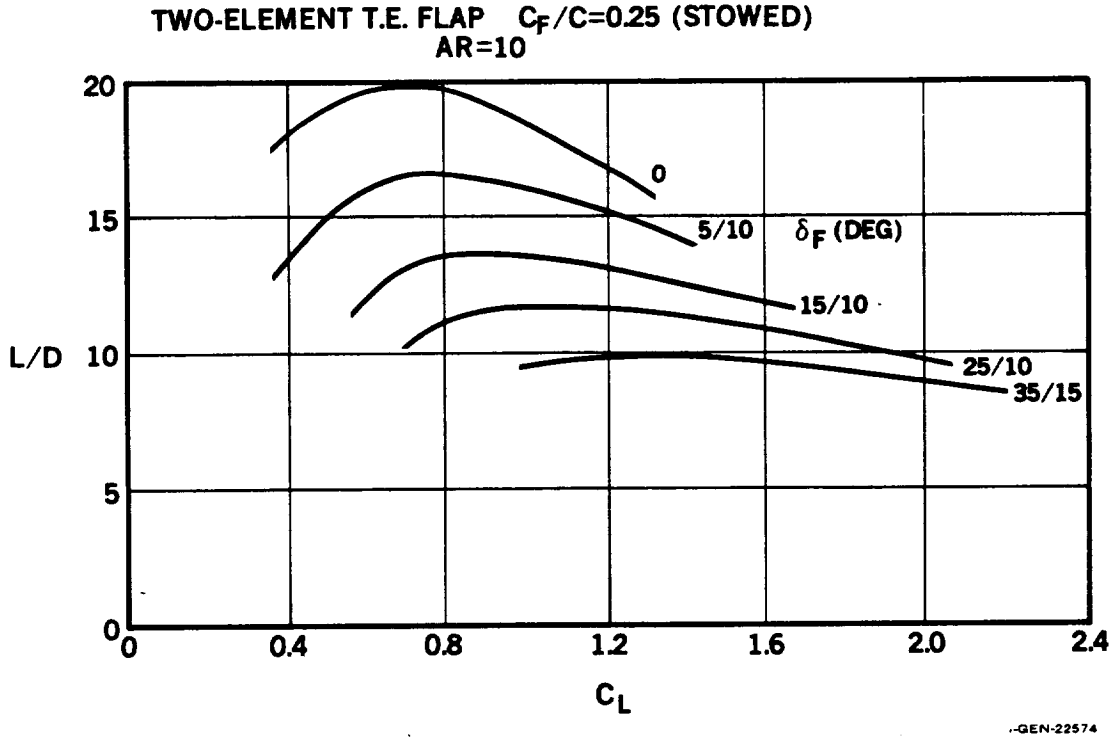

FIGURE 5-31. LOW-SPEED L/D CHARACTERISTICS – SUCTION ON BOTH SURFACES

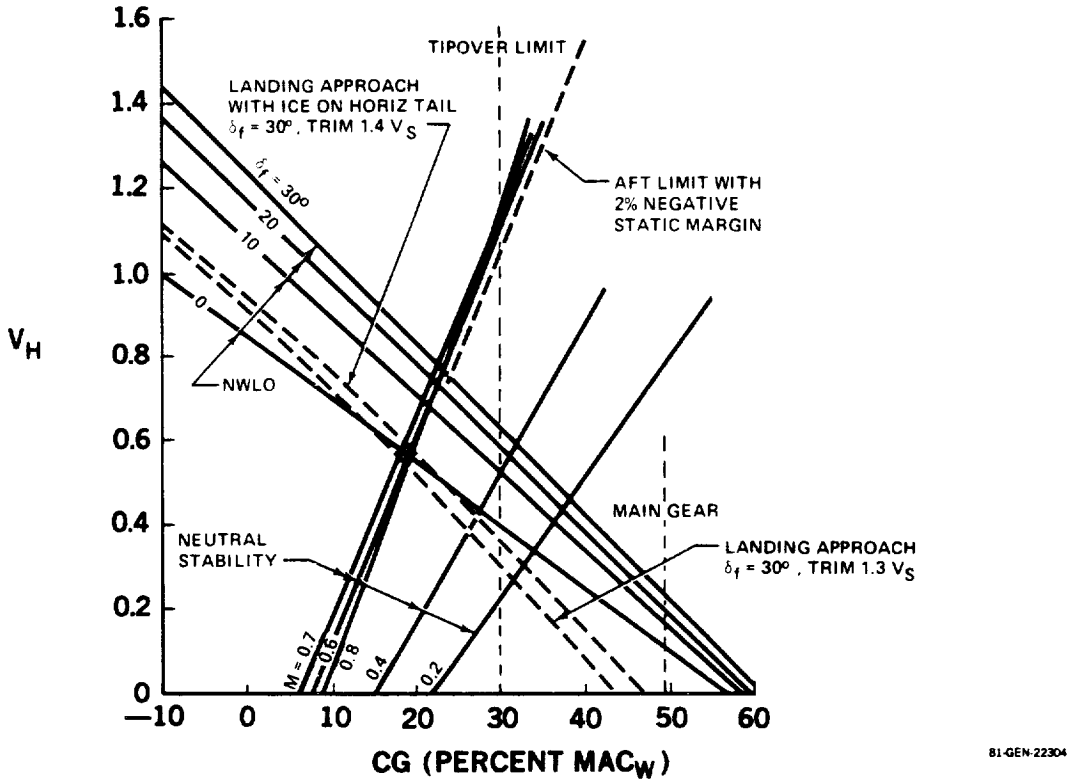

FIGURE 5-32. HORIZONTAL TAIL SIZING – UPPER-SURFACE-ONLY WING LAMINARIZATION

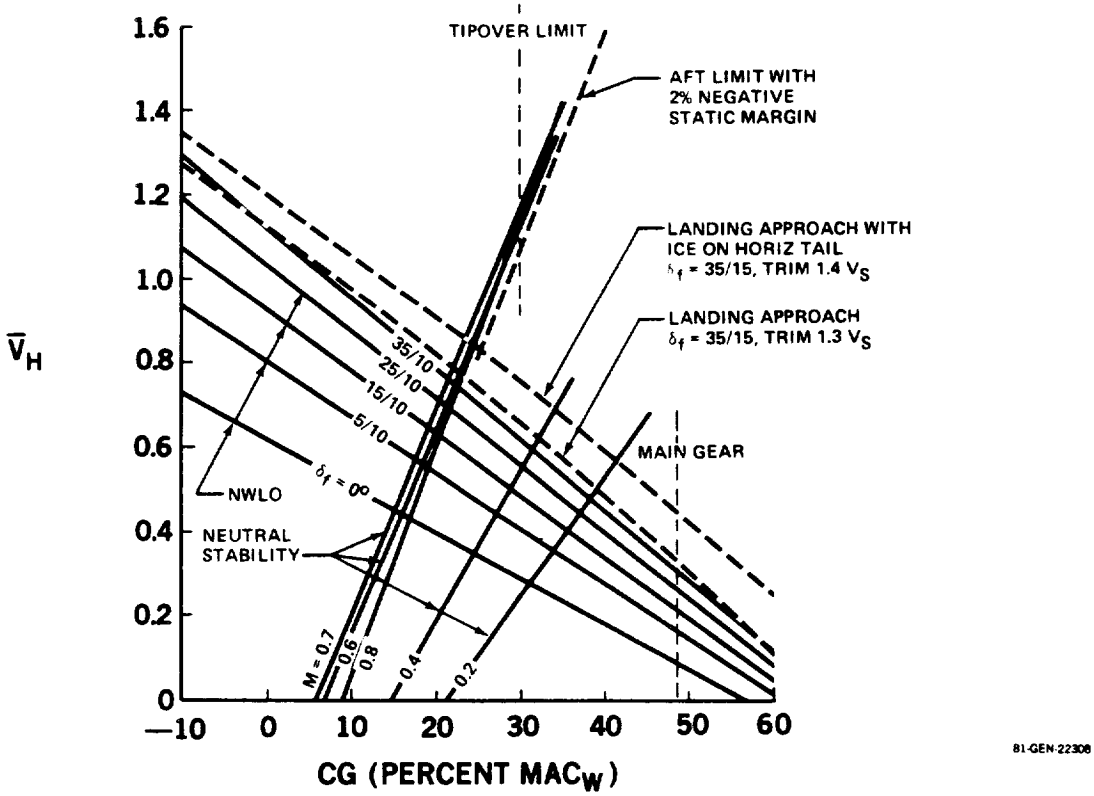

FIGURE 5-33. HORIZONTAL TAIL SIZING – UPPER-PLUS-LOWER-SURFACE WING LAMINARIZATION

- The specific tail volumes were selected to provide 33.5 percent and 31.5 percent c.g. travel, respectively, for the upper-surface-only and the upper-plus lower surface laminarization cases; see Figures 5-34 and 5-35. These c.g. travels are consistent with the aircraft loading and balance requirement and are compatible with DC-9 and DC-10 characteristics, taking into account the cabin length and differences in wing MAC.

In the case of LFC on the upper-surface-only, the flap deflection was subsequently found to be restricted to 12.4^{o} due to second segment climb limitation. This flap restriction would allow the forward c.g. limit to be extended from -3.5 percent to -7 percent increasing the overall travel to 37 percent. Alternatively the tail volume coefficient could be reduced from 1.24 to 1.15 to maintain the 33.5 percent travel with the same c.g. limits.

f. Vertical Tail Sizing - The vertical tail volumes (V_v) shown previously in Figures 5-24a and b, provide a level of directional stability equivalent to that of the DC-9-30 and the DC-10-30 airplanes. The vertical tail volumes of .068 and .0646 respectively for the upper-surface-only and the upper-plus-lower-surface laminarizations provide a low-speed C_{n_β} of .0028. $V_{m_{cg}}$ is not critical since the moment arm of the outboard engine thrust is relatively small.

g. Lateral Control - A brief analysis of the lateral control effectiveness of the upper-surface-only configuration was made using the following simplified procedure.

The lateral control effectiveness of the LFC aircraft was estimated based on DC-10-30 low-speed aileron and spoiler data. Adjustments were made using a series of ratios, to account for differences in the wing area affected by the control surface, in the rolling moment arm of the control surface, in the lift curve slope of the wing, and in the

C-2

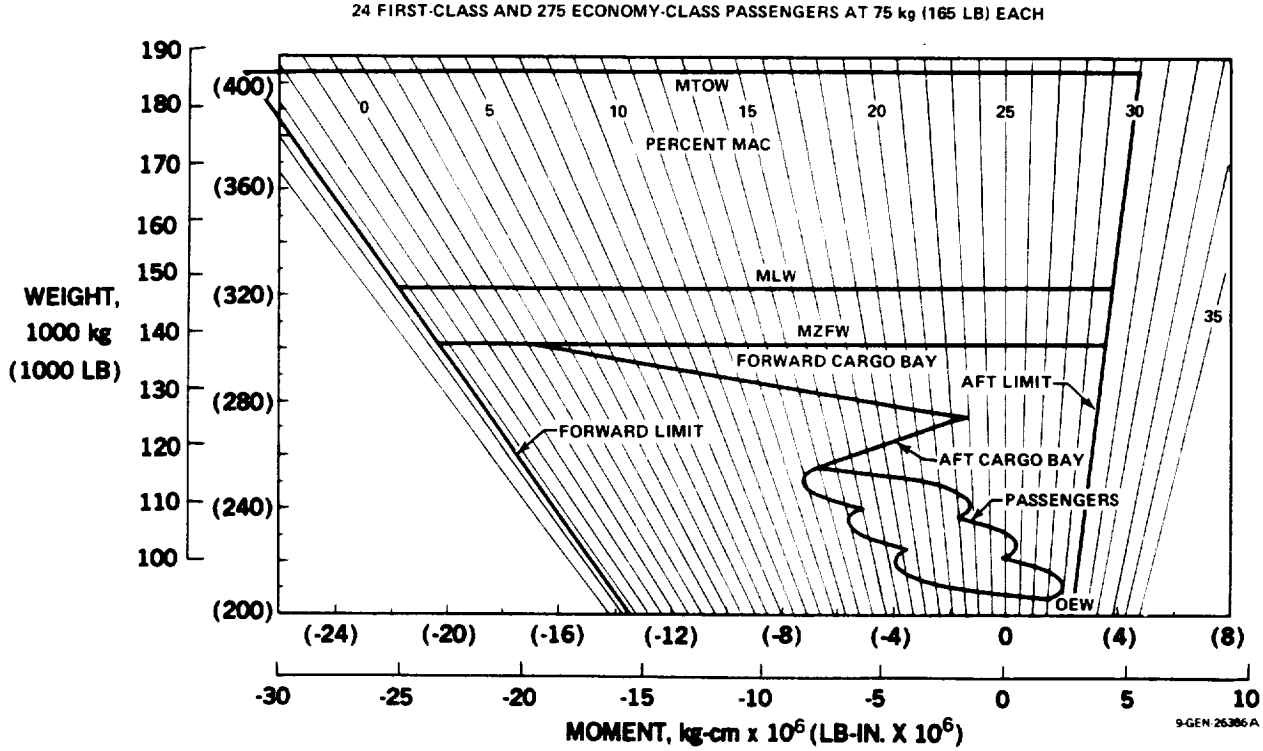

FIGURE 5-34. LFC AIRCRAFT BALANCE DIAGRAM – UPPER WING SURFACE LAMINARIZED TO 85-PERCENT CHORD

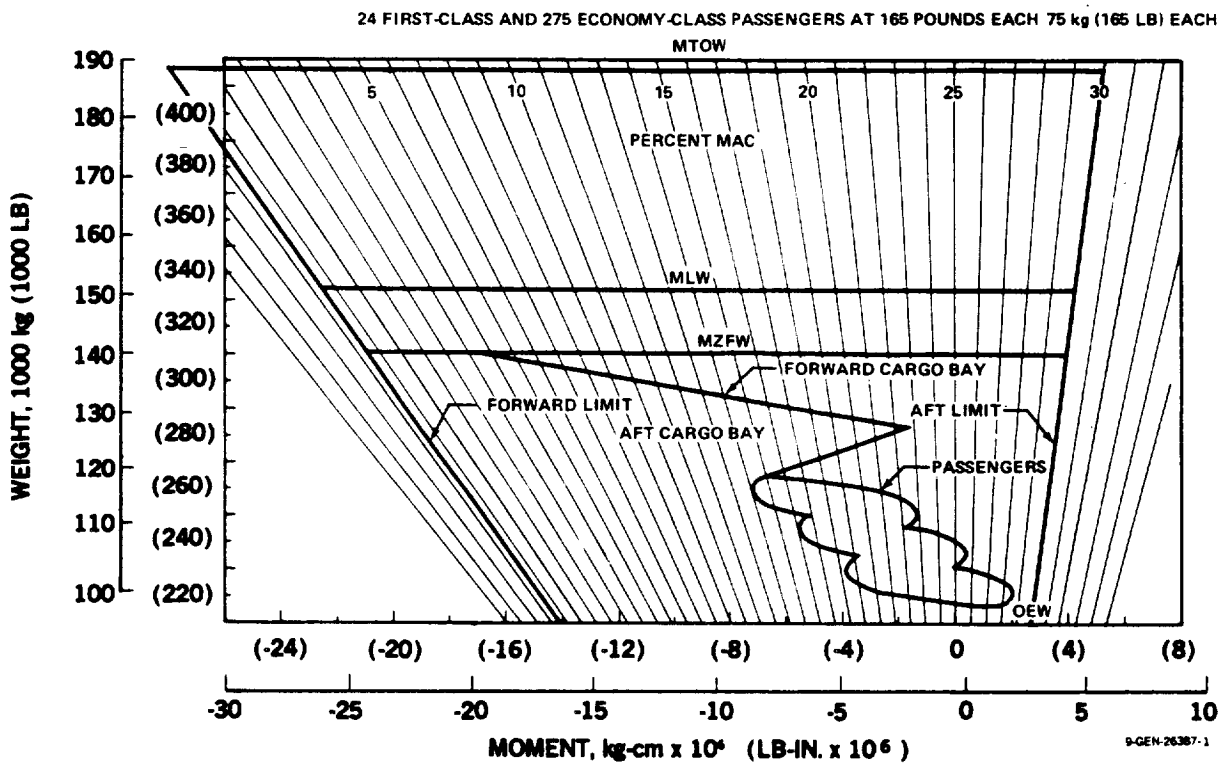

FIGURE 5-35. LFC AIRCRAFT BALANCE DIAGRAM – UPPER AND LOWER WING SURFACES LAMINARIZED TO 70-PERCENT CHORD

effective section angle-of-attack change due to the control surface deflection. This resulted in the following equation, where ($\Delta\alpha'$) is a function of the height and chordwise location of the deflected spoiler trailing edge as indicated by Figure 5-36.

$$(\Delta C_\ell)^{LFC} = \left[(\Delta C_\ell)^{DC10} \frac{\left(\frac{S_{W_a} \ell_a}{S_W b_W}\right)^{LFC}}{\left(\frac{S_{W_a} \ell_a}{S_W b_W}\right)^{DC10}} \frac{(C_{L_\alpha})^{LFC}}{(C_{L_\alpha})^{DC10}} \frac{\left(\frac{\partial \alpha}{\partial \delta_a}\right)^{LFC}}{\left(\frac{\partial \alpha}{\partial \delta_a}\right)^{DC10}} \right]^{Aileron}$$

$$+ \left[(\Delta C_\ell)^{DC10} \frac{\left(\frac{S_{W_{SP}} \ell_{SP}}{S_W b_W}\right)^{LFC}}{\left(\frac{S_{W_{SP}} \ell_{SP}}{S_W b_W}\right)^{DC10}} \frac{(C_{L_\alpha})^{LFC}}{(C_{L_\alpha})^{DC10}} \frac{(\Delta\alpha')^{LFC}}{(\Delta\alpha')^{DC10}} \right]^{Spoiler}$$

This approach indicates a 22-percent increase in effectiveness (at maximum control deflection) of the LFC lateral control system over that of the DC-10-30 in the flaps-up configuration, and 13 percent increase in the landing-flap configuration.

Table 5-17 lists the contributions of each of the major components of the lateral control systems of the two aircraft at maximum control deflection, as well as the damping in roll derivative $(C_{l_p})_A$ The higher value of $(C_{l_p})_A$ shown for the LFC is attributed to the relatively higher aspect ratio and lower sweep angle of the LFC wing. A comparison of the maximum low-speed rolling performance of the two

aircraft is also shown. Included are the wing tip helix angle $\frac{Pb}{2V}$ and the roll rate (p) at an arbitrary speed of 77 m/s (150 knots).

The rolling performance of the LFC aircraft is comparable with that of the DC-10-30 and, by inference, the lateral control system proposed for the LFC aircraft should be adequate.

Table 5-17

LATERAL CONTROL CONTRIBUTIONS COMPARISON

	DC-10-30		LFC AIRCRAFT	
	Flaps Up	Flaps 50°	Flaps Up	Flaps 30°
Control Surface				
Inboard Spoiler (ΔC_R)	0.00428	0.01092	0.01885	0.03260
Inboard Aileron (ΔC_R)	0.00896	0.00878	--	--
Outboard Spoiler (ΔC_R)	0.01948	0.04973	0.02563	0.05022
Outboard Aileron (ΔC_R)	0.01610	0.02195	0.01504	0.02050
TOTAL	0.04882	0.09138	0.05952	0.10332
Damping in Roll $(C_{L_p})_A$ Per Degree	-0.00790		-0.00920	
Rolling Performance				
Wing Tip Helix Angle (Pb/2V) (Radian)	0.108	0.202	0.113	0.196
Roll Rate at 77m/s (150 Kn) p. (Degree/Second)	18.9	35.4	18.6	32.3

5.6.1.2 Wing Structure

Brief descriptions of the structural characteristics of the two LFC wings are presented. Further detailed description and analysis may be found in Section 9.0.

The wing structures of the two LFC configurations are illustrated in Figures 5-37 and 5-38. Complete wing sections were shown on Figure 5-27. The LFC suction panels are supported by the external stiffness of the main wing box. This creates integral ducting which is used to transfer the suction airflow to the dry bay above the suction pump nacelle. Figure 5-39 shows that holes must be provided in the main box skin panels, as illustrated further in Figures 5-40 and 5-41, in order to transfer the airflow to the suction pump. The holes required through primary structure are similar for both LFC configurations.

The main wing box is of graphite epoxy composite construction and the LFC panels are of fiberglass with a porous metal surface. Figure 5-42 shows the cross-section of a typical LFC panel that has a calendered woven stainless steel porous surface, manufactured under the trade name Dynapore. The layers are described as follows:

Layer 1: 80 x 700 + 80 x 80 diffusion bonded Dynapore
.305mm (.012 in) thick porous surface

Layer 2: Perforated 'S' glass laminate 1.4 mm (.055 in) thick
This layer provides support for the surface.

Layer 3: This was subsequently eliminated to avoid moisture entrapment within the perforations of Layer 2, thus avoiding a possible cause of laminar separation due to freezing, also reducing the time required to restore full porosity to the surface layers after exposure to moisture or contamination avoidance liquid.

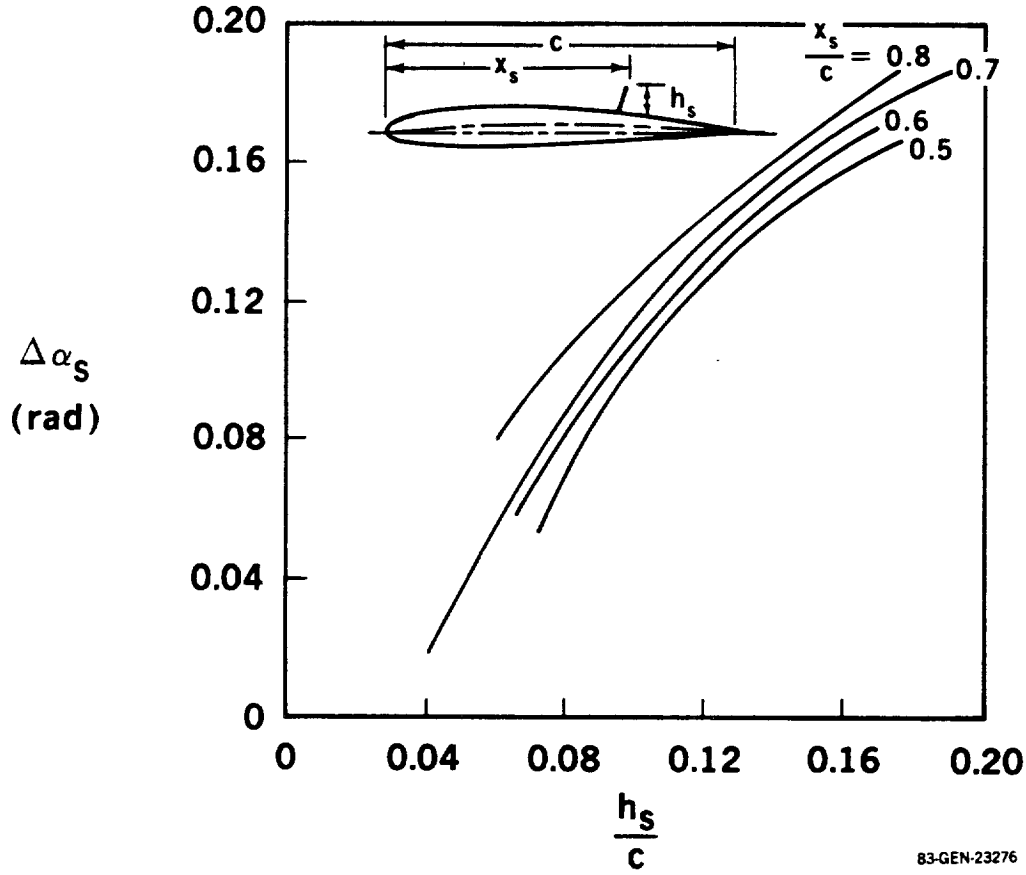

FIGURE 5-36. SPOILER LIFT EFFECTIVENESS AT LOW SPEEDS

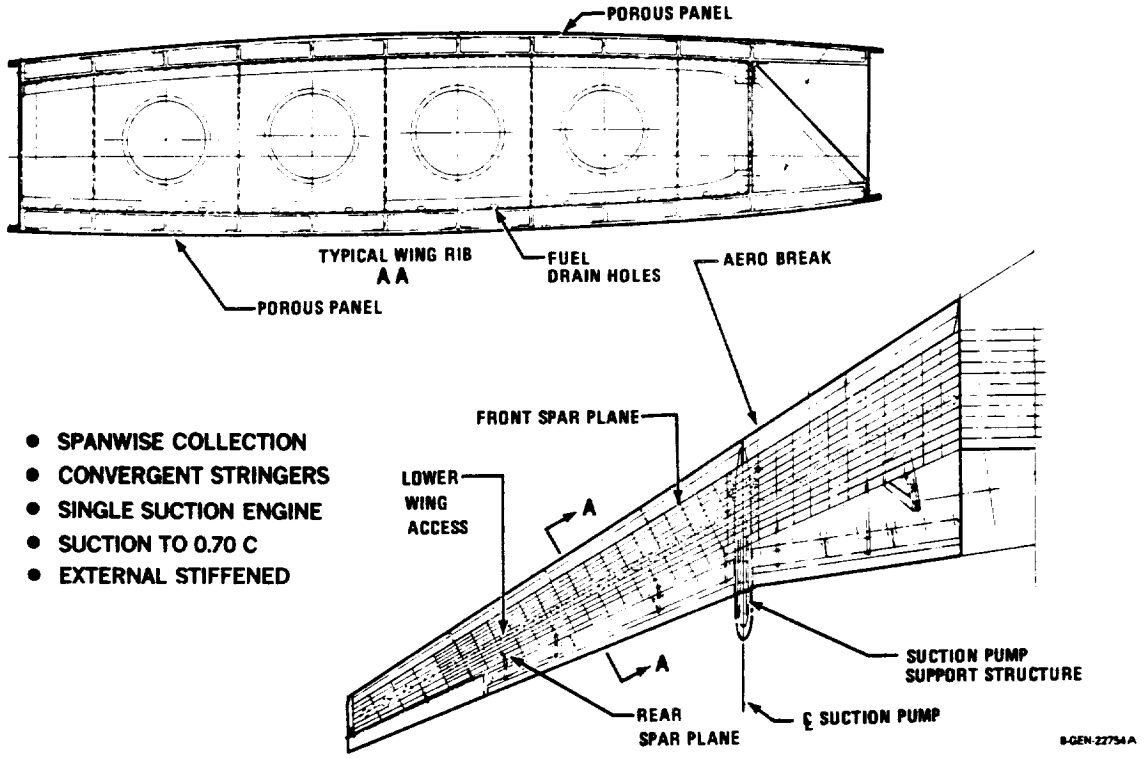

FIGURE 5-37. STRUCTURAL ARRANGEMENT – SUCTION THROUGH BOTH SURFACES

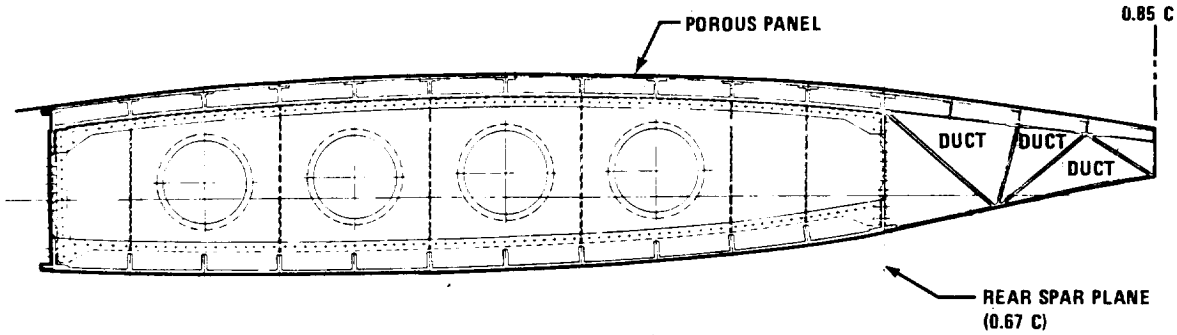

8-GEN-22755

FIGURE 5-38. TYPICAL WING RIB – SUCTION THROUGH UPPER SURFACE ONLY TO 0.85C

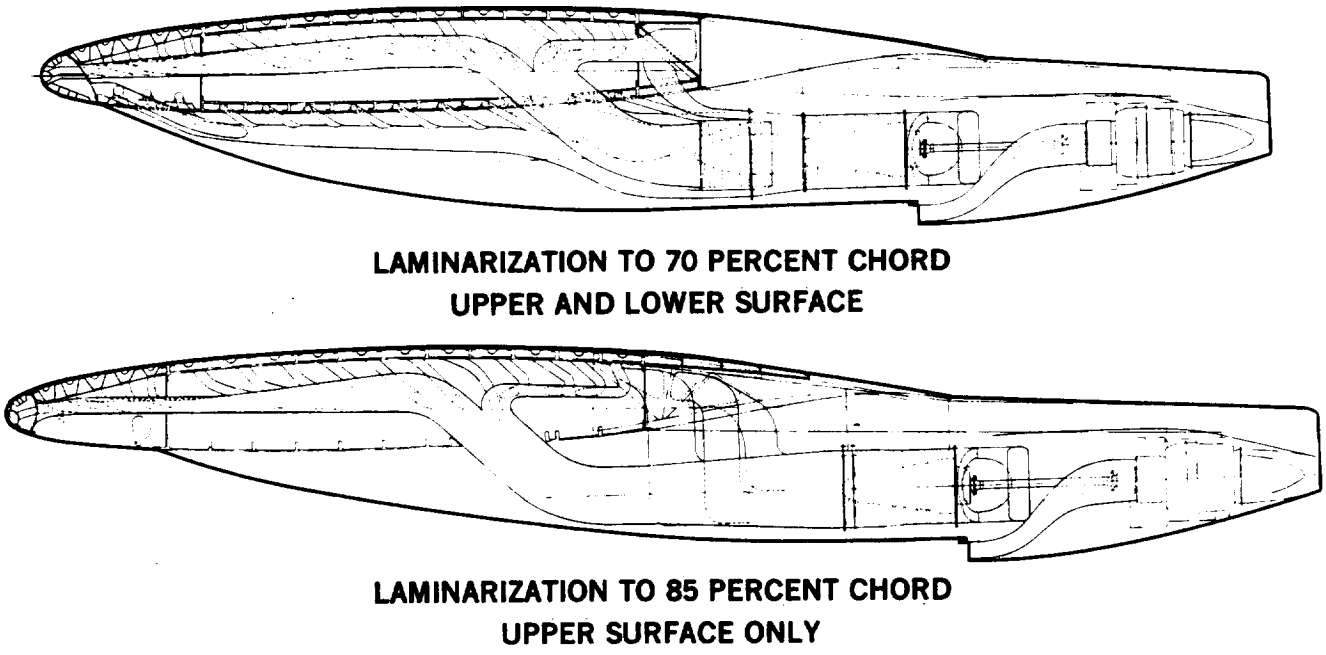

8-GEN-22893

FIGURE 5-39. SUCTION SYSTEM MANIFOLDING INTEGRATION

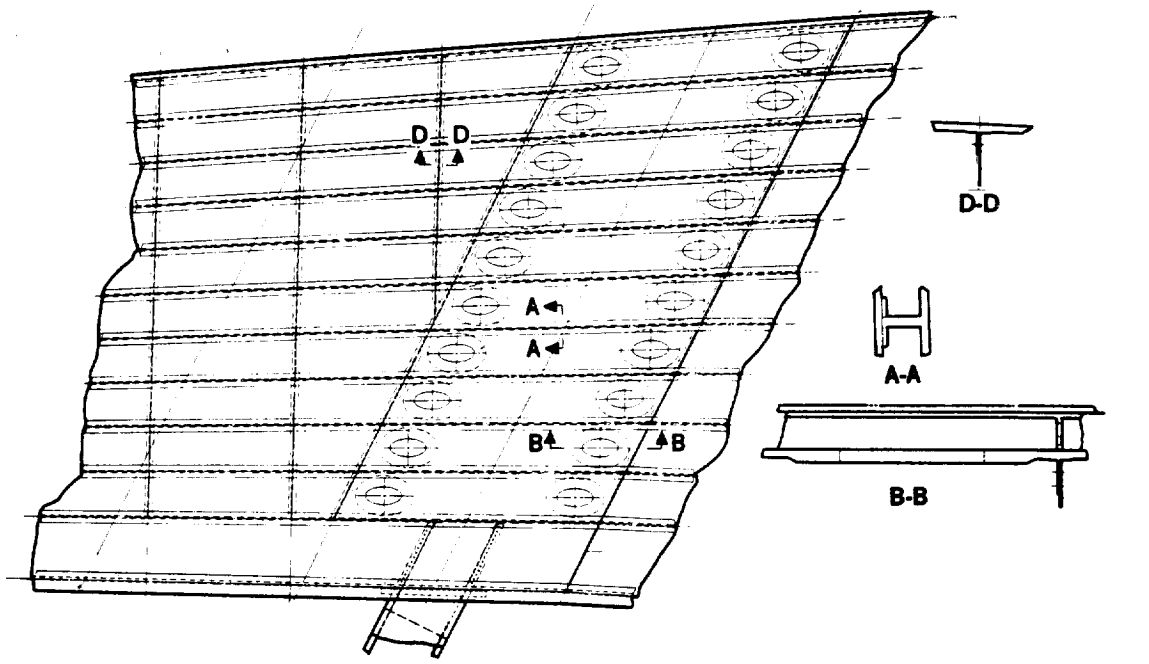

FIGURE 5-40. STRUCTURAL ARRANGEMENT – UPPER WING BOX PANEL AT ℄ OF SUCTION PUMP SYSTEM

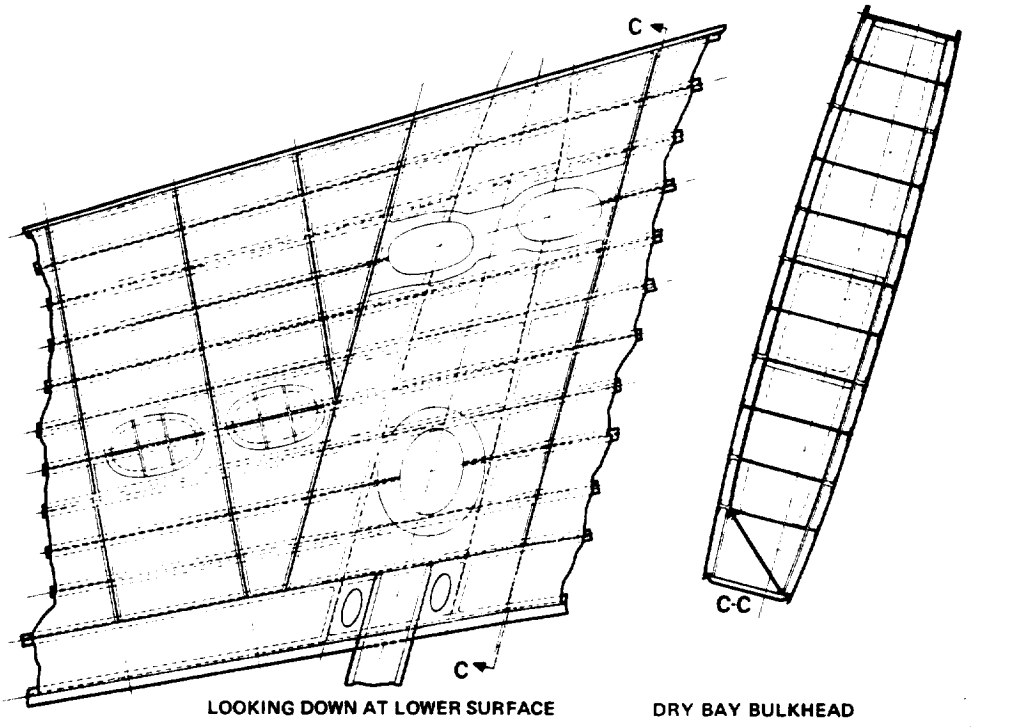

FIGURE 5-41. STRUCTURAL ARRANGEMENT SHOWING LOWER SURFACE AND FUEL BULKHEAD AT ℄ OF SUCTION PUMP SYSTEM

Layer 4: 'E' glass laminated web, .5mm (.02 in) thick. This is now sewn directly to Layer 2 so that Layer 2 becomes part of the base sandwich panel.

Layer 5: 'E' glass back face, thickness .5mm (.02 in) minimum, depends on test results and buckling characteristics.

Substitution of an electron beam (EB) perforated titanium surface for the Dynapore outer layer resulted in improved structural and damage resistance properties. The titanium sheet thickness is .63 mm (.025 in) and the perforations are .063 mm (.0025 in) diameter. After performing satisfactorily as an LFC surface during wind tunnel testing, EB perforated titanium was selected as the LFC panel surface for the final configuration.

The wing leading edge box is where the structural, aerodynamics, suction and environmental problems must all be integrated very compactly. Typical leading edge sections for both LFC configurations are shown in Figures 5-43 and 5-44. The fiberglass corrugations support the surface between nose ribs and provide integral ducting for the suction air. Integration of the environmental systems is covered in the following paragraphs.

5.6.1.3 Wing Leading Edge Protection

This system is described fully in Section 11.0. For LFC on both wing surfaces, the liquid systems must provide complete protection against both icing and insect impingement. Integration of the LFC suction and liquid systems is difficult, particularly if suction is required along the attachment line. One possibility that needs to be investigated is using the same porous surface for both suction air and liquid systems. The purging system and valves required would increase complexity and porosity requirements at the surface would need to be matched for both systems.

The problem is eased considerably with LFC on the upper surface only. A shield is deployed to protect the leading edge region as shown in Figure 5-44. With a large enough shield, the liquid systems would be needed only for ice protection. If the shield is not large enough, there is a tendency for very

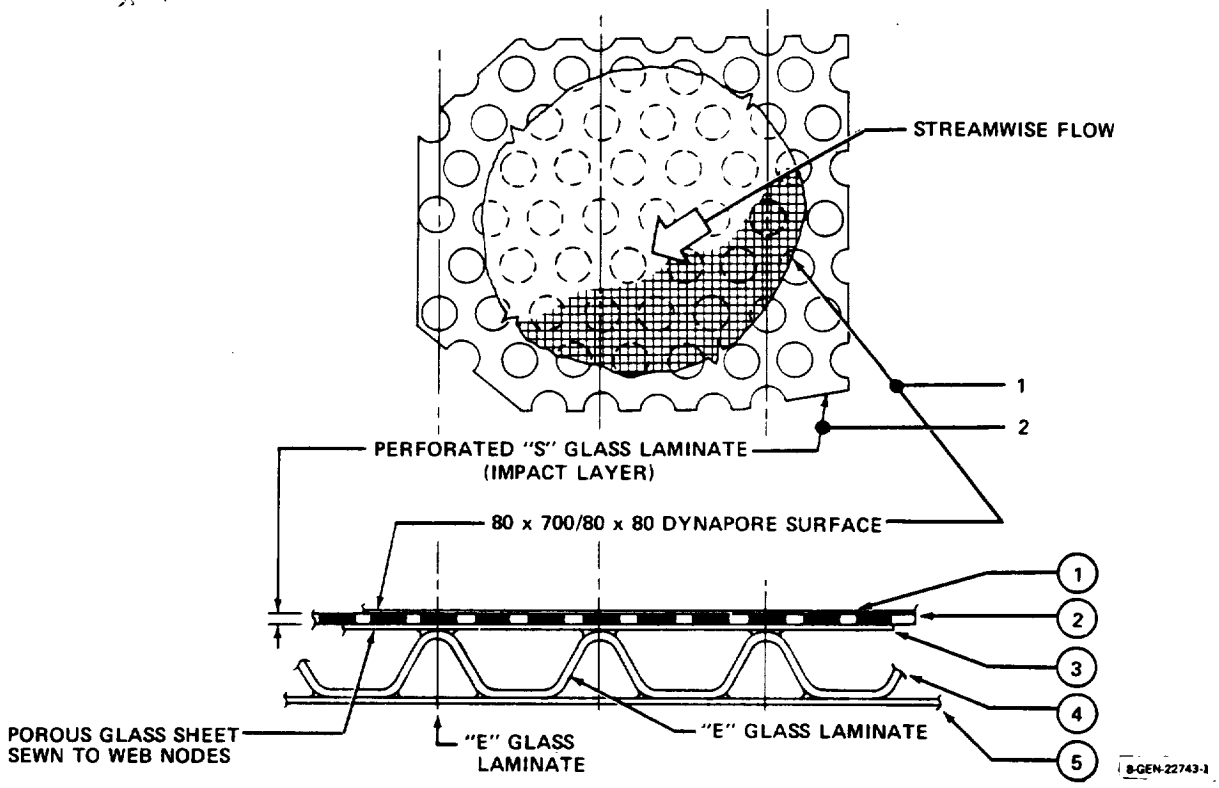

FIGURE 5-42. LFC GLOVE PANEL LAYER IDENTIFICATION

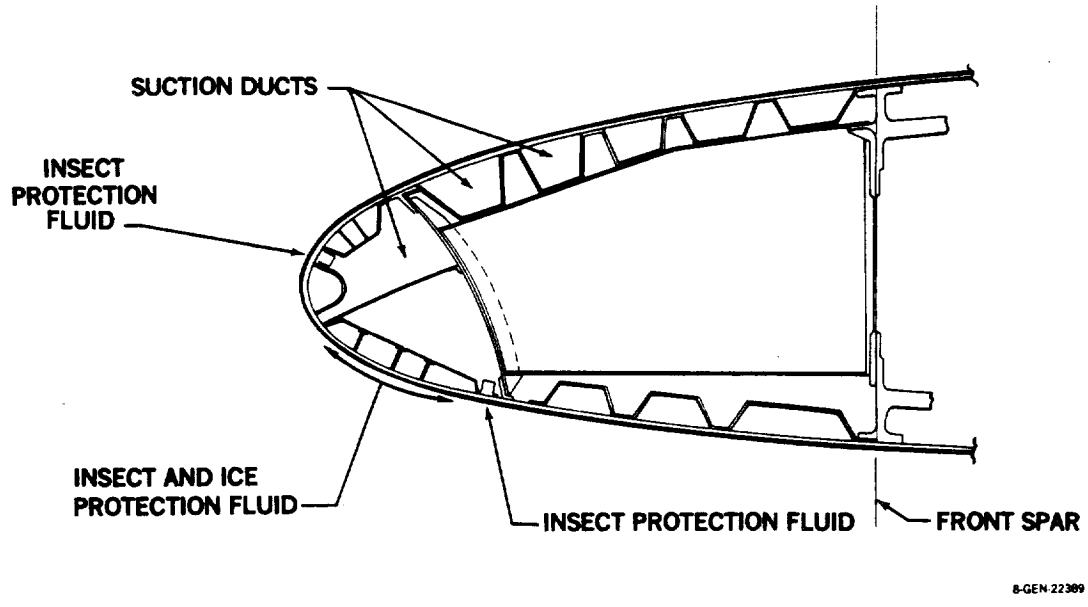

FIGURE 5-43. LEADING EDGE DESIGN – SUCTION ON BOTH SURFACES

small insects to be deflected with the airflow between the shield and the wing and to impinge on the lower leading edge surface. Large insects might not be deflected by the airflow and could contact the upper surface with a glancing impact. Consequently a liquid system is shown for insect protection in addition to the shield, but flight testing may show that this is not necessary. An alternative method of applying protection liquid to the leading edge is to use the shield as a spray-bar as shown in Figure 5-45.

Retraction of the shield into the confined space available near the wing tip can be a problem. One solution is to move the front spar further aft outboard and to use a mechanism similar to that shown in Figure 5-46.

5.6.1.4 Suction/Ducting System

The laminarized planform area, for the upper-surface-only case is illustrated in Figure 5-47. The boundaries of the laminarized areas are practical ones as noted below:

- o A 10^{o} wedge from the wing-fuselage intersection over the upper wing surface
- o The landing gear retraction area.
- o The 80 percent span, 15 percent chord trailing edge flap area.
- o The 20 percent span, 25 percent chord aileron.
- o The area outboard of the wing tip closing bulkhead.

The manifolding at the dry bay area (approximately 40 percent span) for both laminarization cases was shown previously in Figure 5-39. With the suction ducting required further aft in the upper-surface-only case, the suction engine must also be mounted further aft. Detailed technical discussion of the suction ducting, manifolding, and suction engine is included in Section 10.0 of this report.

Additionaldrawings of the two suction ducting systems are shown in Figures 5-48 and 5-49. The ducting and manifolding is considerably simplified for the upper-surface-only case.

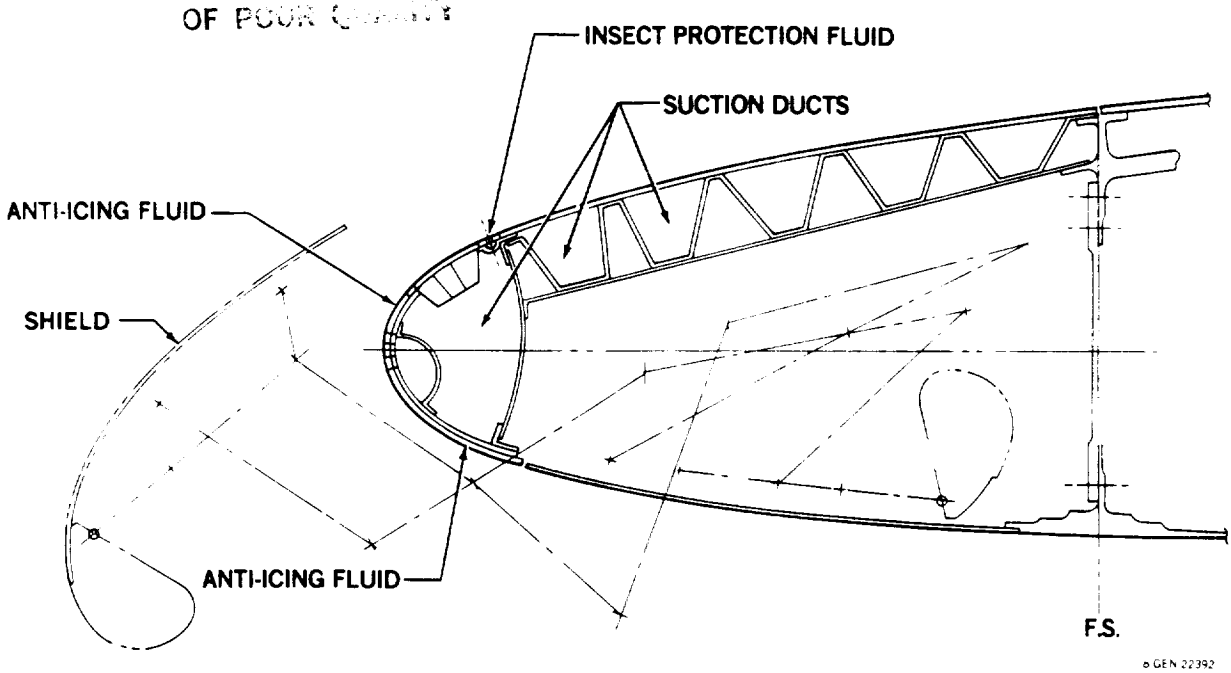

FIGURE 5-44. LEADING EDGE DESIGN – UPPER SURFACE SUCTION ONLY

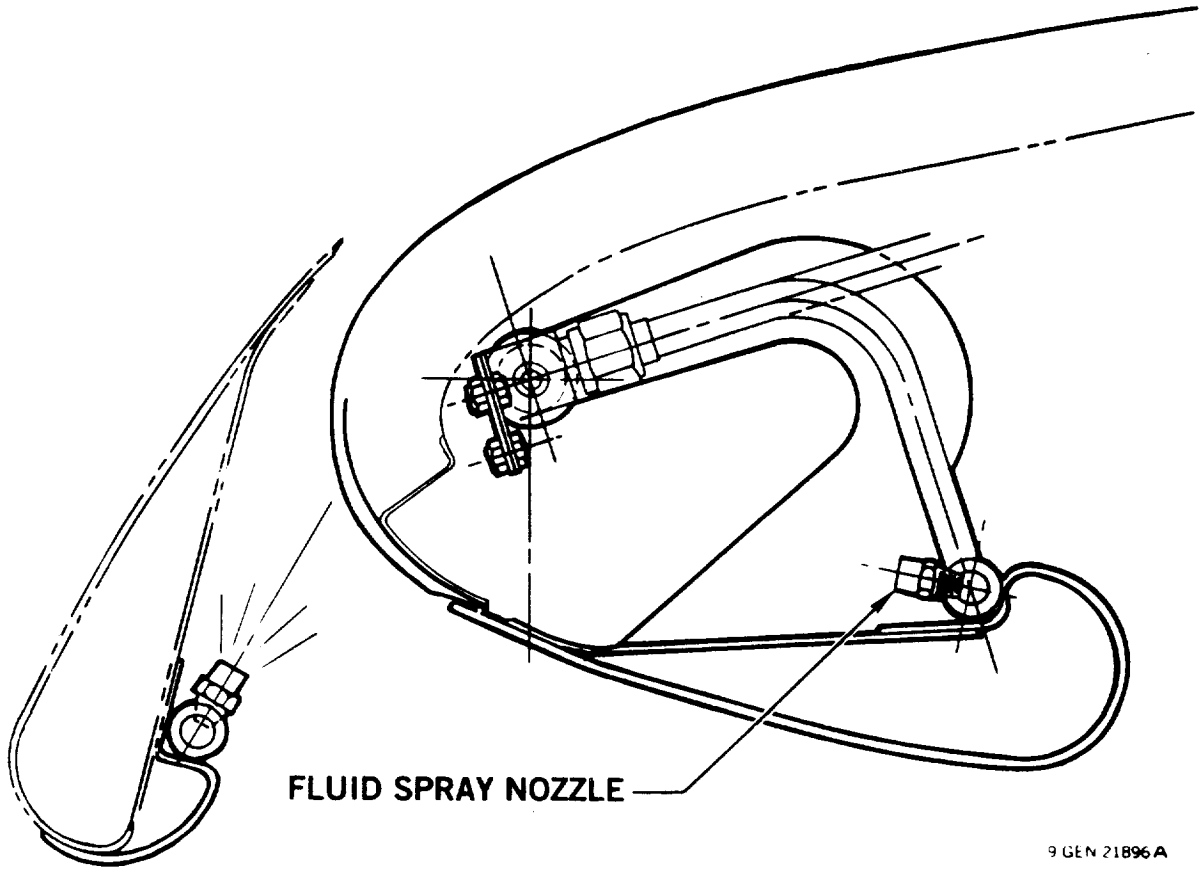

FIGURE 5-45. SPRAY CONCEPT

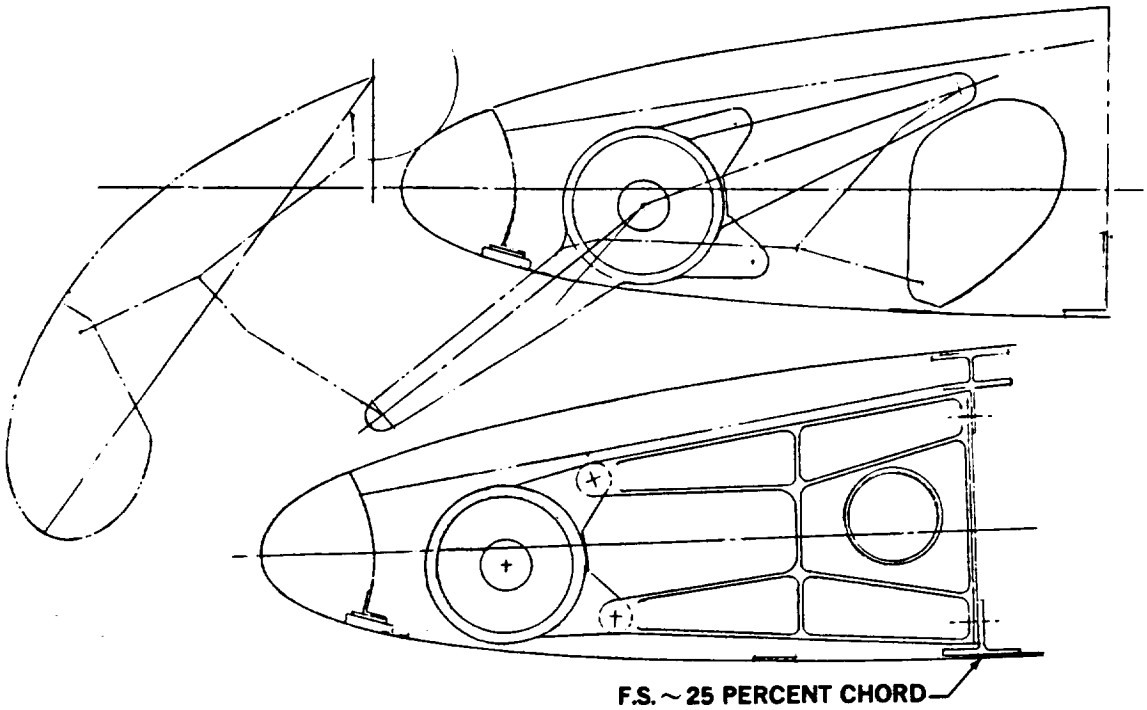

FIGURE 5-46. OUTBOARD WING SHIELD

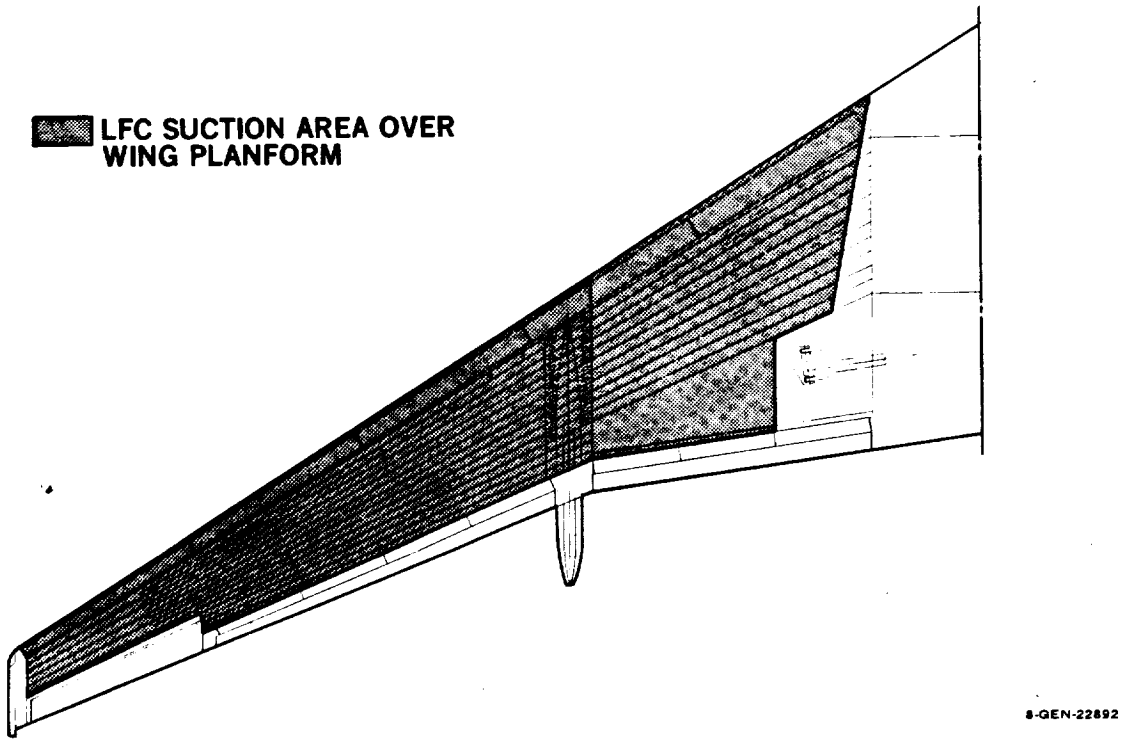

FIGURE 5-47. WING STRUCTURES/SUCTION DUCTING INTEGRATION – UPPER SURFACE ONLY LAMINARIZED

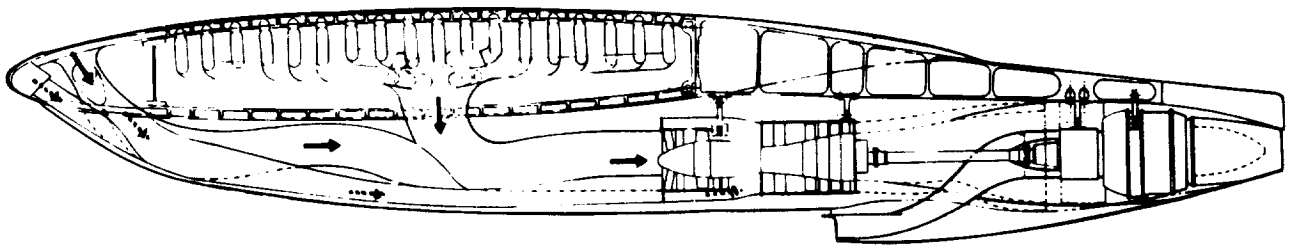

DUCTING FROM UPPER SURFACE

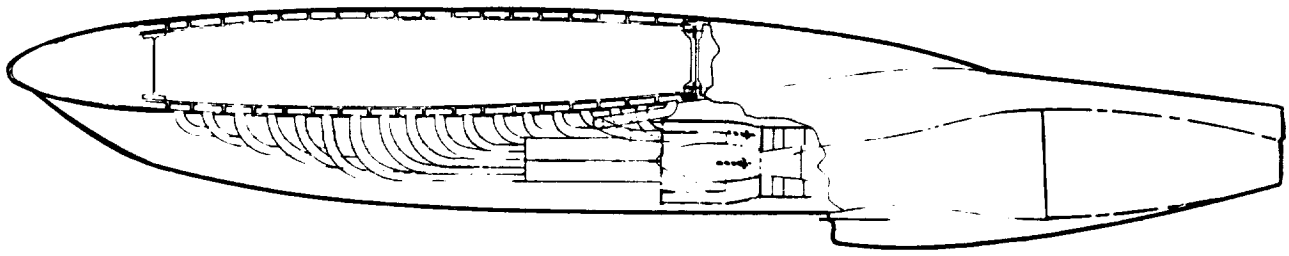

DUCTING FROM LOWER SURFACE

83-GEN-23299

FIGURE 5-48. INTEGRATION OF SUCTION DUCTING IN DRY BAY AREA – UPPER AND LOWER SURFACE LAMINARIZATION TO 70-PERCENT CHORD

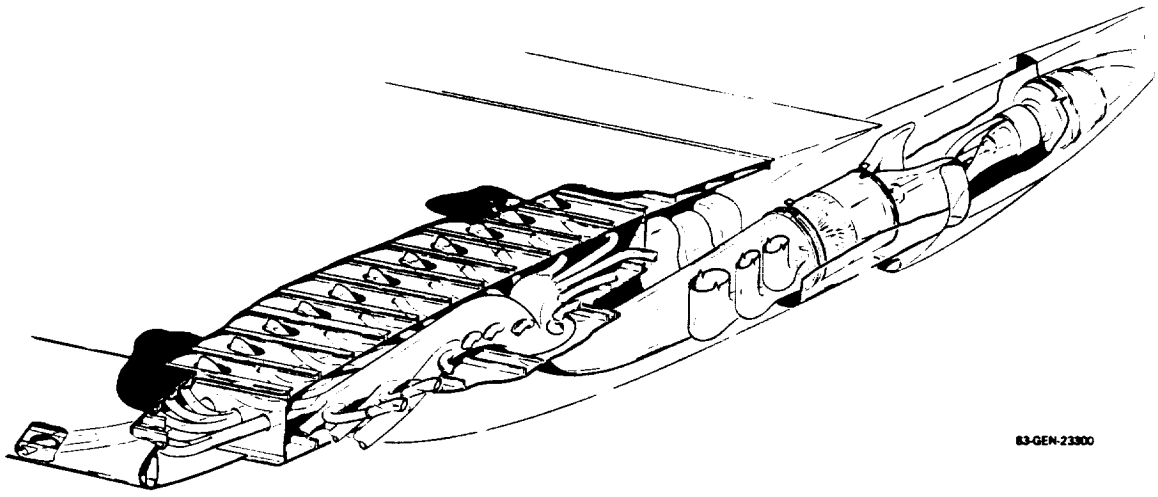

83-GEN-23300

FIGURE 5-49. INTEGRATION OF SUCTION DUCTING IN DRY BAY AREA – LAMINARIZATION OF UPPER SURFACE ONLY TO 85-PERCENT CHORD

5.6.1.5 Weights and Performance - LFC Aircraft

The two LFC configurations shown in Figures 5-24a and b were sized using the K5JA computer program and sizing matrices as described previously under 5.3.7. The study ground rules remained as in Table 5-1. The interior layout, as shown in Figure 5-1, and operational items Table 5-18, were common to both. A comparative breakdown of LFC ducting system weights is presented in Table 5-19.

From the Weight Summary Table 5-20 it can be seen that the upper-surface-only configuration results in a lower takeoff and empty weight and requires less fuel. Table 5-21 shows that the upper-surface-only configuration has a smaller wing area and smaller engine thrust required. Although it has a lower lift-drag ratio, it burns less fuel due to its lower weight. It also has a lower approach speed. There can be no doubt that the "upper-surface-only" configuration is superior. In addition to its better all-round performance, it has all of the advantages listed previously under 5.6.1.

Table 5-18
WEIGHT BREAKDOWN OF OPERATIONAL ITEMS
(SAME FOR LAMINAR AND TURBULENT AIRCRAFT)

	KILOGRAMS	POUNDS
Cockpit Crew	231	(510)
Cabin Crew	590	(1,300)
Crew Baggage and Flight Kits	141	(310)
Oil	120	(264)
Unusable Fuel	227	(500)
Food, Galley Service Equipment and Bev.	1,994	(4,397)
Passenger Service Equipment	542	(1,196)
Potable Water	714	(1,574)
Lavatory Fluids	91	(200)
Escape Slides/Rafts	667	(1,470)
Life Vests	230	(506)
Pallets	794	(1,750)
Containers	1,469	(3,240)
OPERATIONAL ITEMS (TOTAL)	7,810	17,217

Table 5-19

LAMINAR FLOW CONTROL

SUCTION/DUCTING SYSTEM WEIGHTS

		LFC UPPER SURFACE ONLY		LFC BOTH SURFACES	
Takeoff Gross Weight	kg (LB)	183,400	(404,320)	188,660	(415,930)
Wing Area	m^2 (SQ FT)	288	(3,100)	331	(3,560)
Total Wing Weight (Including LFC)	kg (LB)	18,532	(40,855)	20,950	(46,186)
LFC Suction/Ducting System	kg (LB)	2,790	(6,150)	4,550	(10,030)
Suction/Ducting System	kg (LB)	699	(1,540)	690	(1,520)
Ducting-Porous Panel LE Weight Collector Ducts	kg (LB)	2,091	(4,610)	3,860	(8,510)
Suction/Ducting System Weight					
Percent Total Wing Weight		15.1		21.7	
Percent Takeoff Gross Weight		1.5		2.4	
Weight/Wing Plan Area	kg/m^2 (LB/FT^2)	9.67	(1.98)	13.77	(2.82)

Table 5-20

WEIGHT SUMMARY

LFC AIRCRAFT COMPARISON

	LFC UPPER & LOWER SURFACE		LFC UPPER SURFACE ONLY	
	kg	(LB)	kg	(LB)
Wing	20,950	(46,186)	18,532	(40,855)
Horizontal Tail	2,076	(4,577)	1,735	(3,824)
Vertical Tail	1,882	(4,149)	1,733	(3,820)
Fuselage	18,434	(40,640)	18,312	(40,370)
Landing Gear	7,604	(16,763)	7,377	(16,264)
Propulsion System	11,330	(24,979)	10,881	(23,988)
Fuel System	858	(1,892)	803	(1,770)
Flight Controls and Hydraulics	3,222	(7,103)	2,800	(6,172)
Auxiliary Power Unit	490	(1,080)	490	(1,080)
Instruments	794	(1,750)	794	(1,750)
Air Conditioning and Pneumatics	2,075	(4,574)	2,075	(4,574)
Electrical	2,327	(5,130)	2,327	(5,130)
Avionics (Including AFCS)	1,427	(3,146)	1,427	(3,146)
Furnishings	16,400	(36,156)	16,400	(36,156)
Anti-Ice	194	(428)	169	(372)
Auxiliary Gear	28	(62)	28	(62)
Manufacturer's Empty Weight	90,090	(198,615)	85,880	(189,333)
Operational Items	7,810	(17,217)	7,810	(17,217)
Operational Empty Weight	97,900	(215,832)	93,689	(206,550)
Payload	31,298	(69,000)	31,298	(69,000)
Zero Fuel Weight	129,198	(284,832)	124,987	(275,550)
Fuel	59,465	(131,098)	58,409	(128,770)
Maximum Design Takeoff Weight	188,663	(415,930)	183,396	(404,320)

Table 5-21

LFC AIRCRAFT CHARACTERISTICS COMPARISON

5000 N M1 RANGE 69,000 POUNDS PAYLOAD

		UPPER & LOWER SURFACES LFC TO 70 PERCENT C		UPPER SURFACE LFC TO 85 PERCENT C	
POWER PLANT		3 ADVANCED TURBOFANS		3 ADVANCED TURBOFANS	
SLS Thrust/Engine	kN (LB)	145.4	(32,690)	139.8	(31,430)
WING					
Area	m^2(SQ FT)	331	(3,560)	288	(3,100)
Sweepback, c/4	DEG	30		30	
AR		10		10	
Taper Ratio		0.25		0.25	
Airfoil t/c_{AVG}		11.7		10.3	
WEIGHT					
TOGW	kg (LB)	188,663	(415,930)	183,396	(404,320)
OEW	kg (LB)	97,899	(215,830)	93,690	(206,550)
Fuel Burned	kg (LB)	49,745	(109,670)	49,260	(108,600)
Fuel Reserves	kg (LB)	9,709	(21,405)	9,147	(20,165)
CRUISE C_L		0.5		0.56	
L/D		23.1		22.2	
$V_{Approach}$	m/s (KN)	66.9	(130)	64	(124.5)
Takeoff Field Length	m (FT)	2,632	(8,635)	2,615	(8,580)

The economic analysis in Section 6.0 will show that the "upper-surface-only" case also has lower initial cost and lower operating costs. The LFC configuration with suction on the upper wing surface only was therefore finally selected and compared with the turbulent configuration.

5.6.2 Turbulent Aircraft Comparison

The final turbulent aircraft was shown previously in Figure 5-24c. The scissors plot used for horizontal tail sizing is shown in Figure 5-50. As in Study I, the critical forward limit for tail sizing is established by trim requirements at

1.4 V_{stall} with full flaps and ice on the tail. The 21 percent c.g. travel obtained with a horizontal tail volume coefficient of 1.38 is adequate with wing mounted engines. The reduction from 1.52 used in Study I is due to the changes in wing aspect ratio, taper ratio, and airfoil thickness. The latter necessitated a movement of the main gear forward in order to obtain the depth required for housing the main gear.

Figure 5-51 shows the sizing matrix. The increase in takeoff gross weight from 187,243 kg (412,800 LB) for Study I to 191,853 kg (422,964 LB) is primarily due to an increase of operational items (cargo containers and pallets).

Table 5-22 compares the turbulent aircraft characteristics with those of the selected upper-surface-only LFC aircraft.

The LFC aircraft has a higher operational empty weight and wing area but due to its greatly improved lift/drag ratio, it burns 18.2 percent less fuel and the takeoff weight, engine thrust and field length required are lower.

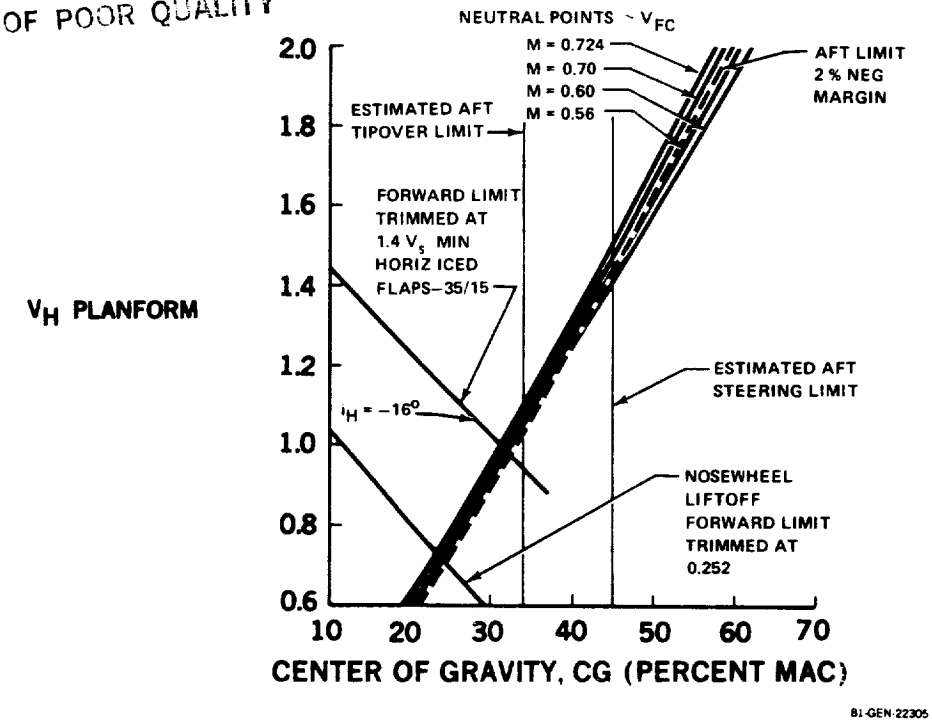

FIGURE 5-50. ESTIMATED CENTER-OF-GRAVITY LIMITS – FINAL TURBULENT CONFIGURATION

ASPECT RATIO = 10.85
M_{CRUISE} = 0.80

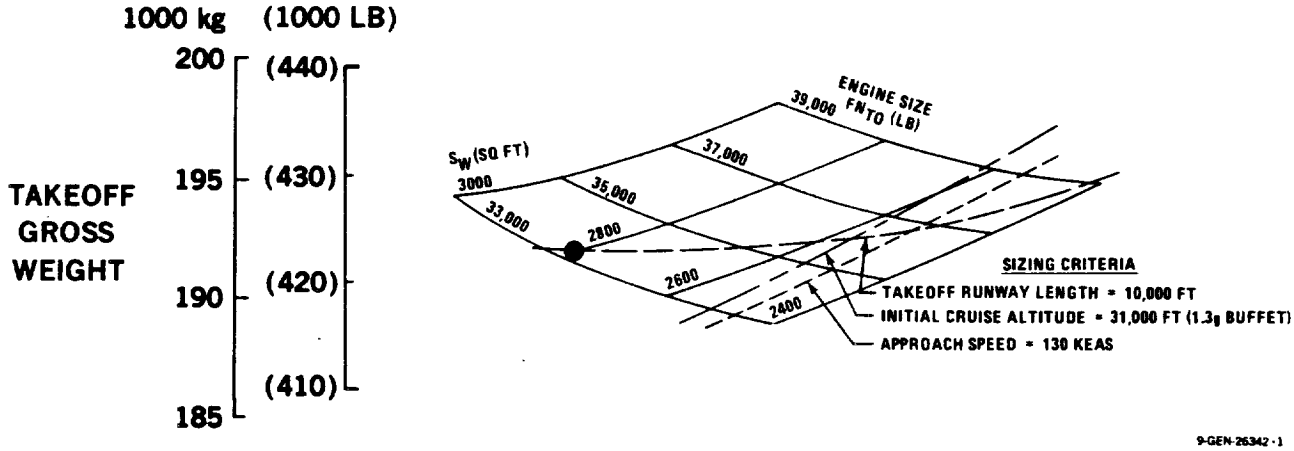

FIGURE 5-51. TURBULENT AIRCRAFT SIZING

Table 5-22

AIRCRAFT CHARACTERISTICS COMPARISON

TURBULENT VS. LAMINAR
5000 N M1 RANGE 69,000 POUNDS PAYLOAD

		TURBULENT		UPPER SURFACE LFC TO 85 PERCENT C	
POWER PLANT		3 ADVANCED TURBOFANS		3 ADVANCED TURBOFANS	
SLS Thrust/Engine	kN/(LB)	147.9	(33,240)	139.8	(31,430)
WING					
Area	m^2(SQ FT)	260	(2,800)	288	(3,100)
Sweepback, c/4	DEG	30		30	
AR		10.85		10	
Taper Ratio		0.25		0.25	
Airfoil t/c_{AVG}		12.7		10.3	
WEIGHT					
TOGW	kg (LB)	191,854	(422,965)	183,396	(404,320)
OEW	kg (LB)	91,401	(201,505)	93,690	(206,550)
Fuel Burned	kg (LB)	60,217	132,755	49,260	(108,600)
Fuel Reserves	kg (LB)	8,936	(19,700)	9,147	(20,165)
CRUISE C_L		0.58		0.56	
L/D		17.5		22.2	
$V_{Approach}$	m/s (KN)	63.5	(123.5)	64	(124.5)
Takeoff Field Length	m (FT)	3,048	(10,000)	2,615	(8,580)

The economic analysis, Section 6.0 will show that even using the study ground rule of only 12¢ per liter (45¢ per gallon) the LFC aircraft has a lower direct operating cost (DOC). At a more realistic cost of 26¢ per liter ($1 per gallon) the DOC for the LFC aircraft would be 6 percent less than for the advanced turbulent aircraft.

5.7 OPERATIONAL CONSIDERATIONS

5.7.1 FAA Regulations

For commercial aircraft to obtain the fullest possible advantage in terms of drag reduction and fuel savings from the use of laminar flow technology, it may be necessary that the Federal Aviation Regulations be modified. Two areas of particular concern are:

- Reserve fuel requirements;
- Dispatch with all or part of the laminar flow control system inoperative.

When new technology is incorporated into new commercial aircraft, the Federal Aviation Administration often issues "Special Conditions" that outline new requirements for the certification of aircraft using this new technology. Such action is likely to occur with the introduction of laminar flow control. An area of special concern to the FAA will be fuel reserves if all or a portion of the laminar flow control system becomes inoperative.

Under present FAA regulations it is very likely that the fuel reserves would have to be determined assuming that the laminar flow control system failed at the most critical time. The FAA probably would not allow the increased fuel consumption resulting from the loss of laminar flow to be taken out of existing fuel reserves. However, for flights over land and with adequate airports available enroute, a modified "re-clearance" procedure could be established. This procedure would permit full advantage to be taken of the fuel savings provided by a fully operational laminar flow control system. In the unlikely event that the system failed enroute on a long range mission, a landing could be made, if necessary, short of the final destination in order to replenish the fuel before continuing to the final destination.

For long over-water operations, the extent that "re-clearance" could be used would depend on the location of suitable airports along the route.

Failure of the laminar flow system does not make the aircraft inoperable or unsafe in any way. Commercial airplanes incorporating laminar flow control would be designed so that they could be dispatched with all or part of the system inoperative. To achieve this capability the manufacturer and the FAA would need to work in close cooperation commencing with the initial design of the airplane and its systems. This dispatch capability may require special conditions to Federal Aviation requirements.

5.7.2 Airline Comments

Discussions have been held with both United Airlines at San Francisco and Flying Tigers Airlines at Los Angeles International Airport. Douglas has agreements with both airlines for consulting on this LFC contract. Both airlines represent large carriers which differ in the principal emphasis of their operation. United is representative of the large domestic and overseas commercial passenger business, and Flying Tigers is concerned with transporting cargo over their long range routes. The long range routes are particularly compatible with LFC.

The discussions included a review of the Douglas laminar and turbulent aircraft configuration drawings and performance. Both LFC concepts and operational aspects were reviewed. The comments of the two airlines, relative to LFC, are consistent. Both airlines felt that with the amount of fuel that could be saved, the acceptability of an LFC aircraft is not dependent on its having a lower DOC than conventional aircraft. When evaluated at the average trip length of the consulted airlines operations, the DOC of the laminar aircraft was considered to be acceptable. The airlines are looking to LFC as both a fuel saving measure and as a hedge against limited fuel allocations.

In the case of United Airlines, the cost of an LFC aircraft would be depreciated over the assumed lifetime of the aircraft. They saw no logical reason for considering LFC as a special case requiring an accelerated rate of depreciation. However, Flying Tigers initially viewed the cost of LFC as a modification cost and, therefore, felt that this cost should be depreciated over a shorter time period, such as five years.

Throughout the LFC aircraft configuration and integration study work, the airlines have reacted positively towards laminar flow. The following summaries of airline comments best express their positive attitude whenever they were consulted.

AIRLINE'S COMMENTS -- CONCEPT

United and Flying Tigers - June 1977

- Both Airlines View LFC Favorably
- LFC is an Attractive Hedge Against Fuel Allocation
- LFC is Acceptable at Same DOC as Conventional
  DOC's Must be Evaluated for Average Trip Length-
  Not at Design Range
- Depreciation Over Life of Aircraft--United
  Depreciation of LFC Over 3 to 5 Years--Flying Tigers
- High Interest in Porous Materials
  --Honeycomb Unsatisfactory in Landing Gear Area--United
  --Honeycomb Unsatisfactory--Flying Tigers
  --Isogrid Unacceptable--Flying Tigers

AIRLINE'S COMMENTS--OPERATIONAL

United and Flying Tigers--June 1977

- Douglas Operating Assumptions are Conservative
- LFC Suction System Should Have Same Reliability As Main Propulsion System
- LFC System Must Not Be Required For Dispatch
- FAA Rules are Subject To Review For LFC Application
- Maintenance of Surface Cleanliness is a Major Concern

AIRLINES' COMMENTS

United and Flying Tigers--May 1978

LFC AFFORDS MAJOR ADVANTAGES

- Fuel Reduction
- Hedge Against Fuel Allocation

UPPER-SURFACE-ONLY LAMINARIZATION UNQUESTIONABLY PREFERRED

- Maintenance Ease and Efficiency
- Elimination of Leakage Problem
- Elimination of Under-Wing Surface Frost Problem

FUEL SAVING ADVANTAGES DUE TO LFC FAR OUTWEIGH

- System Maintenance Costs
- Added Cleaning Required for LFC Aircraft

AIRLINES' COMMENTS

United and Flying Tigers--Sept 1979

Fuel Availability is an Important Consideration

Reduction in DOC Due to LFC More Than Adequate For Serious Consideration by Airlines

Suggested Additional Evaluations Be Made Using

- o Shorter Stage Lengths/Lower Utilization
- o 1980 Economics

Validator Aircraft A Necessary Step

Airline Interest in LFC is Becoming Serious as the Program Advances and Fuel Prices Increase

APPENDIX 5-A

DRAG ESTIMATION

CRUISE DRAG

The estimated cruise drag for the laminar and turbulent baseline aircraft can be broken into three parts: the parasite, the induced, and the compressibility drags, as indicated in the following equation:

$$C_D = \underbrace{\frac{f}{S_w}}_{\substack{\text{Parasite} \\ \text{Drag}}} + \underbrace{\frac{C_L^2}{\pi AR e}}_{\substack{\text{Induced} \\ \text{Drag}}} + \underbrace{\Delta C_{D_C}}_{\substack{\text{Compressibility} \\ \text{Drag}}}$$

Parasite Drag

The form drag is estimated using established form factors from Douglas and Hoerner data. The skin friction coefficients for the turbulent components are based on the method of Van Driest as adjusted for surface roughness by Clutter. A sand-grain roughness level of .024mm (0.00095 in.) is used, which is representative of typical transport aircraft. For the wing of the laminar aircraft without LFC, the sand grain roughness is assumed to be zero. With LFC, the equivalent skin friction drag (wake drag) and the suction quantity are assumed to vary with Reynolds number as shown in Figure 5-A1. These results are based on a preliminary airfoil analysis conducted prior to the start of the base case selection process and are being refined as part of the detailed airfoil design process.

The resulting parasite drag breakdown for the laminar and turbulent initial base case aircraft of Study I is shown in Table 5-A1. The drag due to the fuselage canopy and upsweep, wing twist, and control surface gaps are

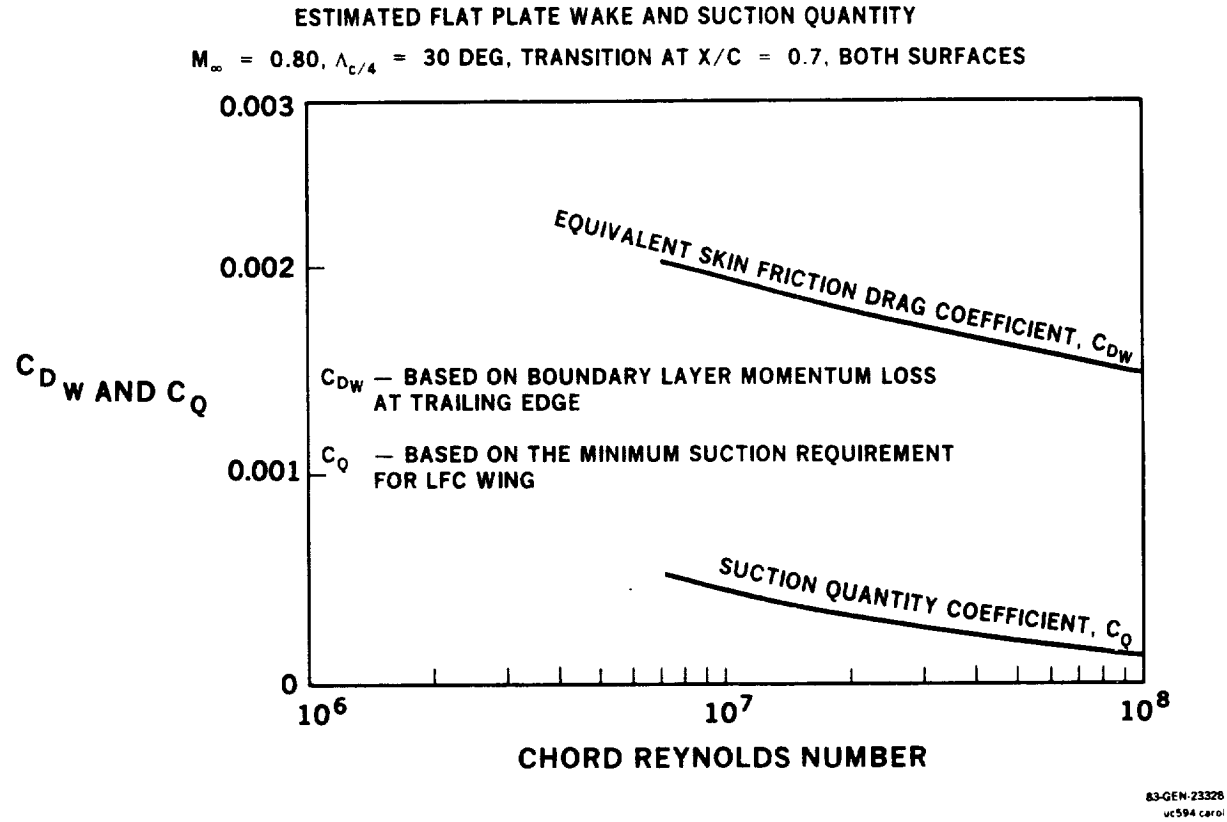

FIGURE 5-A1. PARASITE DRAG – LAMINAR AND TURBULENT

individually accounted for. The miscellaneous drag accounts for items such as steps, vents, etc., and is equal to 7.8 percent of the total friction, form, and roughness drag (average for Douglas transports) for the turbulent base case. Due to the cleaner wing required for LFC, this factor is estimated to be equal to 5.4 percent for the laminar base case. An additional 1.2 percent is included for potential interference drag.

TABLE 5-A1

LFC INITIAL BASE CASE AIRCRAFT
PARASITE DRAG

	Turbulent Base Case		Laminar Base Case With LFC		Laminar Base Case Without LFC	
Friction, Form Roughness	m^2	(Ft^2)	m^2	(Ft^2)	m^2	(Ft^2)
Fuselage	1.649	(17.75)	1.649	(17.75)		
Wing	1.647	(17.73)	1.013	(10.90)	2.246	(24.18)
Flap Fairing	.102	(1.10)	.182	(1.96)		
Horizontal	.421	(4.53)	.396	(4.26)		
Vertical	.261	(2.81)	.346	(3.73)		
Nacelles and Pylons	.593	(6.38)	.619	(6.66)		
Subtotal	4.673	(50.30)	4.205	(45.26)	5.438	(58.54)
Canopy	.010	(.11)	.010	(.11)		
Upsweep	.017	(.18)	.017	(.18)		
Twist	.025	(.27)	.027	(.29)		
Gaps	.018	(.19)	.022	(.24)		
Miscellaneous	.370	(3.98)	.232	(2.50)		
Interference	.061	(.66)	.054	(.58)		
TOTAL	5.174	(55.69)	4.567	(49.16)	5.801	(62.44)
Induced Drag Efficiency Factor e	.819		.922		.832	

Induced Drag

The induced drag is based on the Giesing vortex lattice lifting surface program for inviscid flow plus a factor, based on Douglas flight test data, to account for the variation of parasite drag with lift for the fuselage and wing, due to viscous effects. For the laminar base case, it is assumed that with LFC operating the viscous contribution of the wing to induced drag is equal to zero. The resulting efficiency factors (e) for the base case aircraft are shown in Table 5-A1.

Compressibility Drag

The fuselage compressibility drag is calculated using the current Douglas method based on isolated fuselage wind tunnel data. For the turbulent base case, the wing compressibility drag, which is a function of C_L and Mach number, is calculated using Douglas design charts based on 2-D wind tunnel tests of advanced airfoils. Due to the shock-free design of the laminar base case wing, the compressibility drag is assumed to be zero. Trim drag is assumed to be equal to 25% of the total aircraft compressibility drag, based on current Douglas studies of reduced stability level configurations.

6.0 ECONOMICS ANALYSIS

This section of the report presents the results of the cost analysis generated for the LFC concepts and the turbulent baselines and the aproach that is taken to derive the cost data. Included is a brief narrative of the derivation of the cost data and the ground rules, guidelines and assumptions used. This section includes the acquisition costs for both the turbulent and LFC configurations as they occur in time, along with the operating costs.

6.1 AIRPLANE COST ESTIMATING APPROACH

The cost estimates are used to evalute the LFC concept compared to a turbulent baseline. These estimates are also used to examine the sensitivity of operating cost to fuel price. Proven cost analysis techniques are used to provide a basis for the evaluation. Estimates are derived using a systematic approach to predicting cost behavior in the future, on the basis of current capability and the expected advancements in technology. However, the relationship of technology to cost behavior is more subtle than can be expressed by continuous functions and trend analysis methods. The airplanes in this study are configured partly with current technology design concepts, materials and manufacturing methods; these cost estimates are derived using Douglas standard techniques for advanced design studies. The advanced technology elements require the use of judgement based on scientific and practical experience and background. These judgments are used to modify the existing engineering analysis techniques to reflect the anticipated cost impact of the advanced technology. Experience in cost estimating for advanced technology studies coupled with prototype production and tracking of actual costs (labor and materials) versus the estimates, formed the basis for judgment.

Estimates for the conventional segments of the aircraft are derived using discrete type estimating techniques that parallel the industrial engineering methodology supplemented by parametric cost estimating models.

No attempt is made to establish or justify a market size, a particular market, the number of manufacturers and/or pricing strategies. An arbitrary production quantity of 400 aircraft and a single manufacturer is selected and used in this analysis. The market size could be larger with more than one manufacturer, but this is not relevant to the outcome of the cost comparison between LFC and turbulent designs. It is assumed that an incentive of a 20 percent profit with a production of 400 aircraft is sufficient to attract the manufacture. This establishes the quantity selected and the price level achieved. The methodology incorporates a computation to account for the interest or cost of money with respect to financing the project.

Common guidelines that are applied to each configuration evaluated are presented in Table 6-1. The DOC factors and coefficients used are shown in Table 6-2.

Table 6-1

GENERAL COSTING GROUND RULES

- ROM Costing Level of Estimating
- 1976 Dollars Used Throughout
- 14-Year Aircraft Life
- 5000 Hr-Per-Year Utilization
- 400 Aircraft Production/Single Manufacturer
- 45-Cent-Per-Gallon Fuel*
- Modified 1967 ATA DOC Equations Used
- Addition of Landing Fees & Cabin Attendants
- Factors and Coefficients Based on Douglas Experience With Operators

* Effect of Fuel Cost Variation from $0.45 to $2.50 Per Gallon Included in the Study

Table 6-2

DOC FACTORS AND COEFFICIENTS

Landing Fee	($)	1.70
Cabin Crew	($)	25.48
Cockpit Crew	($)	278.62
Depreciation	(Yr)	14
Insurance Rate	(%)	1.5
Residual Value	(%)	10
Spares	(%)	15
Labor Rate Per Hour	($)	9.23
Labor Burden	(%)	180
Fuel Per Gallon	($)	0.45

6.2 COST SUMMARY

The cost analysis includes the initial baseline configurations of Study I (Section 5.3), the three and four engined configurations of Study II (Section 5.4), and the final configurations of Study IV (Section 5.6). A summary of significant aircraft characteristics considered in the cost analysis is presented in Table 6.3.

A top level summary of the cost data for the configurations examined in this study is shown in Table 6-4. The summary results contain only the flyaway costs and direct operating costs, which are the significant measures. Flyaway cost is defined as the cumulative average of the total quantity produced. Estimates developed for this study are to be considered only as Budgetary and

Table 6-3

CHARACTERISTICS OF CONFIGURATIONS ANALYZED

	STUDY I		STUDY II		STUDY IV		
	Turbulent	LFC-B	LFC-B	LFC-B	Turbulent	LFC-B	LFC-U
TOGW - Kg	186,617	181,650	193,191	195,349	191,853	188,663	183,396
(LB)	(411,419)	(400,469)	(425,913)	(430,670)	(422,964)	(415,930)	(404,320)
ZFW - Kg	120,437	127,459	137,680	139,076	122,699	129,197	124,987
(LB)	(265,519)	(280,999)	(303,532)	(306,609)	(270,506)	(284,830)	(275,550)
MEW - Kg	83,544	90,566	100,827	102,182	83,592	90,090	85,880
(LB)	(184,183)	(199,663)	(222,286)	(225,273)	(184,289)	(198,615)	(189,333)
FUEL - Kg	66,179	54,191	55,511	56,273	69,154	59,466	58,409
(LB)	(145,900)	(119,470)	(122,381)	(124,061)	(152,458)	(131,100)	(128,770)
NO. OF ENGINES	4	4	3	4	3	3	3
THRUST/ENGINE KN	114.32	108.40	148.59	112.54	147.86	145.41	139.80
(LB)	(25,700)	(24,370)	(33,405)	(25,300)	(33,241)	(32,690)	(31,428)

LFC-B = Laminar flow on both wing surfaces
LFC-U = Laminar flow on upper wing surface only

TABLE 6-4
COST SUMMARY

	STUDY I		STUDY II			STUDY IV	
	TURB-4	LFC-B4	LFC-B3	LFC-B4	TURB-3	LFC-B3	LFC-U3
AIRPLANE COST							
FLYAWAY PRICE ($M)	46.35	49.10	52.62	53.99	45.57	48.39	46.52
WITHOUT ENGINES ($M)	—	—	—	—	39.7	42.6	40.9
DIRECT OPERATING COST*							
$/AIRCRAFT km	3.44	3.41	3.44	3.57	3.43	3.41	3.34
($/AIRCRAFT N MI)	(6.38)	(6.31)	(6.37)	(6.62)	(6.35)	(6.32)	(6.19)
¢/SEAT km	1.152	1.140	1.151	1.195	1.147	1.141	1.118
(¢/SEAT N MI)	(2.134)	(2.110)	(2.131)	(2.213)	(2.125)	(2.113)	(2.072)

TURB-3 = TURBULENT AIRCRAFT — 3 ENGINES
TURB-4 = TURBULENT AIRCRAFT — 4 ENGINES

LFC-B3 = LFC BOTH WING SURFACES — 3 ENGINES
LFC-B4 = LFC BOTH WING SURFACES — 4 ENGINES
LFC-U3 = LFC UPPER SURFACE ONLY — 3 ENGINES

*ASSUMING 12¢/LITER (45¢/GALLON) FUEL COST

83 GEN 22061

Planning costs intended for relative rather than absolute use, in consonance with the primary purpose of such costs to be used in the development and comparison of candidate concepts.

The configurations analyzed are presented chronologically with time as the study proceeded. The final three configurations of Study IV are those on which attention should be focused; they incorporate the most recent updated technical parameters, and resultant costs. Comparisons should be limited to those within each particular study. The final LFC configurations are distinguished by the extent to which the LFC is applied to the wing - i.e., upper and lower surface, and upper surface only.

The acquisition and DOC costs of the finally selected LFC configuration with upper surface suction only, and the turbulent aircraft of Study IV are compared in greater detail in Tables 6-5 and 6-6.

Table 6-5

ACQUISITION COST COMPARISON
400 Aircraft-Constant 1976 Dollars in Millions

	LAMINAR (USO)	TURBULENT	DIFFERENTIAL - PERCENT LFC/TURBULENT
LABOR			
Engineering	$ 1,851.8	$ 1,803.5	2.7
Manufacturing	6,208.0	6,042.6	2.7
Manufacturing and Tooling Inspection	1,065.3	1,036.6	2.8
Tooling	971.2	940.4	3.3
Planning	472.5	460.1	2.7
Flight Test and Labs	219.6	213.6	2.8
Engines	IN MATERIALS		
Tech Pubs	144.4	140.8	2.6
Subtotal	10,932.8	10,637.6	2.8
RAW MATERIALS, PARTS, EQUIPMENT			
Engineering Labs	8.2	7.8	5.1
Tooling	74.6	72.2	3.3
Stock List	99.2	96.6	2.7
Raw Materials	984.6	953.1	3.3
Purchased Equipment	3,843.6	3,704.8	3.7
Engines	2,253.9	2,346.6	-4.0
Tech Pubs	0.7	0.7	0.0
Other*	412.1	408.6	0.9
Subtotal	7,676.9	7,590.4	1.1
TOTAL	$18,609.7	$18,228.0	2.1
UNIT PRICE	$ 46.524	45.570	2.1

* "Other" includes vendor tooling, development fixture, nacelle cowl doors

Table 6-6

DOC COMPARISON
Constant 1976 Dollars

	LAMINAR (USO)	TURBULENT
Landing Fee	687	719
Cabin Crew Cost	3,443	3,336
Cockpit Crew Cost	4,297	4,215
Depreciation/Insurance	9,426	8,949
Maintenance	5,830	5,634
Labor	(3,130)	(2,790)
Materials	(2,700)	(2,844)
Fuel*	7,294	8,916
Dollars/Flight	30,978	31,770
Dollars/Aircraft Km (NMI)	3.34 (6.19)	3.43 (6.35)
Cents/Seat Km (NMI)	1.12 (2.07)	1.15 (2.125)

* Assuming Fuel Cost = 12¢/liter (45¢/gallon)

6.3 SENSITIVITY OF DOC COMPARISONS TO FUEL PRICE

The fuel price of $0.12/liter ($0.45/gallon) was stated as a ground rule in the Study Contract NAS1-14632; however, this fuel price became obsolete during the study due to the fuel shortage and associated rapid increase in fuel costs. Consequently, sensitivity to fuel costs, varying from $0.12 to $0.66 per liter ($0.45 to $2.50 per gallon), on the relative DOC advantages of the final LFC aircraft over the turbulent aircraft were investigated and the results are shown in Figures 6-1 and 6-2.

As shown in Figure 6-1, over the life of the aircraft, the LFC aircraft is estimated to save approximately $45 million over the comparable turbulent aircraft, assuming an average fuel price of $0.50 per liter ($1.80 per gallon). This is equivalent to the price of the airplane. Even at $0.12 per liter ($0.45/gallon), the saving would have been $12.5 million.

In terms of comparative percent DOC reduction, Figure 6-2 shows an 8 percent advantage in DOC for the LFC aircraft over the comparable turbulent aircraft at fuel prices predicted for 1981 to 1984. Also shown on Figure 6-2, is the 2 percent advantage in DOC for LFC on the upper surface only compared with LFC on both wing surfaces.

The DOC reduction of approximately 8 percent in favor of the LFC aircraft in the 1990 time period is significant and warrants continued development of the LFC concept.

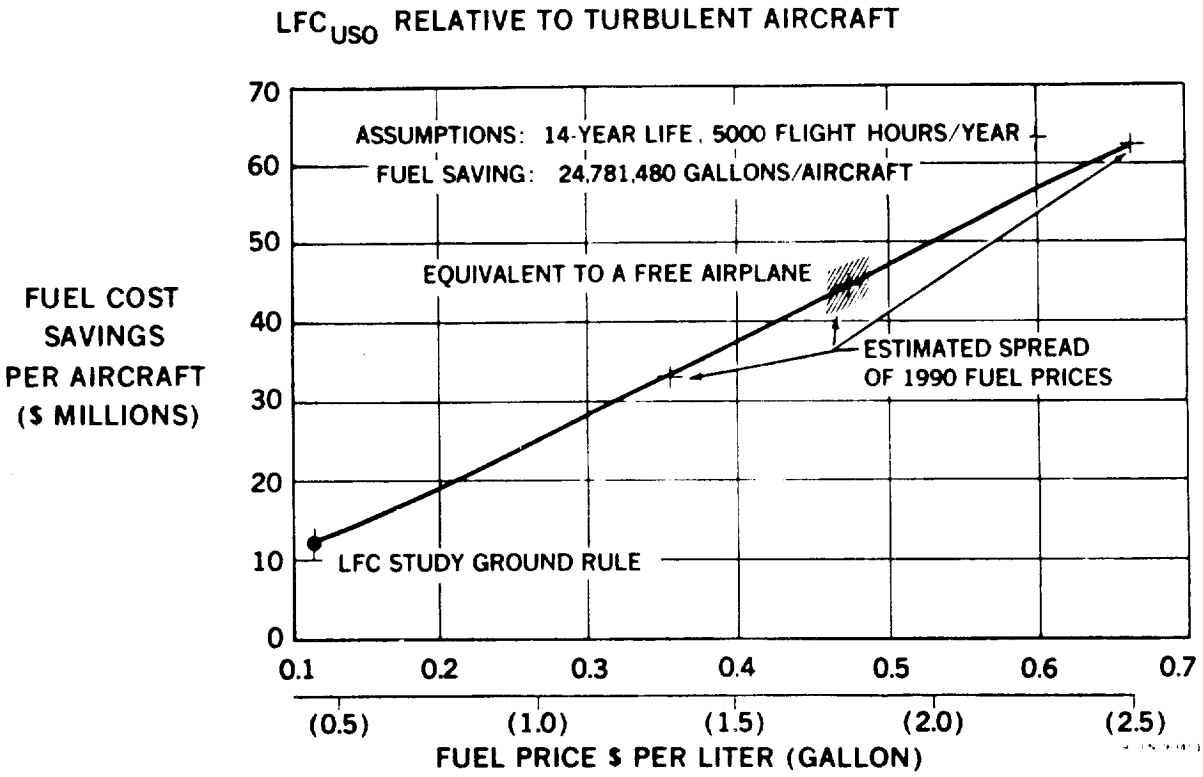

FIGURE 6-1. EFFECT OF FUEL PRICE ON FUEL COST SAVINGS

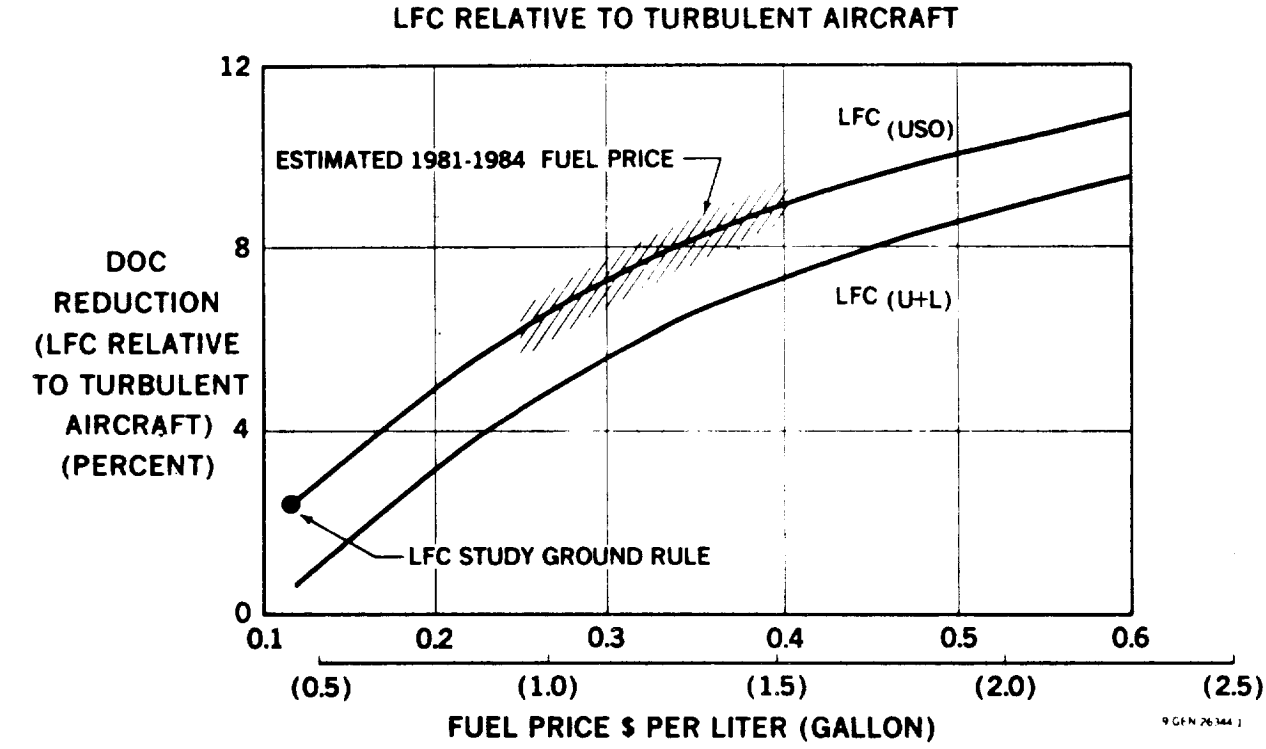

FIGURE 6-2. REDUCTION IN DOC AS A FUNCTION OF FUEL COST

7.0 AERODYNAMIC DESIGN AND ANALYSIS

7.1 AIRFOIL DESIGN AND SUCTION REQUIREMENTS

The purpose of this study was to develop a series of airfoils that would exhibit aerodynamic characteristics compatible with those necessary for successful laminar boundary layer flow control. In addition, it was required to determine the sensitivity of these aerodynamic characteristics to variations in Reynolds number, airfoil thickness and the extent of laminarization. These data were needed to support configuration and suction system design tasks of the overall study.

The procedure used was to develop a series of airfoils having varying thickness-chord ratios and then determine the suction flow quantities and wake drag characteristics of each airfoil as a function of Reynolds number and chordwise extent of laminar flow. Two sets of airfoils were designed corresponding to the normal sections of 25 degree and 30 degree swept wings.

Since it is unlikely that laminar flow can be maintained behind the shock downstream of the supersonic flow region on a conventional supercritical airfoil, the LFC airfoils were designed to remain shock-free. Furthermore, from operational considerations it is important to prevent buffet in the event that laminar flow is lost during flight. This condition requires that aft pressure recovery gradients satisfy separation criteria for turbulent boundary layer flow on the laminarized portion of the airfoil. While the likelihood of suction system failure is remote, the possibility of partial loss of laminar flow due to environmental disturbances must be considered.

7.1.1 Design Guidelines for LFC Airfoils

A two-dimensional infinite swept wing design procedure was used to develop LFC compatible airfoils. The upper surface pressure distribution, normal to the leading edge, was similar for all airfoils. The upper surface pressure peak was constrained to limit the maximum local Mach number to 1.1 near the leading

edge, with gradual supersonic compression to a local Mach number of 1.02 in the vicinity of 65 percent chord. Over the aft portion of the airfoil the adverse gradient was limited so that separation would not occur if laminar flow were interrupted or lost.

The lower surface pressure profile was varied to generate airfoils of different relative thickness and corresponding design section lift coefficients.

A slightly favorable pressure gradient was maintained from the leading edge to 65 percent chord on the lower surface with the adverse gradient near the trailing edge constrained to preserve attached flow with fully turbulent boundary layer.

7.1.2 Airfoil Analysis

Airfoil profiles were developed for the specified pressure distributions using the Tranen code (Reference 7.4-1) which is an inverse transonic analytical procedure. This method is an extension of the 2-D Garabedian airfoil analysis method. Boundary layer analyses and suction requirements for the various airfoils were determined using the Cebeci boundary layer program of Reference 7.4-2. A specialized version of the program was developed to compute suction velocities necessary to satisfy boundary layer stability criteria.

Laminar flow control airfoils based upon the foregoing criteria and methods were developed for a free stream Mach number of 0.8. Two wing sweep angles were considered, 25 degrees and 30 degrees with corresponding normal Mach numbers of 0.725 and 0.70, respectively. Pressure distributions and resulting airfoil geometry for representative cases are shown in Figures 7-1 and 7-2. For the 25-degree swept wing, the design section lift coefficients are 0.73 for the 11.3 percent thick airfoil and 0.54 for the 14.3 percent thick airfoil. Similarly, for the 30-degree swept wing the design section lift coefficients are 0.78 and 0.60 for the 12.8 percent thick and 15.8 percent thick airfoils, respectively.

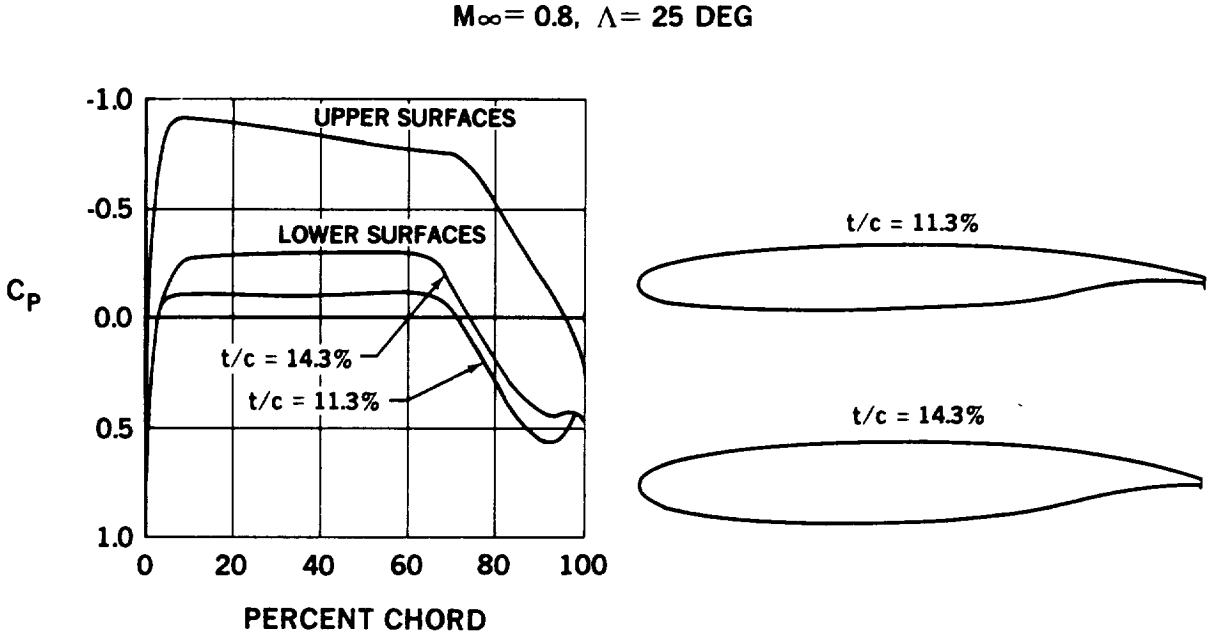

FIGURE 7-1. TYPICAL LFC WING CHORDWISE PRESSURE DISTRIBUTIONS AND AIRFOIL SHAPES – 25-DEGREE SWEEP

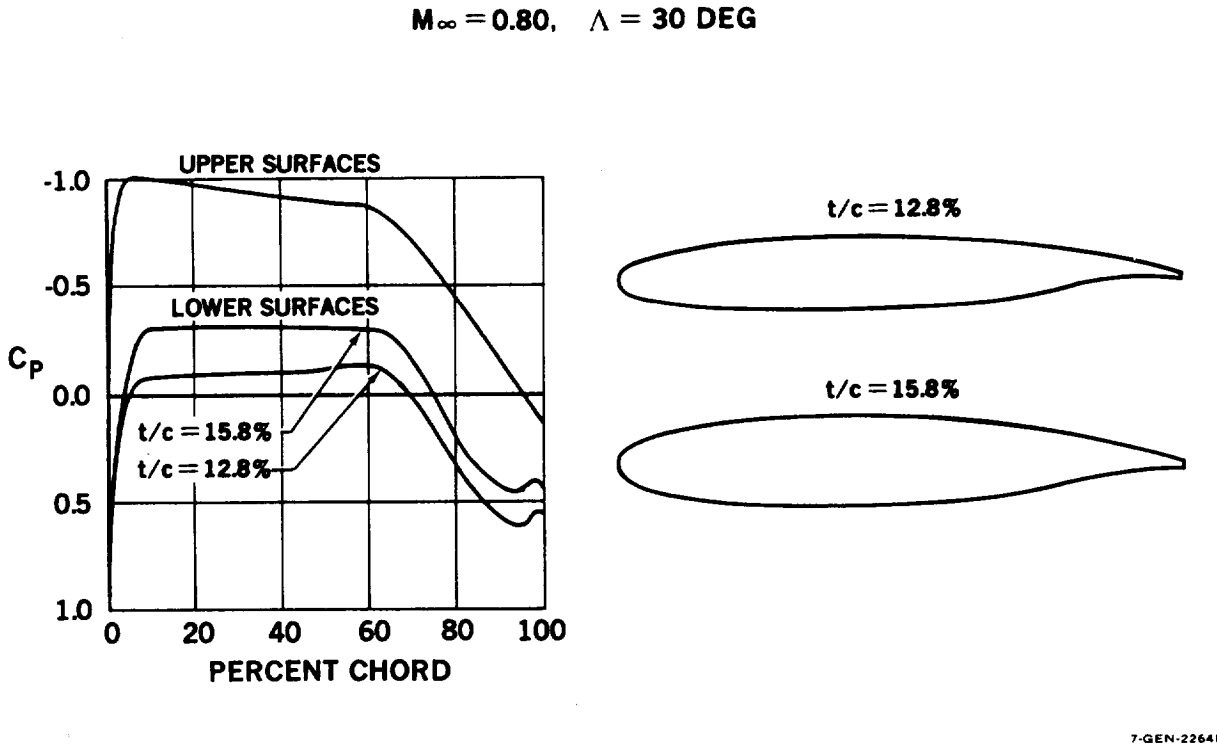

FIGURE 7-2. TYPICAL LFC WING CHORDWISE PRESSURE DISTRIBUTIONS AND AIRFOIL SHAPES – 30-DEGREE SWEEP

Estimated variation of airplane lift coefficient with average streamwise wing thickness is summarized in Figure 7-3. The relationship between two-dimensional design lift coefficient, C_l, and airplane lift coefficient, C_L, is given by:

$$C_L = \frac{C_l \cos^2 \Lambda}{1.17}$$

where Λ is the wing sweep angle and the empirical factor 1.17 compensates for spanwise load distribution and airplane trim effects. For comparison, the corresponding variation of wing C_L and average thickness for a series of advanced supercritical airfoils, on a 30-degree swept wing, is included in Figure 7-3.

7.1.3 Suction Requirements

Suction requirements for the laminar flow airfoils were based on the Cebeci boundary layer analysis for a swept wing (Reference 7.4-3) used in conjunction with the laminar boundary layer empirical stability criteria developed during the Northrop X-21 program (Reference 7.4-4). The analytical procedure and empirical stability relations were combined into the method and computer program described in Reference 7.4-2. A subsequent modification of the computer program provided an interactive mode through a remote graphic terminal. This modification greatly expedited the solution of suction requirements.

The boundary layer stability criteria developed during the X-21 program are listed below:

(1) Attachment line instability-momentum thickness Reynolds number, R_{e_θ}, at the leading edge dividing streamline.

$$R_{e_\theta} = 0.4044 \sin \Lambda_{1.e} \sqrt{\frac{R_c}{\frac{d(u_n/v_\infty)}{d(s_n/c)}}} \leq 100$$

where: $R_c = \frac{U_\infty c}{\nu}$,

u_n = cross-flow velocity in boundary layer, normal to streamline at edge of boundary layer at chordwise station.

(2) Tollmien-Schlichting instability -- Momentum thickness Reynolds number required in presence of streamwise disturbance.

$$R_e \leq \left[7.6 - 106\theta_s^2 \frac{\partial^2 (U_s / U_{s_e})}{\partial y^2} \bigg|_{wall} \right]^3$$

where: $R_{e_\theta} = \frac{\theta_s U_{Se}}{\nu}$;

U_{s_e} = total velocity at edge of boundary layer at chordwise station.

θ_s = streamwise momentum thickness at chordwise station

(3) Cross-flow instability -- cross-flow Reynolds number required in the presence of a component of boundary layer flow as a consequence of wing sweep (sheared pressure gradients).

$$R_{e_n} \leq 1.8 \left[57 - 0.72 \frac{\partial^2 (U_n / U_{n_{max}})}{\partial (y / y_{0.1})^2} \bigg|_{wall} \right]$$

where: $R_{e_n} = \frac{U_{n_{max}} \, y_{0.1}}{\nu}$

$u_{n_{max}}$ = maximum cross-flow velocity.

$y_{0.1}$ = y at $u_n = 0.1\, u_{n_{max}}$, reference dimension of boundary layer cross-flow velocity profile at chordwise station.

Determination of the design suction for a given geometry and pressure distribution was accomplished by computing the suction necessary to satisfy the appropriate stability criteria above. The procedure consisted of a "marching" solution, beginning at the attachment line and progressing downstream. At each chordwise station,the critical instability was identified and the corresponding suction velocity requirement was calculated using an iterative procedure based on an estimated initial value. The results from this procedure are limited in that there is no interaction by which down stream conditions are allowed to affect upstream requirements.

Typical results showing the upper and lower surface suction velocity distributions are presented in Figures 7-4 and 7-5, respectively. These data are for a 30 degree swept wing at M = 0.80 and C_L = 0.502 with three values of wing chord, representative of the root, mid-span, and tip chords of a tapered wing. The different chord lengths change the incident Reynolds number, R_c spanwise. This significantly affects suction requirements in the adverse pressure gradient region over the aft third of the airfoil. Also the chordwise "scale" affects the attachment line suction requirement as the leading edge radius and attachment line Reynolds number vary. The most significant effects of chordwise dimension occur at the leading edge (attachment line) and at the aft pressure recovery region. Strong cross-flow instability conditions are characteristic of the latter region.

7.1.4 Variation of Suction with Airfoil and Flight Parameters

Based on suction velocity distributions for the various airfoils and flight conditions,a total suction flow coefficient can be determined. The suction flow coefficient, C_Q, is obtained by integration of the required suction velocity distribution to the chordwise extent to which laminar flow is maintained. Thus,

$$C_Q = \int_0^{x/c} \frac{v_a}{V_\infty} \, d\left(\frac{x}{c}\right)$$

Using this definition, suction flow coefficients were determined as a function of several operational and configuration parameters.

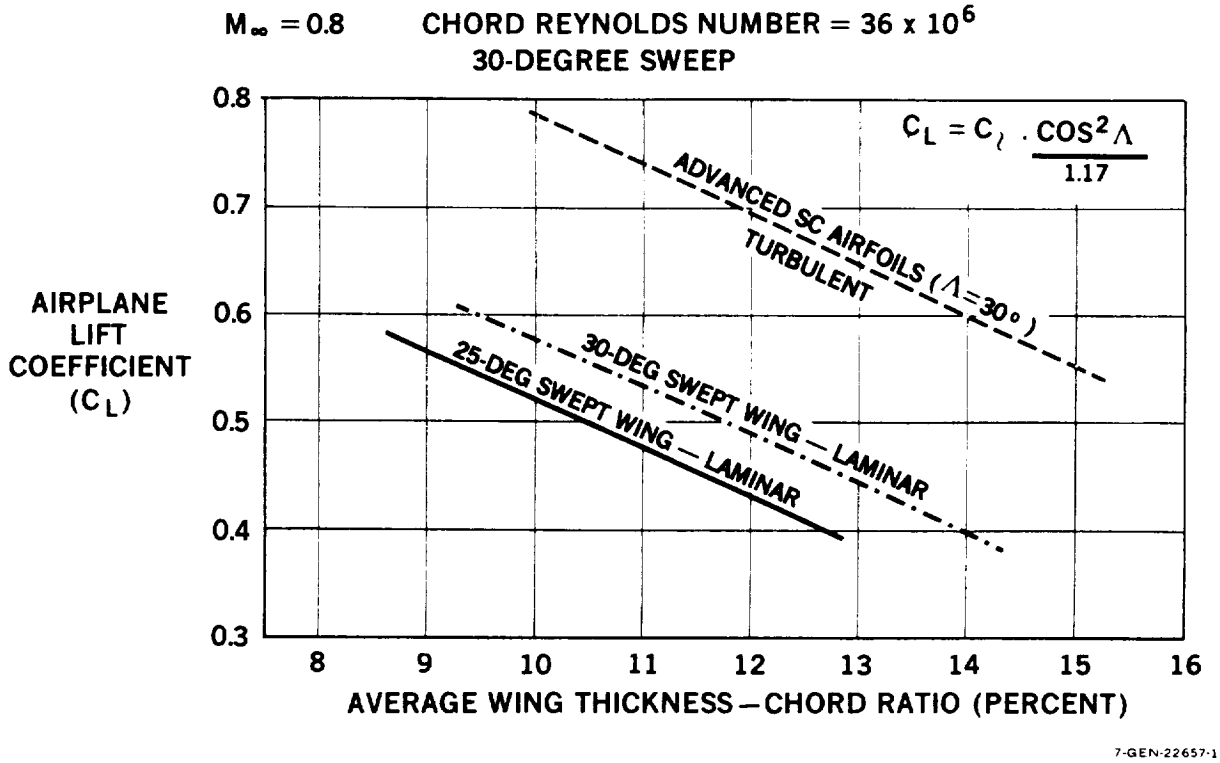

FIGURE 7-3. VARIATION OF DESIGN LIFT COEFFICIENT WITH AIRFOIL THICKNESS

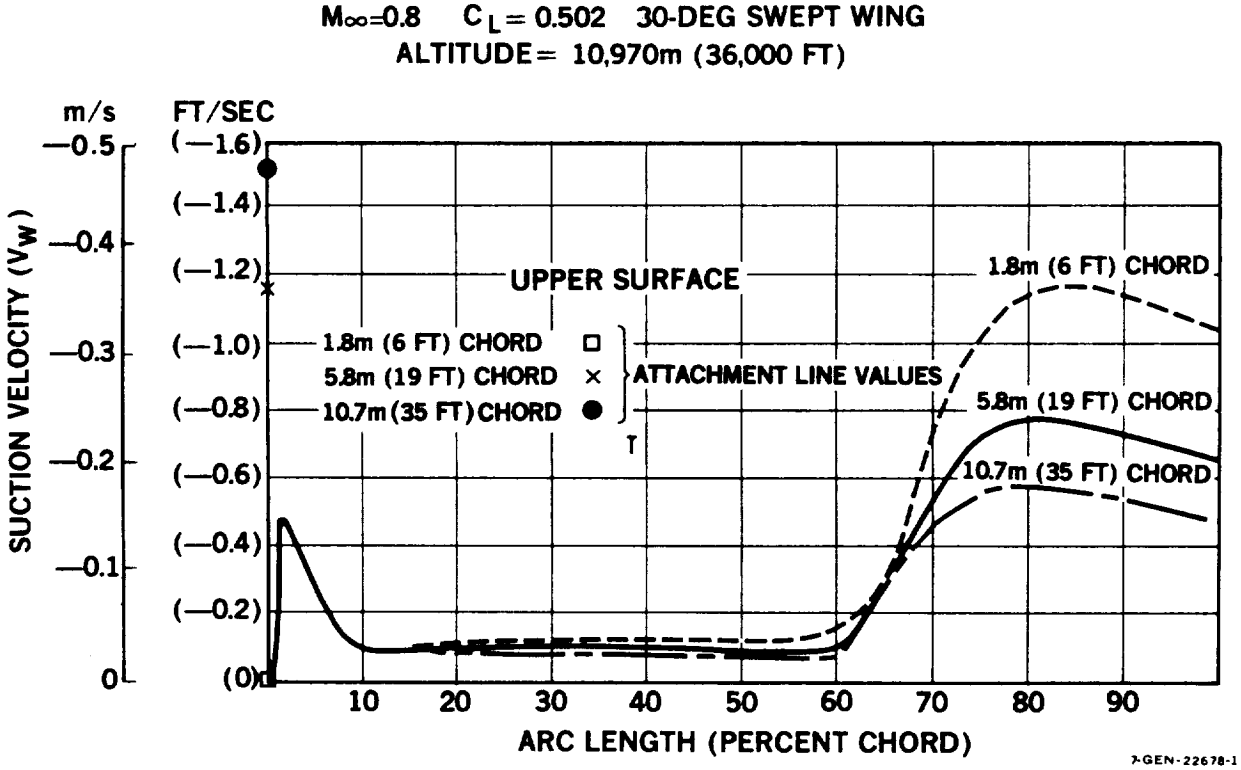

FIGURE 7-4. TYPICAL SUCTION DISTRIBUTIONS — UPPER WING SURFACE

The variation of suction coefficient with airplane design C_L for a 30 degree swept wing with laminarization to 70 percent chord is given in Figure 7-6. As the lift coefficient increases, the lower surface pressure distribution is modified to alleviate the lower surface aft pressure gradient and reduce the suction required on the lower surface. Since the airfoil design criteria require the upper surface pressure profile to remain essentially unchanged with change in lift, the upper surface suction requirement also is unchanged with lift coefficient.

An alternative presentation of suction flow coefficient, as a function of airfoil thickness (in percent chord), is shown in Figure 7-7 and 7-8 for 30 degree and 25 degree swept wings. These data are for suction applied to 70 percent chord and show the same characteristic variation with section lift. The lower surface suction flow coefficient increases with increased airfoil thickness as expected, since airfoil thickness varies inversely with the design section lift coefficient. The variation of C_Q with airfoil thickness, or C_L, is greater for the 25 degree swept wing than for the 30 degree swept wing.

Suction requirements were also computed for a representative 30 degree swept airfoil as a function of chord Reynolds number. Chord Reynolds number was varied by changing unit Reynolds number with fixed chord and by changing chord length for fixed unit Reynolds number. The results are presented in Figure 7-9. Two cases are shown: one with suction to 70 percent chord and one with suction to 85 percent chord. It is evident that the adverse gradients and consequent increased suction requirement (Figures 7-4 and 7-5) result in the total suction flow quantity required to almost double as laminar flow is extended from 70 to 85 percent chord on both surfaces. Included in Figure 7-9 for comparison is the classic assumption of suction varying inversely with the square root of chord Reynolds number. Such an assumption is optimistic with respect to the effect of increasing Reynolds number. The representative airfoil used has a 12.8 percent normal thickness and normal section lift coefficient of 0.783.

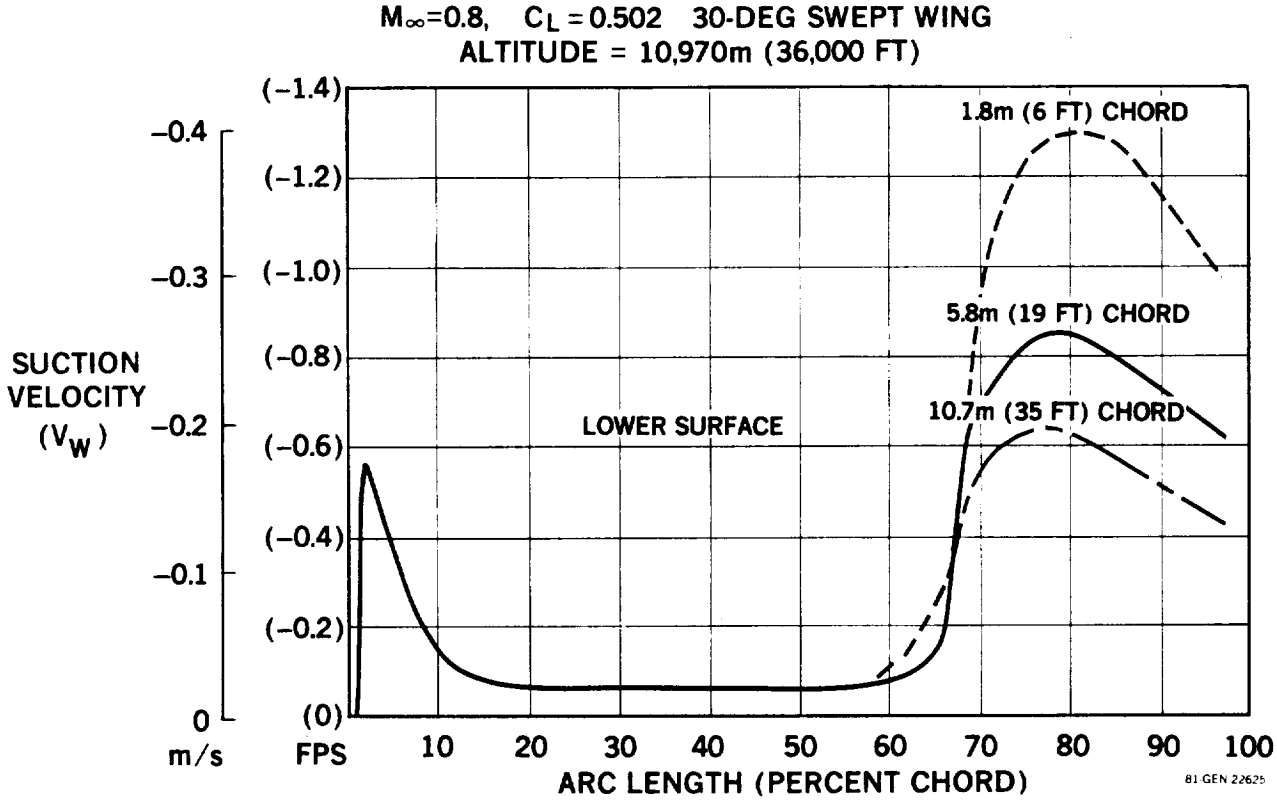

FIGURE 7-5. TYPICAL SUCTION DISTRIBUTIONS – LOWER WING SURFACE

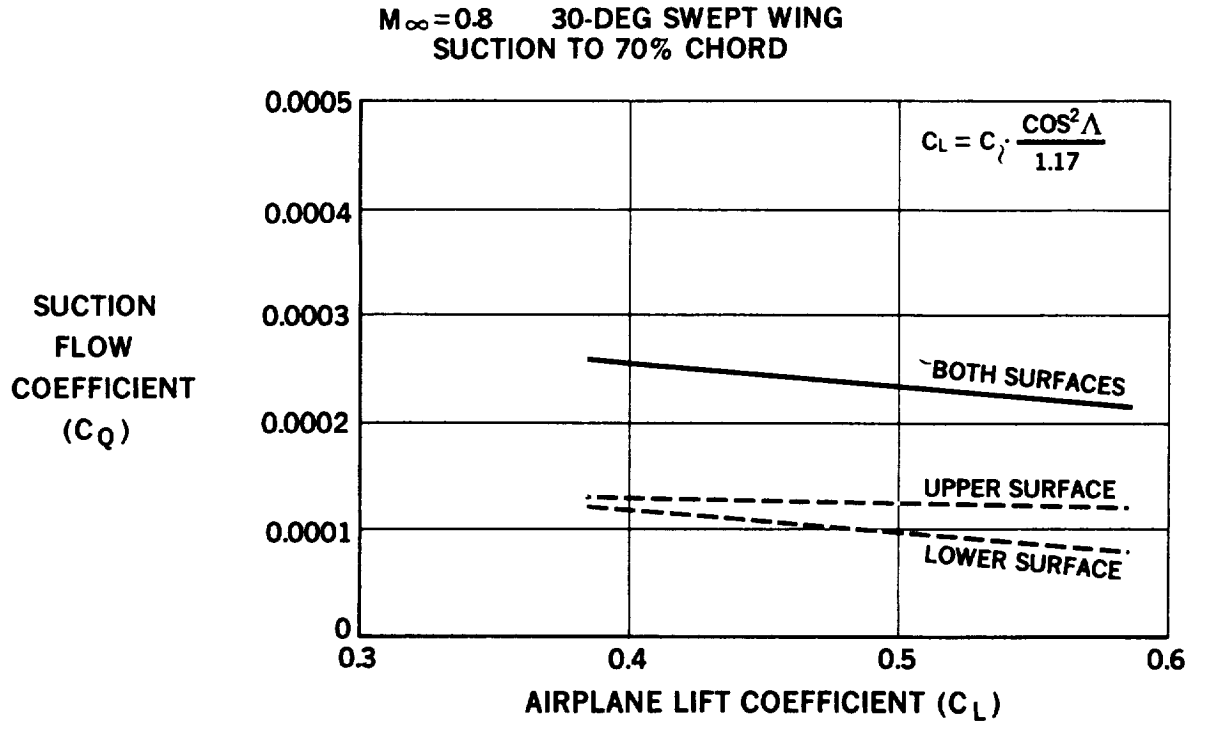

FIGURE 7-6. VARIATION OF LFC SUCTION COEFFICIENT WITH DESIGN C_L

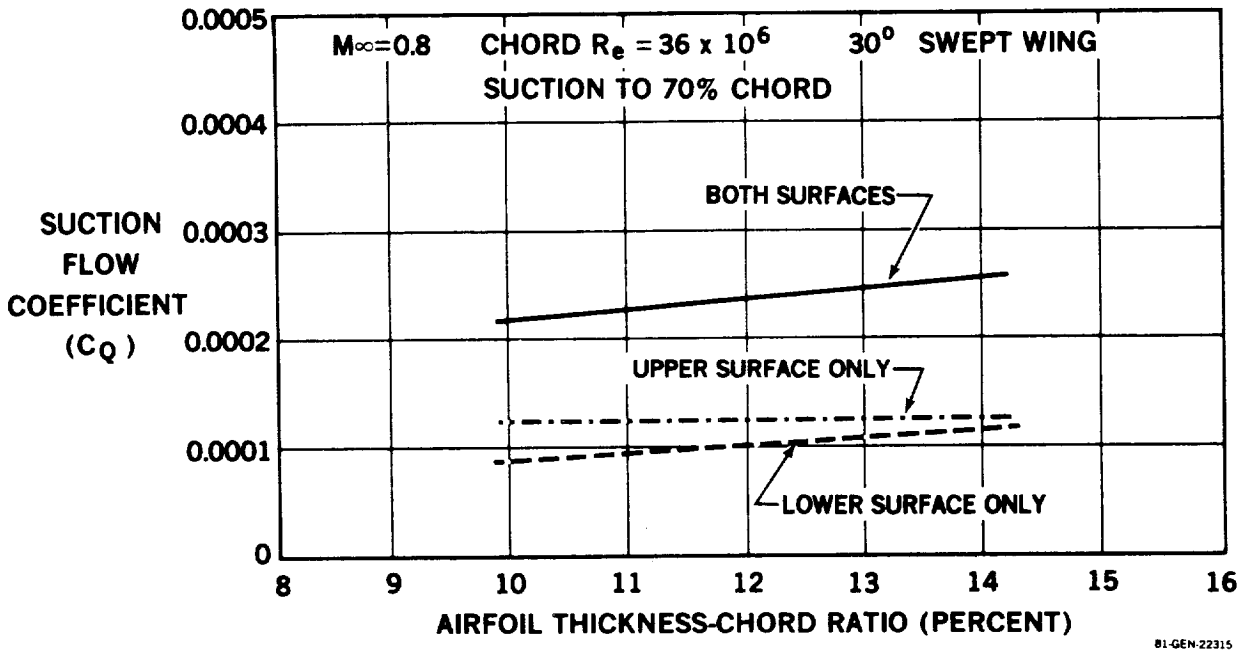

FIGURE 7-7. VARIATION OF SUCTION REQUIRED FOR LFC WITH THICKNESS-CHORD RATIO – 30-DEGREE SWEEP

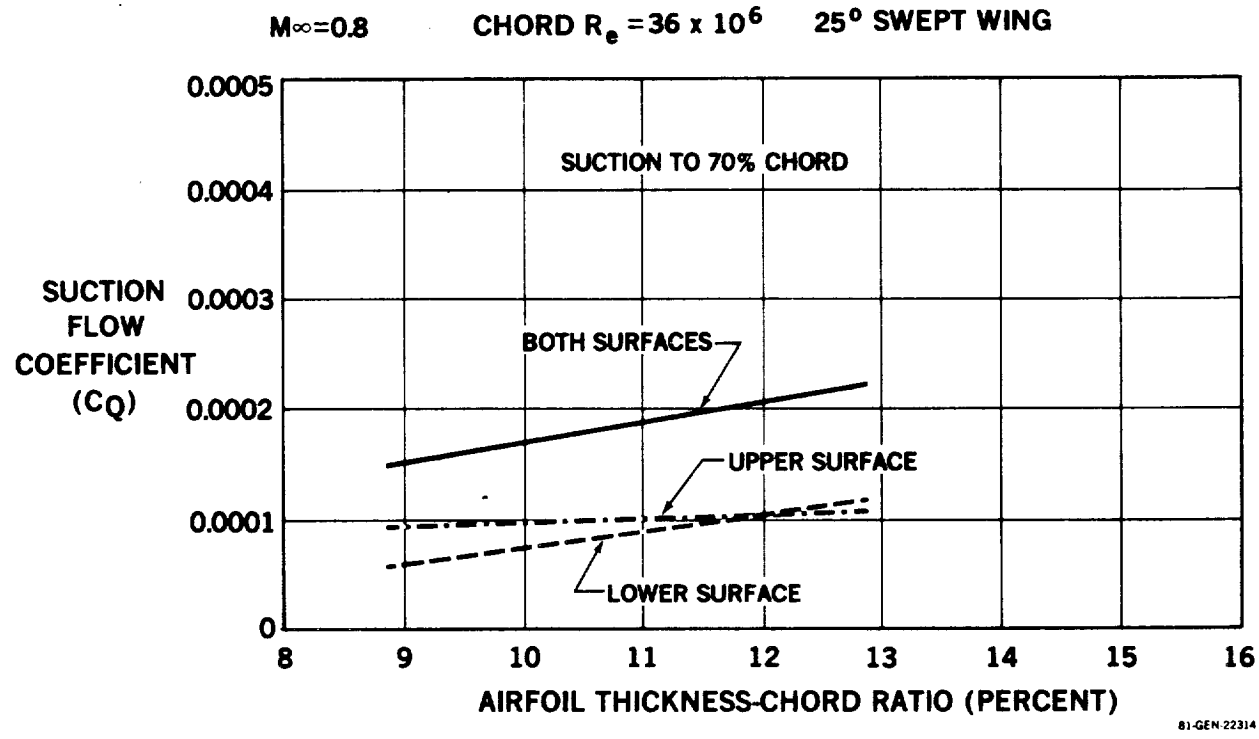

FIGURE 7-8. VARIATION OF SUCTION REQUIRED FOR LFC WITH THICKNESS-CHORD RATIO – 25-DEGREE SWEEP

Airfoil profile drag (wake drag) was calculated for the LFC sections and was found to have only a very small variation with thickness ratio and sweep at the design C_L. This is due to the similarity of the design pressure distributions.

Variation of profile drag for the representative airfoil used in the preceding discussion, as a function of Reynolds number is shown in Figure 7-10. Extending the suction from 70 percent to 85 percent chord reduces the profile drag by approximately one half. However, as noted previously, this extension of laminarization requires a severe increase in suction required. This situation suggests a very practical alternative in which suction is applied on the upper surface only back to 85 percent chord. Profile drag for such a case is included in Figure 7-10. Drag for upper surface suction to 85 percent, without LFC on the lower surface, is only slightly higher than the drag for both surfaces laminar to 70 percent chord.

LFC aircraft configuration studies (see section 5.6.1) showed that using upper surface suction only, to 85 percent chord, resulted in an overall lighter and more efficient aircraft. Greater effective structural depth and a high lift device at the leading edge of the wing are possible with suction only on the upper surface. A lighter wing weight results, which more than compensates for the slightly greater profile drag. In addition this configuration enhances wing accessibility for fueling and maintenance and significantly alleviates requirements for the environmental systems.

7.1.5 Effect of Loss of LFC

Aerodynamic consequences of the loss of LFC were investigated by computing the effect such loss would have on airfoil characteristics. The results are given in Figure 7-11. At constant angle of attack, the section lift coefficient is reduced by 20 percent from 0.783 to 0.625. In order to maintain a constant lift coefficient the angle of attack must be increased by approximately 0.8 degree, from 1.137 degrees to 1.927 degrees. A very significant effect is that with LFC off and constant lift a shock wave forms at 35 percent chord.

$M = 0.80,\ \Lambda = 30\ DEG,\ C_L = 0.50$

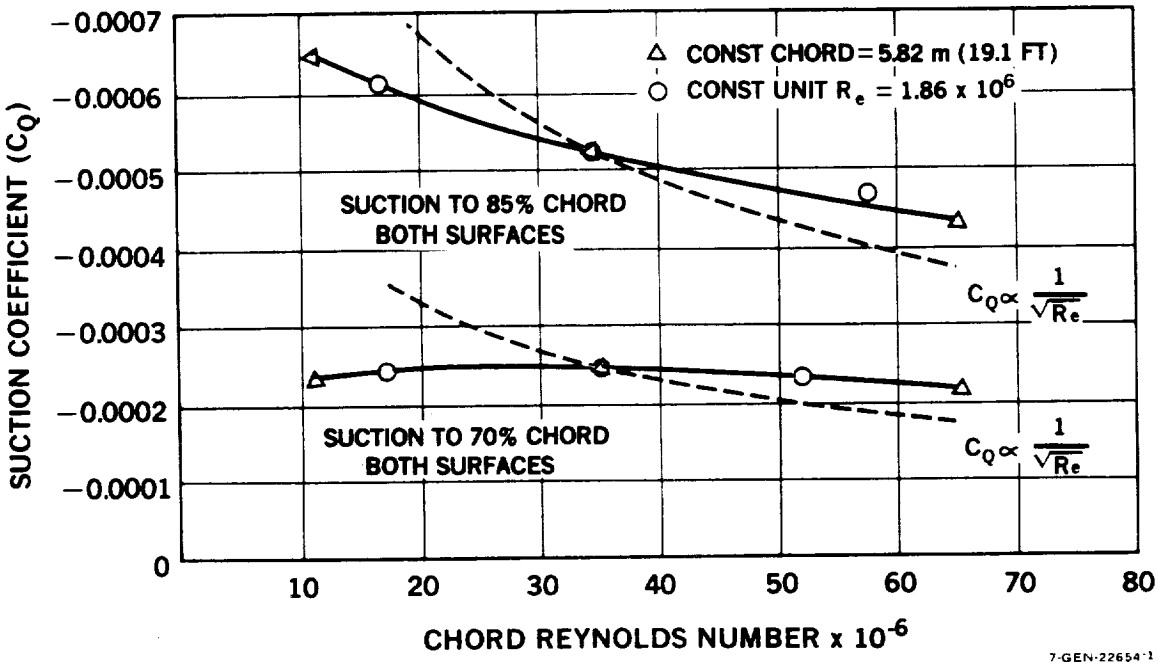

FIGURE 7-9. VARIATION OF LFC TOTAL SUCTION COEFFICIENT WITH REYNOLDS NUMBER

$M_\infty = 0.8$ $C_L = 0.502$ 30-DEG SWEPT WING

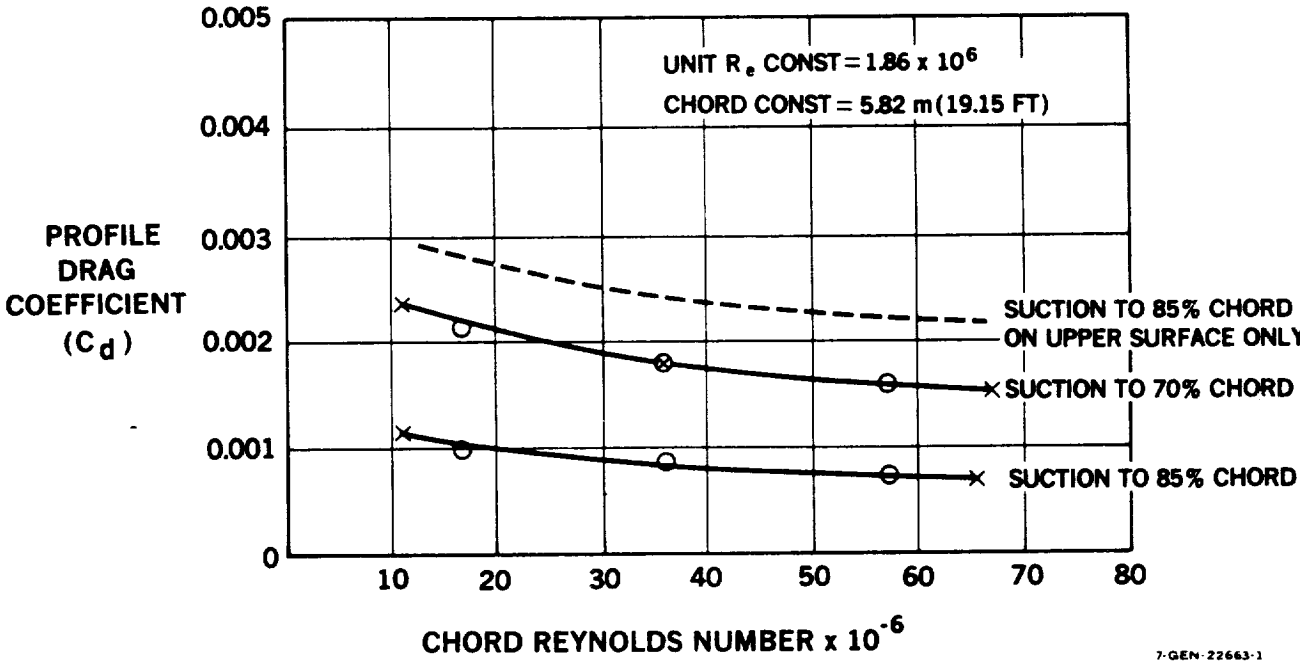

FIGURE 7-10. VARIATION OF PROFILE DRAG WITH REYNOLDS NUMBER

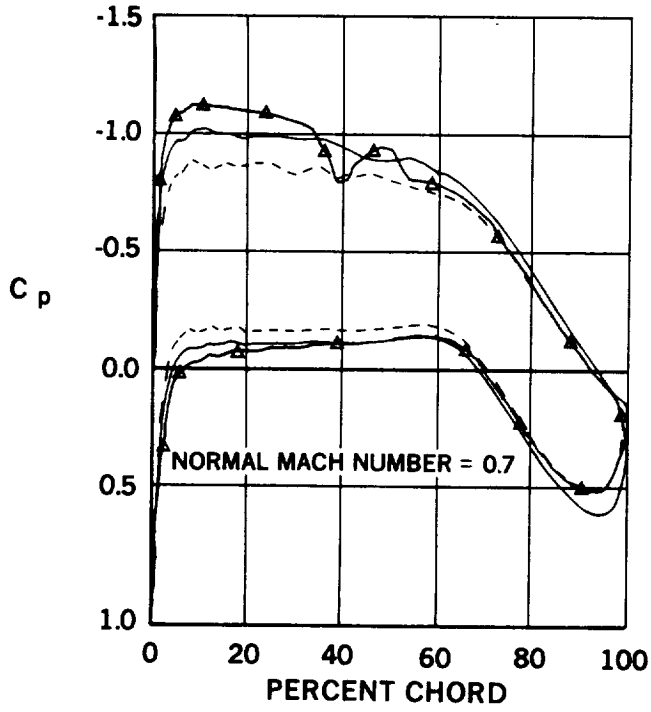

SYMBOL	α	C_ℓ	COMMENT
———	1.137	0.783	WITH LFC
—▲—▲—	1.927	0.783	WITHOUT LFC
- - - - -	1.137	0.625	WITHOUT LFC

7-GEN-22652

FIGURE 7-11. EFFECT OF LOSS OF LFC ON AIRFOIL PRESSURE DISTRIBUTIONS

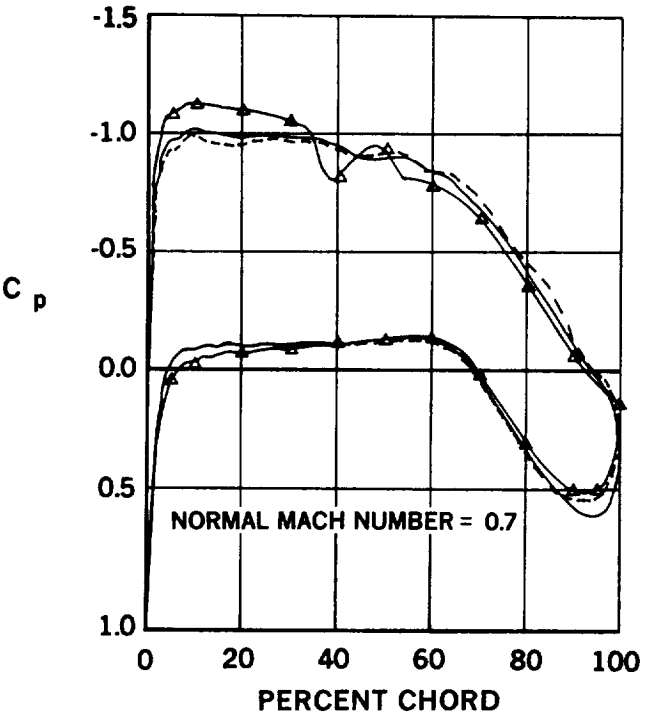

SYMBOL	α	C_ℓ	LFC	S_F
———	1.137	0.783	ON	0
—▲—▲—	1.927	0.783	OFF	0
- - - - -	0.99	0.783	OFF	1.5°

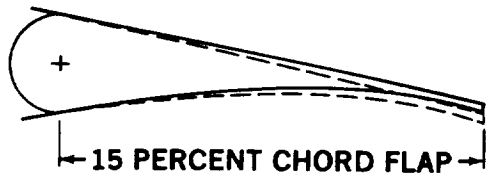

7-GEN-22653

FIGURE 7-12. EFFECT OF TRAILING EDGE FLAP ON AIRFOIL PRESSURE DISTRIBUTIONS

7.1.6 Off Design Conditions

Off-design operation of the representative LFC airfoil was investigated by calculating the pressure distribution and suction requirements for lift coefficients above and below the design lift coefficient. The resulting upper surface pressures and suction velocities are presented in Figures 7-13 and 7-14. When the lift coefficient (angle of attack) is reduced, the pressure peak is also reduced with a similar but more favorable gradient using slightly reduced suction. On the other hand, a small increase in lift coefficient raises the local Mach number, above the design value of 1.1, causing a shock to form near 40 percent chord with possible loss of laminar flow downstream of the shock.

Such velocities in the region of the shock indicate a substantial increase in required suction for the increased lift off-design condition. The local suction values are not considered to be quantitatively correct because there are no reliable methods for predicting suction requirements with a shock present on the airfoil.

7.1.7 LFC Airfoil Design Study Summary

The results of the Airfoil Design study provide the following conclusions:

- Existing analytical aerodynamic design techniques are readily applicable to the design of LFC compatible airfoils having shock-free supercritical flow with a turbulent boundary layer.
- LFC compatible airfoils are significantly thinner than comparable supercritical airfoils.
- Extending LFC beyond 70 percent chord to 85 percent reduces profile (wake) drag by 50 percent while the required suction flow is doubled.
- Trailing edge, small chord trim flaps can provide a ready means of adjusting and maintaining section lift if LFC is lost.
- Operation of the LFC compatible airfoil at off design conditions does not cause any problem at reduced lift coefficients. However, at higher than design lift conditions shock waves appear with a consequent loss of LFC aft of the shock.

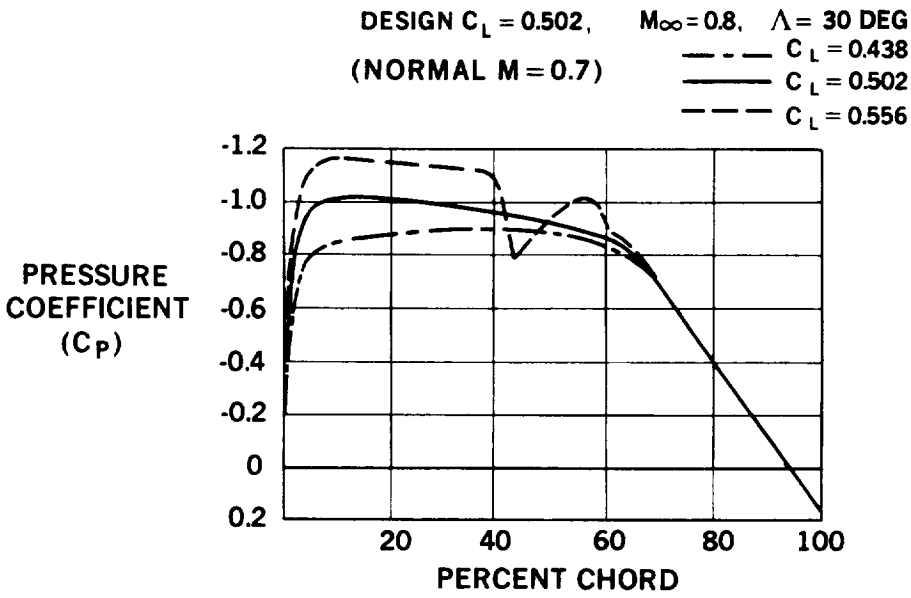

FIGURE 7-13. CHANGE OF AIRFOIL PRESSURE DISTRIBUTION WITH LIFT COEFFICIENT

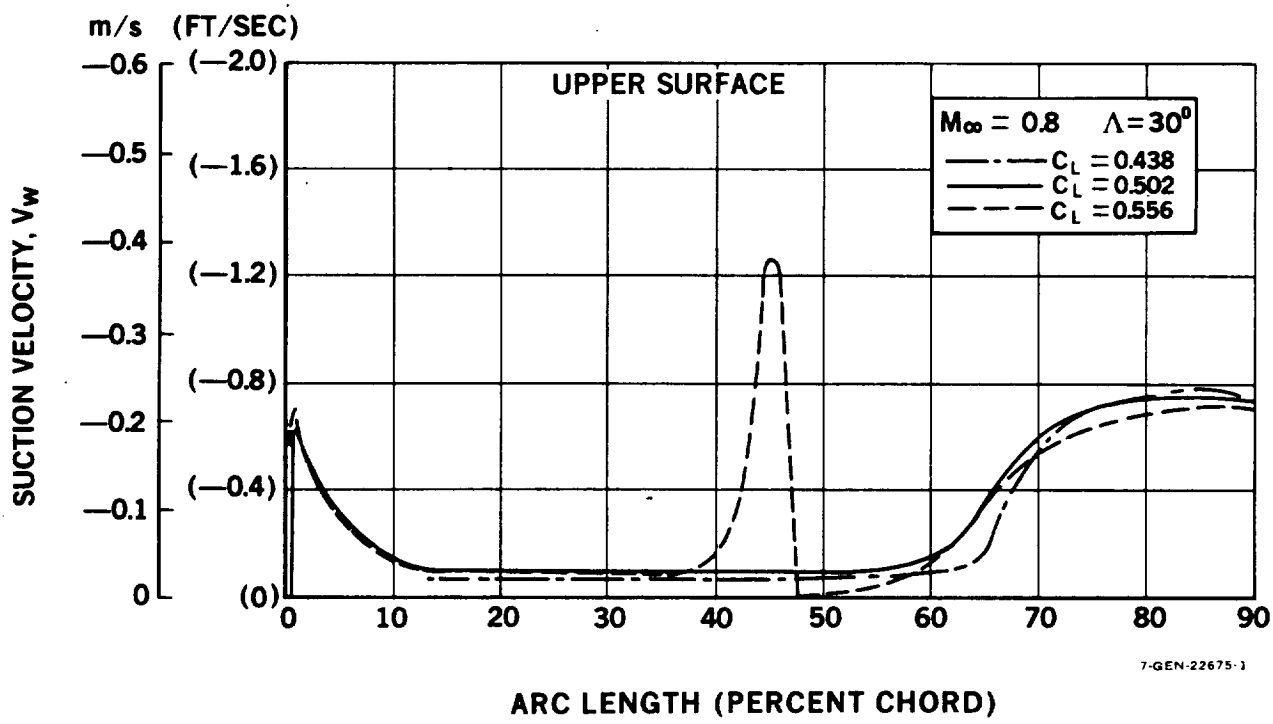

FIGURE 7-14. EFFECT OF CHANGING LIFT COEFFICIENT ON LFC SUCTION VELOCITY DISTRIBUTION

7.2 NUMBER AND LOCATION OF PROPULSION AND SUCTION ENGINES

An investigation was conducted to guide propulsion system configuration development of a baseline LFC aircraft. Three principal items were considered in this investigation.

- o Effect of engine acoustic environment on laminar flow.
- o Number and location of propulsion engines.
- o Number and location of suction engines.

7.2.1 Effect of Engine Noise on Allowable Engine Location

The first phase of the investigation focused on the influence of engine noise on the aerodynamic surfaces where it would be desirable to apply LFC . Near field noise for three candidate engine cycles were estimated. Since difference in overall sound pressure levels (OASPL) were not large enough to affect engine location, only one engine cycle, the Energy Efficient Engine (E^3) type, was selected as the reference for acoustic characteristics and installed engine performance. Allowable acoustic disturbance criteria were developed from X-21A data and alternative engine locations were evaluated. An acoustic map showing contours of OASPL in terms of dB relative to .02mPa (.0002 dyne/cm^2) for the E^3 engine is presented in Figure 7-15.

The interaction of discrete noise frequencies with resonance conditions within the boundary layer should be considered in determining the location of noise induced transition. Unfortunately, detail frequency noise levels are not known for such advanced engines and analytical methods are as yet inadequate to solve the problem, thus a method based on overall sound pressure level was used to assess the possibilities of achieving laminar flow relative to powerplant location.

An estimate of the allowable acoustic environment was made for a standard day flight condition of 0.8 Mach number at 10,670 m (35,000 feet) altitude. This estimate was based upon X-21A criteria presented in Reference 7.4-5. These

criteria were determined in terms of the equivalent sound pressure level, as a function of chord Reynolds number as shown in Figure 7-16. The equivalent sound pressure level is given by the relation:

$$SPL = 20 \log \left[\frac{\Delta \bar{u}}{U_\infty} \gamma M_\infty \frac{P_\infty}{.0002} \right]$$

Where:

$\frac{\Delta \bar{u}}{U_\infty}$ = the ratio of the root mean square disturbance to the freestream velocity.

M_∞ = the freestream Mach number.

γ = the ratio of specific heats

P_∞ = the freestream pressure P_a

Included in Figure 7-16 is a curve showing the X-21A criteria increased by 6dB which was suggested as a result of X-21A flight test experience.

It was also determined during this investigation that at a fixed Mach number, the variation of Reynolds number and ambient pressure at flight levels from 9,140 m to 12,190 m (30,000 to 40,000 feet) is such that the allowable noise level at a given distance from the leading edge is essentially independent of altitude.

The regions affected by engine acoustic environment were estimated for both wing mounted and aft-fuselage mounted engine configurations. By super-position of the engine acoustic field and the allowable noise levels on the aircraft wing planform, an assessment of the extent of detrimental engine noise effects was made.

In the case of the wing mounted engines most of the wing is subjected to an acoustic environment which exceeds the allowable sound pressure levels. The affected area is indicated by the shaded region in Figure 7-17. Since the region shown does not assume any benefit due to shielding of the upper surface by the wing itself, it is probable that the amount of laminar flow achievable would be larger. However, a 10 dB reduction in engine sound pressure level would not increase the laminar flow area appreciably.

$M_\infty = 0.8$ ALT = 10,670 m (35,000 FT)

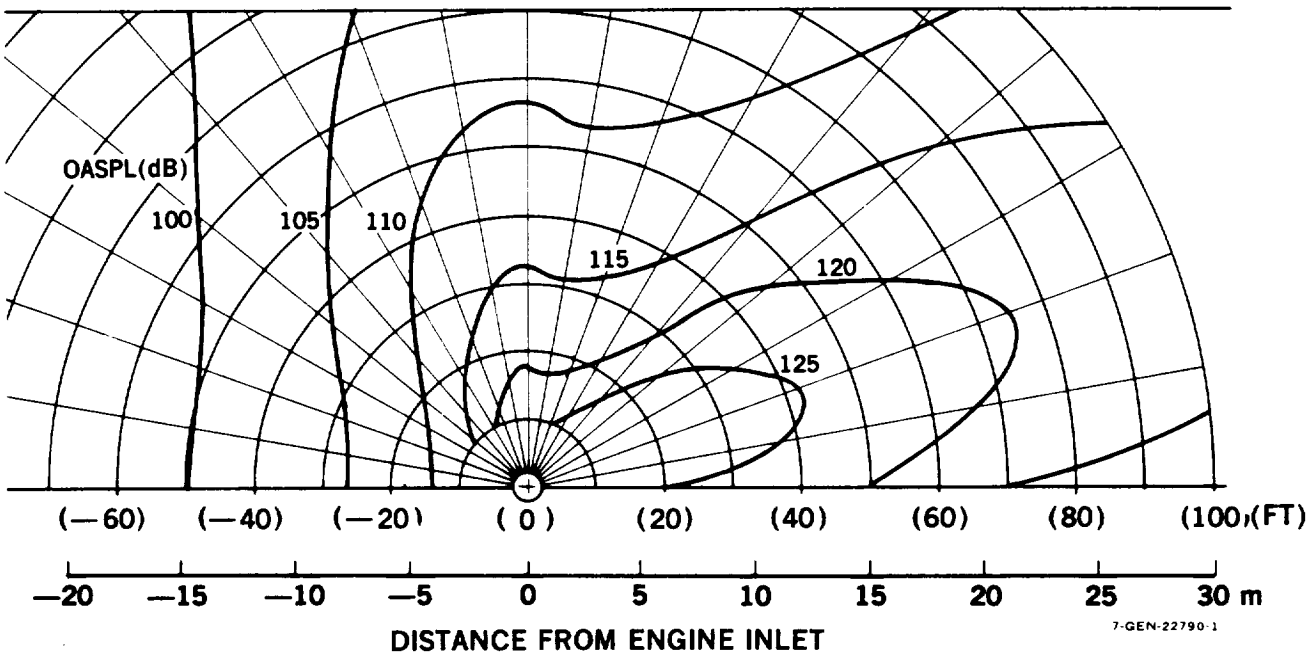

FIGURE 7-15. NEAR-FIELD ACOUSTIC ENVIRONMENT DUE TO ONE ENGINE

$M_\infty = 0.8$ ALT = 10,670 m (35,000 FT)

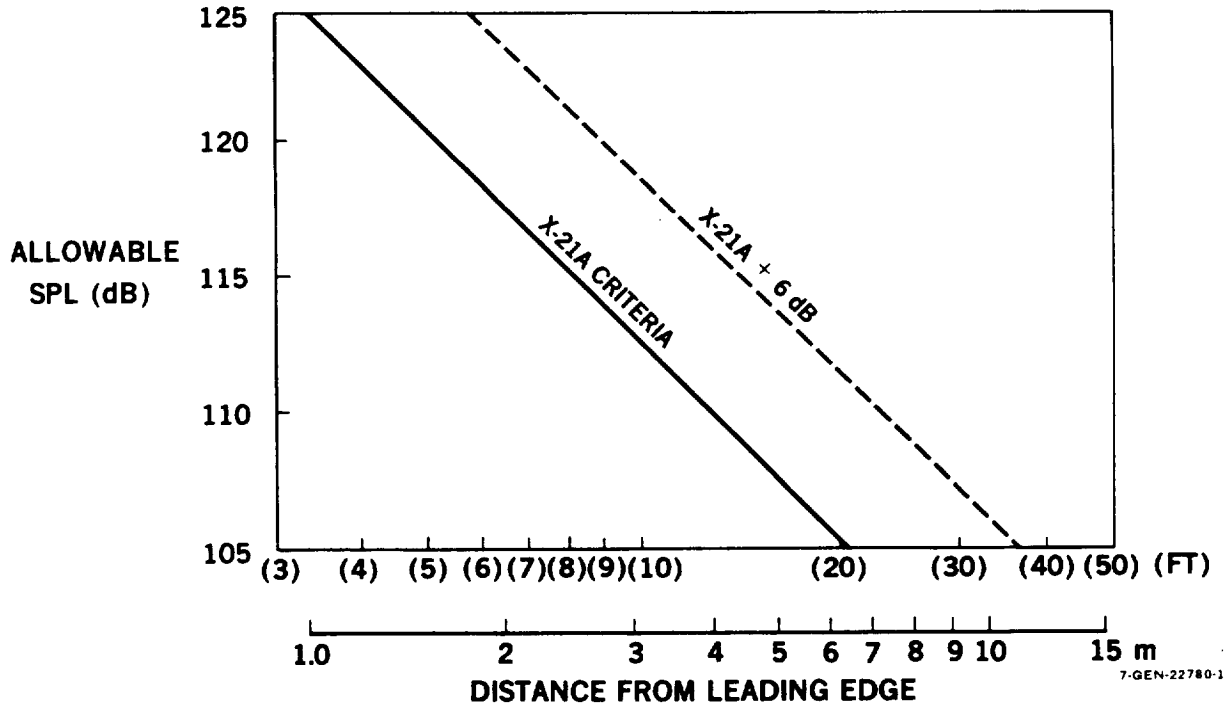

FIGURE 7-16. ALLOWABLE ACOUSTIC ENVIRONMENT

In contrast to the preceding case with wing mounted engines, aft-fuselage mounted engines were found to be compatible with achieving laminar flow on the wing. The areas affected by the engine acoustic environment are exclusively on the tail surfaces as shown in Figure 7-18. Engine induced sound pressure levels for this case were increased 3dB to account for the dual-engine pod concept shown. Most of the vertical tail is not amenable to laminarization so application of LFC on the vertical tail was not recommended. Laminar flow could be established over a significant portion of the horizontal stabilizer. However, unlike the wing which operates over a limited range of lift coefficients in cruise, the horizontal tail lift may vary from positive to negative as center-of-gravity location varies. The complication of a suction system for the horizontal tail, considered along with the limited amount of laminar flow which may be obtained and the inaccessibility of the tail for inspection and cleaning, approx. 15.2 m (50-feet) above ground, resulted in the recommendation to forego LFC on the horizontal tail.

From the investigation of engine acoustic environment effects on laminar flow, it is evident that the engines on an LFC aircraft should be located on the aft fuselage. It is also indicated that tail surfaces may not effectively utilize LFC due to effects of the engine acoustic field.

7.2.2 Number of Propulsion Engines

A study was conducted to evaluate the performance and economic tradeoffs between three and four engine configurations for the baseline LFC aircraft. The aft-fuselage location for propulsion engines was dictated by the need to minimize exposure of the LFC wing to the detrimental engine acoustic environment, as established in Section 7.2.1.

The procedure used to select the number of propulsion engines consisted of sizing both the three engine and four engine LFC aircraft configurations to minimize the takeoff gross weight. This sizing was based upon the design mission and ground rules defined in Sections 4.0 and 5.0. After sizing each

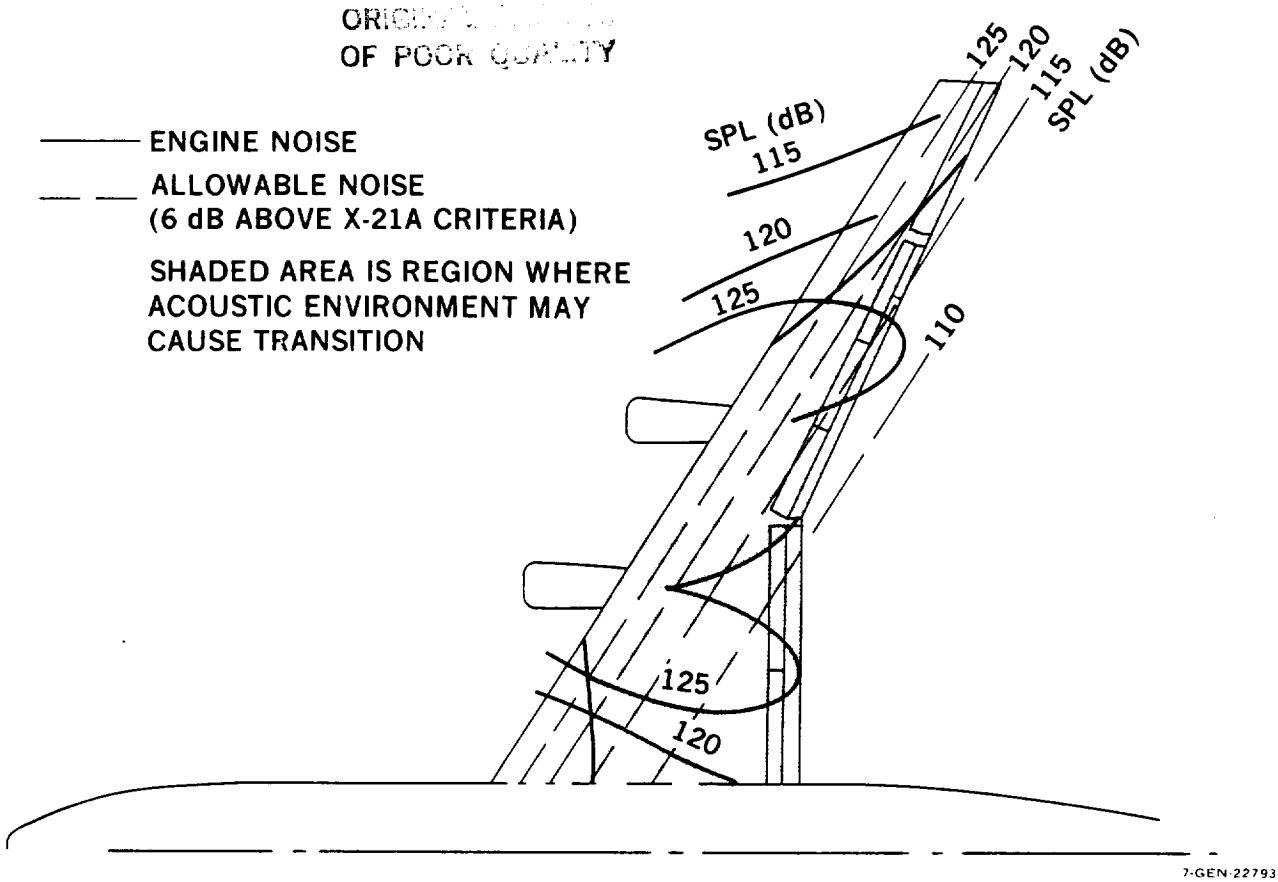

FIGURE 7-17. EFFECT OF ENGINE-INDUCED ENVIRONMENT ON EXTENT OF LFC (WING-MOUNTED ENGINES)

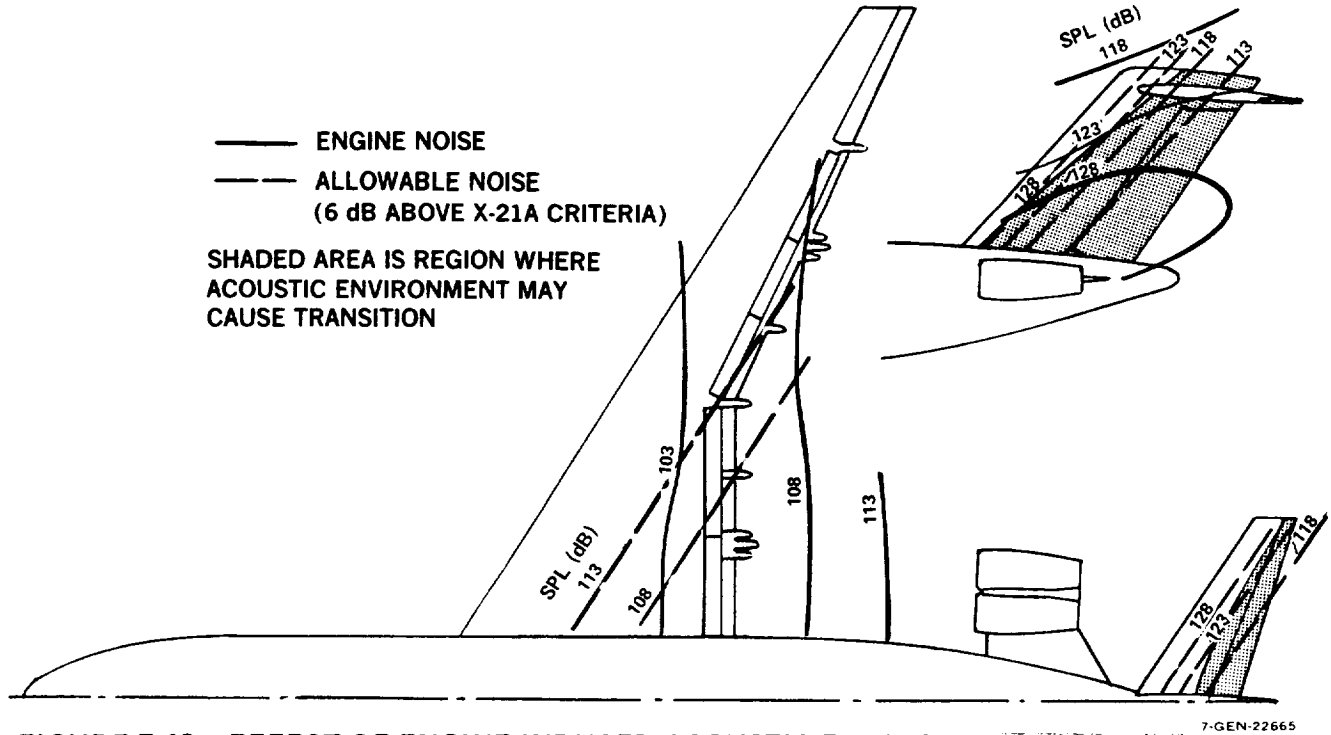

FIGURE 7-18. EFFECT OF ENGINE-INDUCED ACOUSTIC ENVIRONMENT ON EXTENT OF LFC (FUSELAGE-MOUNTED ENGINES)

configuration, direct operating costs were determined. The configuration with three engines which had the lower operating cost was selected for subsequent LFC aircraft. See Section 5.4 for details.

7.2.3 Number and Location of Suction Engines

Investigation of suction system characteristics was conducted to develop overall design, control, and operational requirements. Details of this study and analysis work are described in Section 10.6. A summary of results and conclusions is given in Section 5.5.

The results showed that one suction engine per side, located outboard of the wing planform break was the most suitable arrangement. This configuration is satisfactory for suction on both wing surfaces as well as for suction on the upper surface only.

7.3 ASPECT RATIO, THRUST, AND WING LOADING ANALYSIS

Analysis and configuration development tasks were carried out to evaluate performance parameters and select the aspect ratio, engine size, and wing area for LFC aircraft utilizing two concepts of suction distribution on the wing. The basic concept considered suction on both upper and lower wing surfaces to 70 percent chord, while the alternative concept used suction on the upper surface only back to 85 percent chord. Rationale for this alternative concept is based on the comparison of profile drag coefficients together with significant structural and operational advantages of using suction on only the upper surface of the wing. See Section 5.6.1.

The general procedure used in this analysis consisted of: (1) establishing aerodynamic and structural weight characteristics in parametric form as functions of aspect ratio, wing area, and engine size, (2) calculation of takeoff gross weight (i.e., aircraft size) required for the design mission, and (3) determining operational limits on takeoff field length, initial cruise altitude, and approach speed. Finally, the direct operating cost was estimated for the minimum takeoff gross weight aircraft.

7.3.1 Wing Configuration

Selection of the wing planform for this study was based on concurrent transport design work and wind tunnel test data from the Energy Efficient Transport program. See also Section 5.6.1.1. Wing planforms for aspect ratios of 10, 12, and 14 are shown in Figure 7-19. In each case quarter-chord sweep is 30 degrees and taper ratio is 0.25 for the basic trapezoidal wing. A trailing edge extension, with a trailing edge sweep-back of 8 degrees, is located between the side of the fuselage and 40 percent semi-span station. Design lift coefficient is 0.50 for each aspect ratio and the average thickness is 11.7 percent chord. The thickness-chord ratio distribution is tabulated below:

Semispan Station Percent	Thickness-Chord Ratio Percent
Side of Fuselage	13.82
32.6	11.87
40.0	10.92
80.0	10.92
100.0	10.92

Twist distributions for the 1.0g and rigid reference conditions are shown in Figure 7-20.

The general configuration used in this study was the three engine airplane selected as under Section 7.2.2. Fuselage size was fixed as previously, to be compatible with the 300 passenger, 31,298 Kg (69,000 lb) payload, requirement for the 9260 Km (5000 n.mi.) design mission. Tail areas were initially sized for the nominal wing area. Thereafter the tail volume coefficients were held constant as wing area was varied.

High lift systems were adapted to accommodate each of the two LFC concepts. For the basic concept a 25 percent chord, two element, trailing edge flap was used. A sketch of the flap is shown in Figure 7-21. Because porous suction surfaces extend below the leading edge on the basic LFC wing, leading edge high lift devices were not feasible with suction on both surfaces. The high lift system at the trailing edge for the alternative LFC wing is severely constrained due to the extension of suction to 85 percent chord. Thus the flap was limited to a single slotted configuration having 15 percent chord. However, with LFC on the upper surface only a leading edge device can be used which compensates for the smaller trailing edge flap. The leading edge device also acts as a shield to alleviate insect contamination. The latter high lift system is shown in Figure 7-22.

Weight characteristics for the analysis considered strength, stiffness, and flutter criteria. For the LFC wings it was found that mainly bending stiffness requirements for roll control established the wing structure/weight.

Methods and results of the strength and stiffness analyses are presented in Section 9.1.3. Aeroelastic analyses of the LFC wings were conducted to evaluate the elastic-wing rolling moment due to aileron deflection at varying wing stiffness values. This was done at maximum level flight cruise speed, where it was required that the elastic-wing roll capability be at least 25 percent of the rigid-wing rolling effectiveness in order to assure the desirable level of roll control at high speed. Figure 7-23 illustrates the variation of elastic-wing roll capability with increasing wing bending stiffness for aspect ratio 12. Increased torsional stiffness was also investigated, however, with a 30 degree swept wing, the dominant aeroelastic rolling effects are due to wing bending. The resulting wing bending

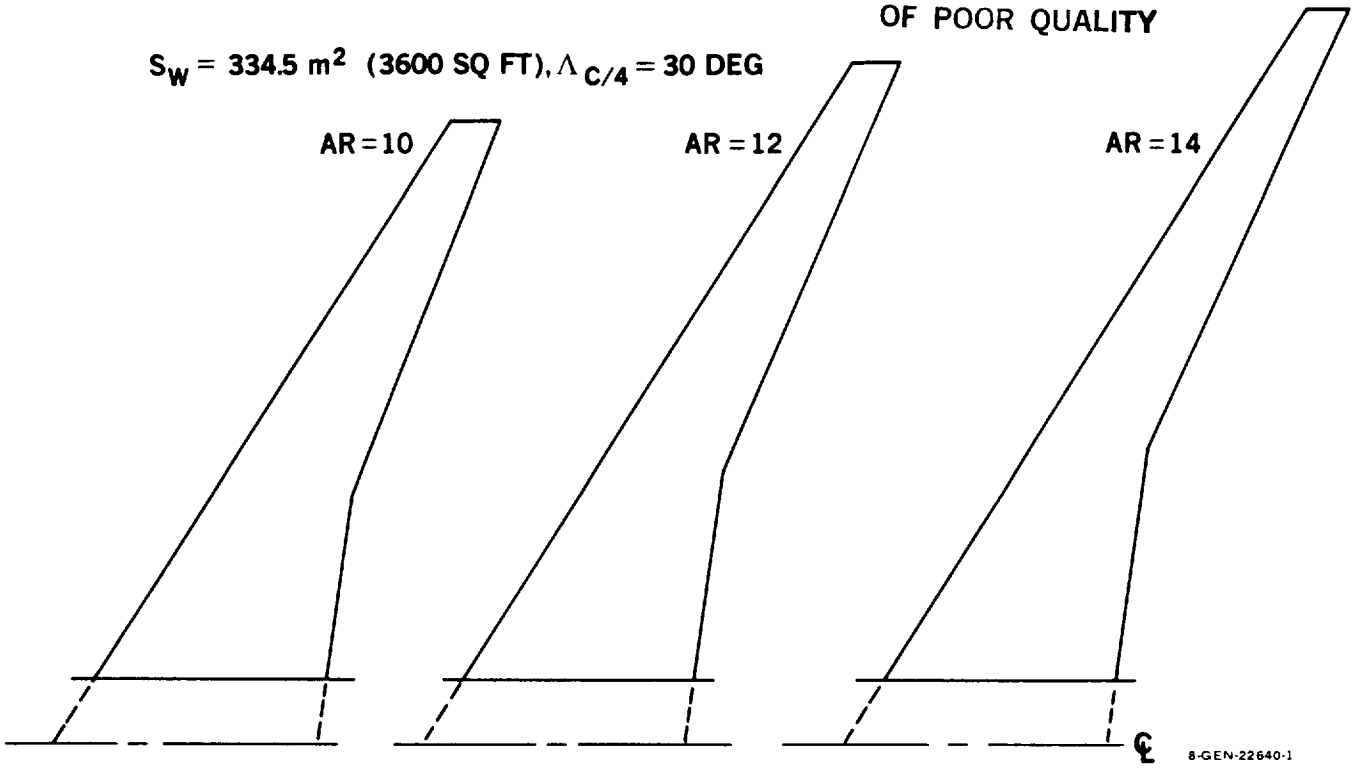

FIGURE 7-19. ASPECT RATIO SIZING WING PLANFORMS

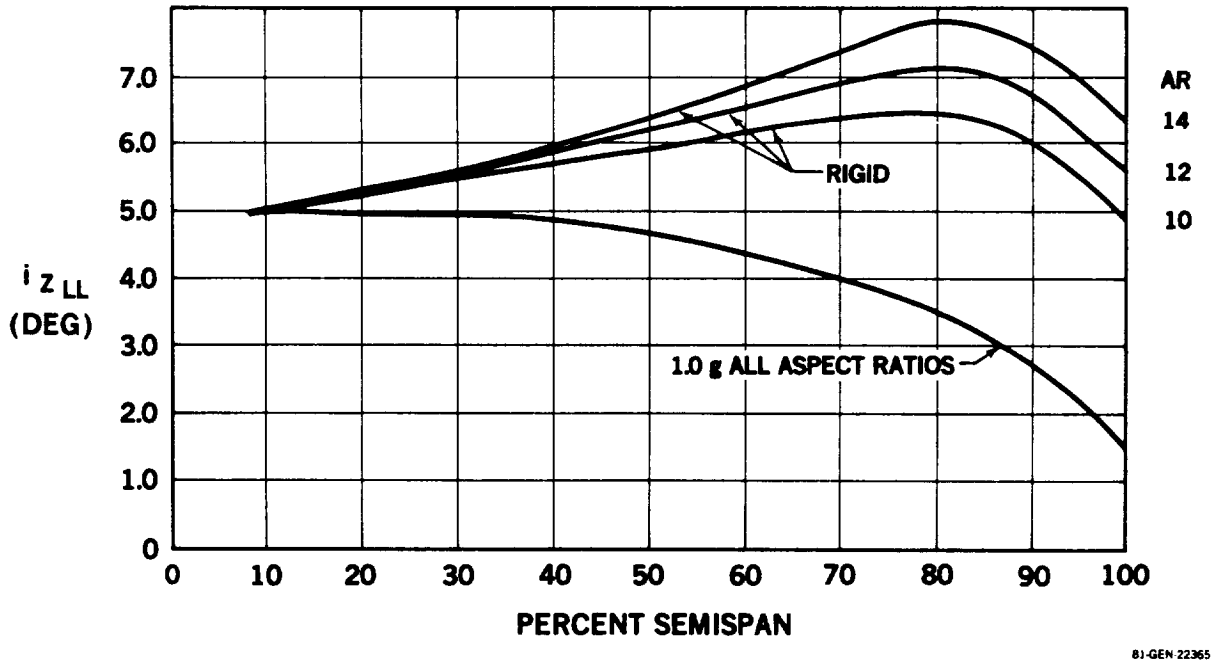

FIGURE 7-20. EFFECT OF ASPECT RATIO ON ANGLE OF ZERO LIFT

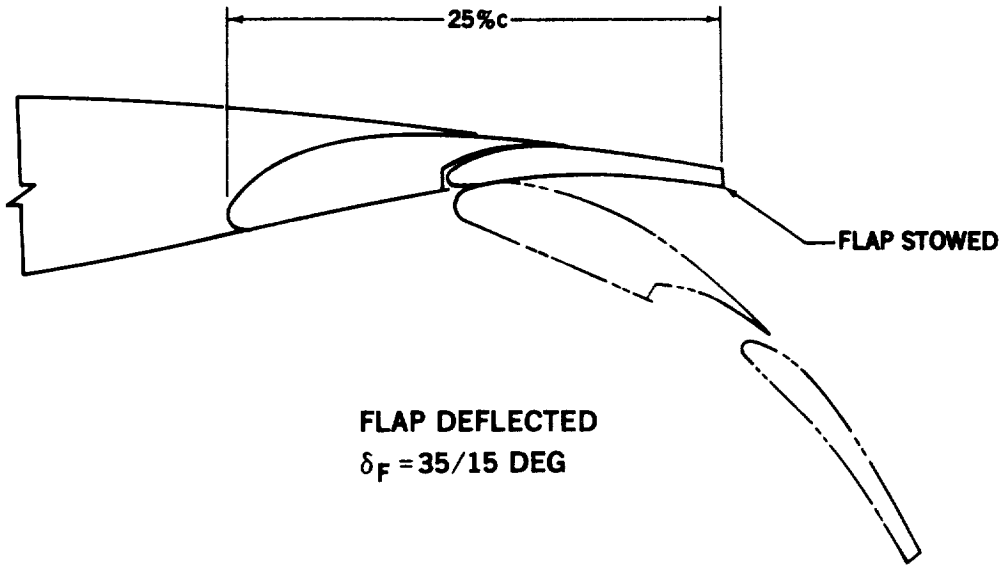

8-GEN-22553-1

FIGURE 7-21. HIGH-LIFT SYSTEM – LFC BASE CASE – SUCTION BOTH SURFACES TO 70 PERCENT CHORD

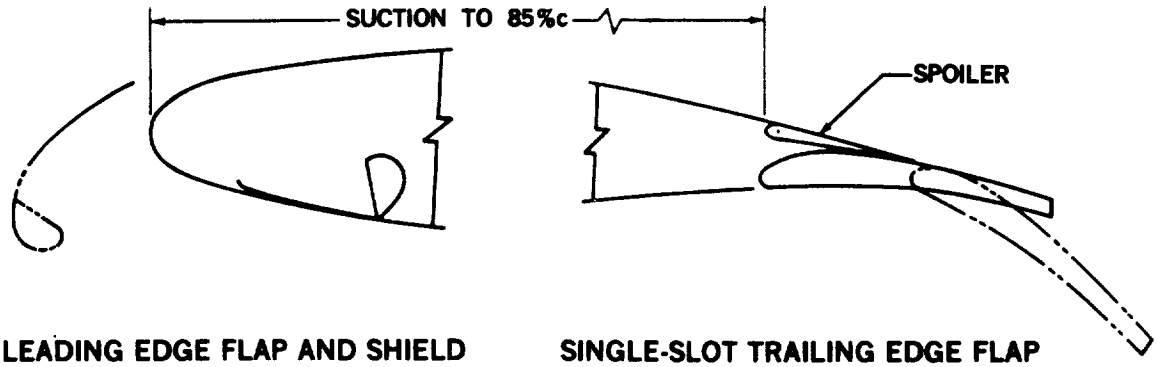

LEADING EDGE FLAP AND SHIELD

C_F/C = 0.10

SINGLE-SLOT TRAILING EDGE FLAP

δ_F = 30 DEG

C_F/C = 0.15

8-GEN-22554A-1

FIGURE 7-22. HIGH-LIFT SYSTEM – UPPER SURFACE SUCTION ONLY

stiffness, and corresponding wing weight factors, are shown as functions of wing aspect ratio in Figure 7-24. Although the weight factor does not increase as rapidly as the bending stiffness factor the weight penalty incurred with higher aspect ratios is clearly evident.

7.3.2 Aircraft Sizing - Base Case

Sizing matrices were constructed for each aspect ratio to graphically show the interrelation between wing area, engine thrust, and takeoff gross weight for the design mission. Mission constraints were then superimposed on the matrix to determine the configuration size parameters for the minimum takeoff gross weight aircraft which meets mission requirements and operational constraints. Figure 7-25 is an example of a sizing matrix for an earlier LFC configuration. Initial cruise altitude limits of 9449 m (31,000 ft) and 10,668 m (35,000 ft) are shown along with the 66.9 m/s (130 KEAS) approach speed cutoff. In this instance the 3,048 m (10,000 ft.) takeoff distance limit did not appear within the limits of the matrix. The design points corresponding to the two initial cruise altitude limits are indicated by the symbols at the intersection with the approach speed limit. Two initial cruise altitudes were considered in order to evaluate the penalty for selecting the higher altitude 10,670 m (35,000 ft) where the likelihood of encountering ice crystals is greatly reduced.

Aircraft configuration and performance parameters are summarized, as functions of aspect ratio, in Figures 7-26a & b for the LFC aircraft with suction on both surfaces corresponding with Figure 7-25. The higher initial cruise altitude requires a slightly larger wing area, larger engines and higher takeoff gross weight. However, fuel burned and takeoff field length are reduced with the larger wing.

Based upon the analytical results and practical operational factors the baseline aircraft was sized to meet the 10,670 m (35,000 ft) initial cruise altitude and have an aspect ratio of 10. Low speed lift curves and L/D characteristics were shown previously in Figures 5-30 and 5-31, and discussed in Section 5.6.1.1.c.

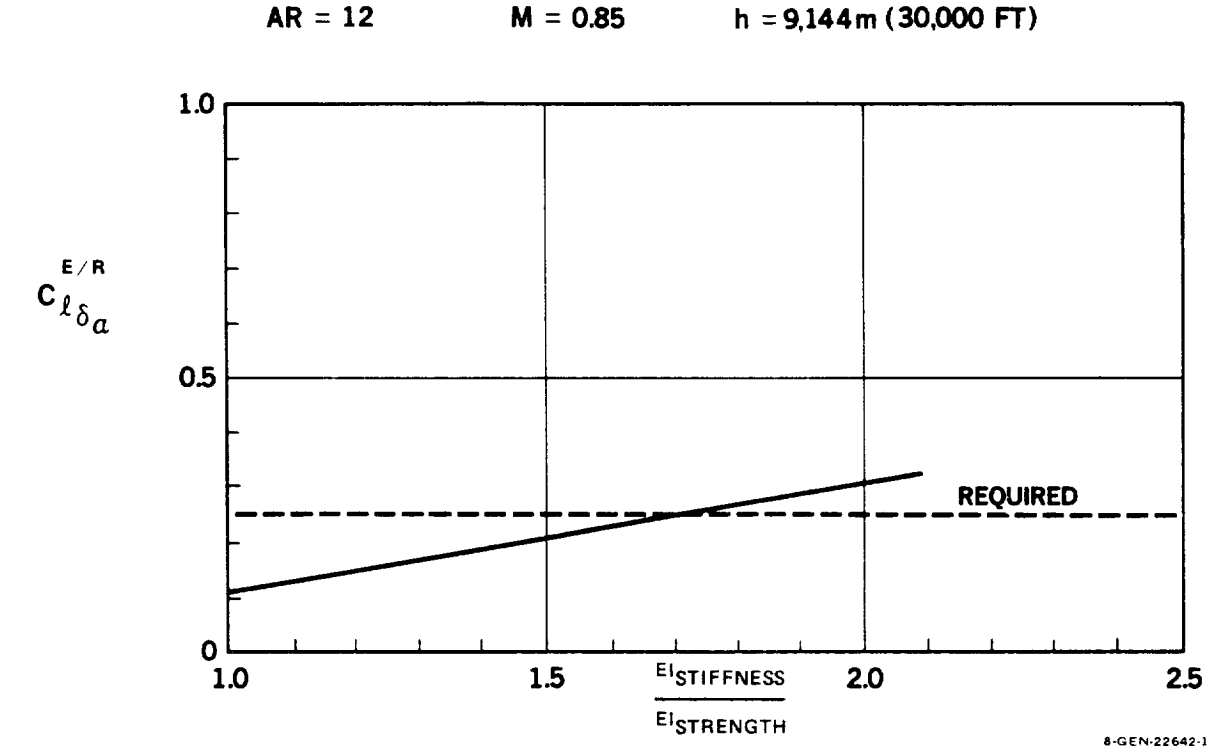

FIGURE 7-23. ELASTIC WING BENDING STIFFNESS CRITERIA

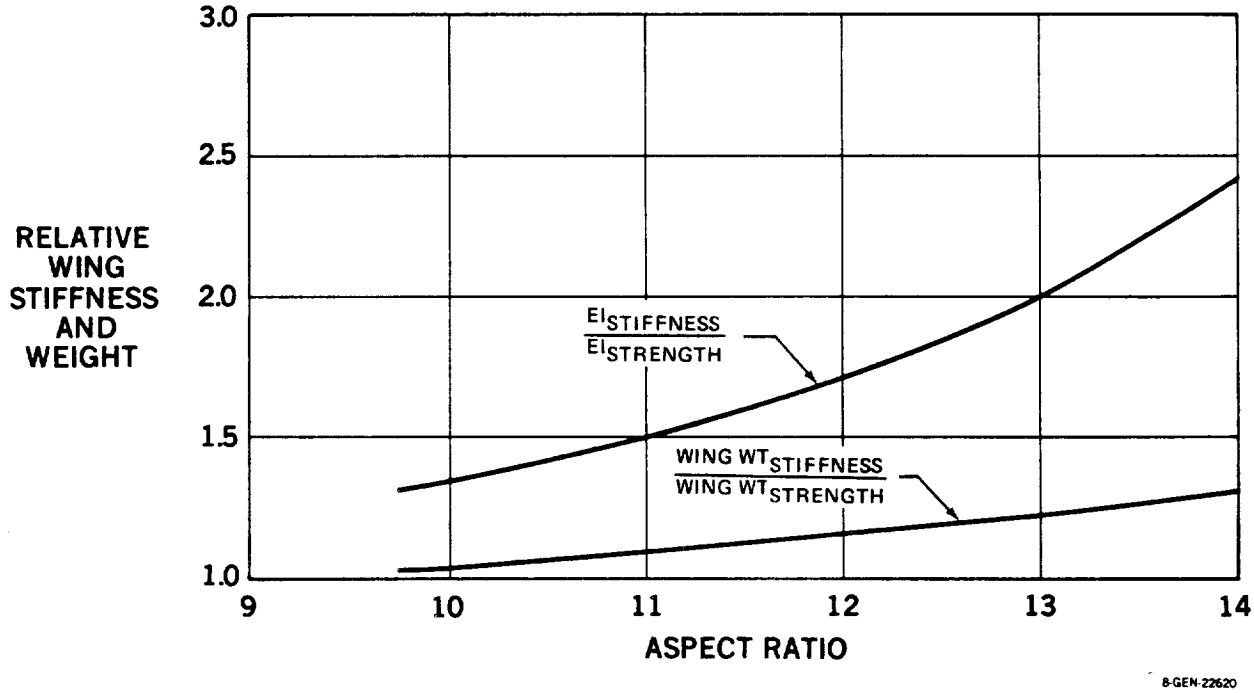

FIGURE 7-24. ELASTIC WING BENDING STIFFNESS AND WEIGHT FACTORS

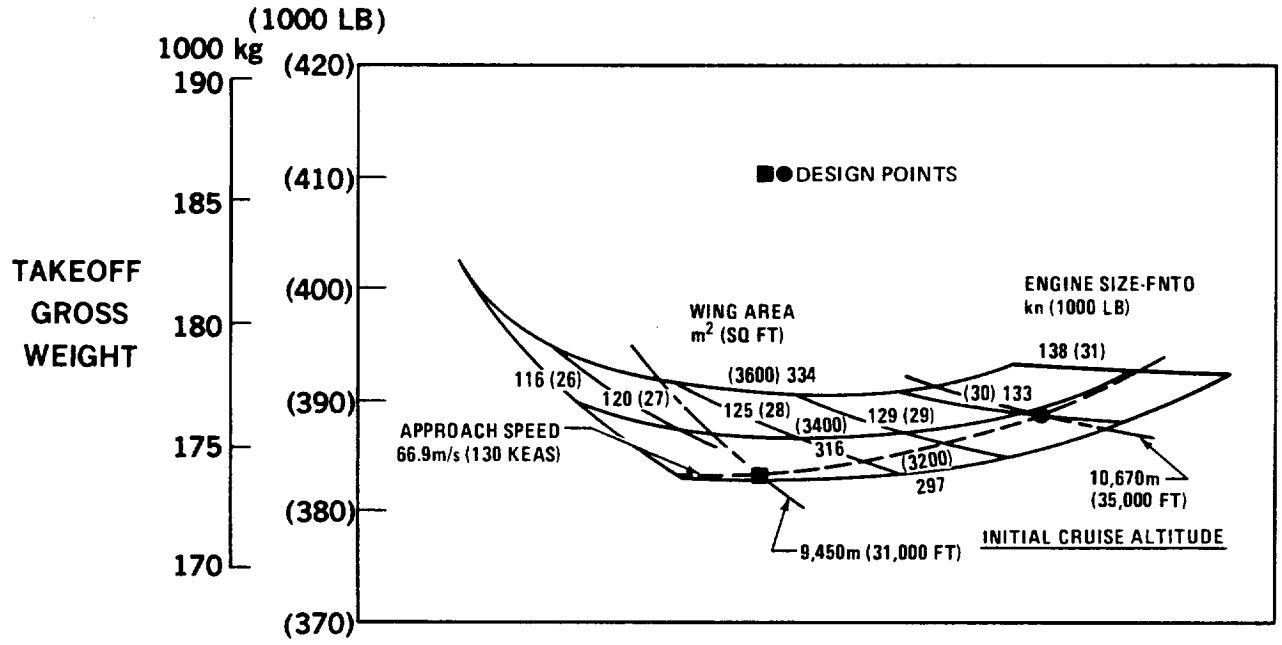

8-GEN-22631-1

FIGURE 7-25. MISSION SIZING MATRIX FOR AR=10 – SUCTION ON BOTH SURFACES

- RANGE = 9260 km (5000 N MI)
- PAYLOAD = 31,300 kg (69,000 LB)
- APPROACH SPEED = 67 m/s (130 KEAS)

INITIAL CRUISE ALTITUDE NOTED

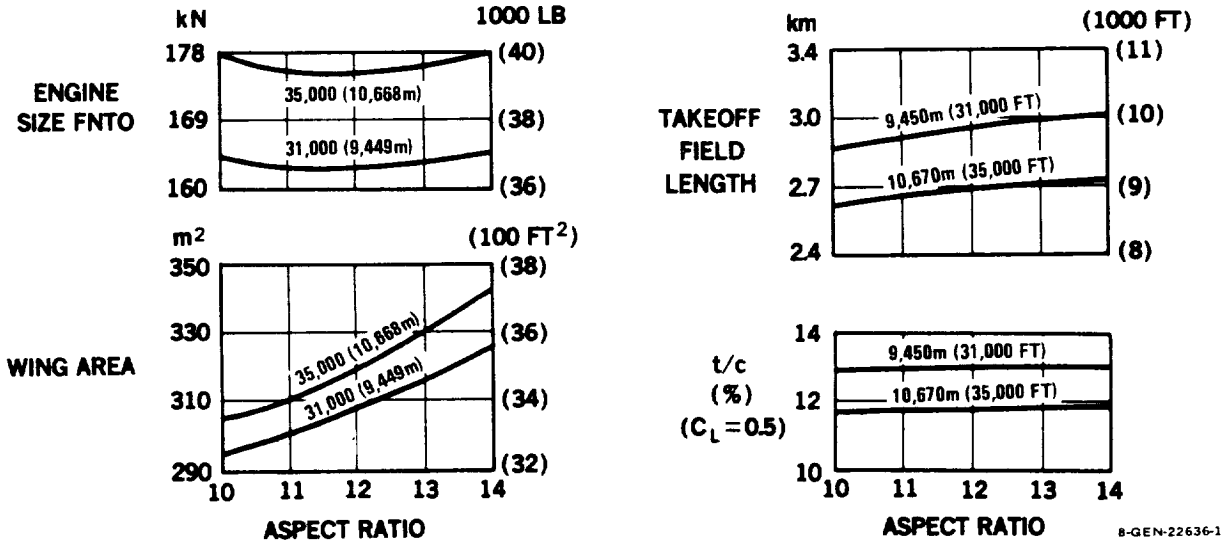

FIGURE 7-26A. ASPECT RATIO SIZING SUMMARY I – SUCTION ON BOTH SURFACES

- RANGE = 9260 km (5000 N MI)
- PAYLOAD = 31,300 kg (69,000 LB)
- APPROACH SPEED = 67 m/s (130 KEAS)

INITIAL CRUISE ALTITUDE NOTED

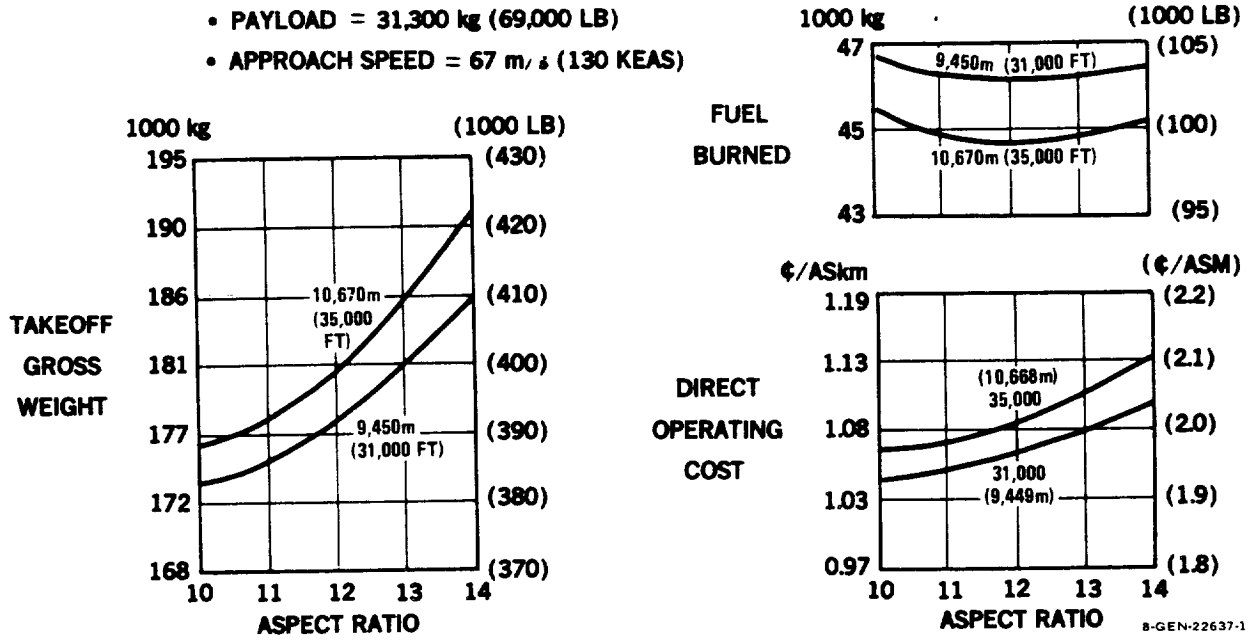

FIGURE 7-26B. ASPECT RATIO SIZING SUMMARY II – SUCTION ON BOTH SURFACES

7.3.3 Aircraft Sizing - Upper Surface Suction Only

The aspect ratio and sizing study for the alternative concept, utilizing upper surface suction only (USSO), benefited from the trends established in the preceding base case. Sizing matrices were constructed for aspect ratios 10 and 12 and only the 35,000 ft initial cruise altitude condition was evaluated. The sizing matrix for aspect ratio 10 is presented in Figure 7-27. In this case the initial cruise altitude became the critical sizing condition.

Performance parameters for the USSO configuration for the two aspect ratio points evaluated are shown in Figures 7-28a & b. These points are superimposed on the summary plots for the preceding basic case. Considering these results and the preceding rationale, an aspect ratio of 10 was also selected for the USSO aircraft. See also Section 5.6.1.1.a. The configuration and performance parameters for the alternative LFC configurations at this stage are compared in Table 7-1. Low speed aerodynamic characteristics, lift curves and L/D ratio, were shown previously in Figures 5-28 and 5-29, respectively.

From the results of the aspect ratio, thrust, wing loading analysis it was recommended that the LFC concept utilizing suction to 85 percent chord on the upper wing surface only, be used for further LFC aircraft development. It should be emphasized that the comparisons were biased in favor of the initial LFC concept because no allowance was made for lower acquisition and maintenance costs that should be credited to the upper surface suction only case.

Later comparisons of updated alternative LFC configurations were presented in Section 5.6.1.5, see Tables 5-20 and 5-21. These showed even more advantages for the USSO configuration.

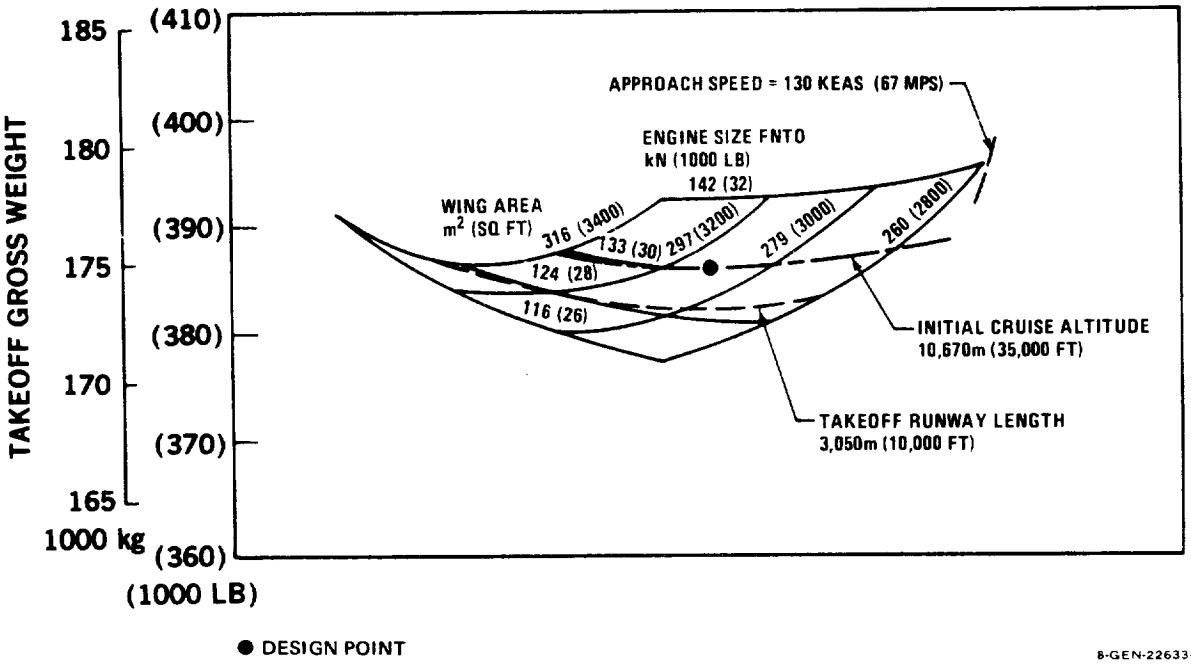

FIGURE 7-27. MISSION SIZING MATRIX FOR AR=10 – UPPER SURFACE SUCTION ONLY

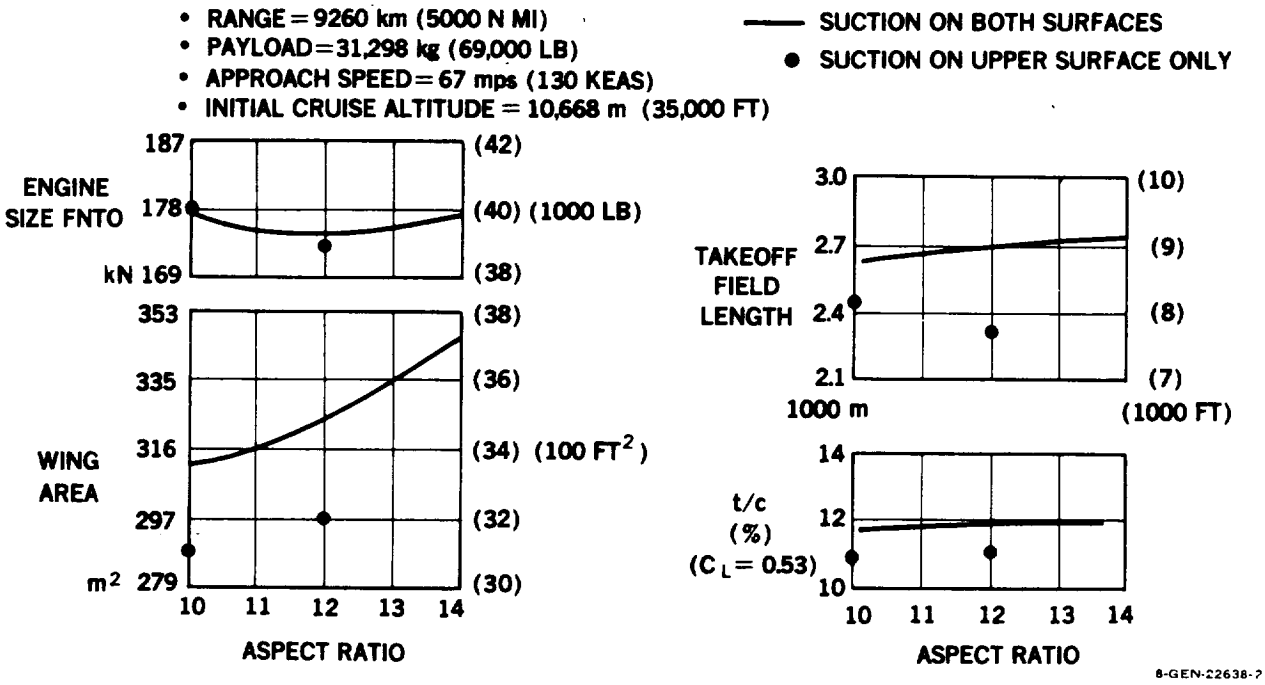

FIGURE 7-28A. ASPECT RATIO SIZING SUMMARY COMPARISON I

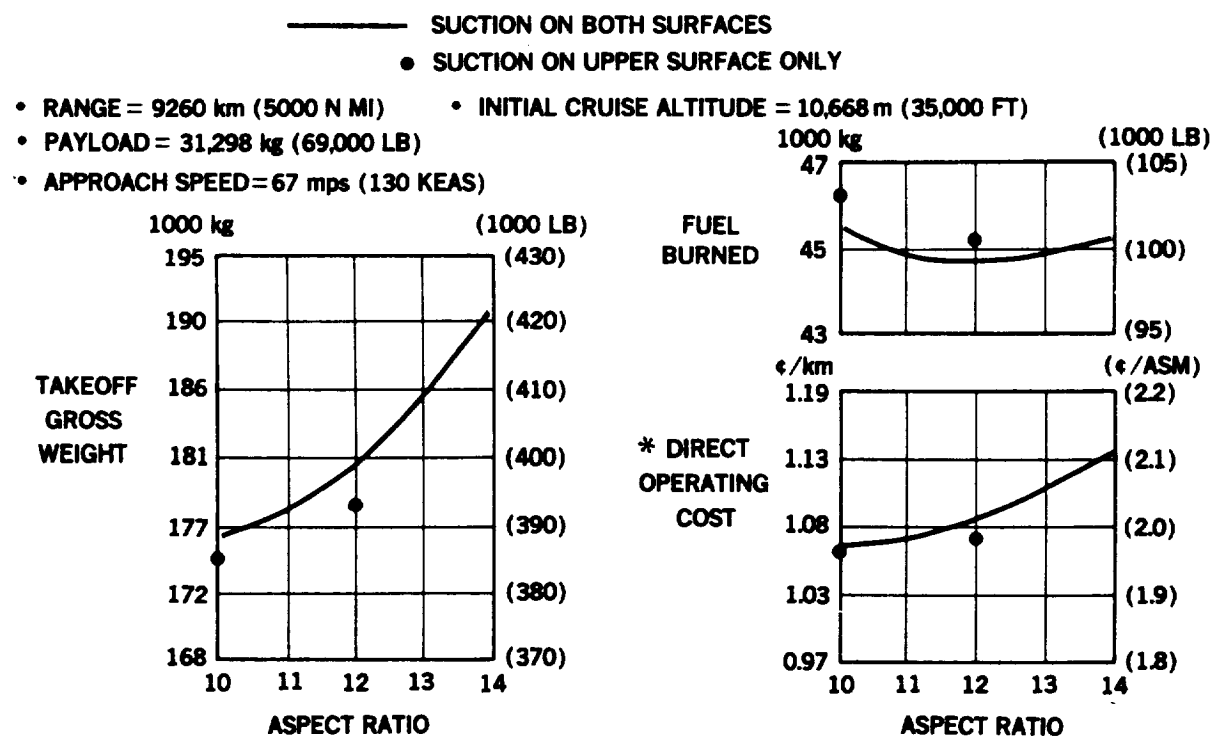

*NO ALLOWANCE FOR LOWER INITIAL AND MAINTENANCE COSTS FOR UPPER SURFACE ONLY

FIGURE 7-28B. ASPECT RATIO SIZING SUMMARY COMPARISON II

Table 7-1

Configuration and Performance Parameter Summary
Sized Aircraft
RANGE - 9,260 Km (5,000 NMI), PAYLOAD 27,215 Kg (60,000 LB)

	Suction Both Surfaces to 70% C	Suction Upper Surface Only To 85% C
Aspect Ratio	10	10
Initial Cruise Altitude m (ft)	10,670 (35,000)	10,670a (35,000)
Wing Area m^2 (ft^2)	311 (3,346)	288 (3,100)
Cruise C_L	.503	.504
$(t/c)_{ave}$	11.7	10.80
Operating Wt. Empty kg (lb)	90,115 (198,670)	87,965 (193,930)
Takeoff Gross Weight kg (lb)	176,275 (388,620)	174,905 (385,600)
Approach Speed m/s (KEAS)	67a (130)	63 (121.7)
Takeoff Field m (ft)	2,667 (8,750)	2,466 (8,090)
Thrust/Engine kg (lb)	13,599 (29,980)	13,608 (30,000)
Total Fuel Burned kg (lb)	45,917 (101.230)	46,847 (103,280)
Suction Engine Fuel kg (lb)	968 (2,134)	1,054 (2,323)
D.O.C. ¢/ASkm (NMI)b	1,065 (1,973)	1,059c(1.962)

a Critical sizing factor

b Fuel 45¢/Gallon

c Reduction of maintenance cost with one surface only not taken into account.

7.4 REFERENCES - AERODYNAMICS

7.4-1 Tranen, T.L.: Analysis and Design of Transonic Airfoils. Report No. MDC A3760, December 1975.

7.4-2 Cebeci, T.; Kaups, K.; Ramsey, J.; and Schimke, S.: A Two Point Finite Difference Boundary-Layer Method for Incompressible and Compressible Two-Dimensional and Axisymmetric Laminar and Turbulent Flows Including Infinite-Swept Wing. Douglas Report MDC J7986, September 1978.

7.4-3 Cebeci, T.: Calculation of Three-Dimensional Boundary Layers. I. Swept Infinite Cylinders Second Small Cross Flow. AIAA Journal, Vol. 12, p. 779.

7.4-4 Nenni, J.P. and Gluyas, G.L.: Aerodynamic Design and Analysis of an LFC Surface. Astronautics and Aeronatics, July 1966, pp. 52-57.

7.4-5 Eichelkrout, W.L.: LFC Aircraft Design Data: Section A-14 Ice Protection Systems. Northrop Report NOR-67-136, April 1967.

8.0 AERODYNAMIC TESTING

Aerodynamic tests conducted during the course of this contract consisted of two substantive test programs which are summarized in this section. The first series of tests were conducted to evaluate the relative aerodynamic smoothness, under conditions of applied suction, of candidate porous LFC surface materials. A second model test program was carried out to demonstrate that suction through a porous surface can sustain laminar boundary layer flow in a representative swept-wing flow situation, where cross-flow instability is a dominant cause of transition. Both test programs were conducted in the Douglas Low Speed Wind Tunnel.

8.1 AERODYNAMIC SMOOTHNESS TESTING

A test program was established to evaluate a variety of candidate surfaces with respect to suitability for application to laminar flow control. Tests were conducted to determine how inherent roughness (surface textures) and porosity characteristics affect boundary layer transition and the ability to maintain laminar flow.

8.1.1 Model Description and Installation

The model consisted of a two-dimensional panel incorporating a removable frame for mounting the porous test specimens. The panel had a total chord of 3050 mm (120 inches) and a thickness of 57 mm (2.25 inches) as shown in the installation diagram and photo, Figures 8-1 and 8-2.

The flat panel was constructed using stock-size square tubing to frame honeycomb areas covered with sheet aluminum. The leading edge section was a 10.2 degree wedge shape. The trailing edge incorporated a full span flap section.

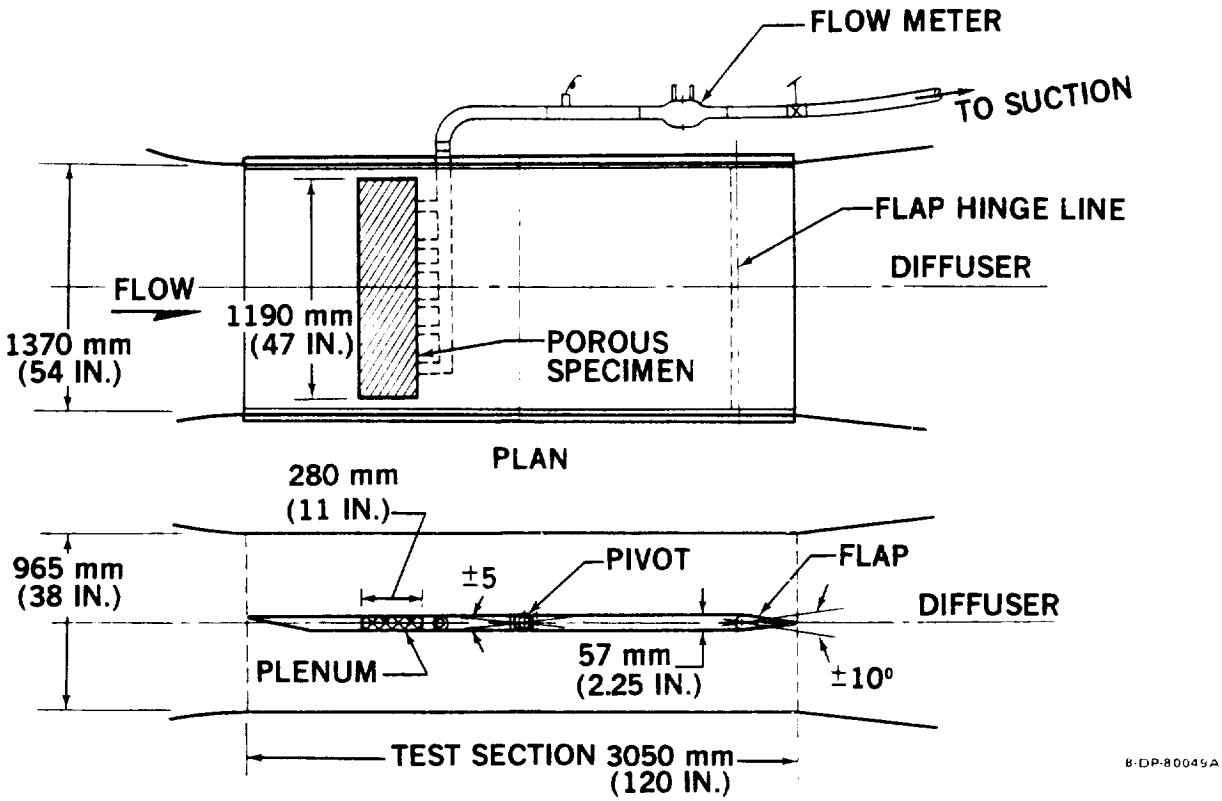

FIGURE 8-1. WIND TUNNEL MODEL TEST FOR LAMINAR FLOW WITH POROUS SURFACE SPECIMENS

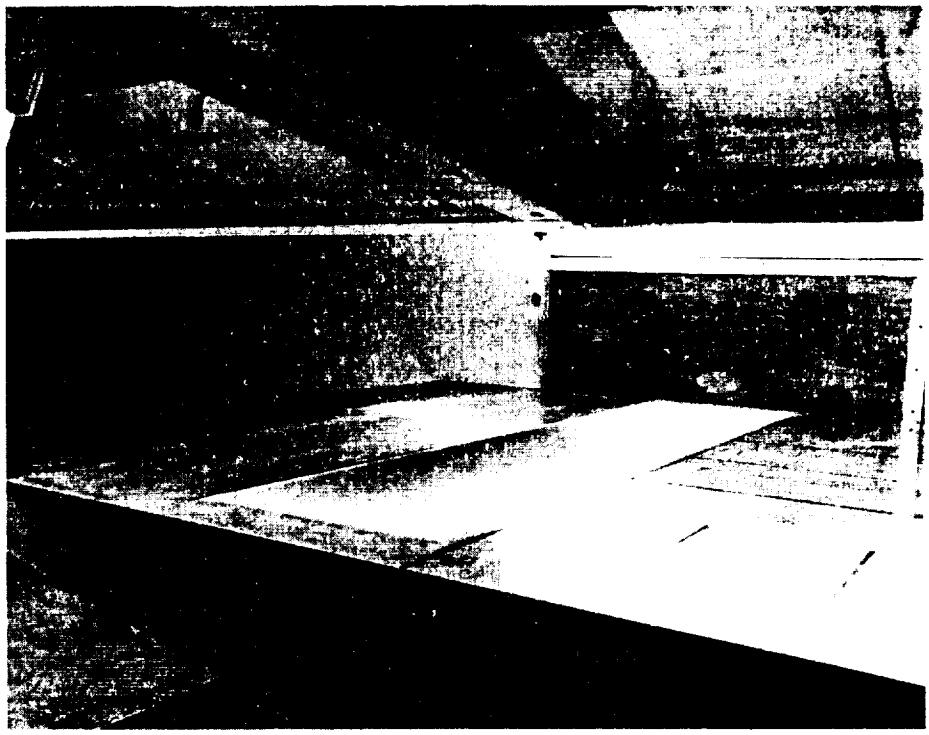

FIGURE 8-2. WIND TUNNEL MODEL INSTALLATION

The radiused nose shape and tangential flat surfaces of the flap formed a trailing edge angle of 11.5 degrees with a trailing edge thickness of 3.18 mm (.125 in). The flap hingeline was located at 90 percent of the panel chord and the flap was manually adjustable to ± 10 degrees deflection.

The panel could be rotated from the horizontal plane, pivoting at 50 percent of the chord length and was manually adjustable to ± 5 degrees of incidence to the tunnel stream. A seal was provided between the ends of the panel and the tunnel walls to prevent leakage and to allow rotational motion of the panel.

8.1.2 Test Specimens

Various 279 x 432 mm (11 x 17 in) effective suction area specimens of porous material were installed in the top surface of the panel between 20 and 30 percent chord. A plenum under the specimen allowed suction through the specimen for removal of air from the boundary layer. A removable cover plate in the bottom surface of the panel provided access for installation and adjustment of interchangeable specimens. The plenum was manifolded to provide an even distribution of suction flow.

Listed below are the surface panel specimens that were tested. Other materials were considered but only those tested are included here. Detail descriptions of the various surface materials and substructures are given in Sections 9.2.1 and 9.2.2.

1. Solid aluminum flat plate - reference surface for transition location without suction

2. Metallized Doweave

3. Sintered fiber metal on Doweave

4. Micro perforated plate (MPP) on Doweave Lockcore

5. Doweave

6. Porous Strips

7. Slotted aluminum

8. Peforated titanium

9. 50 x 250 Dynapore on Isogrid

10. 50 x 250 Dynapore on Honeycomb

11. 80 x 700 Dynapore on Honeycomb

12. 80 x 700 Dynapore (closed) on Honeycomb

13. 80 x 700 Dynapore (open) on Honeycomb

14. 80 x 700 Dynapore (modified) on Honeycomb

8.1.3 Testing Procedure

Due to the large blockage of this model in the tunnel it was necessary to determine the reference (actual) dynamic pressure in terms of the nominal standard tunnel reference pressures. This was done by relating the nominal tunnel dynamic pressure to that measured on a pitot static tube mounted on the tunnel center line at 30 percent chord and midway between the panel surface and tunnel ceiling. The resulting calibration showed that the actual tunnel dynamic pressure, with the model installed, was approximately 87.5 percent of the nominal value for the open tunnel.

Chordwise pressures were measured along the centerline of the model using a length of strip-a-tube attached to the upper surface of the model. The angle of attack and trailing edge flap deflection were adjusted until the stagnation point was on the upper surface and the pressure gradient was slightly favorable-to-neutral over the forward 80 percent of the chord. As indicated in Figure 8-3, a small negative incidence and flap deflection were required.

The solid flat plate was tested first to establish the transition location as a function of chord Reynolds number. This value was then used as a reference to compare the transition location for each of the various porous panels. The reference transition location is shown in Figure 8-4. Testing was conducted with one and three screens installed in the tunnel settling chamber in order to evaluate the effect of the tunnel turbulence level. With three screens in place, the maximum tunnel dynamic pressure obtainable was limited to 1.436 kP (30 lb/ft^2). Most of the testing was therefore done with only a single screen installed.

Transition location was identified by means of a hot-film sensor probe giving a signal which was displayed on an oscilloscope and projected audibly from a speaker. Typical visual display results are shown in Figure 8-5. Transition was identified by judging, insofar as possible, a 50-50 distribution of laminar and turbulent signals in the oscillograph trace. Measurements based upon the visual signal were more consistent than those using only an audio reference. In several instances, Tollmein-Schlichting waves were detected. The resulting signal exhibited a regularity as indicated in Figure 8-5(B) and a distinct high pitched humming sound could be heard on the audio output. This phenomenon is related to the most amplified frequency in the initial transition process, which persisted over a sufficient region to be identified with the hot film sensor.

Each porous specimen was tested by varying the suction flow rate from zero to a maximum corresponding to a flow coefficient, C_Q, value of approximately 0.005. Transition location was determined for several values of C_Q at Reynolds numbers varying from approximately 5.0×10^6 to 11×10^6. Reynolds number variation was accomplished by changing tunnel speed (dynamic pressure). Transition location was considered to be the aft-most point where the boundary layer was observed to change from laminar to turbulent flow. Generally, transition occurred along a slightly irregular spanwise line which was the result of many turbulent wedges finally merging.

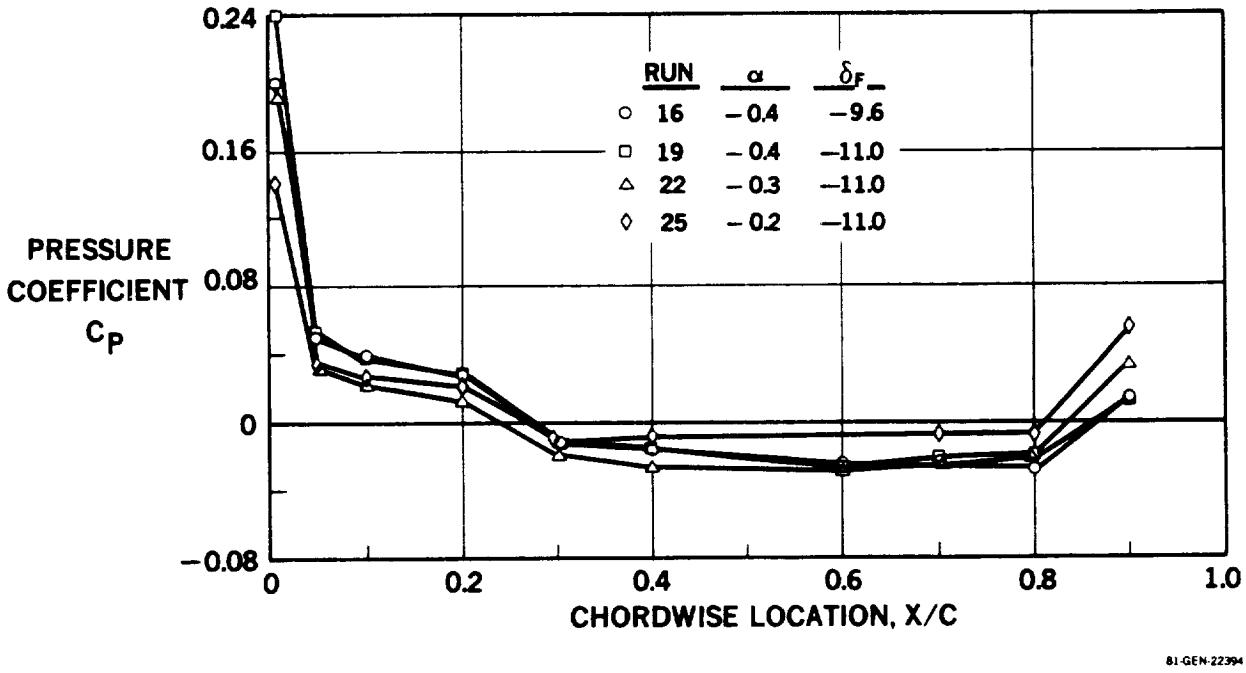

FIGURE 8-3. WIND TUNNEL MODEL – SOLID SURFACE PRESSURE DISTRIBUTION

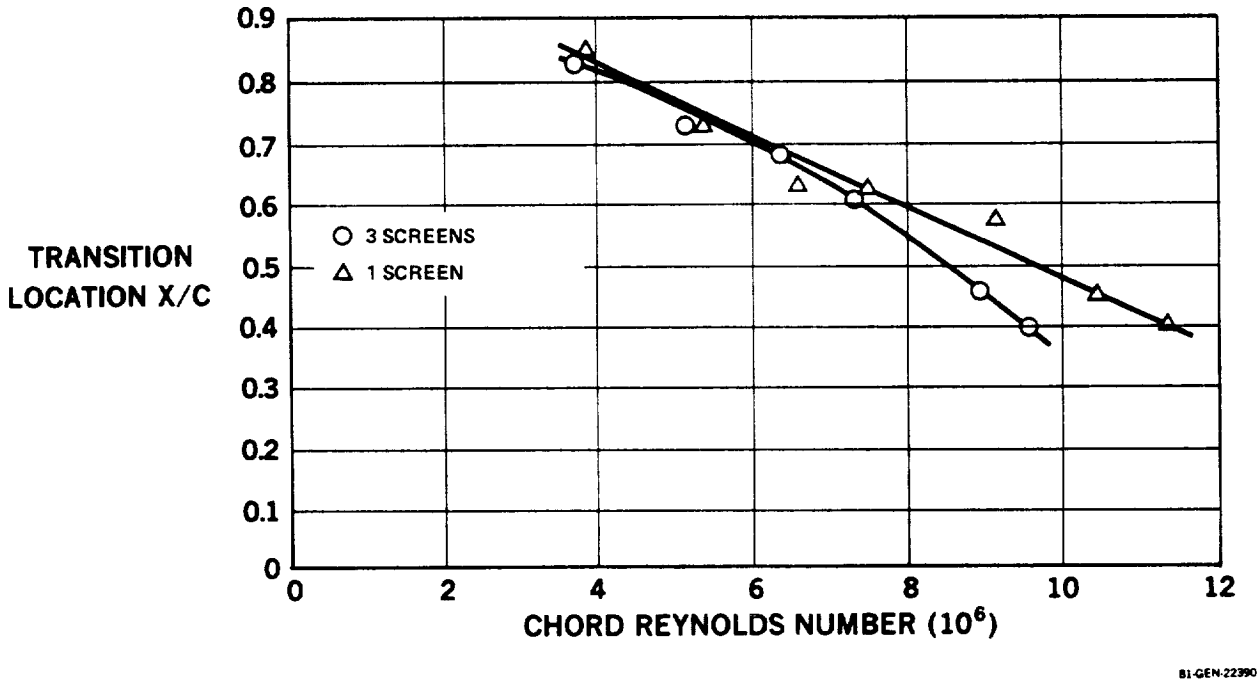

FIGURE 8-4. TRANSITION LOCATION ON WIND TUNNEL MODEL – SOLID PLATE SURFACE

8.1.4 Test Results

Typical results of transition surveys are shown in Figure 8-6 which gives transition location (X_{TR}/C) versus suction coefficient (C_Q) at different chord Reynolds numbers for one surface. Solid symbols denote the reference transition location on the smooth solid surface at the corresponding chord Reynolds number. It should be noted that C_Q is presented on a logarithmic scale. The zero suction and reference transition locations are plotted along the vertical axis.

Comparison of the zero suction and reference transition locations indicates the combined effect of the porous surface texture (roughness) and any inflow/outflow that might be present. Since the pressure gradient is essentially zero in the region of the porous panel, the principal cause in this decrement is assumed to be the surface roughness. The condition of aerodynamic smoothness is defined as occurring when the transition location, with suction applied, is downstream of the reference transition location at the same Reynolds number.

Extension of transition farther downstream as suction is increased provides an indication of the effectiveness of the suction and the amount of suction flow required to maintain laminar flow in the boundary layer. A brief review of results is given below.

Metallized Doweave - The Doweave Specimen did not achieve aerodynamic smoothness at any level of applied suction. It was considered unsatisfactory.

Sintered Fibermetal on Doweave - This specimen achieved some extension of laminar flow with moderate suction ($C_Q > .0001$). However, due to mediocre aerodynamic performance combined with difficult structural features, this material was not considered further.

Microperforated Plate (MPP) on Lockcore - The specimen had a wavy surface originating in the Lockcore truss pattern of the substructure. The results

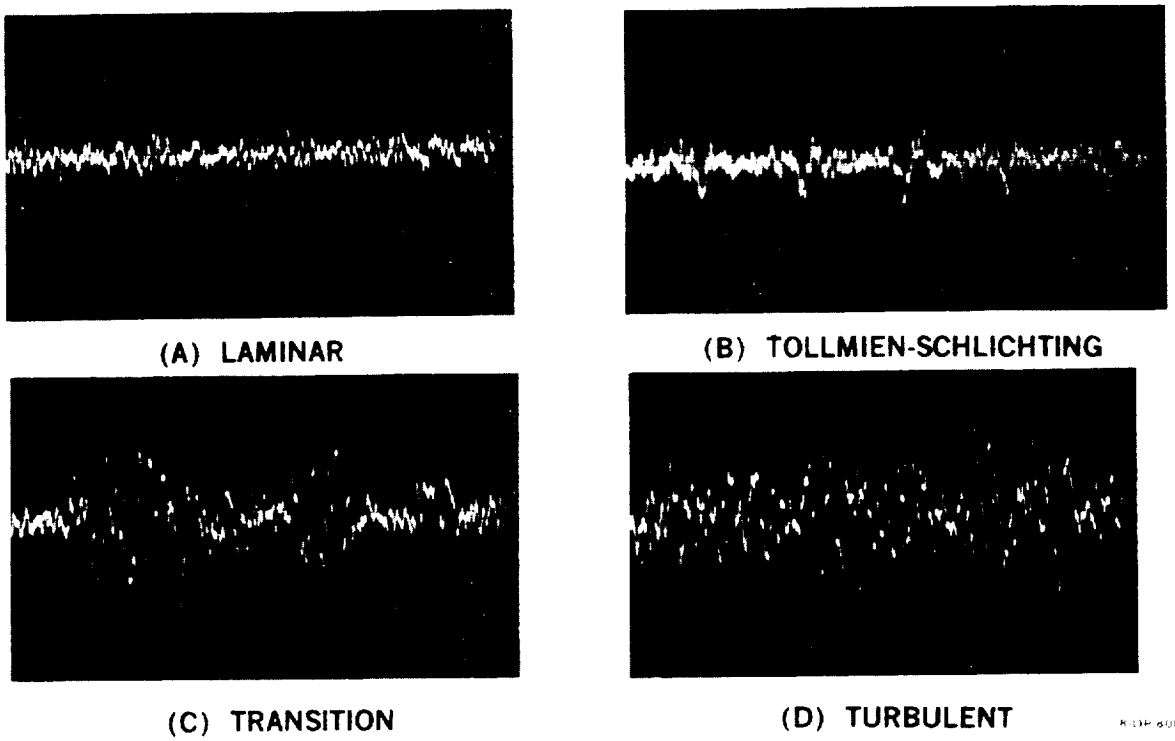

FIGURE 8-5. BOUNDARY-LAYER SIGNATURES – PROBE SIGNAL DISPLAYED ON OSCILLOSCOPE

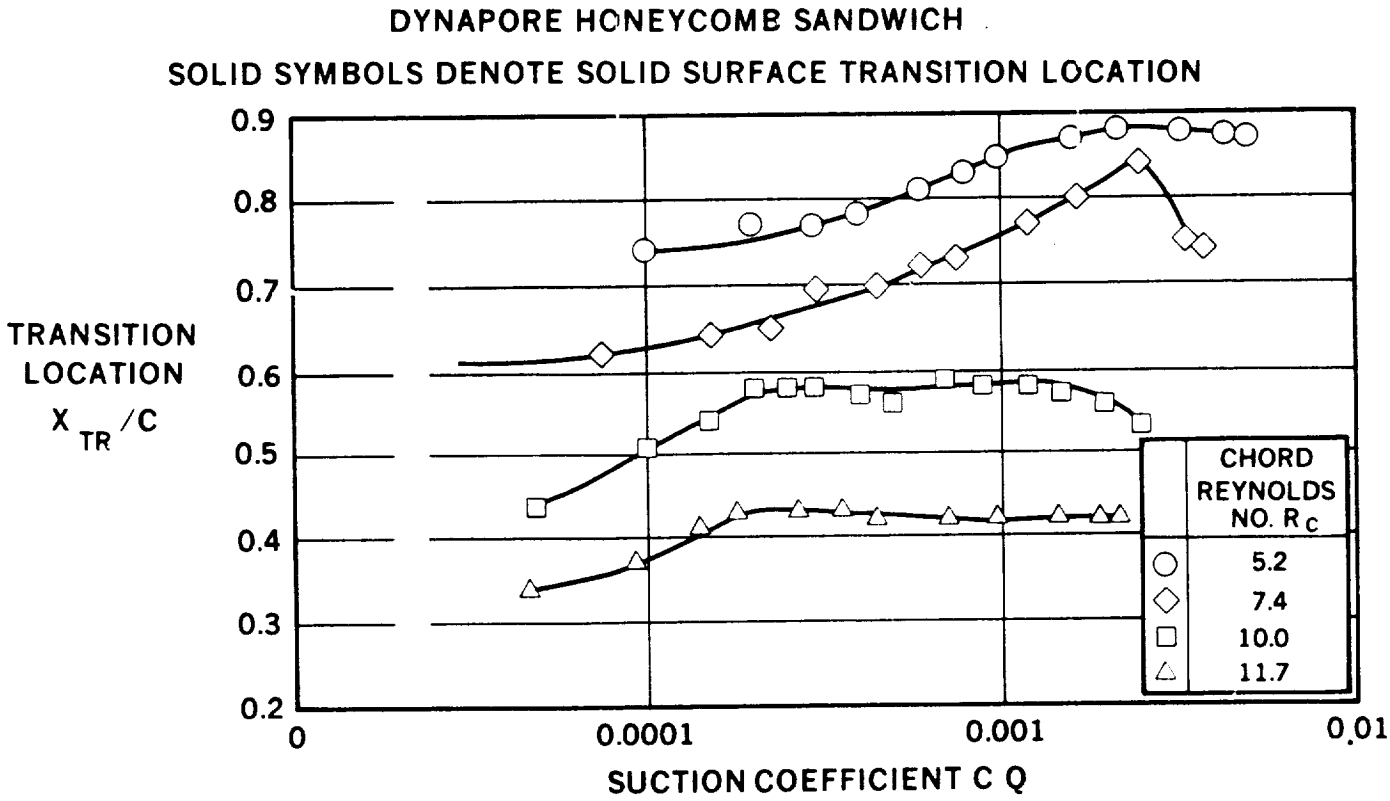

FIGURE 8-6. TYPICAL WIND TUNNEL RESULTS – TRANSITION LOCATION

with suction applied indicated that a satisfactory level of laminar flow could be attained, however, significantly higher suction flow was necessary compared with other specimens tested.

Doweave - This specimen was similar to the metallized Doweave and was unsatisfactory. Although it achieved aerodynamic smoothness at moderate suction values it was subject to complete loss of laminar flow with higher suction flow.

Porous Strips - The porous strip specimen consisted of a Dynapore surface over honeycomb sandwich with nonporous adhesive bonding the Dynapore to the honeycomb. Four porous strips 3.3 mm (0.13 in) wide, were located on the panel. These strips were separated by 72.9 (2.87 in) wide nonporous strips purposely blocked with adhesive. Test results for this specimen indicated that it was effectively smooth with moderate suction coefficients, although at higher suction flows the transition distance was reduced significantly. This was attributed to deflection of the panel surface due to the high pressure differential across the panel, rather than to over-suction. As configured without adequate surface support, this specimen was considered unsatisfactory, however, subsequent tests of the swept wing model with a more substantial sublayer showed very favorable result with porous strips.

Slotted Aluminum - A slotted specimen was included for comparative purposes. This panel had 0.127 mm (0.005 in) wide slots spaced 76.2 mm (3.0 in) apart. Thus the slots were arranged at approximately the same spacing as the preceding porous strips. Performance of the slotted specimen was satisfactory. Transition was delayed to almost 0.8 chord at moderate suction coefficient (C_Q = 0.0017). However, this specimen was sensitive to over suction flows, which caused transition.

Perforated Titanium - Perforated titanium specimens were constructed from .635mm (0.025 in) titanium sheet which had been perforated using an electron beam technique. Holes were nominally .102 mm (0.004 in) diameter and were spaced 1.02 mm (0.04 in) apart in an equilateral triangular pattern. Ribs were provided to support the panel within the frame and minimize distortion of the surface.

Aerodynamic performance of the perforated titanium was satisfactory. Transition was moved farther aft with increasing suction to the maximum suction applied. It was noted in several instances that small foreign particles were caught and held on the surface by the suction through the perforation. The turbulent wedge resulting from the particle disturbance persisted downstream. This phenomenon was alleviated on subsequent testing of the perforated titanium leading edge on the swept wing model by having the perforations elongated to approximately twice the nominal hole diameter. The elongated hole was presumed to be less likely to entrap passing particles in the airstream.

Later development in electron beam perforation technology has produced high quality perforated titanium with a nominal hole diameter of .0635 mm (0.0025 in). This advance in the state-of-the-art appears to have eliminated the contamination problem.

Dynapore - Several Dynapore specimens were tested. The coarser textured 50 x 250 Dynapore surface material was bonded to Isogrid and honeycomb supporting substructures while the 80 x 700 Dynapore material was tested on honeycomb substructure only. Both 50 x 250 Dynapore specimens performed satisfactorily. The 80 x 700 Dynapore specimen with honeycomb substructure had quite irregular porosity due to excessive bonding adhesive. This condition very likely contributed to the susceptibility of the panel to oversuction.

Testing of Dynapore specimens was concentrated subsequently on those having the 80 x 700 surface material. The finer weave of this material provided a smoother surface. However, the finer weave also results in lower strength and stiffness of the porous surface. In order to stiffen the 80 x 700 Dynapore surface, a sublayer of 80 x 80 Dynapore was fusion bonded to the basic surface. Later, since the surface was still more open than desired and to further increase surface strength and stiffness, a perforated fiberglass sublayer (40 percent open) was added beneath the Dynapore layers. The perforated fiberglass sublayer was divided into three spanwise segments with

each segment having different diameter holes 3.18, 4.76, and 6.35 mm, (1/8, 3/16, and 1/4 in), respectively. This was done to determine whether the size of the holes in the sublayer would have any effect upon laminarization of the boundary layer flow. The surface performed satisfactorily and no effect of hole size in the sublayer was detected.

A brief evaluation of the effects of surface damage was made on the last Dynapore specimen tested. Several severe depressions were made in the surface using a spherical tool. In each case a turbulent wedge occurred behind the depression. Laminar flow was restored by simply filling the depressions with tunnel wax and smoothing the surface.

It was determined from tests of these specimens that: (1) Dyanpore is a satisfactory porous surface material for laminar flow control, and (2) within the range of hole diameters tested, there was no observable effect of sublayer hole diameter on the laminar flow or transition location.

A summary of these results is presented in Figure 8-7. Comparative effectiveness for several candidate LFC surfaces is shown for a chord Reynolds number of 8.8×10^6. As a result of these tests, it was concluded that only the 80 x 700 Dynapore and the perforated titanium should be considered further as practical surface materials for laminar flow control using distributed suction through a porous surface. At this point in the program it appeared that Dynapore offered the most promise of successful LFC application because of the limit on the smallest hole diameter available from the electron beam perforation process. Subsequent improvements in the perforation process and the results of subsequent swept-wing model test described in Section 8.2 following, have changed this position significantly and perforated titanium is now the preferred LFC surface.

8.2 SWEPT WING WIND TUNNEL TESTS

The second test program conducted as part of the LFC contract involved testing a swept-wing model in the Douglas Long Beach Wind Tunnel facility. This test program was a cooperative effort in which Douglas IRAD resources provided for design and construction of the basic models and NASA contract funds supported testing and data analysis.

The swept-wing model test was directed toward the primary objective of demonstrating the ability to sustain laminar flow, using suction through a porous surface, under representative full-scale swept-wing flight conditions including practical treatment of surface anomolies such as panel joints. In particular, it was important to demonstrate laminar flow control in the presence of instabilities which are prevalent on a swept wing; namely, cross-flow instability and those resulting from the flow along the attachment line. The basic test provided the demonstration desired first with an all Dynapore LFC surface and then with a perforated titanium leading edge surface. Subsequent testing of the leading edge insert panels was done to evaluate the performance of improved perforated titanium surface material relative to the alternative Dynapore surface. This evaluation was done using an improved substructure which did not require sewing of the fiber glass cloth during fabrication.

Secondary objectives of the swept wing model test included: (1) evaluation of suction requirements relative to analytical criteria, (2) investigation of effects of surface anomolies, panel joints, etc., and (3) development of fabrication techniques applicable to full scale surface panel construction. A description and summary of the swept wing wind tunnel model design is presented in the following paragraphs:

8.2.1 Model Design

In order to provide representative swept wing flow for testing the laminar flow control surface, a large chord model was required. This necessitated the use of special design procedures because of the limited size of the Douglas

Low Speed Wind Tunnel test section which was .965 x 1.372 m (38 x 54 in). The design procedure used to develop the model profile and sidewall fairings is outlined below:

1. The desired pressure distribution was selected from previous airfoil design work for the LFC aircraft configuration. This pressure distribution is shown in Figure 8-8. Although the design pressure distribution shown is for Mach 0.8, this upper surface pressure distribution was selected so that the appropriate pressure profile would exist throughout the LFC test region on the upper surface of the model.

2. Development of the airfoil shape for the model was accomplished using 2-D methods (Tranen, Ref. 7.4-1, and Neumann, Ref. 8.3-1) to obtain the desired upper surface pressure distribution in the presence of the test section floor and ceiling. Numerous iterations were necessary to achieve the required normal profile shown in Figure 8-9. The resulting normal pressure distribution (Figure 8-10) illustrates the strong effects of the tunnel wall restraint and the compromise imposed on the lower surface pressure distribution. It is obvious that the resulting airfoil is relatively thick and causes tunnel blockage of approximately 28 percent.

   Fortunately, the distortion of the lower surface pressure distribution is such that the section lift and resulting structural loads on the model and support structure are reduced.

3. Sweep angle - Originally, variation of sweep angle was considered in order to achieve an attachment line Reynolds number (R_θ) greater than 100. However, the length of the tunnel test section precluded consideration of sweep angles greater than 30 degrees. Reducing sweep would necessitate further increases in airfoil thickness to obtain the increase nose radius required. This was deemed advisable since the airfoil was already inordinately thick. The predicted value of R_θ for this profile at 30 degrees sweep was approximately 90 and it was possible that contamination from the tunnel wall

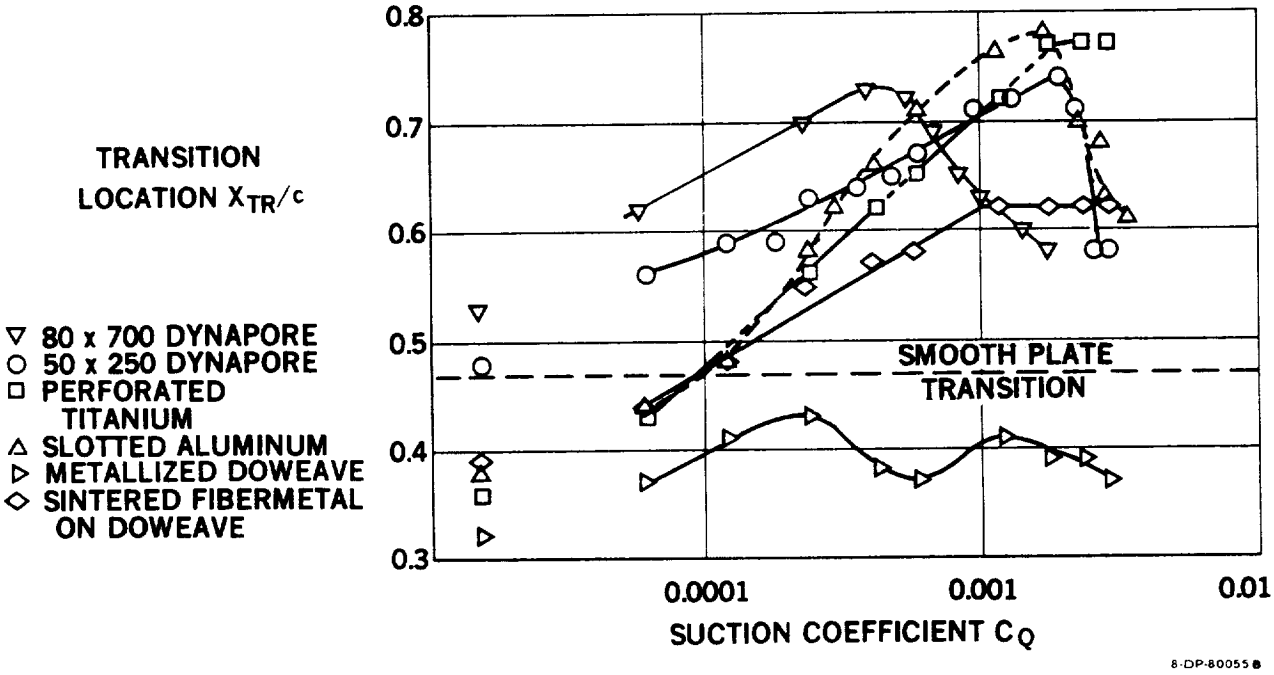

FIGURE 8-7. COMPARATIVE EFFECTIVENESS OF LAMINAR FLOW CONTROL SURFACES

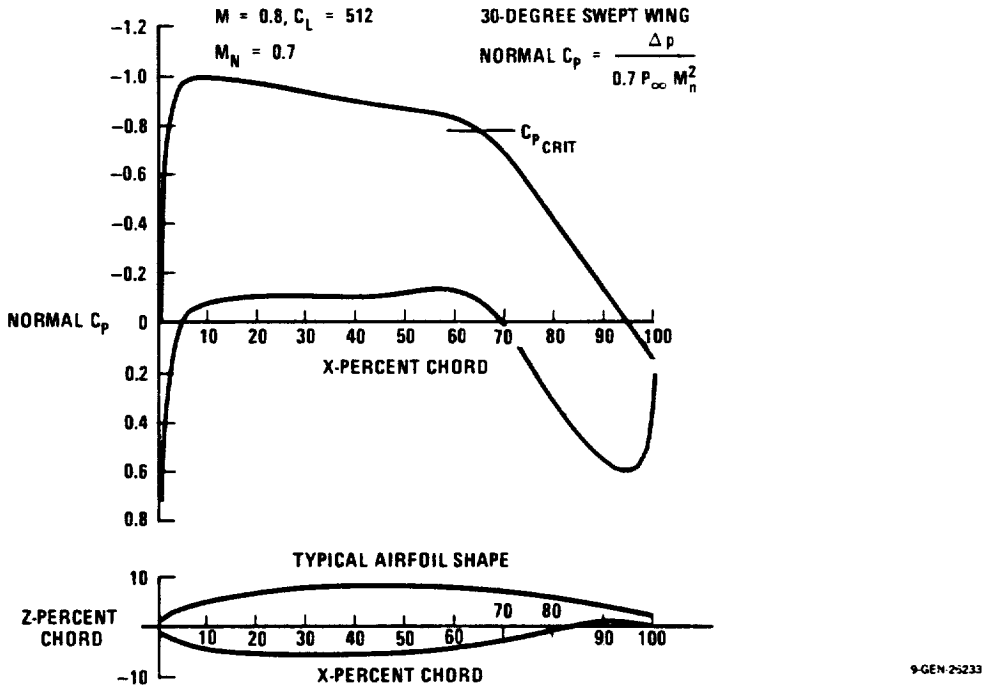

FIGURE 8-8. SWEPT-WING MODEL TEST – REPRESENTATIVE CHORDWISE PRESSURE DISTRIBUTION

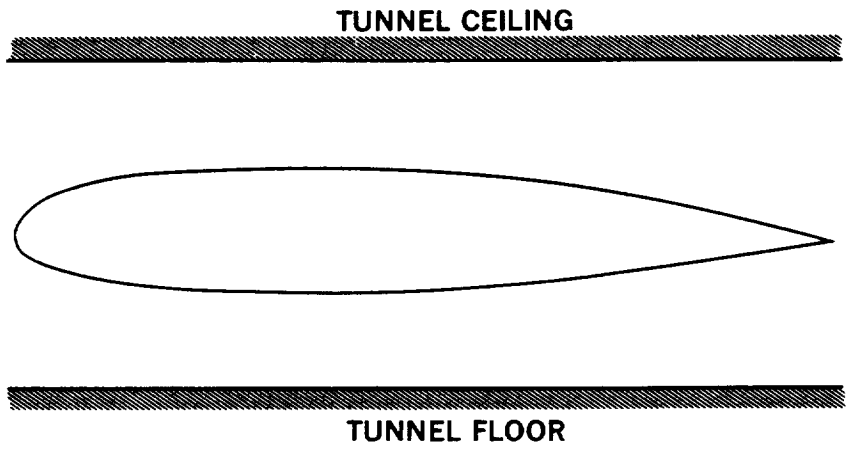

9-GEN-26237

FIGURE 8-9. SWEPT-WING MODEL – AIRFOIL PROFILE IN WIND TUNNEL

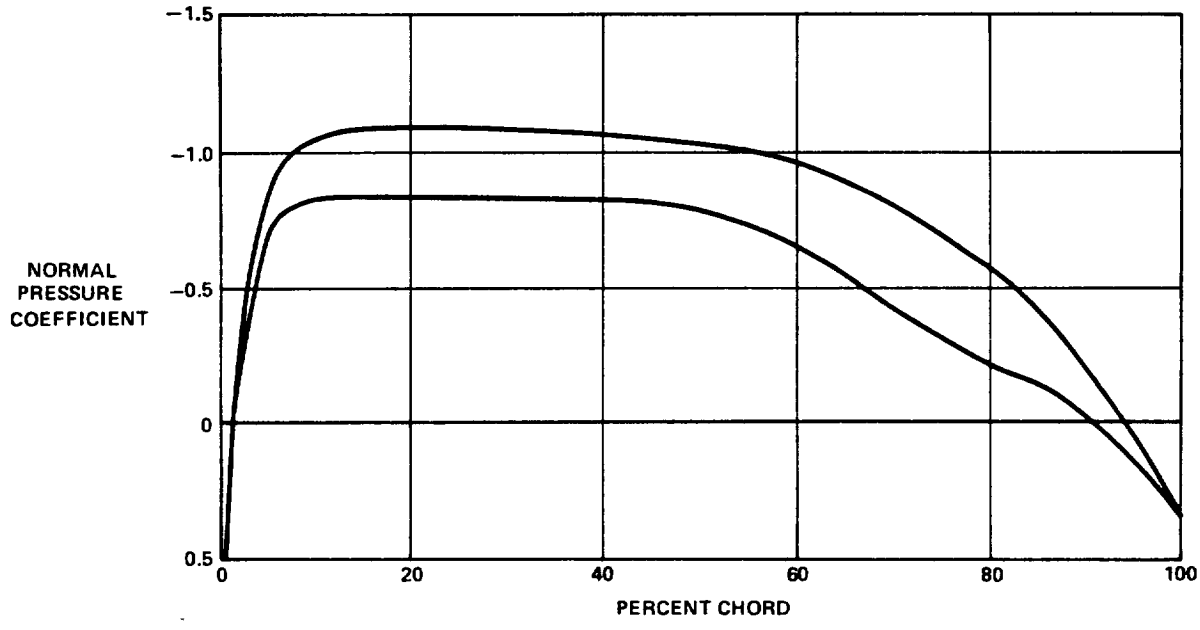

9-GEN-26208

FIGURE 8-10. SWEPT-WING MODEL – CHORDWISE PRESSURE DISTRIBUTION OF AIRFOIL INSTALLED IN TEST SECTION

boundary layer would be sufficient to excite boundary layer instability along the attachment line; it was therefore decided to proceed with the model design using the profile as defined with a sweep angle of 30 degrees.

4. Suction Requirement - Suction velocities for the swept wing model were determined using the X-21 boundary layer stability criteria. Estimated suction requirements for a nominal dynamic pressure 2.15 kPa (45 psf) are presented in Figure 8-11. Cross flow instability establishes the suction level required over the forward 18 percent chord of the model and over the pressure recovery region aft of approximately 65 percent chord. In between the forward and aft steep pressure gradient regions, the suction is determined by the streamwise Tollmein-Schlichting instability criterion.

5. The first step in the development of the tunnel sidewall fairings was to calculate streamline traces for the infinite yawed wing profile, in the presence of the tunnel floor and ceiling, at several vertical stations. After comparison of the streamlines, the one passing through the station 0.005c above the crest of the upper surface was selected as the reference streamline. This streamline is shown in Figure 8-12. The three-dimensional analytical method (Ref. 8.3-1) and computing program (Ref. 8.3-2) were used for these computations.

Verification of the significant influence of the tunnel wall contour is shown in figure 8-13 where the pressure distributions on the upper surface of the model are shown for these spanwise stations. Three-dimensional Neumann calculations were made for the swept wing in the wind tunnel with both straight sidewalls, and with the sidewalls contoured two-dimensionally corresponding to the reference streamline. With straight sidewalls, at the inboard station the pressure peak is suppressed while at the outboard station it is accentuated. The distortion of the pressure profile would be intolerable without contoured walls in the test section.

Practical contouring of the test section sidewalls involved further compromise as illustrated in Figure 8-14. Obviously, the reference streamline, extended two-dimensionally from tunnel floor to ceiling and when translated to be

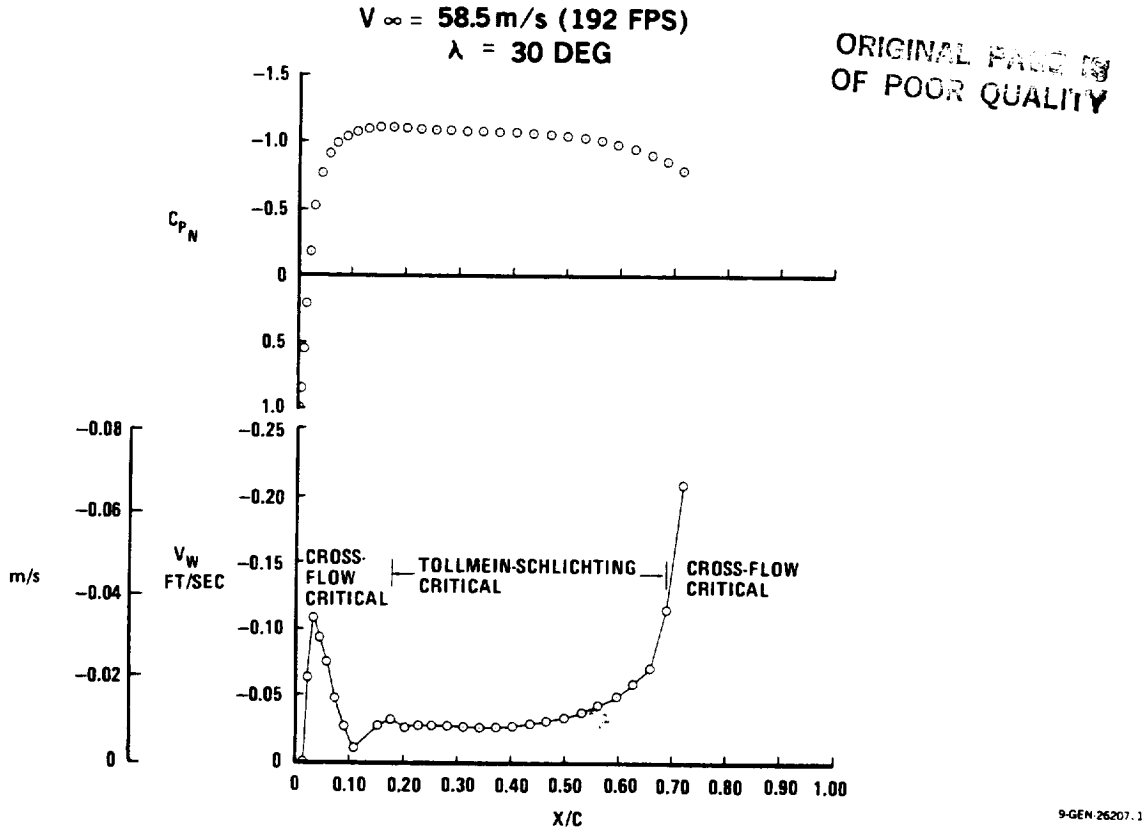

FIGURE 8-11. SWEPT-WING MODEL – UPPER SURFACE PRESSURE DISTRIBUTION AND SUCTION VELOCITY

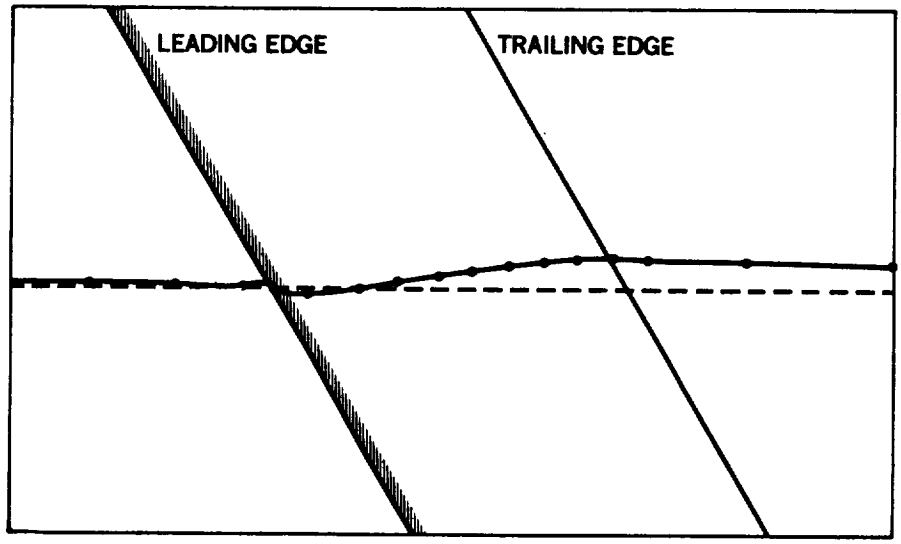

FIGURE 8-12. SWEPT-WING MODEL TEST – REFERENCE STREAMLINE ON UPPER SURFACE-INFINITE YAWED WING

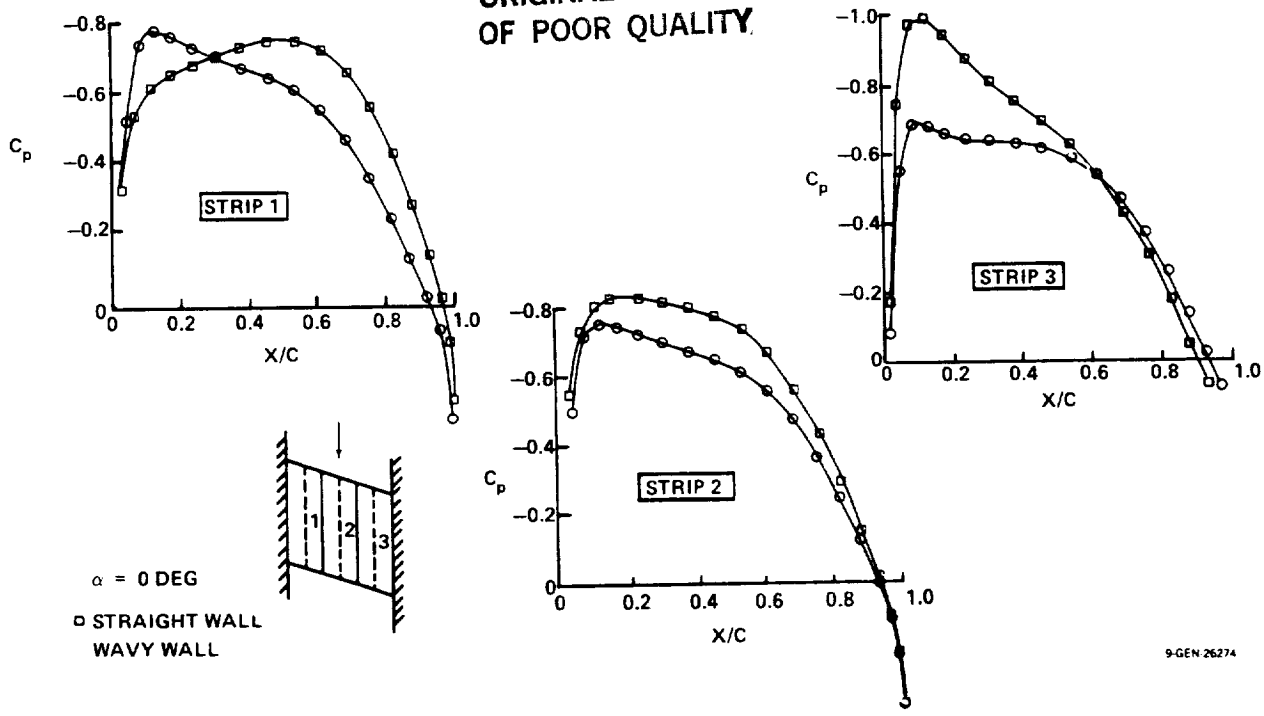

FIGURE 8-13. SWEPT-WING MODEL TEST – EFFECT OF TUNNEL SIDEWALLS ON PRESSURE DISTRIBUTION – WITH SIDEWALLS SHAPED TO MATCH REFERENCE STREAMLINE

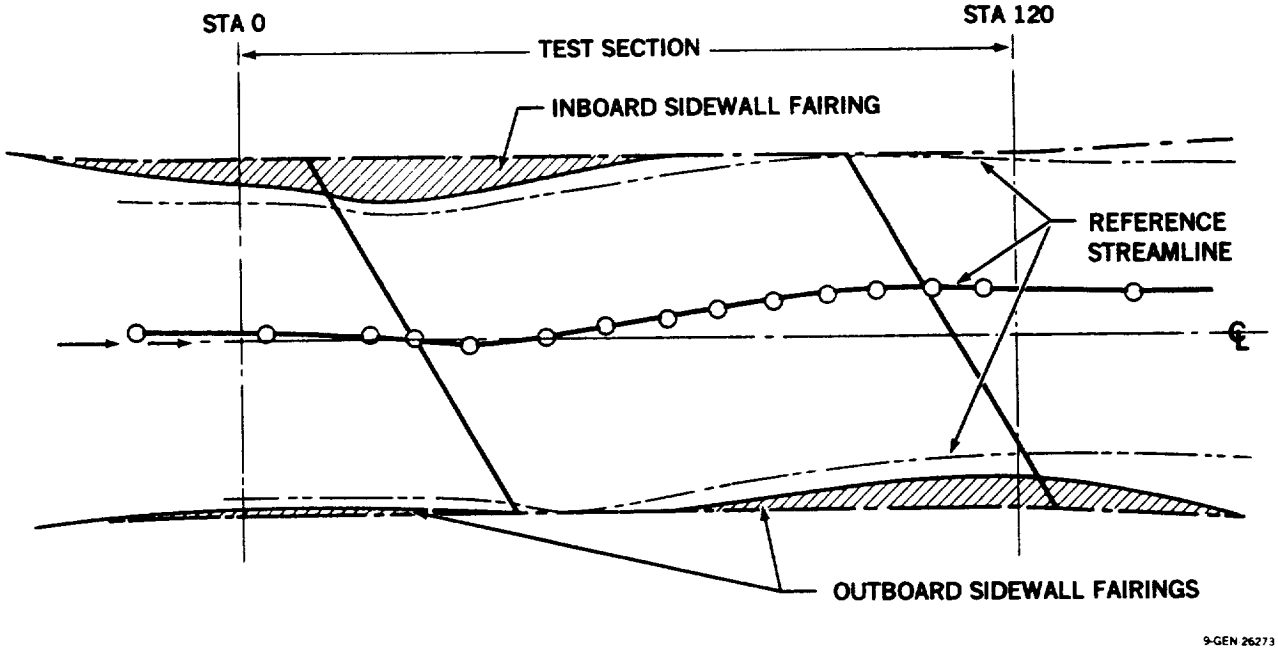

FIGURE 8-14. SWEPT-WING MODEL TEST – SIDEWALL FAIRING DEVELOPMENT

tangential to the test section sidewalls, cannot be reconciled with the tunnel contraction upstream and the diffuser downstream. Hence, the sidewall fairings indicated by the cross-hatched areas in Figure 8-14 were faired using experienced and intuitive judgment. As shown later in Section 8.2.3, the results were satisfactory.

8.2.2 Model Description and Installation

a) The basic model, as noted previously, was a two-dimensional, thirty degree, swept wing. The chord was 1.8 m (6 ft) normal and 2.11 m (6.93 ft) streamwise; the thickness/normal chord ratio was 0.1504. Leading-edge and upper-surface panels were removable as illustrated in Figure 8-15. 15-percent chord, simple trailing edge trim flaps were provided as a means of adjusting the pressure level without having to pitch the entire model. The trim flaps were in three segments so that differential setting could be used to adjust the flow and provide a uniform spanwise pressure distribution. This adjustment was used to compensate for the compromise involved in the design of the sidewall fairings. The basic model structure was built up from aluminum spars and ribs as pictured in Figure 8-16. Aluminum and fiberglass sheet material was used for the non-removable sections of the model surface.

   The LFC test surface extended from below the leading edge at 0.036 chord to 0.70 chord on the upper surface. The juncture between the leading edge panel and the upper surface panel was located at the model front spar (0.18 chord). Non-porous panels were installed for initial testing of the model so that chordwise and spanwise pressure distributions could be obtained and the natural transition of the boundary layer determined. This was used to provide a reference of transition location on a smooth surface and to measure and adjust the surface pressures on the model to the required levels. The Dynapore surface was not amenable to the installation of static pressure orifices and its surface texture, plus its porosity, could not provide a reliable reference for boundary layer transition.

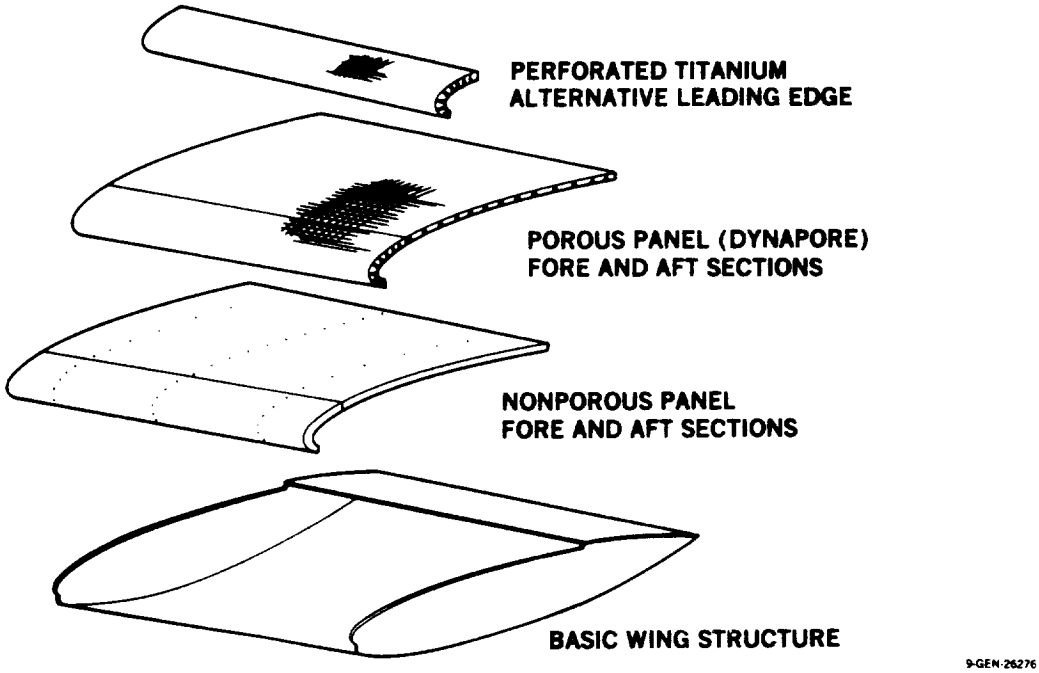

FIGURE 8-15. SWEPT-WING MODEL – COMPONENTS

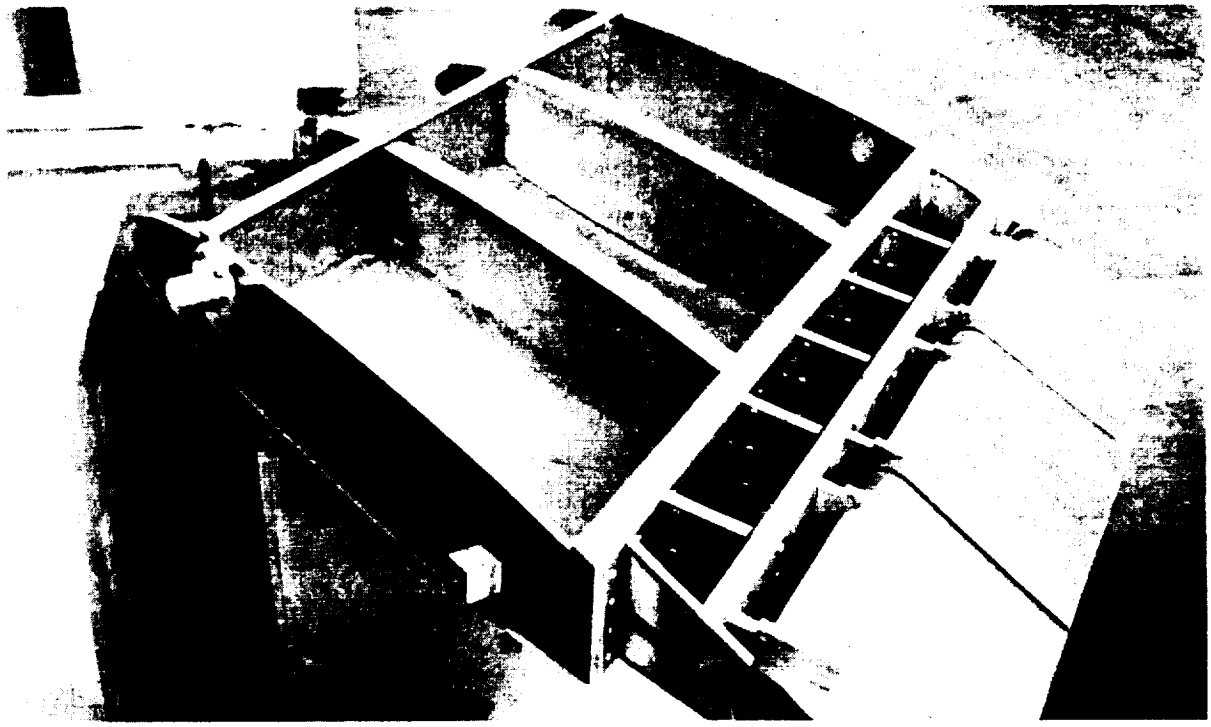

FIGURE 8-16. SWEPT-WING MODEL – BASIC STRUCTURE

The porous surface used initially for testing laminar flow control was Dynapore having an 80 x 700 outer layer diffusion bonded to an 80 x 80 sublayer. This was supported by a fluted fiber-glass substructure which also formed spanwise plenums for the suction system. Due to the high porosity of the Dynapore selected for ease of liquid clearance from the surface, an additional porous fiber-glass metering layer was inserted between the Dynapore and the supporting sublayer. The latter consisted of punched fiber-glass having 6.35 mm (0.25 in) diameter holes distributed to provide a 40-percent open sheet and provided support for the porous surface between the flutes nodes. There were 21 flutes in the leading edge panel and 16 wider flutes in the upper surface panel. On the leading edge panel the nominal distance between node lines (i.e., flute width at the surface) was approximately 17.8 mm (0.70 in). For the panel over the mainbox this dimension was approximately 57 mm (2.25 in). The panel structure buildup is illustrated in Figure 8-17 and a photograph of the Dynapore porous panels is presented in Figure 8-18. The latter shows the suction tubes extending beyond the ends of each plenum. Figure 8-19 shows the basic model during fitting of the upper surface panel.

The alternative leading edge panel utilized a similar substructure. However, the surface material was 0.635 mm (0.025 in) perforated titanium. Perforation of the titanium was by an electron beam process which provided elongated holes, nominally 0.102 x .203 mm (0.004 by 0.008 in), spaced 1.27 mm (0.050 in) along rows. A close-up photograph of the perforated titanium leading edge surface is shown in figure 8-20 and the titanium surfaced leading edge panel is pictured in figure 8-21.

It should be noted that in the construction of the basic model and LFC porous panels, structural joints, welded seams, and the like were to production standards rather than using laboratory or research quality methods. This was in keeping with the primary objective of the test, that was intended to demonstrate LFC under conditions as realistic as possible. A description of the structural design and development of the LFC surface is presented in Section 9.9.

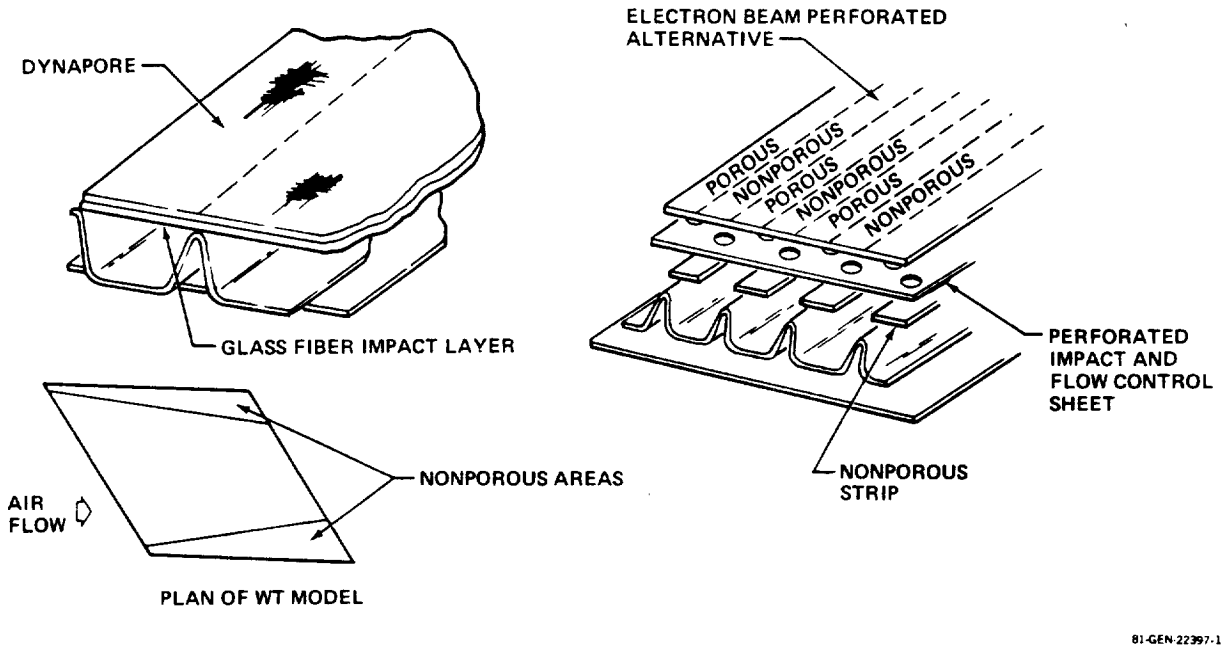

FIGURE 8-17. WIND TUNNEL MODEL – POROUS PANEL CONFIGURATIONS

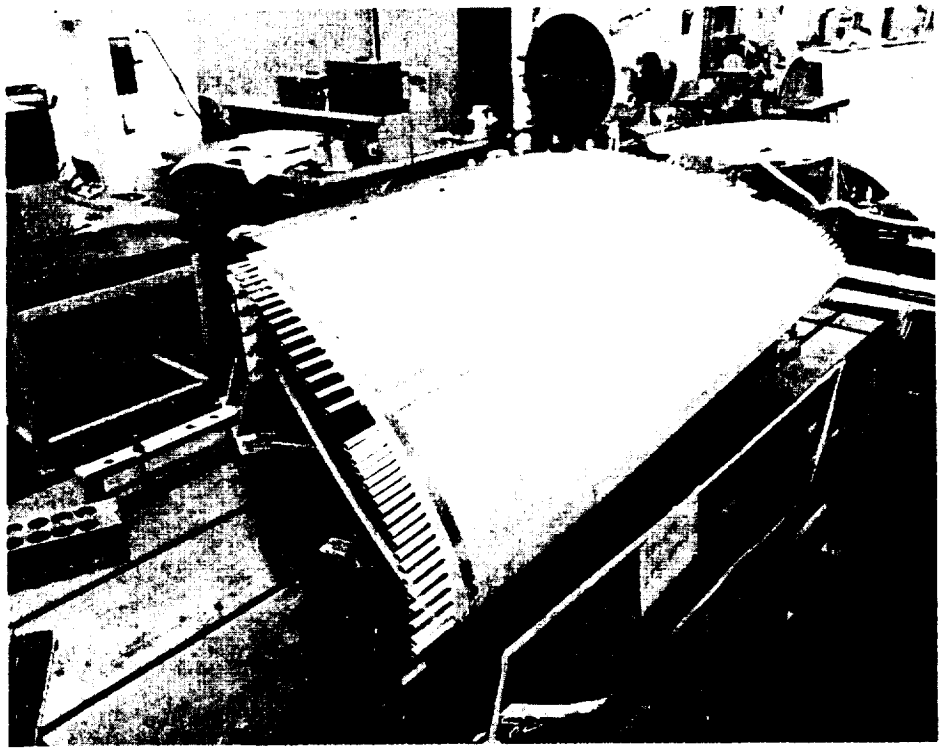

FIGURE 8-18. SWEPT-WING WIND TUNNEL WITH DYNAPORE POROUS SURFACE

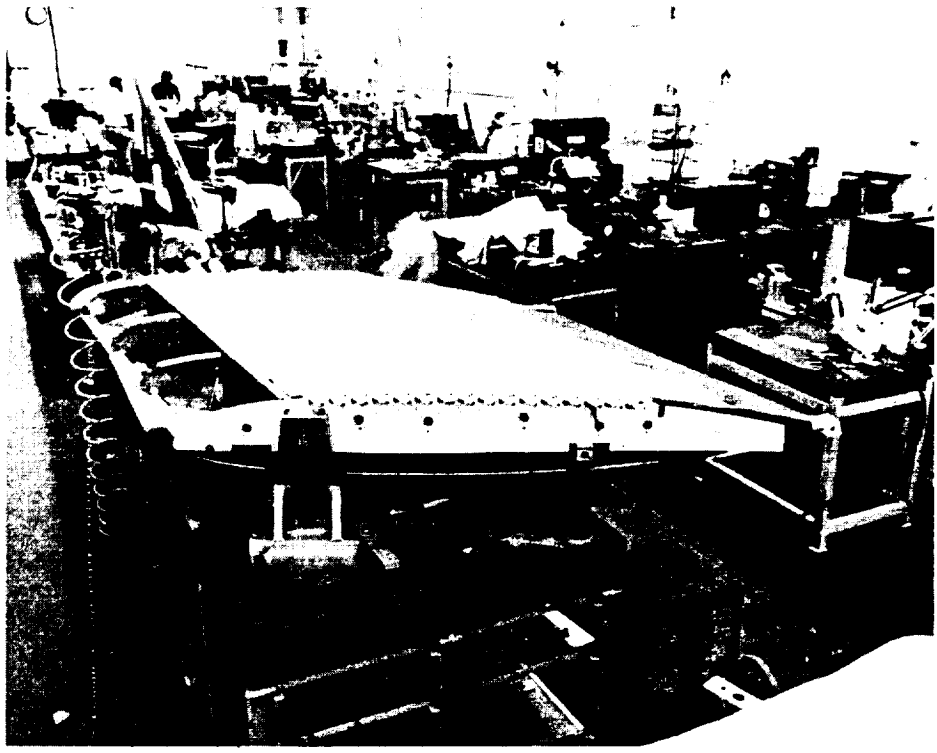

FIGURE 8-19. SWEPT-WING MODEL WITH UPPER POROUS PANEL INSTALLED

FIGURE 8-20. PERFORATED TITANIUM SURFACE NEAR FRONT SPAR JOINT SHOWING NONPOROUS REGION AND WELDED JOINT

Installation of the model with the nonporous panels in the Douglas Low Speed Wind Tunnel is shown in Figures 8-22 and 8-23. These photographs emphasize the size of the model relative to the wind tunnel test section. The test section sidewall fairings were constructed of thin aluminum sheet supported by wooden ribs which were placed horizontally along the sidewalls. The sidewall fairings were fitted into place after installation of the basic model. A plexiglass ceiling was provided with small ports for inserting the transition probe. Figure 8-22 shows the sidewall window used for observation and probing of the leading edge attachment line region.

The suction for the test was provided by an electrically driven vacuum pump. A schematic of the suction system is shown in Figure 8-24 and a photograph of the installed suction systems is shown in Figure 8-25. Individual plenums were connected to the secondary manifolds by 12.7 mm (1/2 inch) plastic tubing. These manifolds allowed rearrangement of the individual suction tubes as testing required. This configuration allowed plenums with generally the same surface pressure and suction requirement to be grouped together and controlled by a single valve. It was not within the available resources of the test program to provide a separate flow meter for each plenum. Twelve Meriam laminar flow elements (meters) were used and the flow was controlled by 12 simple gate valves. The 12 suction flow channels were then connected to the primary manifold which was connected to the suction source through a large gate valve.

b) Leading edge insert model modification

The nonporous leading edge panel was modified to support leading edge insert segments. A sketch of the model with a leading edge insert is shown in Figure 8-26. Figure 8-27 is a photograph of the modified leading edge panel with the insert removed and internal suction lines exposed.

The insert leading edge configuration was selected in order to: (1) allow the leading edge insert segments to be changed without having to remove

C-3

FIGURE 8-21. PERFORATED TITANIUM LEADING EDGE W_{1c} SHOWING SUCTION AND STATIC LINES

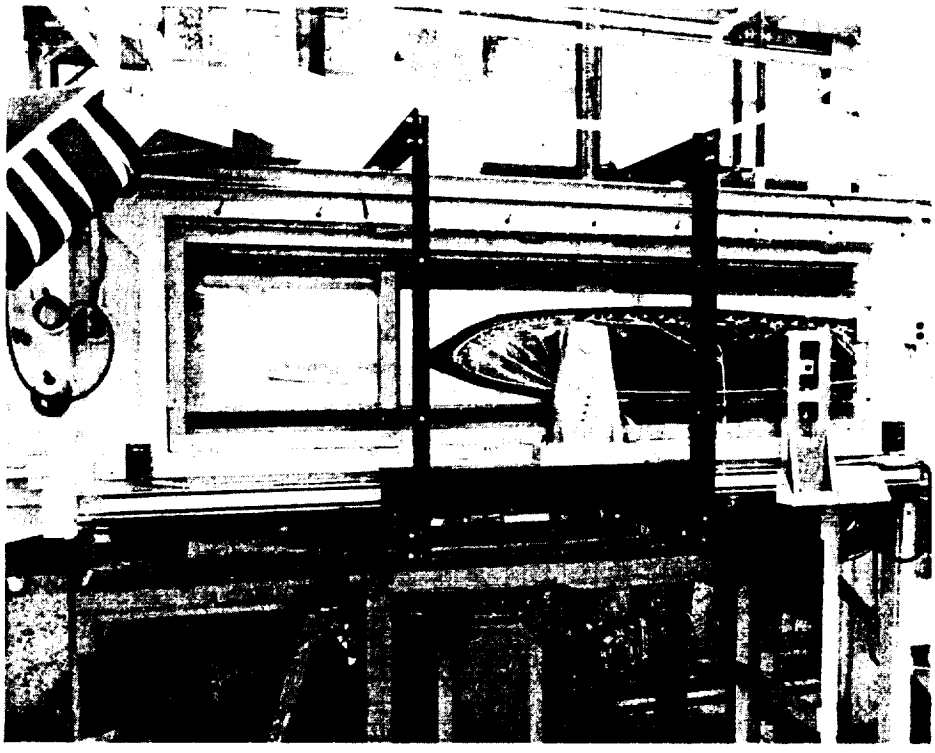

FIGURE 8-22. SWEPT-WING MODEL TEST – MODEL INSTALLATION

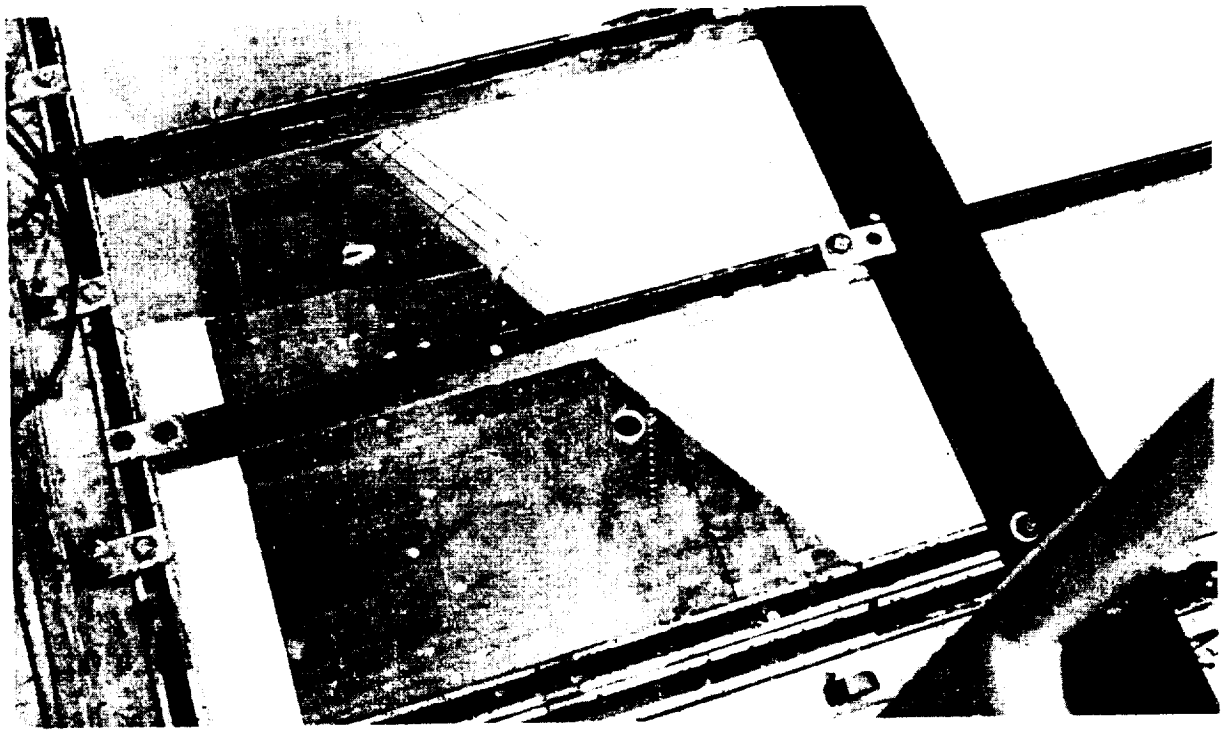

FIGURE 8-23. SWEPT-WING MODEL TEST – UPPER SURFACE AT LEADING EDGE

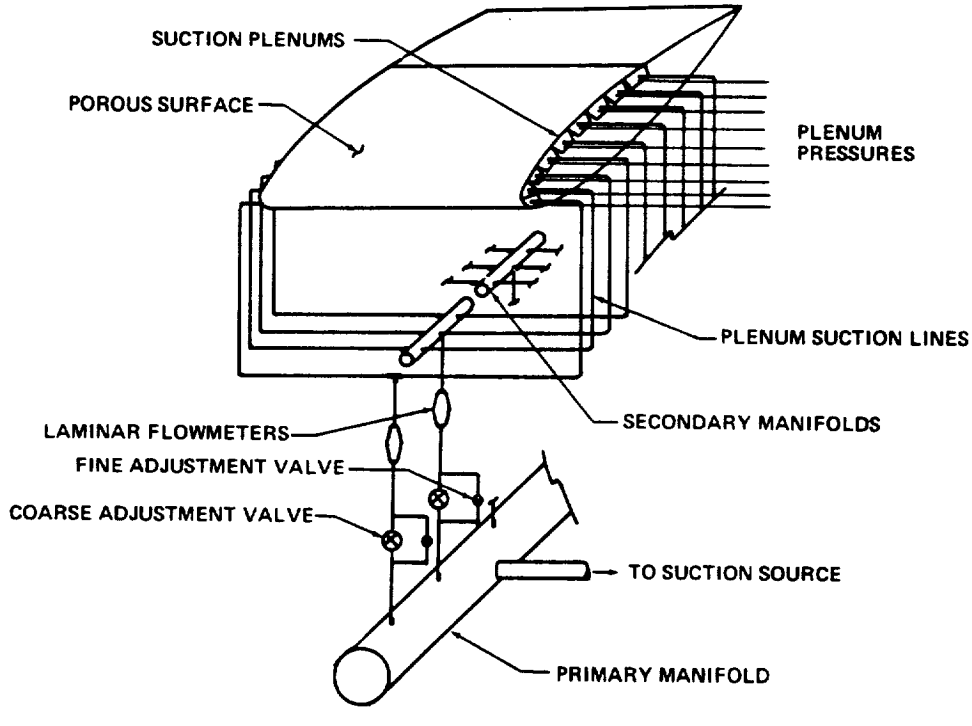

FIGURE 8-24. SWEPT-WING MODEL TEST – SUCTION SYSTEM SCHEMATIC

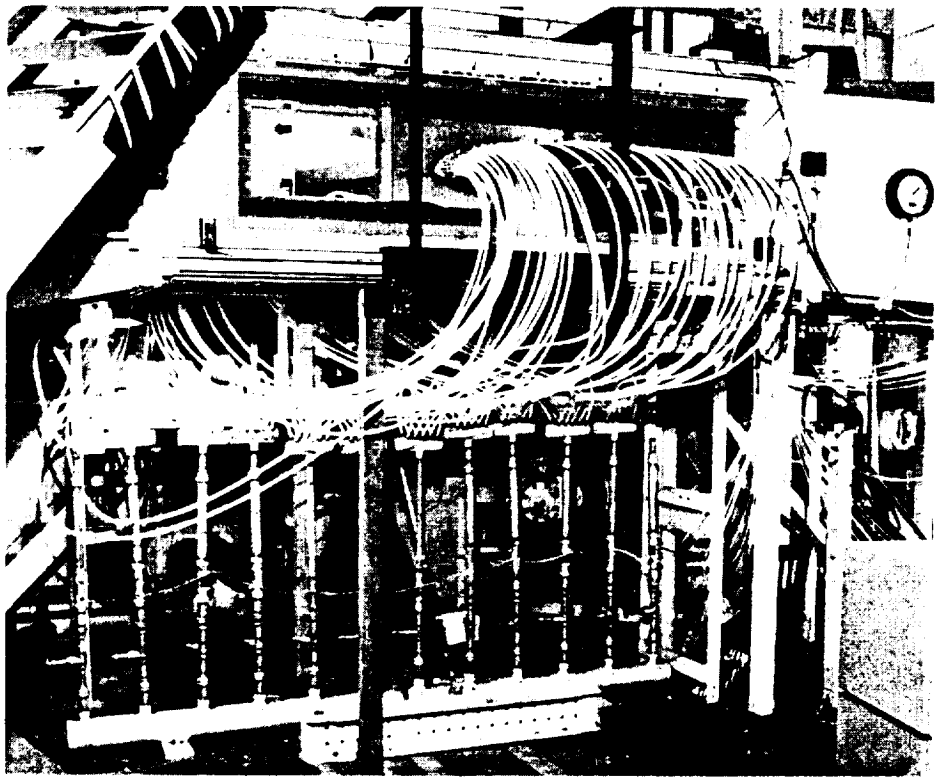

FIGURE 8-25. WIND TUNNEL MODEL WITH SUCTION SYSTEM

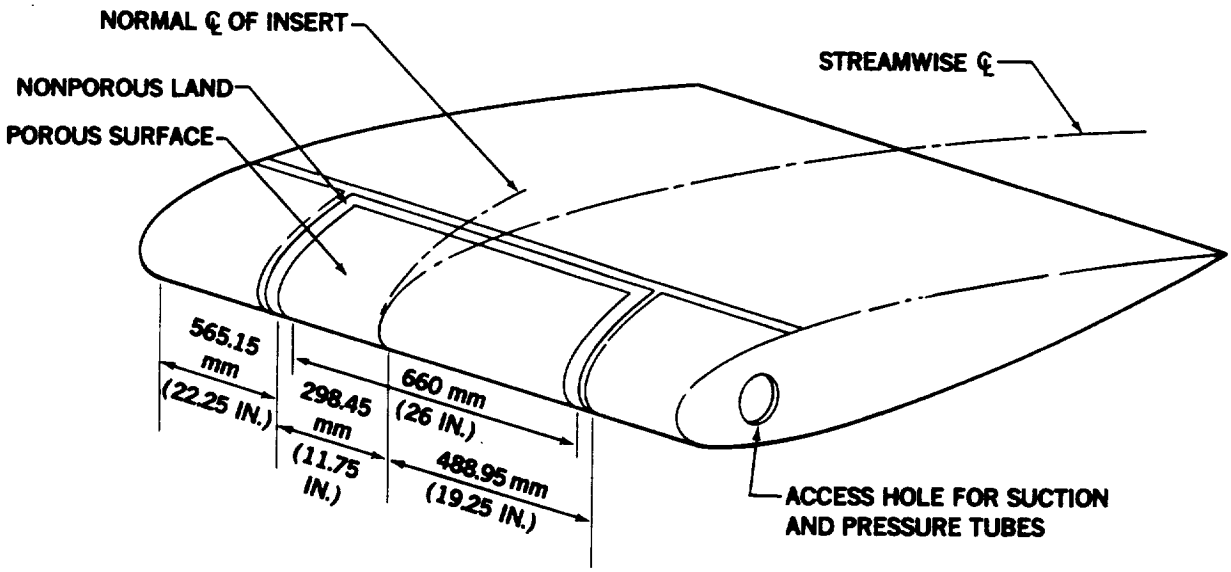

FIGURE 8-26. ARRANGEMENT OF LFC PANEL INSERT IN WING LEADING EDGE

the model from the tunnel, (2) extract suction more realistically part way along the plenums rather than at the ends, and (3) reduce the cost of additional test specimens.

Two insert panels were constructed using an improved substructure which provided a porous strip LFC suction surface. A sketch of the substructure is shown in Figure 8-28. The outermost sublayer formed the bonding surfaces for the porous surface sheet and acted as a baffle between the porous surface and the plenum. Holes 4.76 mm (3/16 in) diameter were drilled in the baffle at approximately 19 mm (3/4 in) pitch.

The first porous surface tested was 80 x 700/80 x 80 Dynapore diffusion bonded to a 0.305 mm (0.012 in) stainless steel sheet perforated with 0.254 mm (0.01 in) diameter holes at 2.54 mm (0.10 in) pitch in a square pattern. The second porous surface tested was the improved electron beam perforated titanium. This titanium surface material was 0.635 mm (0.025 in) thick perforated with 0.0635 mm (0.0025 in) diameter holes spaced 0.813 mm (0.032 in) apart in a square pattern. A photograph of the perforated titanium insert installed in the tunnel is shown in Figure 8-29.

8.2.3 Model Instrumentation

Instrumentation for the swept wing model test was conventional and relatively simple. The nonporous reference surface contained three chordwise rows of static pressure orifices, one row on the tunnel centerline and a row on each side, 381 mm (15 in) from the centerline (static pressure orifices could not be installed conveniently with the porous surfaces). Just aft of the 70-percent chord station, three total pressure rakes each with three tubes, were located similarly on the centerline and 381 mm (15 in) on either side spanwise. The total pressure tubes were at 2.54, 5.08 and 10.16 mm (0.1, 0.2, and 0.4 in) above the model surface. These dimensions were selected to be within the turbulent boundary layer and mostly above laminar boundary layer at the 70-percent chord station. For the leading edge insert panel tests, nonporous leading edge surfaces were available at each end of the porous

FIGURE 8-27. WIND TUNNEL MODEL – LEADING EDGE INSERT REMOVED

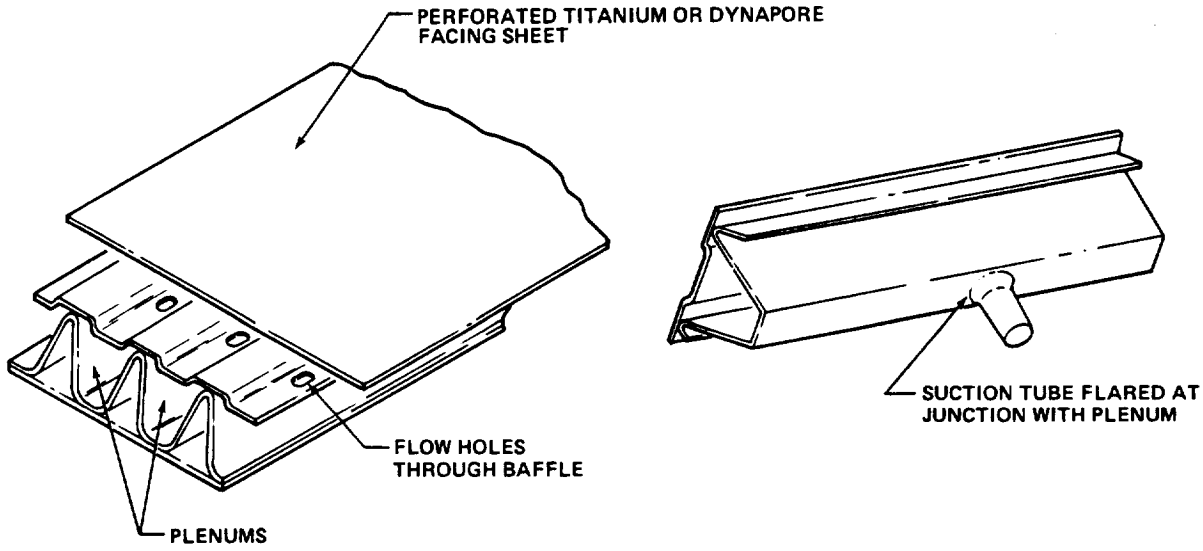

FIGURE 8-28. LEADING EDGE INSERT SUBSTRUCTURE CONFIGURATION AND SUCTION OUTLET TUBING

insert panels. These were used to provide a row of static pressure holes located 38.1 mm (1.5 in) inboard and outboard from the ends of the insert panels. Thirteen pressures were measured in each row.

During testing of the porous surfaces, plenum pressures were measured in each plenum, with suction on and off. All of the surface, plenum, and rake total pressures were measured on manometer boards and recorded photographically.

To obtain flow quantities through each flowmeter, measurement of the upstream pressure and the pressure differential for each flowmeter was necessary. These pressures were measured with a transducer via a scanivalve using a digital voltmeter. A schematic layout of the flow data acquisition is presented in Figure 8-30.

The transition location was determined by ear using a simple medical stethoscope connected to a fine total head probe with its opening held within the boundary layer. Originally a hot film sensor was planned for this purpose, however, the problems of aligning and maneuvering the hot film probe over the curved surface proved to be impractical.

8.2.4. Checkout and Initial Calibration with Nonporous Panels - The first phase of the swept wing test program involved checkout of the basic model installed in the tunnel with the nonporous panels in place. The objective of this phase was to identify and establish the required flow conditions for testing the LFC porous panels with suction applied. The test procedure and results for the nonporous surface is outlined below:

1. Flow Separation Check - Model upper surface and sidewall fairings were tufted to check for expansion separation. With the relatively large diffusion of the flow in the aft portion of the test section, there was concern that separation might occur. The initial runs, up to maximum dynamic pressure, confirmed that no separation existed for the test configuration.

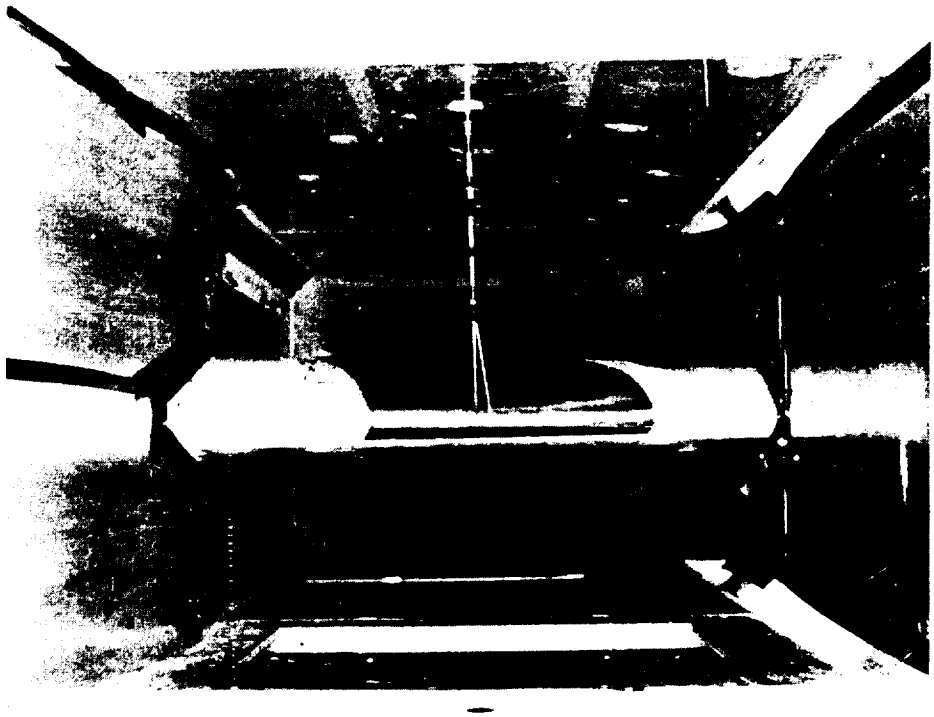

FIGURE 8-29. LFC SWEPT-WING WITH PERFORATED TITANIUM INSERT IN DOUGLAS LONG BEACH WIND TUNNEL

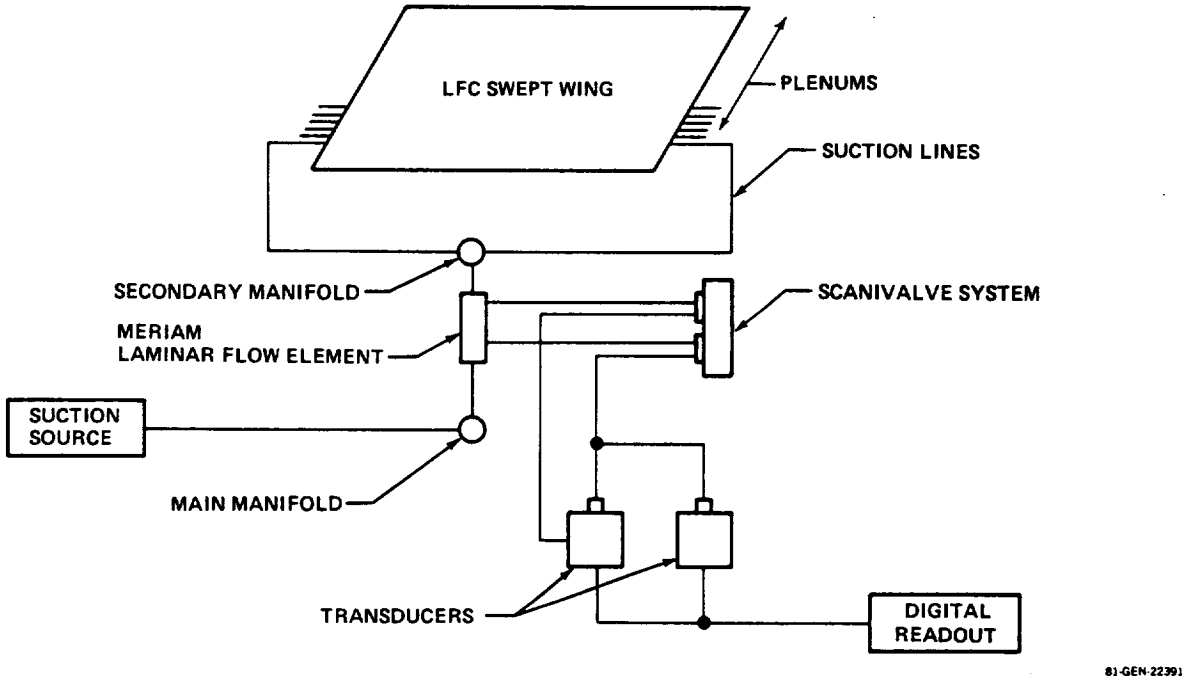

FIGURE 8-30. SCHEMATIC LAYOUT OF DATA ACQUISITION

2. Reference Tunnel Velocity - Due to the exceptionally large amount of blockage with this model, it was necessary to establish the reference dynamic pressure for the test. This was accomplished by locating a pitot static tube in the tunnel ahead of the model on the centerline reference streamline. At the corresponding streamline station the velocity ratio, V/V_{∞} , based upon the analytical (3-D Neumann) value, was 0.9634 (Figure 8-31). This correction was then applied in determination of the tunnel velocity calibration shown in Figure 8-32.

3. Reference Pressure Distribution - The reference pressure distribution for the test was established by adjusting the three trimmer flaps along the model trailing edge. The flaps were first deflected systematically so that the upper surface pressure distribution closely matched the desired pressure distribution (Figure 8-33). Spanwise uniformity was then achieved by differential setting of the trailing edge flap segments. The required flap positions were, nominally.

Inboard	1 degree t.e. up
Center	2 degrees t.e. up
Outboard	1 degree t.e. down

The resulting pressure distributions at the three spanwise stations are compared in Figure 8-34.

It should be noted that the model pressure distribution had a slightly steeper adverse gradient relative to the design value. This was considered acceptable since the steeper gradient imposes a more severe condition for possible crossflow instability.

4. Attachment Line Location - Centerline chordline pressures, near the airfoil leading edge, were used to locate the attachment line as indicated in Figure 8-35. In addition flow visualization (Figure 8-36) verified the attachment line location to be 10.16 mm (0.4 in) (S/C = 0.006) above the leading edge. The resulting value of the attachment line Reynolds number (R_{θ}) was approximately 65 for the maximum test velocity. This value is significantly below the nominal critical value of R_{θ} = 100, and indicated an absence of instability along the attachment line for the test conditions.

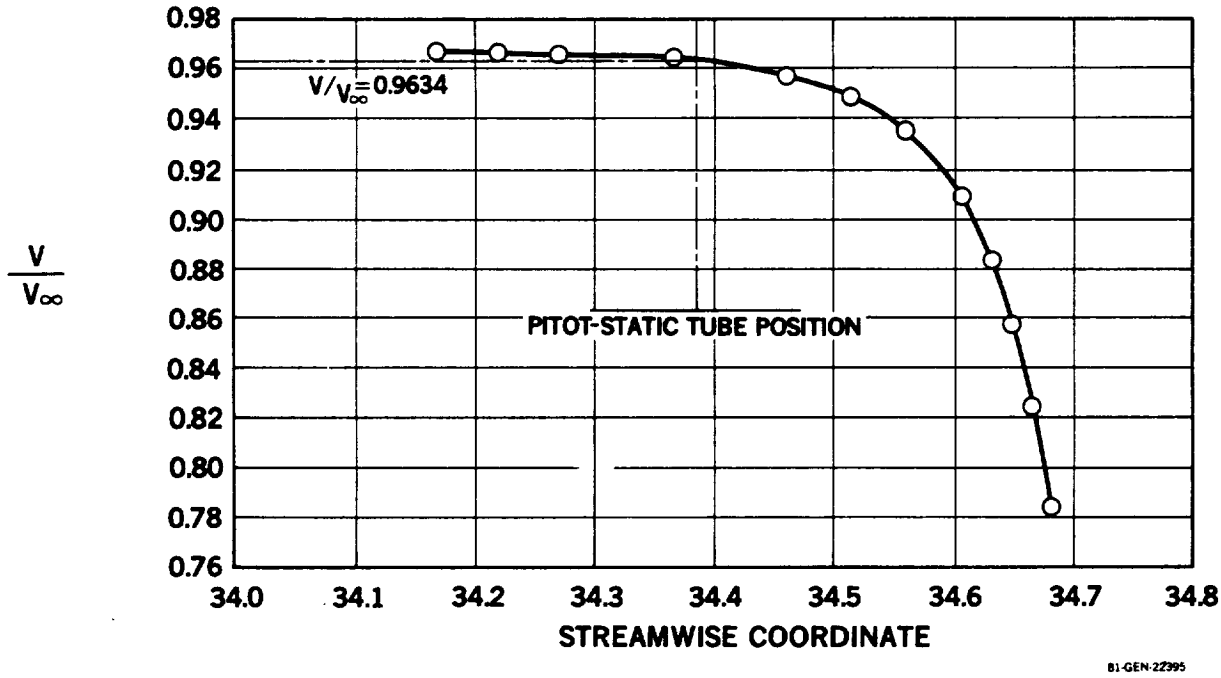

FIGURE 8-31. LFC THEORETICAL STREAMLINE – 14.22 mm (0.56 IN.) ABOVE MODEL SURFACE ON TUNNEL ℄

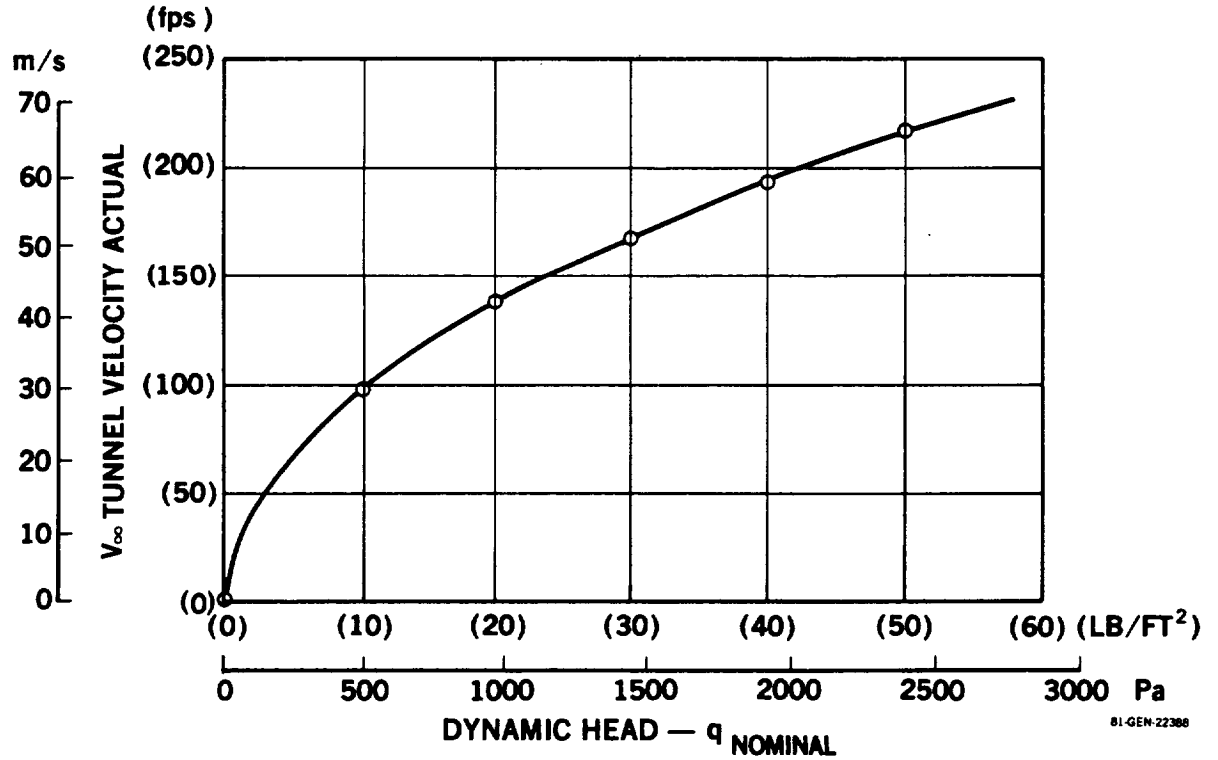

FIGURE 8-32. TUNNEL VELOCITY CALIBRATION – MODEL INSTALLED IN TUNNEL

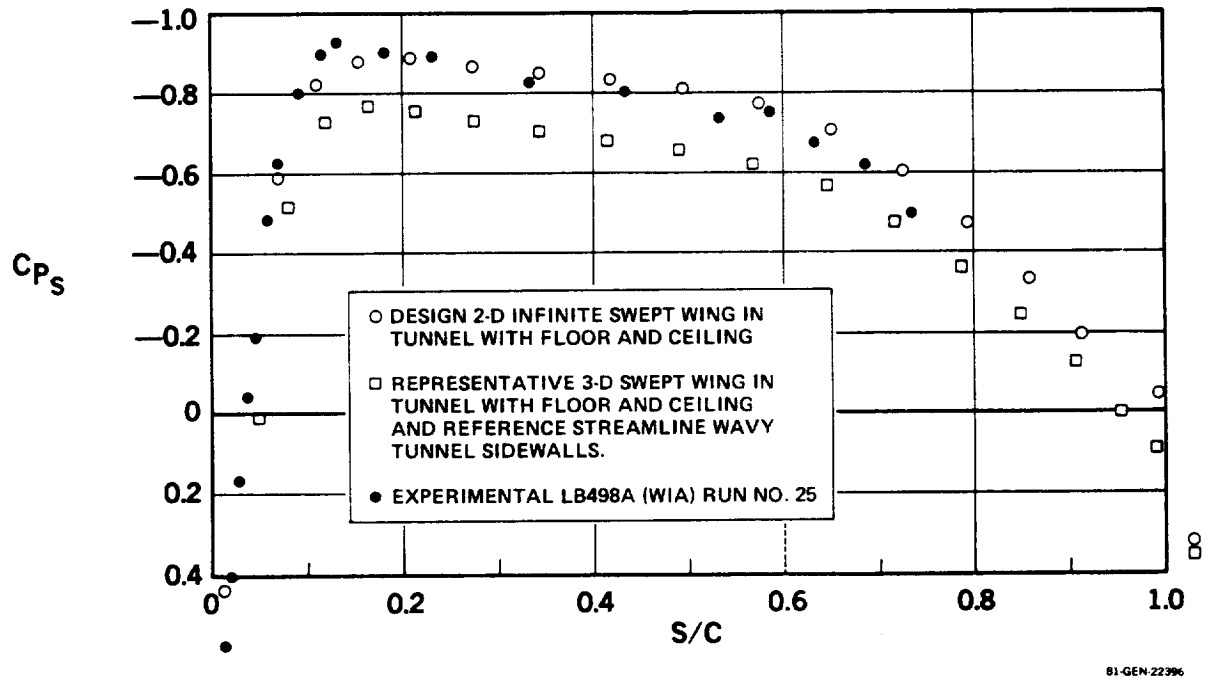

FIGURE 8-33. STREAMWISE PRESSURE COEFFICIENT VERSUS SURFACE STATION

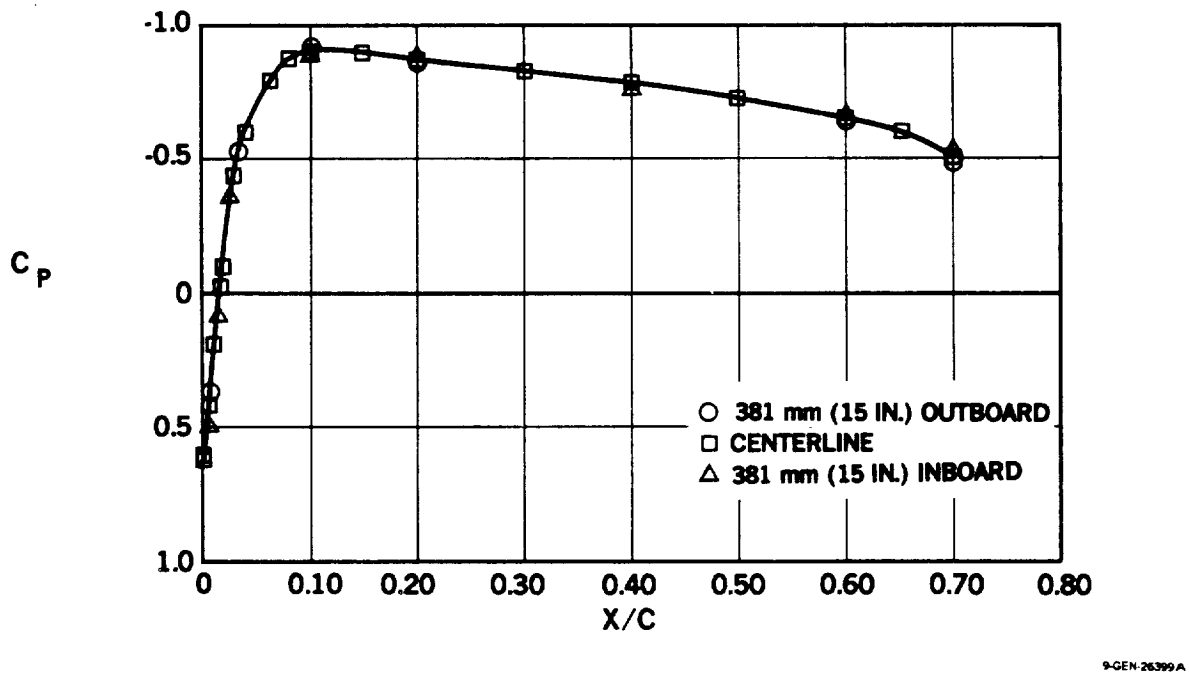

FIGURE 8-34. SWEPT-WING MODEL TEST – SPANWISE PRESSURE DISTRIBUTION COMPARISON

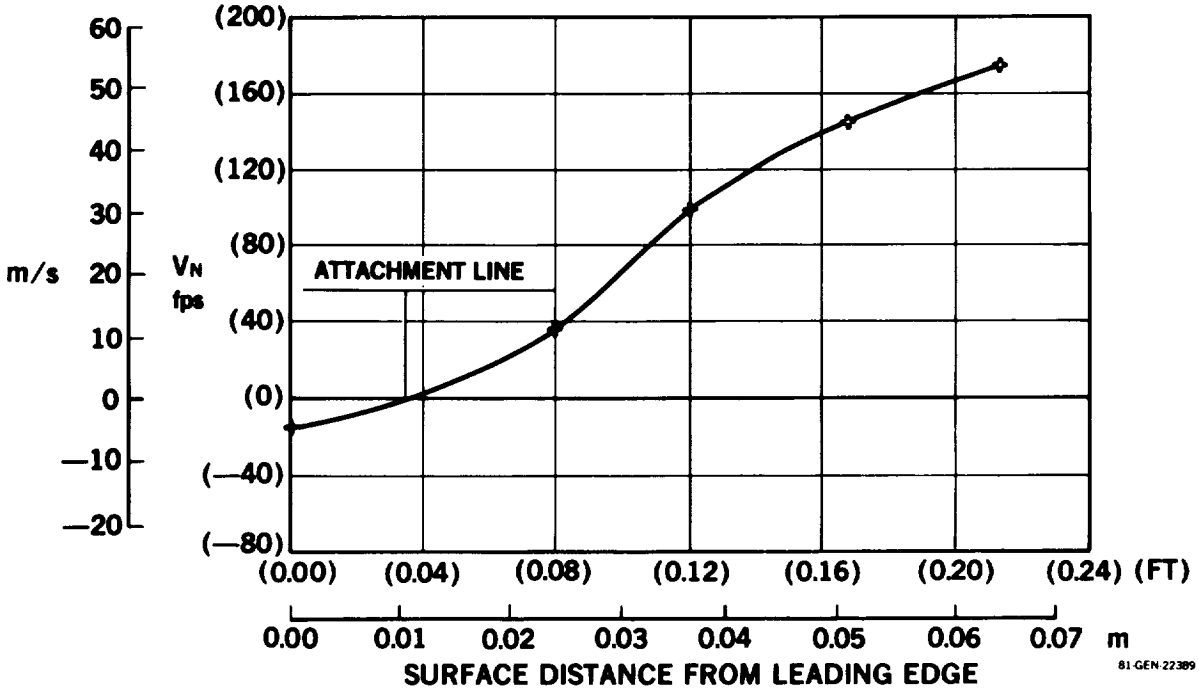

FIGURE 8-35. R_θ EVALUATION – SURFACE NORMAL VELOCITY VERSUS SURFACE DISTANCE

THE ATTACHMENT LINE POSITION IS APPROXIMATELY 0.4 IN. ABOVE LEADING EDGE
VELOCITY q_{NOM} = 50 PSI

FIGURE 8-36. NONPOROUS SWEPT-WING – BASELINE FLOW VISUALIZATION WITH Ti O_2 OIL MIX

During the test, a .635 mm (0.025 in) thick boundary layer tripping strip was placed transversely across the flow along the inboard leading edge in an attempt to induce boundary layer instability and cause transition along the attachment line. This technique failed to cause any transition other than streamwise.

5. Reference Transition Location - Boundary layer transition was located on the nonporous upper surface panel for several test conditions. Transition was determined using a small total head probe attached to a stethoscope. This technique was far more satisfactory than the hot film sensor used in the aerodynamic smoothness testing. The total head probe was: (1) less sensitive to orientation in the airflow, (2) not susceptible to damage while probing, and (3) much more adaptable to probing the curved surface with limited access from ports in the tunnel ceiling.

   The natural transition location for the smooth nonporous upper surface is shown in Figure 8-37 as a function of Reynolds number. A check was made using one screen in the setting chamber; this reduced tunnel turbulence and resulted in the transition location shifting aft by approximately 8 percent chord. Since the purpose of the test was to demonstrate LFC with realistic adverse conditions, the screen was not used for any of the testing with suction. This also allowed the tunnel velocity to be increased.

   For the primary test condition at a nominal tunnel q_{nom} of 2.394 kPa (50 psf), which is equivalent to a Reynolds number of 9×10^6, the natural transition on the nonporous upper surface was located at 8 percent chord.

6. Surface Flow Visualization - As a result of streamwise flow of the excess titanium oxide/oil mixture being used for attachment line flow visualization, the upper surface streamline was traced to beyond 70 percent chord as pictured in Figure 8-38. The surface oil streaks were scaled from the photos and are compared with the reference streamline that was used to develop the sidewall fairings (Figure 8-39). Although these streamlines are not directly comparable, the flow curvature is representative.

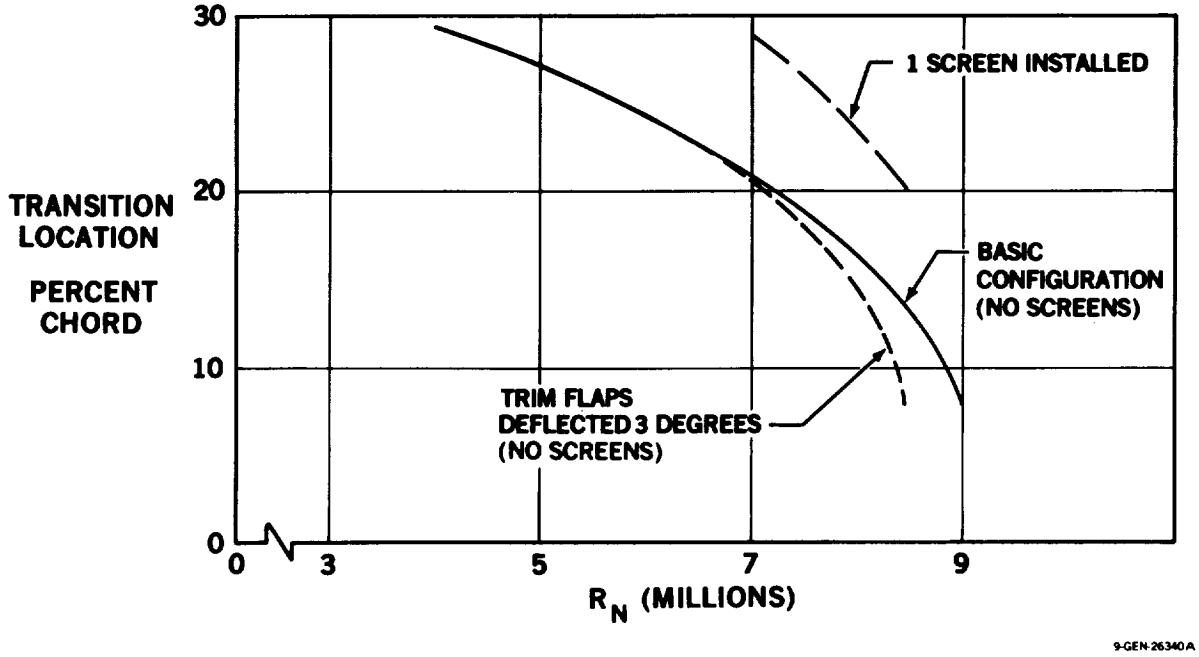

FIGURE 8-37. SWEPT-WING MODEL TEST – NATURAL TRANSITION LOCATION

$\alpha_p = 0^o 57'$; $\delta_{f_c} = -2^o 04'$; $\delta_{f_s} = -1^o 02'$

$\alpha = 0$ DEG TRANSITION FREE

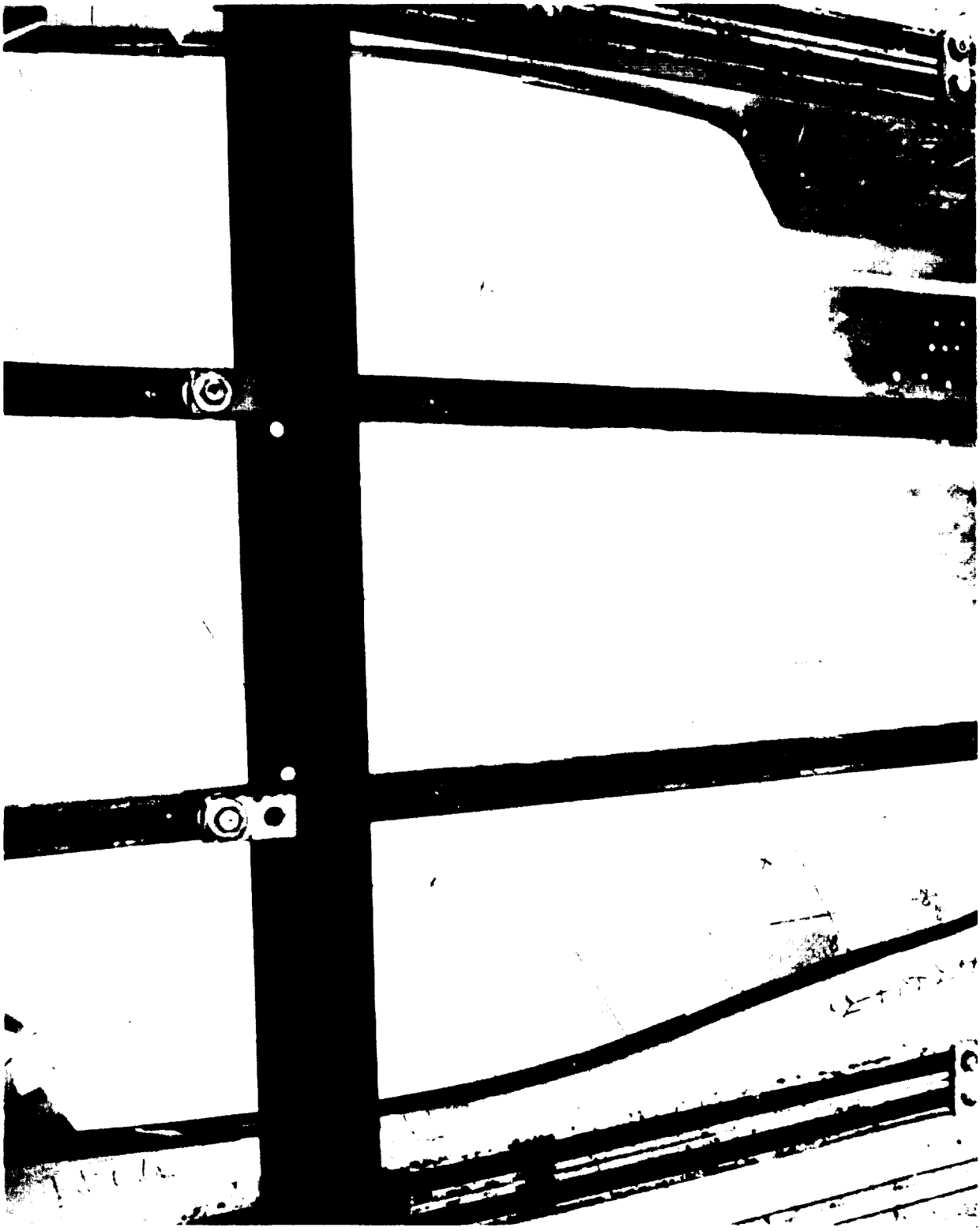

FIGURE 8-38. EFFECT OF CROSS-FLOW ON STREAMLINES WITH NONPOROUS SURFACE ON SWEPT

8.2.5 Calibration and Testing with Porous Surfaces

Testing of the porous surface panels to determine; (1) effectiveness in maintaining laminar flow, (2) the amount of suction required, and (3) effects of surface and suction anomalies, is reviewed in the following paragraphs.

1. Surface Check and Calibration - Prior to installing each porous panel, porosity was checked to determine the porosity of the surface associated with each plenum. This was done by applying suction to each plenum and recording the flow rate as a function of the pressure differential across the surface. During calibration of the basic Dynapore porous panels, it was detected that the resin used for the plenum walls was, in fact, porous. It was therefore necessary to apply additional sealing material in the spaces between the plenums and on the inner panel surface so that leakage through the plenum walls and between adjacent plenums was eliminated insofar as was possible. A routine leakage check was conducted on all subsequent panels.

   Calibration data were reduced to provide a porosity reference value in terms of flow rate, in standard cubic feet per minute (SCFM), at 670.3 Pa (14 psf) pressure differential. Porosity distributions for the basic model porous panels are shown in Figures 8-40 and 8-41. The latter figure shows an expanded porosity comparison for the Dynapore and perforated titanium leading edge panels. Variations in local porosity of the basic surface material together with possible remaining leakage between adjacent plenums and localized internal blockages introduced during fabrication account for the resulting porosity distributions.

   Porosity distributions for the Extension Test Dynapore and perforated titanium leading edge insert panels are presented in Figure 8-42.

2. Basic Model Test Results, Extent of Laminar Flow and Suction Requirements
   The basic swept wing model was tested first with all Dynapore upper surface panels. Suction was varied chordwise to generally minimize the suction flow needed to maintain laminar flow. The extent of laminar flow

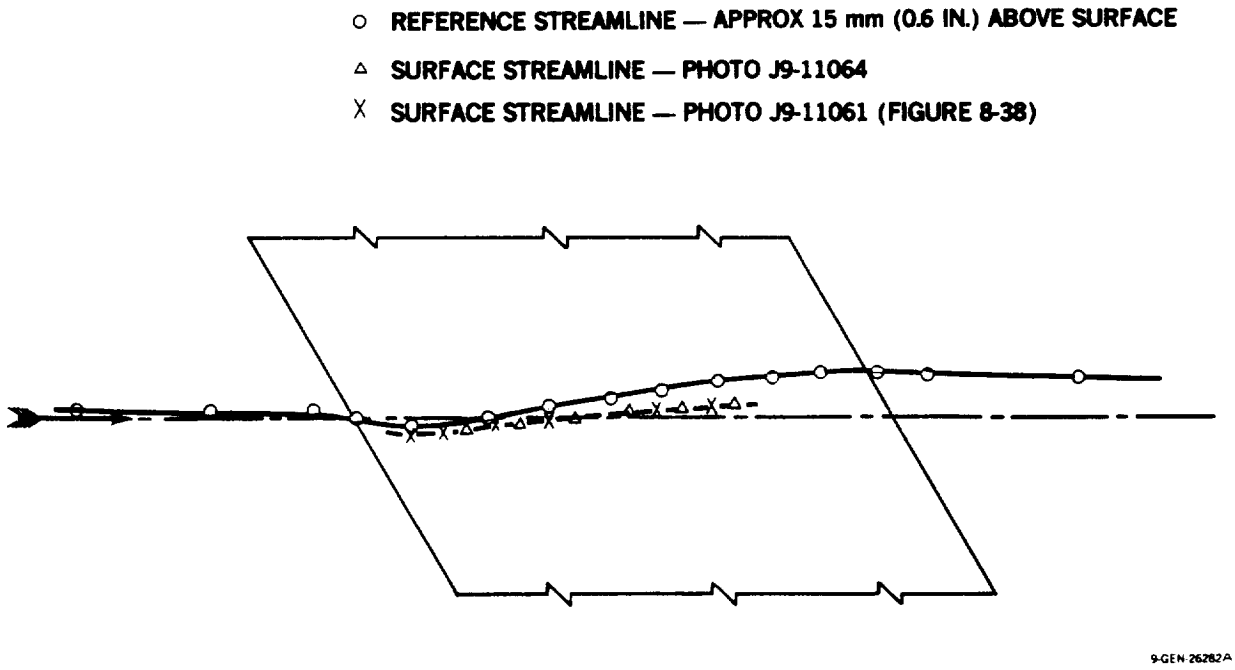

FIGURE 8-39. SWEPT-WING MODEL TEST – COMPARISON OF REFERENCE STREAMLINE AND SURFACE FLOW VISUALIZATION

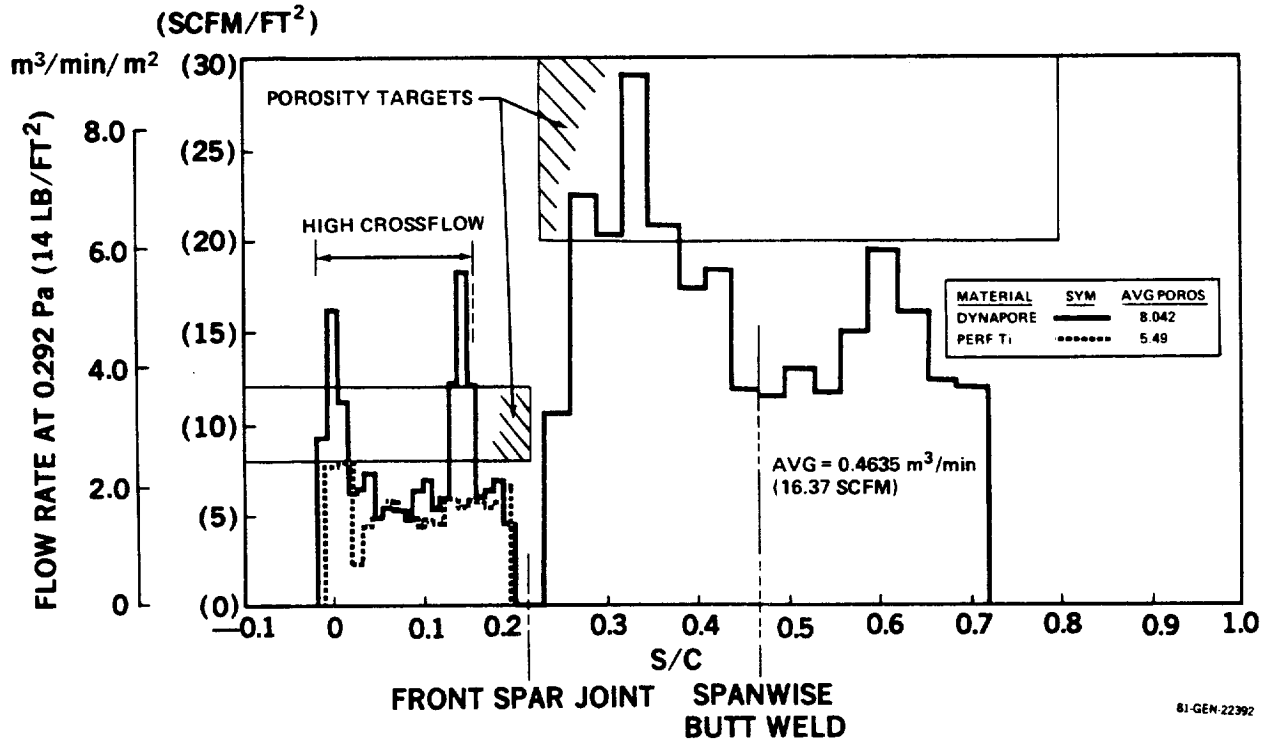

FIGURE 8-40. POROUS SURFACE POROSITY DISTRIBUTION

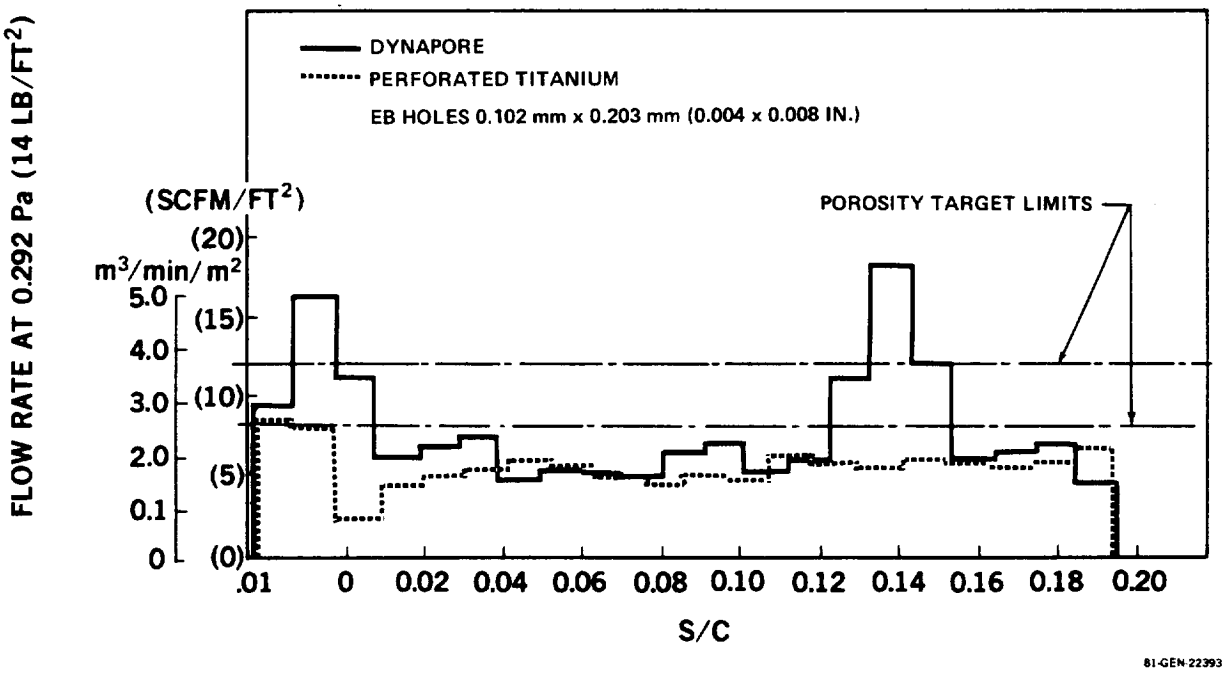

FIGURE 8-41. LEADING-EDGE POROSITY DISTRIBUTION

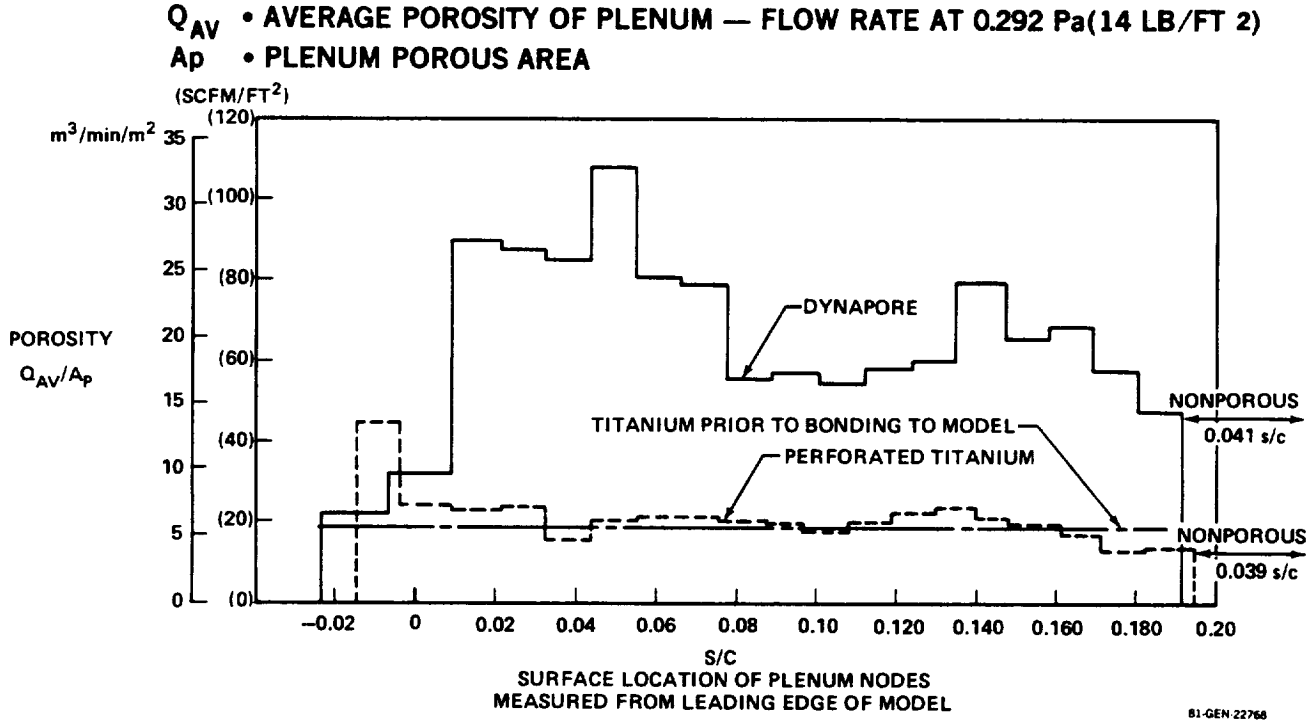

FIGURE 8-42. LEADING-EDGE INSERT POROSITY DISTRIBUTION

obtained with the Dynapore LFC surface is illustrated in Figure 8-43. Application of suction extended the boundary layer transition location to beyond the end of the porous surface at 70 percent chord by as much as 5 to 10 percent of the chord. The extent of laminar flow obtained with the perforated titanium leading edge was essentially the same.

Suction velocity distributions for the basic model, with both Dynapore and perforated titanium leading edges, are shown in Figure 8-44. The stepwise distribution is due to the grouping of several plenums to a single manifold. Included in this figure is the predicted suction velocity required according to X-21 criteria. Suction velocities for the Dynapore surface panels agree quite well with predicted values.

Increased suction ahead of, and behind, the non-porous front spar joint is required. The local increase in suction is approximately equivalent to what would have been required for a porous surface in the non-porous region.

The overall suction level with the perforated titanium leading edge is higher than with the Dynapore leading edge. However, it should be noted that at the time of this test the titanium was only considered as an alternative surface material and the suction values were not refined to the same degree as they were for the Dynapore. The principal objective at this time was to determine whether possible disturbances, originating at the perforations in the thin laminar boundary layer near the leading edge, would cause premature transition. Even with over-suction in the leading-edge region, laminar flow was obtained for the same extent of chord as for the Dynapore.

3. Simulated System Malfunction - During testing with the all Dynapore Surface, an investigation was made of the effect on laminarization of system failures in the form of simulated suction line venting to ambient or blockage at the most critical location. The line feeding plenum number 7 (s/c = 0.025), which was in the crossflow critical region, was selected. Venting #7 moved transition forward to 73 percent chord. Blockage of the same line caused oversuction in other areas but had no detrimental effect upon the extent of laminarization. The conclusions can be drawn that venting of a suction line is more critical to LFC operation than blockage and that blockage would cause an increase in the suction source loading.

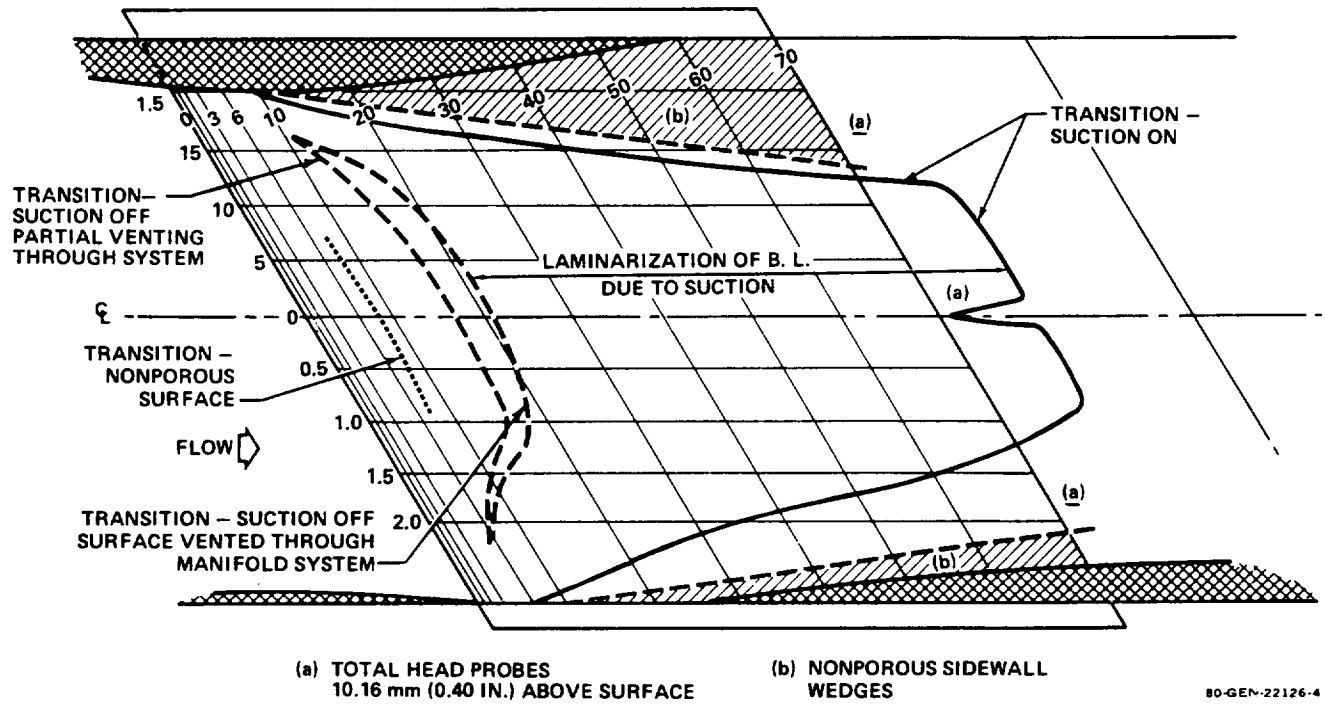

FIGURE 8-43. SWEPT-WING MODEL TEST – EFFECT OF SUCTION ON TRANSITION
q_{NOM} = 2394 Pa (50 PSF)

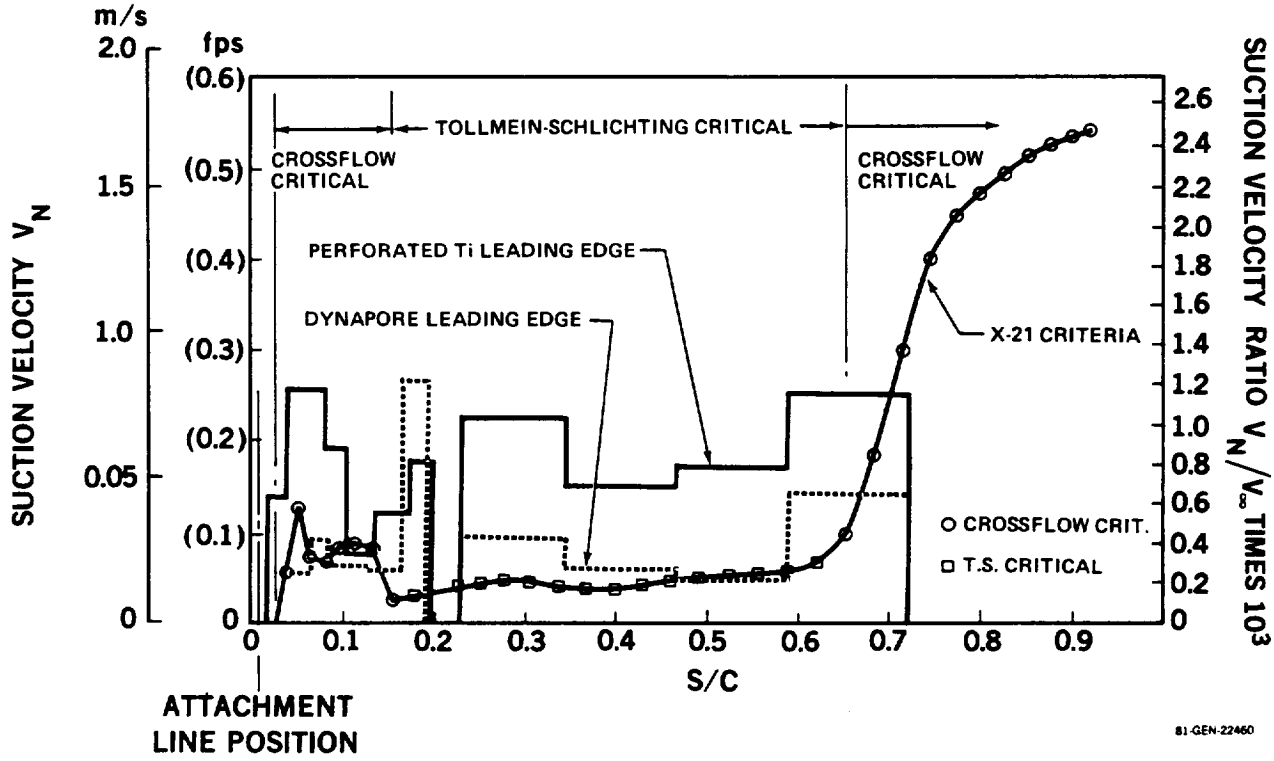

FIGURE 8-44. SWEPT-WING WIND TUNNEL MODEL – SUCTION VELOCITY DISTRIBUTIONS

4. Leading Edge Insert Test Results - The results obtained with the leading edge insert panels are presented in Figures 8-45, 8-46, and 8-47. Because the porous leading edge inserts were limited spanwise, the extent of laminar flow with suction on the insert was reduced by the nominal spread of turbulence from the insert extremities. In this case the prime objective was comparison of the leading edge surface materials with regard to LFC suitability. In spite of its limited span, it was possible to demonstrate laminar flow to beyond 60 percent chord with the new perforated titanium surface using suction to 50 percent chord over the main box regions. The testing effort was concentrated on the improved titanium surface because of its quality and preferred structural characteristics. The increased suction applied ahead of the spar joint for the perforated titanium leading edge insert, shown in Figure 8-47, was computed to compensate for the suction required across the non-porous region at the front spar joint. The resulting laminar flow, to 65 percent chord (Figure 8-46), corresponds to the suction distribution indicated. A similar result would be expected for a Dynapore leading edge insert.

8.2.6 Boundary Layer Stability Analysis

Stability analysis was made of the wind tunnel test results, using the advanced boundary layer SALLY II computer code for comparison. Stability analysis was applied both with and without suction at a nominal tunnel dynamic pressure of 2394 Pa (50 lb/ft^2), which corresponds to a freestream velocity of 66.08 m/s (216.8 ft/sec), and a chord Reynolds number of 8.87×10^6. The boundary layer development was calculated with the experimentally determined pressure distribution to avoid oscillations in the boundary-layer solutions. All stability analysis was done using the envelope method option, that is, the amplification ratios to be integrated were maximized for each selected physical disturbance frequency.

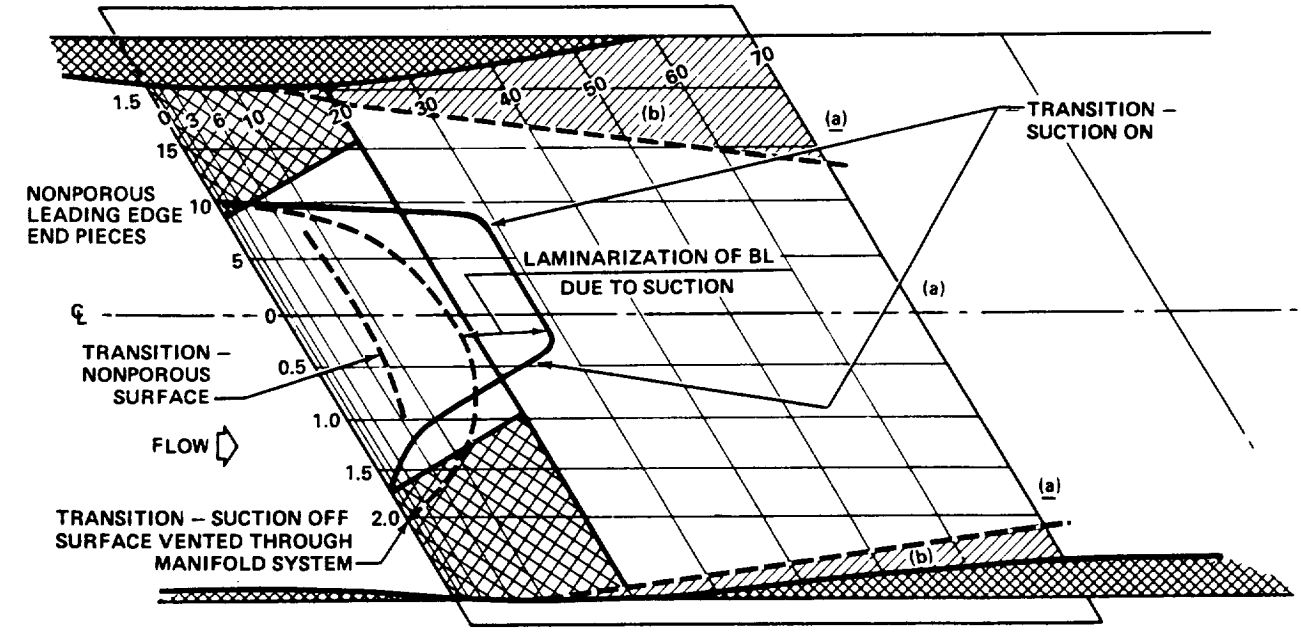

FIGURE 8-45. SWEPT-WING MODEL TEST – EFFECT OF SUCTION ON TRANSITION AT q_{NOM} = 2,394 Pa (50 PSF) – DYNAPORE L.E. INSERT

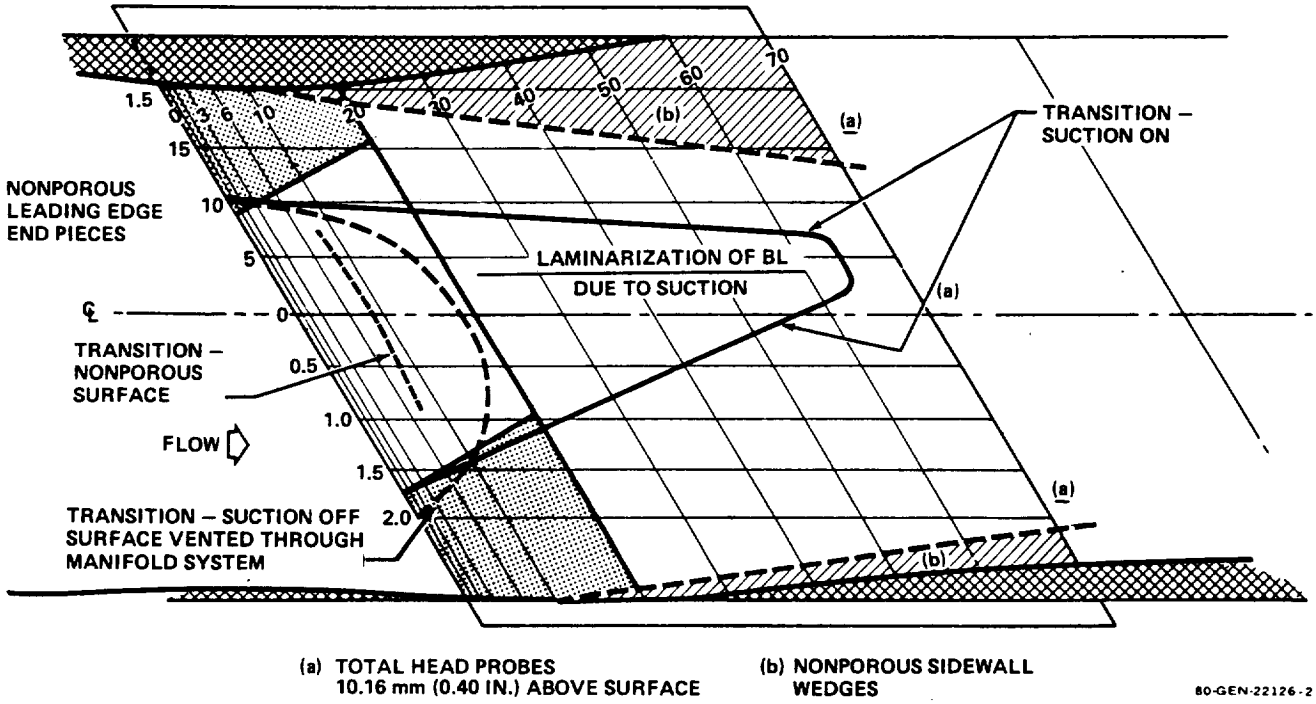

FIGURE 8-46. SWEPT-WING MODEL TEST – EFFECT OF SUCTION ON TRANSITION AT q_{NOM} = 2394 Pa (50 PSF) – PERFORATED TITANIUM LEADING EDGE INSERT*

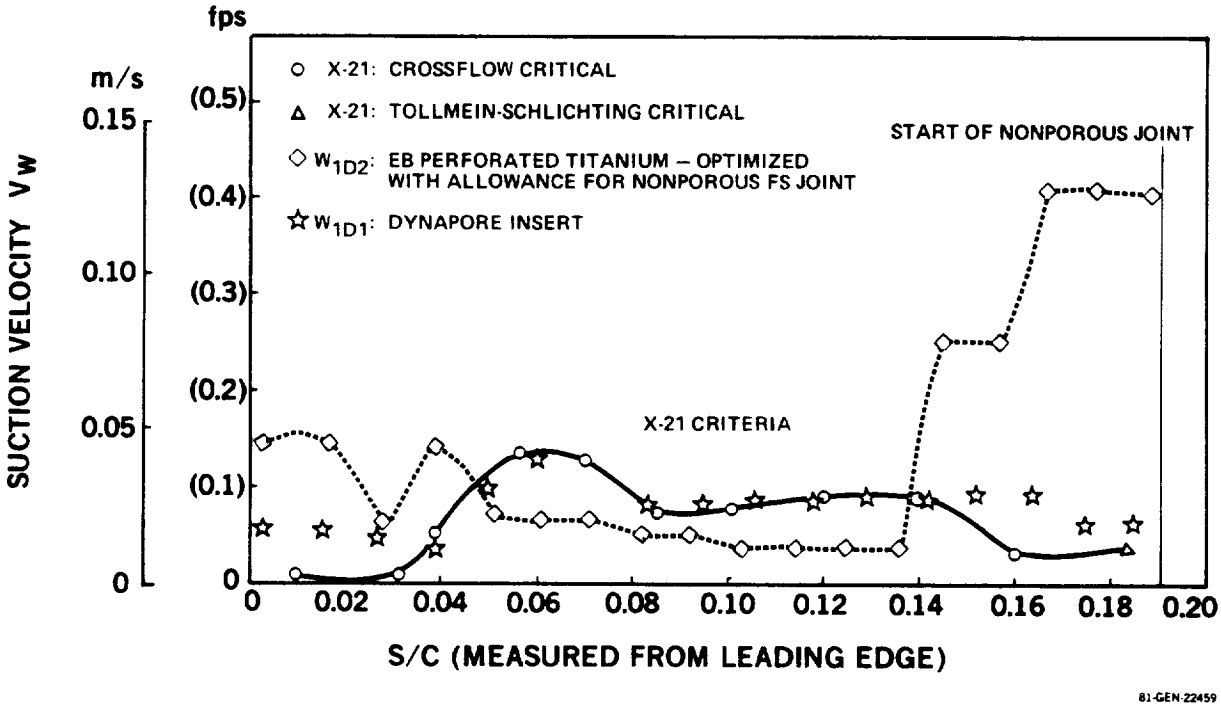

FIGURE 8-47. SWEPT-WING MODEL – LEADING EDGE INSERT SUCTION VELOCITY DISTRIBUTION

(a) No Suction

This case corresponds to tests on the model with non-porous surface. The measured location of the start of transition (assumed to be where the frequency of turbulent bursts recorded by the stethoscope is about once every two seconds) is at $x/c = 0.08$. Since cross-flow instability was suspected of being the transition triggering mechanism, a range of frequencies from 0 to 1500 Hz was considered. The most amplified frequency computed was at 750 Hz, which gave an amplification N-factor of 8.3 at the start of transition. The zero frequency case gave the smallest amplification, indicated by the N-factor of 7.3. The computed range of N-factors is considerably lower than the average N of 10 obtained in low turbulence wind tunnels. The probable reason for this discrepancy is the turbulence level, which in the absence of screens, is about 0.5 percent.

Another interesting feature of the calculated results is that the maximum N-factor for the cross flow barely exceeds 11 before the flow enters the strong adverse pressure gradient on the rear of the airfoil. In view of this, and also considering the fact that the two-dimensional disturbances first start to grow at about $x/c = 0.1$, it is possible to visualize transition occurring at $x/c = 0.2$ or even further aft if this wing were tested under low turbulence conditions. Thus, the relatively high turbulence level may be viewed as a contributing factor to generating a flow which is unstable to cross-flow disturbances, as required by the test objectives.

(b) Porous Surface Suction

As noted earlier, the main difference between the test conditions and calculations is in the smoothing of the experimental suction distribution before boundary-layer calculations. This was necessary because the large discontinuous changes in the suction velocities from one suction chamber to another during the test, when used in boundary-layer calculations, produced an oscillatory solution which made the stability analysis meaningless. In order to eliminate oscillations, a new suction velocity distribution was constructed from the smoothed integrated suction mass flow disdribution. Again, the flow was tested for cross-flow instability in the range of frequencies from 0 to 1500 Hz. On the forward part of the wing the most amplified frequency was 500

Hz, giving an N-factor of 7.75 at x/c = 0.176. The lower frequencies are somewhat less amplified but their chordwise extent reaches an x/c of 0.25 before a stable region is encountered. The maximum amplification factors calculated are less than the values which are considered to be the upper bounds for obtaining laminar flow with suction. Even lower values should be expected on account of the high turbulence level in the wind tunnel which forced the suction to higher levels than anticipated. Reamplification of disturbances on the rear portion of the wing was found only for zero frequency, starting at x/c = 0.596 but the N-factor grew only to 0.67 at the last station calculated. The last station calculated was at x/c = 0.688, or just one step past the end of suction region at x/c = 0.666 because the abrupt termination of suction caused nonconvergent boundary-layer solutions beyond x/c = 0.70. Thus the N-factors corresponding to the measured transition location at x/c = 0.75 could not be calculated.

A search for amplified waves in the two-dimensional disturbance mode was carried out in the frequency range of 1000 to 4000 Hz. Here no amplified disturbances were detected except at the very last station calculated for all frequencies below 3000 Hz. The absence of calculated disturbances in the presence of suction is again probably due to the turbulence level in the wind tunnel which caused considerably higher suction quantities to be applied during tests than were originally estimated.

8.2.7 Conclusions - Wind Tunnel Testing - The wind tunnel testing has demonstrated dramatically the aerodynamic practicality of achieving laminar flow control using distributed suction on a representative wing section with a 30 degrees sweep angle and at an R_e per unit length close to flight conditions.

The results of this test also show that a production quality surface and structural considerations do not preclude establishing and sustaining a laminar boundary layer flow.

The test data indicates that the convenient and relatively simple X-21 boundary layer stability criteria provide a useful means of estimating suction requirements.

The latest progress in electron beam perforation technology has provided a very good surface material for practical laminar flow control.

6.3 REFERENCES - AERODYNAMIC TESTING

6.3-1 Hess, J.L.: Review of Integral-Equation Techniques for Solving Potential Flow Problems with Emphasis on the Surface-Source Method. Computer Methods in Applied Mechanics and Engineering, 5(1975) 146-196.

6.3-2 Friedman, D.M.: A Three-Dimensional Lifting Potential Flow Program. McDonnell Douglas Report MDC J6162/01. September 1974.

9.0 STRUCTURES

9.1 WING BOX DESIGN

For structural efficiency, the LFC surface and suction requirements were integrated with structural design to obtain the maximum effective structural depth within the aerodynamic envelope. The initial aerodynamic definition was for suction back to 70 percent chord on both upper and lower surfaces.

9.1.1 General Requirements

Design Criteria:

- o Manuever load factor = 2.5g
- o Design life = 60,000 hours (crack free). Fatigue scatter factor = 2.
- o Advanced composite material usage and structural technology compatible with 1990-95.

Structural Requirements:
Structure to provide stiff continuous load paths at or near the outer surface, to be fatigue, fracture and damage resistant, environmentally durable and easy to maintain. The requirement for suction airflow through the surface introduced a new factor into considerations of strength, stiffness and environmental resistance.

Aerodynamic requirements:
An extremely smooth wing surface, uniformly porous or slotted with varying suction velocities and close control of pressure drop tolerances.

Suction System requirements:
Maintenance of the required airflow in the main trunk ducts with minimum losses, avoiding right angle turns and constrictions. Metering and control of suction airflow from the surface to the suction pump.

In addition to the integrated discipline requirements, there were four primary structural design questions to resolve:

1) Porous or slotted surface?
2) Integral or gloved LFC surface?
3) Composite or metallic structure?
4) Spanwise or chordwise surface air collection?

9.1.2 Initial Concepts Considered

Initially, twelve concepts were considered and each was assigned a code letter, see Table 9-1. Three wing box materials(composite, aluminum, titanium), porous and slotted surfaces, and a removable glove panel versus an integral LFC surface were the alternatives considered.

Six variations in the suction surface structural design were also considered, as illustrated in Figure 9-1 and described below:

A. CORRUGATED, with air collection spanwise in the flutes.
B. CONVENTIONAL (X-21) and EXTERNAL BLADE (if gloved), with spanwise air collection between the stiffeners.
C. ARCH-WEB, rib support is distributed into a continuous web which separates the fuel tank from the chordwise air collection. The structural cover can be an open grid as shown, a honeycomb sandwich, or a monocoque shell depending on the spacing of the chordwise formers.
D. ISOGRID-STRINGER, an open grid, forms the primary structure through which air is collected spanwise between the stringers. The lower sheet is a fuel pressure barrier and seal.
E. HONEYCOMB, with slotted metallic or "peel ply" porous outer surface. Air is drawn spanwise for short distances within the core and then ducted through the fuel tank to larger ducts in the spar areas.
F. INTERNAL BLADE, (or conventional stringer-stiffened), in which air is collected through a surface panel to a ducting layer entirely outside the primary structure.

With a 1990-1995 technology frame of reference, there should be sufficient time for the development of new and original types of structures, if selected.

TABLE 9-1. INITIAL EVALUATION MATRIX

PANEL / STRUCTURE	INTEGRAL (i)		GLOVE (g)	
	POROUS (p)	SLOTS (s)	POROUS (p)	SLOTS (s)
Composite (c)	A_{cip}	A_{cis}	A_{cgp}	A_{cgs}
Aluminum (a)	A_{aip}	A_{ais}	A_{agp}	A_{ags}
Titanium (t)	A_{tip}	A_{tis}	A_{tgp}	A_{tgs}
	Surface mechanically fastened from inside or permanently fastened. Fab/Assy Scheme I		Surface mechanically fastened from outside. Fab/Assy Scheme II	

The question of a non-removable LFC surface versus removable LFC panels is especially important from an inspection and maintenance standpoint. Integral ducting and integral surfaces could make structural inspection and repair difficult. An early decision, influenced by uncertainty of the durability of the suction surface at that time, was to favor removable LFC glove panels fastened from the outside, to minimize service maintenance costs. It was recognized this would entail fastener smoothness problems and some weight penalty which would be offset by the aircraft performance improvement due to laminar flow and the advantage of having a more easily maintained LFC structure.

Table 9-2 shows some advantages and disadvantages of glove (porous) and integral (slotted) systems. Two separate trade studies, glove versus integral and slots versus porous, were linked in this evaluation by the following rationale: Precision slots must be cut in a metallic material which by virtue of its stiffness attracts load. Slotted panels should therefore be integral with primary structure and fastened accordingly. By contrast, porous materials tend to be of lower stiffness and be less highly loaded. Comparing porous and slotted arrangements, it was concluded that the disadvantages of the slotted systems were more difficult to overcome than those of a porous glove. The listed disadvantages for a porous glove were therefore regarded as areas for design improvement, especially load acceptance. For trade purposes, the porous glove was considered non-structural but attached so as to strain with underlying structure.

TABLE 9-2

GLOVE VERSUS INTEGRAL LFC SURFACE

1. Glove - Porous Panel

Advantages	Disadvantages
o Removable for inspection and repair	o Must strain with structure
o Low sensitivity to variations in porosity	o Glove structure less efficient
o Fewer joints and discontinuities to fair	o Possible clogging and cleaning problem
o Fuel leak seals separable	o Fatigue resistance uncertain at this stage.
o Potential lower fabrication cost	o External fasteners must present a smooth surface.

2. Integral - Slotted Surface

o Efficient structure	o High cost, precision construction
	o Fine slots difficult to machine in corrosion resistant materials
	o Sensitive to suction variations
	o Difficult to inspect for cracks and corrosion in substructure and integral ducts.
	o Difficult to maintain and repair
	o Slots require stiff metallic materials - highly stressed integral design required.
	o Difficult to control slot width under structural loading.

9.1.3 Preliminary Design for Strength

A preliminary wing geometry with an aspect ratio of 12 and a 381 m^2 (4100 ft^2) area, as shown previously in Figure 5-2a, was used to generate loads for sizing the structural sections of the candidate designs. The baseline structural concept selected initially for modeling to determine loads, was a corrugated graphite epoxy wing skin covered with a porous glove panel, concept A, as shown in Figure 9-2. A later version is shown in Figures 9-3a and b. The latter provided spanwise flow channels closely matching desirable structural sizes. The resulting wing shear and moment diagrams are shown in Figure 9-4.

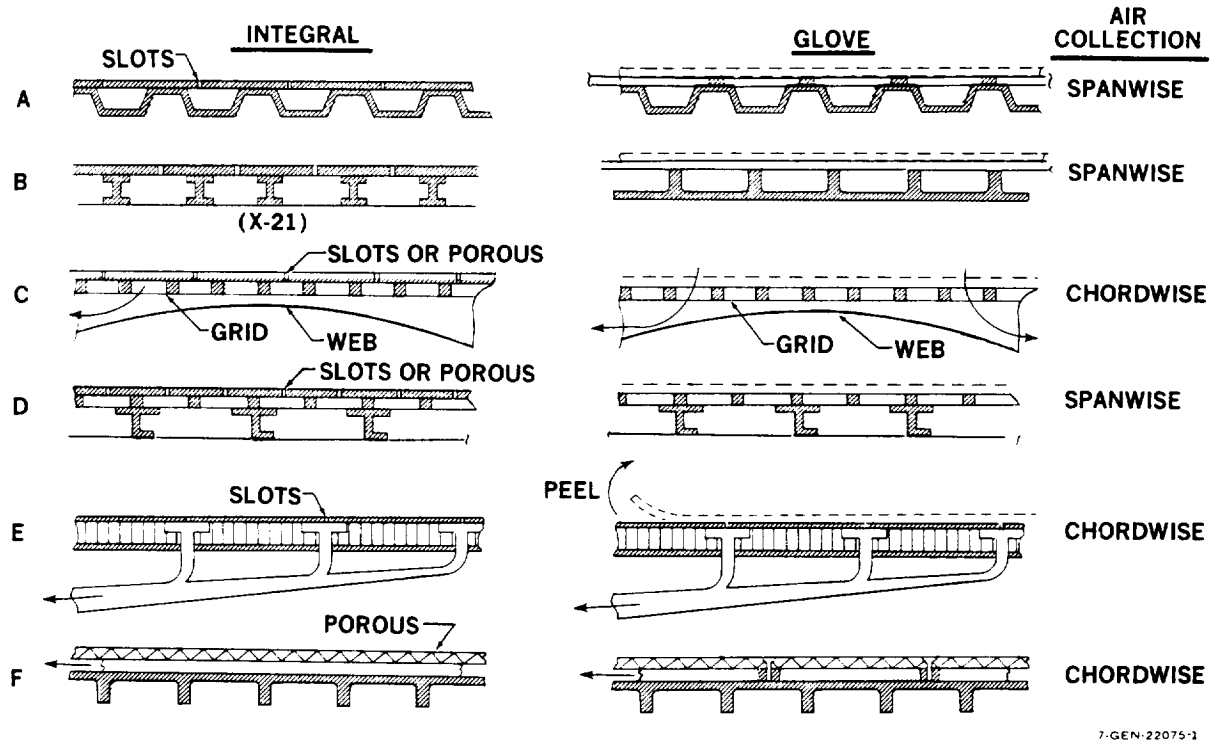

FIGURE 9-1. LFC STRUCTURAL DESIGN CONCEPTS

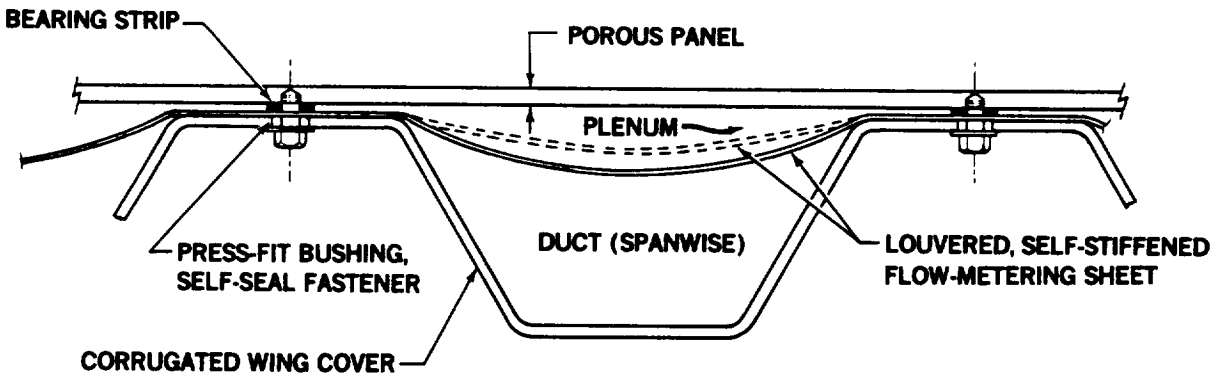

FIGURE 9-2. INITIAL BASELINE STRUCTURAL CONCEPT

- GLOVE CONCEPT
- CORRUGATED PRIMARY STRUCTURE
- INTEGRATED SPANWISE AIR COLLECTION
- CONSTANT NUMBER OF SPANWISE FLOW CHANNELS
- SEE FIGURE 9-3b FOR SECTIONS INDICATED

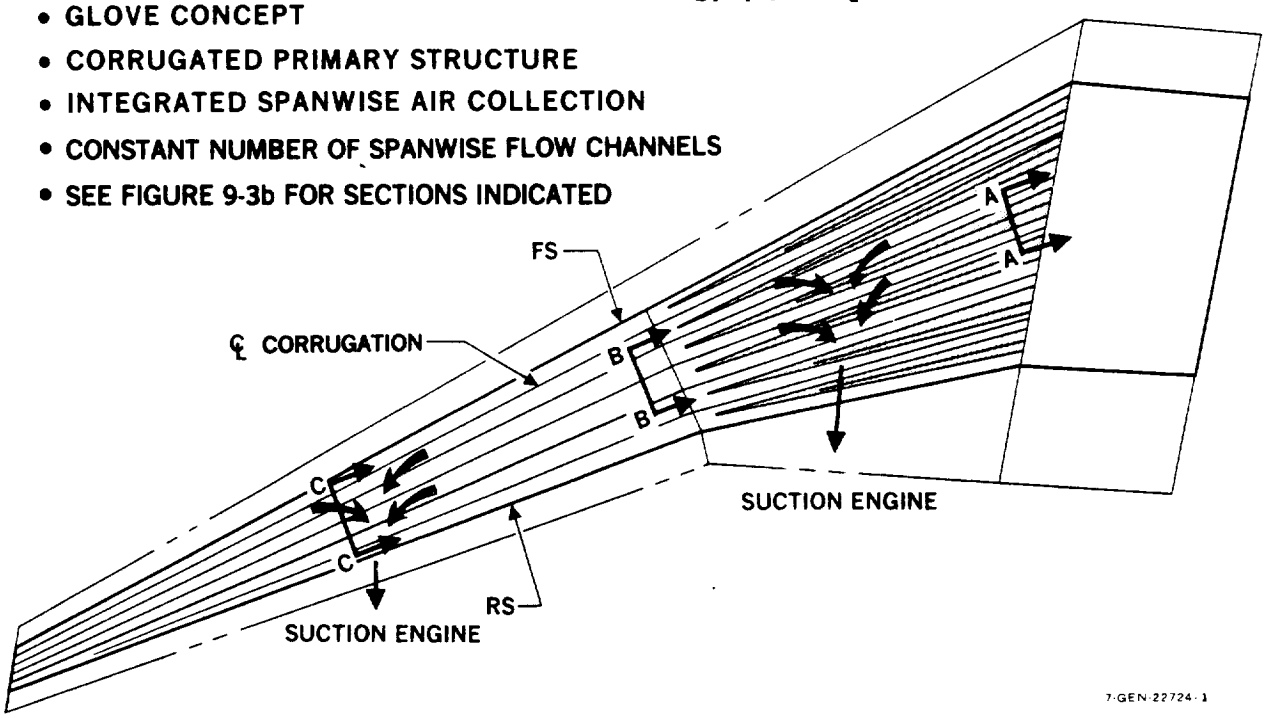

FIGURE 9-3a. BASELINE WING STRUCTURE

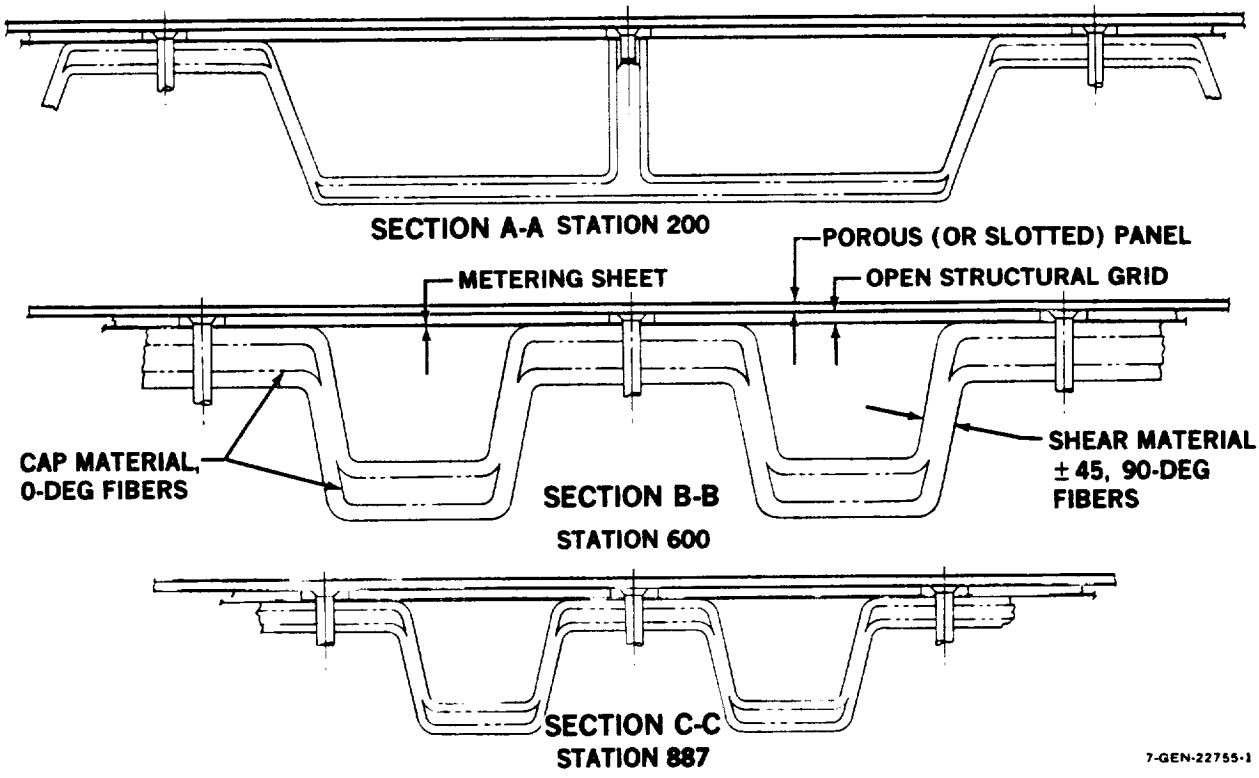

FIGURE 9-3b. CORRUGATED STRUCTURE (COMPOSITE)

Two critical wing load conditions were identified, both gust conditions. The low wing loading of 4.69 kPa (98 psf) made the large wing gust critical. Two fuel conditions were included in the analysis. With fuel outboard maximum bending relief was obtained, resulting in 20-30 percent less bending moment in the inboard wing region. The 3.24g gust response with minimum fuel in the wing produced 40 percent higher shears in the outboard wing and this sized the spar webs.

The bending material effective spread thickness ($\bar{t}$) requirements were generated initially on an Mc/I basis only. This factor ($\bar{t}$) was the significant parameter in the wing bending material requirements used for concept comparison. The bending load intensity peaked at approximately 40 percent span, Figure 9-5, because of the aerodynamic break in planform and thickness controlled by the thickness-to-chord ratio; see Figure 9-6.

The loads and sizing procedures were also run for an aspect ratio 14 geometry for comparison with the initial baseline AR of 12. This produced an even higher peak in the bending load intensity (Figure 9-5). The higher load intensities for the LFC wing were due to aerodynamic requirements for reduced thickness/chord ratios, Figure 9-6.

9.1.4 Flutter Penalty

A preliminary flutter analysis was run using the initial baseline wing bending (EI) and torsional (GJ) stiffnesses for both aspect ratios. The modal representation used in the flutter analysis consisted of three rigid body modes (symmetric and antisymmetric), five uncoupled wing bending modes, five uncoupled wing torsion modes, and one quasi wing-roll mode. This allowed independent variation of bending and torsion rigidities, which is feasible with composite material construction due to directional characteristics of the weave. The strength-only design rigidities were used initially and the analysis of flutter speeds versus percent fuel showed that the most critical loading was with full fuel tanks although even zero fuel produced a flutter speed that was less than the $1.2V_D$ requirement. Substantial increases in wing stiffness were indicated to meet the flutter requirement, see Figure 9-7.

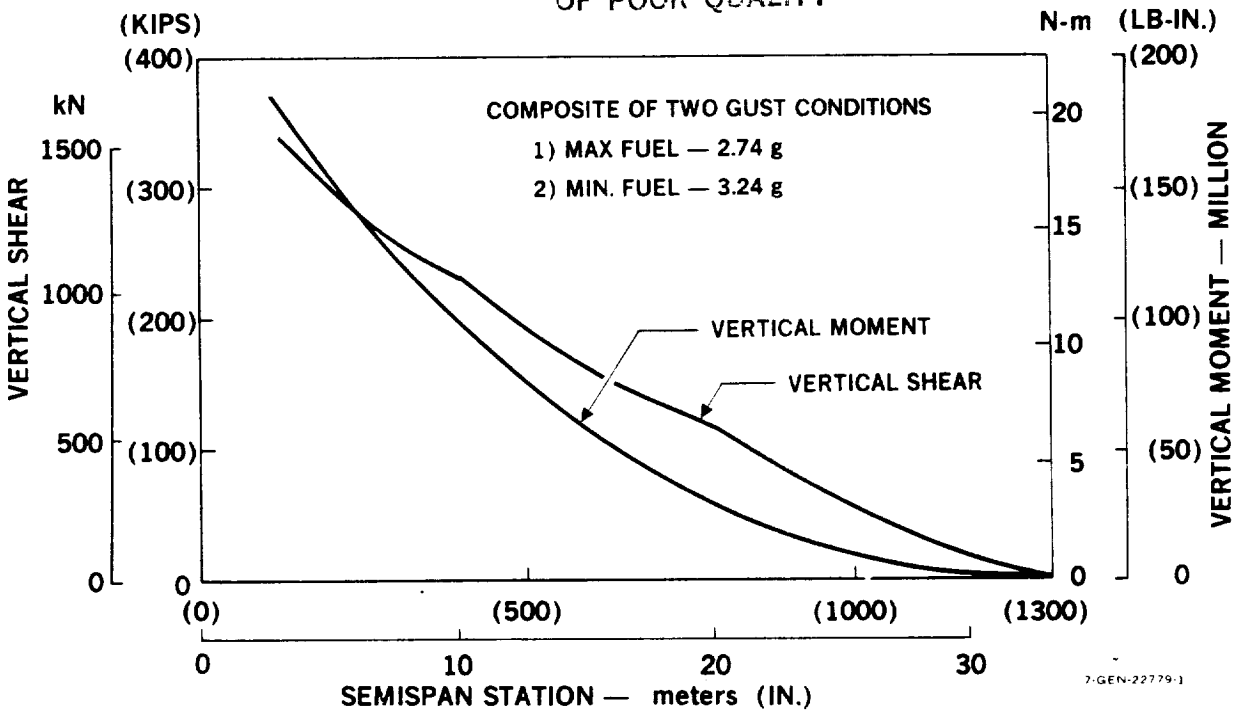

FIGURE 9-4. WING MOMENTS AND SHEARS

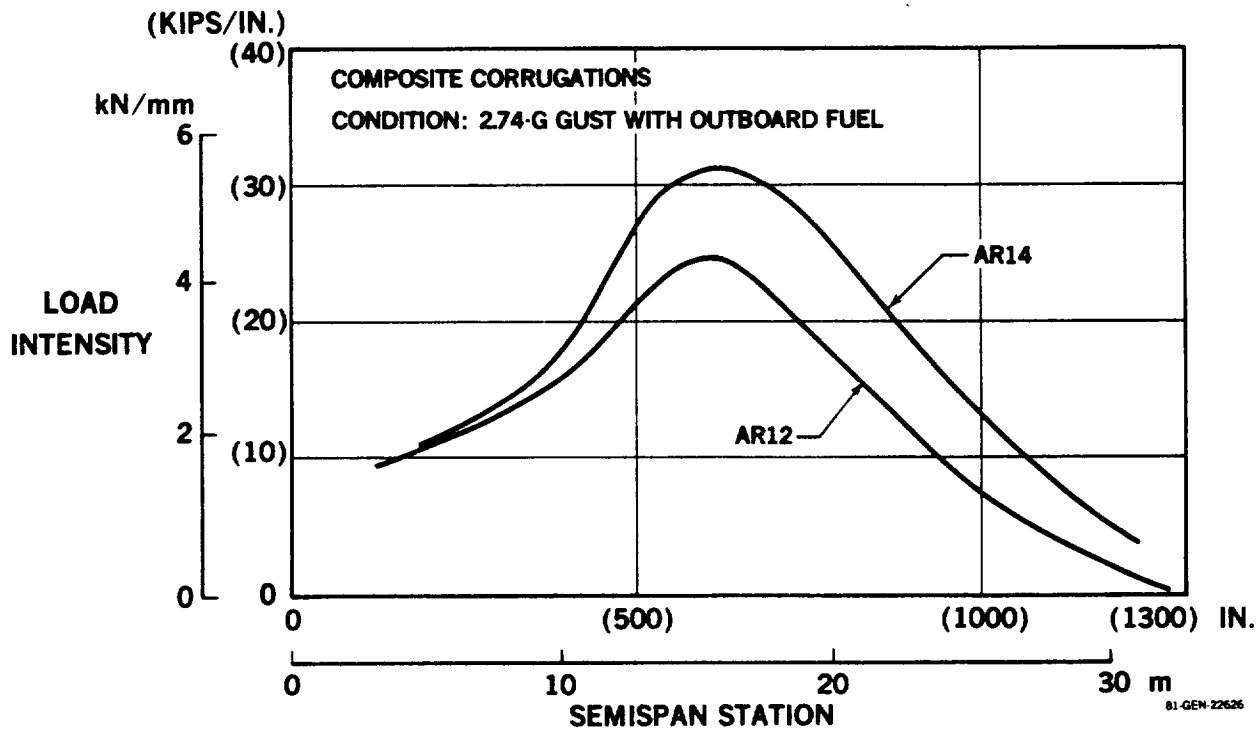

FIGURE 9-5. WING PANEL BENDING LOAD INTENSITY – SPANWISE VARIATION

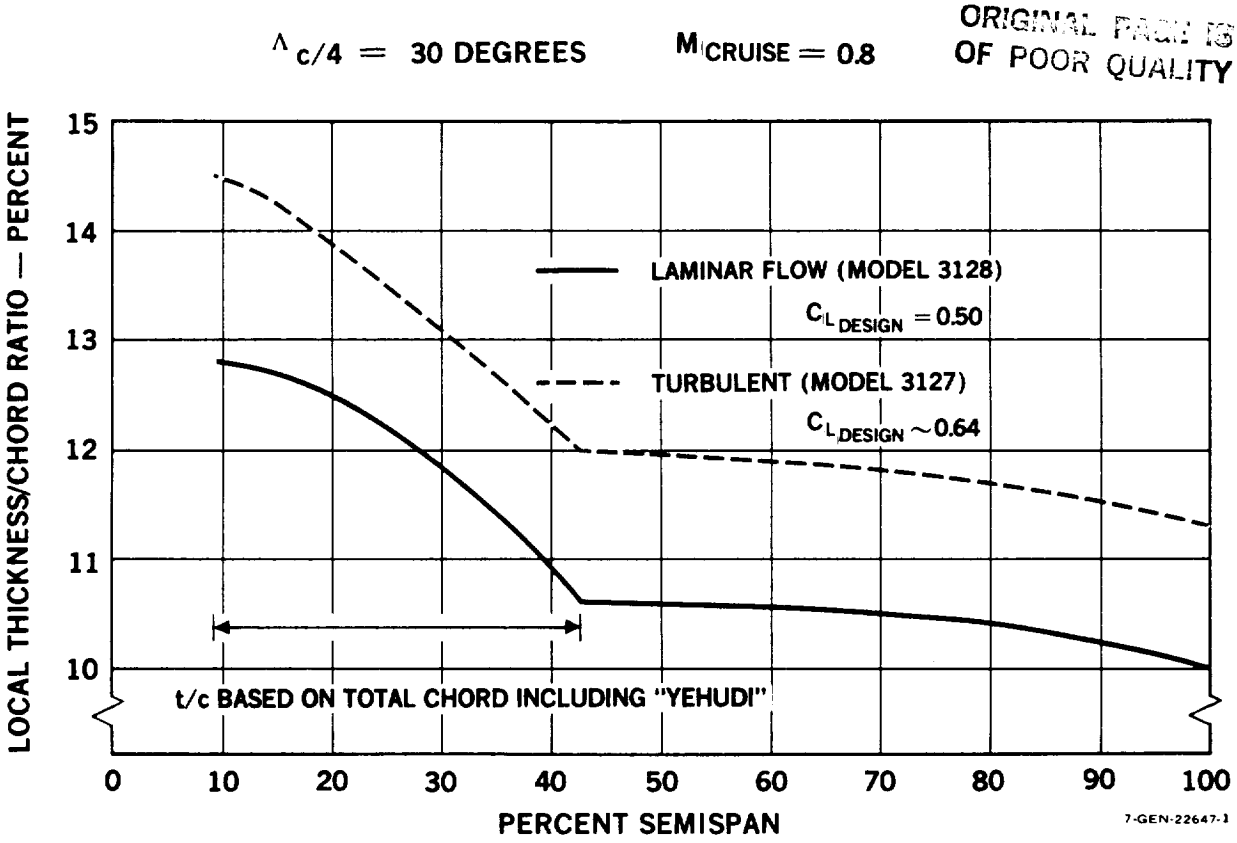

FIGURE 9-6. PRELIMINARY WING THICKNESS DEFINITION

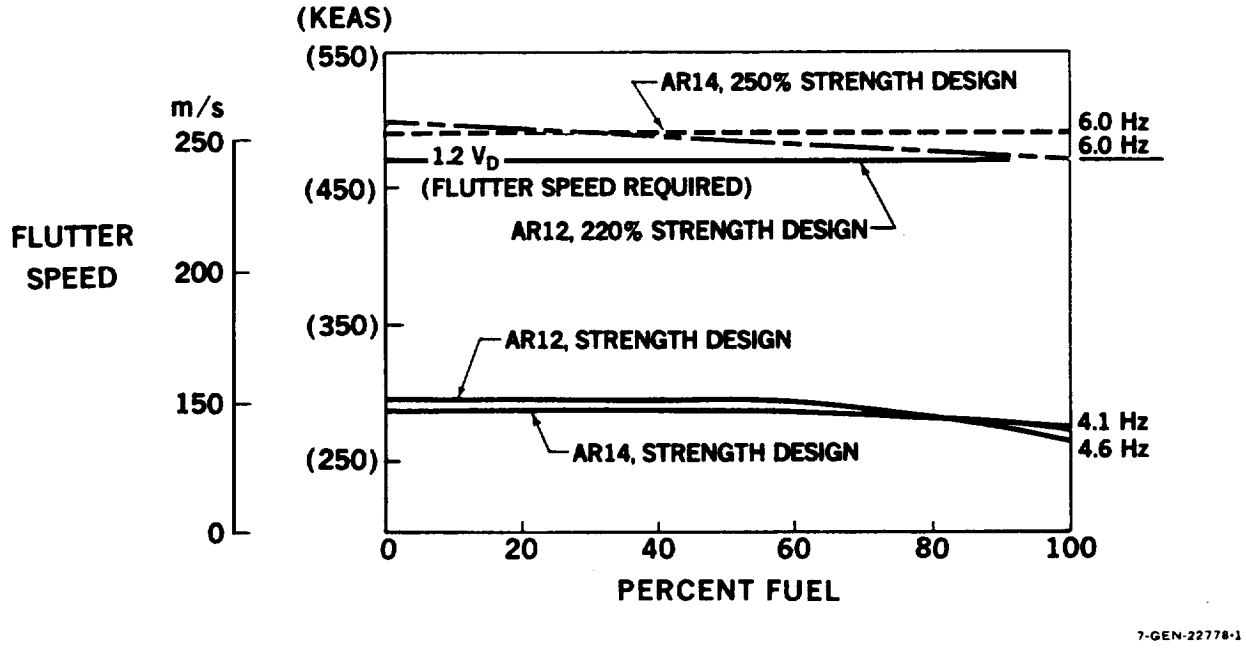

FIGURE 9-7. FLUTTER SPEED VERSUS PERCENT FUEL – INITIAL BASELINE STRENGTH DESIGNED WING

Increasing the bending stiffness (EI) over the strength designed values was found to have no effect on the flutter speed.

The required flutter speed was therefore attained by increasing the wing torsional rigidity (GJ), assuming constant percentage increases over the entire span. A factor of 2.2 times the strength-designed "GJ" values was required for the aspect ratio 12 baseline wing, and 2.4 times for an AR = 14 wing. Future stiffness tailoring along the span could significantly reduce the material required to meet flutter speed, however this analysis highlighted the effect of high aspect ratio on flutter for a 30° swept wing. Metallic wing designs, with a fixed E/G ratio, would incur larger penalties in meeting flutter stiffness requirements than graphite epoxy designs in which ply direction tailoring can be used to augment either EI (bending stiffness - 0° fibers) or GJ (twisting stiffness - 45° fibers) to give minimum weight penalty, see Figure 9-8. The resulting initial wing stiffnesses adjusted for flutter, but before aeroelastic analysis, are presented in Table 9-3.

9.1.5 Evaluation of Initial Concepts

Design sketches were generated for the structural concepts considered. Three of the concepts (arch-web, isogrid and peel-ply) were discarded early for various reasons as discussed in the following paragraphs:

- Concept C, Arch-Web (Figure 9-9) was initially attractive since it promised a very low LFC weight penalty and is geometrically shaped to favor easy integration of chordwise airflow collection and suction air/fuel separation with an efficient structure. The outer structural shell could be slotted honeycomb sandwich or monocoque. For a porous outer suction panel, the structural shell could be of isogrid or sandwich construction. Drawbacks of this design are (1) possible buckling instability for a continuous rib-supported wing cover that would be difficult to analyze, (2) lack of fuel slosh baffles (weight penalty) and (3) difficult fab/assembly sequence. This design could still be attractive for a fuel-free wing or stabilizer.

TABLE 9-3

INITIAL BASELINE WING STIFFNESS DISTRIBUTION
(Strength Designed Wing Stiffened For Flutter Only)

	AR 12 WING - 381 m^2 (4,100 ft^2) GRAPHITE EPOXY STRUCTURE			
	EI DESIGNED FOR STRENGTH		GJ DESIGNED FOR FLUTTER*	
Sta.	MNm^2	Billion Lb-In^2	MNm^2	Billion Lb-In^2
200	4178	1456	3814	1329
296	2936	1023	2594	904
400	1940	676	1685	587
500	1188	414	1111	387
600	720	251	542	189
700	465	162	336	117
800	281	98	227	79
1000	75	26	52	18
	AR 14 WING - 381 m^2 (4,100 ft^2) GRAPHITE EPOXY STRUCTURE			
200	4729	1648	4698	1637
296	3472	1210	3340	1164
400	2376	828	2175	758
500	1550	540	1570	547
600	887	309	717	250
700	591	206	453	158
800	385	134	304	106
1000	132	46	98	34
1200	23	8	17	6

*2.2 GJ factor over strength design for AR 12

2.4 GJ factor over strength design for AR 14

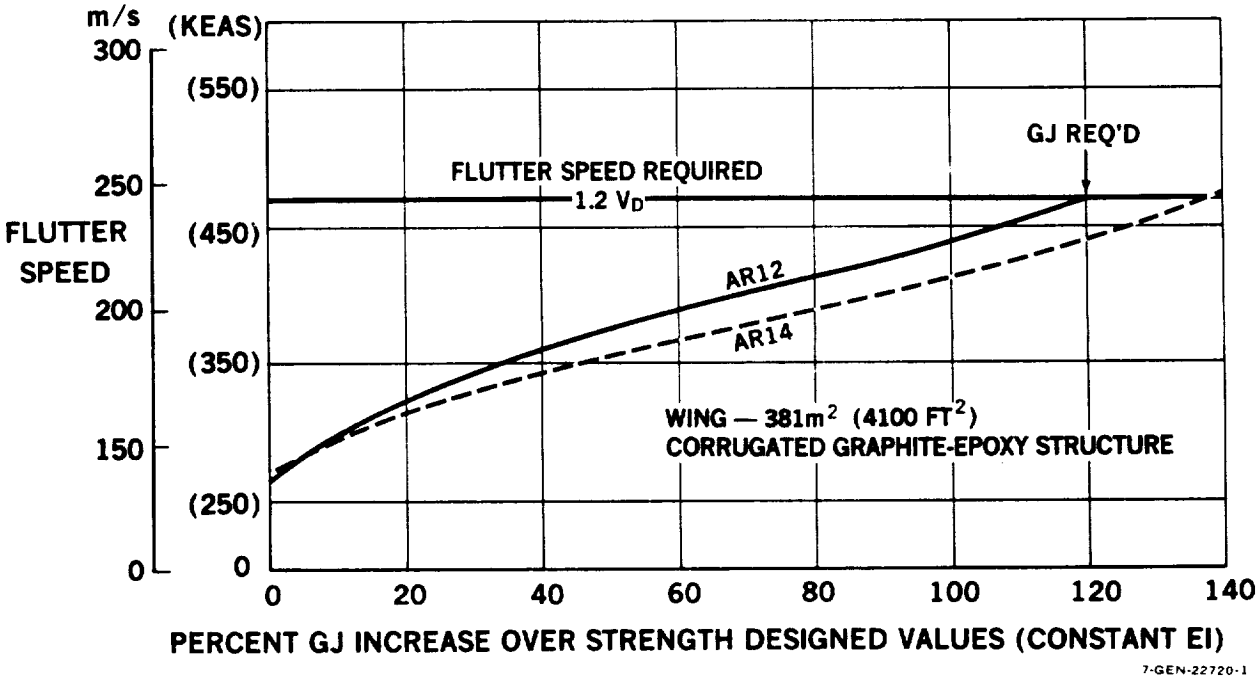

FIGURE 9-8. WING TORSIONAL STIFFNESS INCREASE REQUIRED FOR FLUTTER

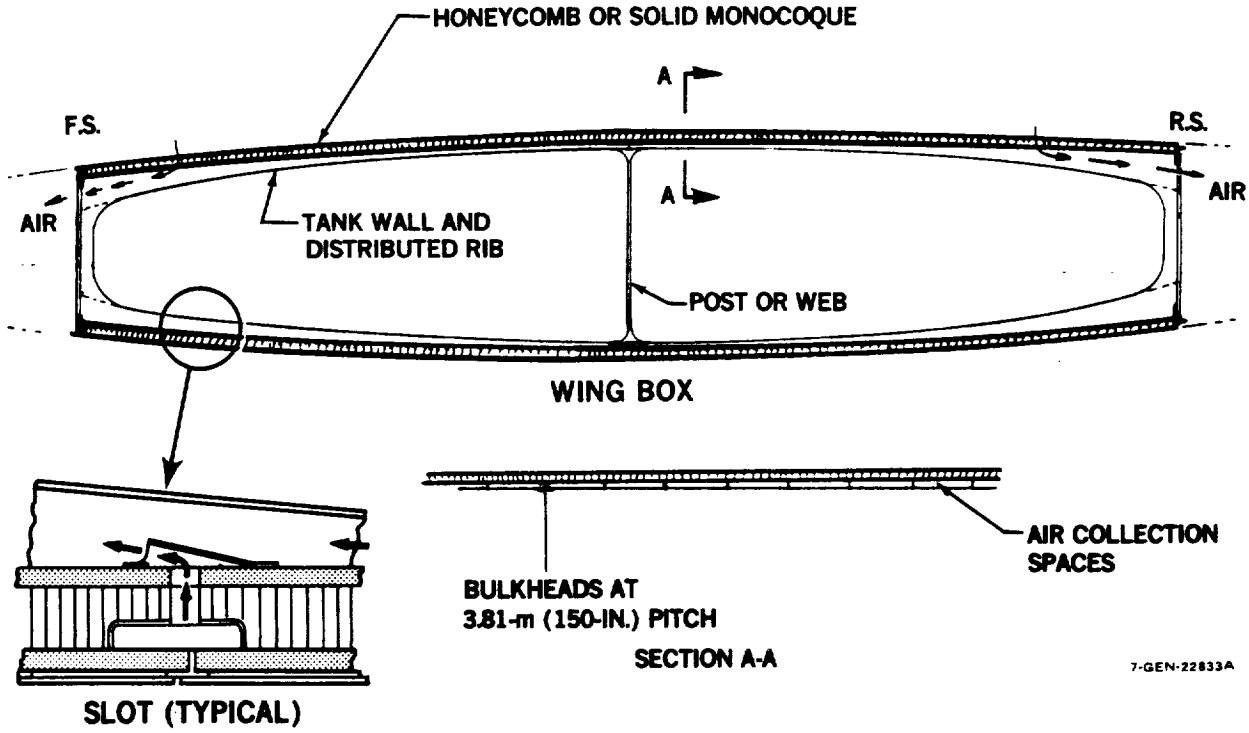

FIGURE 9-9. ARCHWEB-STIFFENED CONCEPT – CHORDWISE COLLECTION – SLOTTED LFC SURFACE

- Concept D, Isogrid-Stringer, Figure 9-10. The isogrid concept studied was of aluminum construction although it would be feasible in graphite epoxy. The isogrid was sized to take an estimated 945.7 kN/m (5400 lb/in) shear load only, since the spanwise grid bars would otherwise be required to take an estimated 4.378 MN/m (25,000 lb/in) bending load intensity and would be very large, penalizing the chordwise grid direction. Stringers were therefore added to take the major portion of the bending load. The spaces between the added stringer were used for air collection and a 1.27 mm (.050 in) diaphram acted as fuel and pressure barrier. The section weight of 51.3 kg/m^2 (10.5 psf) compared unfavorably with the 31.7 - 34.2 kg/m^2 (6.5-7 psf) weight then being obtained for the graphite and/or titanium corrugations and honeycomb sandwich concepts.

- Peel Ply Concept, Figure 9-11. This was a derivative of the corrugated concept "A", except for incorporating an unusual semi-flexible, three-dimensionally porous blanket over air collection holes in the structural skin. This promised to be one of the lightest designs, but cursory materials work with controlled flow resin-impregnated Scott foam under Dynapore surfaces failed to disclose a feasible materials combination for the porous blanket.

  The objective of the "peel-ply" concept was to eliminate mechanical fasteners in the surface yet provide a readily removable surface for cleaning or replacement.

Weight numbers were obtained for other concepts judged to be feasible (Concepts A, B, E, F in Table 9-4). A multi-station analysis using the loads and stiffnesses described previously, provided bending and shear material requirements for the seven remaining concepts. Table 9-4 compares weight efficiency results at the 45-percent semi-span station. This station coincided with peak loading intensity, however an analysis using a larger matrix of stations indicated the same general trends.

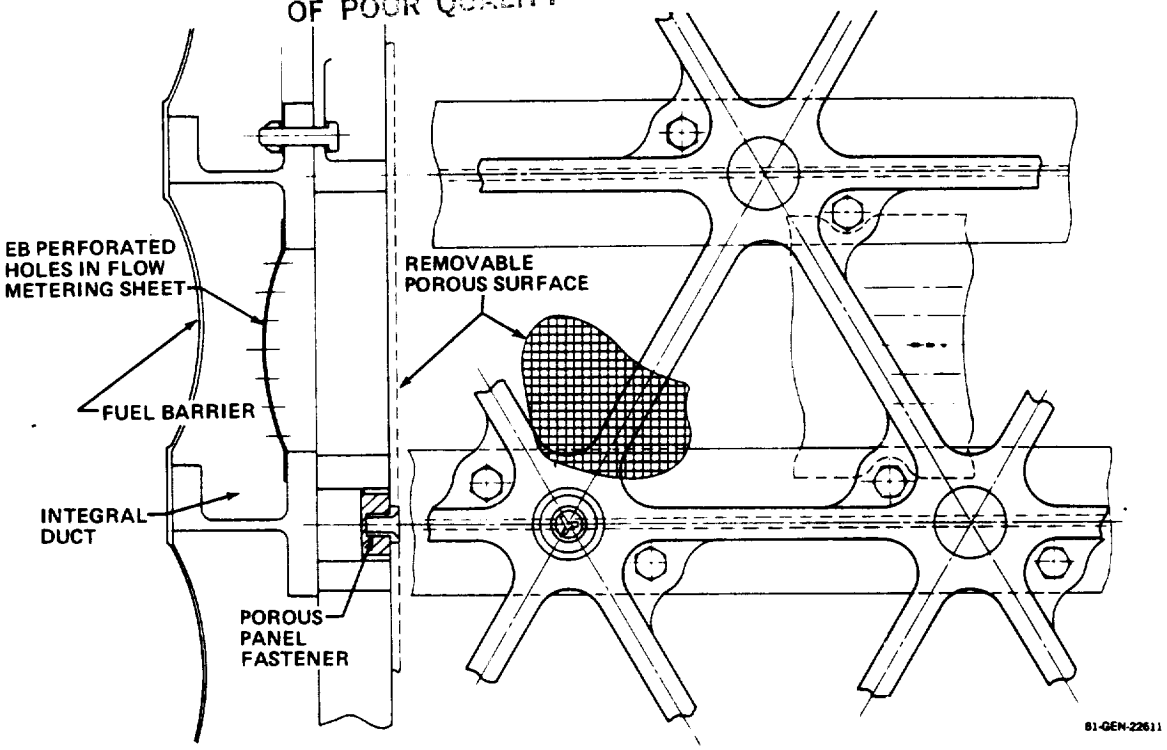

FIGURE 9-10. ISOGRID STRINGER CONCEPT

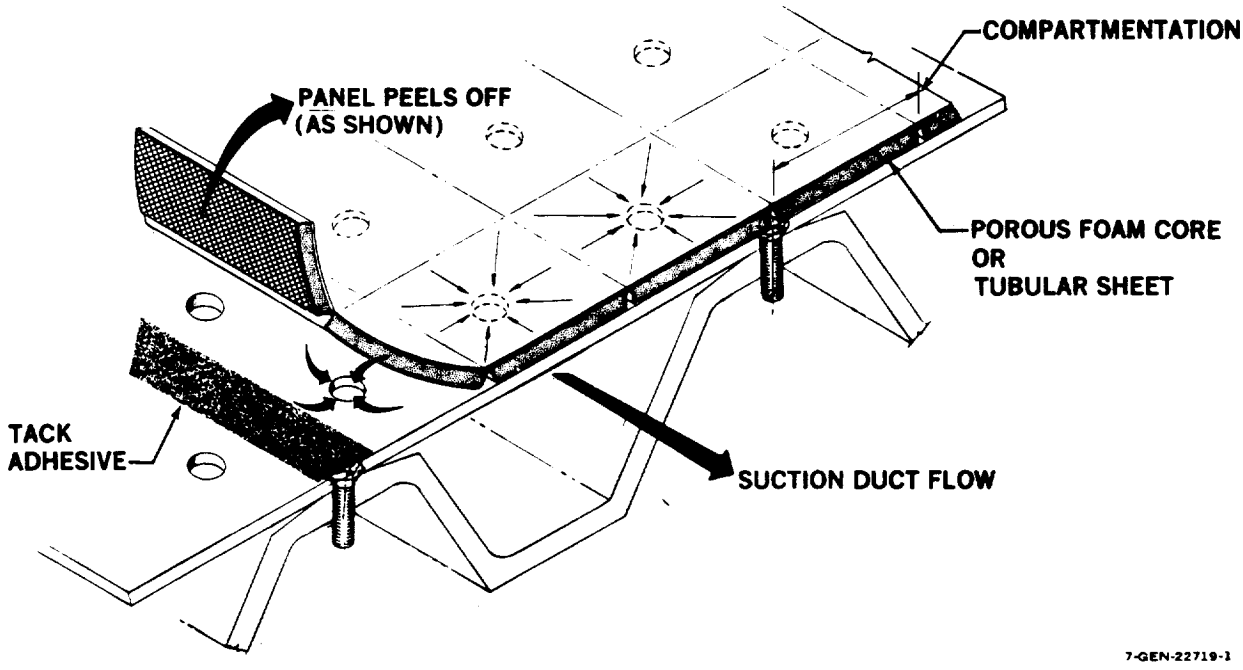

FIGURE 9-11. PEEL-PLY CONCEPT

TABLE 9-4

PRELIMINARY STRUCTURAL DESIGN ASSESSMENT

WING BOX COVER INCLUDING LFC SURFACE AT 45 PERCENT SEMISPAN FOR STRENGTH AND FLUTTER STIFFNESS

STRUCTURAL CONCEPT	BOX STIFFNESS		WEIGHT OF UPPER COVER			RELATIVE WEIGHTS PER UNIT AREA
	GJ-MNm^2 (LB-IN.^{2} BILLIONS)	EI-MNm^2 (LB-IN.^{2} BILLIONS)	kg/m^2 (LB/FT^2)			
			STRUCT	GLOVE	TOTAL	
A. CORRUGATION						
A_{cgp}, COMPOSITE – POROUS 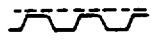	549.9 (191.6)	694.5 (242.0)	46.29 (9.48)	8.93 (1.83)	55.22 (11.31)	ϕ1.52
A_{cis}, COMPOSITE – SLOTTED 	549.9 (191.6)	694.5 (242.0)	46.29 (9.48)	0	46.29 (9.48)	1.28
A_{tgp}, TITANIUM – POROUS 	483.3 (168.4)	744.7 (259.5)	72.11 (14.77)	8.93 (1.83)	81.05 (16.60)	2.24
B. EXTERNAL BLADE						
B_{cgp}, COMPOSITE – POROUS 	553.0 (192.7)	639.1 (222.7)	44.09 (9.03)	10.35 (2.12)	54.44 (11.15)	ϕ1.5
E. HONEYCOMB SANDWICH						
E_{cis}, COMPOSITE – Ti SLOTS 	588.3 (205.0)	721.8 (251.5)	36.23 (7.42)	0	36.23 (7.42)	1.0
F. INTERNAL BLADE**						
F_{agp}, ALUMINUM – POROUS 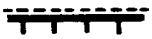	543.0 (189.2)	920.1 (320.6)	95.01 (19.46)	11.42 (2.34)	106.43 (21.80)	2.94**
F_{cgp}, COMPOSITE – POROUS	541.2 (188.6)	646.3 (225.2)	42.04 (8.61)	11.42 (2.34)	53.46 (10.95)	ϕ1.47**

ϕ GLOVE TRADE STUDY COMBINATIONS SELECTED FOR FURTHER STUDY

**RELATIVE OVERALL WEIGHT WOULD BE LESS DUE TO SMALLER CHORD MAIN BOX WITH CHORDWISE AIR COLLECTION

7-GEN-22757-1

Each design was brought to the same level of required stiffness for flutter. The metallic designs incurred greater stiffening weight penalties than the composites since, in meeting GJ requirements, they acquired excess EI material due to the fixed E/G ratio of metallic isotropic materials. The titanium corrugated primary structure was abandoned because it was one of the heaviest designs considered. The aluminum internal blade design that survived earlier screenings was the heaviest, due to the added stiffness penalty. This configuration was closest to conventional wing design.

As expected, the designs with structural material closer to the outer surface were lighter. The honeycomb design illustrated in Figure 9-12, although shown to be the lightest, would be heavier than indicated when the weight of air collection through the fuel tank and joints and attachments are considered; it was not considered further however because Douglas design philosophy for honeycomb structures* is to avoid its use for primary structure. The three glove panel designs with graphite epoxy primary structure are approximately equal in weight when glove panel weights are included. Of these three (corrugated, external blade and internal blade), either of the blade-stiffened designs would be preferred on a basis of probable cost. System weights on a whole-wing basis, including the weight of additional ducting, and relative efficiencies of the spanwise versus chordwise air collection schemes were not considered in this preliminary analysis.

*Honeycomb Design Philosophy. Douglas design philosophy allows the use of honeycomb material for non-structural components, lower life fairings, and replaceable control surfaces if overall evaluation shows it to be advantageous. The reasons for avoiding honeycomb construction for primary structure are:

- It is extremely vulnerable to moisture absorption, corrosion (if aluminum) and delamination. This would apply particularly to an integral air collection LFC honeycomb design where atmospheric moisture is drawn directly into or through the core.

- It is vulnerable to fuel absorption - particularly if the air collection pipes enter the fuel bays through the inner surfaces of the honeycomb sandwich.

- o Attachments and joints are complicated, leading to higher cost - much of the apparent weight advantage may be lost due to heavier joints.

- o Repair is difficult - especially for highly-loaded composite/honeycomb panels.

- o Airline resistance to honeycomb construction is already very strong - due to experience of premature failures in service and costly maintenance procedures.

9.1.6 Aeroelastic Penalty

The stiffness distributions derived for the initial baseline configuration AR 12 and 14 wings, considering strength and flutter requirements only (Table 1) were subjected to an aeroelastic analysis for roll control system effectiveness. Both wings were found to be deficient because of excessive bending and twisting deflection leading to loss of aileron effectiveness at required speeds. Initially, an aeroelastic stiffening factor of 1.5 was applied uniformly spanwise to both EI and GJ of the graphite epoxy structures of Table 9-4. The subsequent multi-station analysis indicated additional stiffness increase would be required to meet the roll stiffness criteria. High modulus GY-70 fiber was therefore introduced in place of T-300 (high strength) fiber material in the $\pm 45°$ plies. This resulted in reduced shear material weight with increased shear stiffness. The T-300 material was retained for the 0° spanwise fibers because of uncertainty about the ultimate strain allowable for GY-70 fibers at this time. The resulting weights for AR 12 are listed in Table 9-5, with an all T-300 weight calculation for comparison. The results clearly indicate the advantage of using GY-70 fibers. The corrugated main box design was the heaviest and the two blade stiffened design weights were not significantly different.

9.1.7 Concept Selection.

The weight of the external blade design was slightly higher than for the internal blade (Table 9-5) but provided the advantage of integral spanwise ducting of increased area compared with the corrugated design. The corrugated design would

TABLE 9-5

WING STRUCTURE WEIGHT

EFFECT OF AEROELASTIC REQUIREMENTS

WITH GY-70 GRAPHITE

Composite Structural Concept	Wing Box Cover Unit Weight*						With LFC Porous Glove Panel T-300 + GY-70	
	Strength/Flutter Only T-300 Fiber		Strength/Flutter & Roll Stiffness					
			T-300 Only		T-300 + GY-70+			
	kg/m^2	lb/ft^2	kg/m^2	lb/ft^2	kg/m^2	lb/ft^2	kg/m^2	lb/ft^2
Corrugated	46.29	9.48	79.05	16.19	51.51	10.55	61.27	12.55
External Blade	44.09	9.03	69.09	14.15	48.19	9.87	57.95	11.87
Internal Blade	42.04	8.61	67.18	13.76	46.87	9.60	56.64	11.60

*Weight/Unit Area at 45 Percent Semi-span

+GY-70 High Modulus Fibers Used in 45 Degree Layers Only.

also incur additional weight penalties because of its inefficiency in carrying chordwise concentrated loads. Another factor against the corrugated concept was that aft of about 65 percent chord the corrugations were not big enough for the increased suction airflow collection, by a factor of two.

An early external blade design sized only for strength and flutter stiffness is shown in Figure 9-13. The exterior paneling was considered at this stage to be fastened mechanically to a glove panel support grid. The grid was then fastened to the split blade stiffened cover below. Flanges were not used to stiffen the blades in order to provide the maximum surface area for porosity; the grid effectively provided both blade stabilization and an outer structural cap. Elements of the trailing edge control system could be readily attached with this design as shown in Figure 9-14, due to the continuous load path provided by the inner structural skin. Rib attachment to the main panel is simplified by the absence of internal stiffeners.

The internal blade structure is shown in Figure 9-15, which also illustrates an option of chordwise air collection. The blades are parallel to each other and to the rear spar, and the wing ribs are attached using separate shear clips as in a conventional wing. Suction airflow from the surface passes through a grid, supported outside the primary wing skin, on chordwise standoff strips. The standoff strips act as chordwise "cross stiffening" and as air flow dividers. The porous outer panel is attached to the grid and can be removed separately. With chordwise collection, the spar location must be moved aft (from.15 chord to .19 chord) to provide space for ducting in the leading edge.

The Internal Blade design is similar to a conventional wing structure with respect to trailing edge control system attachment, Figure 9-16. Air was not ducted spanwise aft of the rear spar with the chordwise collection system because of interference with control system bracketry. Thus both upper and lower surface air is collected forward into the leading edge region where it is ducted spanwise before being ducted into the dry bay at the suction engine. It should be noted that at this stage of conceptual design, LFC suction was being used on both upper and lower surfaces to .7 chord.

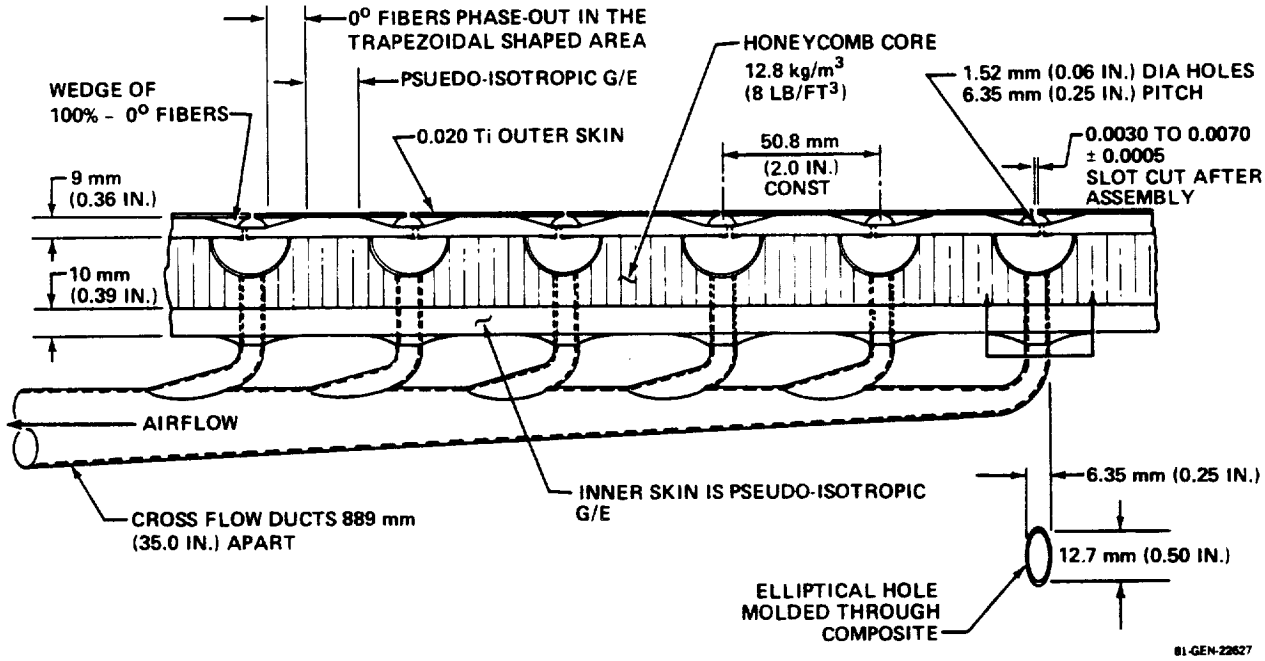

FIGURE 9-12. HONEYCOMB CONCEPT

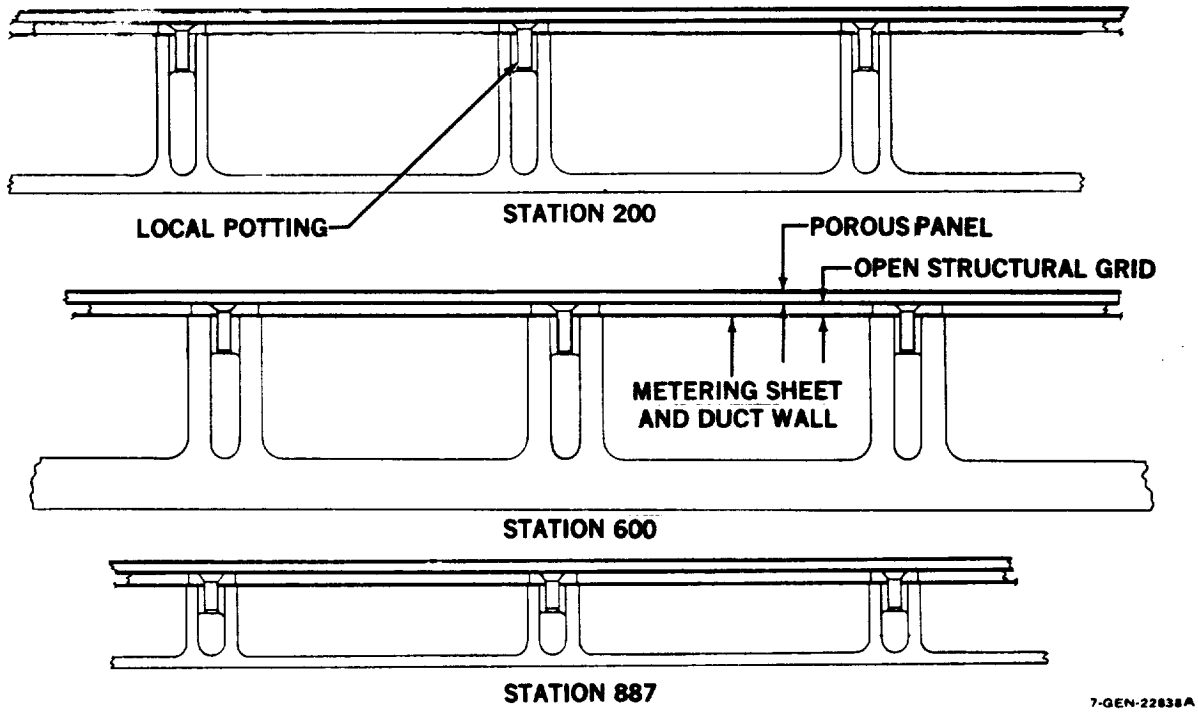

FIGURE 9-13. EXTERNAL BLADE STIFFENER CONCEPT

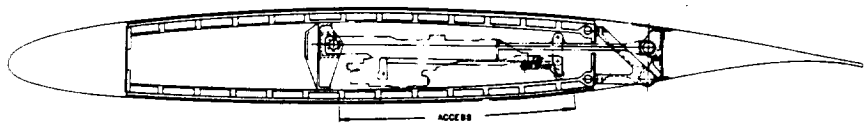

AILERON ATTACHMENT SECTION

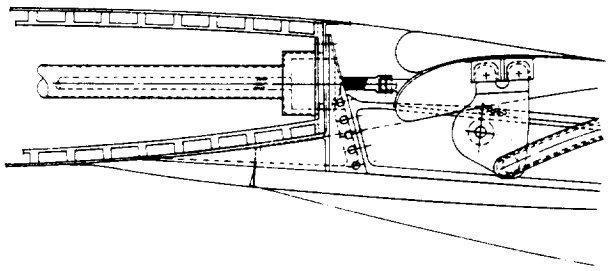

FLAP SUPPORT STATION

SPOILER SUPPORT

7-GEN-22930

FIGURE 9-14. CONTROL SYSTEM ATTACHMENT – EXTERNAL STIFFENER BLADE CONCEPT

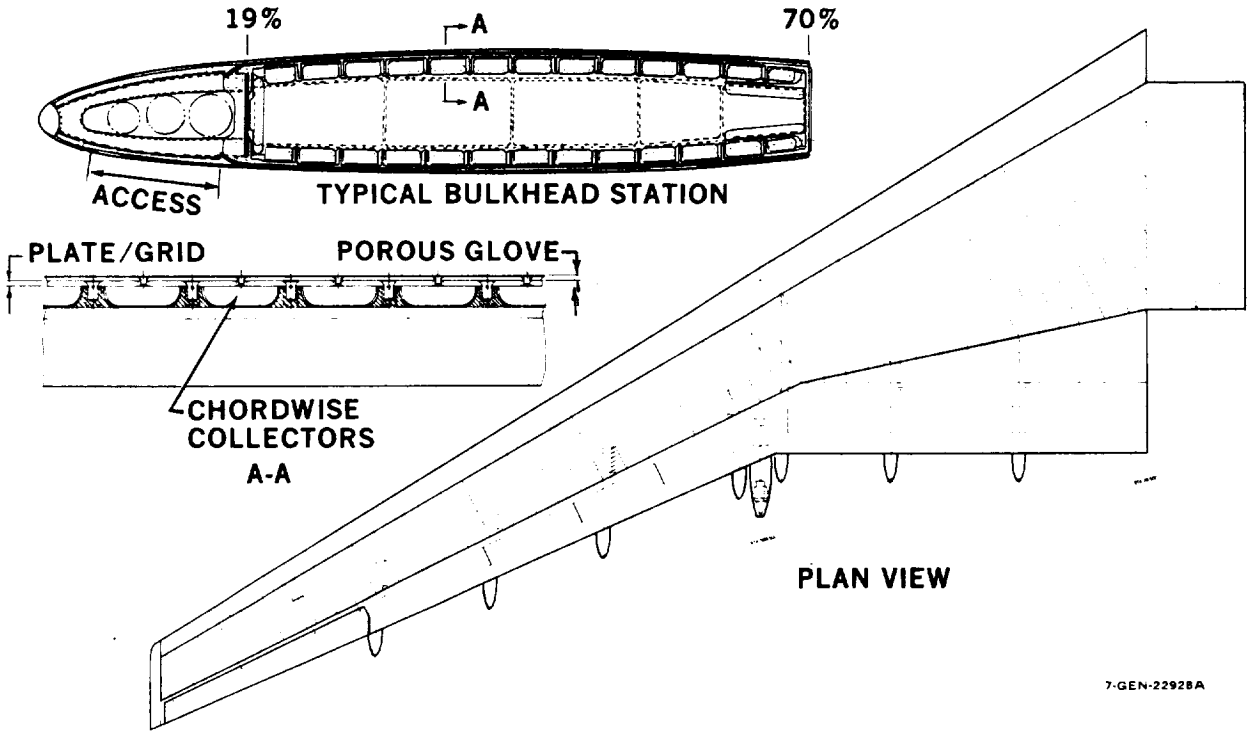

FIGURE 9-15. INTERNAL BLADE STIFFENER CONCEPT – CHORDWISE AIR COLLECTION

The preliminary wing weight comparison of Table 9-6 clearly shows the corrugated structure to be heavier. The trade study was therefore reduced to internal versus external blade configurations and chordwise versus spanwise air collection. A comparison of the blade stiffened designs with only one suction pump/engine installation per side is shown in Table 9-7. In spite of the increased duct size required in the leading edge and the further aft location of the front spar, the internal blade stiffened wing was lighter. With the weight difference being small, the decision was made to proceed with the External Blade stiffening at this stage because of its inherent spanwise air collection capability, but the internal blade stiffened structure would be more efficient if a chordwise suction airflow collection system were finally selected.

9.1.8 Aspect Ratio Study

In order to select the LFC wing planform and thickness ratio, parametric data concerning the effects of aspect ratio and thickness on wing structural weights were produced for use in the aspect ratio trade study discussed in Section 7.3. The general LFC wing concept selected for study was of unconventional material (graphite/epoxy composite) and of unconventional structural configuration (gloved-external stringer); there was therefore no reliable data base for estimating wing weights. A special design/analysis was required making use of conventional analytic tools for strength and stiffness analysis appropriately adjusted for geometry and materials properties. Three cases were carried in parallel for wing aspect ratios 10, 12, and 14. The starting planform family was derived from the initial baseline LFC configuration with suction on both surfaces, however, the wing area was updated to 334 m^2 (3600 ft^2) from the original 381 m^2 (4100 ft^2).

The general procedure used to establish material thickness and volume requirements for weight estimation of each of the three wing geometries was as follows:

a. Define design load conditions. Again, the load factor N_z for gust exceeded the 2.5g maneuver factor by a small amount.

b. Define external design loads and 1.0g twist requirement.

TABLE 9-6

WING WEIGHT COMPARISON
CORRUGATED VS EXTERNAL BLADE STIFFENING

	Corrugated Panels		External Blades	
	kg	(Lb)	kg	(Lb)
Bending Material	13,288	(29,163)	12,796	(28,210)
LFC Box Panels	4,480	(9,876)	4,480	(9,876)
L.E. With Ducts	877	(1,934)	877	(1,934)
Engine/Pump Assemblies*	1,104	(2,434)	1,104	(2,434)
Engine/Pump Nacelles	231	(510)	231	(510)
Ducting to Pumps	413	(910)	413	(910)
Additional Weight (Ribs, Webs, Flaps, Etc.)	10,499	(23,147)	10,282	(22,668)
Total	30,832	(67,974)	30,183	(66,542)

*Two Suction Engines per Side

TABLE 9-7

WING WEIGHT COMPARISON
BLADE STIFFENED STRUCTURES

	External Blades		Internal Blades	
	kg	(Lb)	kg	(Lb)
Bending Material	12,796	(28,210)	12,325	(27,172)
LFC Box Panels	4,480	(9,876)	4,154	(9,158)
L.E. With Ducts	877	(1,934)	1,110	(2,448)
Engine/Pump Assemblies*	683	(1,506)	683	(1,506)
Engine/Pump Nacelles	111	(244)	111	(244)
Ducting to Pumps	409	(902)	409	(902)
Additional Wing Weight (Ribs, Webs, Flaps, Etc)	10,282	(22,668)	10,503	(23,155)
Total	29,638	(65,340)	29,295	(64,585)

*One Suction Engine per Side

c. Establish a structural model geometry and materials allowables for each aspect ratio study wing.

Because of earlier experience on the preliminary baseline (see Section 9.1.6), GY-70 graphite fiber was used at the outset for ±45° plies, but the spanwise fibers remained T-300. The ultimate strain allowable was set at 0.004 for spanwise strains.

d. Establish GJ and EI values distributed along each wing span to meet external loads strength requirements and a 1.0g aerodynamic twist requirement.

At this stage it was noted that for the aspect ratio 14 wing, the high shear stiffness provided by the GY-70 fibers was necessary in the outboard wing merely to meet the 1g aeroelastic twist requirement for obtaining the desired spanwise lift distribution.

e. Establish the weight distribution of each wing represented, as lumped masses along the elastic axis, for the flutter analyses.

f. Calculate the spanwise lift distributions and the aerodynamic centers of pressure.

g. Conduct flutter analyses for the strength designed wing and establish flutter margins and the effect of stiffness variations.
(The wings were flutter free without additional material at this point.)

h. Conduct an aeroelastic analysis for each of the three wings using stiffness distributions established by the strength and flutter analyses.

j. Revise GJ and EI distributions per aeroelastic analysis and calculate the $\bar{t}$ distribution (bending material equivalent thickness) on which to base wing weights. An aeroelastic stiffening for each aspect ratio was found necessary, see Figures 9-17 and 9-18.

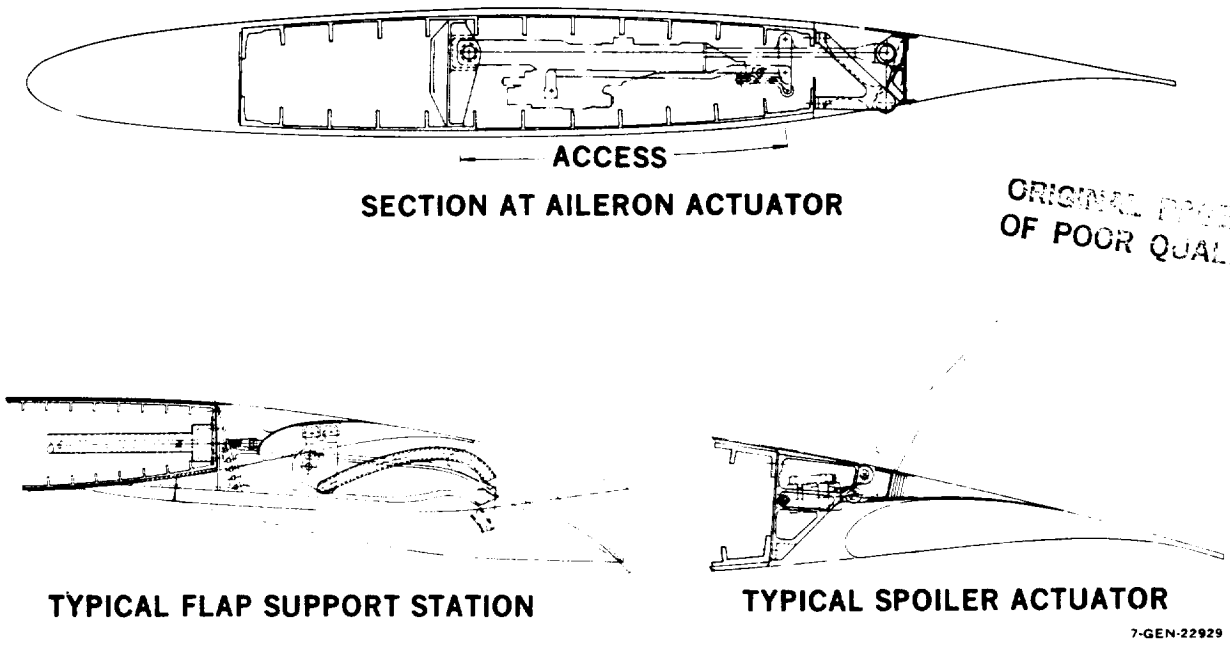

FIGURE 9-16. CONTROL SYSTEM ATTACHMENT – INTERNAL BLADE STIFFENER CONCEPT

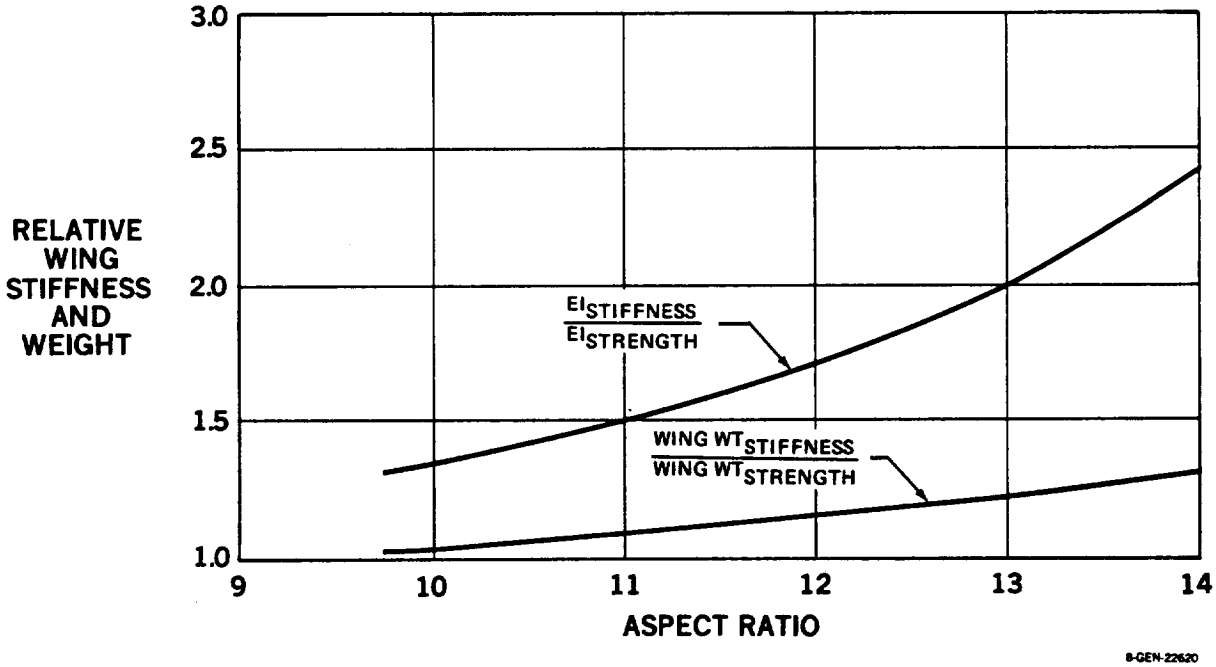

FIGURE 9-17. INCREASED STIFFNESS REQUIRED VERSUS ASPECT RATIO

k. Calculate wing weights for AR = 10, 12, 14.

l. Vary t/c of airfoil and calculate corresponding variations of $\overline{t}$ to meet final strength and stiffness levels. This is subsequently used to define wing weight variations as a function of t/c, see Figure 9-19.

m. Provide weights data for the aerodynamic performance analysis with suction on both wing surfaces.

n. Establish $\overline{t}$ for the "upper surface suction only" configuration to meet the stiffness rquirements, as above.

o. Calculate $\overline{t}$ variations for airfoil t/c variations.

p. Calculate weights and provide input to aero-performance analysis for comparison in "suction on both surfaces" versus "upper surface only" trade study.

9.1.9 Revised Wing Design Details

After the sizing and aspect ratio study, wing aspect ratio 10 and 311 m^2 (3350 ft^2) area were selected for the baseline LFC aircraft, with suction on both surfaces to 70 percent chord. Loads and stiffness requirements were then extrapolated for the new wing. Scope drawings of the wing box structure were prepared. Figure 9-20 shows the planform and a typical rib and Figure 9-21 shows structural details of the wing upper surface at the suction engine dry bay station. Elliptical holes were used to reduce spanwise load stress concentration in the wing skin and allow smooth air collection from each stringer bay. The suction engine support is a box beam cantilever extending from the rear spar. Figure 9-22 shows the lower wing cover at the suction engine. The large hole aft is for routing leading edge and upper surface suction air to the suction pump below the wing. The two holes forward are access door locations and the smaller holes aft are to route air from the lower triangular duct aft of the rear spar. The truss web construction was used to provide the additional ducting area required for the increased suction airflow aft of approximately 63 percent chord.

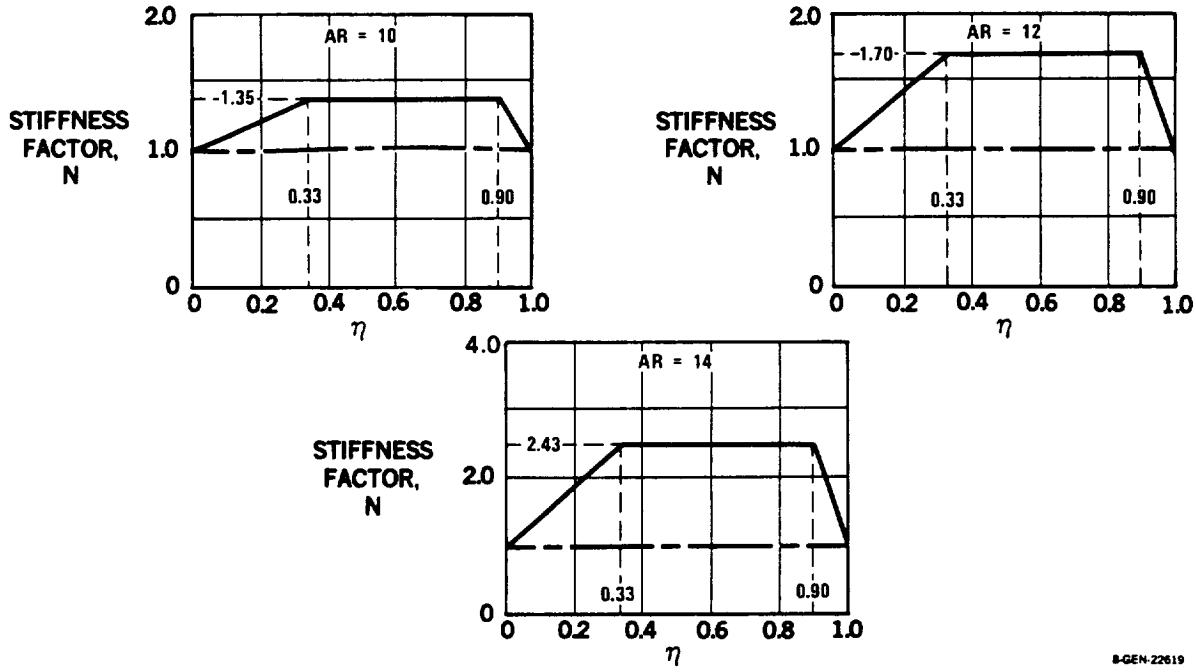

FIGURE 9-18. SPANWISE VARIATION OF INCREASED STIFFNESS

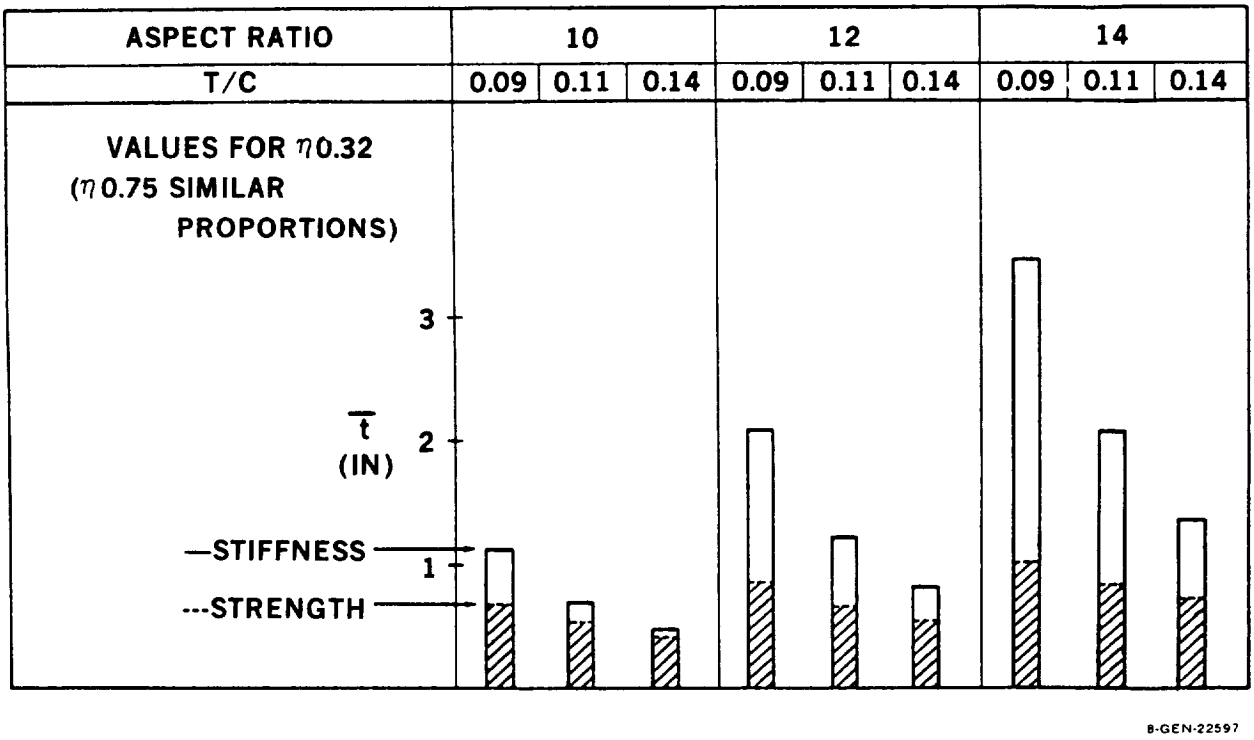

FIGURE 9-19. EFFECT OF THICKNESS/CHORD RATIO ON INCREASED STIFFNESS REQUIRED

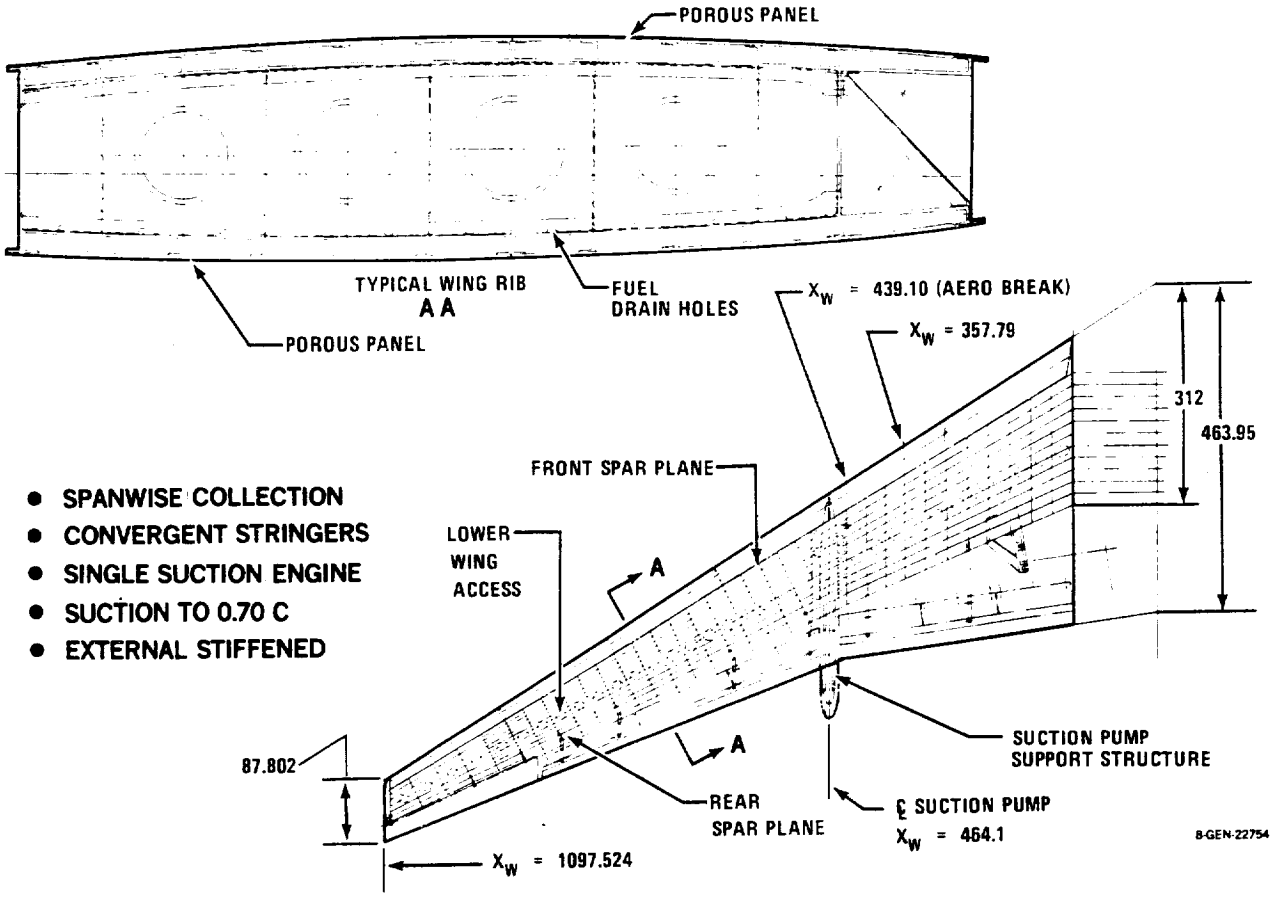

- SPANWISE COLLECTION
- CONVERGENT STRINGERS
- SINGLE SUCTION ENGINE
- SUCTION TO 0.70 C
- EXTERNAL STIFFENED

FIGURE 9-20. STRUCTURAL ARRANGEMENT – SUCTION THROUGH BOTH SURFACES

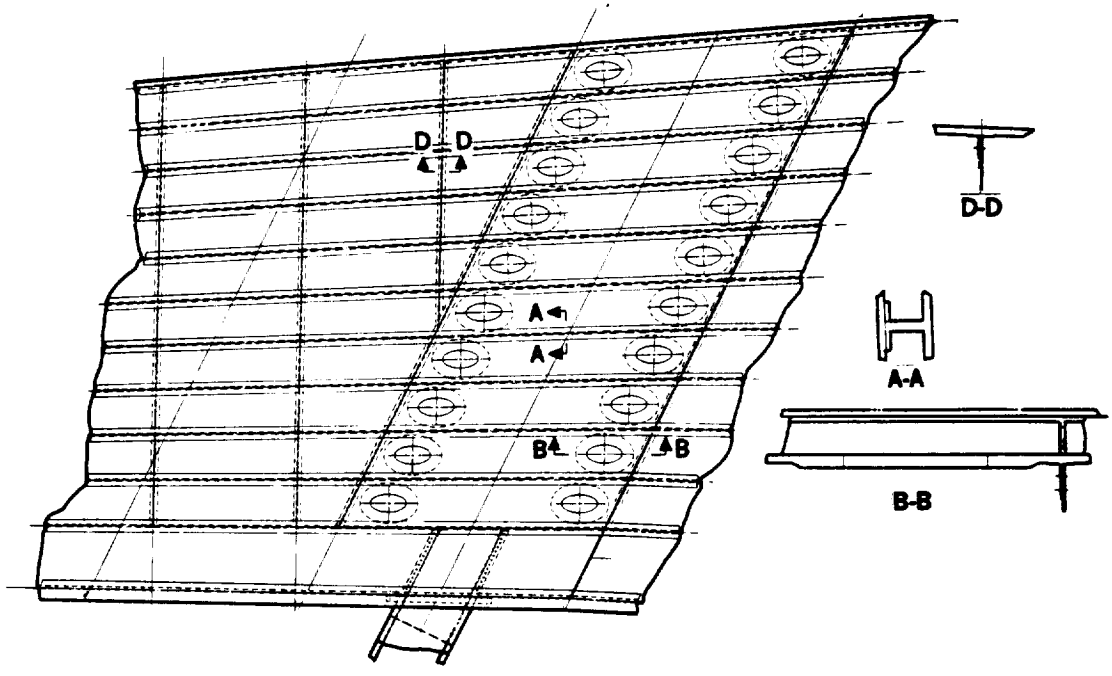

VIEW LOOKING DOWN AT UPPER SURFACE
(GLOVE PANEL NOT SHOWN)

8-GEN-22776

FIGURE 9-21. STRUCTURAL ARRANGEMENT – UPPER WING BOX PANEL AT ℄ OF SUCTION PUMP SYSTEM

A typical rib cross section with upper surface suction to 85 percent chord is shown in Figure 9-23. In this configuration, the spoiler and flap control surfaces were located aft of 85 percent chord and the truss web box extended further aft to provide ducting for the larger volume of upper surface suction air and still provide support for the control surface bracketry and actuators. The lower wing cover was of a more conventional internal blade stiffened skin graphite/epoxy construction. The weight trade study was favorable for this upper surface suction only structure, including the porous panels, compared to the previous baseline configuration with suction on both surfaces. This was primarily due to increased effective structural depth of the wing section without lower surface air collection.

9.1.10 Wing Box Structure Conclusions

- As expected, the wing span (aspect ratio) and wing thickness are dominant parameters in establishing structural bending material requirements, but in all cases wing weight was influenced primarily by aeroelastic stiffness requirements to assure roll control effectiveness.

- Increasing bending stiffness was more effective than increasing torsional stiffness in meeting the aeroelastic requirements with minimum wing weight.

- Flutter was not critical for any of the wings considered.

- GJ flutter margins indicate that further weight reduction could be achieved by optimum balancing of material characteristics to meet GJ, aeroelastic EI, and 1g twist requirements. The optimum would have increased bending stiffness at the expense of torsional stiffness.

- Duct space could also be reduced to some degree in order to increase the effective wing depth, since in this study the stiffener space allocation was never fully utilized for airflow (except at η = .4, AR 14). A reduction of stringer height must, of course, consider stringer/panel compression stability, but this did not appear critical for the proposed mixed modulus graphite composite structure.

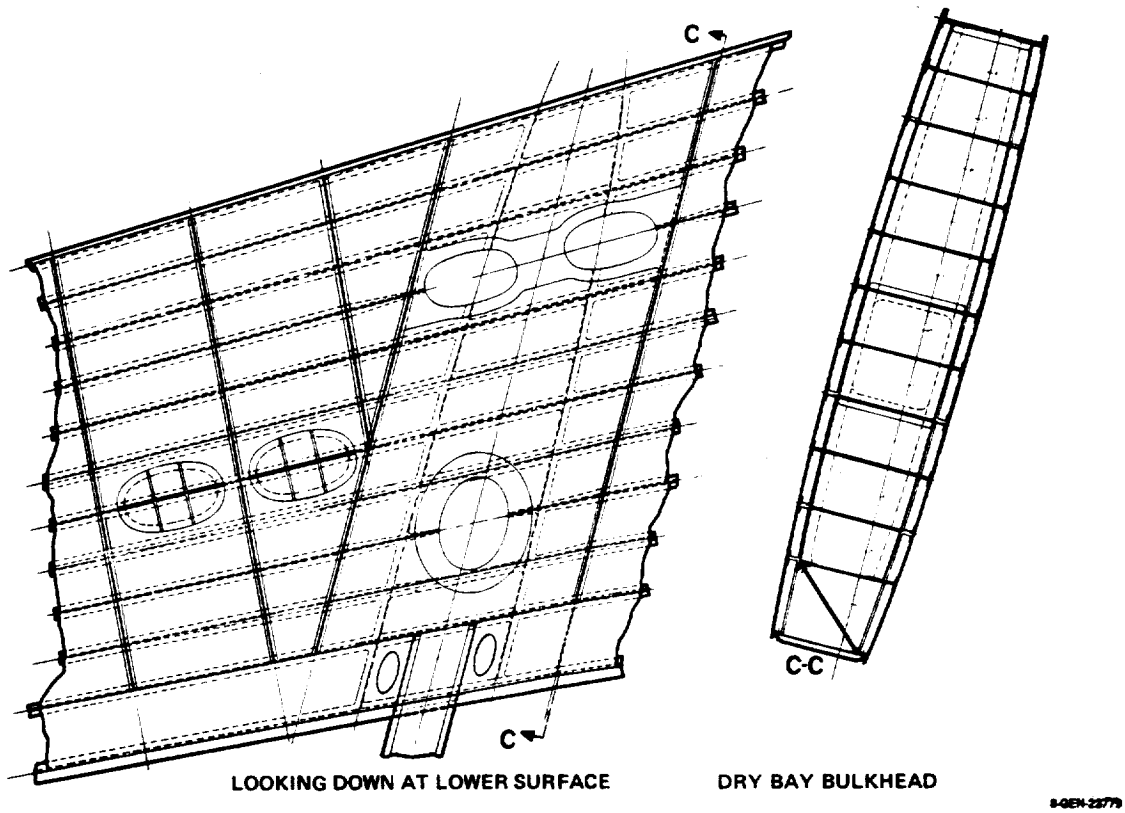

FIGURE 9-22. STRUCTURAL ARRANGEMENT SHOWING LOWER SURFACE AND FUEL BULKHEAD AT ℄ OF SUCTION PUMP SYSTEM

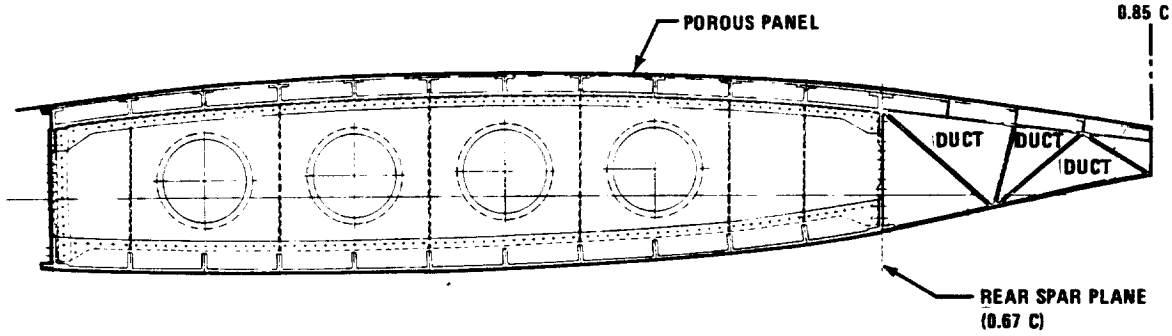

FIGURE 9-23. TYPICAL WING RIB – SUCTION THROUGH UPPER SURFACE ONLY TO 0.85 C

- An aluminum LFC wing of high aspect ratio with reduced effective structural thickness would carry a large weight penalty compared with a graphite epoxy structure.

9.2 POROUS SURFACE SELECTION AND LFC PANEL DESIGN

9.2.1 Initial Survey of Possible Materials & Construction

The selection and development of the porous LFC panel system was dependent on suction air collection requirements, Section 7.1.3, and LFC performance as measured in the Douglas wind tunnel, Section 8.1. Only those porous materials that could meet these basic requirements were considered structurally. Initial experience with porous materials indicated that most were of low modulus and low yield strength; they were therefore not considered to be part of the primary structure. In addition to strength and stiffness the following factors were considered:

- Replaceability in case of damage.
- Porosity - overall, in strips or in geometric patches.
- Smoothness of the surface and at joints
- Initial imperfections and deflection under load to meet waviness criteria.
- Strain characteristics to be comparible with strain levels that could occur in the primary structure.
- Durability in operational environments
- Clogging resistance and cleanability.

Some prior experience with porous panels was obtained under NASA Contract NAS1-14408 "Development of Technology for the Fabrication of Reliable Laminar Flow Control Panels on Subsonic Transports", see Reference 9.7-1. This program suggested suitable porous materials and areas needing further investigation. These included yield, fatigue strength and bondability of 316L stainless steel Dynapore porous sheet; strength of Kevlar 29/Epoxy porous Doweave laminate; resin selection, methods of controlling the porosity of a porous laminate, further investigation of methods of stiffening porous panels for LFC applications and clogging and cleaning of porous surfaces.

The following porous surface materials were considered initially:

- 316L Stainless Dynapore - "Microperforated plate", 50 x 250 and 24 x 110 weaves, used for LFC surfaces.

- Kevlar 29 (Kv 29) Doweave fabric (woven in "basic" weave pattern from 200 denier yarns) and impregnated with Corlar 5134 epoxy resin (250°F curing controlled flow resin, E.I. DuPont) used for porous layers in the body of the panel.

- 80 x 700 Dynapore; other resins and other weaves of Kevlar and glass were variants introduced.

LFC panel constructions considered initially included the following:

- Lockcore - a truss core construction using sewing techniques to mechanically lock the truss nodes to facings, see Figures 9-24 and 9-25. Various composite non-metallic materials can be used, Figure 9-26.

- Composite Isogrid - an interlocking fiber tri-axial grid made from continuous fiber yarns and epoxy, Figures 9-27, 9-28 and 9-29.

- Honeycomb sandwich with porous facings, see Figure 9-30, which contrasts isogrid and honeycomb surface supports as revealed by reticulating adhesive bleed-through at the porous surface in pressure drop test specimens.

The isogrid and honeycomb panel concepts considered require the airflow to be drawn completely through the outer stiffening sandwich before being ducted laterally; this resulted in the need for a double sandwich glove panel or a separate collection structure under the outer sandwich. The Lockcore, on the other hand, already provides a tubular air collection structure once the air is drawn through the outer surface. This feature of Lockcore is an additional advantage.

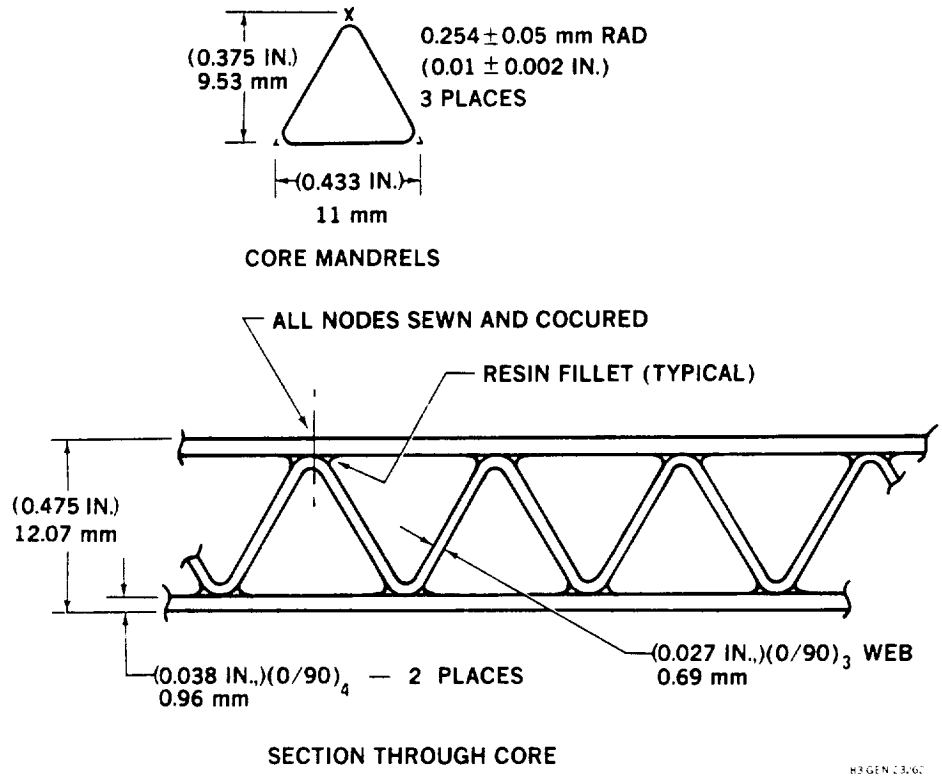

FIGURE 9.24 LOCK CORE BASIC PANEL DEFINITION

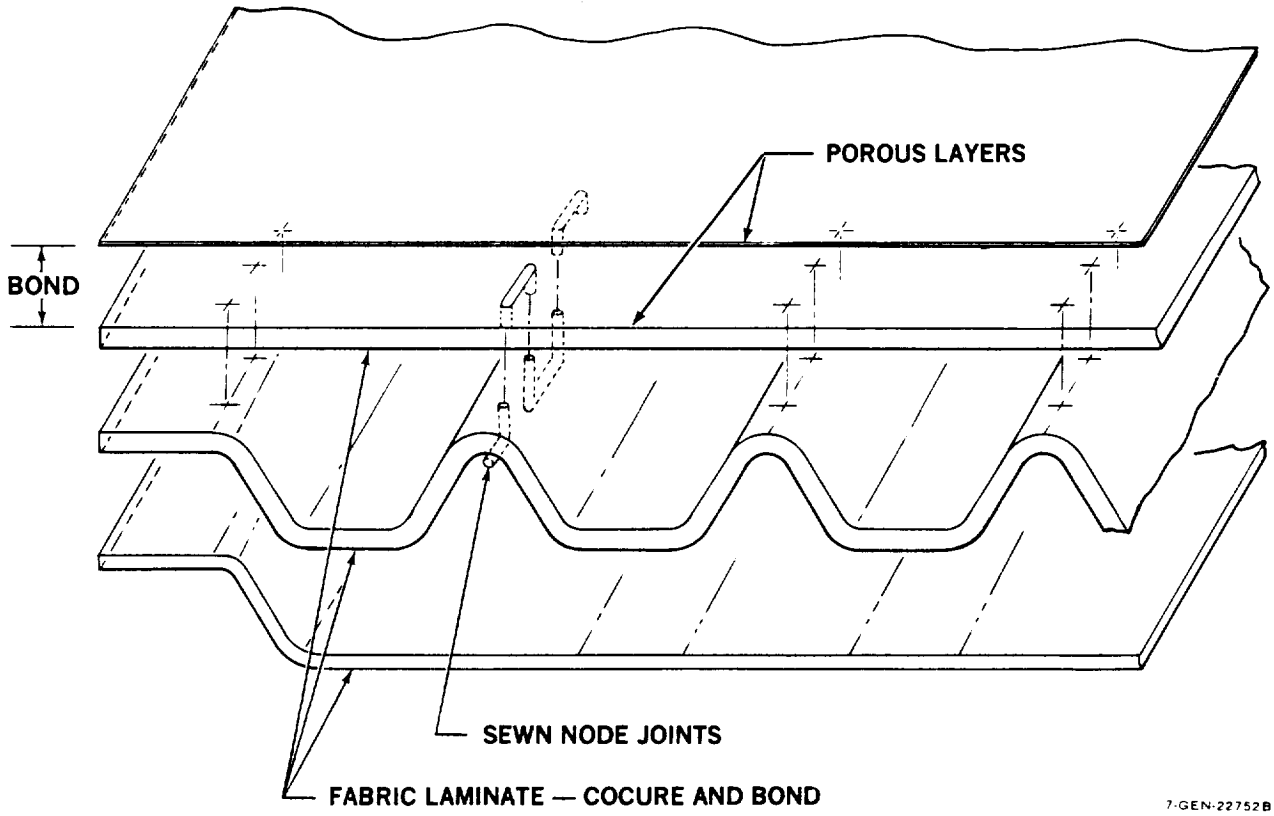

FIGURE 9-25. LOCKCORE PANEL

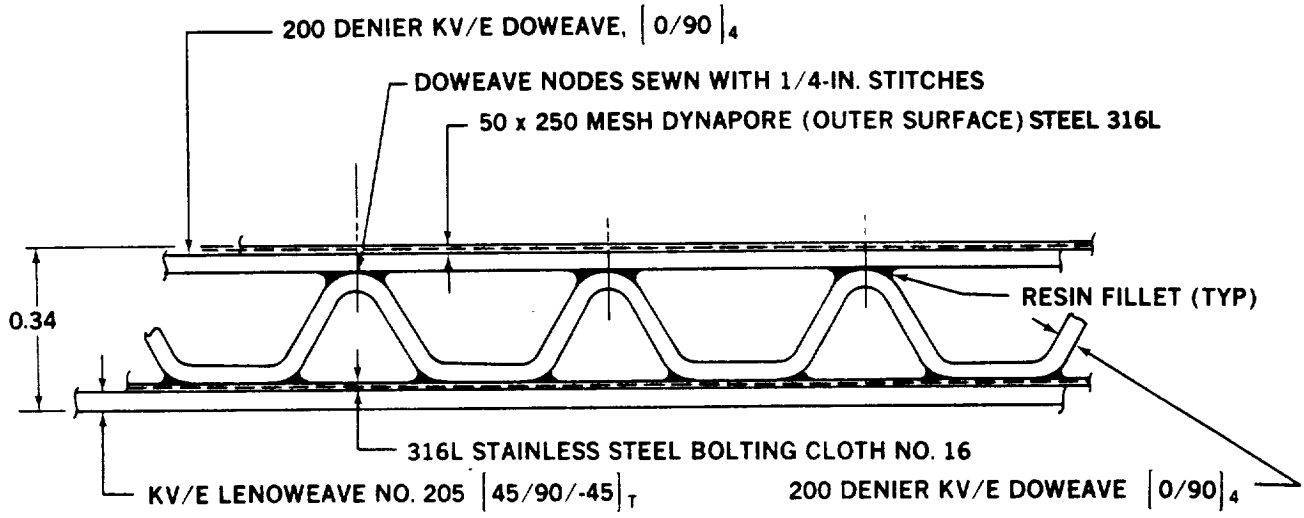

FIGURE 9-26. EARLY MODIFIED LOCKCORE PANEL CONCEPT

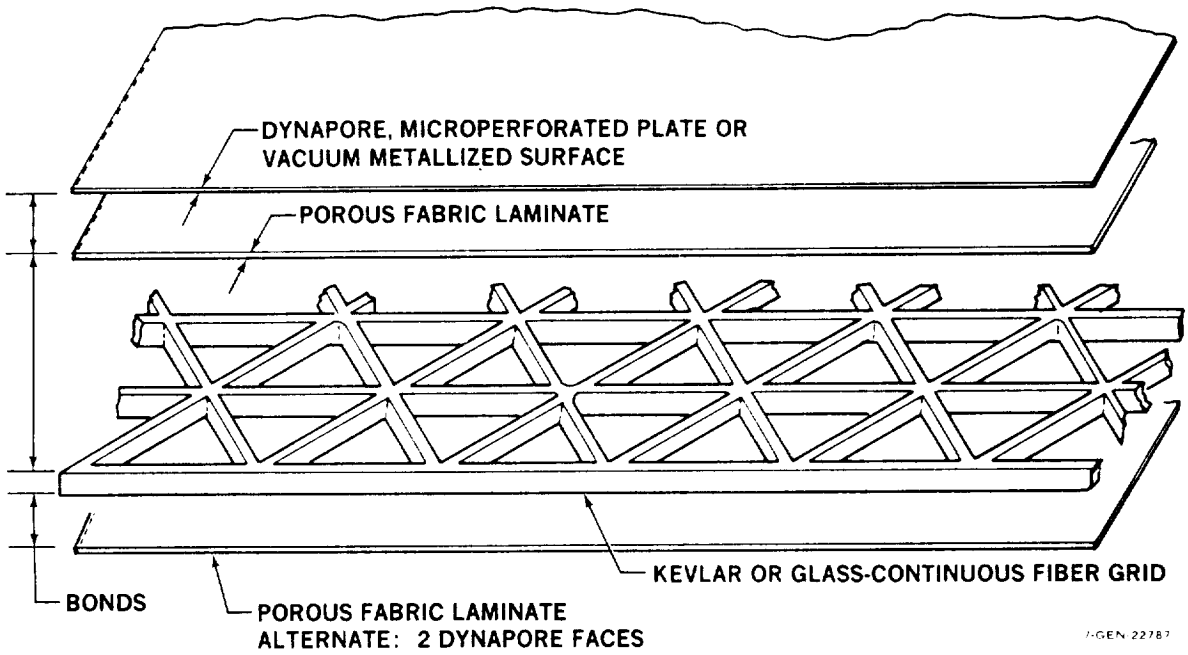

FIGURE 9-27. POROUS ISOGRID PANEL

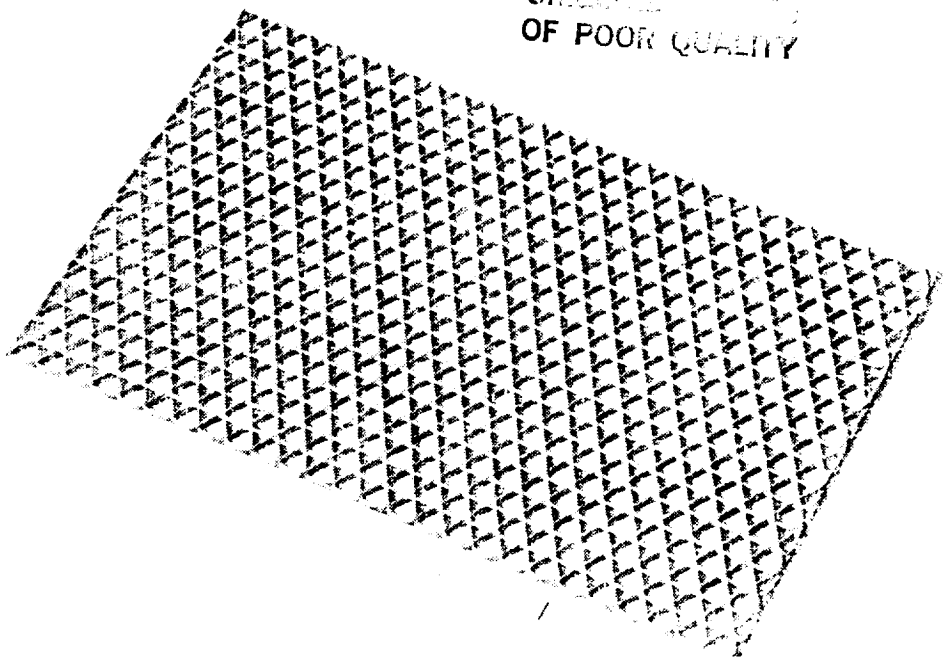

FIGURE 9-28. KEVLAR/EPOXY ISOGRID CORE

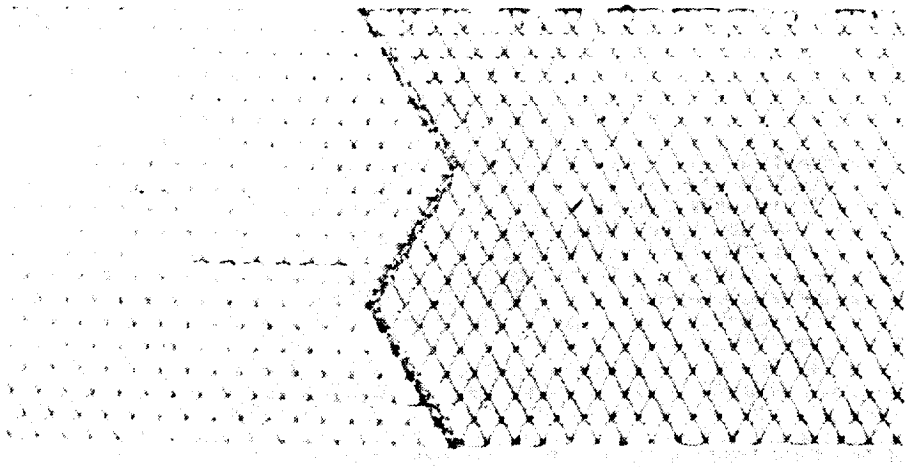

FIGURE 9-29. ISOGRID CORE SPLICE

The exploratory testing included the following:

- o Fabrication Development
- o Short Beam Shear Tests
- o Celanese Compression Tests
- o Block Compression Tests
- o I.I.T.R.I. Tension Tests
- o Sandwich Beam Bending Tests
- o Tension Fatigue Tests
- o Coefficient of Thermal Expansion Test
- o Airflow Testing (including salt solution clogging).

The conclusions from this initial testing are summarized as follows:

- o Of the various constructions studied, the fluted "Lockcore" porous sandwich construction was the most promising for meeting design requirements, so a decision was made to limit further development to this type of construction.

- o It was not necessary to pull suction air entirely through an outer sandwich and initial collection could occur within the integral ducts of the self-stiffened Lockcore sandwich.

- o Although the softness for impact, low yield strength and difficult bondability of the 316L stainless steel "Dynapore" porous surface presented challenges for development into a reliable LFC panel structure, it was the leading material from an aerodynamic standpoint as indicated by the flat plate wind tunnel tests, see paragraphs 8.1 and 9.2.2.

- o The basic Doweave fabric woven from Kevlar fibers and produced as a porous laminate was too porous and lacked sufficient strength and stiffness for suitability as an LFC glove panel support structure. Constructions employing tighter weaves of glass or graphite (rather than Kevlar) fiber were recommended for overcoming these deficiencies. Kevlar was not as good as glass under impact loading with a Dynapore surface.

- Clogging tests with salt (N_aCl) solutions indicated that the Doweave laminate faced with micro-perforated plate clogs relatively little and is easily cleared to its original porosity. Dynapore-faced laminates are susceptible to greater clogging and may clean to lower percentages of their original porosity depending on the original porosity. This tendency needs further investgiation with more representative contaminants.

- Resin content and formulation experience led to selection of E 719 (U.S. Polymeric Co.) resin for continued porous laminate and co-cure bonding work.

- Attempts to "meter down" Doweave with #120 fabric interleaved plies were unsuccessful in controlling the airflow to meet LFC requirements. Much more work with pressure drop technique was indicated.

The conclusions from an additional test program consisting of bending tests of environmentally conditioned Dynapore-faced Lockcore panels and impact tests of various constructions, were:

1) All Dynapore surfaces yield under low impact levels unless supported by sublayers.

2) A titanium surface was far more resistant to surface fracture under impact than Dynapore.

3) An improvement in bond strength bewteen 316L Dynapore and the body of the panel as well as an improvement in cohesive bond strength between underlying layers of the porous non-metallics was necessary.

4) The bending specimens that had been subjected to freezing water and temperature and humidity cycling showed no degradation of strength.

9.2.2 Aerodynamic Smoothness Test Panels

Stiffened porous panels 280 mm chord x 1190 mm span (1 ft x 4 ft), were designed and constructed for wind tunnel testing (see Section 8.0). The panels tested are listed in Table 9-8. They were primarily aerodynamic models not strictly representative of glove panel construction. A Doweave laminate was used for porosity metering under the 50 x 250 Dynapore and Fibermetal surfaces but the panels were found to be consistently too porous compared with predictions based on a series resistance analogy. A bonded honeycomb core support was used to hold the thin Dynapore surfaces flat and rigid under suction pressure, although it would not be adequate to develop necessary panel impact resistances, if used alone under the low-yield surface material. The Dynapore backed with perforated sheet material with holes as large as 6.35 mm (0.25 in) performed satisfactorily but smaller holes would be used to provide acceptable impact resistance. The 80 x 700 Dynapore with a low porosity (25 SCFM/14 PSF) performed the best, so a combination of 80 x 700/80 x 80 surface and perforated fiberglass sublayer (40 percent open perforation pattern) was bonded to honeycomb for additional wind tunnel tests. The resulting porosity of 0.508 $m^3/s/m^2$ @ 670 Pa (100 $SCFM/ft^2$ @ 14 PSF) gave poor results due to an inflow/outflow condition caused by a small pressure gradient over the panel. The panel porosity was therefore reduced to approximately 0.178 $m^3/s/m^2$ @ 670 Pa (35 $SCFM/ft^2$ @ 14 PSF) by the addition of porous glass plies on the backside. This panel worked well and a subsequent test panel of the same average porosity, achieved by using a perforated sublayer containing 3.18, 4.76 and 6.35 mm (1/8, 3/16 and 1/4 inch) diameter holes beneath the 80 x 700/80 x 80 Dynapore surface, worked equally well in the tunnel.

TABLE 9-8

AERODYNAMIC SMOOTHNESS TEST PANELS

(Suction Surfaces)

- Baseline Flat Plate - 3.18 mm (1/8 inch) thick Aluminum sheet
- 50 x 250 Dynapore - Honeycomb Sandwich
- Sintered Fibermetal on Doweave laminate
- 50 x 250 Dynapore - with strip porosity obtained by controlled adhesive blockage.
- 50 x 250 Dynapore on Isogrid stiffening.
- Metallized Doweave laminate.
- Metallized #120 molded fabric surface on Doweave laminate.
- Microperforated Plate (Dynapore) #19 on Doweave Lockcore with flutes running spanwise.
- Slotted Aluminum panel.
- 80 x 700 Dynapore on Honeycomb.
- 80 x 700/80 x 80 Dynapore on perforated fiberglass sublayer - Honeycomb stiffened.
- Electron Beam Perforated Titanium 0.102 mm (0.004 inch holes)

The slotted panel was fabricated by precision machining aluminum sheet and fitting it together with shim spacers during the bonding operation to produce 0.127 mm (.005 inch) slots. The first slotted panel was not smooth enough but a satisfactory test panel was produced after modification of the assembly tool.

The metalized Doweave and metalized #120 fabric surfaces were found to be not smooth enough for laminar flow in the wind tunnel, even though molded against a Mylar sheet. The electron beam perforated titanium panel was procured and tested using a hole pattern suggested by NASA. It is not known whether Dynapore coarser than 50 x 250 would have been too rough, however, the heavier Dynapore was difficult to roll precisely to low porosities during the calendering process. Figure 9-31 shows the effect of calendering on porosity.

9.2.3 Pressure Drop Through Combined Porous Layers

In support of the wind tunnel flat plate tests, pressure drop testing was conducted on various numbers of plies of Doweave that were stacked in alternate weave directions $[0/90]_n$ to avoid uneven porosity distribution in the ply stack. A goal was to discover a method of predicting the porosity of such porous layups and to produce porosity design charts. Figure 9-32 represents an attempt to organize the test data, and indicates the effect of ply stacking of basic Doweave on pressure drop at a single .012 m/sec (.04 ft/sec) flow velocity through the surface. This was the lower limit of velocity through the suction region. The target pressure drop for one facing of a two-faced porous sandwich, assuming no contribution of the core, was 335 Pa (7 psf) as indicated in the right of the chart. The total sandwich ΔP was 14 psf at that flow, with the relationship for separated porous facings assumed to be

$$\frac{\Delta P_1}{V_s} + \frac{\Delta P_2}{V_s} = \frac{\Delta P_{Total}}{V_s}$$

where V_s = suction velocity
and ΔP_i = pressure drop

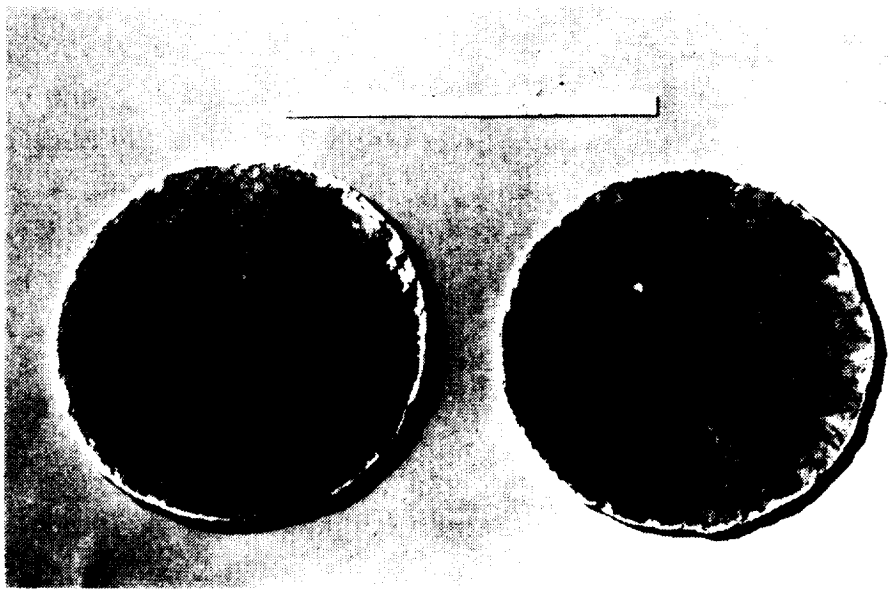

FIGURE 9-30. ISOGRID AND HONEYCOMB CORES BONDED TO DYNAPORE FACINGS

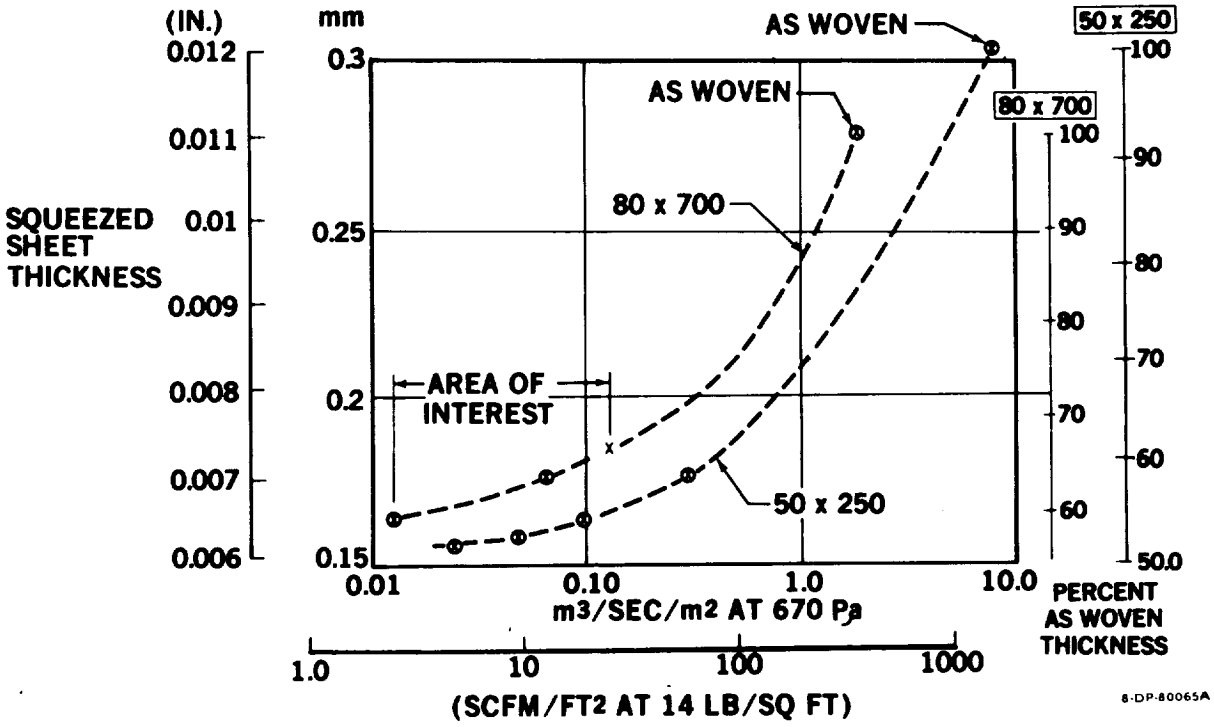

FIGURE 9-31. EFFECT OF CALENDERING ON POROSITY OF DYNAPORE MATERIALS

It was apparent that increasing the number of Doweave plies alone could not produce the required pressure drop. Inserting of (1, 2 or 3) more closely woven #350 fabric plies regularly separated by $(0/90)_n$ Doweave plies, seemed to have a metering effect on the stack. Extrapolation to 5 inserted metering plies indicated that this would produce the required 670.3 Pa (14 psf), however, the panel made for the wind tunnel model in this way was found to have a pressure drop more than one magnitude less than expected.

No simple relationship between the number of plies and the pressure drop could be determined so porosity control using additional porous layers continued to be a "trial and error" process.

9.2.4 Porous Surface Selection

Following the initial survey and testing of a variety of porous surfaces, two were selected for further development. These were: (1) stainless steel Dynapore mesh, and (2) electron beam perforated titanium sheet. These two surface materials were then tested more extensively to obtain the physical and mechanical properties needed for comparison and for LFC panel design.

The evaluation of Dyanpore surfaces was limited to an external 80 x 700 mesh weave diffusion bonded to an 80 x 80 mesh inner weave calendared to a porosity producing 0.813 $m^3/s/m^2$ (160 $SCFM/ft^2$) airflow at 670.3 Pa (14 PSF) pressure, see Figure 9-33. Both 316L and Nitronic 50 stainless steel wire materials were evaluated. In addition, work was conducted on the configuration in which the Dynapore layers were also diffusion bonded to an internal supporting electron beam perforated 316L stainless steel sheet.

The evaluation of electron beam (EB) perforated titanium sheet surfaces was initially with material supplied by the Farrell Company, Connecticut. Testing confirmed the possibility of using EB perforated titanium an an LFC surface and its relative toughness was highly desirable, particularly for leading edge surfaces where high impact resistance is needed.

The smallest holes obtainable from Farrell in 0.685 (.025 inch) thick titanium were 0.102 mm (.004 inch) diameter. There was some concern that suction through holes of this size could trap particles on the surface large enough to cause transition. The use of elongated holes was therefore investigated to reduce this possibility.

The Farrell Company subsequently decided to discontinue EB perforation and additional material was obtained first from Steigerwald in Germany and then from Pratt and Whitney in Connecticut. Pratt and Whitney were able to produce EB perforated holes as small as 0.064 mm (.0025 inch) diameter in 0.64 mm (.025 inch) thick titanium sheet material. This reduced the hazard from possible trapped particles on the surface so development was continued using circular holes only. The maximum ratio of 10:1 in sheet thickness to hole size was confirmed as a limit by Steigerwald, the manufacturers of the electron beam perforating equipment, although Dr. Steigerwald has since stated that his equipment could be modified to produce even smaller holes.

A statistical analysis was made of EB perforated hole sizes. The sampling technique used was to photograph a set of holes using a metalograph (inverted microscope). These photographs were then used to determine hole size variations and obtain a statistical distribution. The results showed very little variation in hole size indicating that a reliable uniform porosity was obtained. Figure 9-**34** shows an example of the uniformity of EB hole sizes and distribution obtainable and Figure 9-**35** shows an electron microscope photograph of an EB perforated hole highly magnified.

The Pratt and Whitney material was of high quality. Sheets of 0.635 mm (.025 inch) thick 6AL4V material perforated with 0.064 mm (.0025 inch) diameter holes spaced 0.813 mm (.032 inch) on centers in a square pattern were obtained and used for wind tunnel testing. Porosity tests indicated a flow rate of 0.014 m^3/s at 670 Pa (30 SCFM at 14 PSF) pressure differential for this material, which was acceptable for the wind tunnel models.

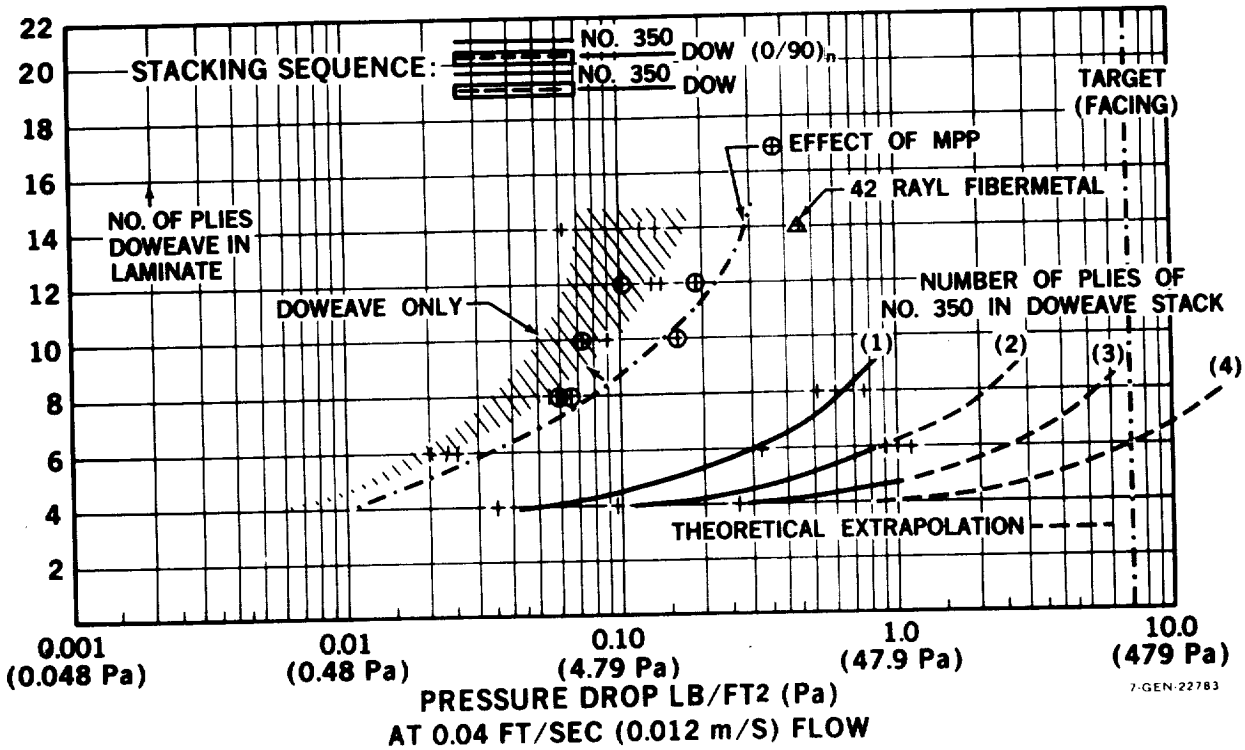

FIGURE 9-32. PRESSURE DROP PANEL DESIGN – POROUS COMPOSITES

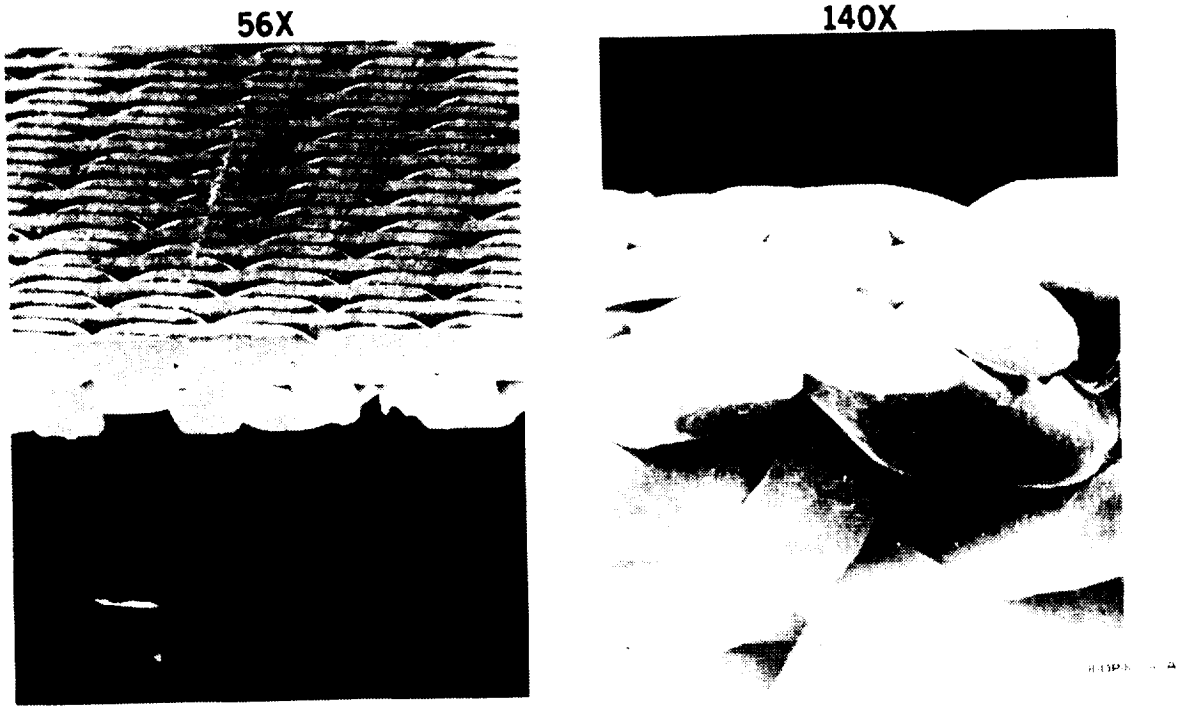

FIGURE 9-33. 80 BY 700 DYNAPORE SURFACE PLUS DIFFUSION-BONDED 80 BY 80 SUBLAYER

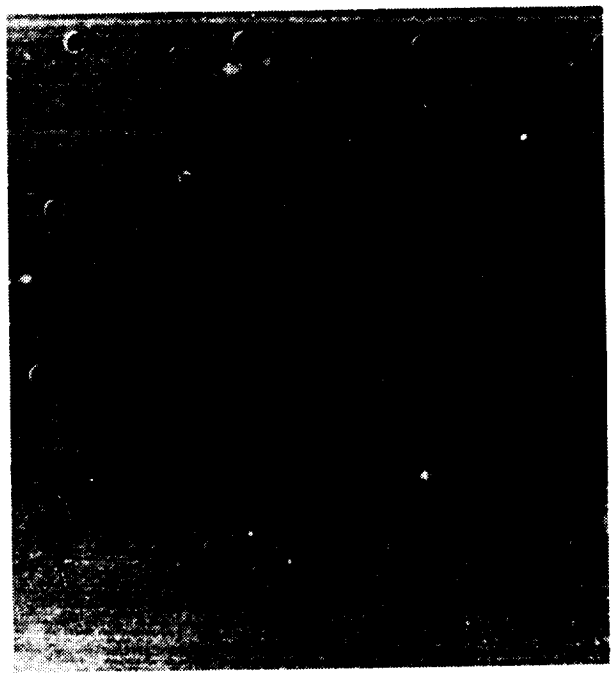

FIGURE 9-34. ELECTRON-BEAM-PERFORATED HOLES

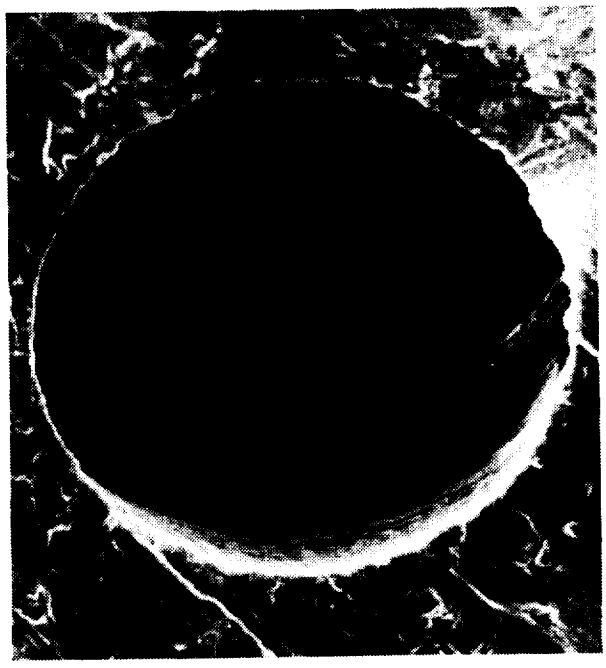

FIGURE 9-35. ELECTRON-BEAM-PERFORATED HOLE

During fabrication development with EB perforated Ti material, it was determined that normal etching and cleaning procedures before bonding would enlarge the hole sizes by about 0.025 mm (.001 inch) diameter. A new preparation procedure was therefore developed using a protective coating applied to the outer surface of perforated titanium. The coating had been developed previously for preferential chemical milling procedures. The coating inhibited enlargement of the perforated holes at the surface and permitted normal etching and cleaning of the interior surface prior to bonding.

Structural testing of Dynapore and EB perforated titanium is described in Section 9.3. The EB perforated titanium LFC surface was finally selected.

9.2.5 Thermal Analysis of Dissimilar Materials

The effect of using dissimilar materials for porous panel surfaces, panel stiffening and for the basic wing structure was considered. The effect on LFC panels, which being securely attached to wing structure, strain to the same extent as the primary structure, is illustrated by Figure 9-**36**. In the example indicated on the chart, a panel material with a 68.9 GPa (10 million psi) modulus would reach a stress level of 186.2 MPa (27,000 psi) when strained with a graphite/epoxy that is allowed to reach 68.6μm (2700 micro-inches) at limit load. A titanium wing structure would be allowed to reach higher strains and would therefore strain the glove material to a higher stress level. A graphite/epoxy basic wing structure results in the lowest glove stress. Thermal strains that may be present, due to the difference between fabrication temperature and service temperature in bi-material systems, must be added algebraically to the load strains to obtain the resulting strain level of the glove material.

The glove panel should be designed to not yield or buckle below wing limit load taking into account any thermal strains present. Thermal strains must therefore be considered when determining the feasibility of structure and panel material combinations. Because of a lack of proportionality indicated by a pronounced "knee" in the stress-strain curve for Dynapore, the secant modulus (E_s) rather than the modulus to proportional limit (E_p) was used in the thermal analysis of Dynapore panels.

The thermal analysis was programmed to accept orthotropic properties of two different layers intimately connected and subject to a temperature change. The program directly solved for single-materials (self-stiffened) Kevlar, glass or steel mesh panels on each of the four primary structural materials: aluminum, titanium, boron epoxy or graphite/epoxy. Multi-material panels were solved in two stages, considering first the bonding temperature of the panel to determine the balanced stresses within the panel layers when they are being assembled to the primary structure, then the effect of temperatures down to -65°F on the combined assembly. The maximum strains in the panel layers occurred at -65°F or room temperature depending on the material combinations and thicknesses. Generally, the thermal strains in the primary structure are very low since it controls the panel strains by virtue of greater cross sectional area. Figure 9-37 summarizes rationale and materials combinations.

In the examples given in Table 9-9, the first column shows the calculated maximum thermal strains induced at -65°F or 70°F for several multi-material panel/structure combinations. It shows the strain available for limit tensile wing loading after subtracting thermal strain from the allowable layer strain. If a layer available strain is less than the structure strain, then that combination is infeasible. The very thin microperforated plate (MPP #21) appears to be infeasible on any structure. 24 x 110 Dynapore on graphite and 50 x 250 Dynapore on titanium wings were indicated as problem combinations although 50 x 250 Dynapore on graphite is feasible. 50 x 250 Dynapore is feasible even with an aluminum wing, at least

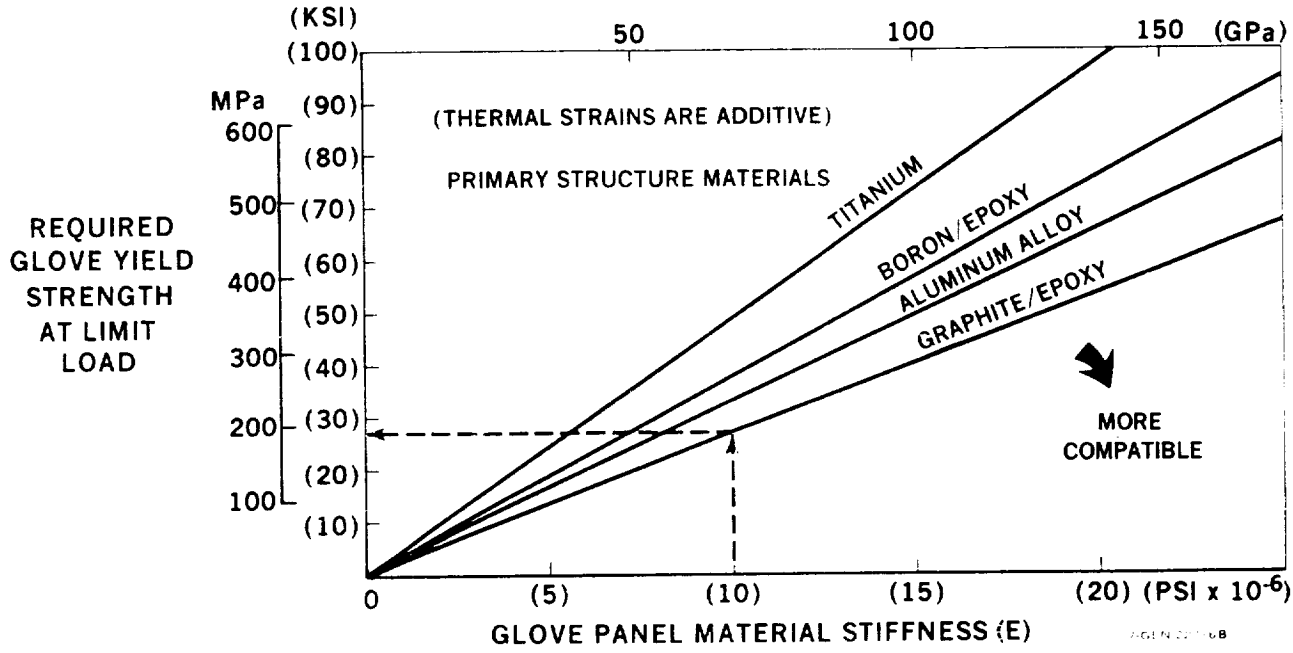

FIGURE 9-36. STRENGTH AND STRAIN REQUIREMENTS FOR LFC GLOVE PANELS

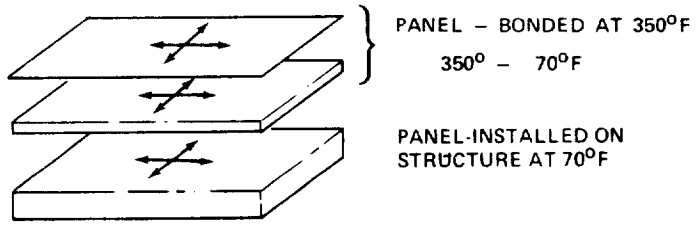

COMBINATION OPERATED AT 70° → –65°F

MATERIALS COMBINATIONS

SURFACE PANEL	STRUCTURE
• ALL KEVLAR/EPOXY	• ALUMINUM
• ALL GLASS/EPOXY	• TITANIUM
• ALL DYNAPORE	• BORON/EPOXY
• DYNAPORE ON KEVLAR/EPOXY LOCKCORE	• GRAPHITE/EPOXY
• DYNAPORE ON GLASS/EPOXY LOCKCORE	
• DYNAPORE ON KEVLAR/EPOXY ISOGRID	
• DYNAPORE ON GLASS/EPOXY ISOGRID	

7-GEN-22756

FIGURE 9-37. THERMAL ANALYSIS – MODEL AND MATERIALS

TABLE 9-9

EFFECT OF THERMAL STRAINS ON RESIDUAL STRAIN
FOR WING LIMIT LOAD STRAIN WITH COMBINED MATERIALS

	MAX. INDUCED THERMAL STRAIN/LAYER AT -65°F OR 70°F μ	LIMIT STRAIN ALLOW μ	MAX STRAIN AVAILABLE (1) FOR LIMIT LOAD μ	FEASIBILITY
PANEL 11A:				
MPP #21	3320	4900 (3)	1580	No
K/E Doweave Lockcore	-370	2800	3170	
G/E #1 Corrugated Struct.		2670	2670	
PANEL 12A:				
50 x 250 Dynapore (Fill Spanwise)	2970	6710	3740	Yes
K/E Doweave Lockcore	-810	2800	3610	
Gr/E #1 Corrugated Struct.	- 10	2670	2680	
PANEL 13A:				
24 x 110 Dynapore	2620	5150	2530	No
K/E Doweave Lockcore	-1070	2800	3870	
Gr/E #1 Corrugated Struct.	- 20	2670	2690	
PANEL 14A:				
MPP #21	2120 (2)	4900	2780	No
K/E Doweave Lockcore	-2060	2800	4860	
Alum. Corrugation Struct.	50	3350	3300	
PANEL 15A:				
50 x 250 Dynapore	1740 (2)	6710	4970	Yes
K/E Doweave Lockcore	-2060	2800	5290	
Aluminum Corrugation Struct.	50	3350	3300	

NOTES: (1) At -65°F, unless noted otherwise.
(2) Maximum thermal strains at room temperature
(3) MPP Properties estimated.

in tension. There was uncertainty about the appropriate stiffness input for a Kevlar isogrid panel stiffening layer and when theoretical KV49 values were used the Kevlar isogrid combinations were infeasible. When glass or lower stiffness Kevlar 29 theoretical values were input the combinations were feasible.

9.2.6 LFC Panels Arrangement

A design study of the porous glove panel structure was undertaken and details of a glove panel design and its assembly to the basic wing structure were drawn. This design provided the basis for glove panel structural testing and development. Figures 9-38 and 9-39 show the arrangement of the panels on the wing.

The LFC panels were trapezoidal rather than rectangular in shape so that all streamwise flow paths would have a reduced non-sucked distance to travel across structural joints, and no joints were made parallel with the stramlines. Sub-surface blockages, such as at node lines, were also angled parallel with the panel end joints. The angled fluting made the panel difficult to analyze structurally, however panel tests showed this arrangement to be stronger than with the flutes at 90° to the stringers. Details of the glove panel at this stage of development are shown in Figure 9-40. The double plate butt splice design shown in Figure 9-41 was used for the chordwise joints. Acceptable smoothness of these panel joints was not established in this program but structural feasibility was demonstrated.

Because of panel length, interior fasteners, or "field fasteners" were used for added support and stabilization, see Figure 9-42. The overall concept showing how the suction flow was controlled and transferred to the integral ducting of the basic wing structure is shown in Figure 9-43.

9.2.7 Superplastic Formed/Diffusion Bonded LFC Panel

To examine the feasibility of using a Superplastic Formed/Diffusion Bonded (SPF/DB) structure for LFC glove panels, a small panel of this type was fabricated. The formed panel is shown in Figure 9-44. The dimples formed in the shallow channels were subsequently machined to create rows of holes and allow suction air to flow from the surface to the integral channels. The resulting panel is shown in

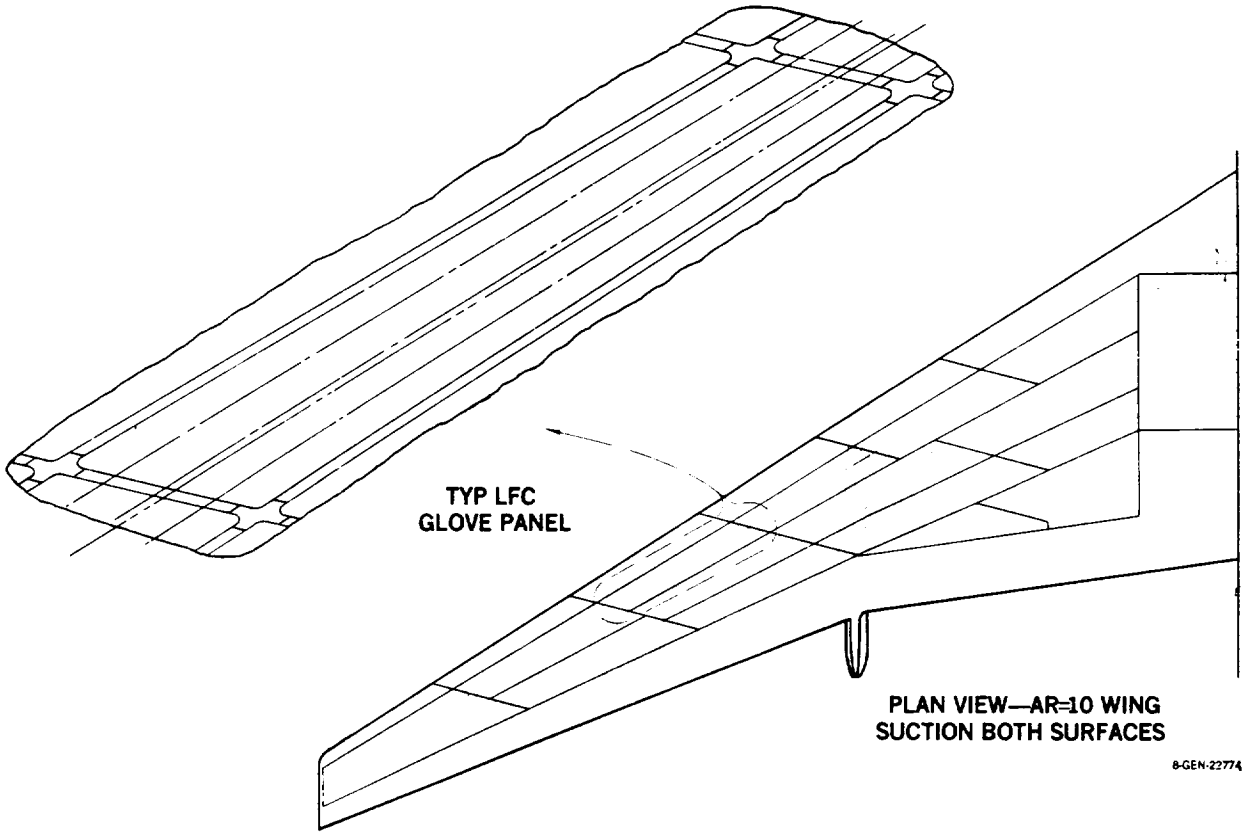

FIGURE 9-38. GLOVE PANEL INSTALLATION

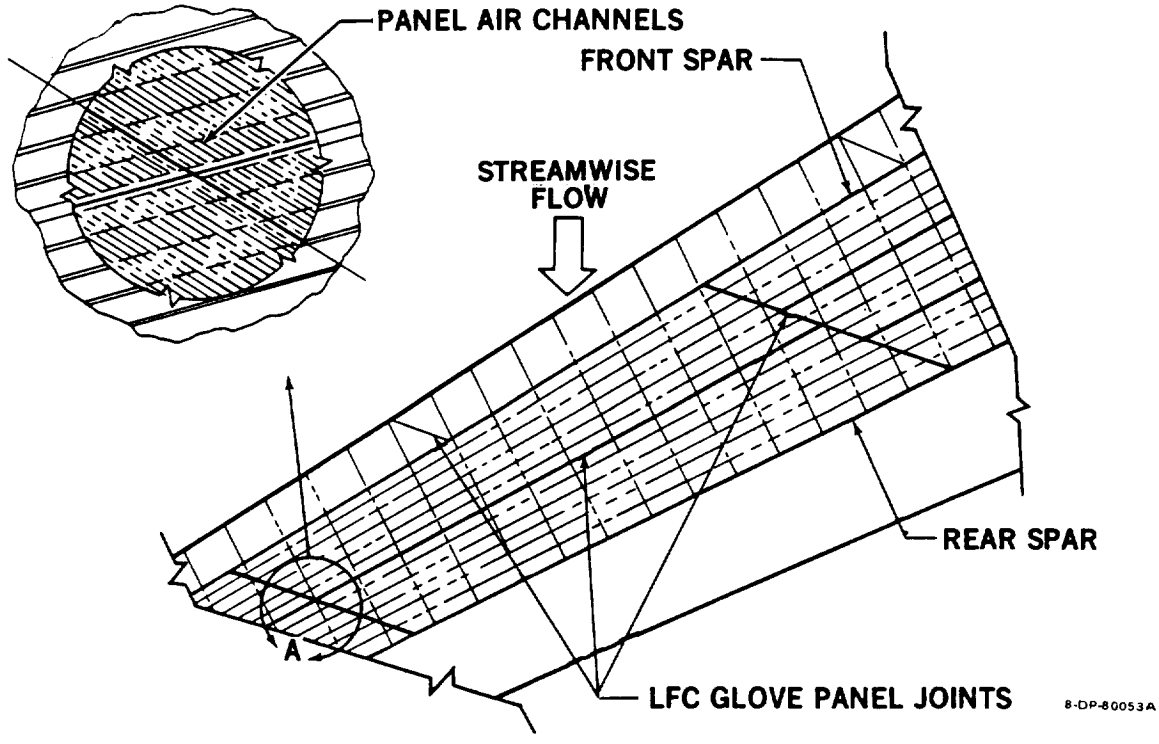

FIGURE 9-39. TYPICAL WING BOX GLOVE PANEL ARRANGEMENT

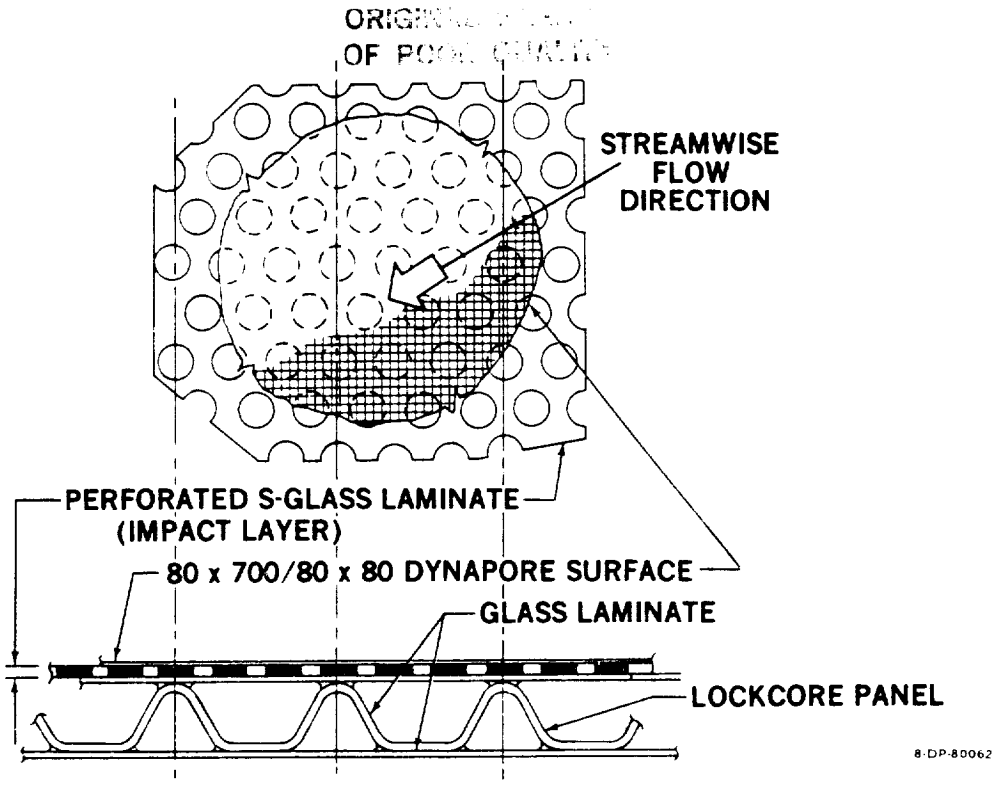

FIGURE 9-40. LFC GLOVE PANEL WITH PERFORATED FIBERGLASS SUBLAYER

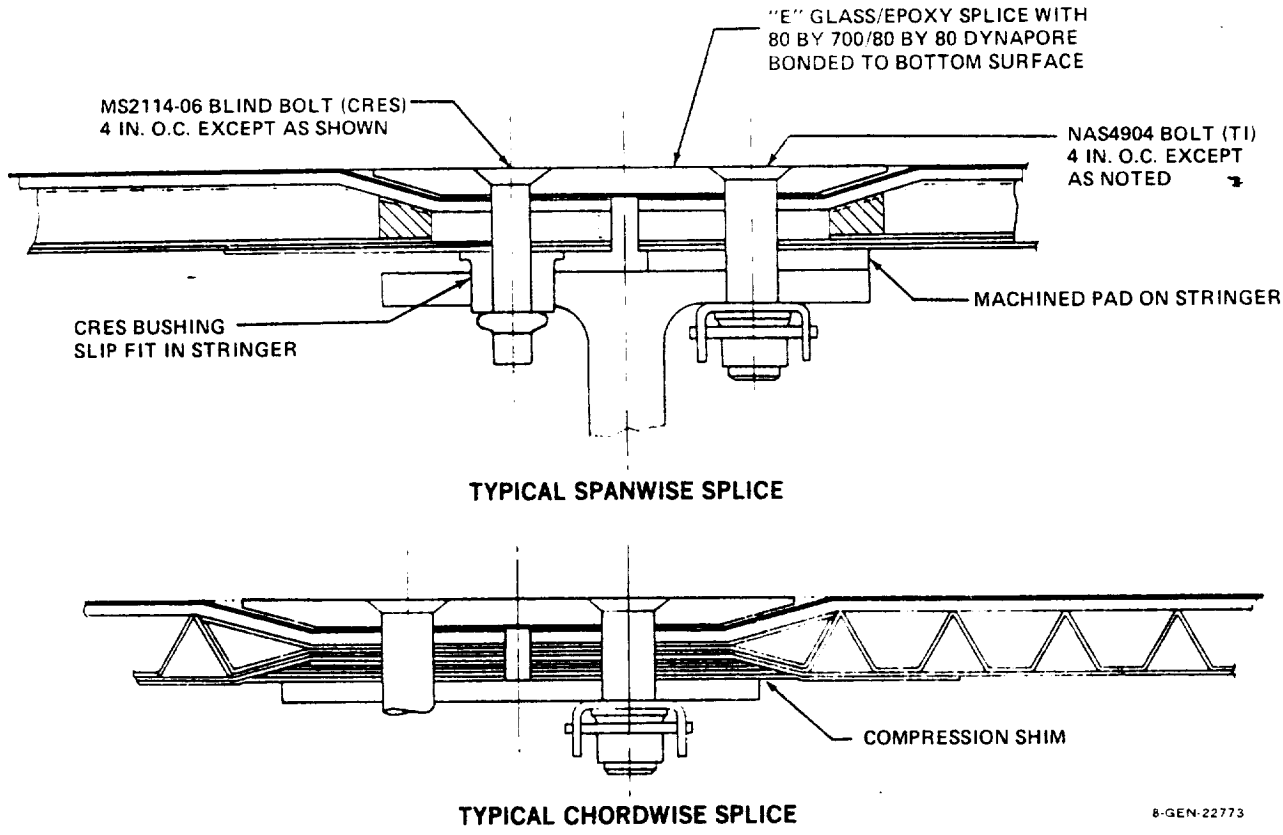

FIGURE 9-41. GLOVE PANEL SPLICES

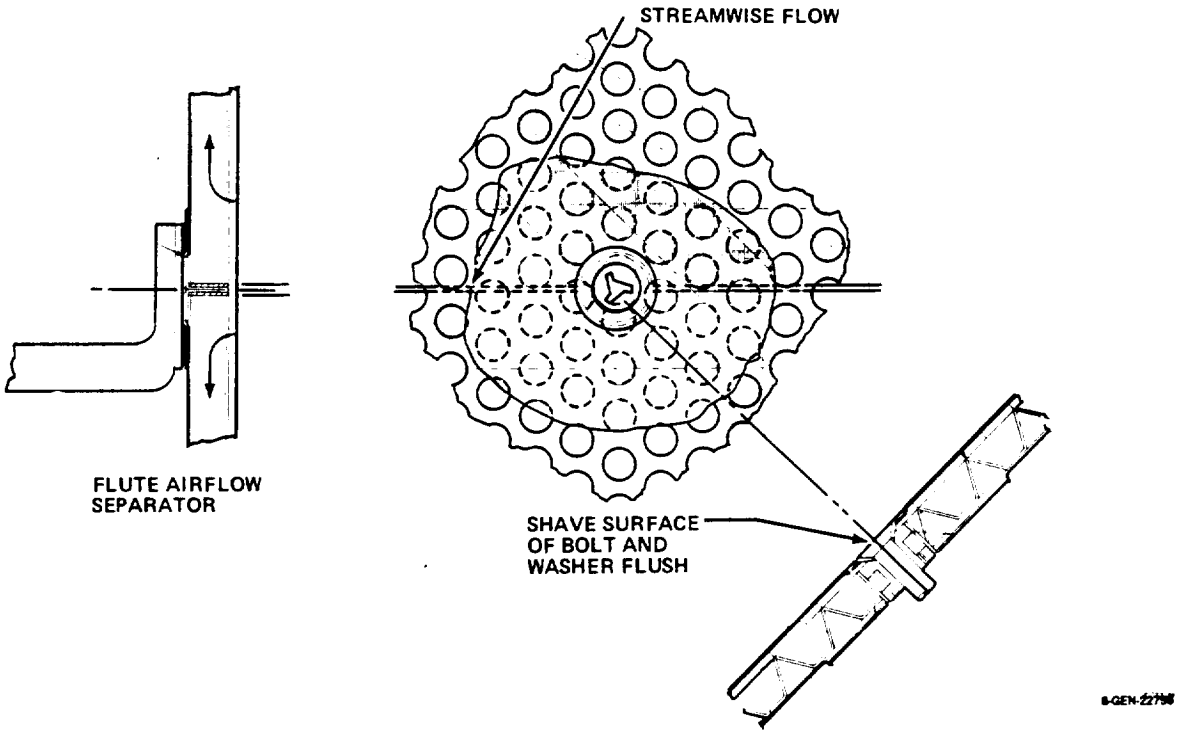

FIGURE 9-42. TYPICAL FIELD FASTENER – LFC GLOVE

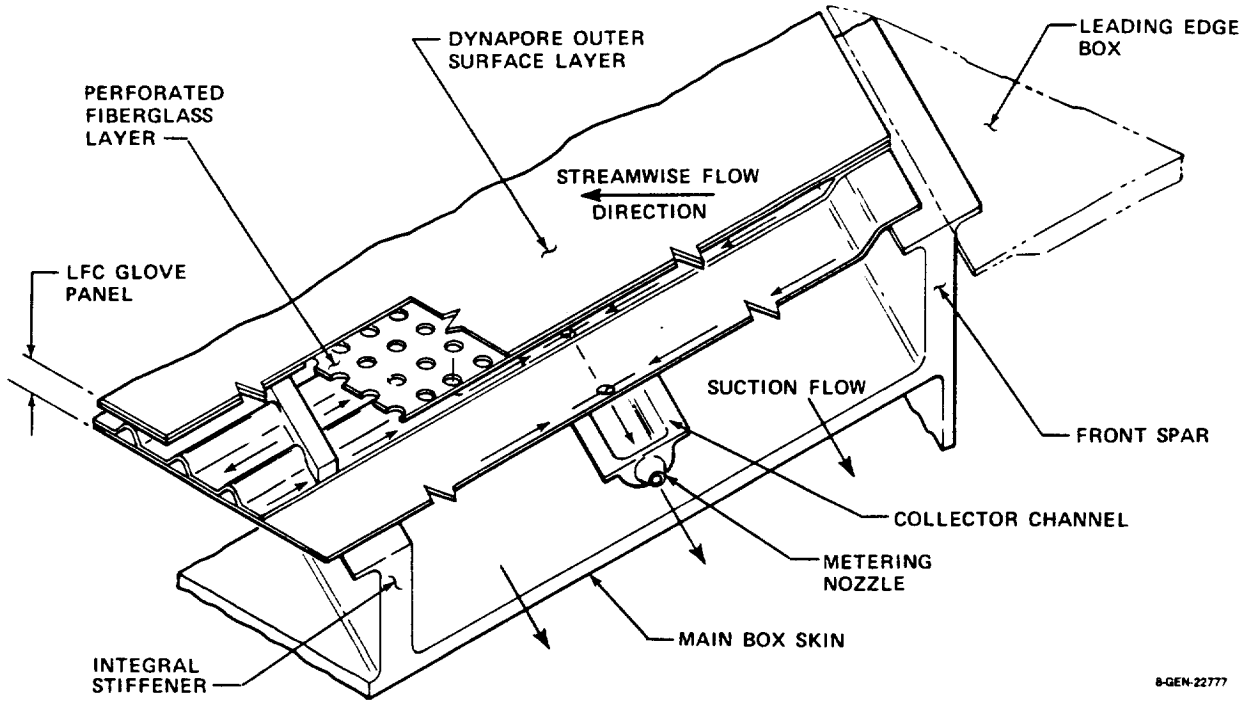

FIGURE 9-43. LFC GLOVED WING STRUCTURAL CONCEPT

Figure 9-45 and an enlarged view of the holes is shown in Figure 9-46. The LFC glove panel could be completed by bonding either a layer of Dynapore or EB perforated titanium to the outer surface. The SPF/DB construction was judged to be acceptable for LFC panels and further development of this concept is recommended.

9.3 STRUCTURAL TESTING

9.3.1 Porous Materials - Strength Properties

To obtain tensile and compressive stress-strain data on porous surface materials, Douglas standard honeycomb bending test beams were used in a four point loading rig. These beams are those normally used for thin composite materials being tested under compression loading. Figure 9-47 shows a typical test beam configuration.

Six beams were fabricated with a 316L Dynapore surface; 3 with an 80 x 700 surface diffusion bonded to an 80 x 80 sublayer, and 3 with an 80 x 700 surface alone. Four similar beams were fabricated with EB holes .0045 x .0073 long in 6AL4V titanium (2 of each with holes in 0° or 90° directions). Strain gages were installed on the beams for testing for strain/yield characteristics. Each beam was tested to a strain of .004 using 2 tests at each of 7 increasing load steps followed by 2 tests at each of 5 decreasing load steps. All initial tests at increasing strains in Dynapore showed that for strain levels up to .002 some small residual strain existed upon unloading which disappears upon reloading up to a strain of .002. For strain levels of .003 and above, the residual strain was reduced after the second loading but did not "disappear" as indicated for lower strain levels.

Prestraining to .003 resulted in no residual strains remaining after loading at lower levels. Both fill and ±45° warp directions in the Dynapore weave were tested. Figure 9-48 shows the stress-strain relationship in tension and compression for 80 x 700/80 x 80 316L Dynapore bonded to a fiberglass sublayer

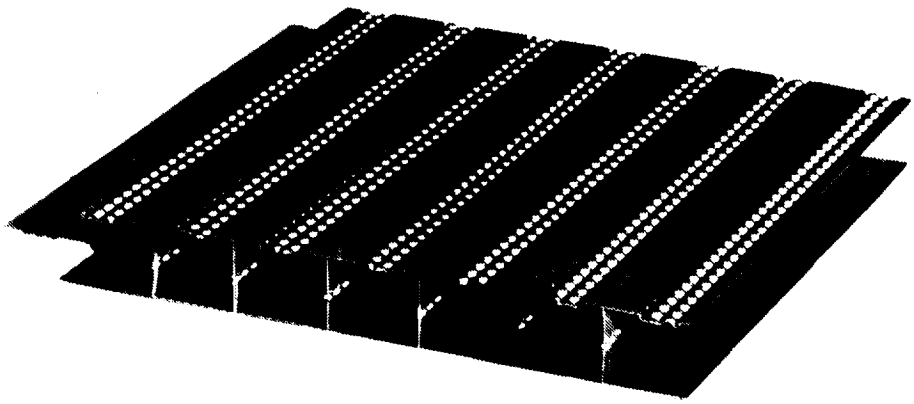

FIGURE 9-44. SUPERPLASTIC FORMED/DIFFUSION-BONDED TITANIUM SANDWICH PANEL – BEFORE MACHINING

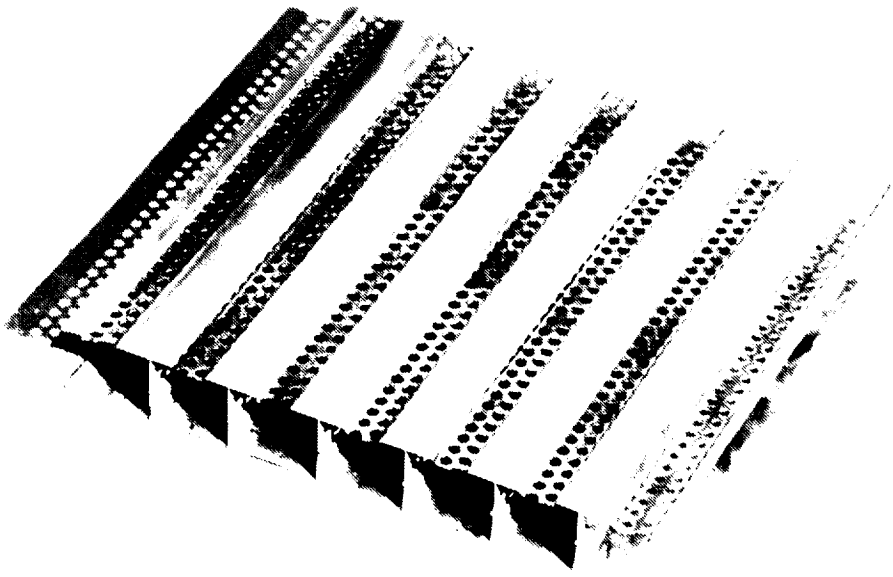

FIGURE 9-45. SUPERPLASTIC FORMED/DIFFUSION-BONDED TITANIUM SANDWICH PANEL

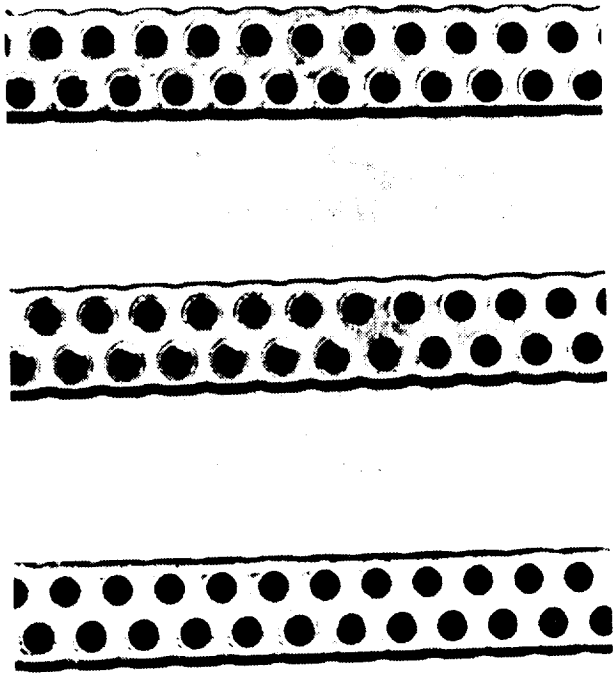

FIGURE 9-46. SUPER PLASTIC FORMED/DIFFUSION BONDED TITANIUM SANDWICH PANEL SUCTION HOLES

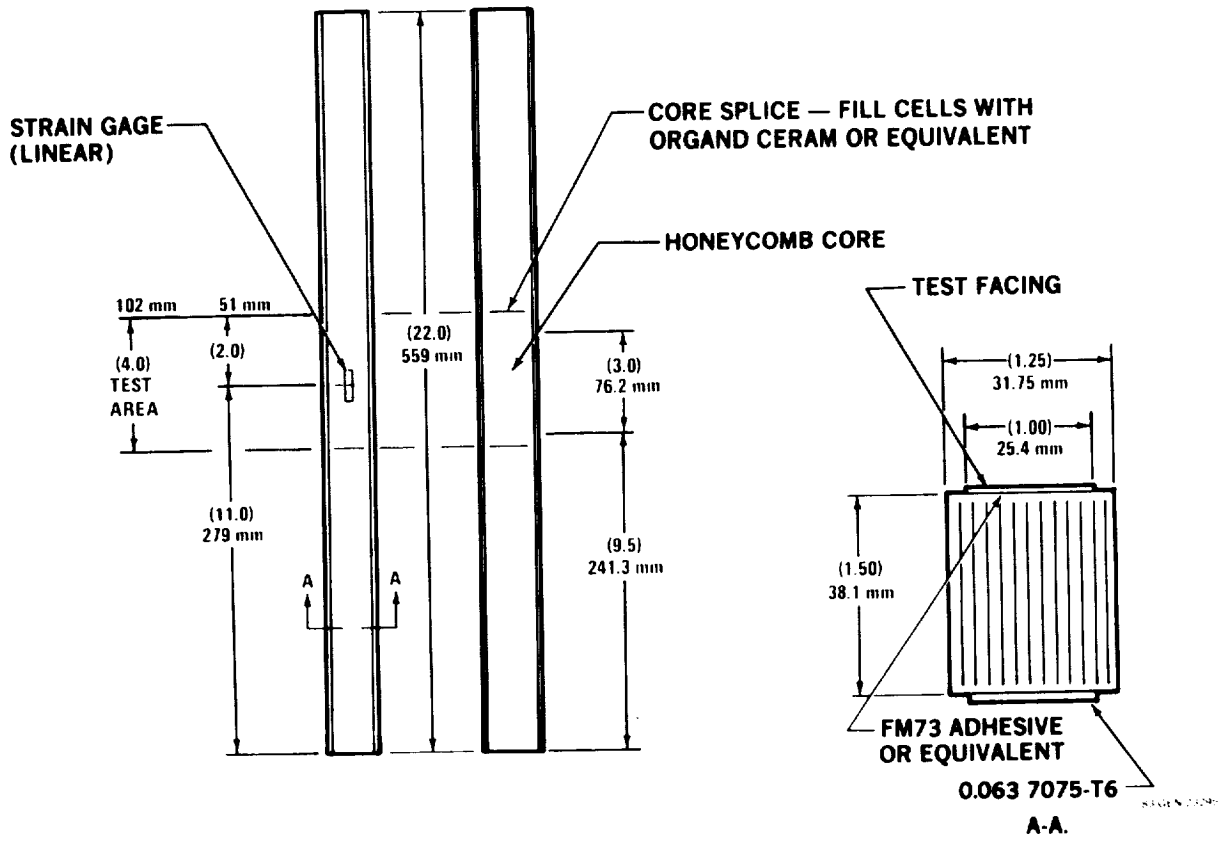

FIGURE 9-47. TEST BEAM

and Figure 9-49 is the stress-strain curve for 80 x 700 Dynapore made from Nitronic 50 wire. The offset of the curve at the axes intercept is the result of thermal stress introduced during the Dynapore to fiberglass bonding process.

Calendered woven metallic materials exhibit a combination of elastic and mechanical strain characteristics depending on load direction relative to the weave. The only requirement for the LFC surface is that the porous material must withstand a limit load strain of ±.0027 without surface deformation after the strain is reduced to the 1g flight condition. The .0027 strain corresponds to a .004 ultimate strain for advanced graphite/epoxy composite materials (current design practice limits ultimate strain in graphite/epoxy materials to ±.003). The test results indicate that some damage may be occurring with the 316L material but Nitronic 50 appears to be still behaving elastically within its limit of proportionality at the required strain level.

All of the 6AL4V titanium faced beams tested with .114 mm x .185 mm (.0045 inch x .0073 inch) long perforated holes exhibited the same stress-strain characteristics as the original sheet materials. The percent porosity was too low to significantly affect the stress-strain relationship up to the .006 maximum strain limit of the tests.

9.3.2 Porous Material - Fatigue

The Dynapore fatigue test beams were as shown in Figure 9-50. Specimens include 316L 80 x 700 warp and ±45° plus an equivalent set using Nitronic 50 wire, as shown in Tables 9-10 and 9-11. Tests were run at "average" reversing strain conditions (R=-2.5) and a design objective of 120,000 cycles at .0016 maximum compressive strain.

Figure 9-51 shows a set of fatigue test sandwich beams with electron beam (EB) perforated test facings. Note that the fatigue beams are wider than the normal one inch wide beam in the foreground which is used for materials properties evaluations. The wider beams are used in the fatigue test rig to prevent loading in the plane of the test facing from the test fixture.

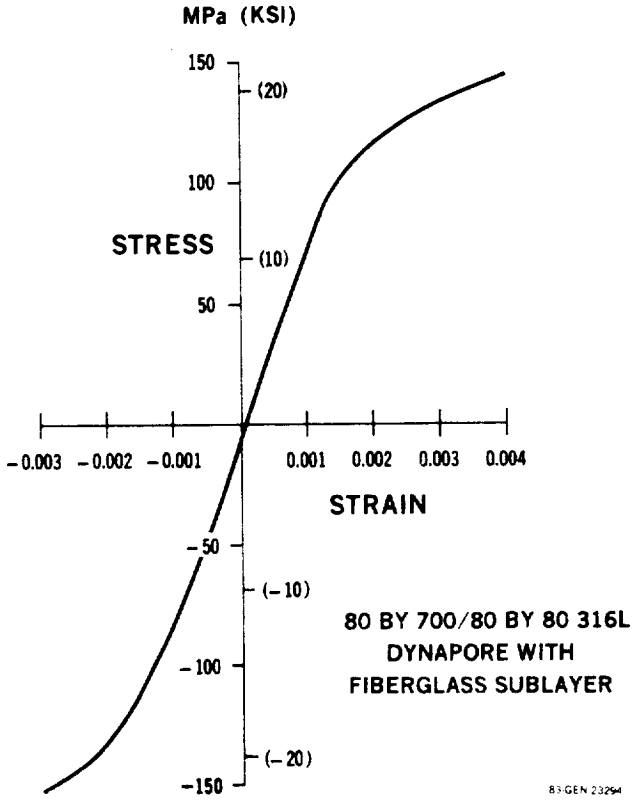

FIGURE 9-48. STRESS-STRAIN CURVE – DYNAPORE ON FIBERGLASS

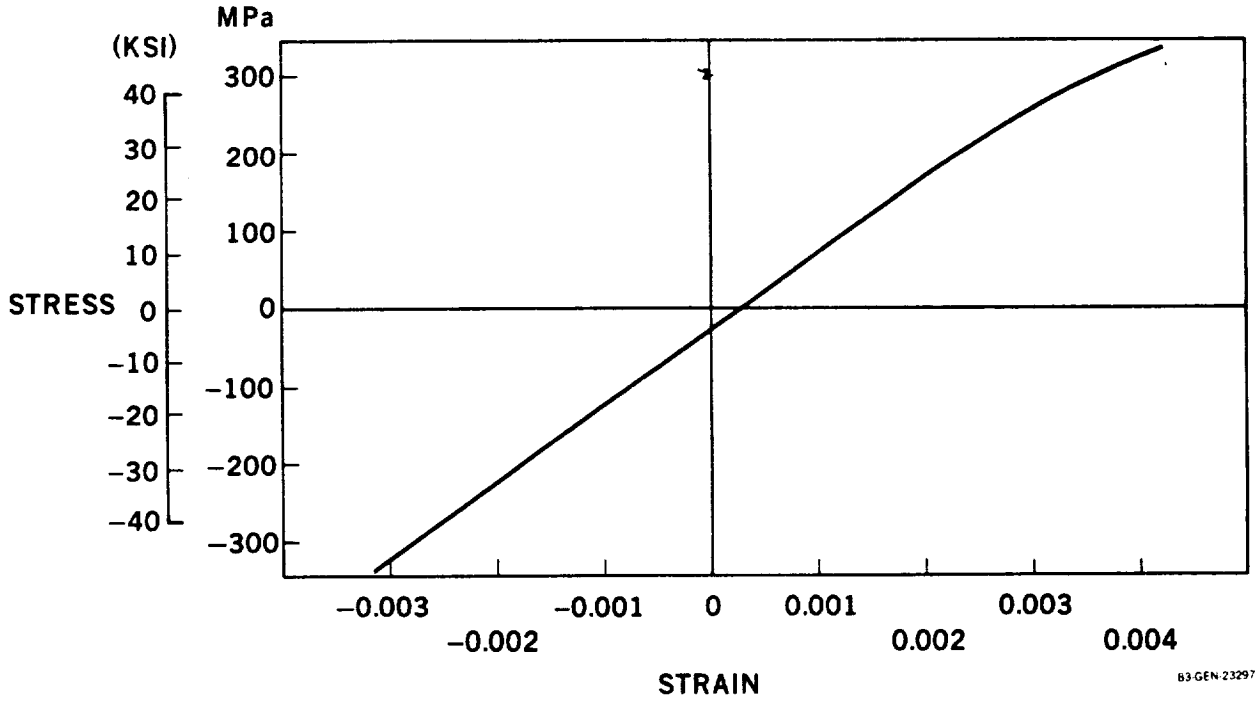

FIGURE 9-49. STRESS-STRAIN CURVE – NITRONIC 50 DYNAPORE

TABLE 9-10

FATIGUE LOADING REQUIREMENTS

	Strain x 10^6		No. Cycles	Test Beams
Tension Compr.	640 -1600	R = -2.5	120,000 or Failure	1 each dash no.
Compr. Tension	-2400 960	R = -2.5	Record Fatigue Cycles to Failure	1 each dash no.
Compr. Tension or Higher as Indicated	-3200 1280	R = -2.5	Record Fatigue Cycles to Failure	1 each dash no.

TABLE 9-11

FATIGUE SPECIMENS AND IDENTIFICATION

Dash No.	No. Beams	Facing Material
-1	3	80 x 700 only, 315L, warp lengthwise.
-2	3	Same as -1 except ±45°
-3	3	80 x 700 Nitronic 50, Warp lengthwise.
-4	3	80 x 700 Nitronic 50, ±45°
	12	TOTAL

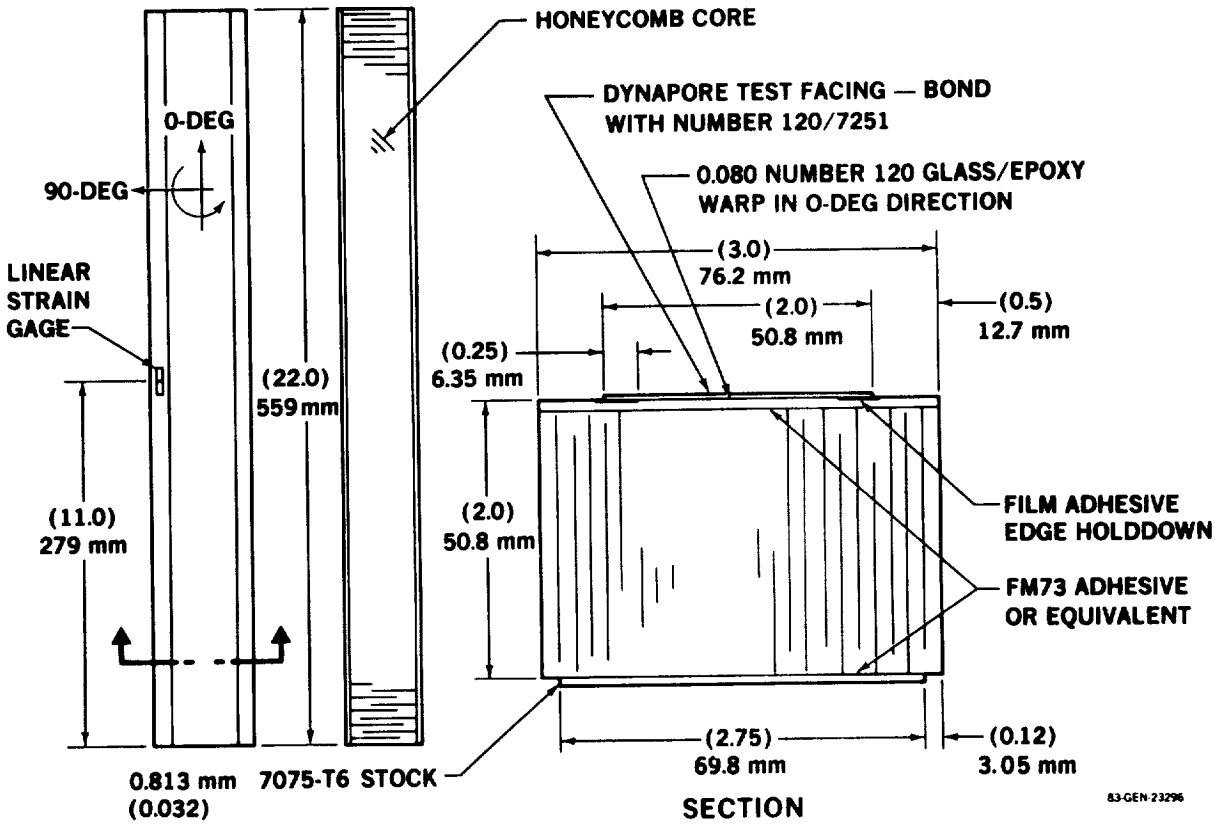

FIGURE 9-50. FATIGUE TEST BEAM

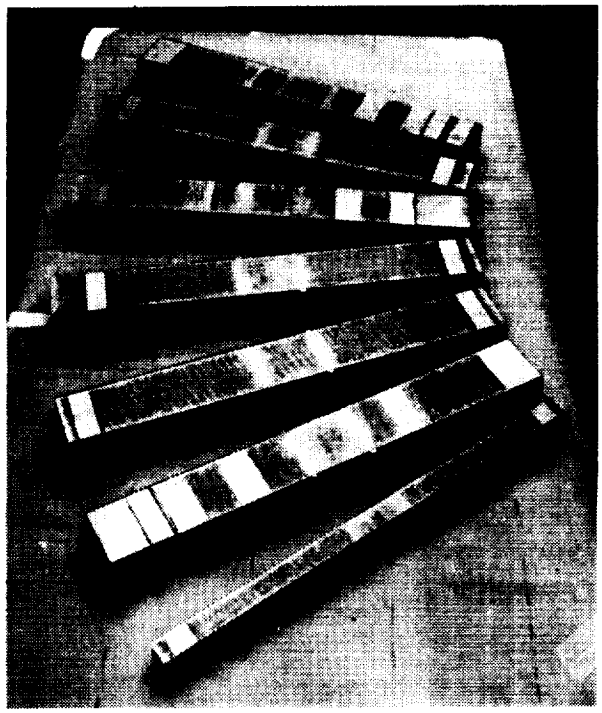

FIGURE 9-51. ELECTRON-BEAM-PERFORATED TITANIUM SHEET FATIGUE SPECIMENS

Fatigue testing of 80 x 700/80 x 80 Dynapore in reverse loading conditions was initially at R=-2.5, 650μ strain in tension and -1600μ strain in compression. This test simulates normal maximum operating stress conditions for a ground to air to ground cycle. The tests showed the material fatigue life capability at this strain to be in excess of 2 million cycles ($>$ 30 lifetimes) for both warp and ±45° orientations.

Due to the high number of cycles to failure on the Nitronic 50 specimens, a cutoff point of 10 million cycles per specimen was established to limit test times. The fatigue tests results on 316L Dynapore, Nitronic 50 Dynapore, and Electron Beam perforated 6AL-4V titanium porous materials are shown in Figure 9-52 together with the target design requirement for the reversed loading conditions.

The Dynapore testing was conducted in 2 directions: parallel to the warp fiber (spanwise on the wing), and ±45° to the warp fiber direction. The perforations in the EB Ti material were approximately 0.114 x 0.185 mm (.0045 x .0073 inches) and the specimens were tested in a direction parallel to the slotted direction, (spanwise orientation on the wing) and perpendicular to the slots (indicated by ll and l respectively in Figure 9-52).

The test results indicate that LFC panel designs using either 316L Dynapore or EB Ti porous surfaces would be adequate for fatigue resistance. The added expense and difficulty in fabricating Nitronic 50 Dynapore is not required to provide fatigue resistance. The EB perforated titanium also exceeds design requirements with holes elongated in either direction.

9.3.3 Impact Testing

The test specimens for the initial impact evaluation of perforated stainless steel backed Dynapore surfaces and electron beam (EB) perforated titanium sheet are described by Figure 9-53 and Table 9-12. The EB perforated Ti sheet materials were purchased from the Farrel Company. The test results are shown in Figure 9-54. It should be noted that the results shown are for maximum depressions which actually occurred at the center lines of the flutes in the substructure.

Final impact testing was conducted using standard Gardner tests on all of the materials listed previously plus a Dynapore surface configuration consisting of Dynapore diffusion bonded to a sublayer of 0.635 mm (.025 inch) thick EB perforated 316L stainless steel sheet with .254 mm (.010 inch) diameter holes spaced 2.54 mm (0.10 inch) on center in a square pattern. The test results are shown in Figure 9-55 together with results for non-perforated materials normally found on leading edges of commercial aircraft. The 0.635 mm (0.025 in) thick electron beam perforated titanium was more resistant to damage than the other materials tested, including conventional leading edge materials of 1.27 mm (0.05 in) thick 7075-T6 aluminum.

9.3.4 Rain Erosion Testing

A total of 44 Dynapore and 20 EB titanium porous surface rain erosion specimens were tested to evaluate their resistance for leading edge surfaces.

Initial rain erosion test specimens were defined as shown in Figure 9-56 and Table 9-13. The testing was arranged through Mr. George Schmitt, Jr., AFML, and was conducted at Wright Patterson AFB. The test facility consists of a powered 2.4 m (8 ft) double arm propeller blade mounted horizontally and the specimens were mounted in the blade tips. A simulated rainfall of one inch per hour was produced with controlled water droplets, which impinged on a pair of specimens as they are rotated. The specimens were tested initially at 179 m/s (400 mph).

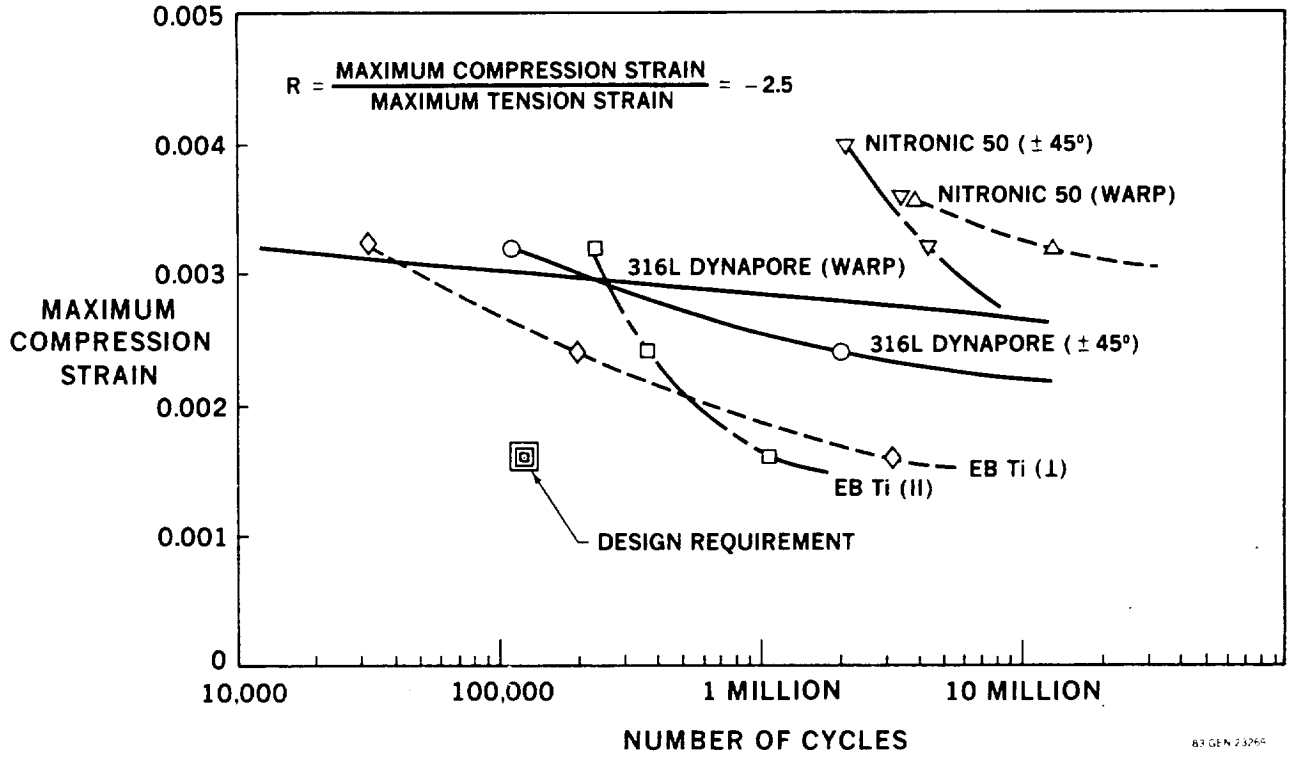

FIGURE 9-52. POROUS SURFACE FATIGUE

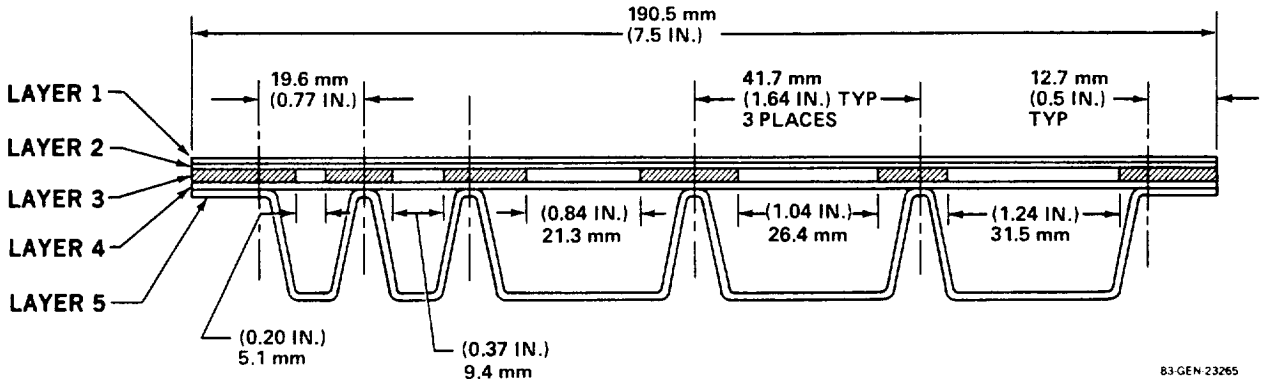

FIGURE 9-53. IMPACT TEST SPECIMEN (SEE TABLE 9-12 FOR DEFINITION OF LAYERS)

TABLE 9-12

IMPACT TEST PANELS

Panel Configuration	Layer 1	2	3	4	5
Dynapore D-1	80 x 700/ 80 x 80 Dynapore	0.508 mm (.020 in) Perf SS (23% open)	2.285 mm (.090 in) Glass/Epoxy Lam (4)	1.016 mm (.040 in) Glass/Epoxy Lam (4)	0.762 mm (.030 in) Glass/Epoxy Lam (4)
Dynapore D-2	80 x 700/ 80 x 80 Dynapore	.508 mm (.020 in) Perf SS (23% open)	1.854 mm (.073 in) (5)	0.991 mm (.039 in) (5)	0.991 mm (.039 in) (5)
EB Perf Ti T-1	EB Perf Ti (See AVI NS-20)	Omit	2.286 mm (.090 in) (4)	1.016 mm (.040 in) (4)	0.762 mm (.030 in) (4)
EB Perf Ti T-2	EB Perf Ti (See AVI NS-20)	Omit	1.981 mm (.078 in) (5)	0.991 mm (.039 in) (5)	0.991 mm (.039 in) (5)

Note: (1) For configurations D1 and D2, resistance spot weld layer 1 to layer 2 approximately 1/4 O.C to simulate a diffusion bonded panel from the vendor.

(2) Sew and cure layers 3, 4, and 5 prior to attach of layers 1 and 2.

(3) Bond layer 1 (or layer 2 if indicated) to cured substructure with film adhesive using strips on layer 3 surface contact area only.

(4) 120/7251 Glass-Epoxy cloth laminate.

(5) T300/5203 Graphite-Epoxy cloth laminate.

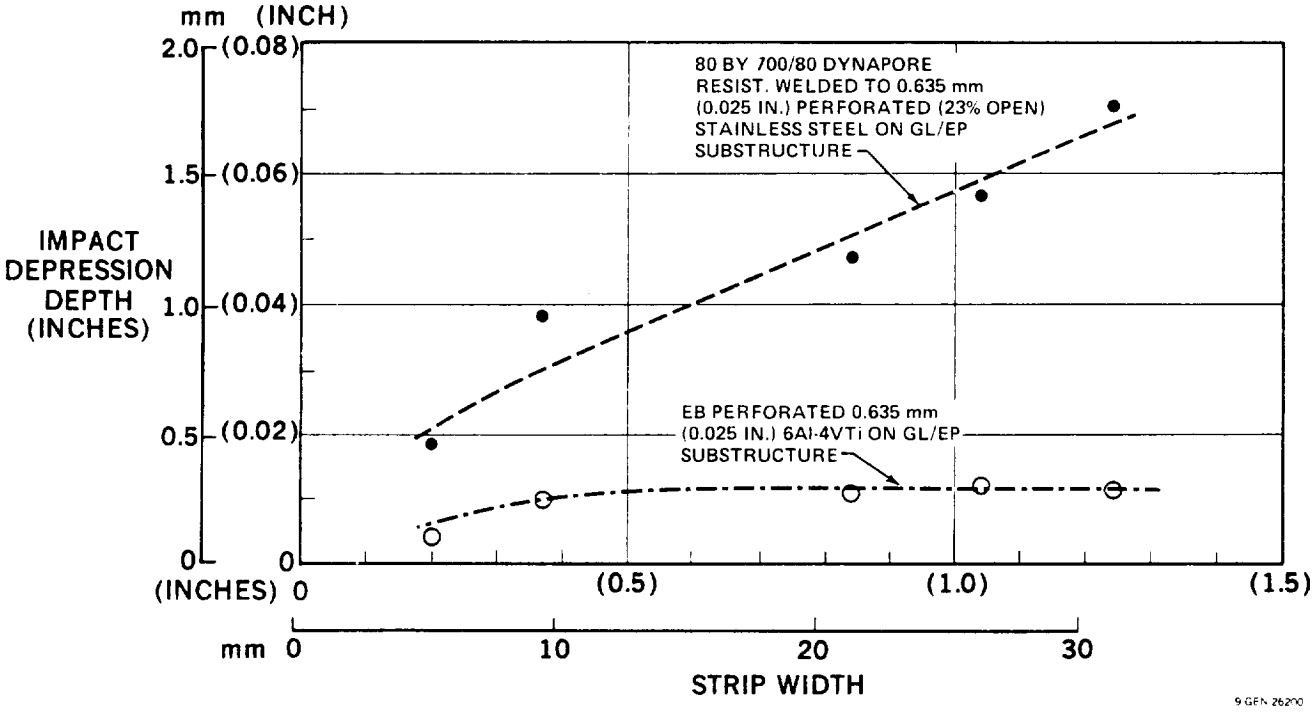

FIGURE 9-54. IMPACT RESISTANCE —2.26 N-m (20 IN.-LB) GARDNER TEST

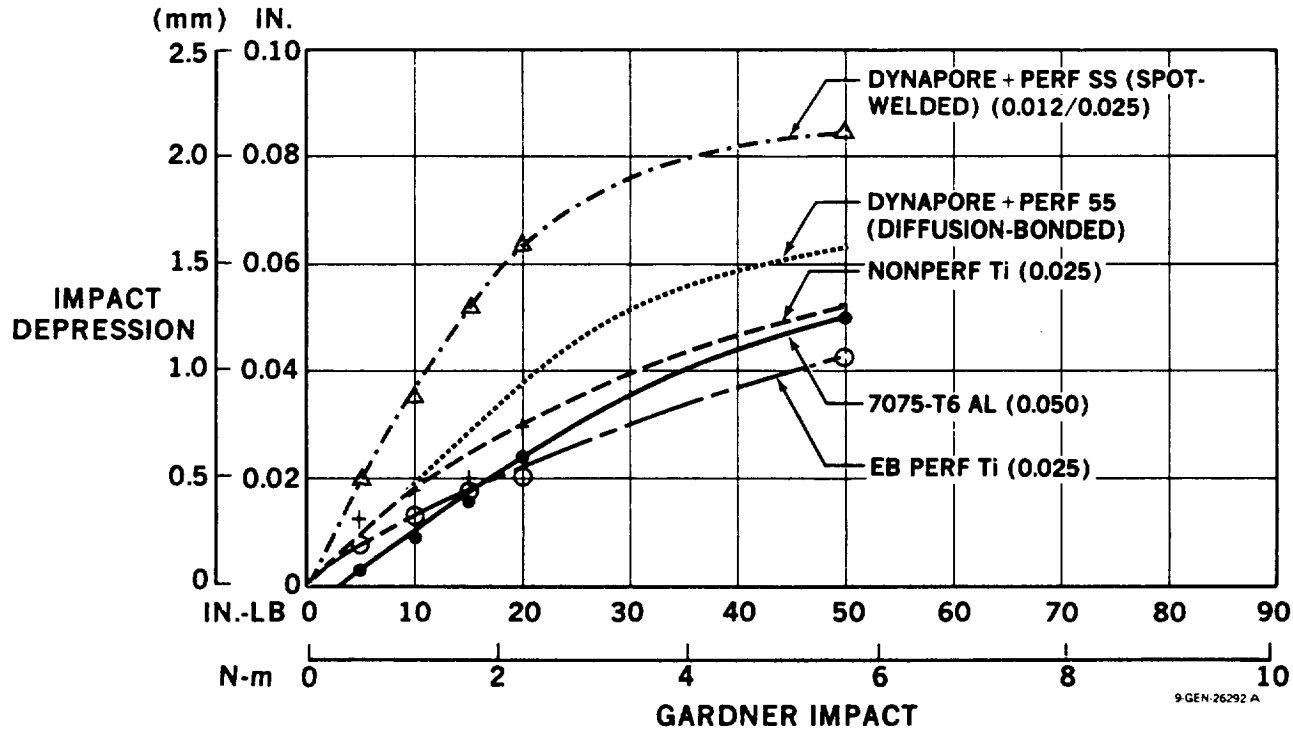

FIGURE 9-55. SURFACE IMPACT-RESISTANCE COMPARISONS

TABLE 9-13
EROSION SPECIMEN MATERIAL CONFIGURATIONS

Specimen Configuration	Layer No. 1	2	3	4	5	6
-501	80 x 700/ 80 x 80 Dynapore	0.508 mm (.020 in) Perforated SS Sheet	2.032 mm (.080 in) (1)	1.27 mm (.050 in) (1)	0.762 mm (.030 in) (1)	1.016 mm (.040 in) (1)
-503	80 x 700/ 80 x 80 Dynapore	0.508 mm (.020 in) Perforated SS Sheet	1.982 mm (.078 in) (2)	1.32 mm (.052 in) (2)	0.991 mm (.039 in) (2)	0.991 mm (.039 in) (2)
-505	.025 EB Perforated Ti Sheet	Omit	2.032 mm (.080 in) (1)	1.27 mm (.050 in) (1)	0.762 mm (.030 in) (1)	1.016 mm (.040 in) (1)
-507	.025 EB Perforated Ti Sheet	Omit	1.982 mm (.078 in) (2)	1.32 mm (.052 in) (2)	0.991 mm (.039 in) (2)	0.991 mm (.039 in) (2)
-509	Same as -501 except bond per note 6.					
-511	Same as -503 except bond per note 6.					

Notes: (1) 120/7251 Glass-Epoxy cloth laminate.

(2) T300/5208 Graphite-Epoxy cloth laminate.

(3) For -501 and -503 configurations, resistance spot weld layer 1 to layer 2 approximately 6.35 mm (.25 in) O.C. to simulate a diffusion bonded material from the vendor.

(4) Sew, cure, and provide suction holes in layers 3 through 6 prior to attach of layers 1 and 2 as shown.

(5) Bond layer 1 (or layer 2 if indicated) to cured substructure with film adhesive on layer 3 contact areas only.

(6) For -509 and -511 configuration, bond layer of 120 fiberglass cloth to internal surface of layer 1 and 2 assembly before bonding per note 5.

Figures 9-57 and 9-58 show typical results of the first series of rain erosion tests. All Dynapore surfaced specimens show damage due to the Dynapore becoming dimpled into the holes in the stainless steel sub-layer. Permanent surface bowing also occurred across flutes. All of the electron beam perforated titanium surfaces show adequate rain erosion resistance. A second set of Dynapore specimens with smaller holes in the sublayer to increase rain erosion resistance was fabricated, configured as shown in Table 9-14. These specimens incorporated a range of smaller diameter hole sizes in the sublayer plus combinations of these sublayers with both Nitronic 50 and 316L Dynapore. These specimens were tested at 179 m/s (400 mph) for 120 minutes, and an additional set was tested at 224 m/s (500 mph) for 60 minutes. An extra set of EB titanium specimens with improved bonding was also tested to check bond strength because of debonding found previously on some samples.

Final results can be summarized as follows:

1. With 80 x 700/80 x 80 or 80 x 700 Dynapore in either 316L or Nitronic 50 material diffusion bonded to perforated stainless steel sublayers, a maximum hole size of 0.381 mm (.015 inch) diameter in the sublayer is allowable to prevent the Dynapore being dimpled into the sublayer holes.

2. All Dynapore specimens diffusion bonded to a 0.635 mm (0.025 inch) thick 316L stainless steel sublayer became permanently bowed across either of the 7.26 mm (0.3 in) or 12.7 mm (0.5 in) gaps in the sublayer. Subsequent analysis shows that a 0.83 mm (0.032 inch) thick layer would prevent depressions at speeds up to 179 m/s (400 mph). Curvature of the surface of a wing leading edge would of course normally increase strength compared to the flat specimens tested and impacts would be lessened by the inclination of the surface other than directly at the leading edge.

3. Nitronic 50 wire Dynapore did not provide increased erosion resistance over 316L Dynapore.

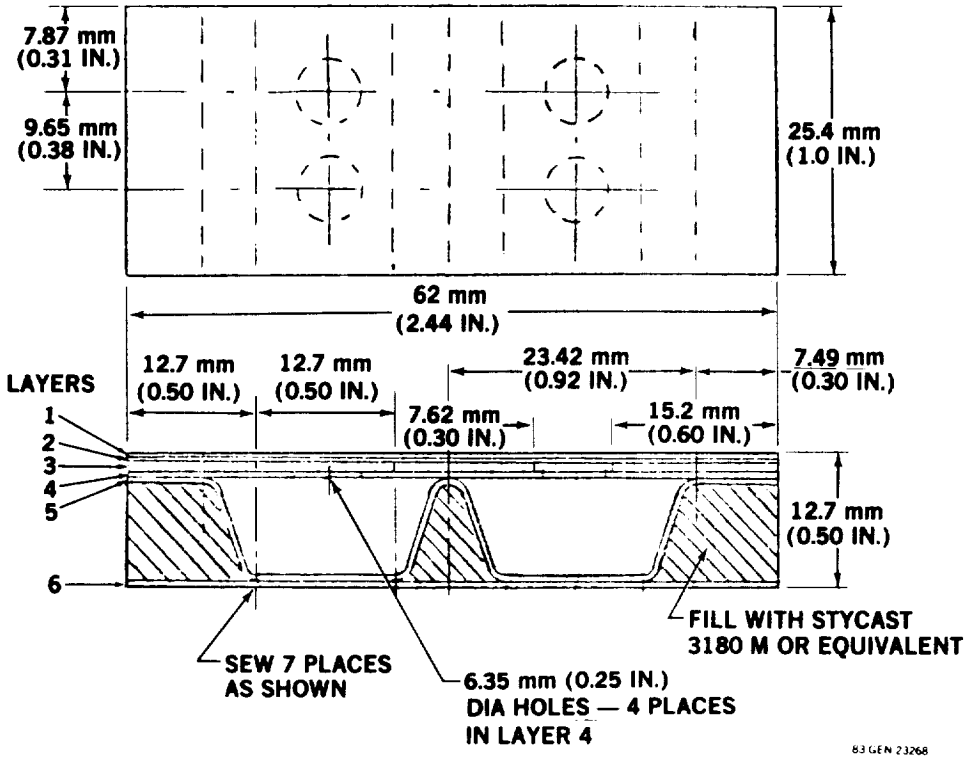

FIGURE 9-56. RAIN EROSION TEST SPECIMEN (SEE TABLE 9-13 FOR DEFINITION OF LAYERS)

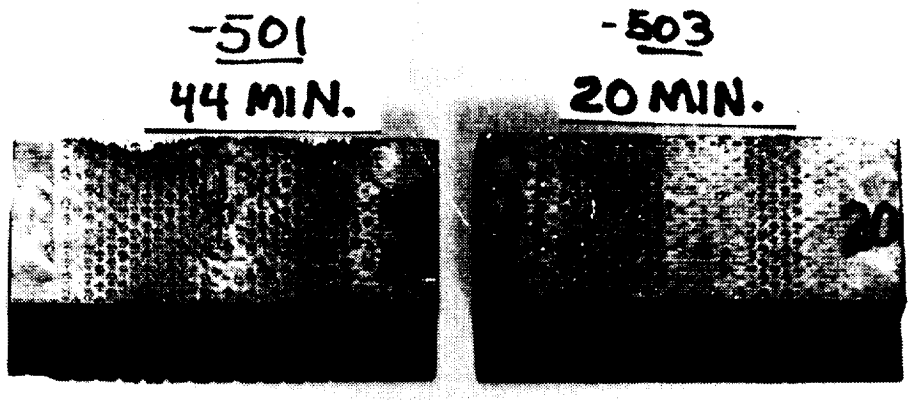

FIGURE 9-57. TESTED DYNAPORE RAIN EROSION SPECIMENS

TABLE 9-14

EROSION SPECIMENS WITH SMALLER SUBLAYER PERFORATIONS

Configuration	Layers 1 & 2 Materials (for other layers see Table 9-13)
NS -501	80 x 700/80 x 80 Dynapore plus 0.635 mm (.025 in) SS sheet perforated with 0.381 mm (.015 in) dia. holes @ 1.143 mm (.045 in) pitch.
-503	Nitronic 50[5] plus 0.635 mm (.025 in) SS sheet perforated with 0.381 mm (.015 in) dia. holes @ 1.143 mm (.045 in) pitch.
-505	80 x 700/80 x 80 Dynapore plus 0.635 mm (.025 in) SS sheet perforated with 0.254 mm (.010 in) dia. holes @ 1.524 mm (.060 in) pitch.
-507	80 x 700/80 x 80 Dynapore plus 0.635 mm (.025 in) SS sheet perforated with 0.152 mm (.006 in) dia. holes @ 2.54 mm (.10 in) pitch.
-509	80 x 700/80 x 80 Dynapore plus 0.635 mm (.025 in) SS sheet perforated with 0.254 mm (.010 in) dia. holes @ 2.54 mm (.10 in) pitch.
-511	80 x 700 Dynapore plus 0.635 mm (.025 in) SS sheet perforated with 0.152 mm (.006 in) dia. holes @ 2.54 mm (.10 in) pitch.
-513	Nitronic 50[5] plus 0.635 mm (.025 in) SS sheet perforated with 0.686 mm (.027 in) dia. @ 1.676 mm (.066 in) pitch staggered.
-515	0.635 mm (.025 in) 6AL4V titanium with EB perforated (elongated) holes 0.102 mm (.004 in) x 0.203 mm (.008 in) long, @ 1.27 mm (.050 in) between holes, and 2.29 mm (.090 in) between rows.

NOTES: (1) 181/7251 glass epoxy cloth laminate.

(2) Sew, cure and provide suction holes in layers 3 through 6 prior to attach of layers 1 & 2 as shown.

(3) Layer 1 to be diffusion bonded to Layer 2.

(4) Bond Layer 2 to cured substructure with film adhesive on Layer 3 contact areas only.

(5) 80 x 700 Dynapore made from Nitronic 50 wire.

4. The bowing of the Dynapore across the flutes is significantly increased at the higher speed of 224 m/s (500 mph). This velocity is higher than is normally required for testing commercial transport aircraft.

5. Electron beam perforated titanium on both glass-epoxy and graphite-epoxy sub-structures was acceptable for rain erosion environments at 179 m/s (400 mph). At 224 m/s (500 mph) slight bowing occurred across the 12.7 mm (0.500 inch) gaps in the sublayer with the flat specimens.

6. Bonding of EB Ti to either glass-epoxy or graphite-epoxy substructures must be carefully controlled to withstand heavy rain enviroments. No bond failures occurred on the Dynapore and titanium specimens with the improved bonds at either test speed.

9.3.5 Compression Crippling Tests

Test specimens were designed and fabricated to evaluate the local crippling strength of the candidate leading edge structure. Figure 9-59 shows the specimen design. Spot welding was used to simulate the diffusion bonded joint between the Dynapore outer surface and the perforated stainless steel sublayer. The substructure design is similar to that used for Dynapore or electron beam porous surfaces. Testing of two specimens indicated a margin of safety in excess of 2 for crippling failures. Figure 9-60 shows a typical specimen tested to failure. The test showed that the leading edge compression design limit would probably be determined by Euler buckling between leading edge rib supports, depending on rib pitch.

9.3.6 Panel Joint Strength

Static tests were conducted on 4 candidate configurations for chordwise joints. The design loads shown below correspond to an ultimate wing strain of 0.102 mm (.004 in). This results in high test loads for test specimens with the stiffer titanium surface.

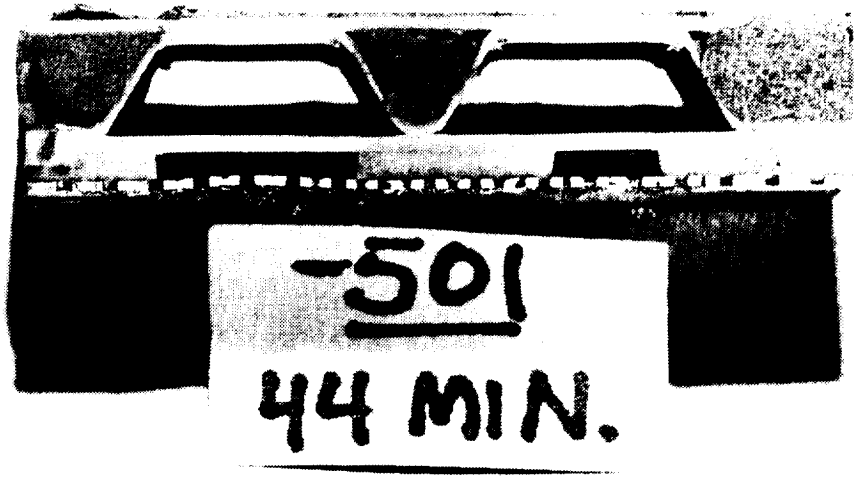

FIGURE 9-58. TESTED DYNAPORE RAIN EROSION SPECIMEN

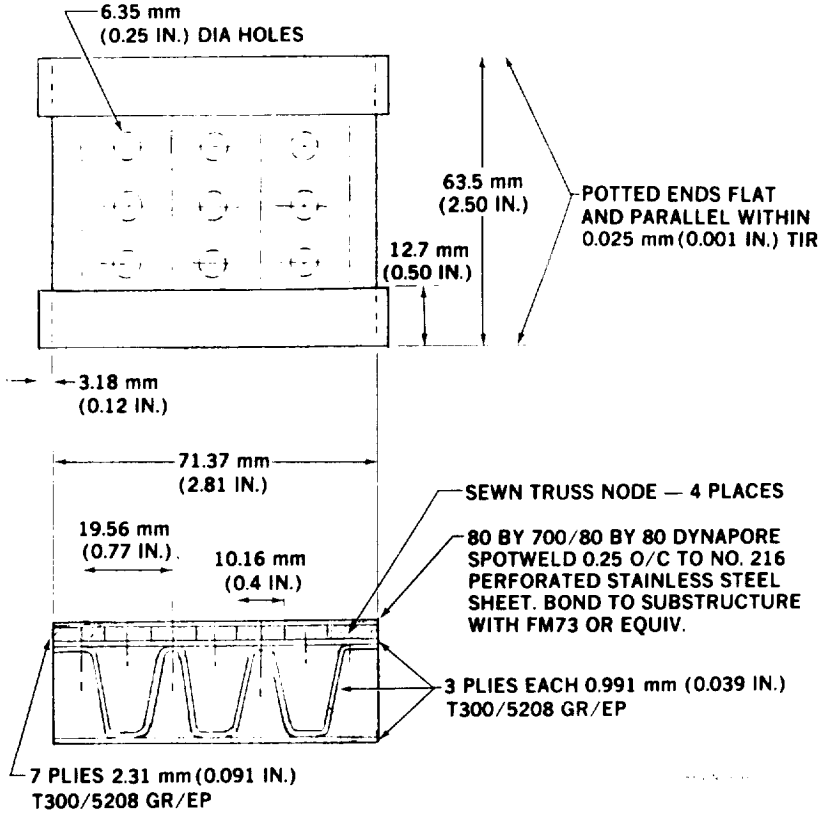

FIGURE 9-59. COMPRESSION TEST SPECIMEN

C-4

Outer Surface Material	Flush Bolt Size 3/8 Dia	5/16 Dia	Compression Load Limit N (lb)	Ultimate N (lb)
Titanium	-1	-505	41,858 (9,410)	62,787 (14,115)
Dynapore	-501	-507	33,273 (7,480)	49,909 (11,220)

Figure 9-61 and Table 9-15 show the test specimen and test schedule respectively and Figure 9-62 shows the compression test set up with a typical specimen ready for test. The test was designed to identify potential strength, fatigue and smoothness capabilities of joint configurations. Configurations -501 and -507 with Dynapore surfaces sustained their ultimate load without failure. Configuration -501 failed at 107 percent ultimate load by delamination of the GR-EP section due to bending adjacent to the simulated rib support. Configuration -507 sustained 107 percent ultimate load without failure (the limit of the test machine).

TABLE 9-15
TEST SCHEDULE
JOINT SPECIMENS

Dwg. Dash No.	Type Test	No. of Specimens	Load/Record
-1	Static Compression	2 pairs	(1) .004 (m/m) strain/check for bearing failures and note joint deflections relative to porous surface
-501 -505 -507			(2) Failure/P_{ult}

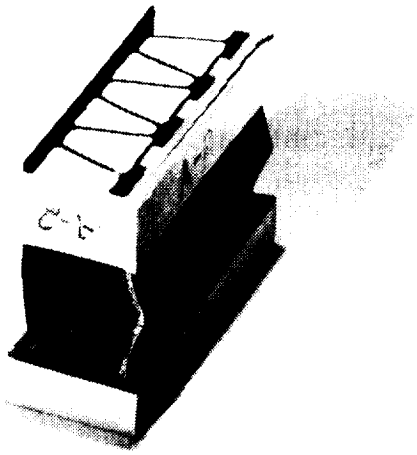

FIGURE 9-60. FAILED COMPRESSION SPECIMEN

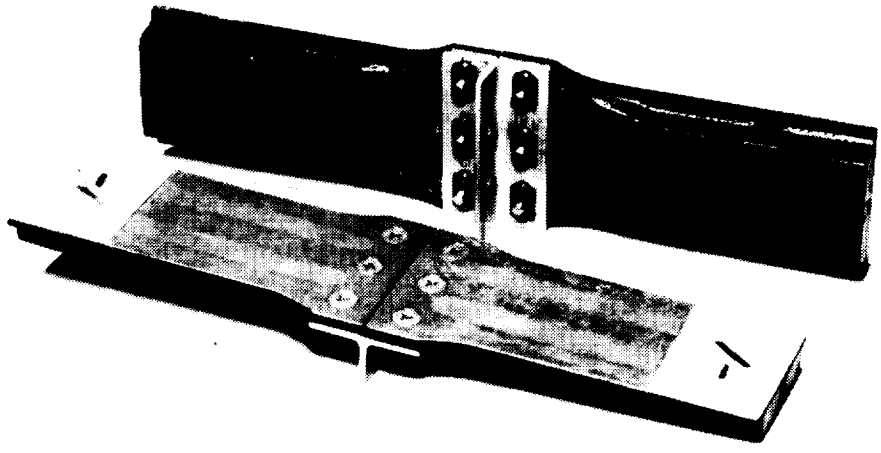

FIGURE 9-61. JOINT TEST SPECIMENS

Configurations -1 and -505 with titanium outer surfaces failed at 67 percent and 87 percent of their limit load respectively due to surface debonding. Post test analysis showed some bonding areas to be below-minimum thickness i.e., bond material starvation. In addition, surface cleaning/bonding procedures were suspect.

Specimens -1 and -505 were therefore rebonded using an improved procedure for porous surfaces that included:

- Taping of the outer surface to prevent excessive thinning of the adhesive layer due to extrusion of the adhesive through the perforations.

- Venting the autoclave vacuum to atmospheric pressure after the autoclave pressure had reached 103 kP (15 psi) to avoid weakening of the bond due to boiling of the adhesive.

- Reducing the time to reach the curing temperature of 121°C (250°F) from one hour to a half-hour, in order to reduce the time spent with the adhesive at a lower viscosity.

- Limiting the time taken between cleaning and etching of the titanium surface and application of the FM73 adhesive to one hour and limiting the time before starting the cure cycle to two hours, in order to minimize contamination effects.

After rebonding, the -505 specimen was retested. Failure occurred in the graphite epoxy supporting structure by separation of the stiffener, due to local bending starting near the simulated rib support, see Figure 9-63. The failing load was (69,948N) 15,725 pounds or 111 percent of the ultimate load. There was no evidence of failure of the bond between the titanium surface and the graphite epoxy structure. The final results of static testing were therefore satisfactory for both the electron beam perforated titanium and the Dynapore

- The rebonded -1 specimen was used for fatigue testing, see Section

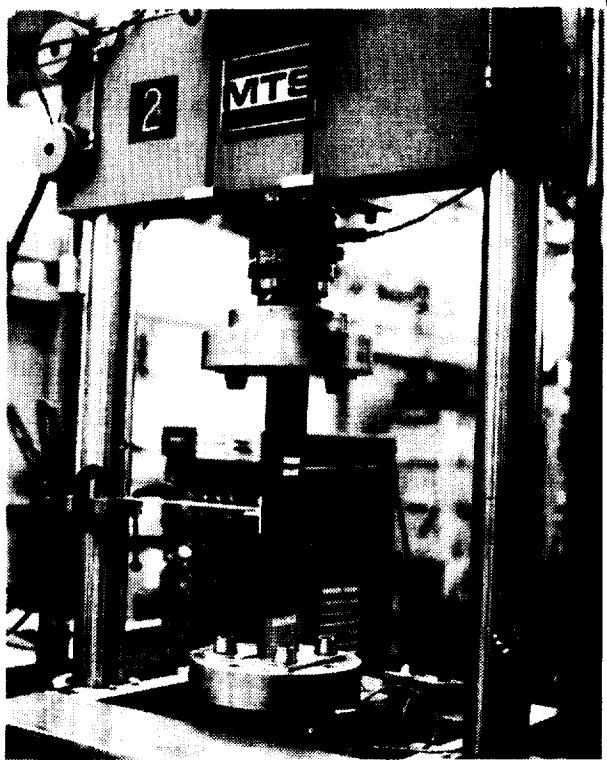

FIGURE 9-62. JOINT COMPRESSION TEST SETUP

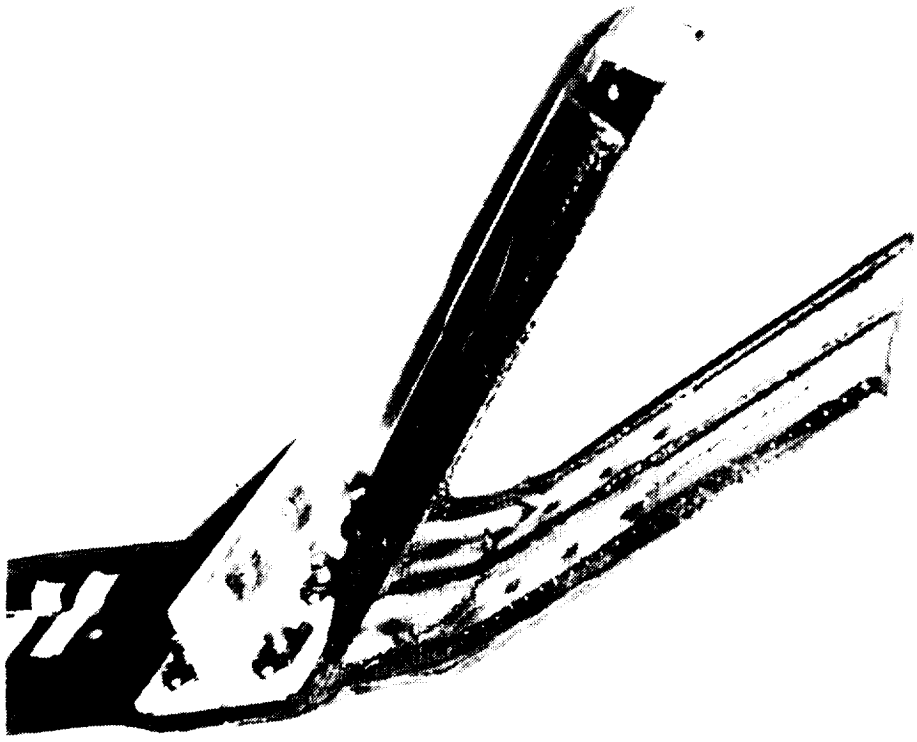

FIGURE 9-63. FAILED COMPRESSION TEST SPECIMEN

During static testing of the joints, 4 deflection gages were used to determine possible waviness and/or steps across the joint. Two gages were placed opposite each other at about 19 mm (.76 in) from the joint and the other two were located about 150 mm (6 in) from the joint gap on either side.

Waviness of about 0.25 mm (.01 in) occurred over a length of 350 mm (12 in) with a step of about 50 μm (.002 in) at the joint under loading conditions corresponding to steady cruising flight. The effects of eccentric loading at the ends of the specimens may have increased the measured deflections.

9.3.7 Panel Joint Fatigue

The design requirement for fatigue was established as a cyclic loading condition with the average compression strain varying from 0.016 percent to 0.160 percent, repeated for 120,000 cycles without failure.

The fatigue specimens were similar to the static test specimens described previously in Section 9.3.6. They were strain gaged on both sides and were tested at a rate of 7,200 cycles/hour in the test machine shown previously in Figure 9-62.

The rebonded EB titanium surfaced (-1) specimen described in Section 9.3.6 was fatigue tested initially to the required 120,000 cycles, then cumulatively at increasing strain levels until failure occurred after 170 cycles at the required ultimate static strength.

Max. Axial Load N	(LB)	Max. μ Strain	(Avg. μ Strain)	Cycles at each Load	Remarks
17,793	(4,000)	1,430	(1,170)	120,000	
26,689	(6,000)	2,190	(1,804)	20,000	
41,813	(9,400)	3,420	(2,790)	20,000	(static limit load)
53,379	(12,000)	4,210	(3,300)	10,000	
62,720	(14,100)	5,840	(4,620)	170	(static ultimate load)

The average strains, shown in parentheses, are the equivalent wing design strains for the upper surface. The maximum strains measured were increased by local bending near the joint due to load path eccentricities. The fatigue strength far exceeded the fatigue strength requirements.

Eventual failure was due to delamination of the outer surface as shown in Figure 9-64, which was taken with the specimen being subjected to an axial compressive load of 17,793N (4,000 lb).

The following results were achieved on the -501 Dynapore specimen:

Max. Axial Load N	(Lb)	Max. μ Strain	(Avg. μ Strain)	Cycles at each Load	Remarks
13,256	(2,980)	1,600	(1,025)	200,000	
29,047	(6,530)	3,200	(2,361)	200,000	
35,052	(7,880)	4,000	(2,963)	200,000	(Static limit load)
44,482	(10,000)	5,080	(3,530)	33,000	'T' support failure

The results show that the -501 joint greatly exceeded fatigue test requirements without failure.

Test results for the -507 Dynapore specimen were as follows:

Max. Axial Load N	(Lb)	Max. μ Strain	(Avg. μ Strain)	Cycles at each Load	Remarks
18,238	(4,100)	1,600	(1,065)	200,000	
39,144	(8,800)	3,200	(2,536)	63,000	7.94 mm (5/16") bolt failure

The bolt failure originated at the junction of the countersunk head and the shank. Although the use of a smaller bolt resulted in a large reduction of fatigue strength, the -507 joint still exceeded the design requirement.

The overall fatigue test result showed that all of the fatigue test specimens exceeded fatigue requirements. Specimens with the 9.55 mm (3/8") bolt were far superior than that with 7.94 mm (5/16") bolt due to induced bolt bending. The results also show that the improved bonding technique for the E.B. perforated titanium surface is satisfactory under both loading conditions.

9.3.8 Panel Development Testing

Fabrication development of the woven steel Dynapore faced fiberglass LFC glove panel included work to meet impact, porosity, bonding and environmental durability requirements. After the panel materials, configuration and fabrication procedure were reasonably well established, mechanical testing of coupons and structural elements was done to determine strength and stiffness properties of the panel constituent materials, both separately and in combinations, representative of the working design. Peel tests after environmental exposure were used to check the Dynapore bond strength during development.

Dynapore (80 x 700/80 x 80) static stiffness and static strain properties were explored. The Dynapore bonded to a perforated "S" glass sublayer was tested for strain recovery, effective stiffness and fatigue strength. Panel assemblies were tested for bending strength/stiffness, compression strength/stiffness, and shear strength/stiffness with alternative core and materials orientations. Two large 356 x 610 mm (14 x 24 inch) shear panels were tested for buckling resistance and to failure with core orientations of 90° and 45° to the shear load direction.

Two panel assemblies 305 x 762 mm (12 x 30 inch) in size were compression tested to assess the strain compatibility between a simulated graphite/epoxy wing cover and the porous glove panel attached to it. One assembly had panel fluting at 90° and another had fluting at 45° to the graphite support stiffeners.

Figure 9-65 shows a 305 x 762 mm (12 x 30 inch) panel before final assembly, and Figure 9-66 shows a panel assembly in the test machine after successful loading to 0.006 strain.

Single fastener joint specimens, representing the initial design for the chordwise glove panel joint, were tested in static tension and tension fatigue. See Sections 9.3.6 and 9.3.7. Static failure occurred at 185 percent of design ultimate. Fatigue failure at maximum limit load occurred at 356K cycles, which is three times the required life.

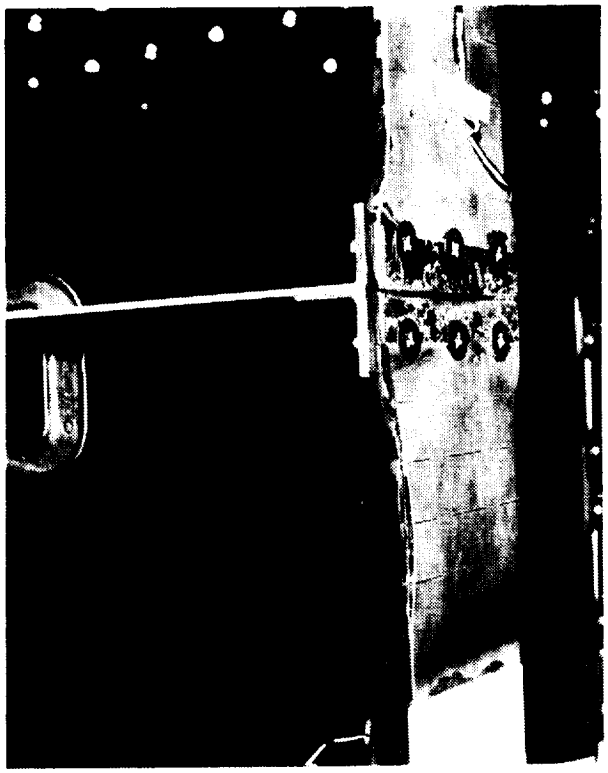

FIGURE 9-64. FAILED JOINT FATIGUE SPECIMEN

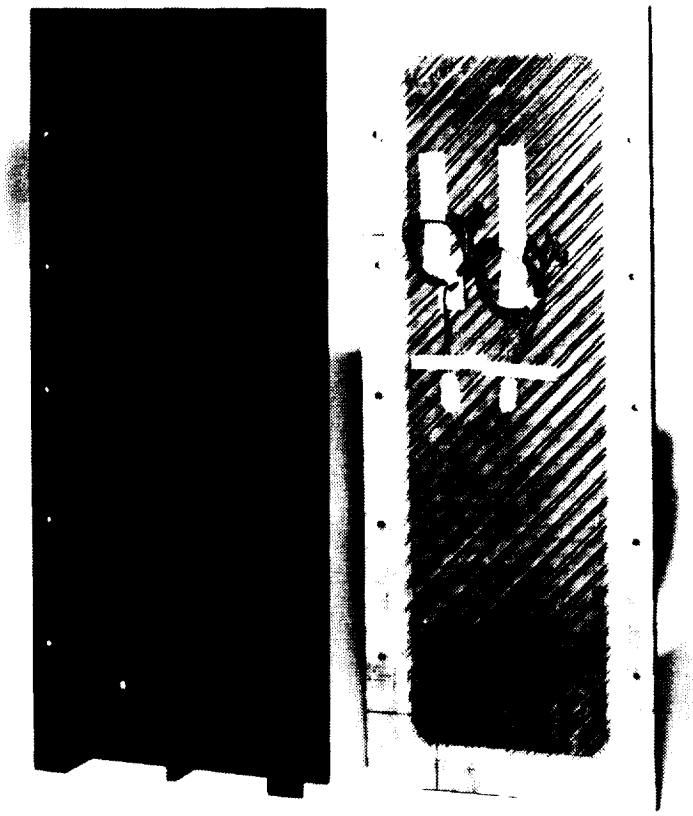

FIGURE 9-65. COMPRESSION TEST PANEL

A 254 x 508 mm (10 x 20 inch) glove panel with a centrally located joint was tested to determine the ability of the surface and joint to conduct lightning discharge currents up to 144 kC 940 KA) magnitude and lightning restrike to 378 kC (105 KA). The resulting damage and discharge capability were acceptable from a safety aspect, but the panel would need to be replaced in service.

9.3.9 Structural Demonstration Component

A large compression panel was tested to verify structural adequacy and fabricability of the LFC porous glove panel/graphite epoxy wing box system, when subjected to compression loading to the required strain levels of 0.004. The design incorporates a simulated wing panel with the porous panel attached to the external stringers, designed to have strain compatibility with the wing structure. The panel size was 2070 x 730 mm (81.5 x 28.75 inch) with an area of approximately 1.4 m^2 (15 ft^2). The test panel was configured for installation in an existing Douglas test fixture for testing on the million pound Baldwin test machine as shown in Figure 9-67.

The design approach was to first design the graphite epoxy J-stiffened compression panel using a simulated rib spacing of 762 mm (30 inch) to control the Euler buckling length, and a stringer height of 38 mm (1.5 inch) with a stringer spacing of 178 mm (7.0 inch). This is representative of wing box structure at the 70 percent span location of the aspect ratio 10 Baseline aircraft wing. The ultimate design strain level of 0.004 was chosen because of an anticipated design constraint for composite wing designs due to damage tolerance and other design requirements. The simulated wing panel was designed in the T300/5208 materials rather than the stiffer mixed graphite concept (T-300/GY-70 fibers) mentioned in Section 9.1.6 to reduce the test load associated with the strain target for the glove panel.

FIGURE 9-66. COMPRESSION TEST PANEL SETUP

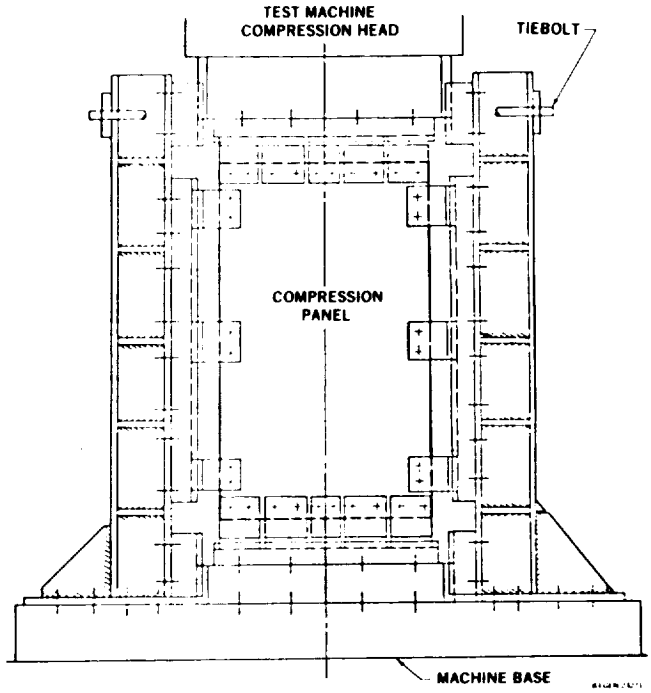

FIGURE 9-67. LARGE COMPRESSION PANEL TEST ARRANGEMENT

The LFC porous glove test panel incorporated the design features of typical longitudinal panel splices at the panel edges. Field fasteners, panel inserts, airflow collection stiffeners and air dams were included to evaluate the structural capabilities of these features and to establish manufacturing feasibility and smoothness of a large panel and the fluted panel stiffening was representative at 45 degrees. A Dynapore porous surface, favored at this time, was used for this test panel. Field fastener spacing was at 15 inches maximum. The combined assembly is illustrated in Figure 9-68 which also shows the strain gage locations.

Computer programmed analyses were used to design both the graphite panel and the porous glove panel. Skin buckling, flange crippling and general buckling were critical elements. Analysis showed that the graphite epoxy panel would require a lod of 1,786 kN/m (10,200 pounds/inch) to reach .004 compression strain. The overall glove panel analysis was conducted utilizing an orthotropic sandwich panel analysis, named TRUSS especially programmed for the glove panel. Supplementary calculations covered element crippling and the panel/graphite structure interaction. The analysis predicted that the glove panel would accept 19 percent of the total test load after graphite epoxy material had been introduced to stiffen the glove panel webs and backfacing.

During testing, buckling of the graphite-epoxy simulated wing box structure occurred between the integral stiffeners at 90 percent of ultimate load and failure occurred at 97 percent of the ultimate design load. Figure 9-69 shows the LFC panel surface in the test rig after failure. Figures 9-70 and 9-71 show failures at the inner face of the LFC panel and the mating face of the GR-EP wing box panel respectively, after disassembly.

Initial delamination of the Dynapore surface was observed to occur at a load equivalent to approximately "1G" flight load. This premature failure was found to be caused by poor surface cleaning procedures prior to Dynapore bonding. Subsequent changes to porous surface designs and bonding methods are expected to correct this failure mode.

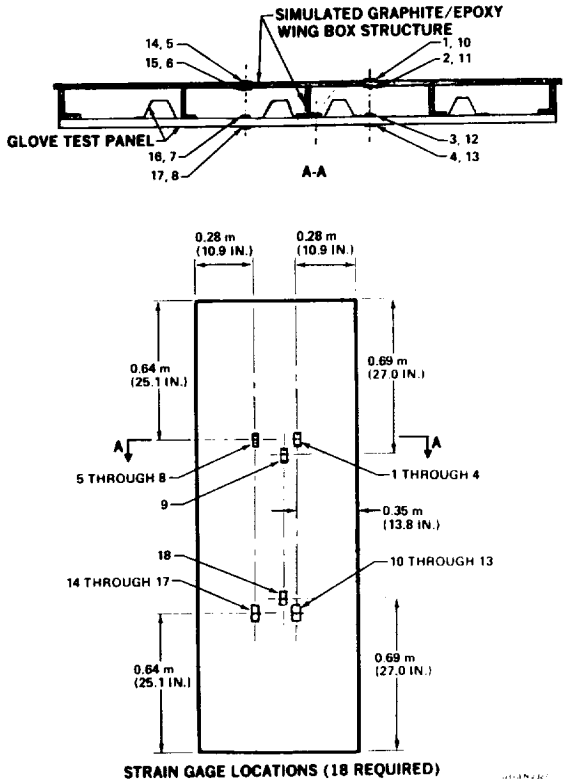

FIGURE 9-68. LARGE COMPRESSION TEST PANEL

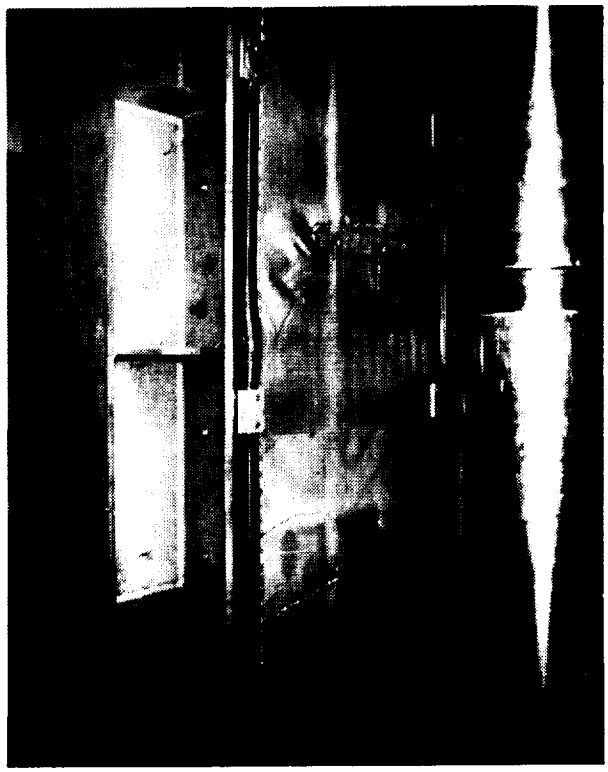

FIGURE 9-69. LFC DEMONSTRATION PANEL FAILURE

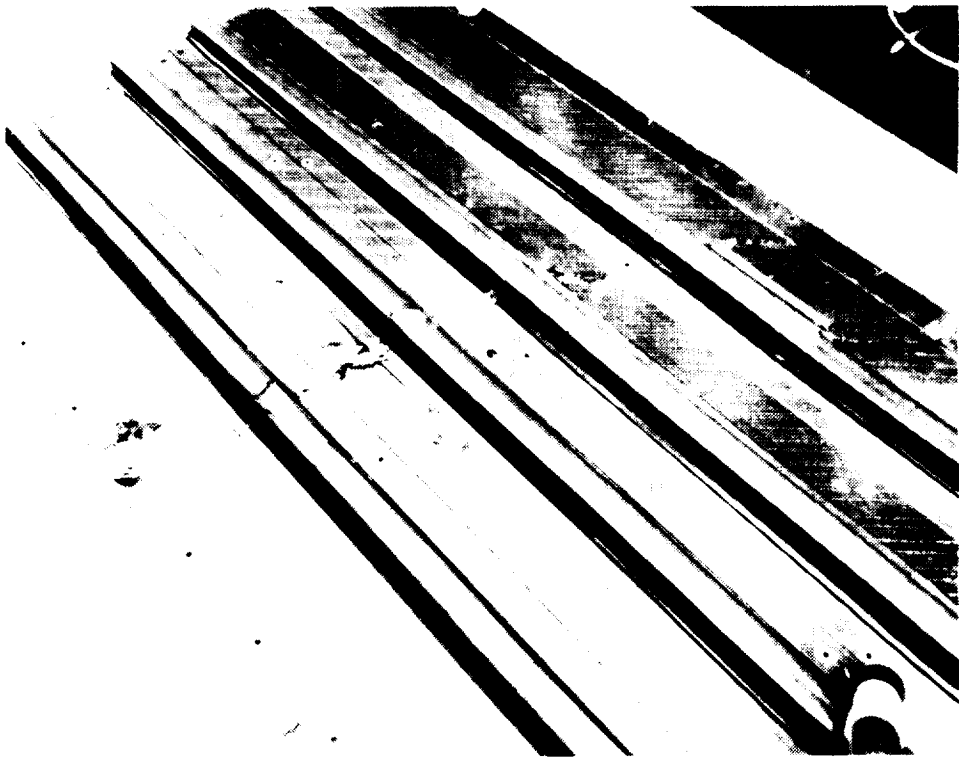

FIGURE 9-70. LFC PANEL FAILURE

FIGURE 9-71. GRAPHITE-EPOXY WING BOX P[illegible]LURE

The average strain gage readings for the GR-EP wing box panel and the LFC panel are shown in Table 9-16, compared to predicted values at increasing loads to failure. Note that the actual strains are all below predicted values at any given load, indicating that the modulus and/or gross-sectional area of the article was higher than anticipated. The results are plotted in Figure 9-72. This shows that the LFC panel was being strained more than the graphite-epoxy wing box prior to the onset of buckling.

The initial failure occurred in the simulated wing structure with a strain level of 0.0037 in the LFC glove panel. It cannot be determined whether the glove panel would have reached the design ultimate strain level of 0.004 but the limit strain level of 0.0267 was easily exceeded.

TABLE 9-16

DEMONSTRATION PANEL STRAIN HISTORY

Strain x 10^6

Strain Locations	Load - % Ultimate									
	10	20	30	40	50	60	70	80	90	97% (Failure)
GR-EP Inner Panel (Average)	288	624	1024	1372	1684	2019	2349	2683	2890	340,000 Lb - No Strain Readings
LFC Panel (Average)	388	716	1062	1403	1867	2310	2670	3027	3410	
Predicted	390	780	1170	1560	1950	2340	2730	3120	3510	

9.4 WING LEADING EDGE DESIGN INTEGRATION

The initial problem addressed in leading edge design was to define geometry and construction requirements for integration of the air suction system and a freezing point depressant (FPD) liquid dispensing system in the same structure. A metallic structure was assumed necessary for impact toughness. Approaches included: (1) suction slots in locally densified porous material with fluid transpiration through remaining porous areas. (2) All porous material with suction and fluid transpiration through alternate porous strips running spanwise. (3) Spanwise porous strips let-in and alternating with solid, slotted material.

The most acceptable approach appeared to be the all porous nose, with an integrated fluid/air supply structure behind the surface. Various sandwich and machined plate concepts were suggested for fluid distribution. One of the controlling fluid system design criteria was the necessity to withstand 345 kPa (50 psi) fluid pressure behind the porous transpiration surface.

9.4.1 Leading Edge Design - Phase I

A section at the 40 percent semispan air collection station of the baseline wing was chosen for the design integration study. The resulting arrangement for upper surface suction only, and with a retractable shield, is shown in Figure 9-73. A sandwich construction with a 3.17 mm (.125 inch) cell honeycomb core, 6.35 mm (.250 inch) thick, supports the outer facing of Dynapore backed up by perforated impact sheet. A complex inner surface is grooved and ducted to provide fluid or air suction at the surface. Materials and fabrication procedures were not well defined at this stage, so the drawings should be regarded only as an initial indication of space and volume requirements for the three integrated systems - structural, air and fluid. Aside from fabricability, the main structural design challenges were impact durability of the outer surface and the peel stresses within the sandwich due to the pressurized fluid. The construction concept assumed a one piece seamless outer surface between approximately 5 percent chord on the lower surface to the joint at the front spar upper flange.

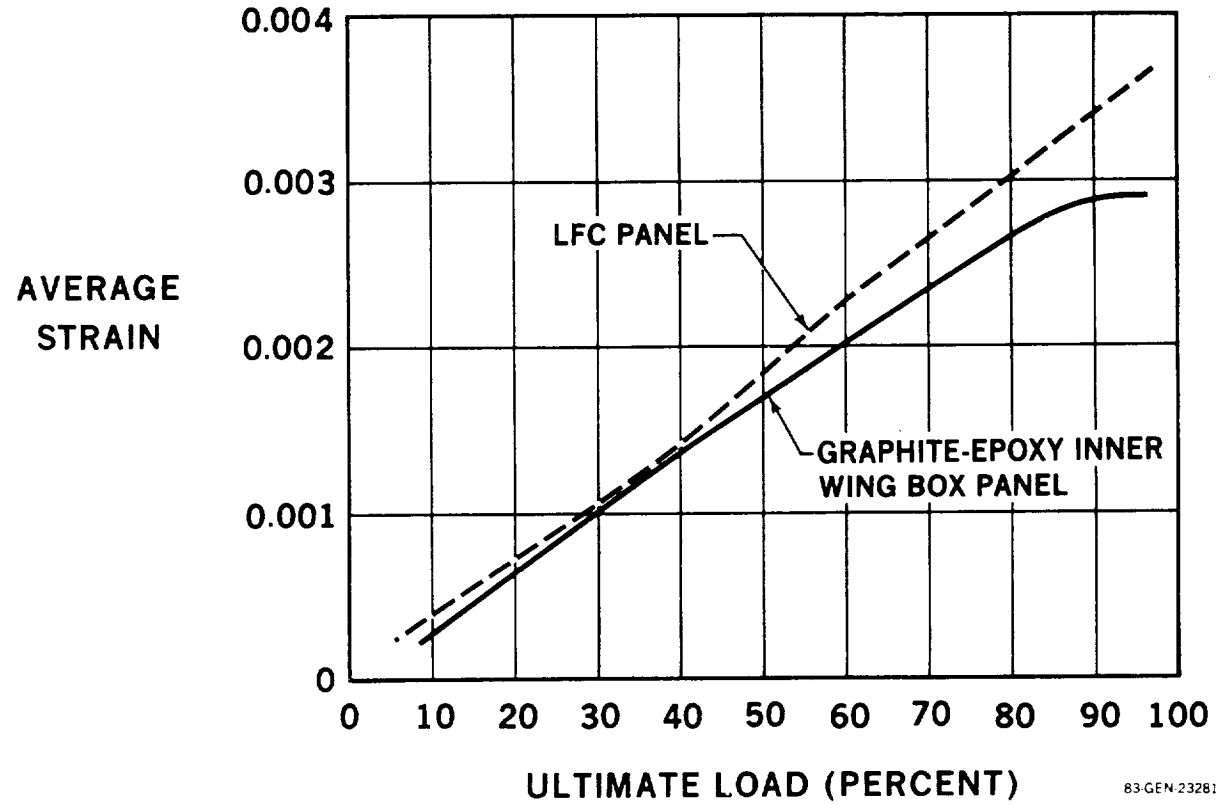

FIGURE 9-72. DEMONSTRATION PANEL AVERAGE STRAIN HISTORY

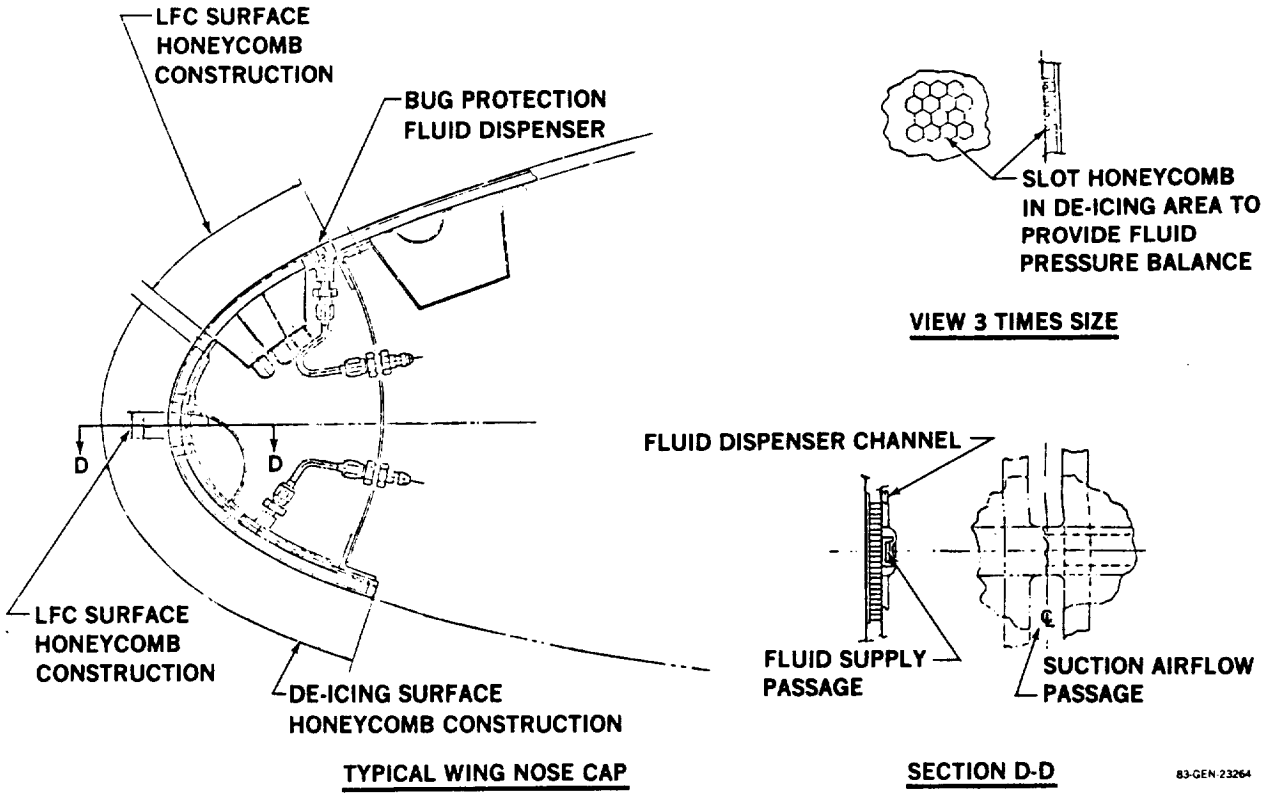

FIGURE 9-73. LFC LEADING EDGE – PHASE I

Before continuing with leading edge structural design, the following complementary studies were undertaken (as reported in Section 11.0);

- o Leading edge protection fluid dispensing testing in the wind tunnel to observe fluid flow characteristics and effects on the surface.
- o Preliminary environmental contamination and cleaning tests.
- o Examination of design parameters to determine required pressure drop and suction flow characteristics of porous surfaces in the leading edge region.
- o Leading edge protection shield bug deflection analysis and consideration of fluid dispensing requirements.
- o Full scale insect impingement tests on a leading edge shape in the icing tunnel.

Considerable effort was expended in evaluating alternatives to the Dynapore/perforated glass honeycomb concept for the critical nose cap region of the leading edge. Improved designs included metallic honeycomb or closely-spaced corrugated surface supports with brazing, welding or diffusion bonding techniques to join surface, subsurface and support structure, and organic bonding. At this stage, a cursory ranking of 10 concepts put in first place a design featuring an electron beam perforated titanium surface, diffusion bonded to slot-perforated backing sheet on a corrugated air collection support structure. It ranked high in toughness, reliability and elasticity.

9.4.2 Leading Edge Design - Phase II

A decision was made to concentrate on using the Dynapore/glass Lockcore glove panel construction in the leading edge region. It was felt that continuity with existing porous panel development would be advantageous. To be consistent with the configuration trade study favoring upper surface suction only, Section 5.6.1, the fluid pressure design requirement was avoided by replacing the fluid protection system with an extendable shield. The objection to chordwise-oriented Lockcore construction, which is not feasible from a fabrication standpoint with curved leading edge contours, was answered by turning the fluted core

spanwise, requiring it to taper in cross section with percent chord lines. Figure 9-74 indicates the first scheme of this type, suitable for a flight test airplane leading edge. This design featured perforated fiberglass under Dynapore; the glass being thick enough to accept major impacts safely. The hinged shield shape although far from ideal from an aerodynamic point of view, could be used to provide insect impingement protection and avoids the cost and complication of a variable camber mechanism.

Concept sketches for a production LFC airplane were generated as shown in Figure 9-75. A "D-duct" accommodates suction for the nose region. Elsewhere suction air is collected from the spanwise flutes into round collection ducts running through support ribs. Surface Concept C shows continuous perforations under the Dynapore. In Concept B, perforations occur only under those Dynapore areas where strip suction is desired, leaving areas for sewing, fastening or adhesive bonding in the intermediate blank strips. Surface Concept A suggests another alternative using larger perforations under small perforations in the surface materials to improve surface backup for impact resistance.

Figure 9-76 shows a design providing easier air collection from the spanwise flutes. It features integral collector ducts which also connect the surface to the supporting ribs. The flutes at the surface would be discontinued at panel splices to control spanwise inflow-outflow. The airflow between the small and large ducts is through metering holes to control the flow. Figure 9-77 illustrates an alternative construction that provides a stiffer complete sandwich structure for the outer surface.

9.4.3 Leading Edge Fabrication

For an initial check on fabricability of the Dynapore/glass laminate construction for the leading edge region, a fiberglass tool was laminated using an existing control surface part to provide the shape. This tool was used for the initial rubber mandrel packing and pressurization fabrication trials. The skin and corrugations were jointed by sewing to strengthen the surface joint.

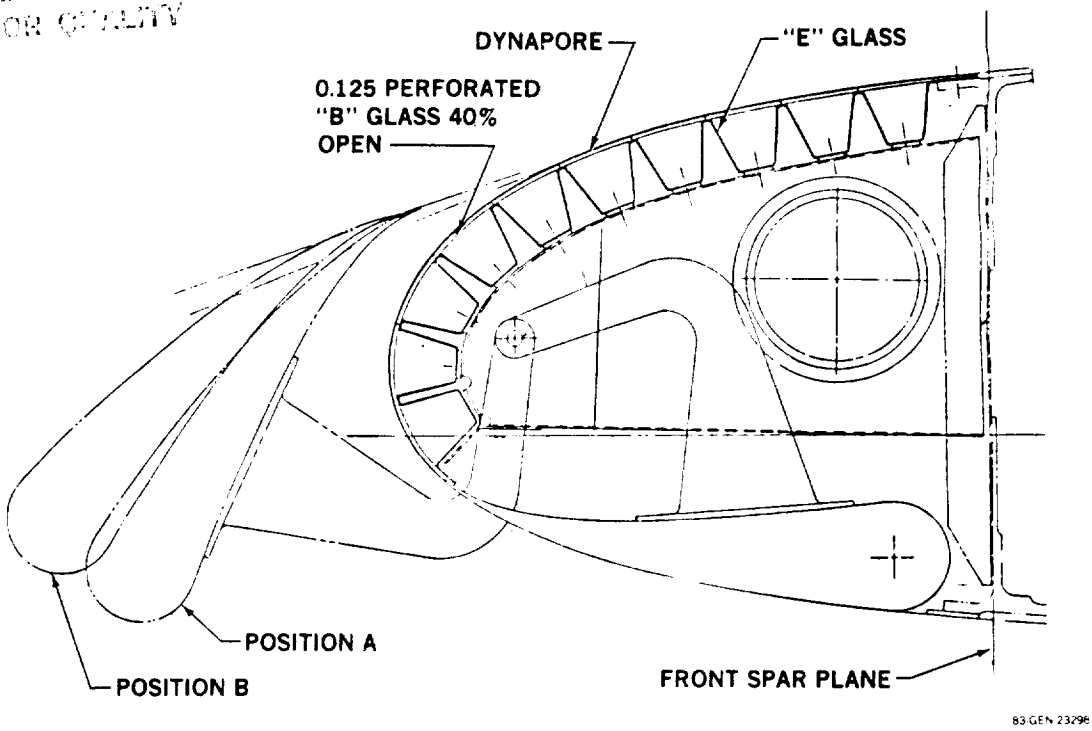

FIGURE 9-74. LFC LEADING EDGE – PHASE II

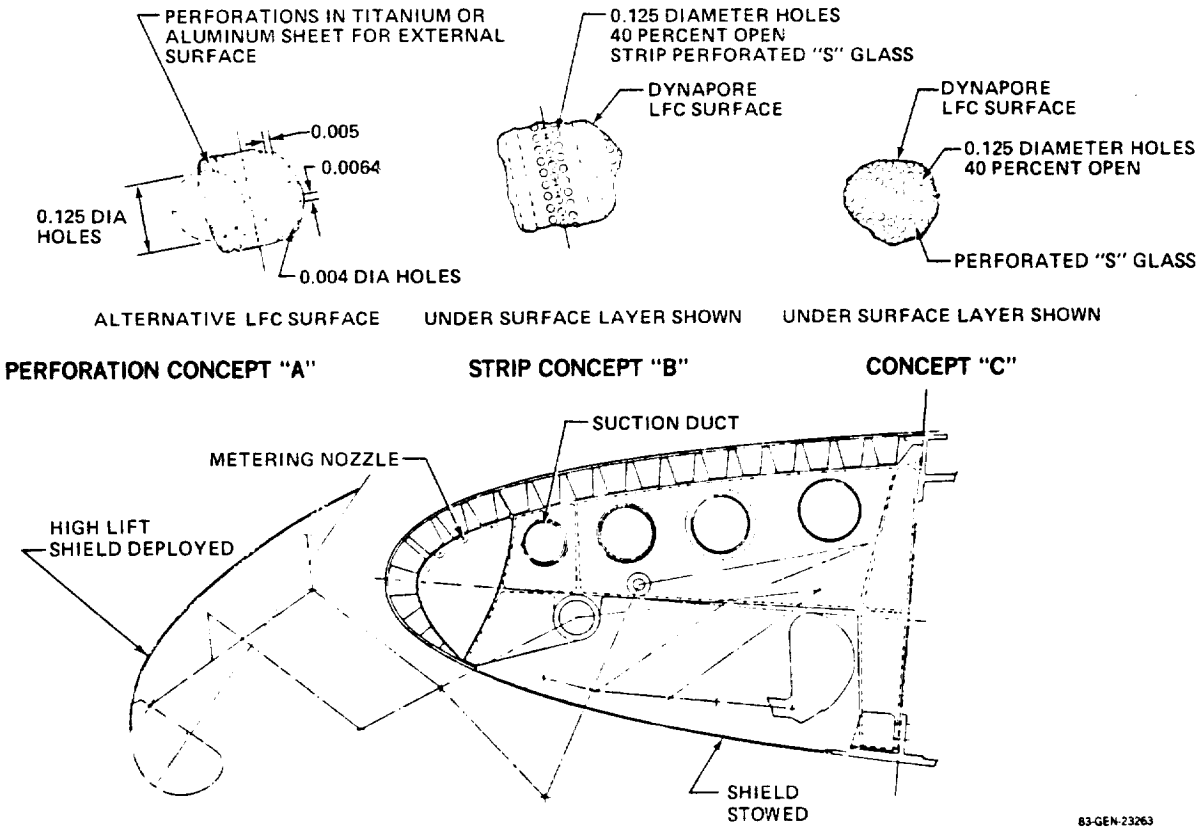

FIGURE 9-75. LEADING EDGE DESIGN – SEPARATE COLLECTOR DUCTS

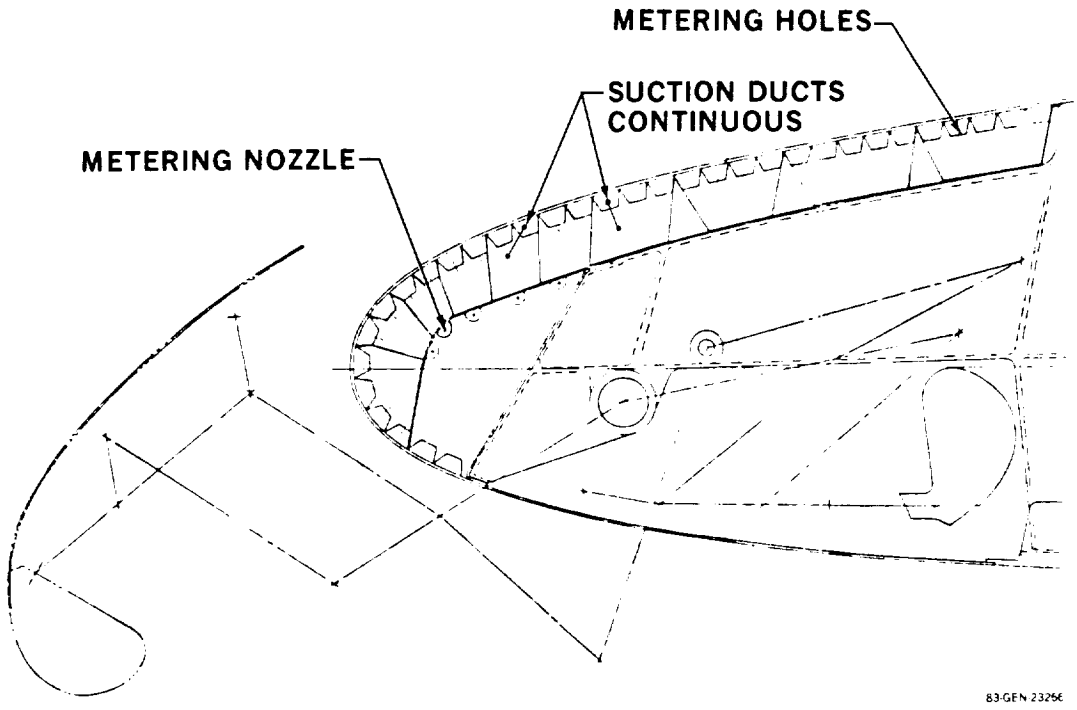

FIGURE 9-76. LEADING EDGE DESIGN – INTEGRAL COLLECTOR DUCTS

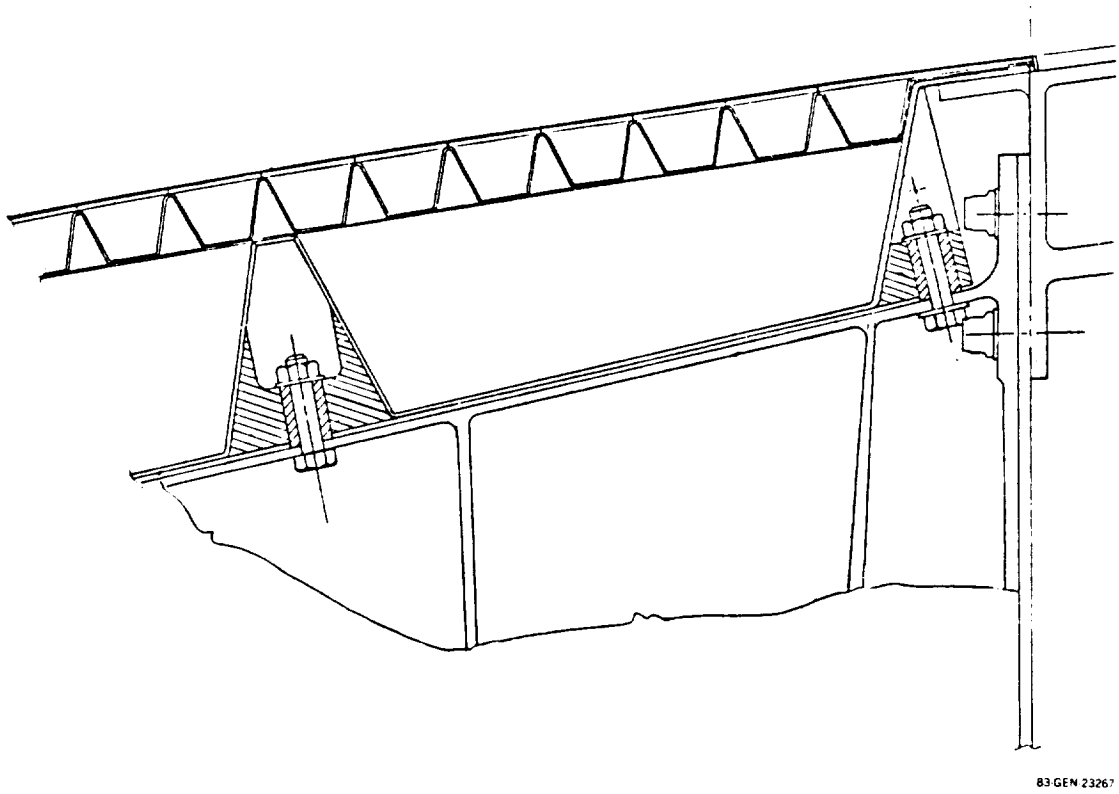

FIGURE 9-77. LEADING EDGE BOX DETAIL AT FRONT SPAR

The co-cure method of fabrication using 345 kPa (50 psi) autoclave pressure produced promising samples and no problems were apparent with that geometry. The test samples are shown in Figure 9-78. One specimen included a second duct layer similar to the design shown previously in Figure 9-76.

Further fabrication experience was gained in producing the wind tunnel model, as described in Section 9.5.

9.4.4 Improved Leading Edge Glove

The porous surface development was finally concentrated on either a Dynapore surface diffusion bonded to a perforated stainless steel sublayer or electron beam perforated titanium. Figure 9-79 shows a design that is suitable for either surface with integral plenum chambers. The porous surface is self-supporting over the integral suction duct span. This type of construction was used for the initial EB perforated Ti surfaced wind tunnel models.

Figure 9-79 also shows a later version of the perforated strip concept designed to reduce weight. The plenum chamber was formed by inserting an aluminum mandrel below the outer surface and by recessing the silicone rubber flute mandrel to conform to the aluminum mandrel shape. Although this configuration did reduce weight, a satisfactory molded leading edge could not be fabricated without some rework after initial curing. Increasing pressure in the autoclave to force the glass-epoxy structure against the molded surface at the flute nodes was not successful. Unfilled voids still occurred along the nodes, which were unacceptable for the subsequent surface bonding process. The wind tunnel model was repaired by filling the voids with epoxy resin, but this would be unacceptable for a flight structure.

FIGURE 9-78. LEADING EDGE – INITIAL CO-CURE ASSEMBLIES

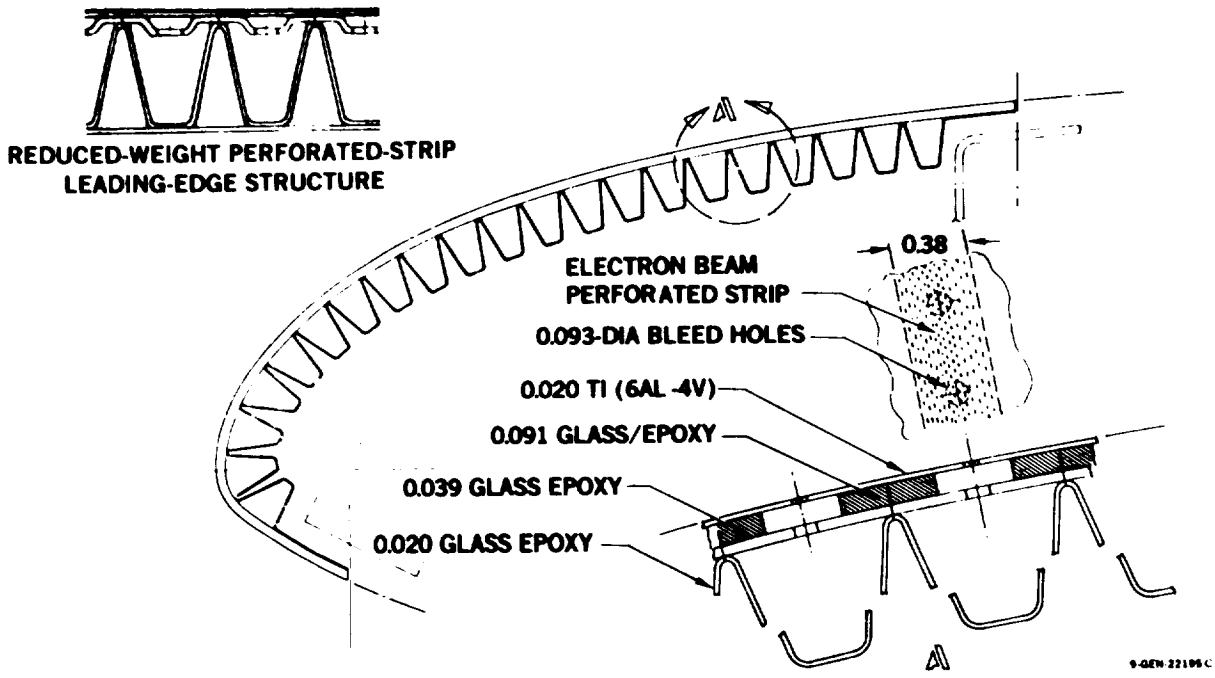

FIGURE 9-79. LEADING EDGE STRUCTURE – Ti SURFACE

Recommendations for future Phase II efforts include studies to omit the plenum chamber and revise the flute geometry to incorporate a flat for bonding at the flute nodes. The use of aluminum mandrels for the flute cavity and rubber mandrels at alternate nodes would permit the precise location of flutes and control of molding pressures during initial curing. The need for sewing would be eliminated, saving production time and cost. This type of construction could also be used for the wing box LFC panels.

9.5 SWEPT WING WIND TUNNEL MODEL - POROUS PANELS

Fabrication of the LFC panels for the swept wing wind tunnel models resulted in a continuation of design and development work on the leading edge and wing box structure glove panels. The initial design for the LFC panels utilized Dynapore porous surfaces as shown in Figure 9-80. An 80 x 700 Dynapore outer surface was diffusion bonded to an 80 x 80 inner mesh. The Dynapore surface, produced by Michigan Dynamics Company, had an initial porosity of 0.813 m^3s^{-1}/m^2 (160 SCFM) at 670 Pa (14 PSF) produced by roll calendaring. This surface was organically bonded to a porous fiberglass substructure designed to reduce the porosity to 0.152 m^3s^{-1}/m^2 (30 SCFM) at 670 Pa (14 PSF).

For initial tunnel/model calibration, a non-porous surface model was fabricated using the same design as the porous model, but with a solid fiberglass surface.

An alternative leading edge panel was developed using an electron beam perforated titanium (EB Ti) surface. This design used a perforated strip concept. Each perforated strip contained several rows of holes feeding suction air to the integral channel of the glove panel, as shown previously in Figure 9-79.

To form the LFC surface panels, a high temperature molding tool was designed and fabricated using a master plaster of the desired aerodynamic shape. Figure 9-81 shows the inside surface of the substructure located in the forming and curing tool. Figure 9-82 is a close-up of the leading edge area showing

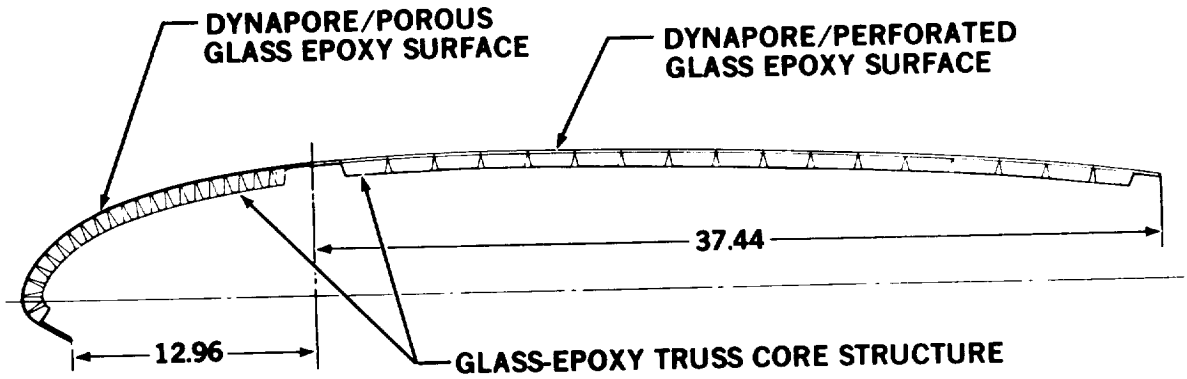

9-GEN 26339

FIGURE 9-80. SWEPT-WING WIND-TUNNEL MODEL LFC SURFACE

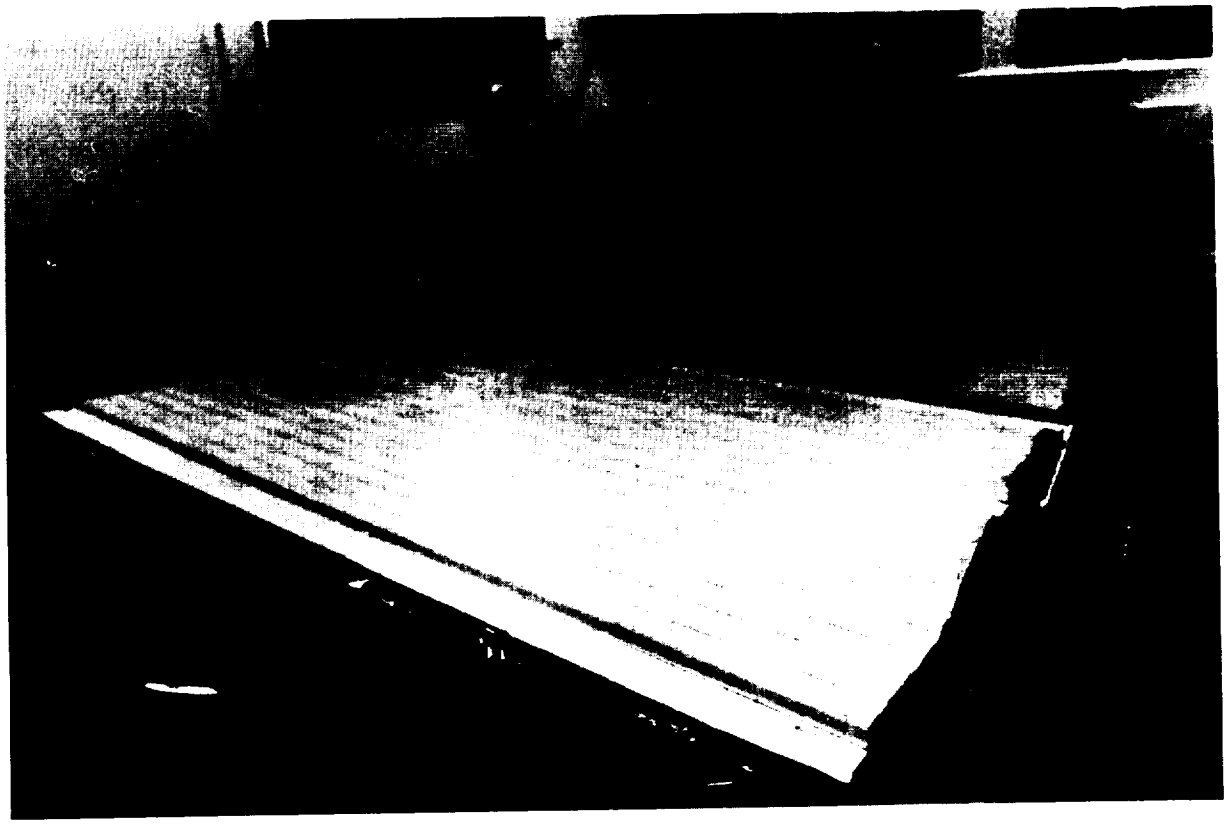

FIGURE 9-81. WIND TUNNEL MODEL SUBSTRUCTURE IN MOLDING FORM TOOL

the nesting of silicone rubber mandrels to form the internal ducting flutes. Figure 9-83 is a view of the cured fiberglass substructure ready for bonding to the porous Dynapore outer surface.

The joining of porous Dynapore sheets in preparation for bonding to the substructure is shown in Figure 9-84. A resistance welding technique was used to provide a lap welded joint with the outer surfaces butted together. Joining strips of 80 x 700 mesh Dynapore were used as butt straps in order to provide continuous porosity across surface joint areas. Surface smoothness and edge hold down were primary requirements.

Considerable effort was needed to develop a process to fabricate and bond Dynapore satisfactorily to the porous sublayer. Excessive variability of the porosity of the fiberglass sublayer was a major problem. A porous surface with a porosity of 0.152 m^3s^{-1}/m^2 (30 SCFM) at 670 Pa (14 PSF) with no more than 30 percent varability over the surface was finally obtained. This was achieved by selecting fiberglass material that was previously checked for high uniformity of porosity after processing. In the event that the relatively high porosity of 30 SCFM was not acceptable for the achievement of laminar flow in the leading edge section, further porosity reductions could be made as required by using suction area reductions through the use of non-porous spanwise strips. However, the use of these strips was not required. During leak tests on the completed LFC panels, it was found that the flute walls were porous. This was corrected by injection and coating of the plenum walls with polyurethane.

For the alternate leading edge panel, an EB Ti surface panel was used with 0.114 mm (.0045 in) wide by 0.193 mm (.0076 in) long holes elongated spanwise and spaced at 1.27 mm (.050 in) on centers in staggered rows 1.27 mm (.050 in) apart. The strip porosity provided by this structural concept created an area blockage of about 50 percent for the test article as shown previously in Figure 9-79. This blockage resulted in an acceptable suction flow for LFC. The elongated hole width was the smallest size available from the Farrel Company, Connecticut, at the time of testing. The elongated hole shape was used to reduce the possibility of particles large enough to trip laminar flow being trapped on the surface by suction.

FIGURE 9-82. WIND TUNNEL MODEL LEADING EDGE AFTER CURING

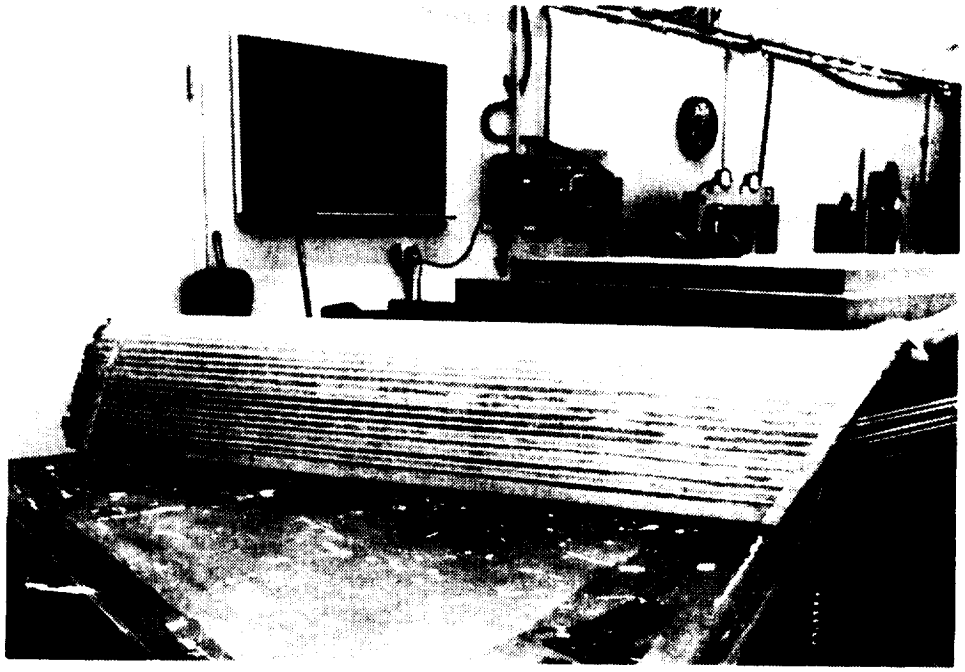

FIGURE 9-83. LEADING EDGE WTM – EXTERNAL SURFACE BEFORE DYNAPORE BONDING

The porous outer surface was preformed by rolling prior to bonding. Figure 9-85 shows the completed leading edge after bonding the perforated surface to the fiberglass substructure. It is ready for trim machining and fitting to the wind tunnel model structure.

Some blockage of the porous surface near the ends of the alternate leading edge was detected on the first EB Ti leading edge test article,due mainly to bonding material flow. The central section of the leading edge did not have any blocked areas.

Additional porous leading edge insert panels, as described in Section 8.2.2 and illustrated in Figure 8-26, were produced subsequently. The type of construction is shown in Figure 8-28. Far better control of porosity was obtained with this design and wind tunnel results, particularly for the EB perforated surface,were greatly improved.

FIGURE 9-84. DYNAPORE LAP SHEAR JOINT WELDING TECHNIQUE

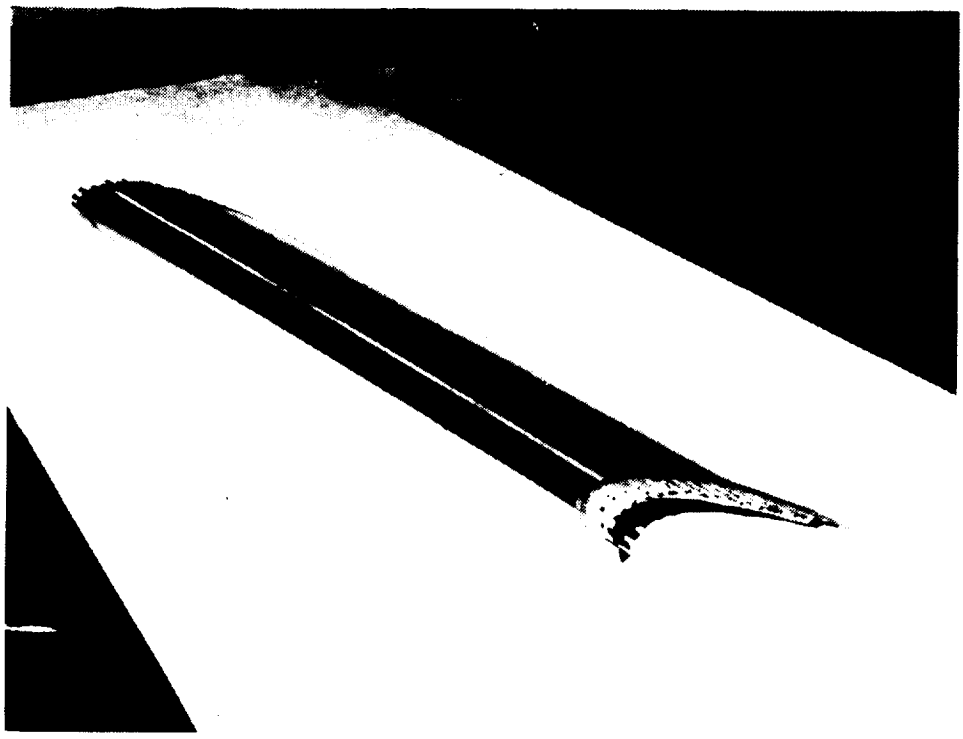

FIGURE 9-85. LEADING EDGE PANEL WITH POROUS SURFACE

9.6 CONCLUSIONS & RECOMMENDATIONS - STRUCTURES

1. An LFC wing structure consisting of an outer glove panel supported by a graphite/epoxy primary wing box structure is a satisfactory arrangement. In addition to reducing wing weight, the use of graphite epoxy material for the primary structure reduces the strain level imposed on the glove panel. The loads at panel joints are correspondingly reduced.

2. The porous surface can be bonded satisfactorily to a fluted fiberglass substructure to form a stiff LFC glove panel.

3. Integral suction airflow ducting can be provided by the flutes in the glove panel, and in the space between the glove panel and the main wing box, utilizing external stiffeners to create separate ducts.

4. Electron beam perforated titanium sheet material is the most desirable porous LFC surface of those investigated, considering strength, damage resistance, rain erosion, uniformity of porosity and ease of fabrication.

5. An all titanium superplastic formed diffusion bonded glove panel is a practical possibility that requires further study.

6. A wing aspect ratio of 10 is practical but results in a significant aeroelastic weight penalty for adequate roll control stiffness. With 30 degrees sweep, wing bending stiffness is the most significant parameter and the graphite fiber selection and orientation should be selected to maximize this characteristic within practical limits.

7. The aeroelastic penalty for an aluminum wing would be far greater.

8. Wing flutter was not critical.

9. Panel joint design must consider local surface deflections due to eccentricities of load transfer, and external smoothness at joints and fasteners. The number of chordwise joints, which are more highly loaded, should be reduced to a practical minimum. Fastening should preferably be from inside to avoid surface imperfections. Joints can be angled relative to the streamlines to reduce the length of surface airflow without suction.

10. The glove panel contour can be controlled by using external molding tools. The finished surface accurately reproduces the mold shape and any slight imperfections in the tool surface are ironed out by the titanium sheet surface of the glove panel.

9.7 REFERENCES - STRUCTURES

Douglas Aircraft Company, "Development of Technology for Fabrication of Reliable Laminar Flow Control Panels on Subsonic Transports," NASA CR-145125, October 1976. (Prepared under Contract NAS1-14408).

10.0 SUCTION SYSTEM

10.1 INTRODUCTION

The goal of the suction system study was the design of a simple, light-weight system to remove the required amount of boundary layer air from those areas of the wing surface where laminar flow is to be maintained. To achieve this aim, the suction system was integrated with the aircraft structure as much as practical. A porous or perforated surface was assumed for the wing surface. Suction air compressors and their power units are located below the wing aft of the rear spar, and the air is exhausted overboard at approximately freestream velocity for minimum drag and suction power required.

As characteristics and performance of various aspects of laminar flow were discovered in the course of the study, the configuration was modified to take advantage of design improvements or to correct newly uncovered problems. For example, when it was shown that approximately the same drag reduction could be achieved by applying LFC to the upper wing surface back to 85 percent chord and eliminating suction on the lower wing surface, this concept was adopted and the manifolding and compressor installation were changed to provide one-step compression for the suction air.

10.2 REQUIREMENTS

Suction flow requirements and surface pressures were based on aerodynamic calculations, discussed in Section 7.1. Typical minimum suction flows (expressed as suction velocity) necessary to maintain laminar flow on the wing are shown in Figure 10-1, together with the corresponding chordwise variation of pressure coefficient. The mass flows were calculated from the velocity, V_w, and free-stream density, incompressible relationships having been assumed in the derivation of V_w. For suction system sizing for the advanced LFC aircraft, the calculated mass flows were increased by a factor of 20 percent to provide for local areas of suction greater than the minimum and to allow a margin for off-design operation.

At the beginning of the LFC study, one of the ground rules established was that no redundancy would be provided in the suction power system. The maintenance of laminar flow on the wing is not a safety item. To provide redundancy for the case of a suction system power unit failure, crossover ducting would be necessary in regions where volume is already at a premium. Also, the size of each power unit would be doubled, which is an additional weight and drag penalty. The system was designed, therefore, with a separate unit in each wing. In case of loss of laminar flow on one side of the aircraft, the asymmetric drag situation can be handled easily with the standard airplane controls, and the additional trim drag penalty is slight.

In the later part of the study, a contamination-avoidance system was defined that requires application of a liquid to the wing surface during flight operations where potentially contaminating conditions exist. To remove remnants of the liquid before trying to initiate LFC, a positive pressure significantly greater than the suction pressure is applied below the surface. The resulting "clearing" airflow is high compared to the suction flow rate in the opposite direction. The requirement to provide this "purging" capability affects the system design and may determine the size of some components.

10.3 POROUS SURFACE CHARACTERISTICS

The desired flow characteristics of the porous surface were originally defined as:

(1) having sufficient pressure drop through the surface during LFC operation so that no outflow of air is induced because of surface pressure variation;
(2) having relatively low pressure drop through the surface even at the higher LFC flow rates;
(3) having a sufficiently open surface to minimize clogging during low-level flight operation.

The porosity, Q, has arbitrarily been defined as the flow, under standard conditions, in cubic feet per second per square foot with 670 Pa (14 pounds per square foot) of pressure differential across the surface.

In the region of the LFC system, item (1) above is important chiefly in regions where the chordwise pressure gradient is steep and the suction velocity is moderate. Figure 10-2 illustrates the effect of porosity in such a region. Air travels through the porous surface into the flute or other collection component below, where the pressure is designated P_{sub}. Some of the surface area is blocked by the attachment of the collecting structure. If V_ℓ is the local velocity into the surface and s is chordwise distance along the surface, ideally:

$$\int_1^2 V_\ell \, ds = \int_A^B V_{th} \, ds$$

where V_{th} is the theoretical suction required, determined by aerodynamic criteria. As the surface pressure at point 1 is higher than at point 2,

$$V_{\ell_1} > V_{\ell_2}$$

To prevent outflow, P_{sub} must be equal to or less than P_2. The maximum allowable porosity, Q_{max}, at which outflow is avoided without the suction flow exceeding the theoretical value is illustrated on the left-hand side of Figure 10-2. Here $P_{sub} = P_2$ and $V_2 = 0$. The dashed line represents the case where the porosity is greater than Q_{max}. To prevent outflow, $P_{sub} = P_2$, with the result that

$$\int_1^2 V \, ds > \int_A^B V_{th} \, ds$$

The right-hand side of Figure 10-2 shows that velocity profile resulting when the surface porosity is less than Q_{max}. Here

$$P_{sub} < P_2 \quad \text{and} \quad V_2 > 0$$

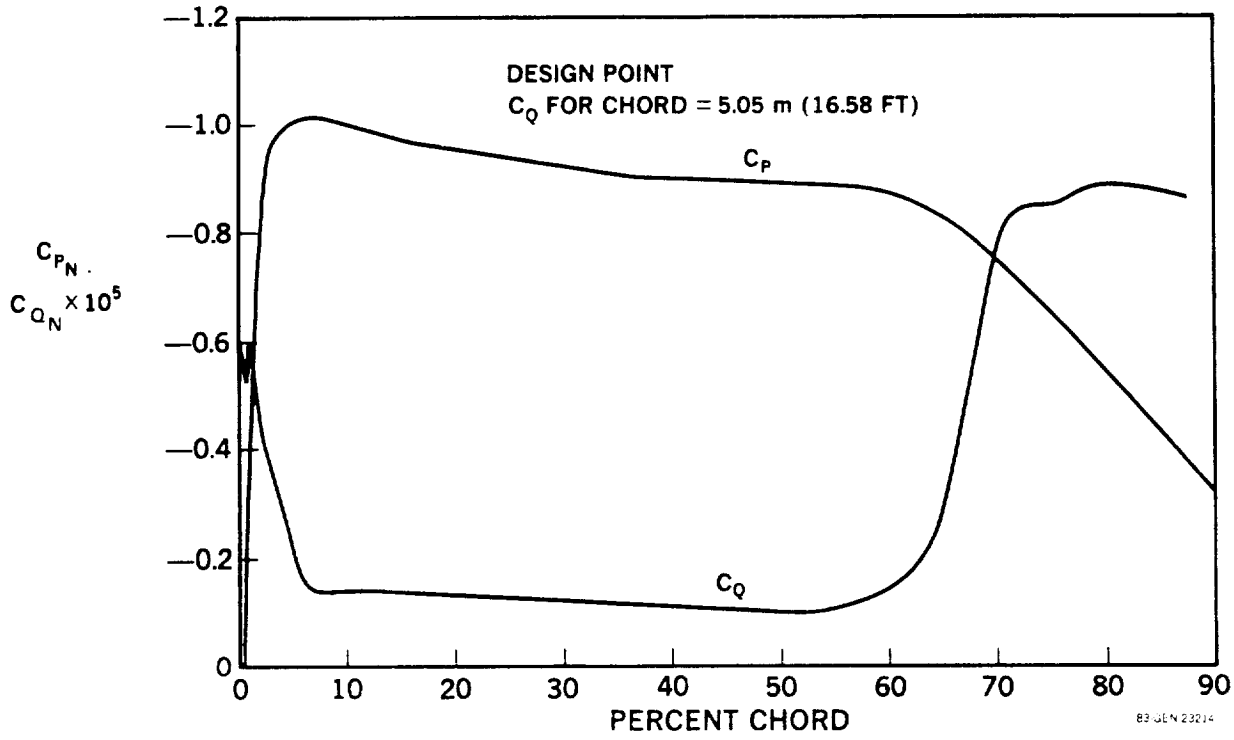

FIGURE 10-1. WING SURFACE PRESSURE & SUCTION REQUIREMENT

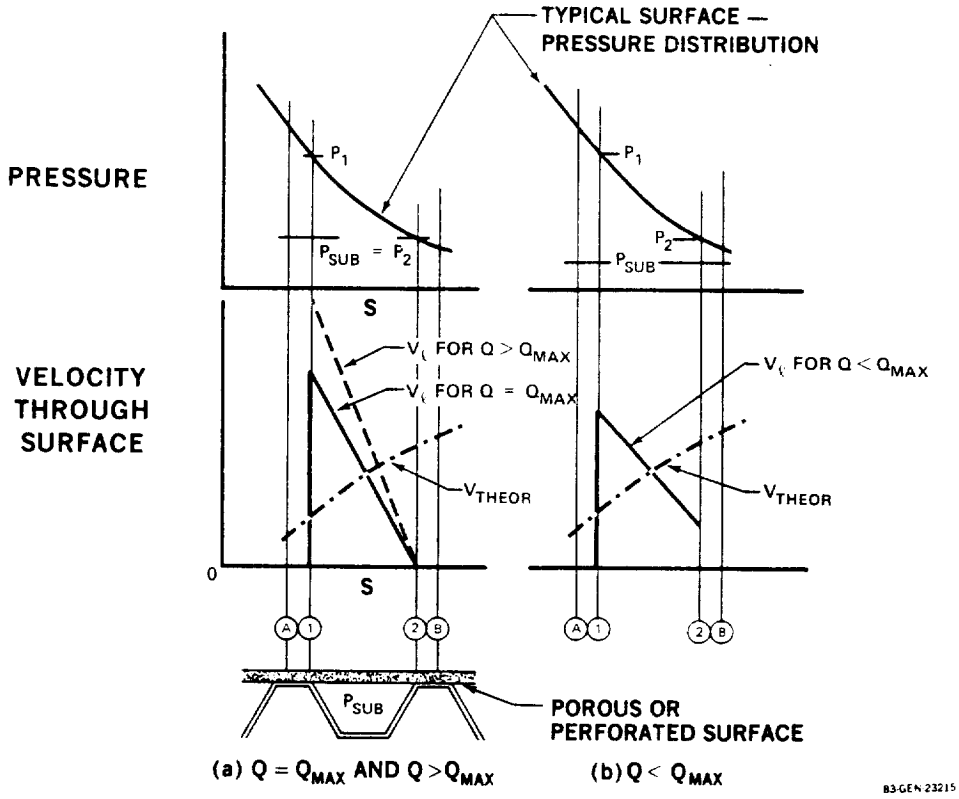

FIGURE 10-2. EFFECT OF SURFACE POROSITY ON SUCTION VELOCITY VARIATION

This condition gives a smoother velocity profile than that achieved with the more porous surface and increased tolerance to off-design conditions.

The widths of the open area and of the blocked portion of the surface both affect the required porosity. Increasing the width of the open area subtended by a flute makes a lower porosity (less open surface) necessary, to match the greater differential in surface pressure that is subtended by the flute. Increasing the percentage of blocked area results in a greater allowable porosity, as the airflow per unit of surface, or V_{ℓ}, is increased, thus increasing the pressure drop through the surface.

During the study of contamination-avoidance procedures, it was found necessary to provide for "purging" the porous surface of the liquid used to prevent contamination before initiating suction for LFC. The pressure differential necessary to purge in a reasonable time was found to be about 6900 Pa (1 psi), see Section 10.7. This pressure differential is an order of magnitude greater than the pressure differential, in the opposite direction, during the suction mode. Surfaces with high porosity have very large airflows during purging. The necessity of a porosity that minimizes the effect of the purging requirement on the size of suction system components becomes a fourth consideration on the above list.

For the flute widths and amounts of blockage that are acceptable from structural considerations, a porosity of 0.061 to 0.076 $m^3/s/m^2$ (12 to 15 $SCFM/ft^2$) at 670 Pa (14 PSF) at the leading edge gives the condition where no outflow exists with the flows approximately equal to the theoretical requirements. If more open porosity were used, more suction would be required, increasing the suction airflow above that required for LFC in order to increase the pressure drop through the surface and avoid outflow. A porosity of about 0.15 $m^3/s/m^2$ (30 $SCFM/ft^2$) at 670 Pa (14 PSF) is proposed for the surface above the wing box and aft of the rear spar. Figure 10-3 shows typical flow characteristics for a porous surface.

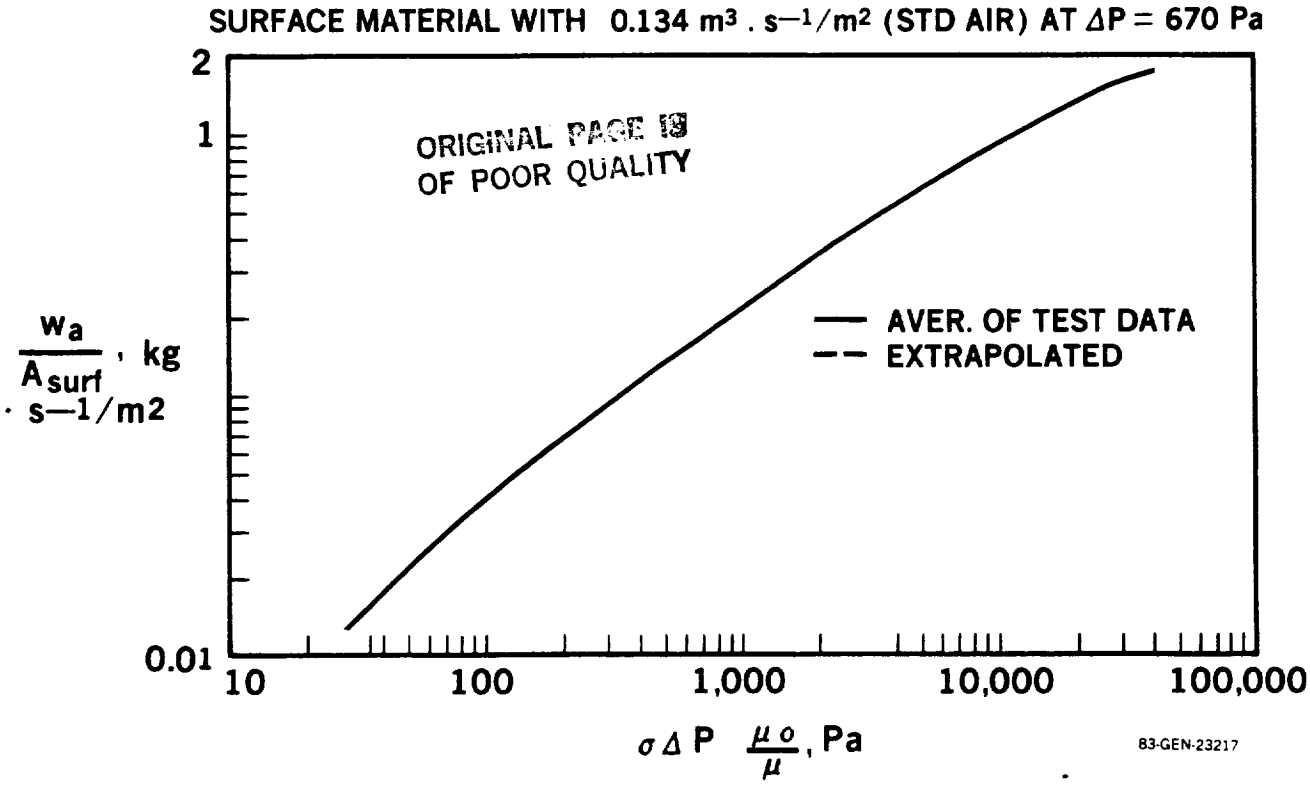

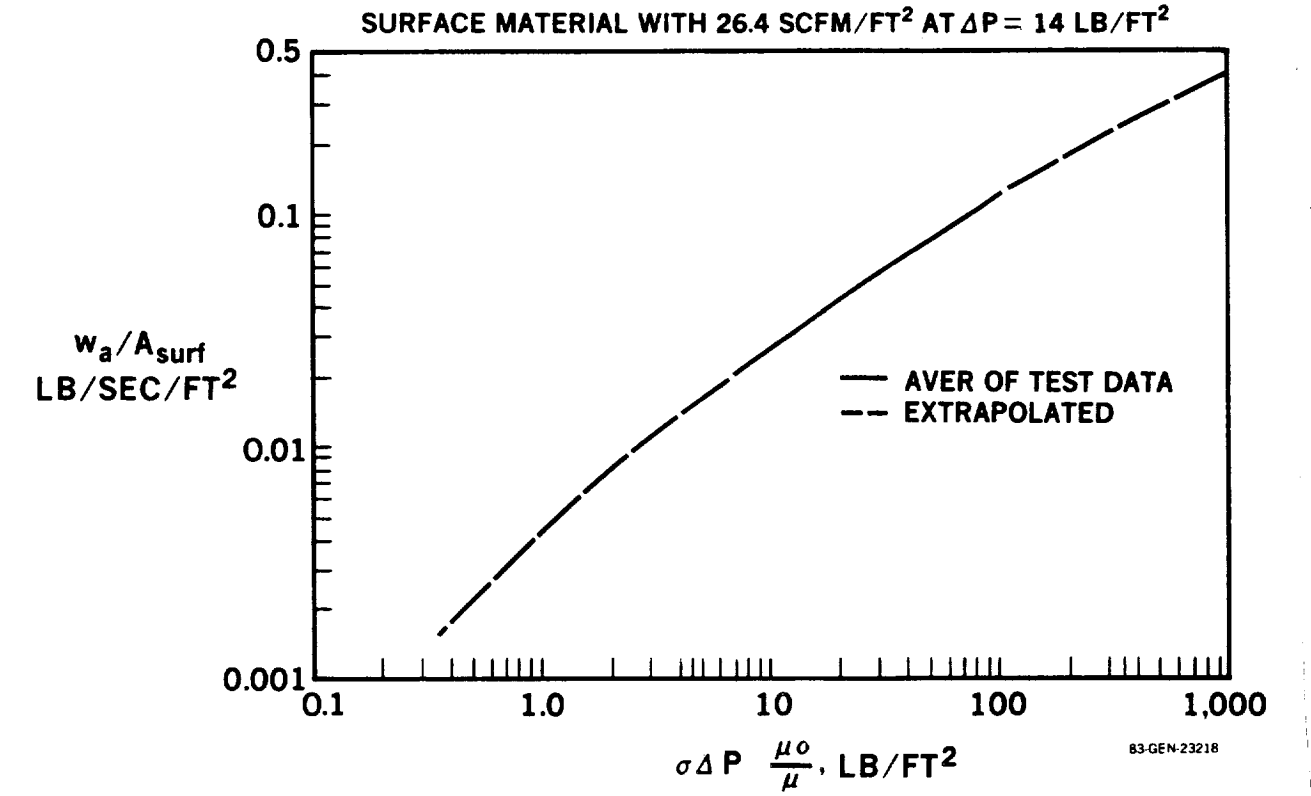

FIGURE 10-3. TYPICAL FLOW CHARACTERISTICS - POROUS SURFACE

10.4 DUCTING

It was desired to have a simple, light-weight, and low-maintenance suction system. To achieve this, the ducting was designed to make use of the aircraft structure wherever possible. In sizing the ducting, the object was to obtain a reasonable compromise between duct size and pressure drop through the system. The pressure drop in the system affects the size and weight of the compressor and its drive unit, and the amount of fuel consumed by the LFC system. Figure 10-4 shows the effect on these parameters of the pressure loss in the system. A pressure at the compressor face of 80 percent of the minimum surface pressure was taken as a goal in the design of the suction system. This provides an allowable 20 percent pressure drop in the system for air from the wing areas where both the surface pressure and the suction requirements are quite low. As was shown in Figure 10-1, in areas where the suction quantity requirements are higher, the surface pressures are generally higher, resulting in an increased allowable pressure drop where the greater pressure drop is likely to occur.

At the beginning of the study, both chordwise and spanwise directions were considered for the initial air collection, as shown conceptually in Figures 10-5 and 10-6. The chordwise method of Figure 10-5 requires a large percentage of the available space ahead of the front spar for ducting the collected air to the compressor and ducting much of the air across the front spar for its entire length is not structurally efficient. The spanwise method makes use of external stiffeners on the main box surface to provide integral spanwise ducting and was selected for the advanced LFC aircraft, although it does require holes in the main box for ducting the suction air to the suction pump below the wing. The suction flow collection system is integrated with the wing structure, as shown in Figure 10-7. The boundary layer air is drawn through the porous or perforated surface into flutes which are bonded to the surface material. The flutes provide both structural stiffness and flow passages. The air travels through the flutes to an opening that leads to an opening into an auxiliary duct. The main flow channels are formed by the surface panel, the integral stiffeners and the wing box skin.

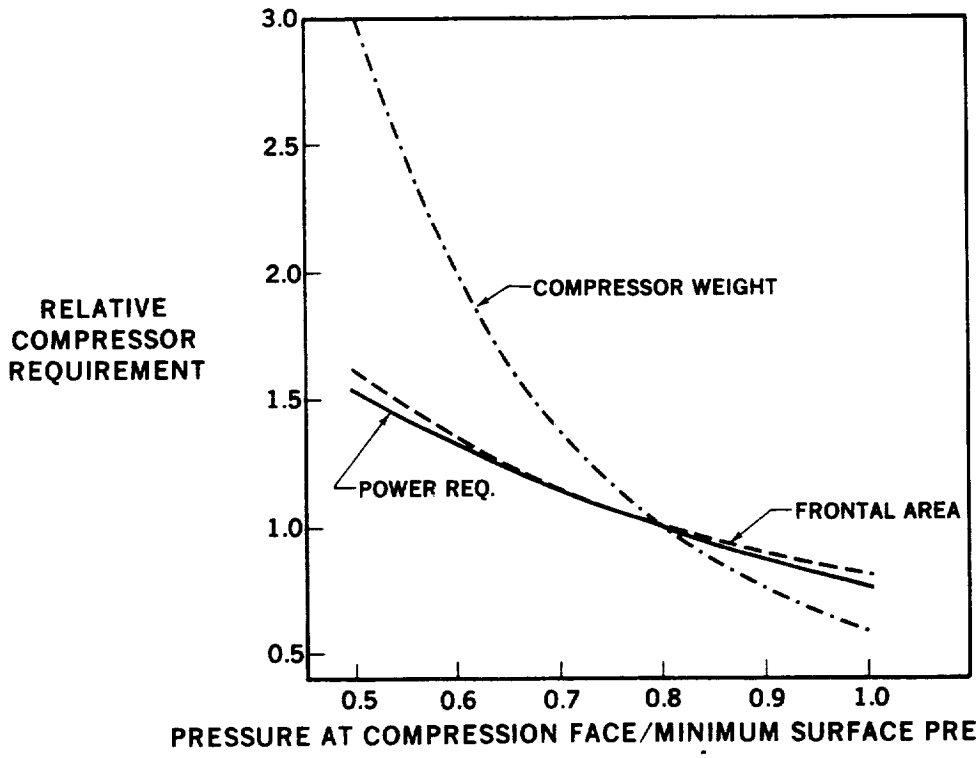

FIGURE 10-4. EFFECT OF SUCTION SYSTEM PRESSURE DROP ON COMPRESSOR REQUIREMENTS (UPPER-SURFACE-ONLY CONCEPT)

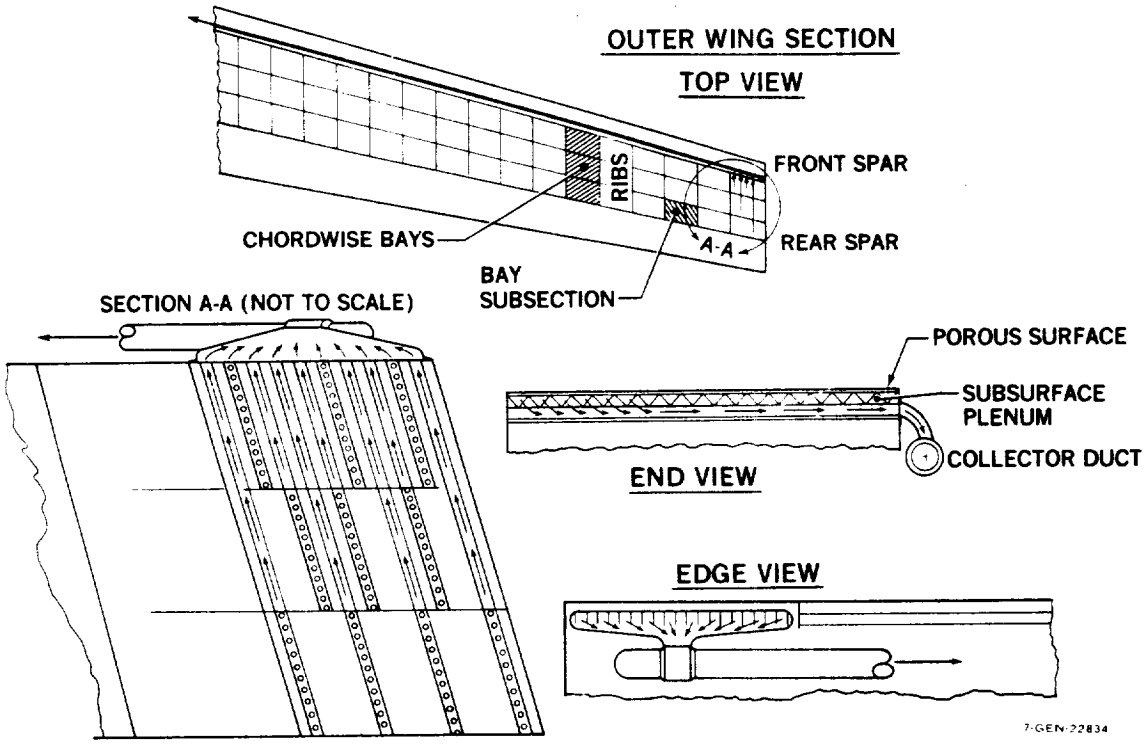

FIGURE 10-5. CHORDWISE AIR COLLECTION SYSTEM

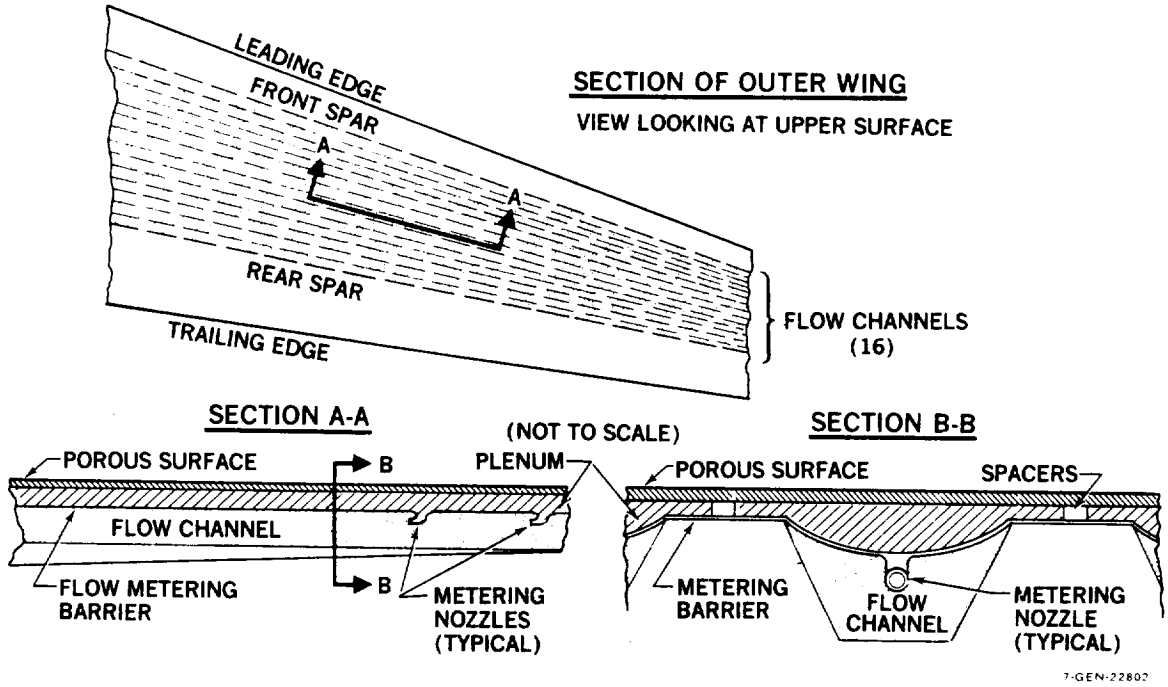

FIGURE 10-6. SPANWISE AIR COLLECTION SYSTEM

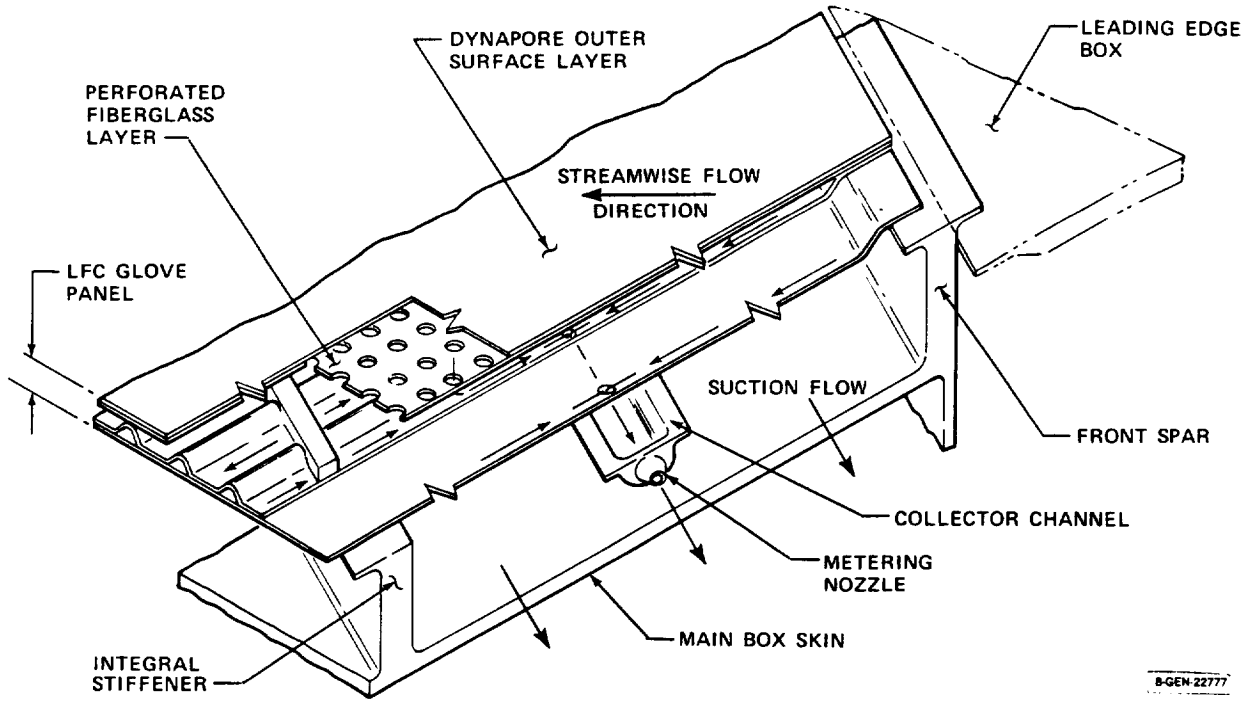

FIGURE 10-7. TYPICAL UPPER SURFACE CONSTRUCTION AND SUCTION SYSTEM

The depth of the wing box stiffeners controls the area available for spanwise ducting of the suction air. The depth of the stiffeners as determined by structural requirements, was assumed initially, and the pressure drops along the integral spanwise ducts were calculated as a function of the spanwise station of suction air collection. The pressure drop was calculated using conventional pipe flow relationships with an assumed minimum friction coefficient of .002. The duct flows are relatively low in the main box region and the Mach number varies from about 0.05 to 0.15 in the spanwise integral ducts.

In the spanwise collection system, it is necessary to provide holes in the upper wing main box skin to conduct the suction air from the spanwise ducts to the manifolds leading to the compressor inlets. The size of these holes is related to the number and location of the suction engines and is discussed in Section 10-6. Figure 10-8 shows a typical detail of the arrangement provided. To keep the structural penalty associated with the cutouts to a minimum, the flow was accelerated to a maximum Mach number of 0.3 in the ducts leading to the manifold. A minimum bend radius of twice the duct inside diameter was maintained throughout the system.

The channels formed by the wing box structural members provide adequate flow area for the region from the front spar back to about 62 percent chord, but beyond this station the suction requirements increase very rapidly. Structural members with greater flow area were devised to provide more flow area in these regions.

For the high flows in the vicinity of the rear spar, the structural/ducting arrangement shown in Figure 10-9 was proposed for the concept with suction on both surfaces. An auxiliary spar provides one boundary, the rear spar another, and the upper and lower wing skins are the remaining boundaries of a region dedicated to the collection of the suction air and its ducting to the vicinity of the suction compressor.

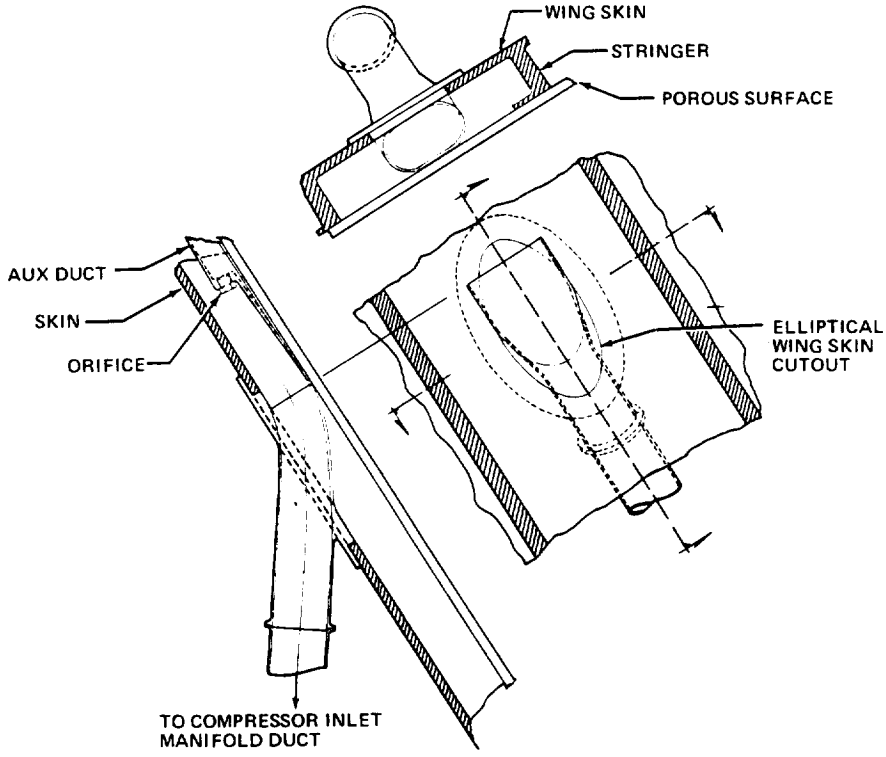

FIGURE 10-8. TYPICAL WING-SKIN CUTOUT FOR SUCTION DUCT

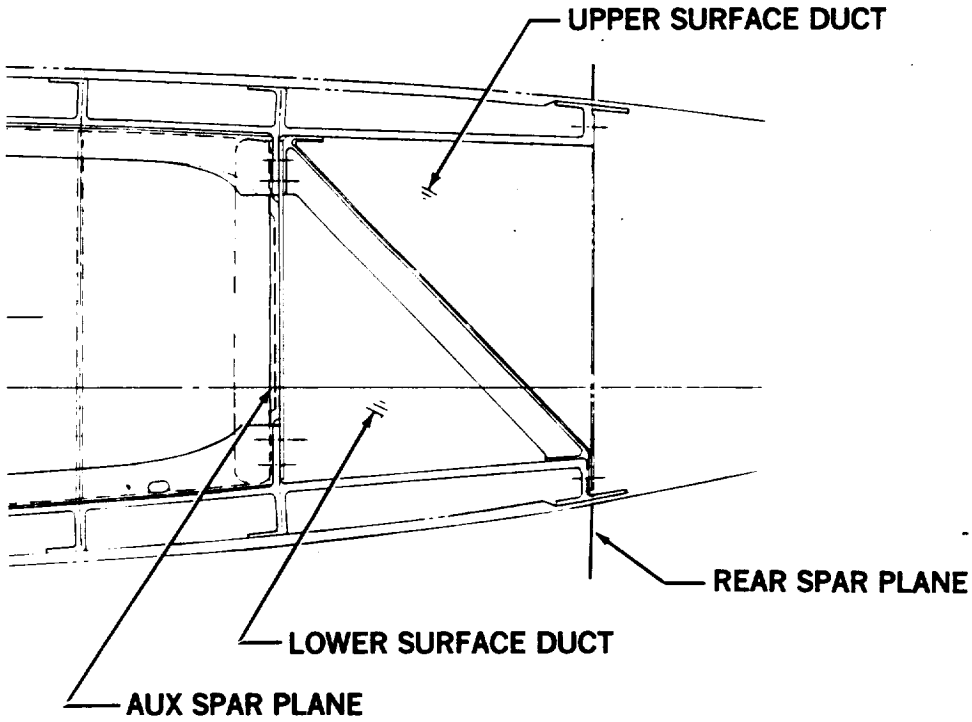

8-GEN-22961

FIGURE 10-9. DUCTING AFT OF REAR SPAR

For the upper-surface-only configuration with suction extending to 85 percent chord, the concept shown in Figure 10-10 provides large flow areas aft of the rear spar. The rear spar, at 67 1/2 percent chord, is farther forward than the 70 percent chord location with suction on both surfaces, but there is still more than adequate fuel volume in the LFC wing. To obtain the desired flow control, four ducts may be desirable rather than the three shown.

As discussed in Section 11.0, a system has been proposed to avoid contamination of the porous surface by applying a liquid to it during takeoff and climb. To remove any residual liquid before LFC operation is initiated, a requirement was defined to provide positive pressure air under the surface for a short period. Because of the relatively high pressure differential required for this operating mode, the airflows through the surface are much higher than those obtained during the LFC mode. Depending on the suction design flow and Mach number, some elements of the suction system can be sized by this purging requirement rather than by suction requirements. This is discussed further in Section 10.7.

10.5 SUCTION PUMP SYSTEM

Air is pumped from the boundary layer by means of compressors. Characteristics and configurations for this part of the suction system were investigated, and the type of compressor and its driving unit were selected for the advanced LFC aircraft. Two units per airplane, one on each wing, were determined to be compatible with the structural and airflow requirements of the concept.

10.5.1 Compressor Design

The general operating requirements for the compressor are:

(1) normal operation at very low inlet pressures;
(2) inlet distortion tolerance;
(3) low noise levels in the critical 1000 to 2000 hertz range;
(4) pressure ratios and airflow capacity to be determined in the study.

A maximum operating altitude of 12,190 m (40,000 ft) was assumed. Typical pressure relationships for the suction system are shown in Figure 10-11. The lowest pressure on the wing upper surface at 12,190 meters (40,000ft) altitude was calculated to be 12.5 kPa (261 lb/ft^2), while the lowest pressure on the wing lower surface is 17.96 kPa (375 lb/ft^2). For the initial baseline aircraft, it was assumed that a suction distribution system could be designed with a 20 percent drop in total pressure from the lowest pressure on the wing surface. This includes a ΔP of 3 percent through the wing surface and a ΔP of 5 percent from the end of the collection duct to the compressor face. The resulting pressures at the compressor face are 10 kPa (209 lb/ft^2) for the upper surface air and 14.36 kPa (300 lb/ft^2) for the lower surface air, compared with a free-stream static pressure P_o of 18.8 kPa (393 lb/ft^2) at 12,190 meters (40,000 ft) altitude.

10.5.1.1 Pressure Ratio. For suction on both wing surfaces, to achieve a compact installation, the upper surface air is compressed to the pressure level of the lower surface air in a "boost" compressor. The two airflows are then combined and compressed in the main compressor before being exhausted overboard. The pressure relationships discussed above indicate a pressure ratio of 1.44 for

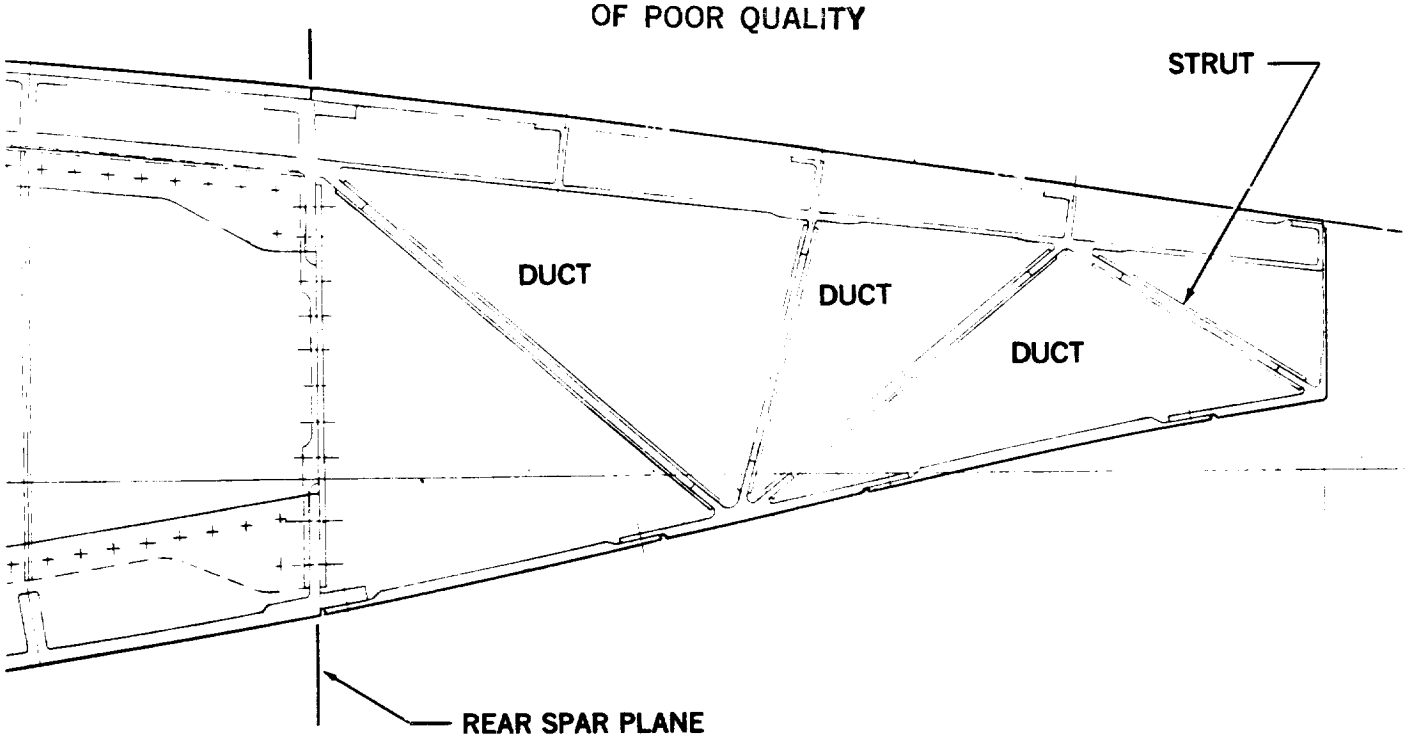

8-GEN-22960

FIGURE 10-10. DUCTING AFT OF REAR SPAR (SUCTION ON UPPER SURFACE ONLY)

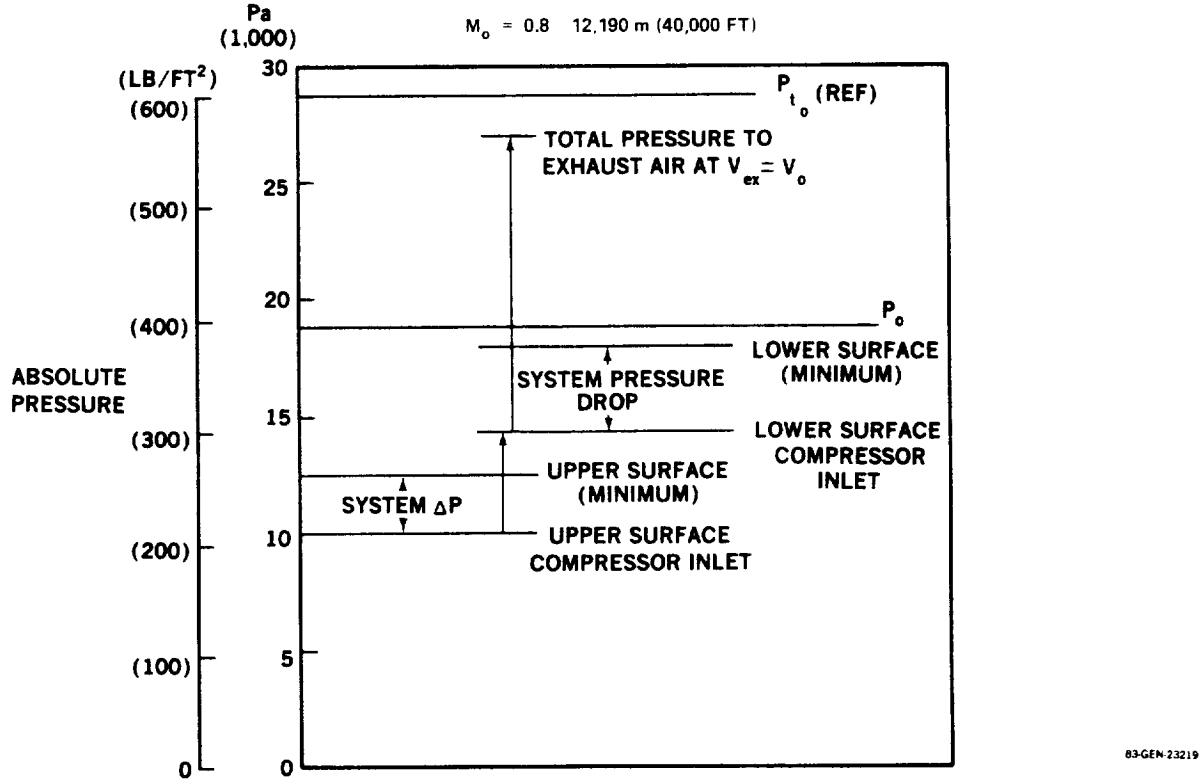

83-GEN-23219

FIGURE 10-11. TYPICAL SUCTION SYSTEM PRESSURES

the boost compressor. The determination of how much the suction air should be compressed in the main compressor before exhausting it in the freestream involves the size of the equipment and the amount of fuel required. At one extreme, the air can be exhausted with a very low velocity, with the attendant penalty of the "ram drag" of the boundary layer air. This results in additional fuel consumption by the main propulsion engines to overcome the drag. The other extreme is to exhaust the air at a high velocity, thereby generating some thrust allowing the main propulsion engines to be throttled back. (The main propulsion engines are sized with the LFC inoperative, so that any thrust available to the aircraft from the suction system does not reduce the size of the main propulsion engines.)

Figure 10-12 shows how the total fuel burned and the size of the drive unit for the compressors vary with the pressure ratio of the main compressor, for a typical cruise condition. The relative exhaust area required for the suction air is also shown in Figure 10-12. At pressure ratios below about 1.7 the necessary area becomes very large. The figure illustrates that fuel consumption is insensitive to pressure ratio over a compressor range of about 1.7 to 2.2. Above a pressure ratio of 2.2, the fuel consumption of the compressor-drive power system increases faster than the benefit of the thrust generated by the higher exhaust velocity. Below 1.7, the increased fuel flow of the main propulsion engines to overcome the ram drag becomes a factor. At a pressure ratio of 1.88, the suction air exhaust velocity equals the freestream velocity. Using this pressure ratio as a design point leaves a margin on each side for off-design operation within the range of minimum total fuel consumption.

10.5.1.2 Compressor Sizing. The airflow capability that determines the diameter of the compressor is usually expressed as $\frac{w_a \sqrt{\theta_t}}{\delta_t}$, where θ_t is the total temperature divided by standard sea level temperatures, and δ_t is the total pressure at the compressor face divided by standard sea level pressure, or the total pressure in atmospheres. The temperature of the air into the compressor is assumed to be the same as the boundary layer recovery temperature (recovery factor = 0.85). The airflow is calculated from the LFC requirement by integrating the suction requirements over the porous surface:

$$w_a = \rho_\infty g V_\infty \int_S C_Q dA_S \quad \text{or} \quad w_a = \rho_\infty g \int_S V_w dA_S$$

For a given Mach number, C_Q, and $C_{p_{min}}$, $\frac{w_a \sqrt{\theta_t}}{\delta_T}$ is independent of altitude.

Most of the study was conducted using values of C_Q and $C_{p_{min}}$ corresponding to a design point condition of Mach 0.8 with the lift coefficient (C_L) required for the initial LFC cruise. However, as discussed in Section 7.1.6, both C_Q and $C_{p_{min}}$ change at off-design conditions so that before specifying a compressor for the suction system, the desired range of operation must be considered.

For an aircraft in airline service, a fixed-area exit for the compressor is desirable. This imposes some limitations oncompressor capability. Figure 10-13 shows a typical compressor map. At 100 percent of rated inlet flow, the exit area is sized for the design point condition at a compression ratio of 2.66. The compressor inlet pressure is 0.53 of the free-stream static pressure to which it is assumed the compressor exhausts. The operating line "A" shows how the airflow and pressure ratio vary at this condition if the compressor RPM is changed.

As discussed in Section 5.3.7 and illustrated by Figure 5-16, the normal operating procedure would be to hold altitude and Mach number during cruise. The wing lift coefficient would then fall until sufficient fuel was burned to allow a step climb to the new cruise altitude, reverting to the original lift coefficient. Figure 10-13 shows the effect on compressor operating conditions of reducing the lift coefficient from a design C_L of 0.56 to a C_L of 0.44. The estimated suction requirements at this point are compared with those of the design point in Table 10-1. Operating line "B" on the compressor map, Figure 10-13, shows typical compressor operation associated with the reduced C_L.

Other off-design conditions, such as off-design Mach number, must be considered when specifying compressor characteristics, particularly if the compressor has been significantly oversized. Care must be taken to avoid both the stall (surge) and the choking regions of the compressor.

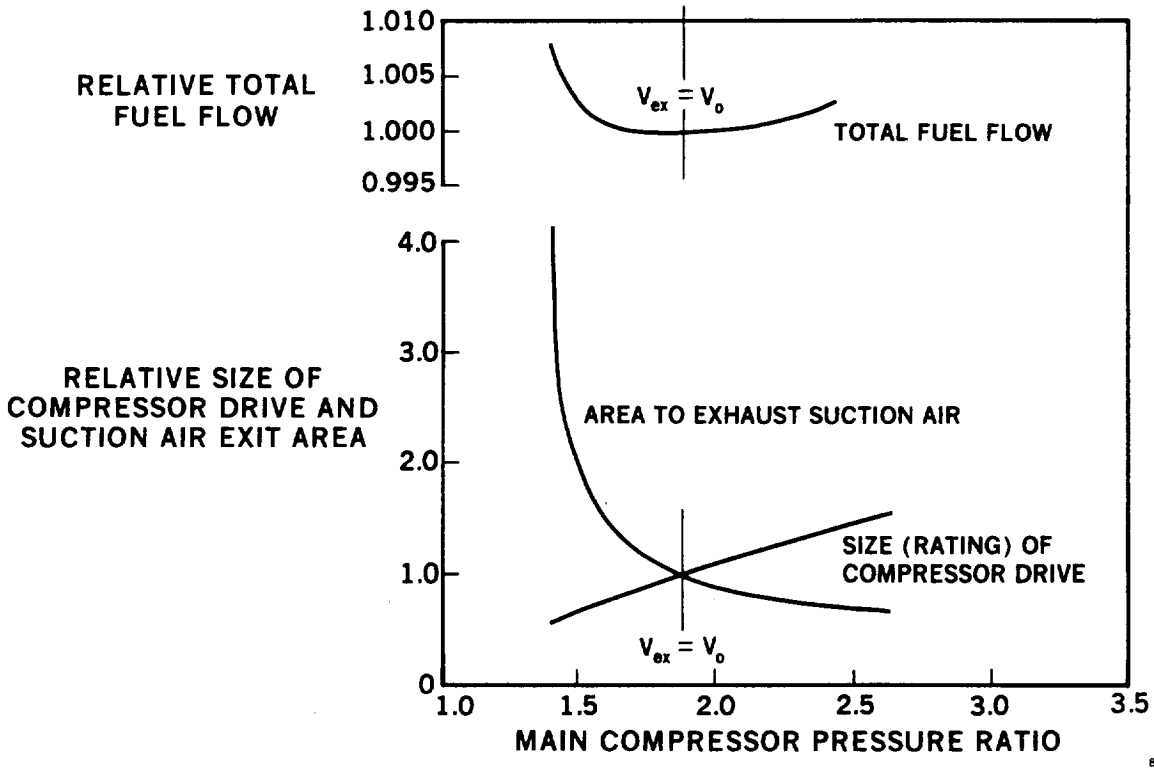

83-GEN-23212

FIGURE 10-12. EFFECT OF MAIN COMPRESSOR RATIO

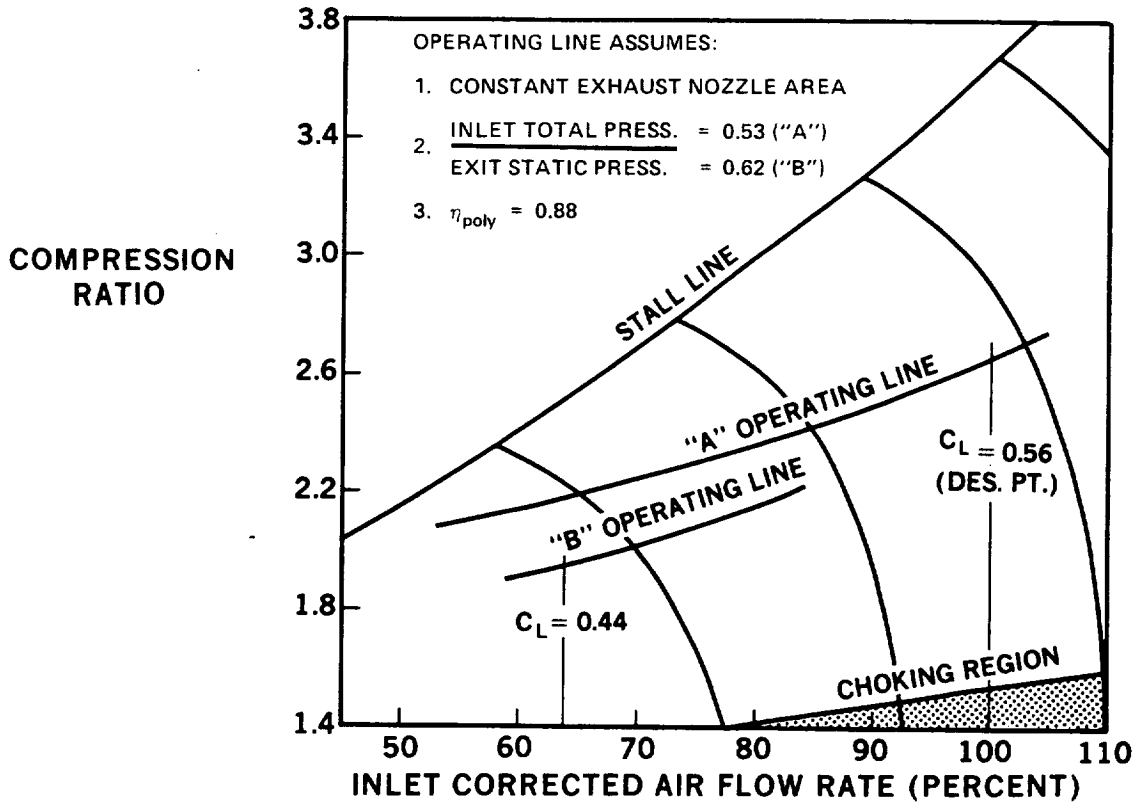

83-GEN-23222

FIGURE 10-13. TYPICAL COMPRESSOR MAP

TABLE 10-1
OFF-DESIGN REQUIREMENTS
Constant Altitude & Mach No.

C_L	Relative Suction Air Flow	C_{P_N} min	ΔP_{sys} approx.	Press @ Compr. Face / Static exit Press.	Relative $\frac{W_a\sqrt{\Theta}}{\delta}$ Compr. Face	Compress. P.R.
0.56	1.00	-1	20%	0.53	1.0	2.66
0.44	0.75	-0.8	15%	0.62	0.64	1.95

10.5.1.3 Compressor Type. Both axial and centrifugal compressors were considered for the advanced LFC aircraft suction system. Their characteristics are compared qualitatively in Table 10-2. The centrifugal type has many characteristics that would make it attractive for application in an LFC suction system. However, the pressure-ratios of 1.44 and 1.88 discussed previously are considerably lower than the typical single-stage pressure ratio of a centrifugal compressor.

For LFC on both wing surfaces, an attempt was made to take advantage of the centrifugal compressor's high pressure ratio to reduce the size of the required equipment. It was proposed to "overboost" the upper surface air and combine the exhaust in an ejector with the air from the wing lower surface, as shown schematically in Figure 10-14. (Although a single-entry impeller is shown, a double-entry design might be used.)

TABLE 10-2. COMPRESSOR COMPARISON

	Centrifugal Relative to Axial
Efficiency (Polytropic)	Δ = 0 to -3 percent
Max Dimension	Larger Diameter*
Weight	Δ depends on pressure ratio - no relative indication
Noise	Lower
Distortion Tolerance	Better
Pressure ratio/stage	Approx 4.0 vs 1.5
Installation Flexibility	Better
Cost	Low
Maintainability	More Rugged
Off-Design Operation	Wider Range

*The increase in diameter over the axial depends on the extent of off-design capability.

Figure 10-15 shows the effect on the main compressor size and fuel flow, assuming no mixing losses in the ejector. The reduction in equipment size was not significant, even with the optimistic assumptions. The installation of the large diameter centrifugal pump and an ejector with a reasonable mixing length proved difficult. Another disadvantage is the "screech" associated with ejectors, which would introduce a potentially strong noise source.

The study indicated a pressure ratio of 1.44 for the boost compressor, to raise the pressure of the upper surface air to that of the lower surface air. This ratio is suitable for an axial compressor, and the geometry of an axial flow compressor lends itself to a concentric installation with the exhaust from the compressor combining with the lower surface air at the inlet to the main compressor. The most efficient pressure ratio for the main compressor has been shown to be in the range of 1.9, which is also lower than would be provided by a single-stage centrifugal compressor. Axial compressors are therefore proposed for the LFC advanced transport. The design should incorporate features to provide distortion-tolerant operation. Blade chord lengths should be relatively long to increase inlet Reynolds number, and the blade-vane spacing should be selected to minimize noise generation.

The above study was completed during the initial period of the contract when suction on both upper and lower wing surfaces was proposed. The decision to use suction on the upper surface only removed one advantage of the axial flow compressor: a single compressor with a compression ratio of about 2.7 replaced the two low-pressure-ratio compressors. The compression ratio of 2.7 is in the range of that of a single stage centrifugal compressor, although the dimensions of the centrifugal type are still a disadvantage. As the compressor type is not a major item at this point, the study was not repeated for the upper-surface only case, and an axial compressor is used for the suction system of the advanced LFC aircraft with suction on the upper surface only.

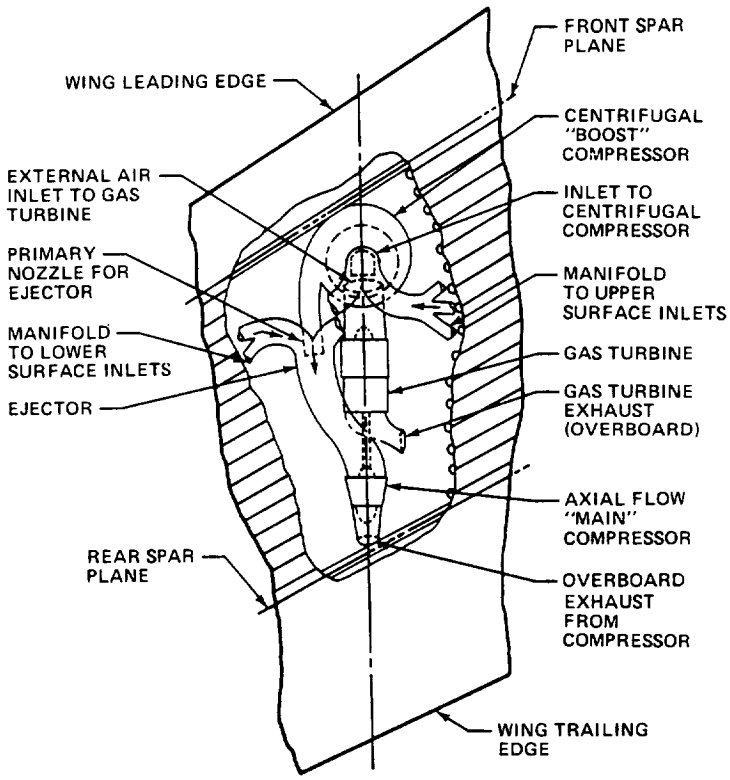

FIGURE 10-14. SCHEMATIC SHOWING USE OF "BOOSTED" UPPER SURFACE AIR TO DRIVE EJECTOR

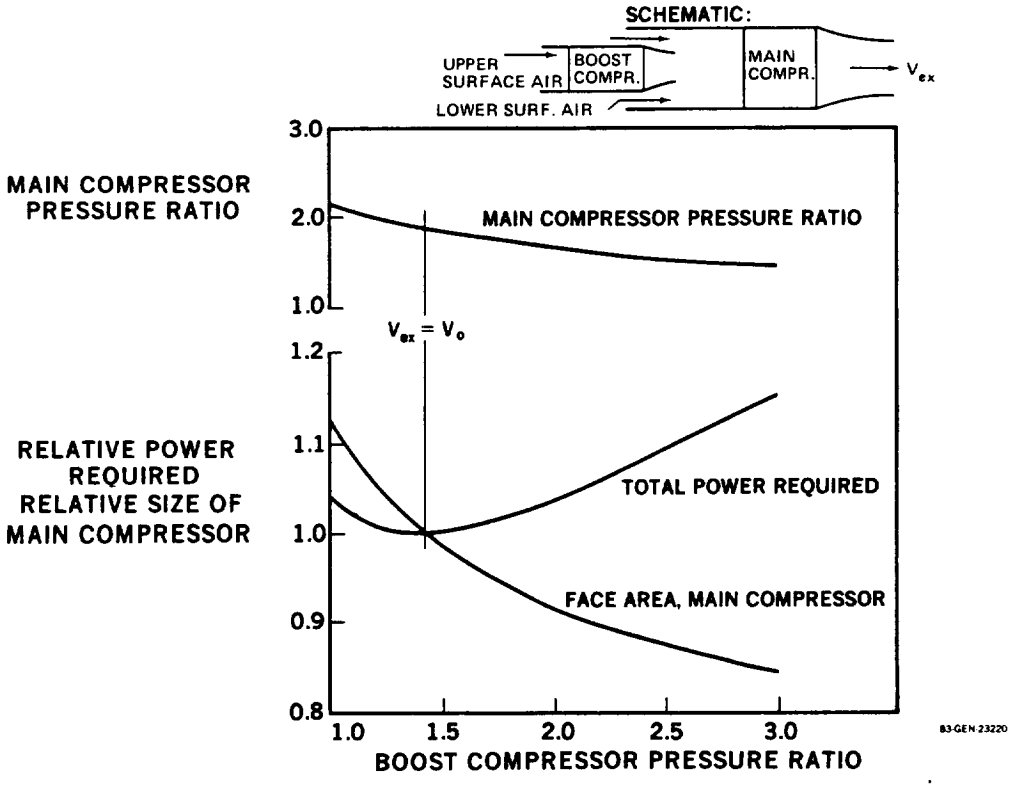

FIGURE 10-15. EFFECT OF BOOST COMPRESSOR PRESSURE RATIO

10.5.1.4 Compressor Efficiency. For the power-required calculations, the polytropic efficiency was assumed to be 88 percent. Present day compressors of large engines have efficiencies of this order and higher. By the 1995 time period, the level of 88 percent should be achievable even with small compressors operating at low inlet pressures. A change of 1 percent in polytropic efficiency would change the power requirement by approximately 1.2 percent.

10.5.2 Power Unit For Compressor

A study was made of power sources to drive the suction-system compressors. A concept with separate engines installed in wing pods was assumed for the initial baseline aircraft.

The order of magnitude of the power required is significant when different types of power sources are evaluated, as some types are not suitable for certain power ranges. The estimated suction power requirements for a typical LFC aircraft are shown in Table 10-3. (Although only the concept with suction on both the upper and lower surfaces was under consideration at the time the power-drive study was performed, a typical upper-surface-only power requirement is included in the Table.) For a 381 m^2 (4100 ft^2) wing area, a total power per airplane of 752 kW (1010 hp) is required at 10,668 m (35,000 ft) altitude. Two turboshaft engines rated at approximately 1100 kW (1500 hp) each at sea level will provide this level of power. For the baseline airplane performance, the specific fuel consumption of an engine of this size in the 1995 era is assumed to be 0.07 gs^{-1}/kW (0.4 lb/hr/hp) under cruise conditions, based on performance of current engines and estimates of performance improvements.

An alternative means of providing power of the required magnitude is by power extraction from the main propulsion engines, either mechanical power or bleed air. With the main propulsion engines in the tail, mechanical power extraction is not practical. Ducting the low pressure suction air from the wing tip to the fuselage, and then aft to a compressor in the tail region is also not practical. It would result in excessive pressure drop, very large space requirements, and severe structural problems.

Table 10-3
Typical Suction Power Required
10,608 m (35,000 ft) M_o = 0.8

Suction on Upper & Lower Surface to 70% Chord

S_w = 381 m^2 (4100 ft^2)

	Suction Airflow per Airplane	Press Compr Face	CPR*	Power / Airflow	Power per Airplane
Upper Surface	5.35 kg/sec (11.8 lb/sec)	1.27×10^4 Pa (265 lb/ft^2)	1.44	30.7 w/gs^{-1} (18.7 hp/lb/sec)	165 kW (200 hp)
Lower Surface	4.54 kg/sec (10 lb/sec)	1.83×10^4 Pa (382 lb/ft^2)			
Upper & Lower	9.9 kg/sec (21.8 lb/sec)	1.83×10^4 Pa (382 lb/ft^2)	1.88	59.3 W/gs^{-1} (36.1 hp/lb/sec)	588 kW (790 hp)
				TOTAL	753 kW (1010 hp)

Suction on Upper Surface to 85% Chord

S_w = 288 m^2 (3100 ft^2)

	Suction Airflow per Airplane	Press Compr Face	CPR*	Power / Airflow	Power per Airplane
Upper Surface	7.24 kg/sec (16 lb/sec)	1.27×10^4 Pa (265 lb/ft^2)	2.66	91.2 W/gs^{-1} (55.5 hp/lb/sec)	660 kW (880 hp)

*For $V_{exhaust} = V_{\infty}$

A comparison was made between using separate turboshaft engines and turbines driven by engine bleed air. A bleed-air-only system and a system where fuel is added to bleed air in a burner ahead of the turbine were also considered. Except for small amounts of bleed for de-icing purposes, engine bleed air used for commercial aircraft applications is normally restricted to a temperature of about 500°K (900°R). At higher temperatures than this, fire-wall type protection must be provided around the ducting, along with a sensing system for leak detection. Table 10-4 summarizes the comparison of the performance of a bleed-only system with a bleed temperature of 500°K (900°R) and one with a bleed air temperature of 683°K (1230°R). The high-temperature bleed system has only a slightly lower overall fuel consumption than the lower-temperature system. The bleed-only systems had about 30 percent higher SFC than the turboshaft and the size of the bleed ducts was incompatible with the very limited space available behind the rear spar. For these reasons, the bleed-only system was eliminated from further consideration.

Figure 10-16 shows power available with air only and with combustion, as a function of turbine pressure ratio (PR) and inlet temperature. The fuel-air ratios required to achieve the turbine inlet temperature of a bleed-burn system with 500°K (900°R) initial air temperature are also plotted in Figure 10-16. With a bleed and burn system, high specific powers can be obtained with fairly low turbine pressure ratios (low bleed-air pressures) at higher turbine temperatures. The bleed-and-burn system was compared to a turboshaft engine at a design-point condition. The same turbine inlet temperature of 1444°K (2600°R) and the same turbine efficiency were used for each system. The assumptions used are listed in Table 10-5. Table 10-6 lists the station cycle parameters calculated for each system. The effect on aircraft fuel consumption is given in Table 10-7. (The SFC penalty for bleed varies with engine cycle and operationg condition, but the value used is typical of an energy-efficient engine operating at about 90 percent of max cruise. The SFC penalty of a bleed system increases with decreased throttle setting, with a constant value of bleed extraction.) The analysis shows a lower overall fuel consumption for the separate turboshaft engine.

Table 10-4

Effect of Bleed Temperature
for Bleed-only System

Bleed Temp	500°K (900°R)	688°K (1230°R)
Bleed Pressure @ engine, P_a (psia)	241 (35)	855 (124)
Bleed Pressure @ Turbine, P_a (psia)	207 (30)	731 (106)
Turbine Pressure Ratio	8	28
Power/airflow, kW/(kg/s) (hp/lb/sec)	205.5 (125)	394.6 (240)
ΔSFC for one percent bleed	1.07%	2%
For aircraft with total fuel flow = 1264 g/s (10,030 lb/hr/airplane) and total air flow = 72.5 kg/s (160 lb/sec)[S_w = 381 in^2 (4100 ft^2)]:		
Power Required = 753 kW (1010 hp)		
Airflow to Turbine, kg/s/airplane (lbs/sec/airplane)	3.66 (8.08)	1.90 (4.2)
Bleed Flow	5%	2.6%
Δw_f due to bleed, g/s (lbs/hr)	67.6 (536.6)	65.5 (520)
BSFC, $gs^{-1}kW$ (lb/hr/shp)	.090 (.531)	.0876 (.517)
Dia pipe (per side), cm (in)	12.7 (5)	4.8 (1.9) duct 9.9 (3.9) duct shroud
Est. Weight of Ducting, kg (lbs)	215 (475)	250 (550)

Table 10-5

Cycle Comparison - Assumptions

Turboshaft compressor ratio = 14.8

Compressor adiabatic efficiency = 0.82

Turbine polytropic efficiency = 0.90

Burner efficiency - From DAC Cycle Program

Fuel heating value = 4.28×10^7 J/kg (18,400 BTU/lb)

0.5% burner ΔP

Nozzle C_V = 0.98

Turboshaft exhaust velocity = V_o (no net thrust)

Bleed-and-burn turbine pressure ratio = 8.0

Bleed Air

500°K (900°R)

241 kPa (35 psia) @ exit of bleed port @ 10.7 km (35,000 ft) altitude

(typical value corresponding to 500°K for adv. technology turbofan)

207 kPa (30 psia) @ burner

Table 10-6

Turboshaft & Bleed-and-Burn Cycles

10,608 m (35,000 ft) Mach 0.8

		Turboshaft	Bleed-and-Burn
Compressor in	P_{t_2}	36.1 kPa (5.23 psia)	- -
	T_{t_2}	247°K (444.5°K)	- -
Burner in	P_{t_3}	534 kPa (77.4 psia)	207 kPa (30 psia)
	T_{t_3}	590°K (1063°R)	500°K (900°R)
Burner	ΔT	854°C (1537°F)	944°C (1700°F)
	$\eta_b \cdot f/a$	.02455	.0270
	η_b	0.95	0.939
	f/a	.0258	.0288
Compr Turbine in	P_{t_4}	531 kPa (77.0 psia)	-
	T_{t_4}	1444°K (2600°R)	-
Power Turbine in	P_{t_5}	195 kPa (28.3 psia)	206 kPa (29.9 psia)
	T_{t_5}	1170°K (2106°R)	1444°K (2600°R)
Power Turbine Out	P_{t_6}	27.4 kPa (3.93 psia)	25.7 kPa (3.73 psia)
	T_{t_6}	761°K (1370°R)	933°K (1679°R)
Power Turbine	ΔT	409°C (736°F)	511°C (920°F)
	Power/airflow	495 $W/g \cdot s^{-1}$ (301 hp/lb/sec)	644 $W/g \cdot s^{-1}$ (392 hp/lb/sec)
	BSFC	.052 $g \cdot s^{-1}/kW$ (.309 lb/hr/hp)	.045 $g \cdot s^{-1}/kW$ (264 lb/hr/hp)
Nozzle	Pressure Ratio	1.147	1.075
	$V_{exhaust}$	237 m/s (779 ft/sec)	192 m/s (629 ft/sec)

Table 10-7

Comparison of Fuel Required by Turboshaft
and by Bleed-and-Burn System

Assumed for Main Engines:

No-bleed SFC = 16.7 $g \cdot s^{-1}/kN$ (0.59 lbs/hr/lb)

1% increase in bleed - 1.07% increase in w_f

Engine fuel/air = 0.0174

Fuel Consumption for Turboshaft:

$w_f = 0.052 \cdot (kW\ req)$, g/s (from Table 10-6)

$[w_f = 0.309 \cdot (hp\ req)$, lbs/hr]

Fuel for Bleed-and-Burn:

w_f = fuel for turbine + fuel for bleed - savings for exhaust thrust

bleed air flow = $\frac{kW\ req}{.644}$, g/s $[= \frac{hp\ req}{392}$, lbs/hr]

savings = SFC x exhaust velocity x bleed air mass flow

$w_f = 0.045\ (kW\ req) + 0.029\ (kW\ req) - .005\ (kW\ req) = 0.069\ (kW\ req)$, g/s

$[w_f = 0.264\ (hp\ req) + 0.171\ (hp\ req) - .029\ (hp\ req) = 0.406\ (hp\ req)$, lb/hr

Comparison:

$\frac{\text{Bleed-and-Burn Fuel}}{\text{Turboshaft Fuel}} = 1.3$

A qualitative comparison of the two systems is summarized in Table 10-8. The turboshaft engine has the advantage of being independent and self-contained, with the attendant merits of ease of installation, maintenance, and ground check. The bleed-and-burn system requires a slightly smaller turbine, and eliminates the requirement for a compressor for the power drive. The major disadvantage of the bleed-and-burn system is the requirement for a pressurized, relatively high temperature duct running from the main engines in the tail area, through the fuselage, and down part of the wing span. This must be done without compromising the safety of the aircraft.

When the time comes to build an LFC aircraft of a given size, and to choose a power source for its suction-air compressors, the principal criterion will be either the direct operating cost or the return-on-investment. Another factor is hardware availability. At this future time, detailed design and cost studies will be made of all available engines including turboshafts of the required size and turbines that might be incorporated in a bleed-and-burn system. For this conceptual study, however, the turboshaft engine shows three definite advantages:

- o Lower fuel consumption
- o Better operational flexibility
- o No hot air ducting through wing and fuselage.

For these reasons, the decision was made to use a turboshaft engine to drive the compressor in this study.

Table 10-8

Qualitative Comparison of Suction Power Systems

Item	Turboshaft	Bleed-&-Burn System
Ground Check	Self-contained	Requires high-temp., press. gas supply
Effect on Main Engine	None	Penalties increase as main engine throttled. If LFC bleed + a/c bleed exceed normal engine bleed quantity limits, special engine devel. required
Weight	Inlet, compressor, starter	Ducting through fuselage and part of wing
Drag	Slightly larger dimensions for turbo-machinery	Slightly smaller pod for turbo-machinery
Wing Volume	None	Bleed air ducts from fuselage to burner
Availability	Could be "off-the-shelf", depending on size aircraft	Special equipment with development & certification program.
Installation	Conventional podded turboshaft	Leak-detection provision where duct near critical structure or equipment. Blow-out provisions if duct runs through low-volume, sealed compartment.

10.6 SUCTION ENGINE ARRANGEMENT

In the wing box, the suction flow collection system is integrated with the structure, as shown in Figure 10-7. The boundary layer air is drawn into the main air ducts formed by the suction panels, integral stringers, and wing skin. The air flows spanwise to the suction engine location, where it is ducted from the individual channels into manifolds merging into inlets for the suction compressors. The number and location of the suction engines must be such that the flow in the ducts does not undergo excessive pressure loss, and the size of the cutouts required in the wing structure to remove the air is compatible with the structure dimensions and allowable stress levels.

10.6.1 Number of Suction Engines

With the small compressors and engines that are required by the LFC aircraft suction system, there are advantages in having fewer, larger engines rather than more smaller engines to provide a given total capacity. Reynolds number effects and clearance and minimum gage considerations combine to make the larger units more efficient and proportionally smaller and lighter. For the LFC aircraft, there is also a weight penalty for each collection station where the air must be ducted from the spanwise flow channels, through a dry bay, and manifolded into inlets for the suction "pumps" (compressors). A drag increment is incurred, likewise, for each engine pod. When direct-operating cost (DOC) is considered, keeping the number of engines to a minimum is important as both initial and maintenance costs are sensitive to the number of engines. In particular, maintenance labor costs are almost directly proportional to number of engines, with size having very little effect. Because of this, the number of engines is an important factor in airline acceptance.

The number of suction engines affects the suction-engine-out situation but because safety was not affected, a decision was made early in the LFC study not to provide redundancy or cross-ducting because of the large amount of additional weight, volume, and complexity involved. With one suction engine/

side, laminar flow would be lost on that side only in case of a suction engine shutdown. Laminar flow would be maintained on the other wing, and normal flight, with an increase in drag over half the wing surface, would continue following throttle and trim adjustment. With two suction engines/side, laminar flow could be maintained on approximately three-quarters of the wing surface if one outboard engine were shut down. Failure of an inboard engine would result not only in loss of laminar flow on the quarter of the wing surface sucked by that engine but also on a portion of the adjoining outboard wing surface. As the shutdown rate per engine is independent of engine size, the increased fuel consumed because of loss of laminar flow from suction-engine failure is roughly independent of the number of engines.

The concept of one suction engine per airplane was rejected for two reasons:

(1) for safety and for low noise levels in the cabin, jet engines in the passenger region of commercial transports should be avoided whenever possible; and (2) preliminary calculations showed large penalties from increased duct sizes and pressure drops, resulting from ducting air the entire semi-span.

10.6.2 Location of Suction Engines

With one suction engine/side, the location of the engine must also be considered. Placing each engine in the wing root has the same disadvantages as the centrally located single engine mentioned above. A midwing location may require a dry bay to provide space for removing suction air from the wing box ducts, combining all the suction flows, and ducting the air to the compressor. For the design mission of the LFC advanced aircraft, ample fuel volume remains despite the inclusion of dry bays. A logical position for the location of the dry bay, compressor, and suction engine is at the "wing break" point, which is at 40 percent of the semi-span for the baseline configuration. The structural discontinuity in the flap system is avoided. Flow distributions and pressure drops were calculated for the wing box suction air as a function of location

along the span. Figure 10-17(a) shows typical cumulative flows from each direction. Over the greater part of the surface between the front and rear spars, the required suction flow per unit area of wing surface is quite low, of the order of 3×10^{-2} m/s (0.1 ft/sec), and is independent of the wing chord. With the wing blade height selected by structural considerations, the calculated pressure drop in this region varies with span as shown in Figure 10-17(b). Pressure drop was calculated by conventional "pipeflow" relationships. The dashed line in this figure represents the pressure if the pressure drop were assumed to be twice the conventional driction drop. Even with this assumption, the pressure at the 40 percent semi-span meets the goal assumed in the definition of compressor and power requirements.

The area requirements for removing air from the wing box ducts were calculated as a function of Mach number and spanwise location, with the results shown in Figure 10-18. The location of the engine just outboard of the 40 percent semi-span station results in approximately equal cutout area requirements for the air from the inboard and from the outboard wing surfaces.

Layouts were made of the ducting and engine installation with the engines located below the wing just outboard of the wing break. The inboard bulkhead of the "dry bay" is located at 40 percent semi-span, the wing break point. For the wing geometry used in the layout (AR = 12), the engine centerline is at 41 1/2 percent semi-span. Figure 10-19 is a profile view of the installation study showing the suction pump, engine and duct manifold arrangements for LFC suction on both wing surfaces and for suction on the upper wing surface only. In addition to the multiple holes in the wing box upper surface, a large hole is required in the lower surface for ducting the suction air to the compressor. The compressor rotors are aft of the rear spar for safety reasons and to facilitate ducting air to the inlet with a minimum of severe turns. The drive unit is axially coupled aft of the compressors, and the installation enclosed in a faired pod under the wing. The aft mounting of the turboshaft is advantageous both for safety and for minimizing the noise transmitted to the laminar wing boundary layer.

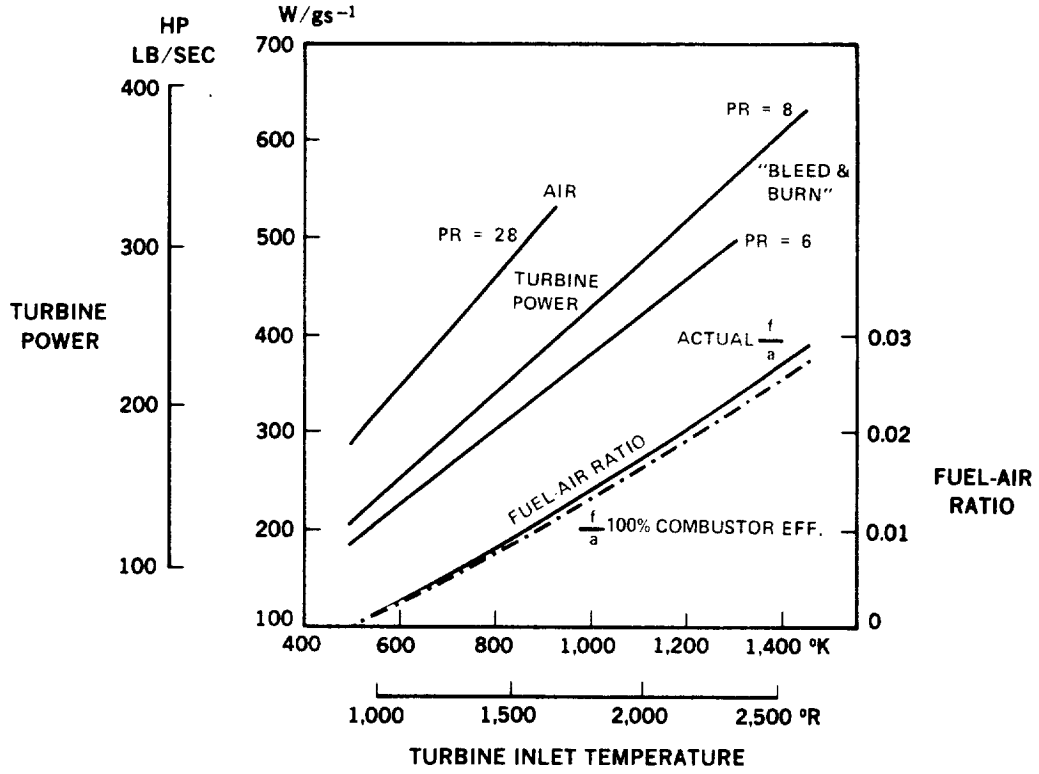

FIGURE 10-16. TYPICAL "BLEED & BURN" SYSTEM RESULTS (500°K BLEED AIR)

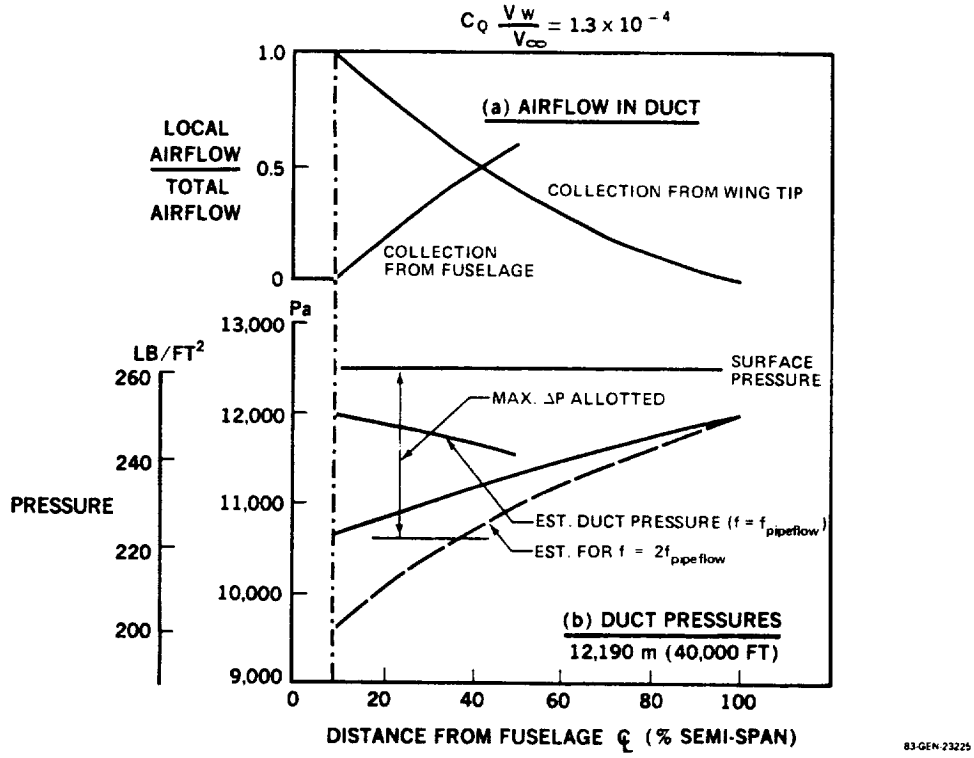

FIGURE 10-17. SUCTION AIRFLOW IN WING-BOX DUCTS

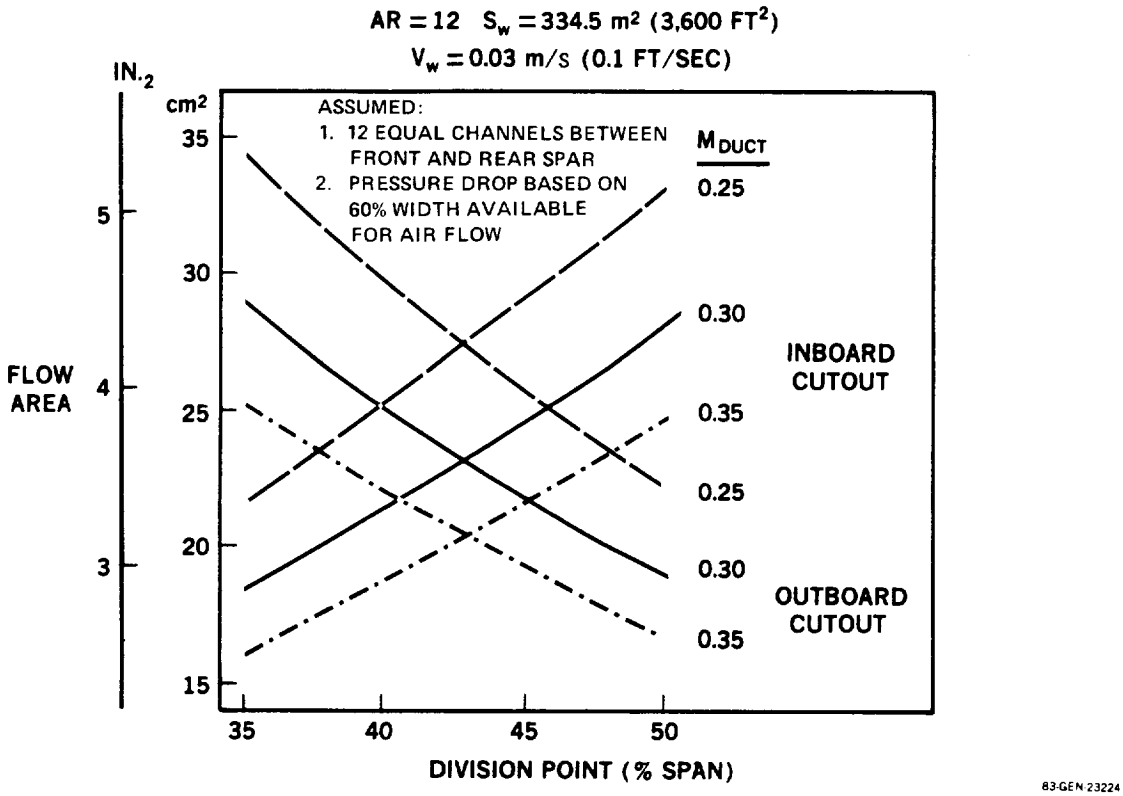

FIGURE 10-18. TYPICAL AREA FOR WING-BOX-DUCT CUTOUTS (UPPER SURFACE)

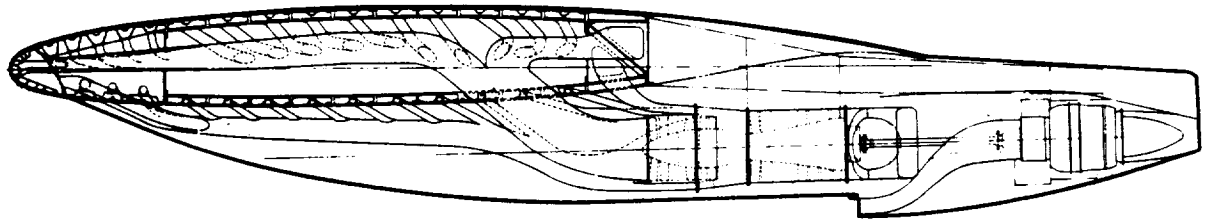

LAMINARIZATION TO 70 PERCENT CHORD
UPPER AND LOWER SURFACE

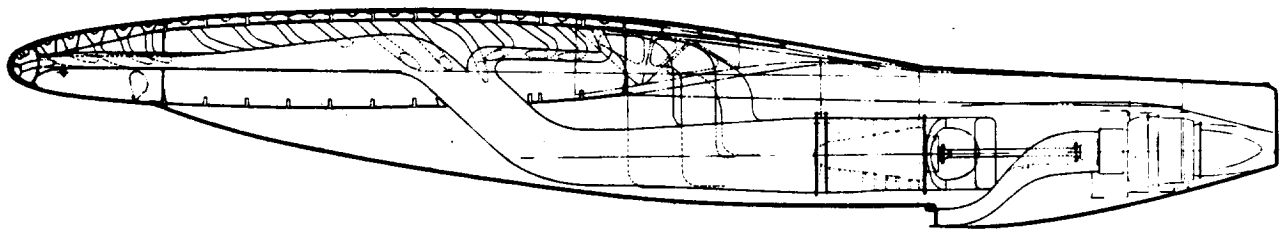

LAMINARIZATION TO 85 PERCENT CHORD
UPPER SURFACE ONLY

8-GEN-22893

FIGURE 10-19. SUCTION SYSTEM MANIFOLDING INTEGRATION

The alternative LFC airplane configuration with suction on the upper surface only but with the suction continued further aft shows that ducting air from the surface back to 85 percent chord requires the suction pump and engine to be located further aft, but the overall arrangement is greatly simplified. Refer also to Figures 5-48 and 5-49.

10.6.3 Number and Location - Conclusions

The study layouts demonstrate that a configuration having one engine/side, with the engine located just outboard of the "wing break", is a feasible concept for the LFC basline aircraft. This configuration results in acceptable pressure losses in the ducting system, and is compatible with the proposed wing structure. Moving the engine outboard results in more pressure drop and larger cutout areas for the flow from the inboard region, as well as reducing the vertical dimensions in the wing for installing the ducting to the engine. The pressure drop and area increases would be even greater if the engine location were moved to the wing root region. For these reasons the decision was made to use two suction engines per aircraft located each side at the wing break.

10.7 POSITIVE-PRESSURE PURGING SYSTEM

During the development of the surface-contamination-control system (Section 11), a procedure was defined for application of a liquid to the surface during takeoff and climb for contamination avoidance and ice protection. Some of the liquid remains on, or in, the surface, and would impede the flow of LFC air if allowed to remain when suction is initiated. Tests demonstrated that a pressure differential of 6900 P_a (one psi) applied across the porous surface would remove the liquid and return the surface to approximately its original porosity in one minute. Tests on perforated materials indicate that a lower pressure increment may be sufficient for clearing these surfaces. A lower pressure requirement reduces the magnitude of the situation discussed below, which is based on the original 6900 P_a (one psi). See Section 11.6.2.4.

Ram air is a convenient source of positive pressure, having sufficient pressure to supply the required differential for purging all LFC porous surfaces except in the attachment line area. Pressurized cabin air can be used as a source for this part of the system.

The greater pressure drop across the surface during the "purging" mode results in an order-of-magnitude greater airflow. Unless the Mach number in a duct or other component is very low in the suction mode, the positive-pressure flow will "choke" before the surface has been cleared. A comparison of typical suction and "purging" conditions is made in Table 10-9. In the suction case, the values of pressure coefficient, C_{P_N}, and suction flow quantity, C_Q, are representative of those in the wing box region behind the front spar. The second column shows the flows encountered with the application of 6900 P_a (one psi) pressure differential across the surface at 7,620 m (25,000 ft) altitude. In this condition, the critical flow quantity, $w\sqrt{\theta}\sqrt{\delta}$, which determines area requirements, is almost eight times its value during LFC operation. If some part of the suction system is designed for even a moderate Mach number, such as the wing-duct cutout, which is designed for 0.3, the surface area over which the positive pressure can be applied is appreciably smaller than that from which the suction air is drawn. A system of valving can be devised to permit sequential purging of the wing box surface where it is not desirable to increase flow areas to accommodate the positive-pressure flow requirements. This is illustrated in Figure 10-20. The upper schematic shows the LFC mode with continuous suction applied to the whole LFC surface. The lower schematic illustrates how the purging flow to the porous panels can be reduced. Groups of valves could be opened in sequence to limit the duct Mach number. The number of sequences needs to be kept to a minimum to avoid excessive time being taken for purging.

For wing surface regions, where the suction flow is high, such as aft of the rear spar, the ratio of purging flow to suction flow is reduced and continuous purging could be achieved with acceptable duct Mach numbers. Figure 10-21 shows that with a suction C_Q of 1×10^{-3}, the purging flow Mach numbers are acceptable even with moderate Mach numbers in the suction mode.

Table 10-9

Typical Parameters in Suction & In Purging Modes

Surface Porosity = 0.134 $m^3 \cdot s^{-1}/m^2$ @ ΔP = 670 Pa

(26.5 $SCFM/ft^2$ @ ΔP = 14 lb/ft^2)

Location	Item	Suction Mode	Purging Mode
Freestream	M_∞	0.8	0.7
	Altitude	10,668 m (35,000 ft)	7620 m (25,000 ft)
	P_∞	23.9 kPa (499.4 lb/ft^2)	37.65 kPa (786.4 lb/ft^2)
	q_N	8.04 kPa (167.9 lb/ft^2)	9.69 kPa (202.3 lb/ft^2)
Surface	C_{pN}	-0.92	-0.8
	Pressure	16.5 kPa (345 lb/ft^2)	29.9 kPa (625 lb/ft^2)
	Temp	243°K (437°R)	262°K (472°R)
	σ	0.1935	0.3246
	μ/μ_o	0.872	0.926
	C_Q	*1.29 x 10^{-4}	-3.36 x 10^{-3}
Across Surface	w/A_{swt}	.0234 kg · s^{-1}/m^2 (.0048 $lb/sec/ft^2$)	.40 kg · s^{-1}/m^2 (.082 $lb/sec/ft^2$)
	$\sigma\Delta P_{\mu/\mu}$	53 Pa (1.1 lb/ft^2)	2418 Pa (50.5 lb/ft^2)
	ΔP	239 Pa (5 lb/ft^2)	*6895 Pa (144 lb/ft^2)
Under Surface	P_t	16.3 kPa (340 lb/ft^2)	36.8 kPa (769 lb/ft^2)
	$\frac{w\sqrt{\theta}}{A_{surf}\ \delta}$	0.134 kg · s^{-1}/m^2 (.0274 $lb/sec/ft^2$)	1.05 kg · s^{-1}/m^2 (.2152 $lb/sec/ft^2$)

*Determines airflow through surface.

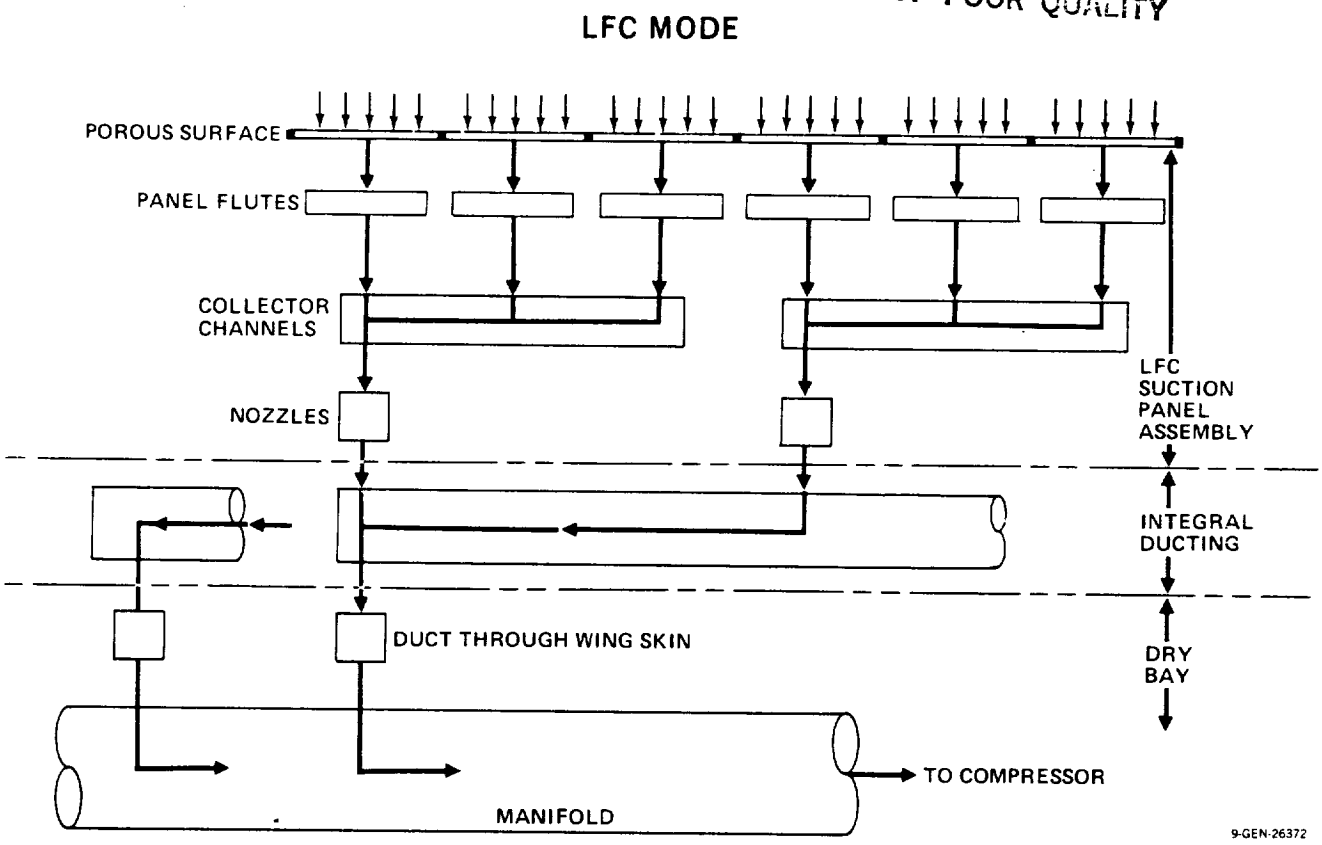

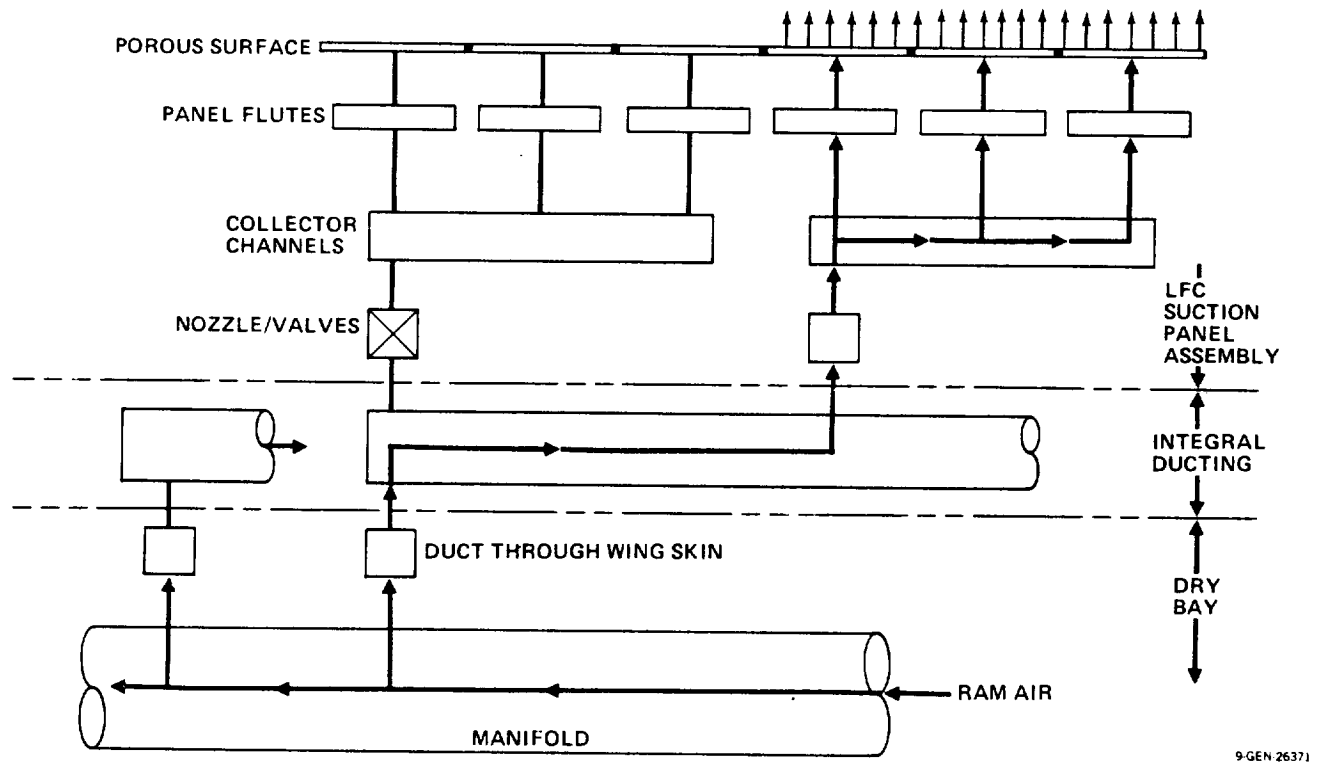

FIGURE 10-20. SCHEMATIC OF SUCTION SYSTEM

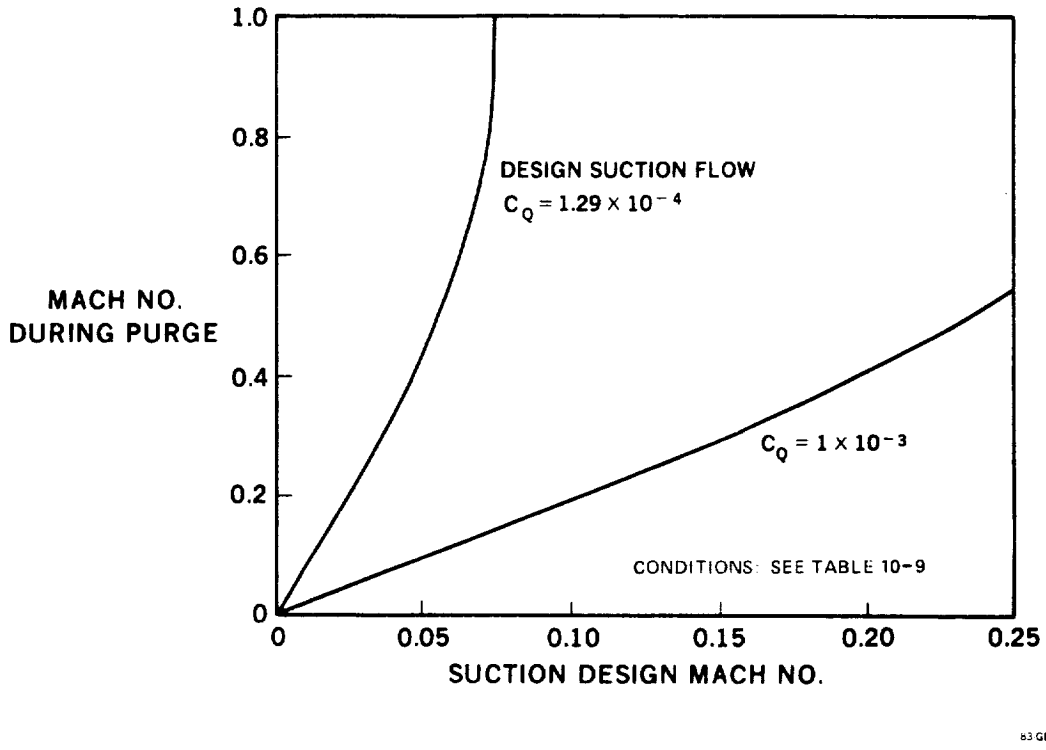

FIGURE 10-21. EFFECT OF SUCTION DESIGN MACH NUMBER ON PURGING MACH NUMBER WITH POSITIVE PRESSURE

10.8 SUCTION/PURGING CONTROL

The controls for the suction system can be more fully defined after completion of the planned development, test, and flight demonstrator activities. More information is required on such items as the permissible amounts of over- and under-suction, the effect of spanwise differences in suction quantities, actual pressure drops in suction-system components, etc. The general control concept now proposed for the advanced LFC aircraft provides chordwise pressure variation by means of valves between the ends of the main flow ducts and their inlet to the collection manifold. Calibrated nozzles are used at the end of each collector channel to take care of spanwise variations in main-duct pressures. If the sequential application of positive pressure to purge the surface proves to be necessary, selector valves can be incorporated with the control nozzles. The selector valves could also be used to prevent flow through the LFC system during flight with LFC off.

The control systems should be designed to increase flight crew work load as little as possible.

10.9 SUMMARY - SUCTION SYSTEM

Design studies and analysis indicate that the system proposed for pulling LFC air from the wing surface through a porous or perforated skin into a collection system in which the flow ducts are incorporated with the wing structure is practical. A dry bay, located on the outboard side of the wing "break", contains a manifold for collecting air from the spanwise ducts and conducting it to the inlet of a compressor. A pod beneath the wing encloses the suction compressor and its power source, a turboshaft engine, as well as part of the manifold.

Flow requirements have been estimated to ensure their compatibility with the wing structure. A method has been devised to provide positive pressures beneath the wing surface to remove any residual fluid before LFC operation is initiated.

While some suction system requirements need to be defined quantitatively, or more accurately, no major problems can be discerned that should discourage the proposed orderly development of the concept.

11.0 ENVIRONMENTAL SYSTEMS

11.1 INTRODUCTION

The ultimate goal of the LFC program is to develop an aircraft design that will achieve laminar flow during cruise flight conditions in an economical and practical manner. One foreseeable problem that could interfere with the attainment of this goal is the contamination of the wing leading edge due to insects, airborne particles, and/or ice. The wing must therefore be protected from any surface accumulations that would create a turbulent boundary layer during normal cruise; laminar flow would not be required during climbout or during an icing encounter.

Early studies have shown that roughness on the wing leading edge due to the residue of impacted insects can be sufficient to create a turbulent boundary layer. Possible approaches are to:

(a) Add a protective system to the aircraft that will either prevent insects from impinging on critical LFC surfaces, prevent adhesion and buildup of roughness after insect impingement, or remove insect contamination.

(b) Reduce the insect aerial population near airports to an acceptable level and do not incorporate a contamination prevention system.

(c) Accept the reduced aircraft performance resulting from insect contamination and do not incorporate a contamination prevention system.

An economic trade-off analysis could determine which approach would result in the most profitable mode of operation. However, this evaluation assumes that a contamination avoidance system and some form of wing ice protection is required.

A major concern in the evaluation of the various contamination avoidance concepts is whether the ice protection and suction requirements can be met in the space available in the wing leading edge. In view of the limited space envelope and

viscosity on pressure drop at low temperature and pressure. The functional dependency must be determined experimentally and is influenced by the condition of the air flowing through the porous media. The major concern with regard to the contamination avoidance system is the effect of temperature on viscosity and surface tension of liquids. These parameters affect the performance of spray nozzles and porous media, the ability of liquid to cover a surface and flow aft, and the pressure required to purge liquid from a porous suction surface.

Current large commercial aircraft use hot air to provide ice protection. A cursory review of the space requirements indicates that this concept may not be feasible. Another change from normal ice protection design is the consideration of runback. De-icing and anti-icing systems presently used on commercial aircraft can be permitted to melt some of the ice cap. This water flows aft along the wing until it freezes. The frozen runback remains on the surface because it is aft of the area that is heated by the ice protection system. This condition is intolerable for an LFC aircraft where the roughness could cause transition of the boundary layer.

Some of the considerations included in the feasibility evaluation are listed below:

(a) Effectiveness of the concept in protecting the wing against contamination.

(b) Compatibility of the contamination avoidance system with an ice protection system, the aerodynamic performance of the wing, the structural integrity of the wing and materials involved, and the requirements of agencies such as the Environmental Protection Agency (EPA).

(c) Compatibility of the contamination avoidance system with the LFC suction system with regard to (a) clogging of the suction passages and (b) physical space limitations imposed by the suction system installation.

(d) Ability of the contamination avoidance system to be manufactured and maintained to meet the maximum allowable roughness requirements of the LFC system.

the possible interaction between systems, consideration must be given to ice protection when evaluating the contamination avoidance system. Since the contamination avoidance and ice protection systems must provide coverage of the same area, and in many cases can use the same techniques, it would be advantageous to use a common system for the two functions. Further definition of the suction system space requirements may make this necessary.

In addition to the design of active contamination avoidance and ice protection systems, this section of the report reviews the peculiar effects of other environmental contaminants on LFC aircraft design and operation. Dust, sand, exhaust products, and other airborne contaminants can be drawn into, or settle on, the suction surface. The suction material must be relatively insensitive to these factors and maintenance methods must be established to restore the original system characteristics.

Erosion due to rain, hail, or sand has caused severe roughening of the wing leading edge for airlines operating in semi-tropical areas. The structural implications for the wing surface are considered elsewhere. However, erosion also is considered in the selection and design of the contamination avoidance and ice protection systems.

Another environmental factor that influences LFC aircraft operation is the frequency and severity of atmospheric ice crystal encounters and their disruption of laminarization. If ice crystals in the cruise altitude regime caused loss of LFC with significant frequency, the cruise altitude would need to be changed. This section includes a discussion of the problem and a review of presently available data. A program is recommended to provide the basis for a quantitative analysis of the effect of ice crystans on the economics of LFC aircraft operation.

The effect of operational pressures and temperatures on the suction and contamination avoidance system performance is also evaluated in this section. For the suction system, consideration is given to the effect of density and

(e) General practicality of the design including such factors as system weight, availability of materials, and limitations due to manufacturing techniques.

(f) Compatibility of the contamination avoidance system with the aircraft environment, especially considering rain, ice, and sand erosion.

(g) Operational considerations such as ground support requirements, periodic maintenance, flight restrictions and operational procedures.

A review of each concept with respect to these factors provides an indication of feasibility and also a measure of confidence in the ultimate successful implementation of the concept.

11.2 CONTAMINATION AVOIDANCE AND ICE PROTECTION SYSTEM REQUIREMENT

The major considerations for the contamination avoidance system are the distribution and characteristics of airborne insects, the extent to which smoothness must be maintained, compatibility with other LFC systems and structure, and compatibility with normal operation and maintenance procedures.

(a) Insect Population and Characteristics - The contamination avoidance system must prevent contaminants that will trip the boundary layer from adhering to any portion of the wing in which laminar flow is to be maintained. For the LFC aircraft to be economically viable, this objective must be achieved for the large majority of flights. One method of achieving this goal is to use a shield forward of the wing that may also act as a high-lift device.

To analyze the effectiveness of a shield, it is necessary to calculate the trajectory of an insect subjected to the aerodynamic forces of an approaching aircraft. To accomplish this, it is necessary to know the drag-to-weight ratio of the range of insects that are expected to be encountered. Figure 11-1, taken from Reference 11-1, presents the frequency that insects of various weights were encountered during

experiments conducted at very low altitudes. Reference 11-1 also states that 54 percent of the roughness generated due to insect impingement occurs during the ground run, about 33 percent during climb to 305 m (1000 feet) and the remaining 13 percent while continuing the climb to 1524 m (5000 feet). Hence, the values shown in Figure 11-1 for insect distribution near the ground are very significant to the study of insect impingement. Figure 11-2 shows the ballistic coefficients of twelve species of small insects with wings removed. The ballistic coefficient represents the ratio of drag-to-weight of the insects tested. It can be seen that for the range of insect weights that are expected to be encountered (Figure 11-1), the ballistic coefficients range from 0.1 to 0.2. Wings would only increase this value slightly.

Most insects are confined to the so-called terrestrial zone (from ground level to 91.4 m (300 feet) although for insects occurring up to 1500 m (5000 feet), the insect density appears to be a continuous function with respect to altitude. Figure 11-3 taken from References 11-1 through 11-6 illustrates both of the foregoing statements. The large variation in insect population found by different investigators is also apparent.

References 11-7 and 11-8 present data relative to the height of insect deposits on a wing leading edge. The data indicate that insect deposit can range in height from 0.381 mm (0.015 inch) to 0.762 mm (0.030 inch) near the stagnation point. The height range decreases rapidly to a value of 0.152 mm (0.005 inch) to 0.302 mm (0.008 inch) within a distance of a few percent of the chord from the peak value, and then decreases more slowly with increasing distance from the leading edge. Figure 11-4 is a crossplot of the data for constant values of ε (deposit height). The region in which protection is required to avoid deposits greater than 0.102 mm (0.004 inch) high, is forward of about 8 percent chord on the upper surface. For the airfoil used in the study, this coincided with a tangent of about 7 degrees to the surface.

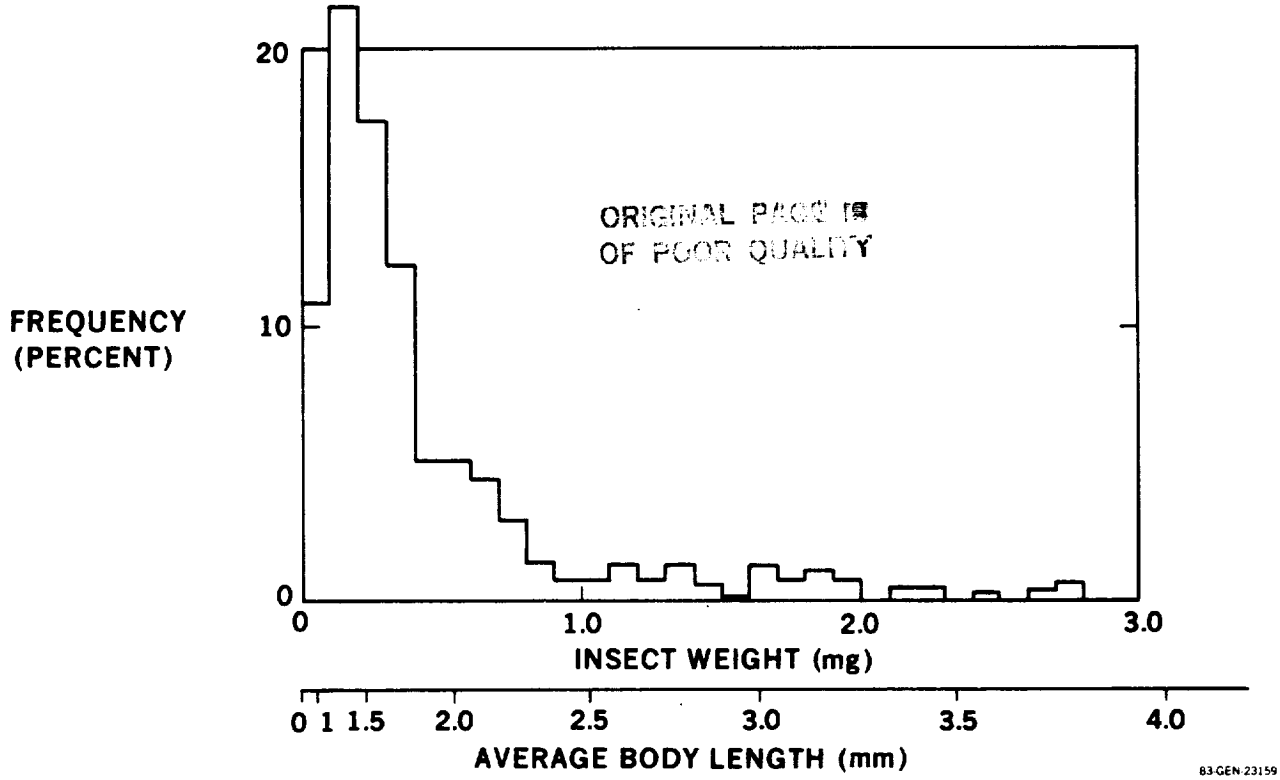

FIGURE 11-1. INSECT FREQUENCY VERSUS WEIGHT – NEAR THE GROUND (FROM "ROUGHNESS DUE TO INSECTS" BY W. S. COLEMAN)

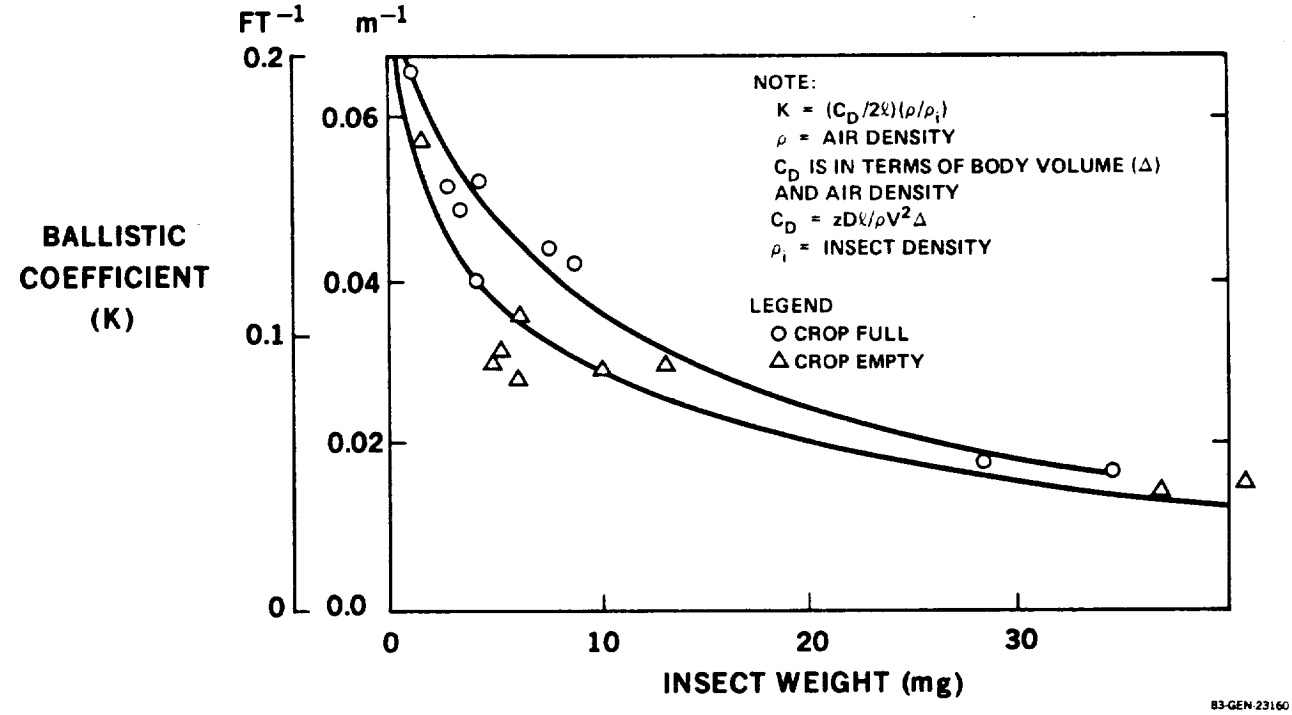

FIGURE 11-2. INSECT BALLISTIC COEFFICIENT (K) VERSUS WEIGHT (FROM "ROUGHNESS DUE TO INSECTS" BY W. S. COLEMAN, USING SMALL INSECTS WITH WINGS REMOVED)

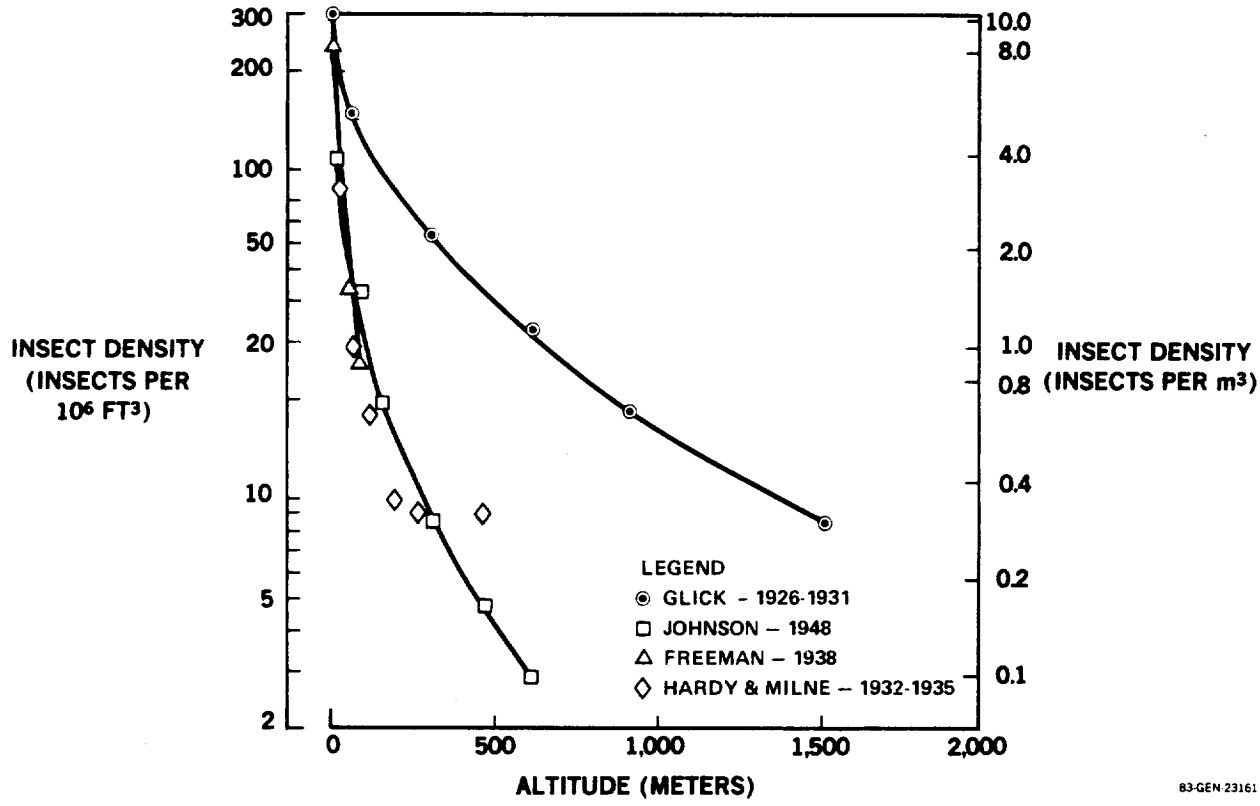

FIGURE 11-3. INSECT POPULATION DENSITY VERSUS ALTITUDE

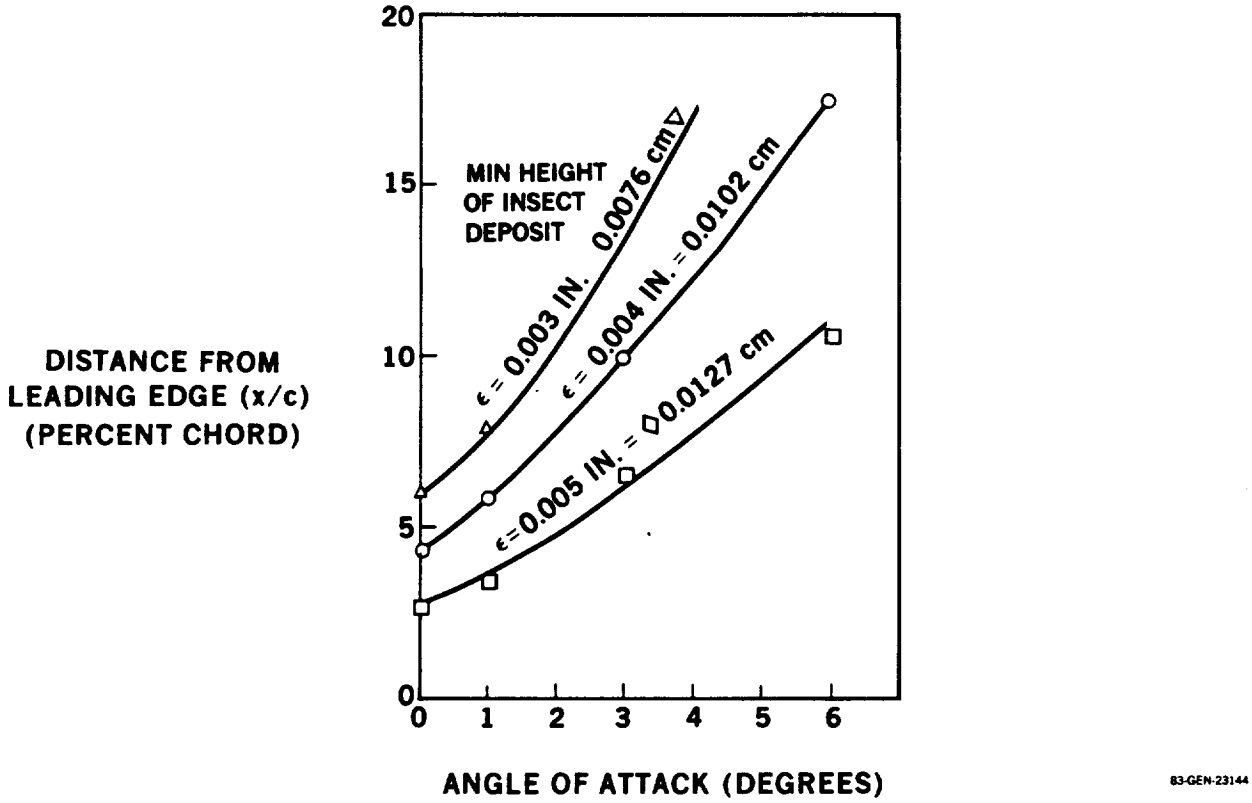

FIGURE 11-4. EFFECT OF ANGLE OF ATTACK ON LIMIT OF INSECT IMPINGEMENT (NACA 66-009 AIRFOIL AT $R_C = 6.9 \times 10^6$) FROM REFERENCE 11-7

It is apparent that the insect density varies greatly due to geographical and seasonal factors. Therefore corresponding operational requirements will also vary. A contamination avoidance system that is effective at all altitudes below 305 m (1000 feet) should be adequate in a temperate climate but some data indicate that protection up to 1524 m (5000 feet) may be required under semi-tropical conditions. Each of the candidate systems is evaluated on its ability to provide contamination protection up to 305 m (1000 feet) altitude as a minimum and up to 1524 m (5000 feet) as a design goal.

(b) Roughness Criteria - The permissible roughness is a function of cruise altitude, the chordwise distance from the attachment line (similar to stagnation point of two dimensional flow), and the type of roughness. A maximum allowable height of 0.102 mm (0.004 inch) was used for system evaluation and preliminary design, based on Reference 11-9.

(c) Ice Protection/Contamination Avoidance System Compatibility - The ice protection system must not allow water to run back into an area from which it cannot be removed and could subsequently freeze. All thermal systems (such as hot air and electrical heating) permit some runback that will trip the boundary layer and are unacceptable. The ice protection system must be certificable by the FAA and must meet the requirements of FAR 25. Laminar flow is to be maintained after encountering continuous maximum icing condition or intermittent maximum icing condition as defined by FAR 25.

(d) Space Compatibility - The contamination avoidance system must be designed within the space constraints of the leading edge box and be compatible with the space requirements of the structure and the suction system. Of particular concern are the volume requirements of a Krueger-type shield that protects the leading edge against contamination which must also be properly sized and located for aerodynamic performance. Another potential conflict of requirements is the liquid dispensing versus suction area requirements, especially in the region of attachment line travel.

(e) Suction System/Contamination Avoidance System Compatibility - It is highly desirable to use the same surface material and liquid for the contamination avoidance system and for the ice protection system. To effect this integration, the porosity requirements of the two systems and the spreading characteristic of the liquid must be compatible. Also, the liquid must not clog the porous surface after low altitude application or a method must be devised to clear the porous surface.

(f) Aircraft Operational and Maintenance Compatibility - The contamination avoidance system should not require special flight procedures that will seriously degrade performance or affect safety. Consideration must also be given to crew workload, worldwide availability of materials, environmental pollution, and ground maintenance including the ability to fabricate, install and replace all system components.

11.3 POSSIBLE SYSTEMS CONSIDERED

The selection of several candidate concepts was the first step in arriving at a feasible contamination/ice protection system for the LFC aircraft. The task included:

- Compilation of all conceivable methods that could be employed to protect the LFC aircraft from the effects of contaminants and/or ice. This includes methods obtained from a review of LFC literature, similar industrial applications, and brainstorming sessions.

- Formulation of a theoretical basis and conceptual design for each conceivable method. In some cases, this would include a rough order of magnitude analysis to assess the effect of the parameters involved.

- Evaluation of each method to determine the critical technical areas that require development in order to assure feasibility.

- o Initial evaluation of the various concepts to eliminate infeasible approaches in order to concentrate the effort on those that offer the greatest probability of success and/or the most advantageous solution to the problem. This provided a list of candidate systems for more detailed design studies.

The various contamination avoidance concepts considered fall into five main categories: mechanical, liquid, electrical, disposable covers and surface materials. Each category is discussed separately since many of the problems involved are common to all concepts in a given category.

11.3.1 Mechanical Systems

Mechanical systems that will result in a wing surface tha meets the smoothness criteria for laminar flow have been subdivided into three types: shields, covers and scrapers. Generally, the mechanical systems require some mechanism to deploy, operate and stow the apparatus; this may require rigorous control of tolerances to meet the smoothness requirements.

Designing an ice protection system compatible with mechanical cover or scraper systems is not simple, but a preliminary design for a possible electric deicing system is presented in Reference 11-10. There is concern, however, regarding the implementation of the electrical heaters into the LFC suction surface and about the power requirements of such a system.

11.3.1.1 Retractable Shield - Reference 11-11 describes wind tunnel tests of a shield concept in which a curved plate was extended forward through a slot on the upper surface. A degree of insect protection was obtained using this approach; however, aerodynamic and mechanical problems were created relative to increased drag, pitching moment, weight, and wing surface smoothness.

If suction is not required on the lower surface, a shield similar to a variable cambered Krueger (VCK) could be deployed. The primary purpose of the shield would be to prevent impingement of insects on the fixed wing. Secondary benefits, such as providing ice protection and high-lift, could also be obtained.

To protect against contaminants, the shield would be extended during all aircraft operation below 1524 m (5000 feet) including taxi, takeoff, climb, descent, approach, and landing. Full ice protection would require the shield to be extended during all icing conditions unless wing leading edge ice protection were provided independently. Extension of the shield could require special operating procedures with possible restrictions on speed. A thorough study of the operational impact of shield deployment during icing conditions is necessary to determine the acceptability of this approach or the need for supplemental ice protection.

An alternative is an internally stowed shield. The rigid shield would normally be stowed in the wing leading edge cavity forward of the front spar. It would be deployed through a slot in the lower wing surface near the leading edge.

The size of the shield would be restricted by the space available forward of the spar after the installation of the suction system and structure.

Figures 11-5 and 11-6 show two possible mechanical shield leading edge protection systems.

11.3.1.2 Retractable Cover - This concept may also be retractable. A cover differs from a shield in that it is in direct contact with the protected surface.

A thin foil cover such as 0.061 mm (0.002 inch) thick mylar, could be extended across the leading edge. After flight through the contaminated region, the cover could be retracted. A continuous drive could be used to pull the cover along the wing from a stored roll in the fuselage.

The exposed drive mechanism would need to meet the aero smoothness requirements.

11.3.1.3 Mechanical Scraper - Early designs and tests of a variety of mechanical scrapers using wires and felt pads indicated that this method might be feasible (References 11-8 and 11-11). In these designs, some type of external frame was used to support the scraper. The felt pad, which would be more compatible with an LFC surface, was propelled along the leading edge of the wing by either mechanical or aerodynamic forces.

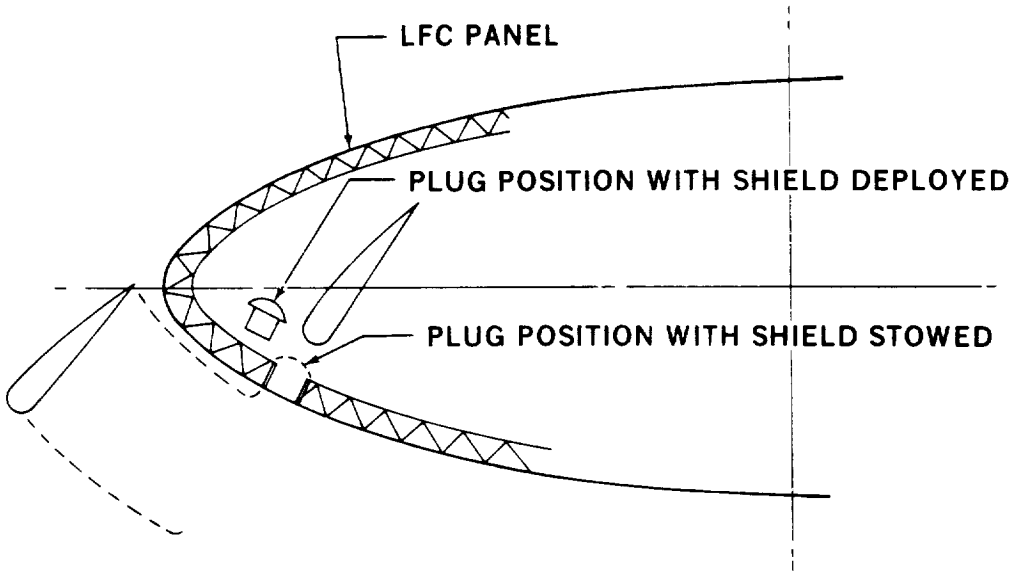

FIGURE 11-5. PRELIMINARY CONCEPT OF INTERNALLY STOWED SHIELD

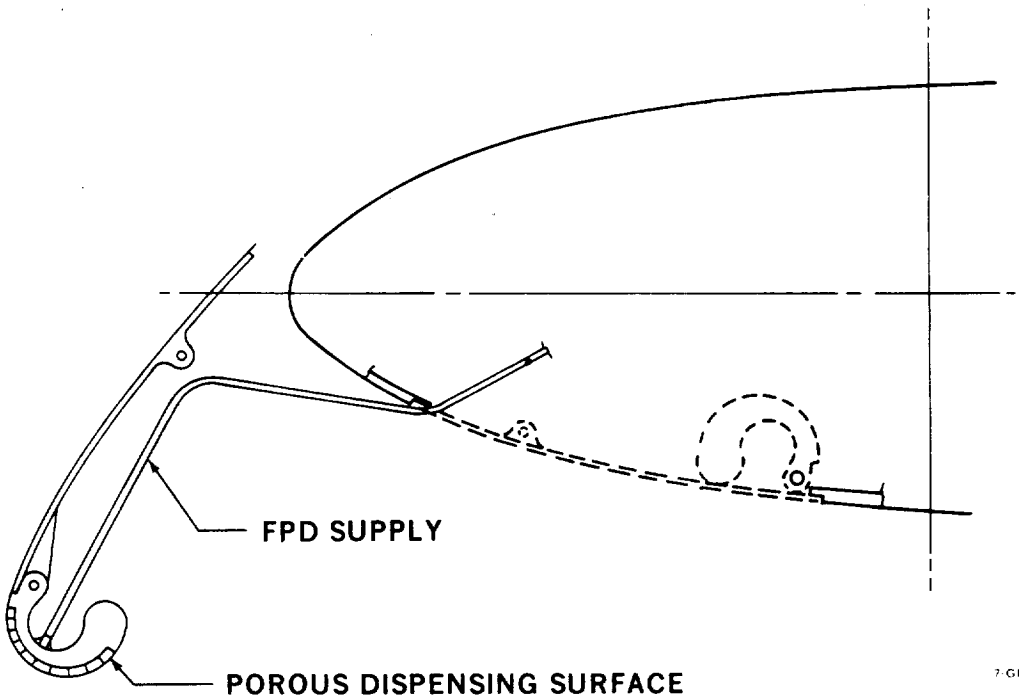

FIGURE 11-6. PRELIMINARY CONCEPT OF RETRACTABLE SHIELD

11.3.1.4 Recommended Approach - Mechanical System - The most practical approach for a mechanical system is the use of a Krueger-type shield with laminar flow on the upper wing surface only. A high lift Krueger flap is currently being used on commercial aircraft and a shield of this type could provide substantial protection against contaminants and ice. Analyses and tests will be required to determine if supplemental protection is needed.

A completely retractable shield may also be feasible for an LFC aircraft with laminar flow on both upper and lower wing surfaces.

With an adequate shield, the wing suction system would be completely free from contamination protection requirements; and with the shield performing as a high lift device it would also improve the aerodynamic performance of the aircraft. The shield could also be designed to meet the ice protection requirement, further simplifying the suction system design.

11.3.2 Liquid Systems

Liquids could be used to protect surfaces against deposits by acting in any one of three basic ways:

(a) A film of liquid over the surface could cushion the impact of the contaminant and maintain the deposit in a semi-liquid state preventing adhesion to the metal surface.

(b) A liquid could be used as a washer to dissolve the excrescence and/or the bond between the deposit and aircraft surface.

(c) A liquid spray could be used to erode the excrescence by the impact force of the impinging droplet.

These methods can be used separately or in conjunction with each other; they may be used continuously, intermittently, or after the encounter in the case of a washer or spray system.

The liquid system can be used for both insect protection and ice protection if the fluid acts as a freezing-point-depressant (FPD). Freezing-point-depressants have been used in anti-icing and de-icing applications for the protection of propellers, wings, cowls and other surfaces for many years. The fluids used for FPD are usually mixtures of alcohol (ethyl, methyl or isopropyl) and ethylene glycol. The most fully developed method of distributing the FPD on a wing leading edge is through a porous surface, although the use of spray nozzles is also feasible.

For LFC, two potential problems are common to all liquid systems. (1) Clogging of the suction orifices with liquid or contaminants (even when the suction system is not active) will require special procedures during flight to expel the liquid from the porous materials. Periodic ground cleaning procedures may also be required to remove any cumulative residue. (2) Runback of the liquid and contaminants to surfaces further aft on the wing where any residue could be deposited if not removed by aerodynamic forces. Laboratory and wind tunnel tests of the various concepts with candidate LFC surface materials are required to evaluate these problems for a specific design. In general, the liquid would need to have a low enough viscosity for it to move quickly across surfaces and avoid these problems. Additional considerations in the selection of a suitable liquid are wetting ability to provide good spreading over the surface to be protected, low evaporation rate to maintain the protection over the complete impingement area, a low freezing point, and a low surface tension to aid purging of the pores.

11.3.2.1 Liquid Film - With sufficient continuous application of a liquid film over the wing leading edge, contaminants impinging on the wing would be cushioned and carried aft by the liquid to a point at which they would be blown off the wing by aerodynamic forces. One method of applying the liquid film is by a means similar to that used for the TKS fluid de-icing system (Reference 11-12). The TKS fluid de-icing system consists of a fluid reservoir, pump, filter, metering unit and liquid distribution panel at the surface. The distribution panel is a porous metal section that is an integral part of the

wing and substitutes for the wing leading edge. By means of this porous leading edge, the fluid is exuded over the surface in and on both sides of the stagnation region. The de-icing fluid spreads in a limited region on dry surfaces and is miscible with water to enhance spreading when flying through a moist atmosphere. If system activation were delayed until after formation of an ice cap, the fluid would spread throughout the ice cap to de-ice the surface. The fluid reduces the freezing point of the ice resulting in a slush that is blown away (Reference 11-13). The TKS de-icing system is currently used on the Short Brothers Skyvan SC.7 and the Hawker Siddeley HS125 executive jet aircraft.

Other methods of introducing a freezing-point-depressant that appear to be feasible include the use of other types of porous panels, leading edge orifices, or spray nozzles. It may be possible to use the porous LFC suction surface to distribute the freezing-point-depressant. The final choice of the type of fluid distribution system will be influenced by the space available and the roughness criteria. Figures 11-7 through 11-9 depict some of the schemes considered for a liquid leading edge protection system.

The performance of a liquid film protection system was investigated by Coleman (Reference 11-11). Coleman reported a definite increase in the flow requirement at higher ambient temperatures. In the normal icing temperature range of 30-35^{o}C about 0.069 Kg/s/m^2 (0.85 lb/min/ft^2) of water would be required to keep the surface clean. At 50^{o}C the required flow rate is increased by 50 percent. These flow rates result in a feasible system weight for a reasonable area of coverage. Coleman used a solution of water with 2 to 30 percent detergent added to assist in distributing the fluid over the surface to be protected.

Some of the potential problem areas of a liquid-film/freezing-point-depressant system for contamination and ice protection are:

(a) Space limitations - The requirements of the suction system in terms of both the surface area in which suction is required and the ducting and support structure within the wing severely limit the space available for fluid distribution panels. If space limitations negate

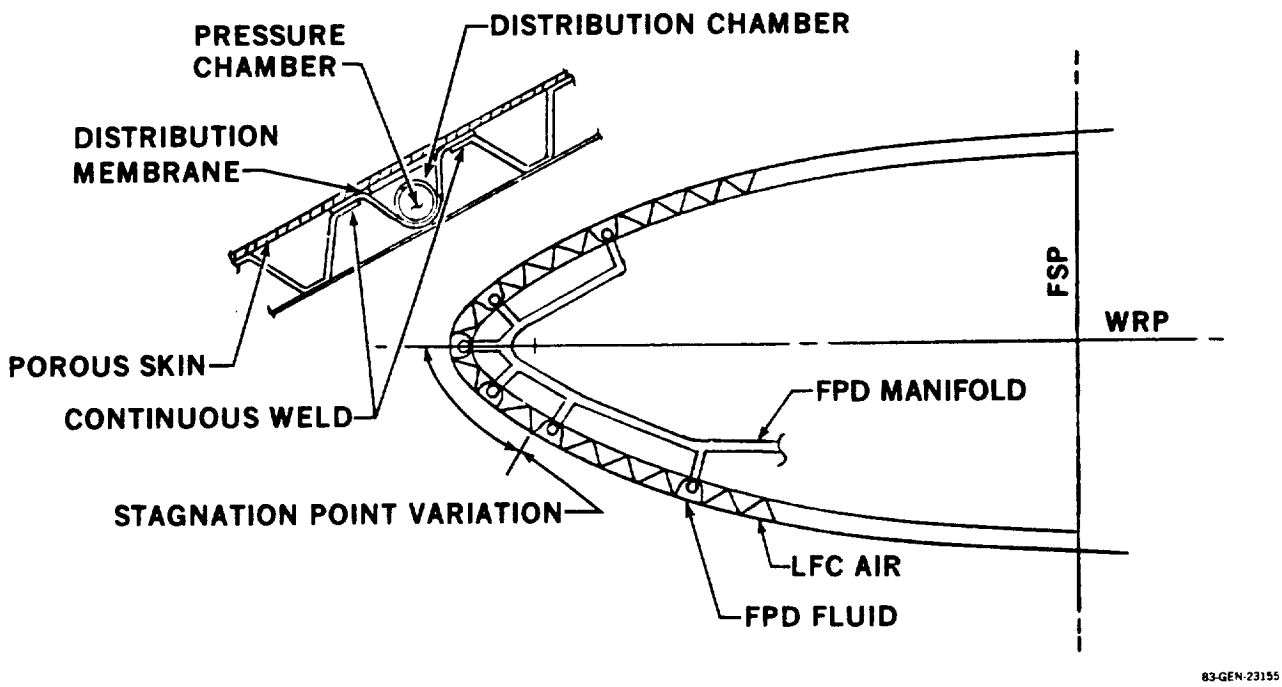

FIGURE 11-7. FREEZING POINT DEPRESSANT LEADING-EDGE DISTRIBUTION STRIPS WITH ALTERNATE AIR AND FPD PASSAGES

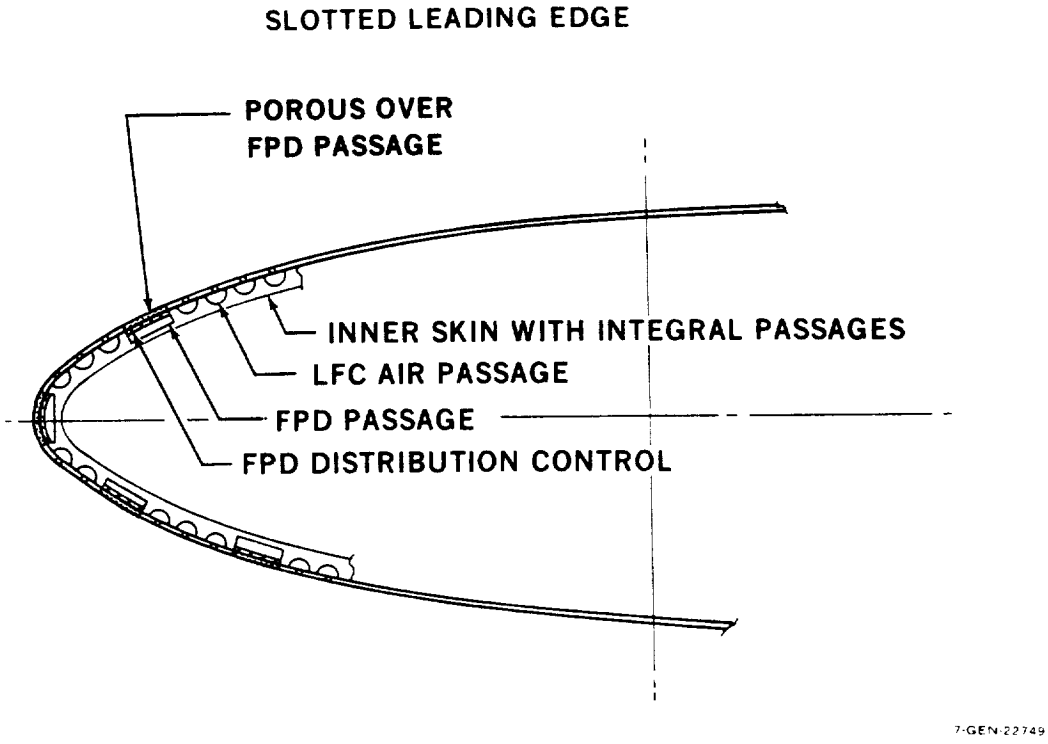

FIGURE 11-8. PRELIMINARY CONCEPT OF FREEZING-POINT DEPRESSANT DISTRIBUTION SYSTEM

the use of porous panel distribution, the liquid film concept may still be feasible using a spray type distribution system. Mounting the spray nozzles on a Krueger-type shield is possible.

(b) Leading Edge Erosion - An early problem associated with TKS porous panels was that water hitting the pores produced an explosive erosion effect. Several layers of steel calendared wire cloth presently used, resist erosion better than previously used materials and appear to be adequate for in-service use. Rain erosion tests were run on Dynapore and electron beam perforated surfaces. See Section 9.3.4. The calendared wire cloth used by TKS is much coarser than that investigated as an LFC surface.

11.3.2.2 Washer System - A washer system could apply a cleaning fluid to a contaminated surface to weaken or dissolve the bond between a deposit and the aircraft surface. This system may be used alone or as part of a liquid-film system that also cushions the impact of an insect or a water spray that erodes the deposit. The unique feature of the washer system when compared with a liquid-film is that the washing fluid may be dispensed in a single application after the contamination encounter. This may result in a lower weight system. However, the more stringent requirements of a cleaning fluid will tend to make it more difficult to find a fluid compatible with a freezing-point-depressant ice protection system. Feasibility of the washer system depends primarily on locating a good cleaning agent that is also a freezing-point-depressant. Lachmann has demonstrated the feasibility of one type of washing system in Reference 11-9.

11.3.2.3 Erosion by Water Spray - When a liquid drop collides with a solid surface it exerts a localized pressure and then flows out radially from the point of impingement (Reference 11-14). In the case of a water drop colliding with a glass plate, the flow velocity immediately after the impact has been found to approach ten times the value of the impingement velocity (Reference 11-15). The radially flowing liquid then exerts a shear force on the surface of the solid over which it is running and a pressure force on any protrusion that it encounters. The combination of impact pressure, flow shear force, and flow pressure acting on a protrusion can be made to exceed either the cohesive or adhesive bond strengths and remove the contaminant.

Lachmann reported the results of insect removal by water spray in a wind tunnel (References 11-8 and 11-9). The tests evaluated the effect of jet size, water pressure, wind speed, and fluid properties. A two percent solution of liquid soap in water was found to work well probably due to the combined effect of erosion and washing as described previously. Lachmann concluded that "it is feasible to wash fly deposits off a wing leading edge by water jets and that the quantity of water required is....little more than.... 1.5 kg/m (1 lb/ft) length of leading edge...".

Tests by NASA using a JetStar aircraft were less encouraging; hard-shell portions of insect remains were not eroded. It would seem that a more comprehensive investigation is required.

11.3.2.4 Recommended Approach - Liquid System - Considering the functional, operational, and compatibility requirements defined in the INTRODUCTION, a liquid system that would appear to have the best change of success for contamination avoidance of the wing leading edge would include the following features:

(a) Distribution - spray nozzles, mounted on the shield, to minimize the complexity of the wing leading edge design and the conflict of space requirements with the suction system, although dispensing the liquid through the porous surface would use less liquid and is preferable if a practical design could be achieved.

(b) Fluid Properties - must include some form of freezing-point-depressant, contain a wetting agent, have low viscosity, and low surface tension.

(c) Flow Control - optimal operation would include variable or intermittent flow capability and ability to maintain a constant flow over a reasonable temperature range.

11.3.3 Electrically Powered Systems

A number of electrical/magnetic phenomena could be utilized for removing insect deposits, ice or other contaminants. The Russians have developed an Electro-Impulse (EI) de-icing system to shed ice. Ultrasonic vibration has been used to clean contaminated surfaces. Home ovens are being self-cleaned by pyrolysis and electrical heating is a possibility. Magneto-hydrodynamic forces have been used to divert flow fields. Each of these concepts was evaluated for applicability to the LFC contamination protection requirement.

11.3.3.1 Electro-Impulse - This de-icing concept is based on the forces developed by an induced magnetic field in the aircraft skin. A pulse of electric current is passed through a coil located in close proximity to the skin to be de-iced. The magnetic field created by the coil induces eddy currents in the conductive skin panel. The interaction of the magnetic field and induced currents causes mutual repulsion between the skin and coil (Reference 11-16), creating a hammer blow effect that sheds the ice formed on the surface.

The major problem areas anticipated with the use of the E-I system are (a) the space limitations due to the suction system requirements, (b) the requirement for the E-I system to deflect the skin coupled with the expected rigidity of the LFC outer panel, and (c) the possibility that the E-I system will not shed insect deposits. Generally, the E-I system ice shedding capability increases as ice cap thickness increases. The small mass of contamination may not produce the forces necessary for shedding.

Although direct use of the E-I system for insect protection may not be feasible, the E-I principle may be used with a coating. The coating may be a simple protective film or an electrically conductive film. A simple protective film would be removed in a manner similar to de-icing. The high energy impulse would accelerate the skin and the coating would break loose due to inertial forces. An electrically conductive coating would be subjected to an electro-magnetic repulsion force in addition to the inertial forces and may, therefore, require a lower energy pulse for removal.

11.3.3.2 Ultrasonic Vibration - A commonly used method of industrial cleaning is the immersion of a contaminated part in a liquid bath that is subjected to ultrasonic vibration. This cleaning method uses the "brushless scrubbing" effect of cavitation produced by the ultrasonic pressure waves. The process is especially effective for intricate parts and/or difficult to remove contaminants (Reference 11-17).

A conceivable inflight use of ultrasonic vibration would be to provide a large volume of fluid over the wing and simultaneously vibrate the surface. Practical considerations would include the thickness of the liquid layer required to sustain cavitation, the length of time that the liquid would need to be applied, and the physical installation of the transducers.

In view of the large quantity of liquid necessary to sustain cavitation, the difficulties expected in designing the transducers, and the space limitations expected to be imposed by the suction system, an in-flight ultrasonic cleaning system does not appear to be feasible. However, there may be justification for consideration of ultrasonic cleaning for ground use.

11.3.3.3 Thermal Decomposition - Contamination due to insect deposits can be removed by the application of heat. If the aircraft surface is heated sufficiently, either the bond between the insect deposit and aircraft would be weakened or the insect deposit would be thermally decomposed. In either case, the surface would be cleaned in a manner similar to that used for self-cleaning ovens.

Two major considerations must be evaluated before pyrolysis can be said to be feasible: compatibility of thermal decomposition requirements with material temperature limits and available electrical power. Self-cleaning ovens are usually operated at temperatures above 455°C (850°F) which is well above an acceptable temperature for aluminum. The power required to maintain this temperature level also appears to be excessive even if segmental cyclic heating is used. Based on these considerations, thermal decomposition of insect deposits does not appear to be a practical approach for insect protection.

11.3.3.4 Magnetohydrodynamics - Theoretically, MHD can be used to deflect the flow field and thereby control insect impingement. Two considerations have ruled this approach out immediately: the high magnetic field strengths required in practical applications and the need for an electrically charged fluid to produce the force.

11.3.3.5 Recommended Approach - Electrical System - None of the electrical systems appear to be feasible by themselves as an insect protection system. The electro impulse system might be feasible, however, if used in conjunction with a coating.

11.3.4 Disposable Covers

A number of investigations have been made of covers or coatings applied to the wing leading edge prior to takeoff and removed after the insect encounter. These covers may be categorized by the method of removal (dissolving, electrical, mechanical, or thermal) and by the form of the cover after removal (large sheet, small pieces, liquid or vapor). Four major concerns are common for these systems: (a) contamination of the environment, (b) effect of the disposed cover on the aircraft, (c) ground support and (d) the cover does not eliminate the requirement for an ice protection system on the fixed wing after the cover is removed.

11.3.4.1 Temporary Coating - A coating applied on the ground could protect the surface during takeoff and climb. The coating would be automatically released and would not interfere with cruise performance of the aircraft. Three categories of temporary coatings were investigated: polishes, controlled adhesion coatings, and subliming coatings.

A wax coating, polish or a release agent containing silicone, oils or teflon will reduce the adhesion of contaminants. These materials could be used in conjunction with a fluid system but fluid spreading would be difficult. If highly effective, they could conceivably be used without supplemental insect protection. A number of coatings are available as listed in Table 11-1. The major concern with a polish type coating is that the buildup of the coating may block or interfere with the suction perforations. Polishes would not be compatible with a porous suction surface.

TABLE 11-1. AVAILABLE COATINGS

GENERAL CATEGORY	IDENTIFICATION	SOURCE AND COMMENCS
TEMPORARY		
1. Waxes, polishes, and release coatings	Lethison release agent	Kemco Co., L.A.
	Cab-o-Sil Std	Cabot Corp.
2. Controlled Adhesion	Controlled Adhesion	DeSoto Corp. (not presently active but development could be reopened).
PERMANENT		
1. Teflon	Fluorocarbon, Teflon PFA	Dupont, available through applicators, applied by powder coating techniques.
	Teflon S958-211 and 954-101	Dupont, still available
2. Hard Surface	Abrasion resistant coatings	3M Co., available through Aerospace representative. Will coat samples for testing. Some wet material available in 1977.
	Formica UHM	Formica Corp., still available.
	Astrocoat RM-115 pi (Polyurethane)	Olin-Mathieson Chemical Corp. Available from Sterling Lacquer Corp.
	"Silicone" type hard coating	Dow Corning Corp., will coat sample and supply experimental quantities on request
3. Silicone	Insulgrease G-660 & G-635	GE Corp. Still available.
	Silicone coatings	GE; a group of these products is under evaluation at MDAC-West
	Silicone oil additive, Tec700	Tec Chem Corp. Monterey Park
4. Hydrophylic Coating	Under Development	3M Co., available through Aerospace Rep. Will coat samples for testing
5. Anti-Stick	Anti-Stick	3M Co.

A controlled adhesion coating could be applied prior to takeoff. Shear forces could be used to peel or flake the coating from the surface. Consistent adhesion control would be difficult as well as the problems previously described for polishes.

A subliming coating is conceivable which will have evaporated due to low pressure and airflow prior to reaching cruise altitude. This type of temporary coating is discussed under "Thermally Removed Coatings".

11.3.4.2 Chemically Removed Coating - A film may be applied to the wing leading edge prior to takeoff and washed off after climbing through the insect envelope. The film could be a gel or viscous fluid and remain in place for the initial climbout. Insects would impinge on the film and be trapped without impinging on the wing surface.

Tests run by Coleman (Reference 11-18) indicated that this system is probably feasible. Glycerine, glycerine and gelatine, and soap in methanol were tested. Glycerine by itself did not completely protect the surface. A mixture of 60 percent glycerine, 30 percent gelatine, and 10 percent wetting agent provided complete protection. Soap in methanol required much more water for removal. Conceivably, the washer system used to remove the soluble film could also be used for ice protection.

Two potential problem areas need to be explored before feasibility can be established: (a) find a material that is easily dissolved and will not clog the suction pores and (b) ensure that the insect residue is blown off the wing surface and does not adhere during its travel across the wing surface.

Although this method appears to be feasible, the complex ground operating procedures required to apply the coating reduce its attractiveness. This type of system should be considered further if some of the more desirable approaches prove impractical.

11.3.4.3 Electrically Removed Coating - As discussed previously, a coating may be removed by accelerating the skin or coating by means of the Electro Impulse (E-I) principle. Although no experimental work has been performed on this system, it is conceivable that a metalized sheet or coating could be applied prior to takeoff. After climbing above the insect envelope, the cover could be removed in one of several ways. If an E-I system is used for ice protection, the same system can be used to fragment a coating into small pieces which would be dispersed by aerodynamic and wind forces. A sheet-type cover, similar to that used by Lachmann (Reference 11-9), could be removed by a single E-I coil located at the wing leading edge near the root. Pulsing the E-I coil could be made to repulse the corner of the cover and initiate a tear along the leading edge. Aerodynamic forces could be made to complete the ejection of the cover in two halves. A metalized cover could also be held in place by magnetic force. After climbout above the insect level, the magnetic attraction could be interrupted and aerodynamic forces or electromagnetic repulsion used to remove the cover.

11.3.4.4 Mechanically Removed Cover - The contamination sensitive surfaces could be covered during takeoff and initial climbout. Upon reaching a predetermined altitude which is well above the insect envelope, the cover would be jettisoned. Lachmann described such a design in Reference 11-9 and Coleman reported work as long ago as 1945 by Smith and Higton (Reference 11-11) on this concept.

A variety of materials has been studied for this application including paper, tracing linen, cellulose sheet, plastic spray, and lacquers. To date, the greatest success has been achieved using a self-adherent, thin cellulose fiber matting. The cover was slit along the leading edge by a cutter that was subsequently retracted into the fuselage. Aerodynamic forces removed the cover.

One concern relative to the use of this system is whether the Environmental Protection Agency would allow ejection of the cover over land. A biodegradable cover would probably solve this problem; however, a cover that meets this additional requirement has not been found to date. Ground maintenance requirements are also a concern.

11.3.4.5 Thermally Removed Coating - The leading edge can be protected against contamination due to insect impingement by the application of a coating that is removed by heat. A layer of ice formed on the leading edge and subsequently removed by a thermal de-icing system is a feasible example of such an approach. Other general subcategories are:

(a) A flammable coating that is removed by an ignition source, e.g., an electric spark. The method was mentioned by Coleman (Reference 11-11) and rejected on the ground of safety.

(b) A volatile coating that is boiled off or evaporates in flight. This method was also mentioned by Coleman who reported unsatisfactory results during early tests. Although this method is probably feasible using thicker coatings and/or different materials, practical considerations minimize its attractiveness.

(c) A coating that melts, decomposes, or sublimates; e.g., an ice cap. Coleman experimented with this type of system and concluded that a layer of ice 6.3 to 9.5 mm (1/4 to 3/8 inch) thick should suffice to protect the wing from insects. On extremely hot days, a thicker layer would be required. An integral intensive cooling system in the wing leading edge would be needed. Sustaining an ice cap on the wing without cooling equipment would appear to be impractical due to the typical delays in takeoff clearance at many high density airports.

An ablative material can be envisioned that could be applied quickly on the ground and would be stable up to at least 93°C (200°F). A thermal ice protection system could be used to remove the ablation material at high altitude. Although this method is probably feasible, it does not appear attractive.

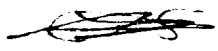

11.3.4.6 Recommended Approach - Disposable Cover - Disposable covers have three major disadvantages: contamination of the atmosphere, possible aircraft damage, and ground maintenance requirements. Soluble and electrically removed covers appear to have a low to moderate chance of success. Further investigation and testing is warranted to assess their practicality if the more promising approaches prove to be infeasible.

11.3.5 Special Surface Coatings for Contamination Avoidance

A permanent coating may be applied to the wing leading edge to either prevent contamination or to facilitate contamination removal. Three types of surfaces have been considered: (a) icephobic or anti-stick materials that have low bond strengths with ice or insect deposits, (b) elastic materials that cushion insect impact, and (c) hydrophylic materials that are easily cleaned.

11.3.5.1 Anti-Stick Coatings - A low bond strength between the ice or insect deposit and the wing surface can be achieved using any one of three basic approaches: (a) use of a superslick or icephobic material that possesses inherent low bond properties, (b) use of additives that cause a surface to exude oils or similar substances, and (c) use of a very hard, smooth surface. It has been postulated that aerodynamic forces would shed ice and other deposits from such surfaces. A number of coatings including Teflons, silicone elastomers, fluorocarbon elastomers, and greases (see Table 11-1) have been tested in icing tunnels. To date, no coating has been found that provides auto-release of the ice formed under these similated conditions (References 11-19 and 11-20) although some of the coatings did reduce the forces required to release the ice, compared with an untreated aluminum surface.

Four other major concerns exist in the use of anti-stick coatings: (1) Is the coating compatible with the roughness and waviness criteria for LFC? (2) Is the coating sufficiently resistant to rain, dust, and ice erosion to be practical? (3) Is the coating compatible with the suction system, i.e., can the coating be applied and not interfere with holes, slots, or porosity? And (4), will an anti-stick material shed insects? Limited experience on the Jetstar aircraft indicates poor insect shedding characteristics.

C-5

In view of the high probability of a negative answer to most of these questions, it is concluded that an anti-stick coating by itself is not a feasible insect protection system. However, it appears that anti-stick materials could be used in specialized applications with other insect/ice protection systems such as washers, shields, or vibrators. Their presence may increase the primary system efficiency enough to result in an overall weight and cost saving.

11.3.5.2 Elastic Coatings - Elastic coatings proved to be effective in cushioning the impact of insects at low velocity. By avoiding disintegration, the elastic coating prevents contamination by reflecting the insect from the surface. Three millimeter-thick, solid rubber and foam rubber with shore hardness 10-35 proved to be effective at velocities up to 56 m/s (108 kn) (Reference 11-21).

Some of the problem areas anticipated with the use of elastic coatings are: (1) erosion at moderate to high speeds, (2) ineffectiveness of insect protection at high speeds, and (3) incompatibility with suction and ice protection systems. Like anti-stick surfaces, elastic coatings do not appear to provide adequate insect/ice protection by themselves, but may prove useful in conjunction with other insect protection concepts.

11.3.5.3 Hydrophylic Coating - A hydrophylic material has an affinity for water so that it is easily cleaned with a water or alcohol rinse. One such coating is under development (Table 11-1) but to date no contamination tests have been conducted. Data are limited due to the newness of this concept. Further advances in hydrophylic materials development should be monitored to establish usefulness of this concept. The Jetstar program has investigated two hydrophylic coatings with results about the same as for the "superslicks".

11.3.6 Contamination Protection - Initial Conclusions

The preliminary evaluation of the various concepts that could provide contamination and/or ice protection for the LFC aircraft wing leading edge indicates that a number of approaches offer promise of being feasible.

Three approaches were selected as offering the best chance of success or having unique characteristics that are desirable for the LFC aircraft.

(1) A shield that normally forms part of the wing lower surface that can be extended to a position in front of the leading edge. The shield would contain a liquid system for contamination and ice protection.

(2) Spray nozzles located in the wing leading edge or in the aft face of a shield, that distribute a washer/deicing fluid over the impingement area. The distributed liquid is required to inhibit the adhesion of insects and act as a freezing-point-depressant.

(3) A liquid system similar to (2) above except that the spray nozzles are replaced by a porous distribution panel in the wing leading edge.

11.4 SHIELD PRELIMINARY DESIGN AND PERFORMANCE EVALUATION

Investigations were conducted to determine the compatibility of the various shield concepts (rigid, folding and variable camber) with the space constraints and the performance requirements of the LFC aircraft. This section presents the results of design and analytical studies and the resulting design recommendations.

11.4.1 Preliminary Design Studies

Feasible installations of the three types of shields are shown in Figures 11-10 through 11-12. Figure 11-10 shows a rigid shield with a simple hinged deploying mechanism. Although this concept limits the shield size and location of the trailing edge, the simplicity and compactness of the design may make it suitable for early flight tests and in areas of limited space. This concept would provide the least aerodynamic benefit to the aircraft. Flexible hoses are used for the liquid supply lines and are routed along and supported by the hinges. An alternate design using rigid tubing and swivel fittings is also feasible.

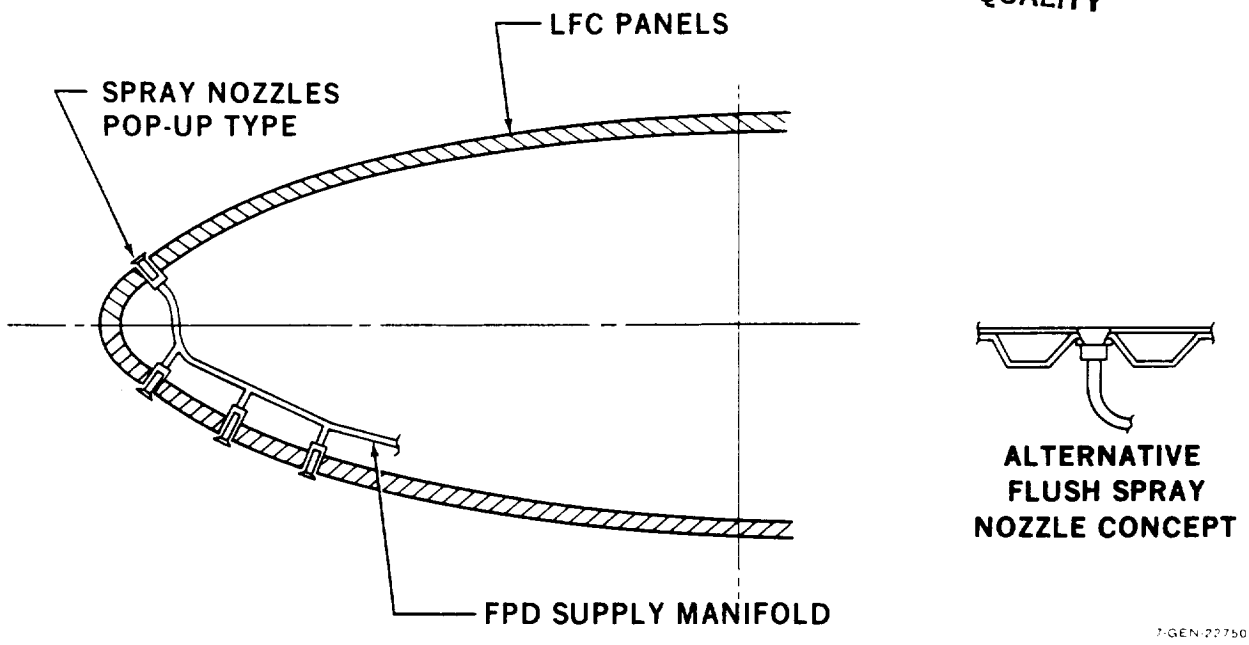

FIGURE 11-9. PRELIMINARY CONCEPT OF FREEZING-POINT DEPRESSANT SPRAY ON FIXED LE

(1) SHIELD SURFACE MAY BE USED FOR FPD DISTRIBUTION
(2) ELECTRICAL IMPULSE DE-ICING MAY BE USED ON TIP

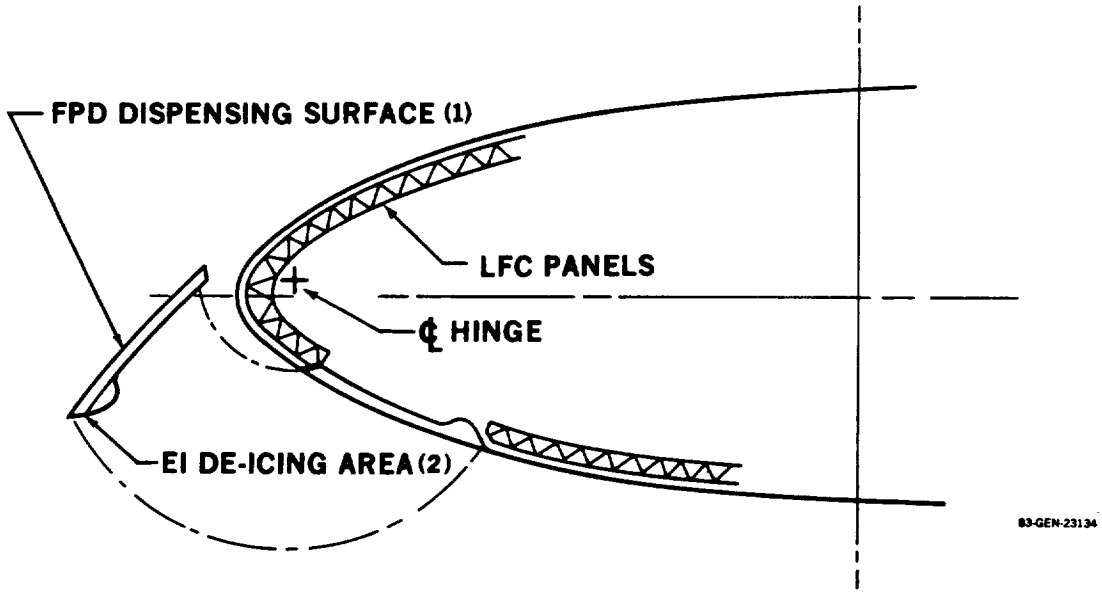

FIGURE 11-10. RETRACTABLE SHIELD – DEPLOYED FOR INSECT/ICE PROTECTION

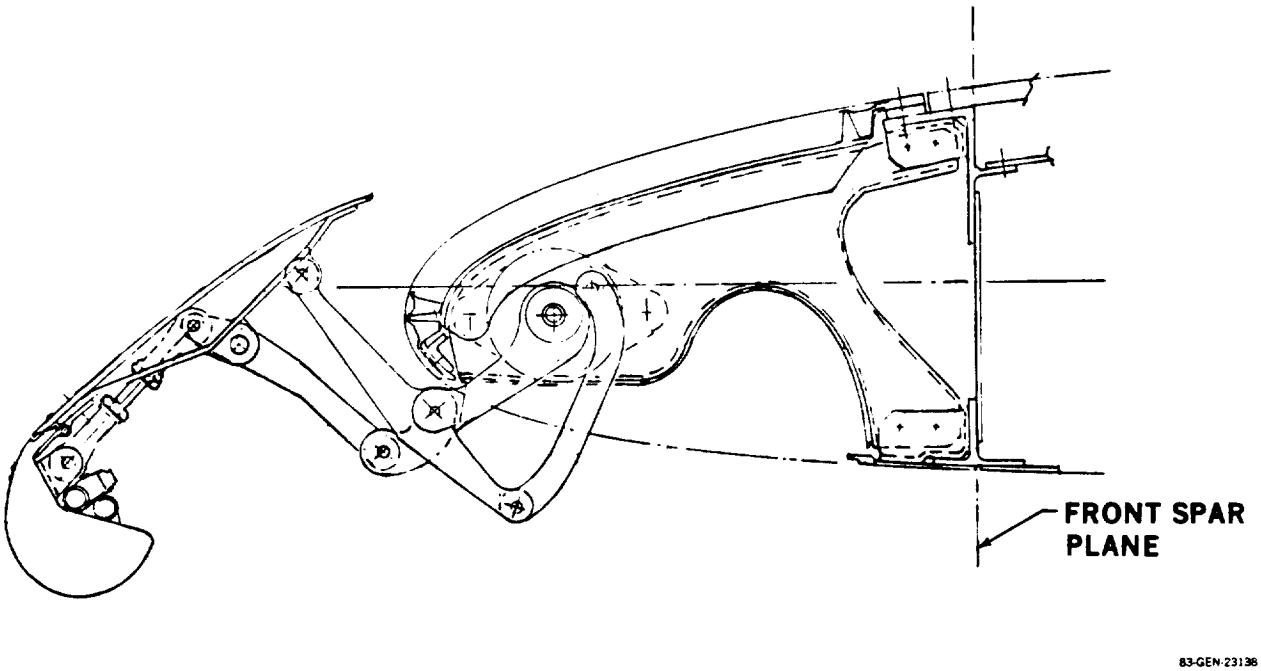

FIGURE 11-11. FIXED CAMBER SHIELD (EXTENDED)

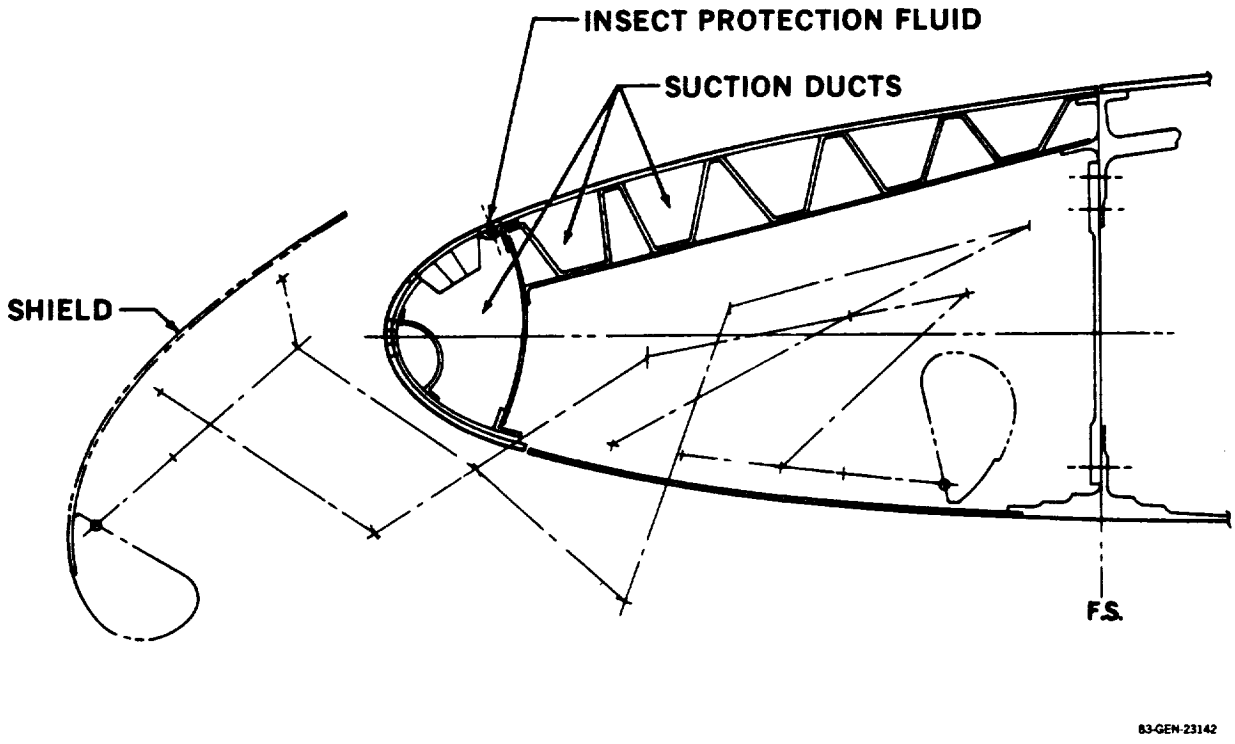

FIGURE 11-12. VARIABLE CAMBER SHIELD (EXTENDED)

The fixed-camber, folding-shield concept (Figure 11-11) permits the use of a larger shield with increased protection for the upper wing surface. The complexity of the linkage and drive mechanism will require a more extensive development effort than the rigid design.

The variable-camber shield shown in Figure 11-12 combines the good shielding qualities of the folding shield with high lift capability and is the most likely arrangement to be used in a commercial application. The length of the shield shown in the Figure is 12 percent of the chord length. The contour of the shield is similar to the high lift device designed for a Douglas Advanced Commercial Aircraft. This design was used for many of the preliminary shielding effectiveness analyses.

If ice protection of the shield is required for aerodynamic or stowage considerations, two methods are feasible. Flexure of the variable-camber devices would provide some de-icing capability as on current commercial applications. The preferred method is the use of a freezing-point-depressant applied through a porous distribution panel as described in Section 11.5.

11.4.2 Contamination Avoidance Effectiveness Analyses

As the laminar flow aircraft encounters an insect or other potential source of contamination, the insect will be affected by the flow disturbance of the approaching aircraft. The initial position and motion of the insect relative to the wing determine whether or not the insect will impinge on the wing and create a source of turbulence. This problem is very similar to the problem of ice accretion on a wing leading edge, for which a number of analytical solutions are available (References 11-22 through 11-24).

11.4.2.1 Computer Programs - The most applicable tool available at Douglas for this type of analysis is computer program H9PB, "Water Impingement on Two-Dimensional, Multi-Element Airfoils". This program has the capability of analyzing the trajectory of a droplet in the flow-field induced by an airfoil

composed of as many as ten elements. An iterative, stepwise solution is used to solve the differential equations of motion in cartesian coordinates. The coefficient used in the equations to described the drag-inertial characteristics of the droplet is $\frac{C_D R_e}{24 K}$, where

C_D is the drag coefficient

R_e is the Reynolds number based on air properties, droplet diameter and droplet relative velocity

K is the inertia parameter $\frac{2}{9} \frac{r^2 Vo \rho_w}{C \mu a g}$ from Reference 22

Coleman, in Reference 11-25, derives similar equations for insect trajectories using a drag-inertial coefficient defined as $\frac{C k Vd}{Vo}$, where:

C is the chord length

k is the insect ballistic coefficient in $(length)^{-1}$ units

Vd is the insect relative velocity

Vo is the free stream velocity

To permit insect trajectory analyses, computer program H9PB was modified so that the insect ballistic coefficient (k) and airfoil chord (C) would be substituted in appropriate places for the droplet parameters.

Flow field velocities and body coordinates were generated by a separate computer program using the Neumann method for angles of attack of 0^o and 90^o. These data are input to program H9PB which modifies them for the angle of attack being considered. Special techniques are provided to obtain sufficient accuracy of the flow field near body surfaces.

The output of computer program H9PB includes a tabulation of the coordinates of the droplet (or insect) relative to the airfoil as the particle moves towards the airfoil. Particle and air velocities are also tabulated. To facilitate the evaluation of the data, a graphics computer program was developed to display the trajectory output data of H9PB.

11.4.2.2 Shielding Analysis - Three existing airfoil designs, available from the Douglas Advanced Commercial Aircraft (ACA) program, were used as the basis of the study. (1) A two-element section at the 90 percent span wing station was used to evaluate the wing tip and zero flap conditions. (2) A four-element section at the 80 percent span wing station was used to evaluate the effect of full flaps (50^{o}). And (3), a model at 13 percent with a flap angle of $27\ 1/2^{o}$ was used to evaluate the inboard airfoil which has a much blunter leading edge that extends above the shield.

Another major variable in the analysis is the angle of attack. Contaminants may impinge on the wing leading edge during the takeoff roll, rotation, and climbout. During this time, the aircraft angle of attack may vary from 0^{o} to 9^{o}. To determine the range of airfoil angle of attack, it is necessary to add the wing incidence angle. Figure 11-13 shows the wing twist used to determine the local incidence angle. Note that the wing tip is at -2^{o} when the wing root is at $+5.5^{o}$. Angles of attack of -4^{o}, 0^{o} and 15^{o} were used to bracket the anticipated range of wing section angle of attack with respect to the free stream. Other parameters that were varied during the analysis included insect, the ballistic coefficient (k), the airfoil chord length (C), and the aircraft velocity (Vo).

A number of runs were made to correlate the results of the insect trajectory analysis with results of droplet analyses under identical conditions. A 900 micron droplet trajectory was found to be almost identical to an insect trajectory with a k of 0.66/m (0.2/foot). An insect having a k of this value weighs about 0.8 mg. A spherical droplet weighing 0.8 mg would have a diameter of 1150 microns.

11.4.2.3 Trajectory Analysis -

(a) Flaps Retracted - The two-element airfoil section at the 90 percent wing span location was chosen to represent the wing tip and the main wing area after flaps have been retracted. An insect ballistic coefficient of 0.66/m (0.2/ft) was used. This represents an insect weighing about 0.8 mg which is heavier than about 90 percent of the insect population. Two angles of attack were selected: 0^{o} to represent the worst condition for impingement above the shield and $+15^{o}$ to represent the worst condition below the shield.

Figure 11-14 presents the results of the trajectory analysis at 0^{o} angle of attack. A small amount of impingement is noted above the shield and none below. The trajectory analysis predicts that insects starting at a position between 0.030 and 0.035 chord lengths above the leading edge will impinge on the wing. This represents a shielding effectiveness of about 94 percent.

The fact that insects impinge on the wing above the shield does not necessarily mean that the resulting contamination will cause turbulence. Based on data from Reference 11-25 it can be seen that insects that impact at an angle of less than about 7^{o} with respect to the surface do not leave a residue greater than 0.102 mm (0.004 inch) height. The maximum angle of impact from Figure 22 is 5^{o} which implies that the insect residue will be less than 0.102 mm (0.004 inch) height, and should not cause transition.

Figure 11-15 presents similar results at an angle of attack of 15^{o}. Since the shield is designed for LFC on the upper wing surface only, impingement as shown is acceptable.

(b) Landing Flaps - A four-element airfoil section model at the 80 percent wing span location was available for this analysis from the Douglas ACA program. The flaps were extended to 50^{o}, representing the approach and landing situation. Three angles of attack (α) were considered:

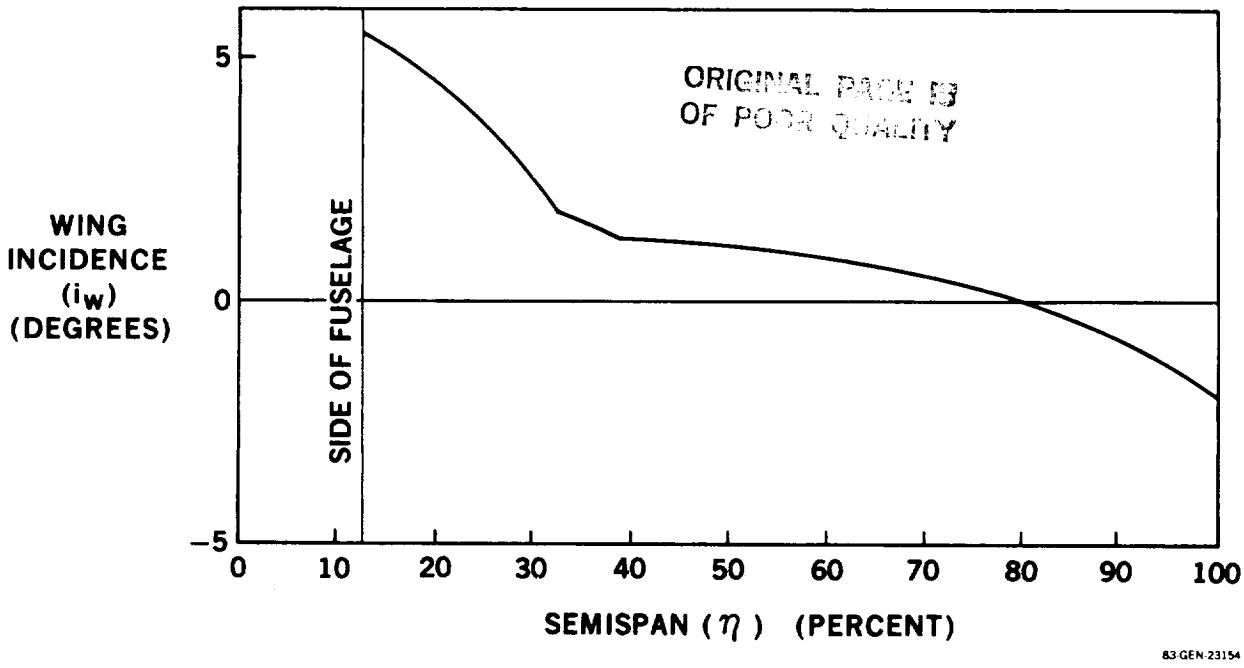

FIGURE 11-13. LFC WING CHARACTERISTICS

ACA WING AT 90-PERCENT SPAN LOCATION

INSECT AERO COEF (K) = 0.200 PER FT
ANGLE OF ATTACK = 0.0 DEGREES

CHORD LENGTH = 2.22 m (87.4 IN.)
AIRSPEED = 74.6 m/s (145 KIAS)

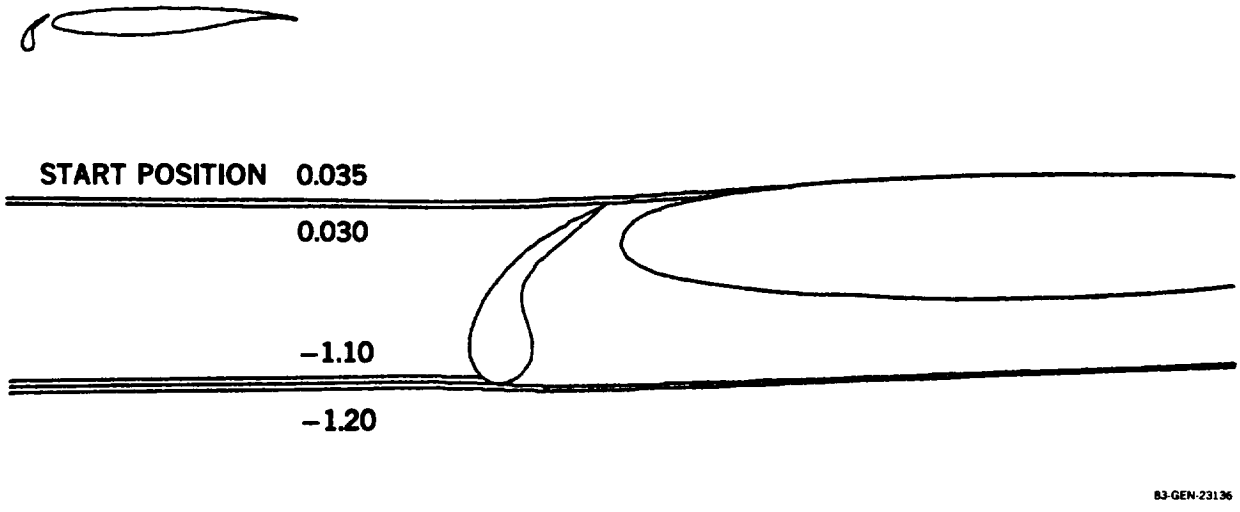

FIGURE 11-14. INSECT TRAJECTORIES – SEA LEVEL, TAKEOFF

-4^{o} and 0^{o} representing the landing roll out phase which is the worst case for impingement on the wing upper surface and $+15^{o}$ representing the approach and flare out phases during which impingement under the shield is critical.

Figure 11-16 presents the results of analyses at $\alpha = 0^{o}$ and insect ballistic coefficient (k) of 0.1. The results indicate that insects will not impinge on the upper surface under these conditions.

Figure 11-17 presents similar results at $\alpha = -4^{o}$. Impingement is possible only with very dense insects ($k > 0.1$).

Figures 11-18 through 11-20 present the results of an analysis at $\alpha = +15^{o}$ illustrating the effect of k varying between 0.1 and 0.35. The concern is that the lighter insects would be forced upward by the airflow between the shield and the wing and impinge near the wing leading edge. In cruise, the attachment line point is in the region of $\pm$ 0.6 percent of a chord length from the leading edge and, therefore, any point above the -0.6 percent point should be considered as the "upper surface" and must be protected.

Figure 11-18 shows no critical impingement for large or dense insects. The other figures in this group show that light insects that start in a narrow band (0.5 to 1.0 percent chord wide) could impinge near the wing leading edge.

If it is assumed that the wing without the shield would intercept insects in a band 10 percent of chord wide, the Krueger is about 90 percent effective in shielding the leading edge under the foregoing conditions. At lower angles of attack or flap setting, the shield would be more effective. It is not essential to have fully effective shielding in the landing configuration because the leading edge could be wiped clean before takeoff.

ACA WING AT 90-PERCENT SPAN LOCATION

INSECT AERO COEF (K) = 0.200 PER FT
ANGLE OF ATTACK = 15.0 DEGREES
CHORD LENGTH = 2.22 m (87.4 IN.)
AIRSPEED = 74.6 m/s (145 KIAS)

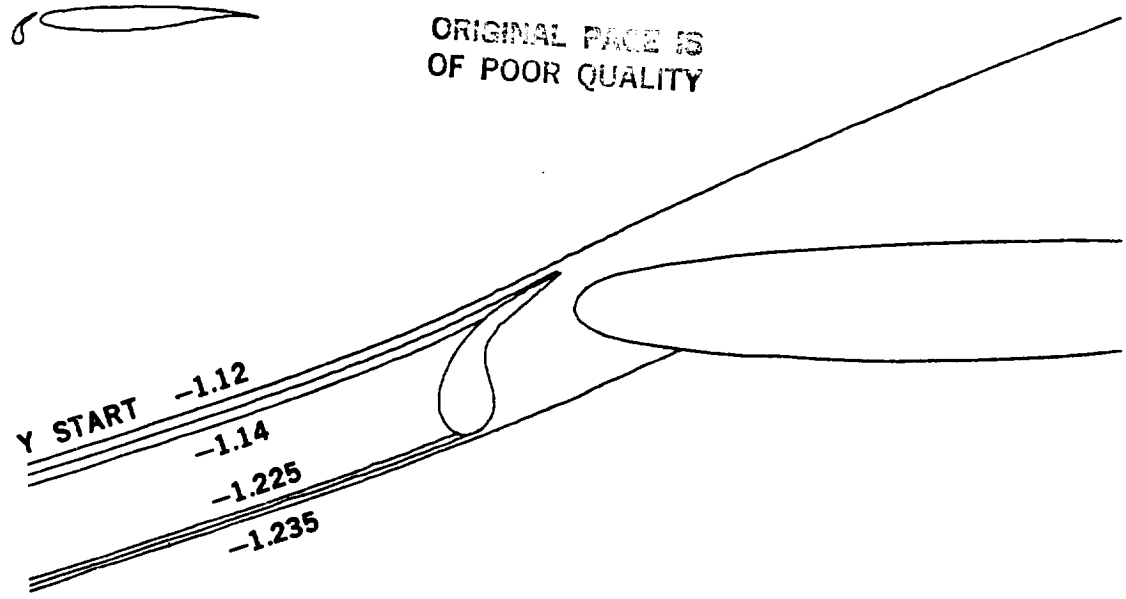

83-GEN-23139

FIGURE 11-15. INSECT TRAJECTORIES – SEA LEVEL, TAKEOFF

ACA WING AT 80-PERCENT SPAN LOCATION

INSECT AERO COEF (K) = 0.100 PER FT
ANGLE OF ATTACK = 0.0 DEGREES
CHORD LENGTH = 2.47 m (97.1 IN.)
AIRSPEED = 74.6 m/s (145 KIAS)

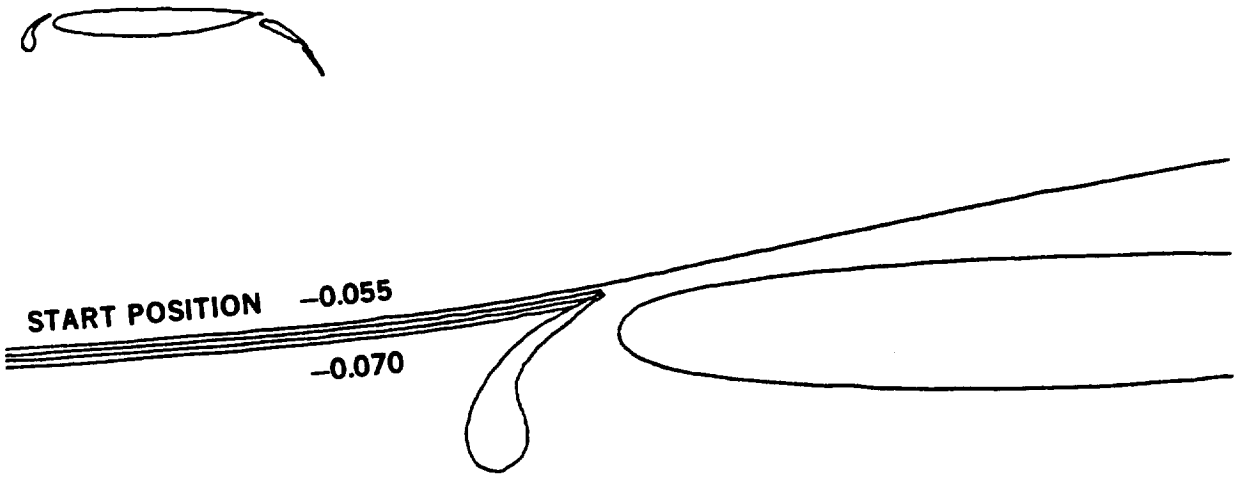

83-GEN-23143

FIGURE 11-16. INSECT TRAJECTORIES – SEA LEVEL, TAKEOFF

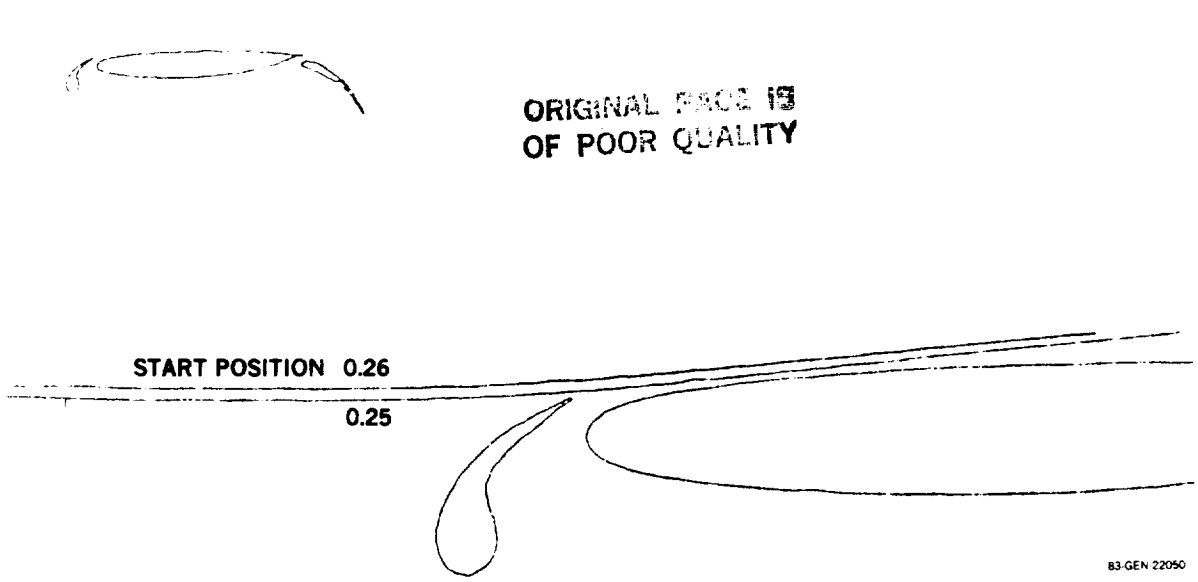

FIGURE 11-17. INSECT TRAJECTORIES – SEA LEVEL TAKEOFF, –4-DEGREE ANGLE OF ATTACK

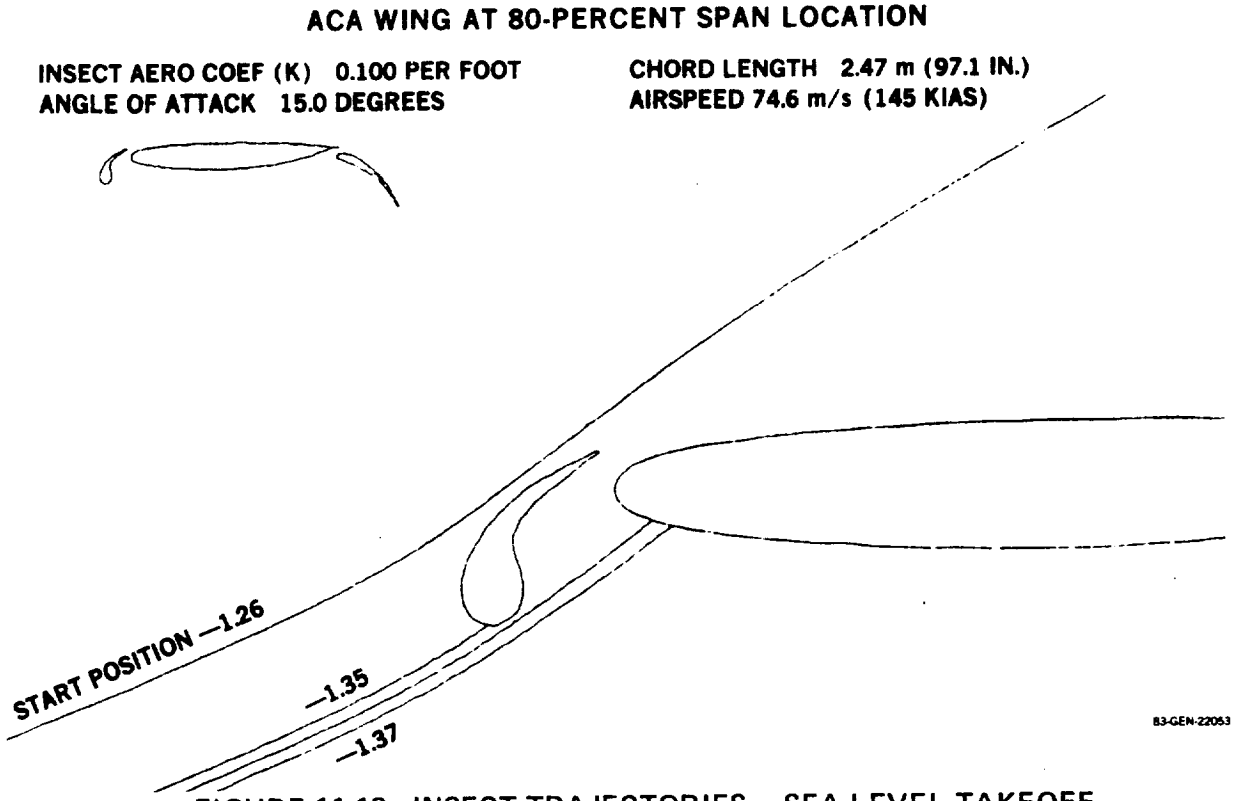

FIGURE 11-18. INSECT TRAJECTORIES – SEA LEVEL TAKEOFF, 15-DEGREE ANGLE OF ATTACK

ACA WING AT 80-PERCENT SPAN LOCATION

INSECT AERO COEF (K) = 0.250 PER FT
ANGLE OF ATTACK = 15.0 DEGREES
CHORD LENGTH = 2.47 m (97.1 IN.)
AIRSPEED = 74.6 m/s (145 KIAS)

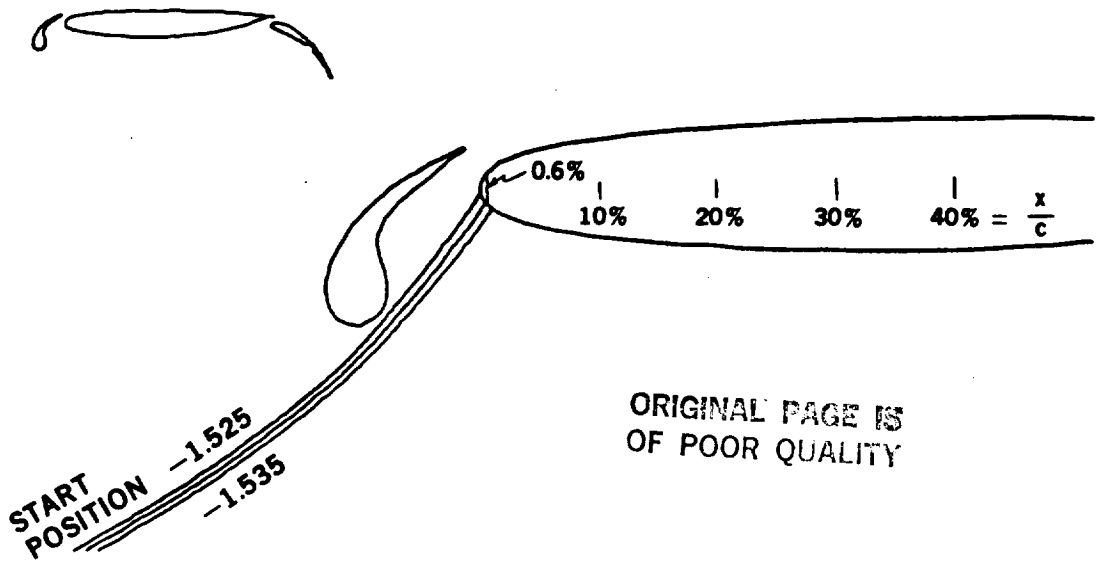

83-GEN-23141

FIGURE 11-19. INSECT TRAJECTORIES – SEA LEVEL, TAKEOFF

ACA WING AT 80-PERCENT SPAN LOCATION

INSECT AERO COEF (K) = 0.350 PER FT
ANGLE OF ATTACK = 15.0 DEGREES
CHORD LENGTH = 2.47 m (97.1 IN.)
AIRSPEED = 74.6 m/s (145 KIAS)

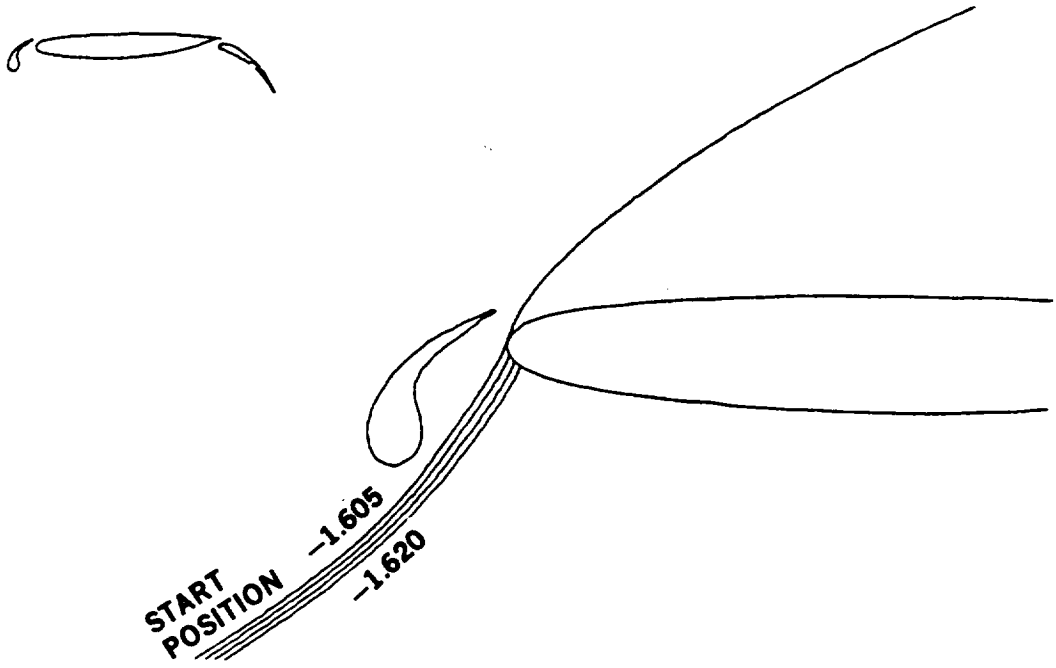

83-GEN-23140

FIGURE 11-20. INSECT TRAJECTORIES – SEA LEVEL, TAKEOFF

(c) Takeoff Flaps - A four-element airfoil section model of the 13 percent wing span location was available for this analysis from the Douglas ACA program. The flaps for this model are extended 27 1/2^{o} to represent the takeoff configuration. The inboard wing section selected is much more blunt than the section outboard of the suction engine and is therefore more susceptible to insect impingement.

Figure 11-21 presents an insect trajectory at $\alpha = 0^{o}$ and $k = 0.2$. It is apparent that insects would impinge on the upper surface at an angle steep enough to create protuberances greater than 0.102 mm (0.004 inch) in height. Figure 11-22 shows a similar condition with the angle of attack increased to 15^{o}. Again, impingement on the inboard leading edge region is predicted. The band in which insects will impinge on the leading edge is about 1 percent of the chord length.

11.4.2.4 Effectiveness Analysis - Conclusions - Based on the results of the trajectory analyses, it is concluded that a Krueger-type shield will provide substantial contamination protection in the critical stagnation region. The analysis indicates three potential areas of concern:

(1) In the inboard area where the wing thickens, impingement could occur on the wing upper surface to an extent that would disrupt laminar flow unless supplementary liquid protection were provided.

(2) In the wing tip area where the angle of incidence is negative, the computer program predicts that impingement could occur on the upper surface during the ground roll. However, since upwash and ground effects are not included in the analysis, there is a high probability that the extent of impingement would not pose an operational problem.

(3) The computer program predicts impingement by light particles travelling under the shield at a high local angle of attack. Considering wing twist and thickness, the inboard wing is more susceptible to this condition. However, the deposit left by a light particle is not expected to be thick enough to disrupt laminar flow.

ACA WING AT 13-PERCENT SPAN LOCATION

INSECT AERO COEF (K) = 0.200 PER FT
ANGLE OF ATTACK = 0.0 DEGREES

CHORD LENGTH = 2.47 m (97.1 IN.)
AIRSPEED = 74.6 m/s (145 KIAS)

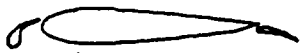

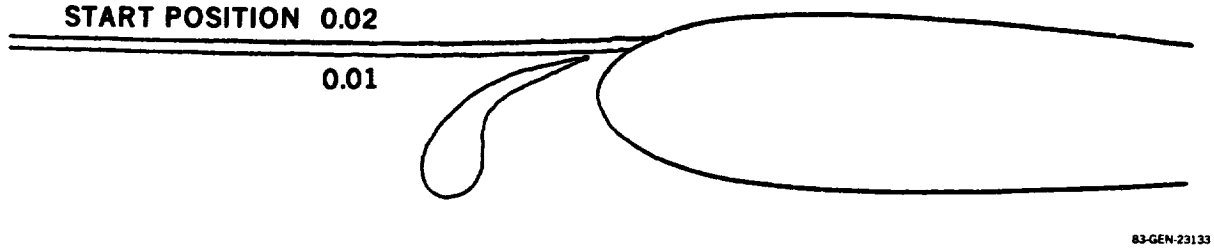

FIGURE 11-21. INSECT TRAJECTORIES – SEA LEVEL, TAKEOFF

ACA WING AT 13-PERCENT SPAN LOCATION

INSECT AERO COEF (K) = 0.200 PER FT
CHORD LENGTH = 10.16 m (400 IN.)
AIRSPEED = 74.6 m/s (145 KIAS)
ANGLE OF ATTACK = 15.0 DEGREES

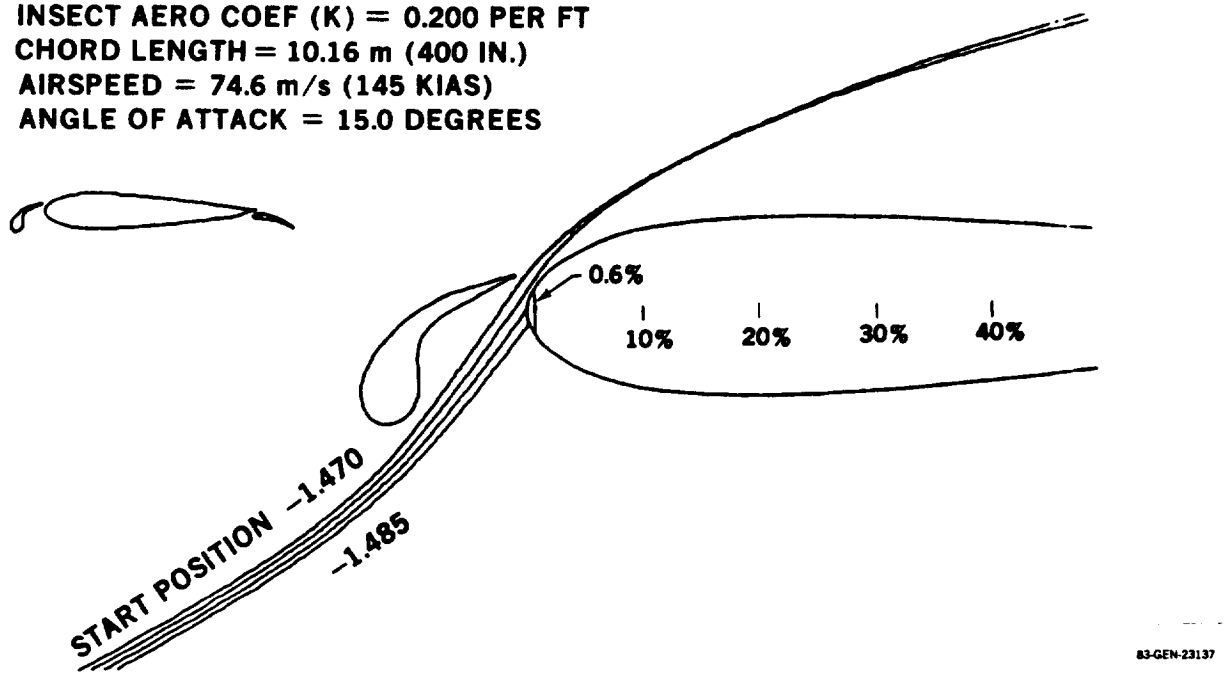

FIGURE 11-22. INSECT TRAJECTORIES – SEA LEVEL, TAKEOFF

11.4.3 Wind Tunnel Test of Shield Effectiveness

To determine the practical effectiveness of the shield concept, insect impingement testing was done in the Icing Tunnel Facility at NASA Lewis Research Center. The model was a DC-9 wing tip on which a representative fixed leading edge shield was installed. Insects were released upstream from a series of containers set at an angle to the plane of the wing so that a number of streamlines were represented along the span. This arrangement is illustrated in Figure 11-23.

The test results supported the theoretical analysis. Angles of attack ranged from -4 degrees to +7 degrees. At an angle of attack of -4 degrees, insect contamination of the upper surface occasionally exceeded a critical height of about 0.1 mm (.004 inch). This indicated that a more extensive shield or a supplementary liquid protection system may be required in the wing tip region, where negative angles of attack would exist during taxiing and at takeoff roll.

11.4.4 Shield Operational Use

The shield would be extended on the ground prior to brake release to provide protection from airborne contaminants and ice during the ground roll and climbout. Normally, the shield would be retracted at or below 1524 m (5000 feet) on climbout, depending on flight test experience. If icing conditions are anticipated at higher altitudes, shield retraction could be delayed. The shield would normally be re-extended during descent at altitudes below 1524 m (5000 feet) or under icing conditions.

Normally, icing conditions are not encountered at the cruise altitudes associated with LFC aircraft operation. In the very unlikely event that icing conditions are encountered during cruise that result in the loss of laminarization, the flight could be continued in the turbulent mode or the shield could be extended and the wing de-iced. The actual operating procedure will vary depending upon the experience of the particular airline operator. The possibility of encountering such icing conditions would vary with route structure and seasonal conditions.

11.5 SHIELD ICE PROTECTION SYSTEM

Except for infrequent occurrences, icing conditions are only encountered at the lower altitudes of commercial aircraft operation. Generally, this limits consideration of ice protection system performance to takeoff, initial climb-out, descent, landing and holding during either departure or landing. Large accumulations of ice are the result of continued exposure of the surface to icing conditions for long periods of time. The most severe icing encounter found during the analysis of the DC-9/DC-10 fleet was a 15 minute departure hold followed by a 30 minute landing hold.

The combination of the Shield/Liquid-Film ice protection system is capable of providing protection during all of these flight conditions. If operated as a de-icing system, a fluid capacity for three cycles per flight should be adequate. For an anti-icing system a capacity for one hour of operation should be sufficient. For operational flexibility, the liquid storage capacity should be sufficient for two flights.

A schematic diagram for a liquid-film ice protection system is shown in Figure 11-24. Additional porous panel dispensing units would be fed in parallel using multiple flow-metering valves as required.

The supply tank, pump, filter and check valve would be mounted on a panel in the pressurized area of the fuselage. The supply tank would include a sight gage and a remote indication of fluid level. A slight positive pressure could be provided by the pneumatic system (or other suitable source) if desirable for pump operation.

Typically, a piston type positive displacement pump with an integral relief mechanism, driven by a 28 volt d.c. motor, would be used and the flow rate would be pre-set on assembly. The system would be designed so that the normal operating pressures fall within the constant flow region of the pump characteristic. Due to the increase in fluid viscosity, operation at low temperatures (i.e., below $-40^{o}C$) will give rise to higher pressures, and under these conditions the pump output flow rate falls so that the pressure does not exceed a pre-set value.

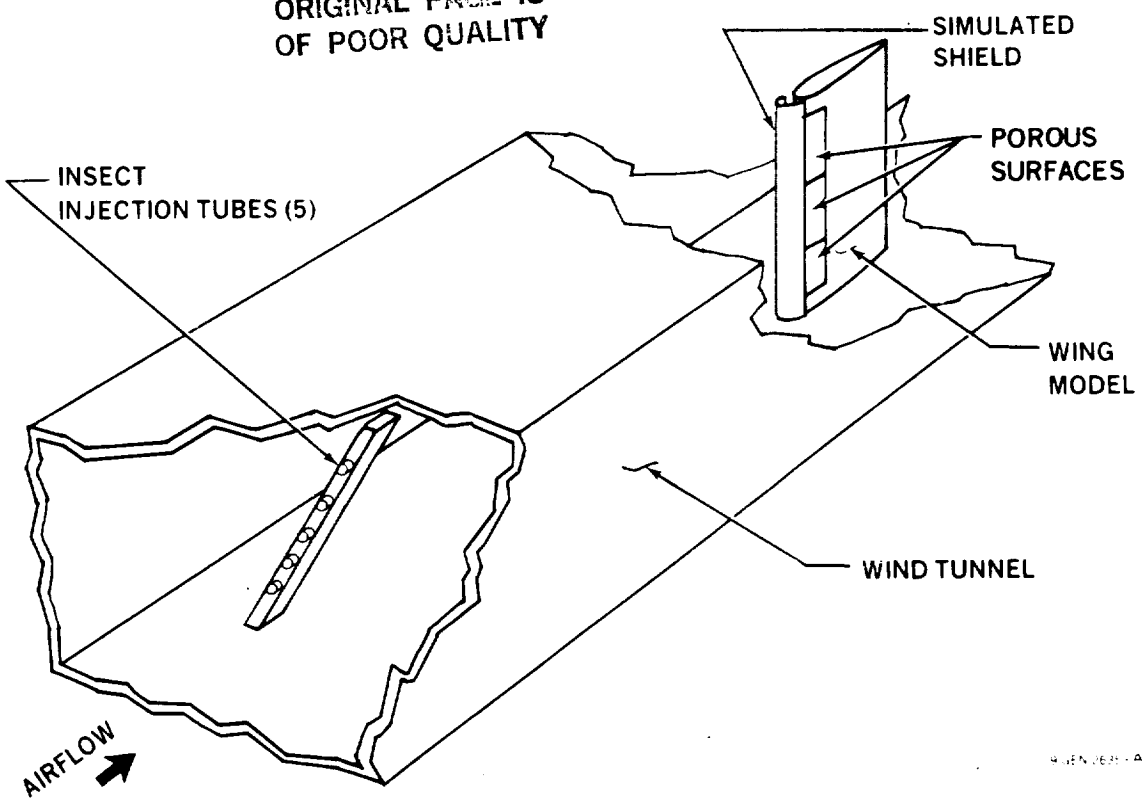

FIGURE 11-23. INSECT IMPINGEMENT TESTS IN LEWIS ICING TUNNEL

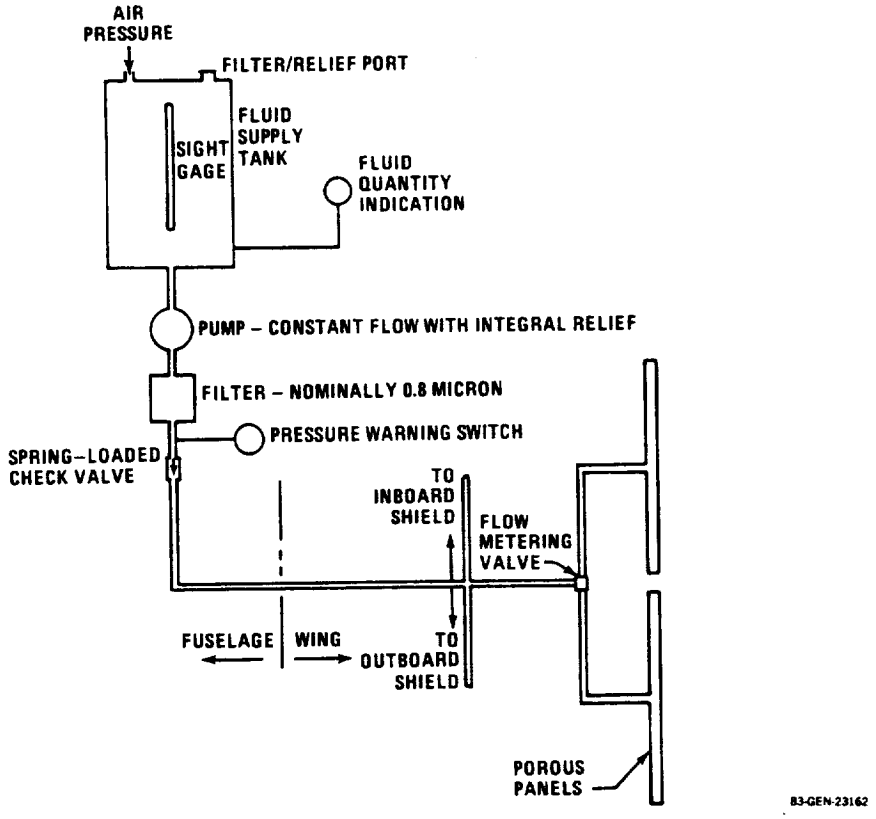

FIGURE 11-24. SCHEMATIC DIAGRAM OF LFC L.E. ICE PROTECTION SYSTEM

A fine filter (nominally 0.8 micron) is required to prevent blockage of the porous panels by contaminants introduced with the fluid. A bypass and a differential pressure indicator are unnecessary. The pressure drop across the filter would vary widely due to the viscosity variation as a function of temperature. A spring-located check valve would minimize loss of fluid during maintenance operations or during flight with the pump OFF.

It is envisaged that the porous panels would provide an active region as shown in Figure 11-25 and would be divided into individual panels about four feet long.

The system can be operated in either the de-icing or anti-icing mode. Generally, anti-icing requires about twice the flow rate needed to de-ice and may require a longer period of operation. For example, three de-icing cycles could be achieved in fifteen minutes compared to an estimated one hour capability required for an anti-icing system. Using these ground rules, the weight of fluid required for anti-icing is eight times that required for de-icing. To provide ice protection capability for two flights, a typical LFC large transport aircraft would require about 82 kg (180 lb) of liquid based on a de-icing system and 653 kg (1440 lb) based on an anti-icing system. A combined system that anti-ices the wing in frontof the engines and de-ices the remainder of the wing would minimize the liquid required to provide adequate protection. De-icing forward of the engine is not acceptable due to the possibility of large ice particle shed from the wing entering the intake.

11.6 LIQUID-FILM PRELIMINARY DESIGN AND PERFORMANCE EVALUATION

Numerous studies have shown that once insects adhere to the wing surface, it is extremely difficult to remove them. The liquid-film concept prevents adhesion by coating the wing leading edge with a thin film of liquid. The liquid cushions the impact, prevents adhesion, and carries the insect debris aft along the wing and off the trailing edge.

Two methods were considered as a means of applying the liquid to the wing:

(1) a porous distribution panel through which the liquid was forced, and

(2) spray nozzles mounted on the aft face of a Krueger-type shield and directed toward the wing leading edge.

The term liquid-film will be used to denote the former concept. Performance and design of the spray system is discussed in Section 11.7.

11.6.1 Preliminary Design Studies

The liquid-film system can provide integrated ice protection and contamination control. A freezing-point-depressant (FPD) that has good spreading properties and other properties compatible with aircraft use (non-toxic, low flammability, etc.) is required to protect against both insects and ice. Other properties such as viscosity and surface tension may be critical to ensure that insects are swept off the wing and that the liquid can be cleared from the small pores of the porous suction surface. The recommended liquid formulation is discussed in detail in Section 11.6.3.

The system schematic would be identical to that of the shield ice protection system shown in Figure 11-24, except that the flow and liquid capacity would be increased. The description of system components and functional operation presented in Section 11.5 also applies. The unique features of the liquid-film system for the LFC aircraft are associated with (1) variable flow rates to meet the requirements of both ice protection and contamination avoidance

with reasonable quantities of liquids, (2) integration of the liquid-film distribution panels with the LFC suction panels in the stagnation region, and (3) selection of a FPD fluid compatible with an LFC aircraft using porous suction surfaces.

Analyses of the trajectories of insects indicate that the upper surface dispenser must protect against direct impingement for distances slightly less than 10 percent of the chord length whereas the lower surface dispenser must provide protection to at least half the chord length.

A unique problem exists in the attachment line region when attempting to keep the wing leading edge completely wetted. The liquid will stream away from the attachment line and, therefore, a dry area will tend to form whenever the attachment line lies in an area outside of the dispensers. For this reason, liquid should be dispensed onto the entire region through which the attachment line travels. On the LFC aircraft the region through which the attachment line travels also requires suction. These conflicting requirements necessitate either (a) a system that can alternatively provide liquid dispensing or suction capability for the same surface area or (b) a system that meets the suction requirements in a series of narrow spanwise strips permitting liquid dispensers between the suction areas. All concepts that were developed to interconnect the suction and liquid systems were felt to be impractical from the reliability and maintainability points of view.

With separate liquid and suction systems, spanwise liquid distribution channels could be molded into the laminated glass substructure. A single chordwise liquid distribution channel could then be used to connect the inlet with the spanwise channels.

For a takeoff through a contaminated area, the liquid-film system that protects the attachment line region would be turned on prior to taxiing to the runway. Gravity and wind would ensure a fairly complete initial coverage of this portion of the wing while the aircraft is in the static condition. During the ground

roll the position of the attachment line will depend on flap position, wing incidence with respect to the fuselage, and the effect of the ground plane. It is expected that some portions of the leading edge would start to dry, but during rotation all regions that have started to dry would be completely rewetted. Similar changes in angle of attack as gears and flaps are retracted would again rewet any dry areas. Attachment line travel during acceleration and oscillations of the attachment line during climbout would continue to rewet areas that started to dry. It is expected that a fluid that does not dry in twenty seconds could keep the attachment line region wetted.

High flow dispensers would be used to form a liquid-film over the wing leading edge aft of the attachment line region using the high-initial-flow/low-sustaining flow method developed during tests described in Section 11.6.4. During the initial phase of the ground run, the leading edge would be completely wetted by the use of a high flow rate for a short time (less than ten seconds). The surfaces would then be kept moist by a low sustaining flow. At a pre-selected time or altitude, possibly 1520 m (5000 feet), high flow would be used to wash off all debris over the trailing edge of the wing. The regulator supplying the high-flow system would require two pressure settings to provide the capability for the foregoing operation.

In order to ensure a smooth surface in the critical leading edge region, the entire surface would be of one piece construction from the upper surface at the front spar, around the leading edge to about 6.5 percent of a chord length aft of the leading edge on the lower surface. This subassembly would consist of the nose "D" duct with the suction and liquid-film ducting installed and the upper suction surface with spanwise metering ducts. The upper and nose regions would be attached to the main structure using internal fasteners. The remainder of the leading edge cavity surface would be provided by a lower panel assembly extending to the front spar. The nose section would contain the spanwise collector ducts in addition to the suction surface and metering ducts. The lower panel could be removed for maintenance and to gain access to the internal fasteners attaching the upper panel. Internal panels in the "D" duct would provide access to the liquid-film system and nose ducting.

11.6.2 Experimental Evaluation of the Liquid-Film Concept

Tests were conducted in the Douglas Low Speed Wind Tunnel to investigate four key aspects of the liquid-film concept:

- o Liquid Distribution: the ability of the liquid to completely cover the wing leading edge.
- o Removal of Debris: the ability of the liquid to transport contaminants off the wing.
- o Residual Film: the degree of surface roughening caused by the liquid residue and its effect on laminarization.
- o Clogging and Clearing: the effect that the liquid has on the suction surface porosity and methods of clearing a porous surface if it becomes clogged with liquid.

The flat plate test model used previously for laminar flow evaluation of porous surface specimens in the wind tunnel was used for these tests. Two of the 3 m x 1.2 m (4 ft x 1 ft) specimens were modified by adding three 13 mm x 124 mm (5 in x 4.9 in) liquid dispensing plenums to the underside of the specimens. The two specimens were designated as follows:

-517 50 x 250 Dynapore (a Dutch weave cloth made of 316L stainless steel wire with 50 wires per inch warp and 250 wires in the fill direction. Bonded by sintering and callendered to produce a smooth surface and obtain the desired resistance to airflow.)

-541 Perforated titanium with 0.102 mm (0.004 inch) diameter holes, spaced 1.02 mm (0.040 inch) on-centers, in a square pattern.)

11.6.2.1 Liquid Distribution - To ensure that the liquid-film, contamination-avoidance system will prevent insects from adhering to the wing leading edge, it is necessary to completely cover the region in which impingement occurs. Wind tunnel tests were conducted to explore potential problems and possible solutions

in three areas: (1) the formation of rivulets, (2) the uniformity of distribution and edge effects, and (3) the avoidance of dry areas in the range of chordwise travel of the attachment line (i.e., the stagnation region for two dimensional flow).

The runback of de-icing liquids tends to form into rivulets in a short chordwise distance depending on liquid characteristics and flow rate. To assure complete coverage of the wing leading edge, it would be necessary to reapply the liquid at a chordwise distance less than that in which rivulets would form. One objective of the wind tunnel tests was therefore to determine the distance (in the flow direction) over which the FPD liquid would provide complete coverage and to determine the effect of fluid flow rate on this distance.

To ensure uniform fluid distribution, the resistance to the fluid flow across the surface must be significantly greater than the fluid pressure drop in the spanwise distribution channel. A de-icing system of similar design (Reference 11-12) manufactured by TKS Corporation of England uses a porous sublayer of high pressure drop Provic sheet to ensure uniform spanwise distribution. Since the flow was interrupted at the end of each channel, the tests also evaluated the effect of this interruption on the ability to provide complete liquid coverage of the wing.

The final area of concern is the attachment line region. To ensure complete protection, the TKS de-icing system distributes liquid over the entire region of attachment line travel. This is done to prevent a dry area when the attachment line falls between two dispensing plenums. This ideal implementation method may not be achievable on the LFC aircraft due to conflicting suction system and structural requirements. An acceptable compromise system is one that permits spaces between dispensing channels if it can be shown that the space will not dry out during the time period in which the attachment line falls into this region. One purpose of the test was to determine the time taken for the surface to dry out after being fully wetted.

Tests were conducted on the perforated titanium and Dynapore panels to evaluate the effect of liquid flow rate, tunnel dynamic pressure (q), and tunnel-to-suction plenum differential pressure, on the ability of a liquid to completely cover the test panel aft of the liquid distribution plenum. The liquid used during these tests was 100 percent ethylene glycol which is a typical freezing point depressant (FPD) that possesses good wetting capabilities.

Table 11-2 summarizes data on the effect of differential pressure between the suction plenum and local ambient on the ability of the liquid to coat the wing surface. The data show that when the suction plenum was open to laboratory ambient the flow quickly broke into rivulets. This was because the differential pressure forced the liquid through the porous material instead of allowing it to flow aft. The data from the run in which the plenum-to-local-ambient pressure was equalized demonstrates improved coverage 178 mm (7 inches) aft of the dispenser. Based on these result it was concluded that the suction plenum pressure should be equal to or greater than local ambient pressure to achieve the most efficient liquid distribution.

Tunnel dynamic pressure (q) was varied from 478.8 to 2394.0 Pa (10 to 50 psf) to determine the effect of q on the distribution of the liquid. For the same flow of liquid, a definite improvement in coverage was noted as q was increased.

A number of test runs were made to determine the liquid flow rate necessary to provide complete coverage. It was found that a high initial flow rate was required to wet the entire surface. The flow rate was then reduced incrementally and the effect on surface coverage was observed. Figure 11-26 presents representative results which indicate that a sustaining flow of 0.251 cm^3/s for a 127 mm span (0.92 in^3/min over 4 inches) was the minimum flow necessary to maintain surface wetness after an initial flow rate of about 1.092 cm^3/sec (4 in^3/min). The results also indicate that the flow necks to an extent dependent on the flow rate. To prevent dry areas, the plenums must be overlapped and, if possible, the ends of the dispenser should be provided with a slightly higher flow rate than for the basic panel.

TABLE 11-2

EFFECT OF SUCTION PLENUM TO

LOCAL AMBIENT DIFFERENTIAL PRESSURE

Tunnel 'q' Pa	(psf)	Liquid Flow Rate cm2/3	(in^3/min)	Suction Plenum Pressure	Percent of Total Coverage at Various Chordwise Distances from L.E. 25mm(1 in)	102mm (4 in)	178mm (7 in)
47.8	(10)	1.35	(4.95)	Ambient*	58	12	0
1436	(30)	1.37	(5.02)	Ambient*	61	12	0
1436	(30)	1.14	(4.16)	Ambient*	52	0	0
1436	(30)	1.14	(4.16)	Tunnel**	38	28	27

* Ambient indicates that the suction plenum was open to laboratory ambient pressure and was negative with respect to the local pressure in the wind tunnel.

** Tunnel indicates that the suction plenum was sealed so that the pressure in the plenum was equal to the local pressure in the wind tunnel.

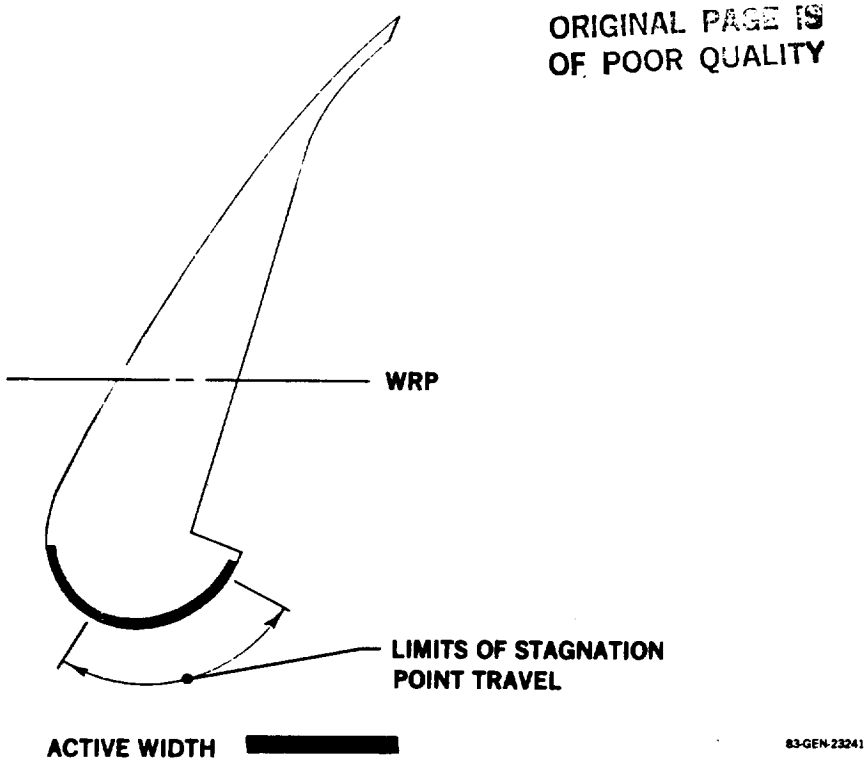

FIGURE 11-25. FIRST APPROXIMATION OF ACTIVE POROUS PANEL WIDTH REQUIRED ON SHIELD FOR ICE PROTECTION

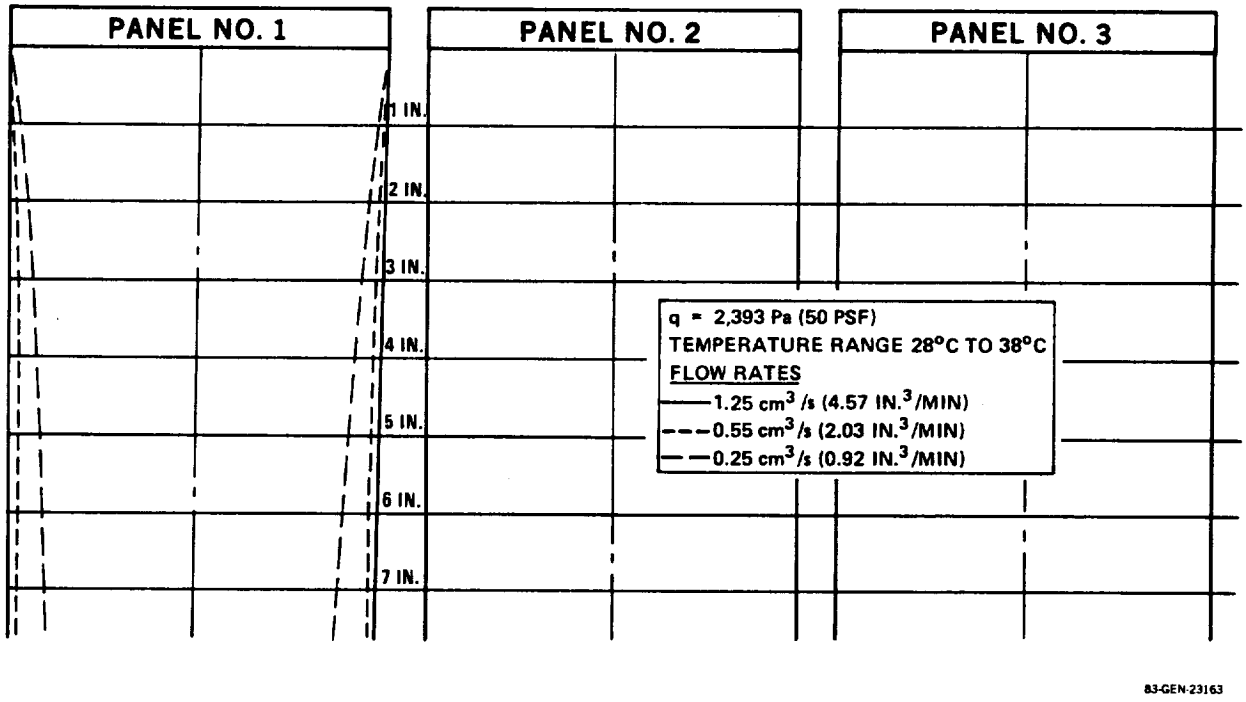

FIGURE 11-26. FPD LIQUID FLOW TESTS IN LOW-SPEED WIND TUNNEL PERFORATED TITANIUM PANEL – ONE PLENUM

During the tests, it was observed that the porous surface would stay wet after the glycol flow was discontinued, for periods of 20 seconds to one minute. The time during which the surface would remain wet decreased when water was added to the glycol. The maximum time that flow can be disrupted will depend upon the viscosity and evaporation rate of the final fluid formulation.

11.6.2.2 Removal of Debris - The liquid-film concept of contamination avoidance requires that the liquid first prevents adhesion of the insect to the wing surface and second lubricates the surface so that insect remains or other contaminants are transported off the wing. Particles larger than 0.01016 cm (0.004 inch) in height have been shown to affect boundary layer transition and therefore the liquid-film system must prevent their adherence and remove them from the wing.

To evaluate the removal of contaminants, glass beads 0.15 mm (.006 inch) diameter were used to simulate debris. Initial tests indicated that aerodynamic forces would blow particles off of a dry wing but would not remove particles from a damp or wet surface. Additional runs showed that the application of a glycol at a high rate for a short time caused most of the particles to be transported off the 0.305 m x 1.22 m (1 foot x 4 feet) panel but did not completely remove the particles from the 3.05 m (10 foot) long test section. The ability of water to permit removal of particles from both the perforated titanium panel and aluminum afterbody was demonstrated. Based on observations during the test runs, it was evident that the high viscosity of the glycol was the predominant factor in causing particles to adhere to the surface. The evaporation rate appeared to have a minor influence. Three conclusions can be drawn from the results of testing:

(a) Aerodynamic forces will not maintain the level of cleanliness required for an LFC aircraft.

(b) To ensure complete removal of contaminants from the wing, the fluid viscosity must be less than that of 100 percent ethylene glycol.

(c) A viscosity slightly greater than that of water is acceptable.

11.6.2.3 Residual Film - When the ethylene glycol evaporates from the surface, a film remains that could appear rough to the freestream. Tests to evaluate this residue were conducted. Visual inspection indicated that the film of glycol that remained on the perforated titanium was extremely smooth. The residue on the 50 x 250 Dynapore was slightly rougher and on smooth aluminum, beads of glycol formed. During clogging/clearing test runs on panel LFC-17 (80 x 700 Dynapore), visual inspection indicated that the residue was extremely smooth with the glycol diluted with 40 percent water or 30 percent water/10 percent alcohol.

Measurements of the chordwise distance to the transition point as a function of suction rate indicated that the residual glycol film had a negligible effect on the extent of laminar flow.

11.6.2.4 Clogging and Clearing - Whenever a liquid covers any portion of the porous material on the wing surface, the possibility exists that the liquid will lodge in the pores and reduce the surface porosity. This situation could be encountered (1) during flight or ground operations in rain, or (2) when the liquid-film contamination-avoidance or ice protection system is operated. Hence, the liquid could be either water or the contamination-avoidance liquid which will probably be some mixture of glycol, water, and additives to inhibit corrosion.

To ensure proper operation of the suction system during cruise, the liquid must either be prevented from entering the porous surface or must be cleared out of the pores before it freezes or the viscosity increases substantially. Conceptually, a system can be envisioned in which the suction manifolds are always pressurized slightly to prevent the liquid from entering the pores.

A more practical approach is to provide a high positive pressure in the suction system for a short duration after encountering the liquid to clear the porous surface.

The results of early tests in the wind tunnel indicated that liquid does degrade the surface porosity severely, resulting in up to 82 percent reduction in suction airflow. Attempts to clear the panel using the suction system in a reasonable time were unsuccessful with suction levels as high as 958 Pa (20 psf). Further exploratory tests confirmed that unreasonably high suction levels would be needed to clear trapped liquid from the porous material. Tests also indicated that water was expelled far more easily from the porous surface than ethylene glycol which required a relatively high pressure. As a result of these findings, glycol mixtures were used for subsequent clogging/clearing tests and pressure was used to expel the liquid.

Further testing was done in the wind tunnel to include the effect of aerodynamic forces on clogging and clearing. Test panel LFC-17 (80 x 700 Dynapore) was used, which incorporated the most recent fabrication and design concepts. The panel was not modified to add liquid distribution plenums. Instead, the liquid was applied externally upstream of the test section using a spray tube. The liquids tested were 60 percent ethylene glycol/40 percent water, and 60 percent ethylene glycol/30 percent water/10 percent alcohol and suction plenum pressures ranged from 96 to 3352 Pa (2 to 70 psf). Figure 11-27 presents results in which a glycol mixture was cleared from the porous specimen in about fifteen minutes at a pressure slightly below 3352 Pa (70 psf). The pressure tapered off during the test because of reducing flow restriction. The unclogged porosity of the test panel was 0.61 $m^3/s/m^2$ at 670 Pa (120 $SCFM/ft^2$ at 14 psfg).

At this point it was decided that a more comprehensive investigation was needed. Two approaches were taken:

(1) Specify a liquid formulation that best meets the requirements of the contamination-avoidance/ice protection functions and possesses the physical properties allowing it to be easily expelled from a porous surface. The results of this investigation are presented in Section 11.6.3.

(2) Systematically evaluate clogging and clearing of porous panels to determine the influence of surface porosity, overall porosity, and liquid properties on the required clearing pressure and time, as follows:

The basic wind tunnel setup previously described in Section 8.1.1 was modified to allow filtered plant air to pressurize the plenum under the porous test specimen and a 280 mm x 1190 mm (11 inch x 47 inch) aluminum panel insert was modified to permit the installation of 152 mm x 305 mm (6 inch x 12 inch) porous panels. Candidate contamination-avoidance liquids were sprayed on the test section from a pressurized supply tank. The physical properties of these liquids are presented in Table 11-3 and Figure 11-28.

The evaluation of the various construction techniques and liquid formulations followed a standardized procedure. Each specimen was airflow tested in the "as-manufactured" condition to establish the overall porosity with no airflow over the surface. Next a calibration curve of airflow versus pressure drop was established at the test conditions, wind tunnel q = 479 Pa (10 psf). This calibration curve was used as a reference to calculate the percent clogging due to the liquid. With the tunnel operating at a q of 479 Pa (10 psf) and with a slight positive pressure of about 249 Pa (1 inch of water) maintained in the plenum, the candidate liquid was sprayed upstream of the test specimen until the entire specimen was coated with liquid. The plenum pressure was then increased to the test value and time measured as the pressure passed through 2758 Pa (0.4 psig). A constant plenum pressure was maintained as the panel cleared. Flow versus time was recorded to indicate the effectiveness of the plenum pressure in clearing the liquid from the porous surface. Characteristics of the various porous surface specimens that were tested are presented in Table 11-4. Initial pressure drop versus flow measurements were made on each specimen. The value of the flow per unit surface area at a differential pressure of 670 Pa (14 psf or 2.69 inches of water) was used as a measure of the openness of the porous material and is termed "porosity".

TABLE 11-3

PHYSICAL CHARACTERISTICS OF TEST LIQUIDS

	Water (Reference)	33% Denatured Ethyl Alcohol 67% Water	60% Propylene Glycol Methyl Ether, 40% Water	60% Ethylene Glycol, 40% Water
Density (gm/cc)	1.000	0.962	0.950	1.076
Freezing Point (°C)	0	-16	-41	-57
Viscosity at 20°C (cs)	*	*	*	*
Surface Tension @ 25°C (dynes/cm)	72	34.5	36.7	52
Flash Point (°F) T.C.C.	None	82	125	>212
Toxicity**, LD 50	Not Applicable	13.7 ml/kg	9.3 ml/kg	7.4 ml/kg

* See Figure 11-28

** Refers to the oral dose that kills 50% of exposed rats, expressed in ml of chemical per kg of body weight.

NOTES:

1. WIND TUNNEL OPERATED AT q = 10 PSF = 1,915.2 Pa
2. PLENUM PRESSURE 4.2 PSF WHILE APPLYING LIQUID (4.2 PSF = 201.1 Pa)
3. LIQUID APPLIED EXTERNALLY (60% GLYCOL, 30% WATER, 10% ALCOHOL)
4. PLENUM PRESSURE INCREASED AS SHOWN.

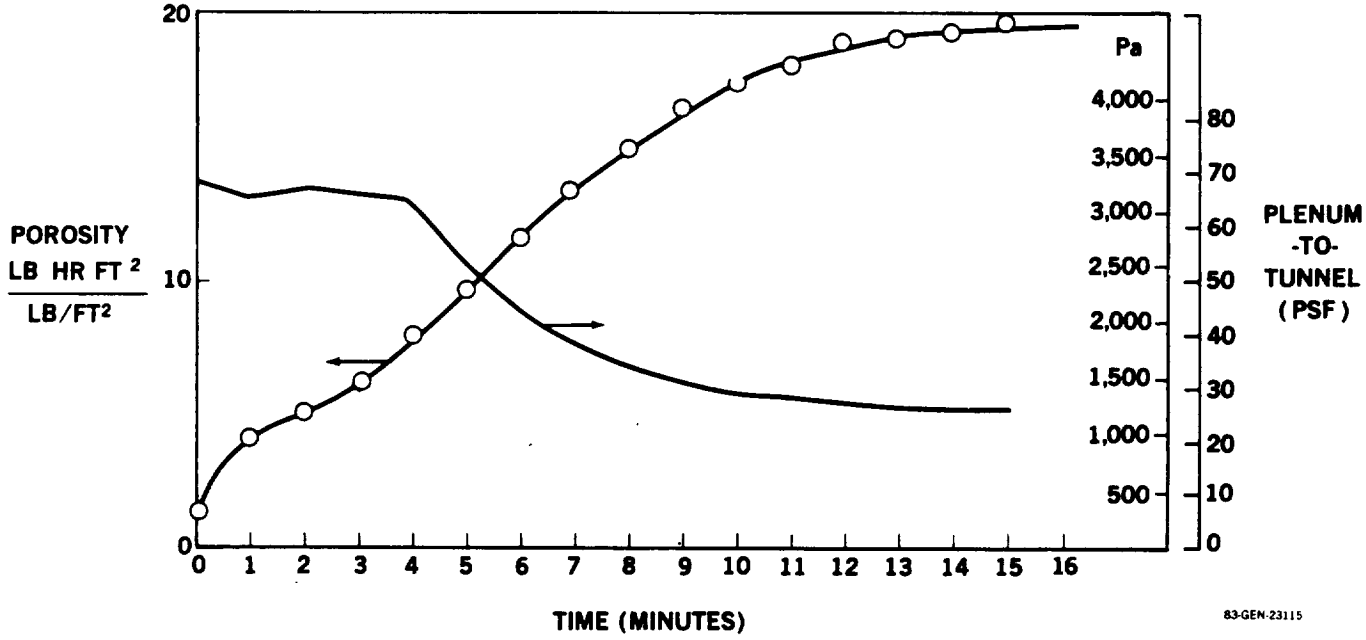

FIGURE 11-27. CLOGGING AND CLEARING OF POROUS MATERIAL (SPECIMEN LFC 17 IN LOW-SPEED WIND TUNNEL)

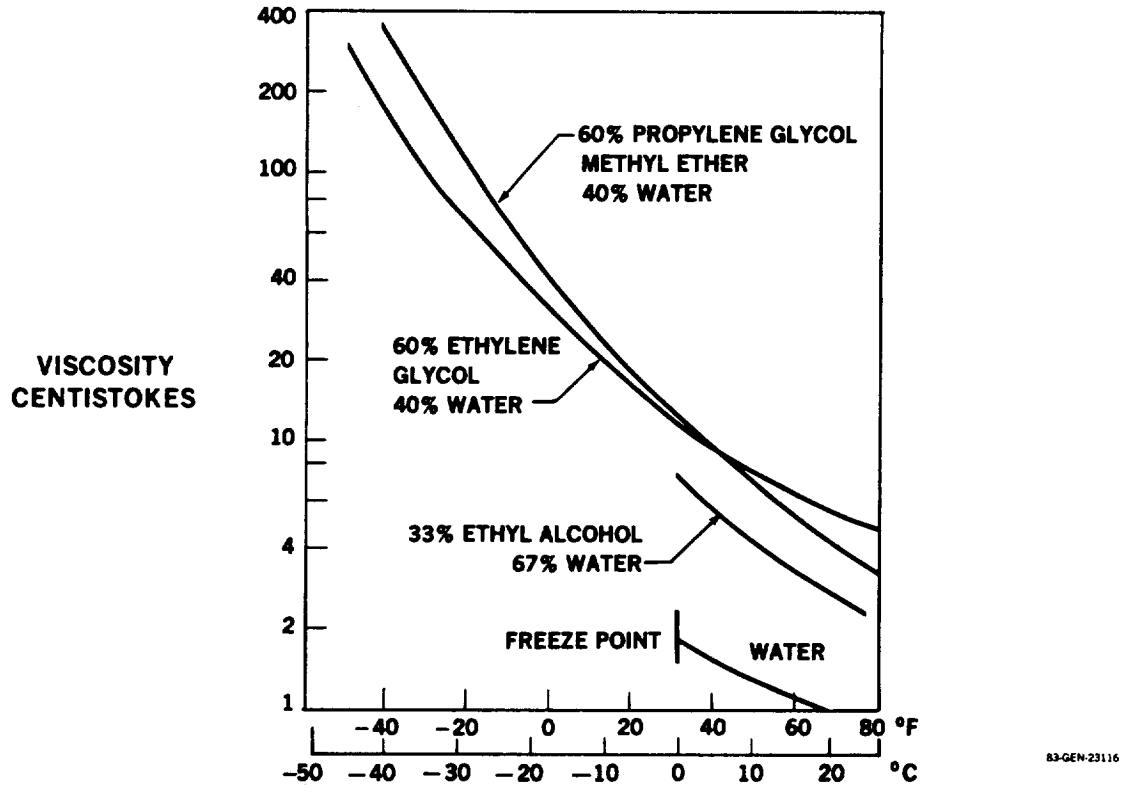

FIGURE 11-28. VISCOSITY VERSUS TEMPERATURE FOR CANDIDATE LIQUIDS

TABLE 11-4

CONSTRUCTION AND OVERALL POROSITY* CLOGGING AND CLEARING TEST SPECIMENS

Specimen Designation	Surface Material**Porosity $m^3/s/m^2$@670Pa	Surface Material**Porosity (SCFM/FT^2 @ 14 psf)	Glass Cloth	Overall Porosity $m^3/s/m^2$@670Pa	Overall Porosity (SCFM/FT^2 @ 14 psf)
S1	0.142	(300)	3 plies of 194 cloth	0.342	(67.3)
S2	0.142	(300)	1 ply of 120 weave	0.099	(19.5)
S3	0.142	(300)	2 plies of 120 weave	0.037	(7.2)
S4	0.077	(164)	3 plies of 194 weave	0.264	(52.0)
S5	0.077	(164)	1 ply of 120 weave	0.095	(18.7)
S6	0.077	(164)	2 plies of 120 weave	0.076	(14.9)
S7	0.038	(80)	3 plies of 194 weave	0.113	(22.3)
S8	0.038	(80)	1 ply of 120 weave	0.074	(14.6)
S9	0.038	(80)	2 plies of 120 weave	0.051	(10.0)

*Porosity is used to indicate the openness of the pores or capillary paths through the porous material and is the flow per unit surface area at 670Pa (14 psf) differential pressure.

**All specimens were made from 80 x 700/80x80 Dynapore surface material and used a glass cloth impact layer with 6.35mm (1/4 inch) diameter holes.

Prior testing had indicated that the primary force that prevented the liquid from being expelled from the porous material was due to capillary action. It was not clear, however, to what extent viscous forces also retarded the clearing process. It is assumed that for a given liquid the capillary forces are controlled by the pore size at the surface whereas the viscous forces are controlled by the flow resistance across the entire specimen including both the Dynapore and the epoxy-filled glass. The porosity of the Dynapore provides an indication of the pore size at the surface.

Figures 11-29a and 29b present results from the clearing tests of the 152 mm x 305 mm (6 inch x 12 inch) specimens at two pressure levels. The results show that surface porosity has a definite influence on the ability to clear the liquid from the material whereas no definite tendency is seen as a function of overall porosity.

Figures 11-30 and 11-31 show the relationship between the pressure required to obtain an arbitrary level of clearing versus surface porosity and overall porosity, respectively. Although there is a great deal of scatter in the data, the results show that clearing pressure is affected by surface porosity. No such dependency is seen as a function of overall porosity (note the data point at .0508 $m^3/s/m^2$ (10 SCFM per sq. ft.) in Figure 11-31. Assuming that capillary forces are the dominant factor, the clearing pressure would be inversely proportional to the surface pore diameter (which can be represented by the square root of the surface porosity). The line on Figure 11-30 which is drawn with a slope of -1/2 supports this premise. Based on these data, it appears that capillary forces (and hence liquid surface tension and surface porosity) dominate the clearing process and that viscosity has no consistent effect.

To further explore the effect of liquid properties on the required clearing pressure, various liquid formulations were tested. Typical results are shown in Figures 11-32 through 11-34. A dramatic reduction in the pressure required to clear the specimen is noted when the liquid is changed from aqueous

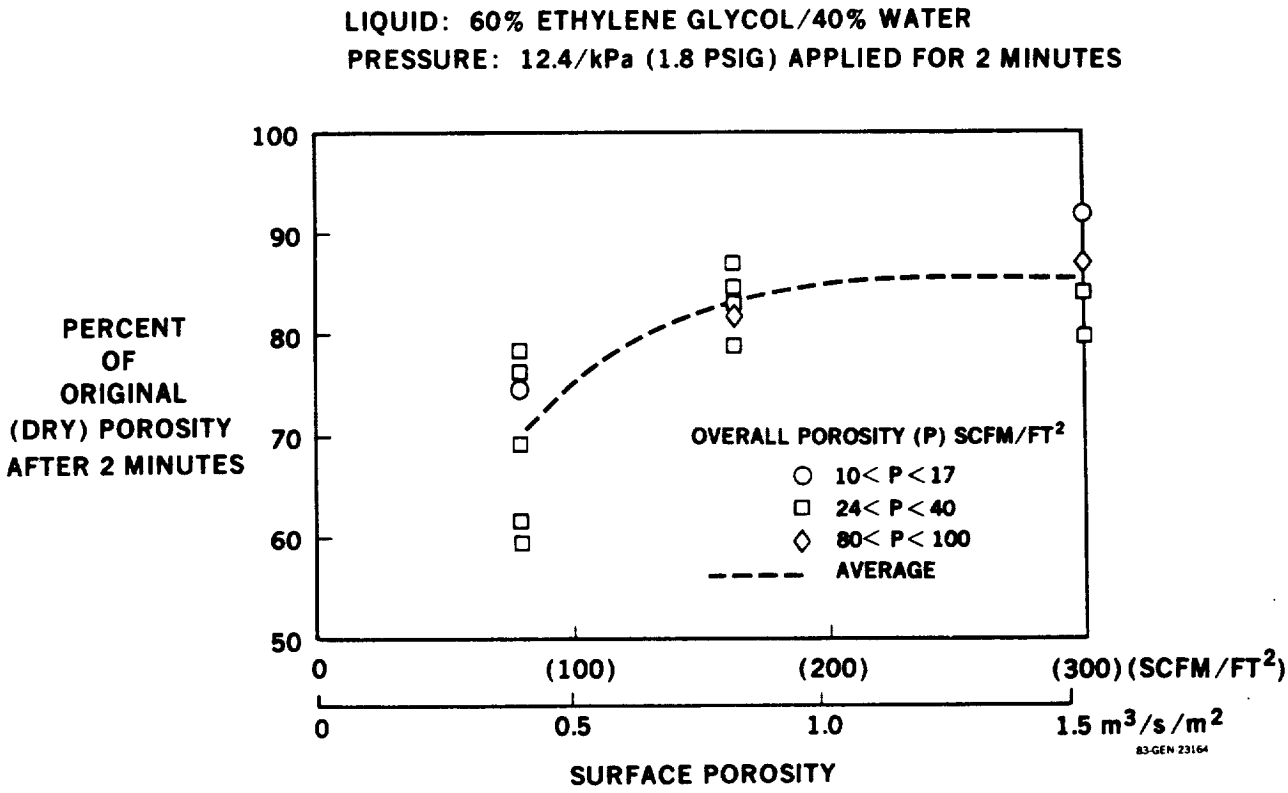

FIGURE 11-29.A EFFECT OF POROSITY ON LIQUID CLEARANCE AT 12.4 kPa PRESSURE

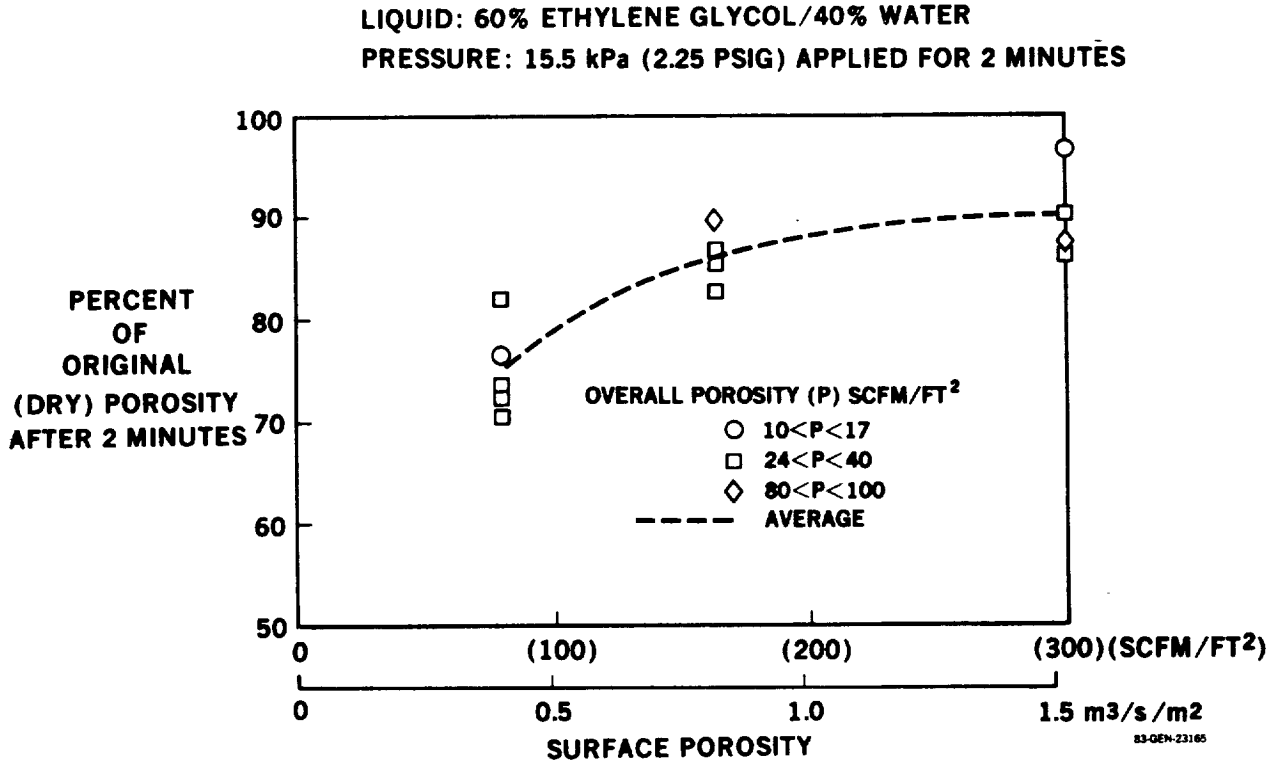

FIGURE 11-29.B EFFECT OF POROSITY ON LIQUID CLEARANCE AT 15.5 kPa PRESSURE

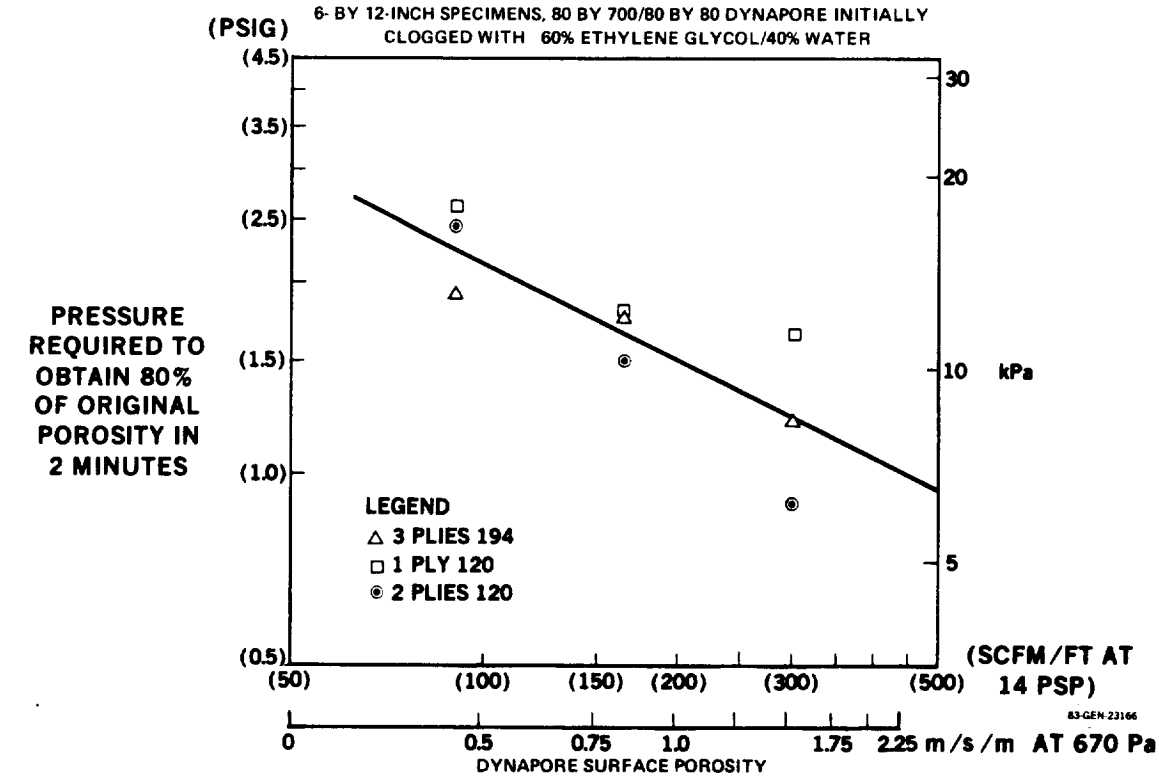

FIGURE 11-30. EFFECT OF SURFACE POROSITY ON LIQUID CLEARANCE

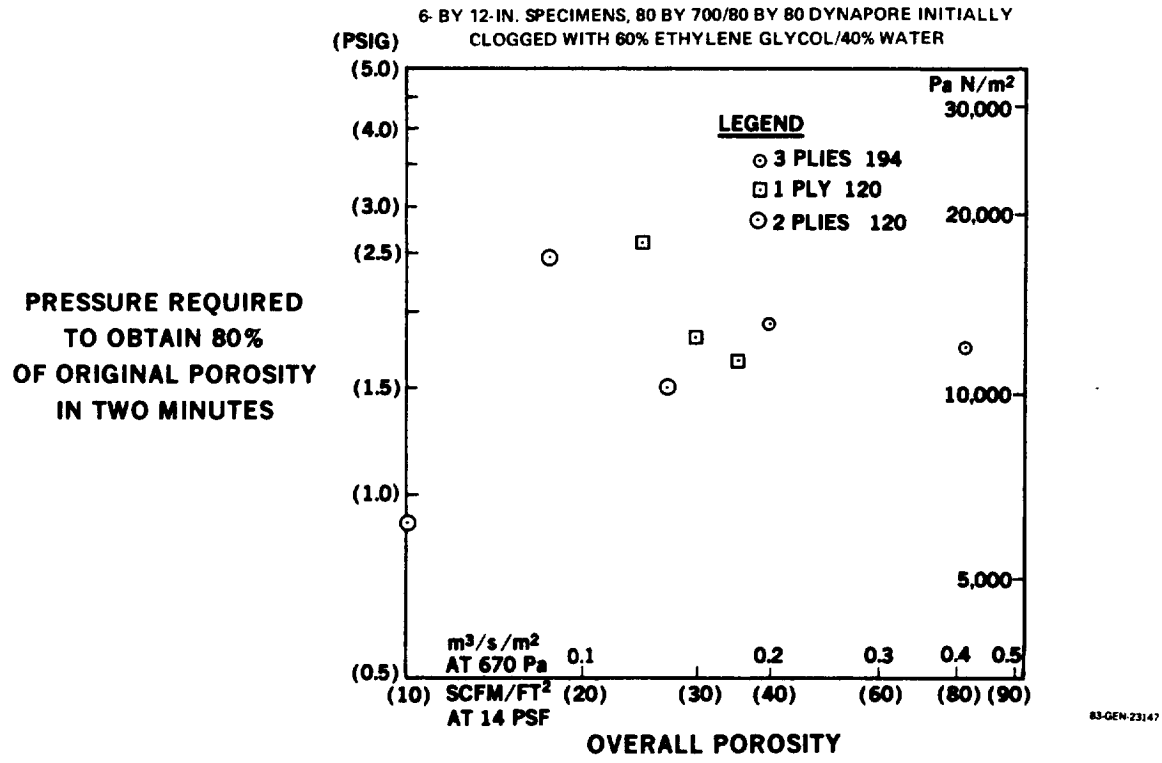

FIGURE 11-31. EFFECT OF OVERALL POROSITY

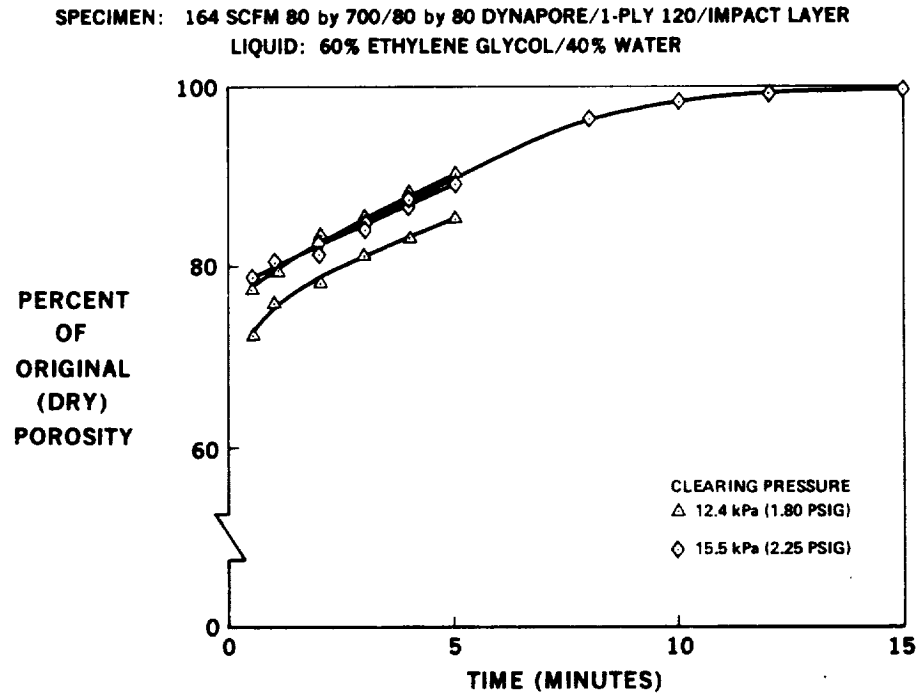

NOTE: EACH 6- BY 12-IN. SPECIMEN WAS SATURATED WITH LIQUID IN THE LOW-SPEED WIND TUNNEL AT A q OF 479 Pa (10 psf). POSITIVE PRESSURE WAS APPLIED AND THE TIME TO REACH A PRESSURE OF 3.1 kPa (0.45 PSIG) WAS MEASURED

83-GEN-23196

FIGURE 11-32. TIME TAKEN TO CLEAR DILUTED ETHYLENE GLYCOL

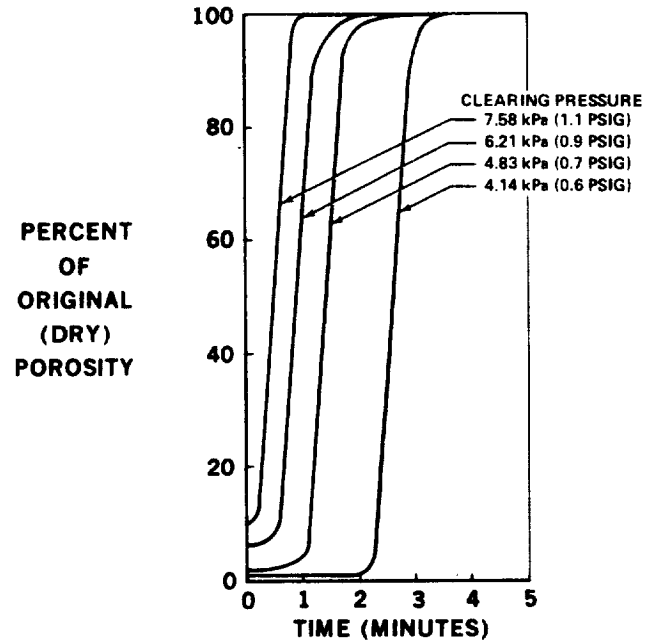

NOTE: EACH 6- BY 12-IN. SPECIMEN WAS SATURATED WITH LIQUID IN THE WIND TUNNEL AT A q OF 479 Pa (10 PSF). POSITIVE PRESSURE WAS APPLIED AND THE TIME TAKEN TO REACH A PRESSURE OF 3.1 kPa (0.45 PSIG) WAS MEASURED

83-GEN-23197

FIGURE 11-33. TIME TAKEN TO CLEAR DILUTED ETHYL ALCOHOL

ethylene glycol to an alcohol or propylene glycol methyl either (PGME) mixture. Figure 11-34 also shows that a porous surface that meets the porosity and smoothness requirements of the LFC aircraft can be cleared after being saturated with liquid by applying 6.894 KPa (one psi) of internal pressure for one minute.

Table 11-5 summarizes the pertinent liquid properties and required clearing pressures. A relationship is apparent between clearing pressure and surface tension. No such relationship is apparent between clearing pressure and viscosity.

To further investigate the ability of positive pressure to clear the surface of contamination avoidance/ice protection liquid, combinations of three fluids on three porous surfaces were tested. Porosity was measured as a function of time and pressure for each combination and the qualitative pattern of fluid removal was determined visually. The test results provide an indication of which materials and liquids would have the best clearing properties in flight. Specimens measuring 127 mm x 254 mm (5 inches x 10 inches) were fabricated from the following materials:

Specimen	Materials
-503	80 x 700 Dynapore plus perforated stainless steel sheet
-509	80 x 700/80 x 80 Dynapore plus perforated stainless steel sheet.
-515	Titanium perforated with 0.102 mm x 0.203 mm (.004 inch x .008 inch) holes.

The liquids tested were 60 percent ethylene glycol - 40 percent water; 57 percent propylene glycol - 43 percent water; and 60 percent propylene glycol methyl ether (PGME) - 40 percent water.

Clearing pressure was supplied through a plenum directly beneath the specimen and an airstream with a dynamic pressure of 220 Pa at approximately 23^{o}C was directed over the specimen parallel to its surface.

TABLE 11-5

PROPERTIES OF TEST LIQUIDS

	60% Ethylene Glycol/40% Water	33% Denatured Ethyl Alcohol/ 67% Water	60% Propylene Glycol Methyl Ether/40% Water
Surface Tension (dynes/cm)	52	34.5	36.7
Viscosity (cs)	5.6	2.75	4.4
Clearing Pressure* (psi)	(1.8)	(0.67)	(0.54)
kPa	12.4	4.62	3.72

*Pressure required to obtain 80% of the initial (dry) porosity in two minutes.

The test results are summarized in Figures 11-35 and 11-36, which show the time to reach 98 percent porosity versus pressure. The porosity changed very slowly with time above 98 percent porosity, making determination of time to 100 percent porosity largely arbitrary. Approximate times to 100 percent porosity were 5 to 15 seconds longer than the time to 98 percent porosity for all materials with PGME; ethylene glycol and propylene glycol were not 100 percent cleared from any specimen in less than 2 minutes for the pressure ranges of 0 to 14,000 Pa for -503 and -509 and 0 - 10,000 Pa for -515. No data are shown for ethylene glycol or propylene glycol on the -503 specimen or for propylene glycol on the -509 specimen because 98 percent clearing did not occur within two minutes with any of these combinations for pressures up to 20,000 Pa.

The results indicate the -515 specimen and PGME are the material and liquid combination with the best clearing characteristics. This is consistent with observation of liquid removal from the surface. Most of the liquid was removed by run back along the surface. The Dynapore specimens, however, retained liquid in their surface structures, inhibiting complete run back. Evaporation accompanied final clearance of the PGME from the Dynapore specimens, but the ethylene glycol and propylene glycol did not evaporate.

Because of the rapid drop in vapor pressure as temperature is lowered, final clearing of PGME by evaporation cannot be relied upon in flight conditions. Run back will be the primary mechanism for liquid removal. A smooth surface, such as perforated titanium, and a liquid possessing low surface tension and low viscosity, such as PGME, are therefore recommended as having the best clearing characteristics. The optimum clearing pressure can be determined in a flight test program, where the low temperature effects of higher viscosity and higher surface tension and the effects of a higher airstream velocity will be taken into account.

SPECIMEN: 164 SCFM 80 by 700/80 by 80 DYNAPORE/1-PLY 120/IMPACT LAYER
LIQUID: 60% PROPYLENE GLYCOL METHYL ETHER/40% WATER

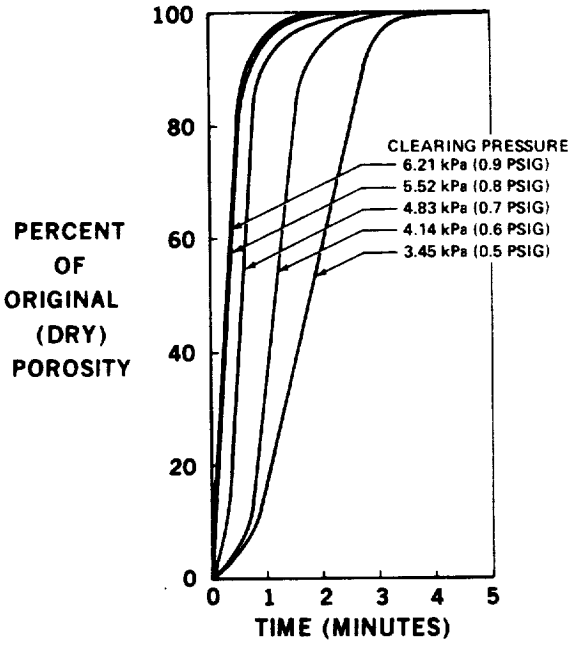

NOTE: EACH 6- BY 12-IN. SPECIMEN WAS SATURATED WITH LIQUID IN THE LOW-SPEED WIND TUNNEL AT A q OF 479 Pa (10 PSIG). POSITIVE PRESSURE WAS APPLIED AND THE TIME TAKEN TO REACH A PRESSURE OF 3.1 kPa (0.45 PSIG) WAS MEASURED.

83-GEN-23198

FIGURE 11-34. TIME TO CLEAR DILUTED PGME

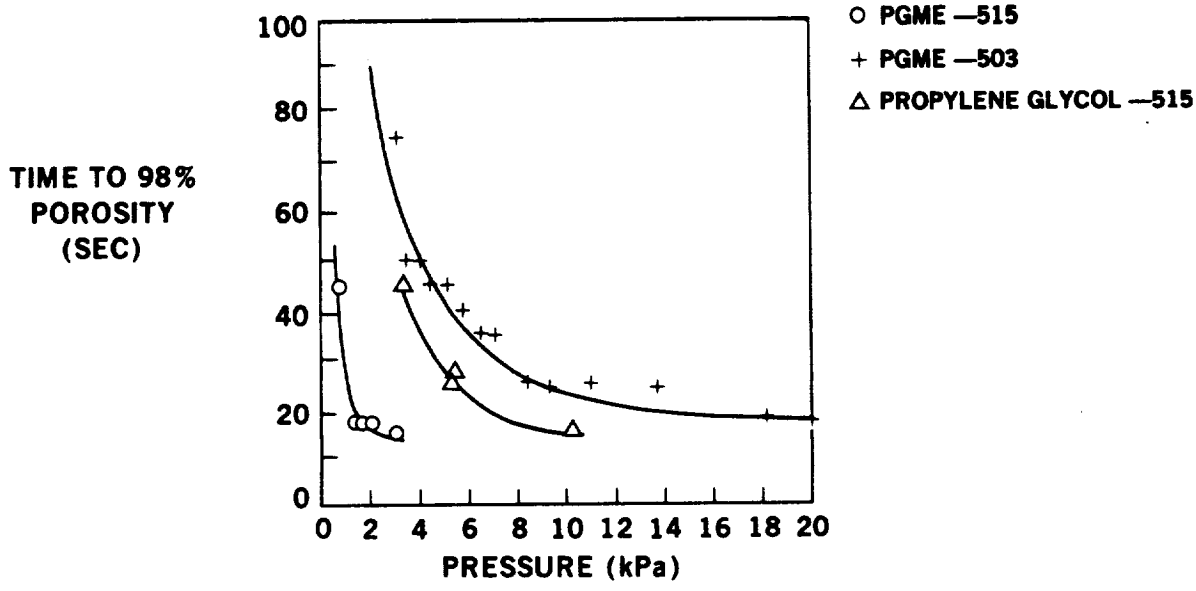

83-GEN-23152

FIGURE 11-35. LIQUID CLEARANCE TIME VERSUS PRESSURE

11.6.3 Liquid Formulation

The liquid used for contamination-avoidance and ice protection must meet many requirements to ensure proper system operation and compatibility with the overall aircraft operation. Some of these requirements have not been fully defined at this time.

(a) Freezing Point - Unless all of the contamination avoidance liquid in the wing tubing is purged after each application, the liquid in the unheated wing will be cooled by the ambient temperature which at cruise altitudes can be as low as $-70^{o}C$. Allowing for a $25^{o}C$ ram temperature rise, an aircraft skin temperature of $-45^{o}C$ can be expected. The ice protection system will be required to operate following a descent into icing conditions after being cold soaked during cruise to this temperature. During descent, the tubing and liquid in the wing will warm up somewhat. The system may also be required to operate during cruise to eliminate small amounts of ice that could disrupt laminar flow. It is therefore a design goal that the ice protection liquid have a freezing point of $-45^{o}C$ or less to permit operation during cruise.

(b) Surface Tension and Wettability - These two interrelated properties of the liquid affect (1) the ability of the liquid to form a film over the entire wing surface without breaking up into rivulets, and (2) the pressure required to clear a porous surface that has been clogged with liquid. To enhance its wettability, the liquid should possess a low surface tension and low contact angle (θ) between the liquid and metal.

The pressure required to clear a clogged porous surface is related to the pressure exerted by capillary action which is proportional to the product of the surface tension and the cos θ. A liquid with a good wettability (i.e., low θ) will be difficult to clear from a porous

surface unless it also has a low surface tension. Since good wettability is essential, the selection of a liquid with the lowest possible surface tension is necessary to minimize the pressure required to clear the liquid out of the porous material.

During operation in rain or icing conditions the liquid may be diluted with water, therefore, it is required that the product of surface tension and cos θ be minimized for all aqueous solutions of the contamination-avoidance/ice protection liquid formulation.

(c) Viscosity - The liquid viscosity and its variation with temperature affects three areas of operation. First, the liquid viscosity must be low enough to allow the transport of insect remains in a chordwise direction. The viscosity must also be low enough to prevent the formulation of globules on the surface that would also create turbulence. A final concern is the variation of viscosity with temperature. The liquid pressure drop through the surface must be sufficient to ensure uniform spanwise distribution. Over the temperature range from $-40^{o}C$ to $+50^{o}C$, the viscosity of typical glycols changes by a factor of 100. These viscosity variations will be reflected in corresponding changes in liquid flow and/or pressure drop across the suction surface. Over the range of ambient temperatures in which insects are active it is desirable to maintain a constant flow. This would require a pressure across the suction surface of at least five times the minimum operating pressure. For adequate ice protection the liquid flow required at $-40^{o}C$ is less than that required at $0^{o}C$ so that the pressure increase for ice protection need not offset the full viscosity change.

(d) Volatility - Evaporation rate will also influence the ability of the liquid to coat the surface and to permit insect remains to be transported off the wing. The most critical region that is influenced by volatility is the area of attachment line travel. As discussed in Section 11.6.2.1, dry areas may form if the liquid film is removed by the airstream in less than about twenty seconds.

(e) Miscellaneous Liquid properties - The liquid must possess properties that are generally required for fluids used on aircraft. For instance, the liquid should be non-corrosive and have a reasonable boiling point. Two properties that will require special consideration are flammability and toxicity. Since the liquid is applied external to the wing, it must not create a fire hazard. Both a reasonable flash point and low concentration of the vapors in air are required to avoid a fire hazard. Low toxicity is needed to minimize the environmental impact due to the liquid-film system.

(f) Summarizing the foregoing discussion, the physical property requirements of the liquid to be used for contamination-avoidance/ice protection are as follows:

1. Freezing point < - 45^{o}C
2. Surface tension < 40 dynes/cm
3. Good wettability
4. Viscosity: The exact limits have not been defined. In general, the viscosity should be low enough to prevent the formation of globules as the liquid runs back along the surface and the ratio of viscosity at cold temperatures to that at maximum temperature should be minimized.
5. Low volatility
6. Low toxicity
7. High flast point
8. Low corrosivity.

(g) Candidate Liquids - A number of candidate liquids were evaluated to find a suitable formulation. Alcohols, including glycol, form the basis for the common de-icing agents and were therefore considered first. Five glycols were evaluated: ethylene, diethylene, triethylene, tetraethylene and propylene. A 70 ± 10 percent glycol/ 30 ± 10 percent water solution is required to satisfy the freezing point requirement. Aqueous propylene glycol has the lowest surface tension: 40 dynes/cm at 70°F compared to about 52 dynes/cm at 77°F for either ethylene or diethylene glycol. However, propylene glycol is too viscous at temperatures below -10°C.

Some of the glycol ethers offer improvement in both viscosity and surface tension characteristics over the aqueous glycol solutions. Over thirty formulations were screened. Some of the more promising are listed in Table 11-6.

TABLE 11-6 CANDIDATE GLYCOL ETHERS

Name	Manufacturer	Freezing Point °C	Viscosity at 20°C CP	Surface Tension dynes/cm	Flash Point °C (°F)
Butyl CELLOSOLVE	Union Carbide	-70	6.4	27	60 (140)
Methyl CARBITOL	Union Carbide	-85	3.9	40	147 (188)
Butyl CARBITOL	Union Carbide	-68	6.5	34	101 (214)
PROPASOL Solvent P	Union Carbide	-80	2.8	26	48 (119)
PROPASOL Solvent M	Union Carbide	-95*	1.9	29	33 (91)
PROPASOL Solvent DM	Union Carbide	-80*	5.2	33	75 (167)
DOWANOL EE	Dow	-100*	1.8	28	43 (109)
DOWANOL PM	Dow	-97*	1.7	28	36 (96)
DOWANOL DPM	Dow	-82*	3.4	29	78 (175)

*Pour Point

Both ethyl and methyl alcohol meet the freezing point, surface tension, and viscosity requirements but have low flash points. Silicate ester based fluids such as COOLANOL (manufactured by Monsanto) and fluoronated hydrocarbons

also possess good physical properties but are expected to have an unacceptable impact on the environment. Typical properties are listed in Table 11-7.

TABLE 11-7. CANDIDATE ALCOHOLS, FLUOROCARBONS AND HEAT TRANSFER FLUIDS

Name	Manufacturer	Freezing Point (°C)	Viscosity at 20°C (cp)	Surface Tension (dynes/cm)	Flash Point °C (°F)
Ethyl Alcohol	--	-117	1.2	22.8	Low
Methyl Alcohol	--	- 98	0.6	22.6	Low
"Freon E2"	Dupont	-123*	1.1	12.9	High
"Freon E3"	Dupont	-190*	2.2	14.2	High
COOLANOL 15	Monsanto	-140*	2.0	21.0	77 (170)
COOLANOL 25	Monsanto	-120*	5.4	25.0	163 (323)

*Pour Point

One of the most suitable liquids for insect/ice protection is propylene glycol methyl ether (PGME), the basic constituent of DOWANOL PM and PROPASOL Solvent M. The major concern in the use of this fluid is its low flash point of 35°C (95°F). The use of an aqueous solution of 60 percent PGME/40 percent water raises the flash point to 52°C (125°F). Considering the extremely low concentrations that will be present after mixing with the free stream, the flash point of 52°C (125°F) is considered to be acceptable. This liquid formulation is recommended and has been used as the basis of additional investigations.

11.6.4 Liquid-Film System Test and Analysis Summary

(a) System Performance - The results of the tests conducted in the Douglas Low Speed Wind Tunnel indicate that complete coverage of the wing leading edge surface can be achieved for a downstream chordwise distance of at least 254 mm (10 in.) by applying 9.9 $cm^3/s/m$ (10 cu in/min per foot) of span. While applying the liquid, the suction plenums should be pressurized to at least local ambient pressure to prevent the liquid

from being forced through the porous surface. To avoid irregular coverage, the ends of the distribution plenums should be overlapped. The pressure drop through the surface must be sufficiently greater than the spanwise pressure drop in the panel to obtain uniform distribution. During the wind tunnel tests glycol kept the surface moist in excess of twenty seconds after liquid application.

The wind tunnel tests indicated that a liquid with a viscosity as great as that of 100 percent ethylene glycol will not transport contaminants off the trailing edge of the wing, whereas water did keep the wing clean. This was confirmed by the JetStar tests program (Reference 11-26) in which a water spray was effective in preventing adhesion of insects on the wing and transporting the debris off the wing. The recommended solution of 60 percent propylene glycol methyl ether/40 percent water has a viscosity about 1/5 that of 100 percent ethylene glycol.

Tests also indicated that the residue from the ethylene glycol after evaporation did not significantly affect transition of the boundary layer.

Based on the results of Douglas wind tunnel tests and NASA Jetstar flight tests, it is concluded that a liquid-film system meets all of the system performance criteria. One concern that will be evaluated during subsequent flight testing is the limits of operation during low ambient temperature operation, especially considering the increase in viscosity at low temperature.

(b) Compatibility: Tests were conducted to evaluate the compatibility of the liquid and the porous surface. The major concern was that the liquid would be held in the pores due to capillary action and would clog the porous surface when suction would be required. Test results indicated that both water and glycol substantially reduced the porosity of Dynapore materials. LFC levels of <u>suction</u> failed to restore the porosity in a time compatible with flight operations. Water was

cleared from the pores by a very low positive pressure; however, a positive pressure of one psig was required to clear the propylene glycol methyl ether mixture from the pores. Based on these test results, it appears that a liquid-film insect protection system can be made compatible with a porous surface suction system by the following procedure. Following any application of a liquid to the porous surface (either by operation of the insect/ice protection system or by flying through rain), the suction system will be pressurized to a level of about 7 kPa (1.0 psig) for about 1 minute. The exact values will be determined after the selection of the final suction surface configuration and the liquid formulation.

Design studies also showed that the liquid-film system can be made compatible with the suction system, ice protection system, structure, and space restraints in the leading edge area. The choice of the low toxicity fluid propylene glycol methyl ether should make the system compatible with Environmental Protection Agency (EPA) requirements. The liquid-film system is not expected to significantly protect the outer surface against erosion due to sand, dust, hail or rain and normal structural design requirements would apply to these conditions.

Based on the results of studies to date, it is concluded that the liquid-film system can be made compatible with other LFC system requirements. Some concern remains regarding the flammability of the liquid. However, as previously stated, the low concentrations of the fluid in the air make the probability of fire extremely remote. Caution in handling, ventilation design, and isolation from ignition sources should be stressed.

11.6.5 Liquid-Film System Design

A central supply panel is envisioned which will include storage, pumping, filtering and pressure/flow control functions. The storage tank would have a capacity of about 0.42 m^3 (110 gallons) and would contain about 390 kg 860 pounds) of usable fluid. This quantity of fluid would provide contamination protection for the entire wing during takeoff and landing as required below 1524 m (5000 feet) altitude for two flights. It would also provide three de-icing applications per flight for the wing and ice protection for the shield.

To avoid clogging the porous surface, the filters must be effective down to the 1 to 2-micron range. A flow control valve will provide constant flow whenever the ambient temperature is above about $0^{o}C$. Below this ambient temperature, flow will be controlled by the system pressure drop and will decrease with decreasing temperature. This control scheme will provide adequate fluid to protect the wing leading edge from contamination without subjecting the system to excessively high pressures during cold ambient temperature operation.

A breakdown of the weights estimated for the portion of the system within the fuselage of a 300 Passenger aircraft is listed in Table 11-8.

TABLE 11-8. LIQUID SYSTEM WEIGHTS

	Kg	(Lb)	Kg	(Lb)
Fluid Weight				
Shield Ice Protection:	82	(180)		
Attachment Line Region:	82	(180)		
Hi Flow, Upper Surface:	226	(500)		
Total Fluid			390	(860)
Tankage			20	(44)
Pump, Motor, Filter, Regulator			20	(44)
Total System Weight			430	(948)

Fabrication, Operation and Maintenance - The liquid-film system employs concepts that have been used for ice protection of commercial and military aircraft for over 30 years. The only area of concern is the integration of the liquid and suction plenums in the wing leading edge area. Further detail design work is necessary to demonstrate that an easily fabricated design can be devised.

The contamination-avoidance or ice protection system should pose no operational restrictions. Flight testing is required to determine whether laminarization can be achieved after operation of the liquid-film system at low ambient temperatures. Operation of the contamination-avoidance system can be made completely automatic except for an ON/OFF switch using inputs of altitude, static air temperature (SAT), airspeed, and possibly flap position. Operating procedures for the ice protection system will be similar to those used on current aircraft.

Maintenance of both liquid-film systems will be similar to that of current aircraft applications. Care must be exercised in the design phase to reduce the possibility of leaks. Access in the wing leading edge for inspection and maintenance is improved with the upper-surface-only LFC concept. In either case, the plenums could be integral with the surface panel. Excessive leakage would require panel replacement and overhaul. It may be possible to design a removable insert which would contain the ice protection plenums. Further effort is required in this area to develop a practical design.

11.7 SPRAY SYSTEM PRELIMINARY DESIGN AND PERFORMANCE EVALUATION

An alternative method ofapplying liquid over the surface of the wing leading edge is the use of a spray system. Used in conjunction with a shield, two methods of implementing the spray concept were considered. Figure 11-37 illustrates a "shield spray" in which the spray nozzle is mounted on the aft face of the shield and directed toward the wing leading edge. Figure 11-38 illustrates a "wing spray" in which a pop-out nozzle is mounted in the turbulent lower surface of the wing leading edge and the spray is directed forward and slightly upward. Aerodynamic forces cause the liquid to be distributed across the leading edge. The shield spray is utilized when the shield is deployed while the wing spray can be used when the shield is retracted. A schematic diagram of a liquid supply system suitable for either spray nozzle arrangement is shown in Figure 11-39.

During take-off through a contaminated region or in icing conditions, the shield provides the primary contamination avoidance function. Earlier studies indicated that a supplemental system may be required near the wing tip at minimum angle of attack and for the inner wing if a thick inboard wing section is used. This augmentation of the shield can be provided by operating the shield spray system as required during take-off and climb or descent. Normally

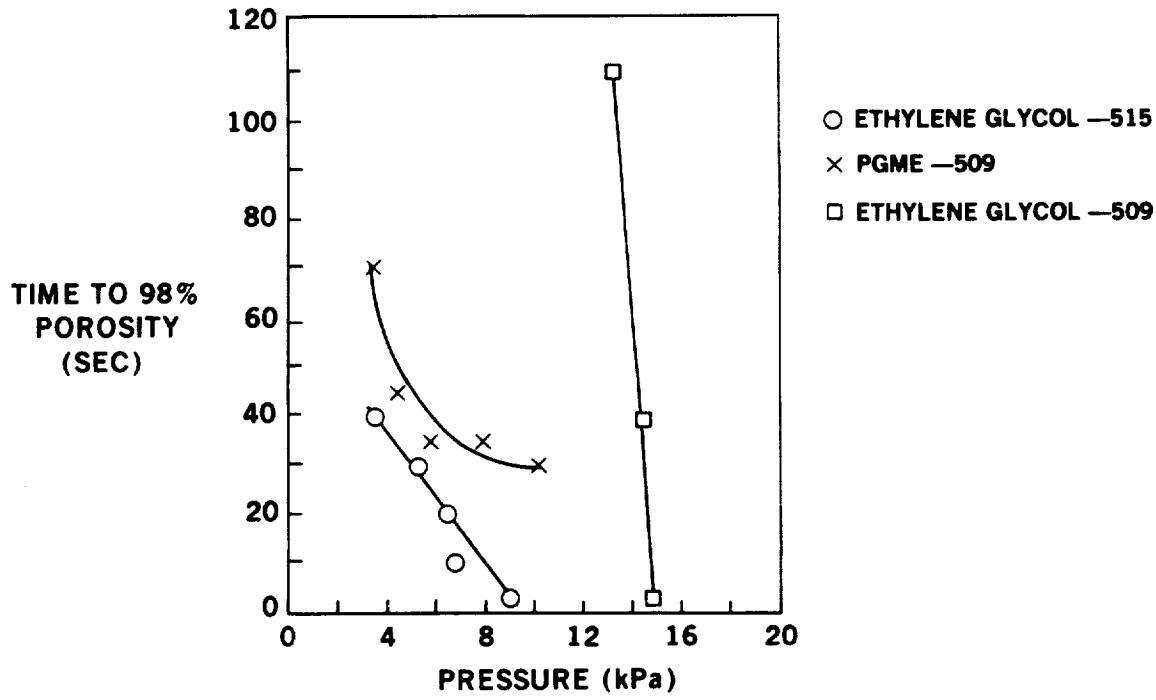

FIGURE 11-36. LIQUID CLEARANCE TIME VERSUS PRESSURE

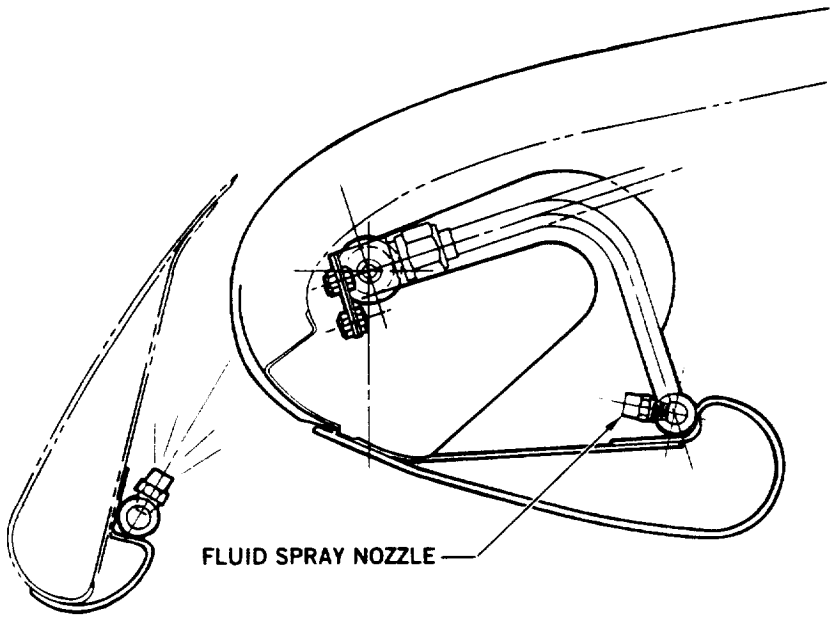

FIGURE 11-37. SHIELD SPRAY CONCEPT

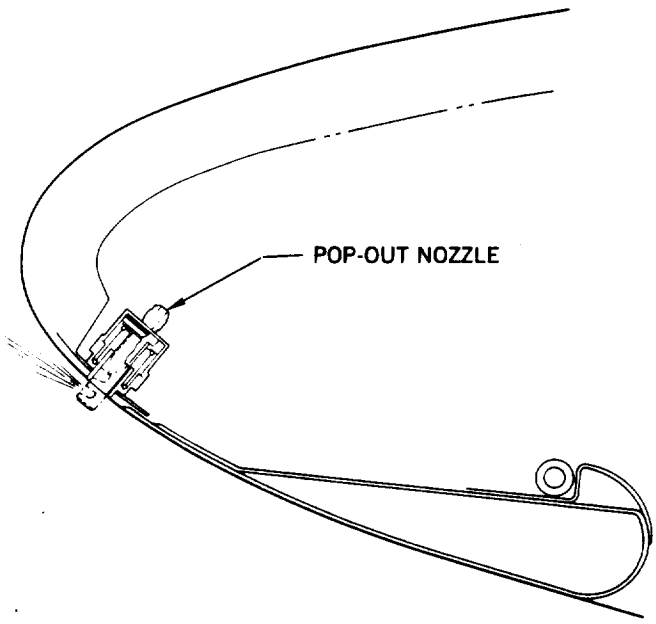

FIGURE 11-38. RETRACTABLE NOZZLE CONCEPT

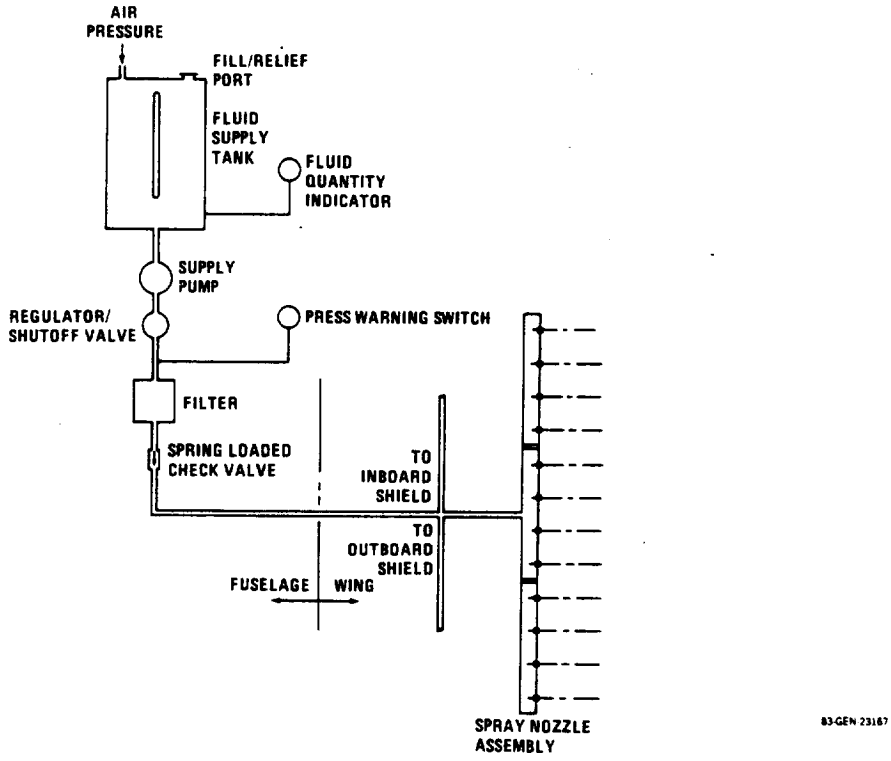

FIGURE 11-39. SCHEMATIC DIAGRAM OF LFC LEADING-EDGE CONTAMINATION-AVOIDANCE SYSTEM (SHIELD SPRAY CONCEPT)

the shield spray would be shut off and the shield retracted at about 1524m (5,000 feet) altitude. When icing conditions are anticipated between 1524m (5,000 feet) and the cruise altitude, there are two options:

(a) To keep the shield extended through the icing condition and use the shield spray to de-ice the wing if required.

(b) To retract the shield and use the wing spray system to de-ice after reaching initial cruise altitude.

Light icing conditions could be encountered on rare occasions at cruise altitudes. This would be insignificant for a turbulent aircraft but LFC could be lost during and after such an encounter unless the ice cap were removed. Either spray system could be used during these encounters.

Freezing point depressants have been used in numerous ice protection applications generally operating in an anti-icing mode. Liquid sprays have been used to remove ice and snow on the ground, however, the liquid was heated and used at higher flow rates than would be practical for an airborne application. To the best of our knowledge, no data are available to indicate the effectiveness of a freezing point depressant liquid spray for de-icing. Icing tunnel and/or icing flight tests will be required to determine de-icing capability.

11.7.1 Shield Spray System Evaluation

The evaluation of the shield spray system feasibility includes:

(a) The effect of the high velocity airstream between the shield and wing on the droplet trajectory.

(b) The selection of a nozzle to provide the desired distribution of droplet size and velocity.

(c) Droplet breakup due to high relative air-to-droplet velocities.

11.7.1.1 Liquid Droplet Trajectory - Douglas computer program H9PB, "Water Impingement on Two-Dimensional, Multi-Element Airfoils" has the capability of analyzing the trajectory of a droplet in the flow-field induced by an airfoil composed of up to ten elements. This program was originally written as a wing ice protection design tool and considers a small, supercooled droplet starting at about ten chord lengths forward of the wing. The computer program calculates the droplet trajectory and determines the catch on the wing. The program was modified so that an arbitrary starting location, velocity and direction could be input for a single droplet.

The amount of droplet deviation from a straight line would be expected to be a function of:

(a) Inertial forces (droplet mass and initial velocity).

(b) Aerodynamic forces (aircraft altitude, airspeed, angle of attack, flap angle, etc.).

(c) Trajectory (initial droplet angle and chord length).

Parametric analyses were conducted to obtain a first-order indication of the significance of the various parameters and to obtain preliminary design values. An existing airfoil model which is representative of the wing outboard of 40% span was used for this portion of the study. The range of variation of the parameters is tabulated below:

Altitude:	Sea level to 4752m (15,000 feet)
Airspeed:	118 to 165 m/s (230 to 320 KIAS)
Angle of Attack (α):	0^{o} to 10^{o}
Flap Angle:	0^{o}
Chord Length (C):	1778mm (70 inches)
Initial Droplet Velocity (Vd):	15 to 122m/s (50 to 400 fps)
Initial Droplet Angle* (ϕ):	25^{o} to 35^{o}

*ϕ is defined as the angle between the nozzle center line and wing reference plane.

The droplet diameter was varied from 2,000 microns down to the minimum size that would impinge on the wing leading edge.

A large number of trajectories were calculated to find the limiting drop size that is tangent to the wing upper surface for each set of conditions. Figure 11-40 is a plot of these results for a specific nozzle orientation. A value of $\phi = 30^{o}$ was selected to minimize the loss of liquid resulting from small drops being blown above the wing and large drops impinging too low so that they flow over the wing lower surface. Figure 11-40 shows that the shield spray will be most efficient at $\alpha = 0^{o}$ and least efficient at $\alpha = 10$. Outboard portions of the wing may require the spray for insect protection at low angles of attack (while the aircraft is on the runway during take-off and landing). The thick inboard section may require spray at both high and low angles of attack. The center section of the wing probably will not require liquid for insect protection. To obtain a conser-

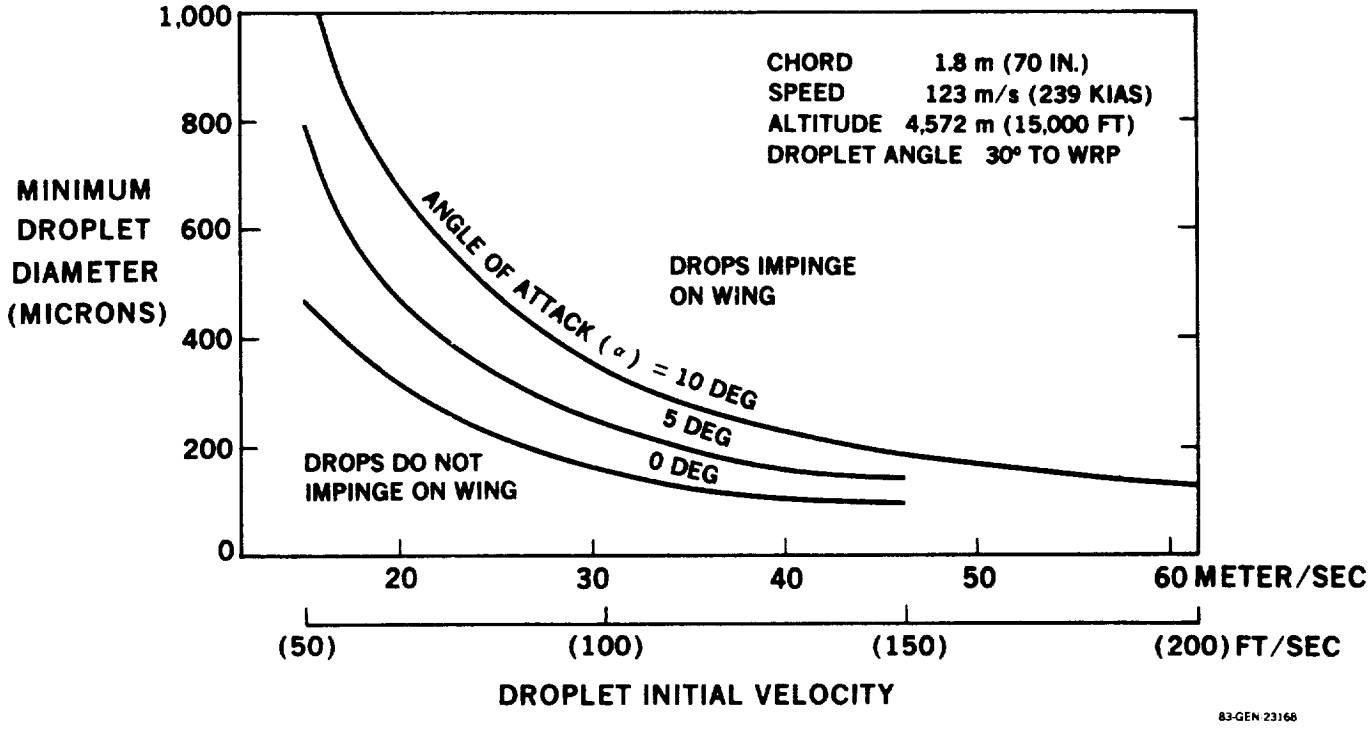

FIGURE 11-40. MINIMUM DROPLET DIAMETER TO IMPINGE ON WING VERSUS INITIAL DROPLET VELOCITY (DC-9 ICING TUNNEL WING WITH SHIELD)

vative estimate of the shield spray system, the preliminary design is based on $\alpha = 10^{0}$.

11.7.1.2 Nozzle Selection and Performance - Nozzles are available for numerous specialized applications such as cleaning, painting, combustion, manufacturing, cooling/humidifying, agriculture, etc. The flat spray nozzle appears to be the most suitable for the LFC application. This section compiles some of the performance characteristics available for flat spray nozzles. Much of the information was obtained through the courtesy of Spraying Systems Company.

A typical flat spray pattern is shown in Figure 11-41 (Spraying Systems Co. Drawing No. 13777). The pattern is "full" as contrasted with the "hollow" cone pattern also shown. The flat spray is characterized by a narrow band of liquid in one direction and a wide spray angle that can be generally specified between 15^{0} and 110^{0} in the other direction at 276 Pa (40 psig) nozzle pressure. The actual spray coverage is reduced from the theoretical value based on a nominal spray angle as the nozzle pressure and spray distance are increased.

A theoretical nozzle capacity can be calculated based on the assumption that the nozzle frictional losses are small with respect to the nozzle pressure so that all of the pressure is transformed into kinetic energy. Based on this assumption and the continuity equation,

$$Q_T = 456 \; A \sqrt{p} \times \sqrt{\rho o / \rho}$$

Where: A is the nozzle area in square feet.
p is the nozzle pressure in psf
ρ is the liquid density in lb/cu. feet
ρo is the density of water at 70^{0}F in lb/cu. feet
Q_T is the theoretical nozzle capacity in gpm

The distribution of droplet sizes that are formed by a nozzle ejecting a liquid into air is described by the median volume diameter:

The Median Volume Diameter is that diameter of droplet, above or below which is found half the mass (or volume) of the spray.

NOZZLE NO.	PRESSURE IN PSI	CAPACITY IN GPM	*PARTICLE SIZE DIA IN MICRONS PERCENT OF THE VOLUME OF LIQUID IN DROPS LESS THAN THE DIAMETERS SHOWN BELOW		
			2%	50% MEDIAN VOL DIA	98%
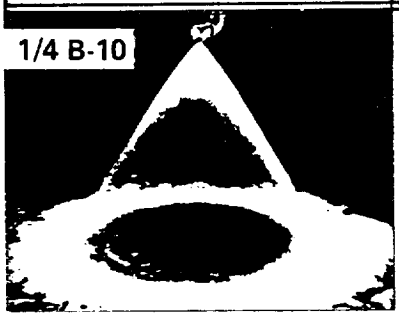 1/4 B-10 *WhirlJet.* NOZZLES HOLLOW CONE SPRAY PATTERN	10	1.0	. 200	. 645	● 1,300
	40	2.0	. 170	. 545	. 1,000
	100	3.2	. 140	. 440	. 880
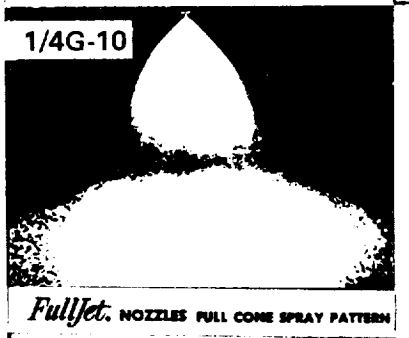 1/4G-10 *FullJet.* NOZZLES FULL CONE SPRAY PATTERN	10	1.0	. 700	● 2,910	● 5,500
	40	1.9	. 400	● 2,040	● 3,900
	100	3.0	200	. 1,240	● 2,750
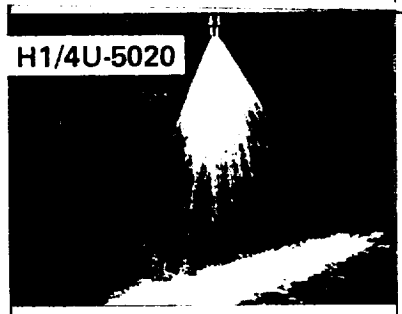 H1/4U-5020 *VeeJet.* NOZZLES FLAT SPRAY PATTERN	10	1.0	. 420	. 1,355	● 2,910
	40	2.0	. 350	. 1,180	● 2,700
	100	3.2	. 290	. 910	● 1,650

*BASED ON VOLUMETRIC MEASUREMENTS (0.001 INCH EQUALS 25.4 MICRONS).

NOTE: PARTICLE SIZE ESTIMATES ARE BASED ON SPRAYING WATER AT ROOM TEMPERATURE UNDER LABORATORY CONDITIONS AND SHOULD BE USED AS APPROXIMATIONS ONLY.

FIGURE 11-41. VISUAL AID FOR COMPARING RELATIVE PARTICLE SIZES OF NOZZLES WITH EQUAL CAPACITIES AND SPRAY ANGLES

83-GEN-23169

Figure 11-42 presents the median volume diameter for a series of Spraying Systems Co. flat spray nozzles as a function of pressure. Figure 11-41 also presents the 2, 50 and 98 percentile droplet sizes for flat spray nozzles at various pressures. Assuming a normal distribution, the 2 and 98 percentile values correspond to 2.05 standard deviations. It can be seen from Figure 11-41 data that the standard deviation varies with nozzle pressure and differs above and below the median volume diameter.

Using the foregoing data, a relationship can be derived between initial droplet velocity (Vd) and nozzle pressure (p):

$$Vd = 1.0159\ \eta \sqrt{p}$$

Where: p is the nozzle pressure in psf

Vd is the nozzle droplet velocity in fps

η is the nozzle efficiency (dimensionless)

The above relationship between initial velocity and pressure permits a comparison to be made between the requirements of Figure 11-40 and the mean droplet diameter (dm) produced by a given nozzle at the same conditions. For instance, a pressure of 1158kPa (168 psig) is required to provide an initial droplet velocity of 13.9m/s (150 fps) (assuming a nozzle efficiency of 95%. At this velocity, Figure 11-40 shows that droplets smaller than 190 microns will not impinge on the wing leading edge at an angle of attack of 10^{o}.

Assuming a requirement for 90 percent of the liquid spray to impinge on the wing and a normal spray distribution with a standard deviation of 0.0332 dm (Figure 11-41), a mean droplet diameter (dm) of 331 microns is required. Comparing this requirement with the nozzle performance characteristics (Figure 11-42) indicates that a nozzle such as Spraying Systems Co. Nozzle 9506 with a nozzle orifice diameter of 1.57mm (0.062 in) will best approximate the desired spray distribution. As will be seen from considering droplet shattering, a smaller diameter nozzle at a higher operating pressure and a higher duty cycle may be more suitable for the final design. For preliminary design purposes, a 9502 nozzle, with an orifice diameter of 0.91mm (0.036 in) and a 1785kPa (255 psig) operating pressure were selected. This combination will require a 22 percent duty cycle to give the flow rate necessary for contamination-avoidance. The duty cycle being the percent of total time in contamination that the spray is ON. The performance chart of Figure 11-43

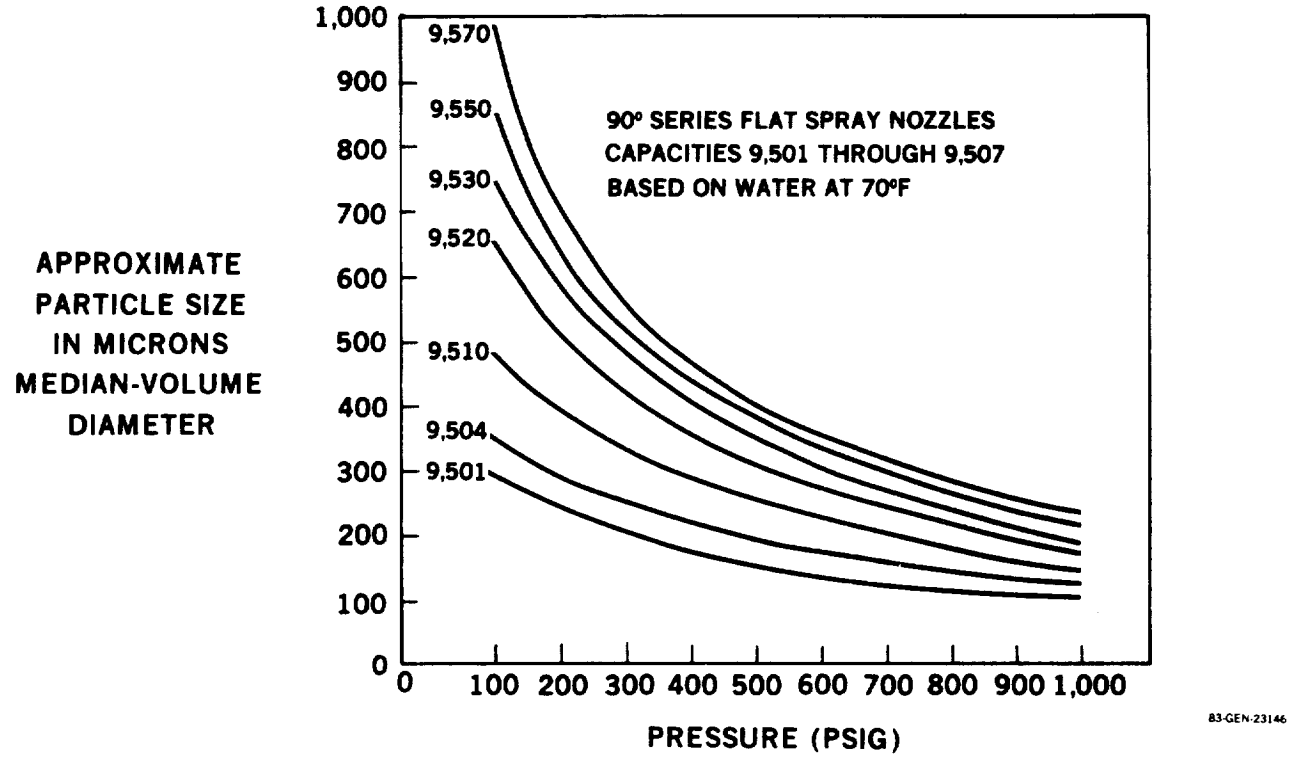

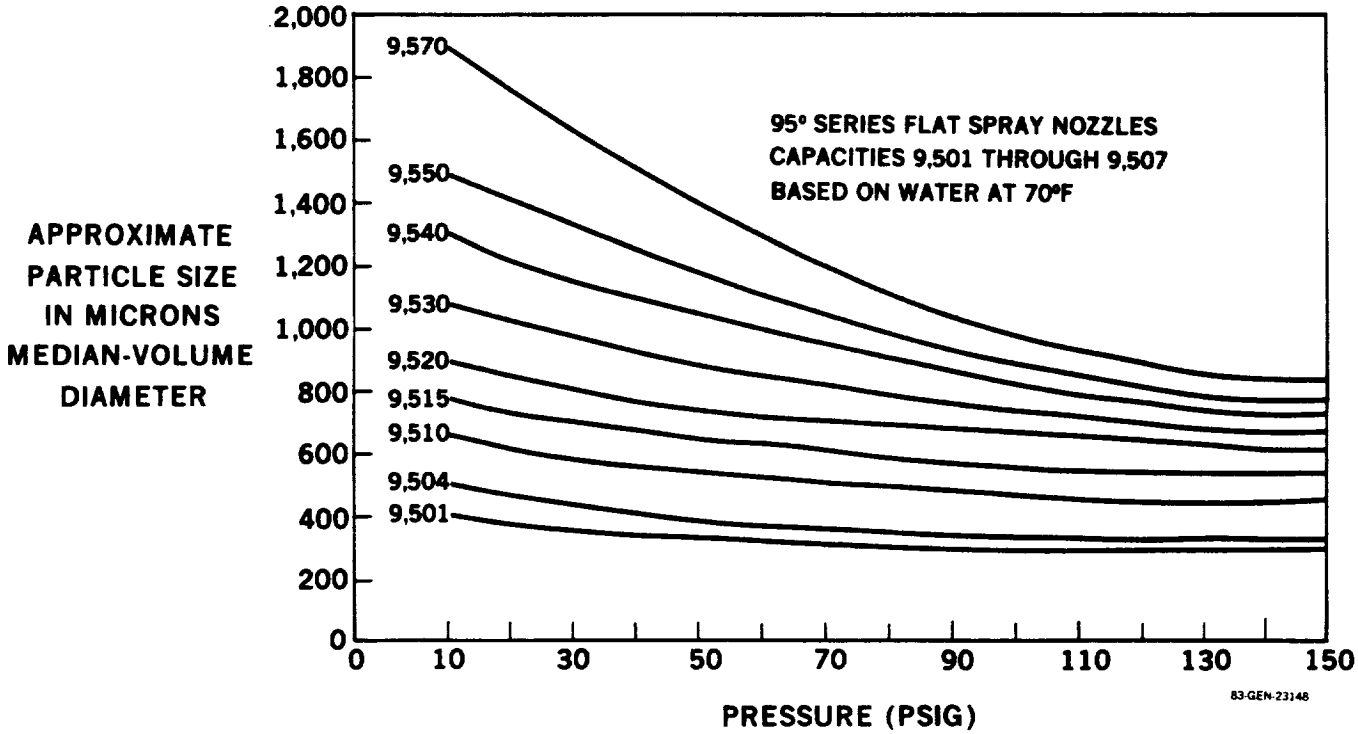

FIGURE 11-42. SPRAY PARTICLE SIZE VERSUS PRESSURE

was obtained by crossplotting the required nozzle characteristics as calculated above (for various initial velocities and impingement efficiencies) against the nozzle spray characteristics.

Based on Spraying Systems Co. data, a 9502 nozzle operating at 1758 kPa (255 psig) will result in a median volume diameter of 233 microns. Assuming that the droplet size distribution shown in Figure 11-41 for 690 kPa (100 psig) is valid for higher pressures, the droplet distribution at the design condition is as shown in Figure 11-44. Superimposed on this figure is the minimum drop size at $\alpha = 10^{o}F$ for any initial velocity, which is 140 microns. Thus droplets with a diameter less than 140 microns will not impinge on the wing. Figure 11-45 is a plot of cumulative volume of drops and indicates that about 11 percent of the volume of the spray will be in droplets with a diameter less than 140 microns.

11.7.1.3 Droplet Shattering - As the droplets travel between the shield and the wing leading edge, high relative airflow velocities can be encountered which could cause the droplet to shatter. To determine the extent to which droplet shattering will affect the spray system performance, the relative velocity of the droplet was calculated using data from computer program H9PB. A typical result is shown in Figure 11-46. Based on data from Wolfe and Anderson (Appendix A), the maximum droplet diameter that will not shatter was calculated as a function of relative velocity, Figure 11-47. By comparing Figures 11-46 and 11-47, it can be seen that droplets of 400 microns and smaller will not shatter over most of the trajectory. However, the minimum relative velocity to shatter will be exceeded during the last 0.02 chord lengths of travel. Since the time required for the droplet to travel across this distance is of the same order as the time to shatter, it is not possible to predict the outcome with any degree of certainty. The high relative velocity is encountered at high angles of attack and at a location above the leading edge. The velocity encountered by droplets impinging lower on the wing leading edge will be less than that shown in Figure 11-46 and the tendency to shatter reduced. Because of the difficulty in analyzing the transient shattering of drops, wind tunnel and/or flight tests will be required to optimize the nozzle characteristics.

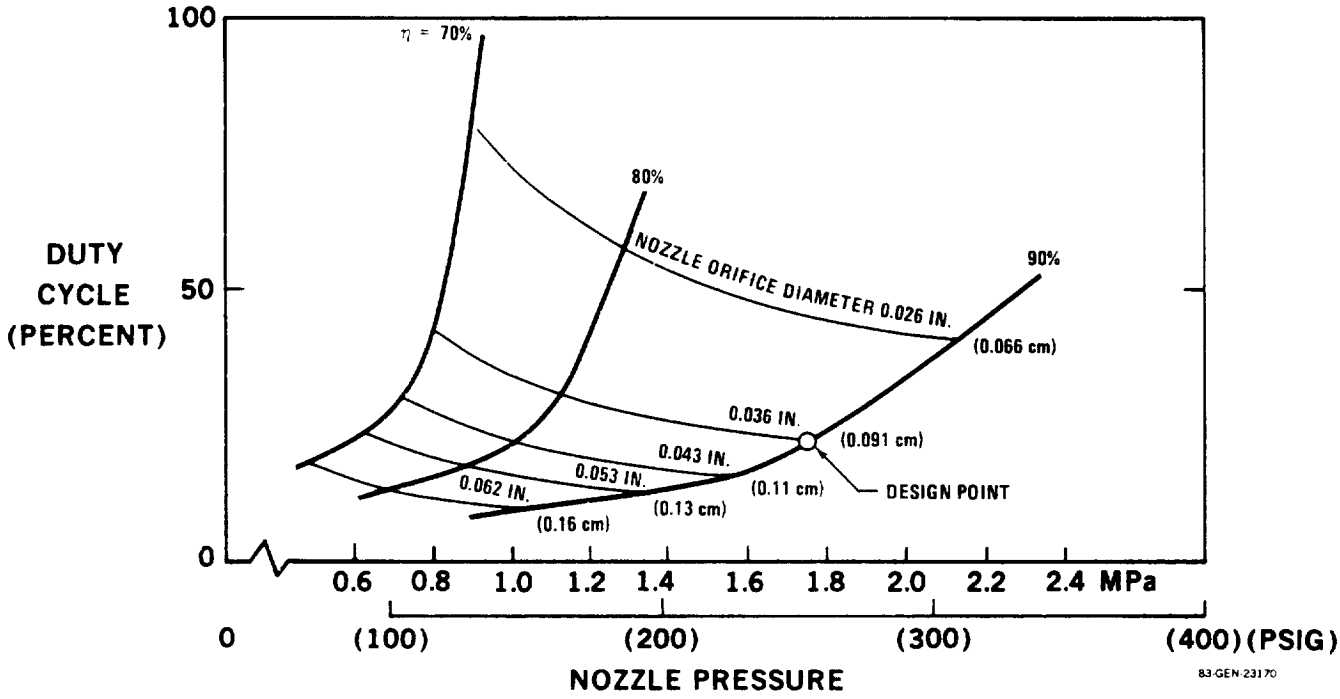

FIGURE 11-43. SHIELD SPRAY PERFORMANCE DC-9 ICING TUNNEL MODEL (0° FLAPS, α = 10°)

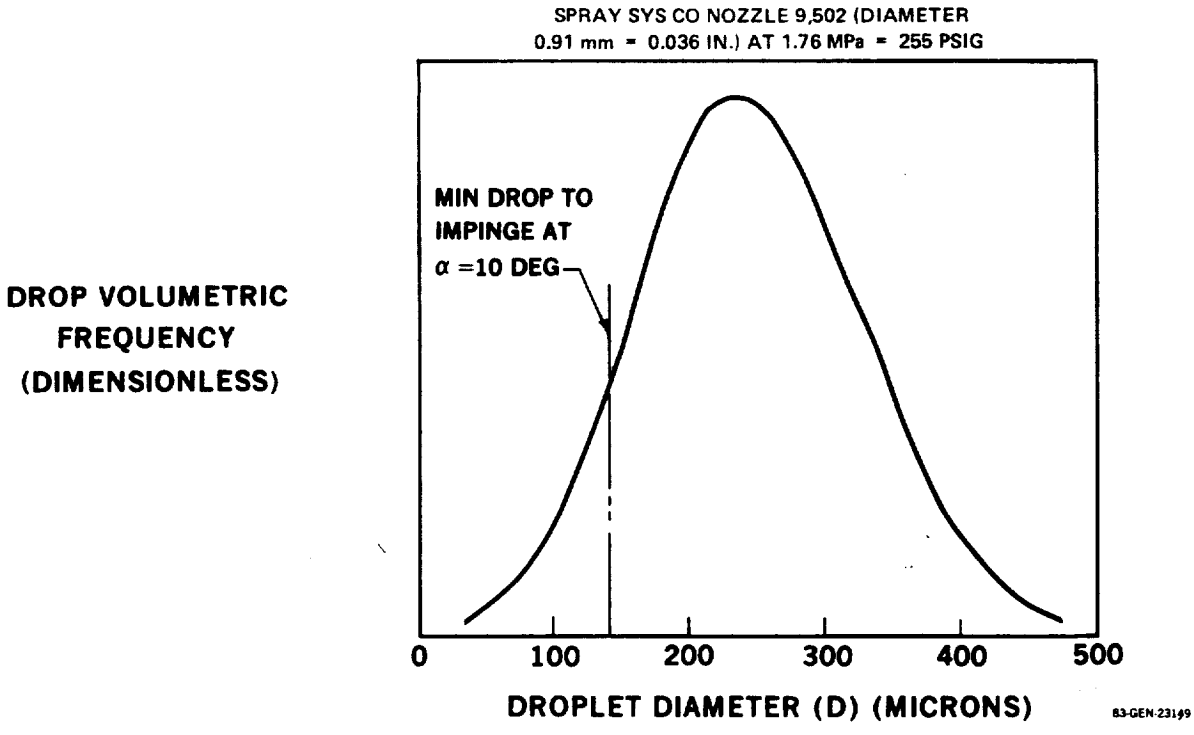

FIGURE 11-44. DROP SIZE DISTRIBUTION

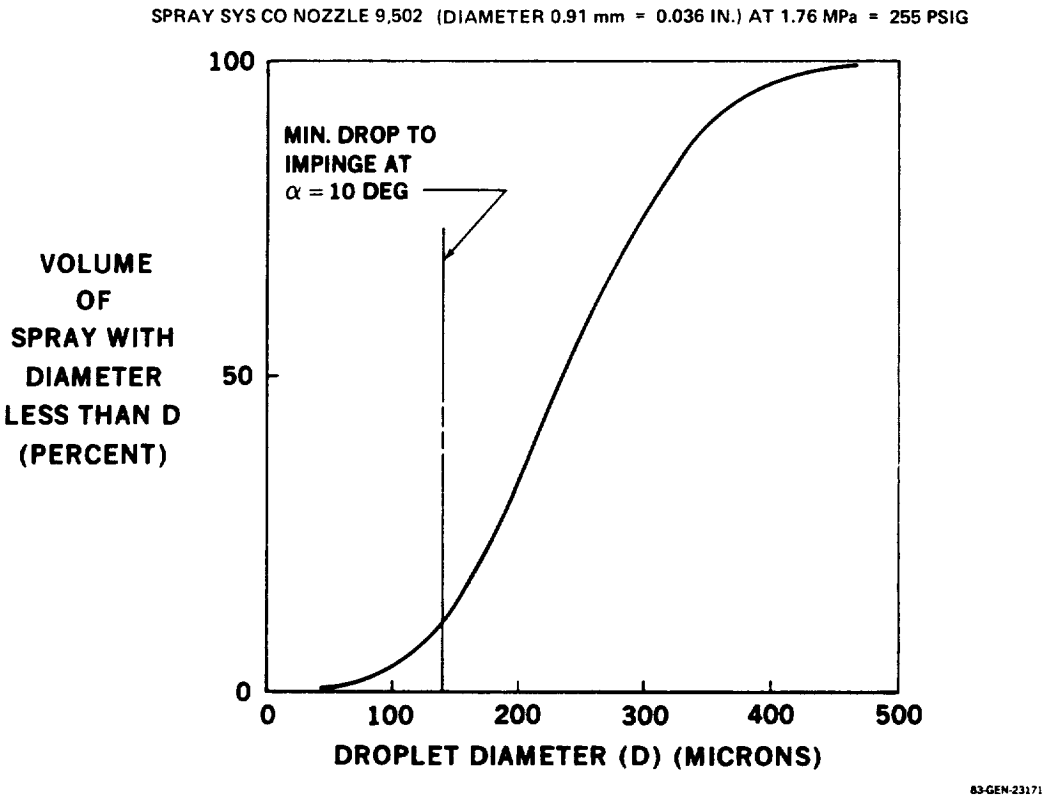

FIGURE 11-45. CUMULATIVE DROP SIZE DISTRIBUTION

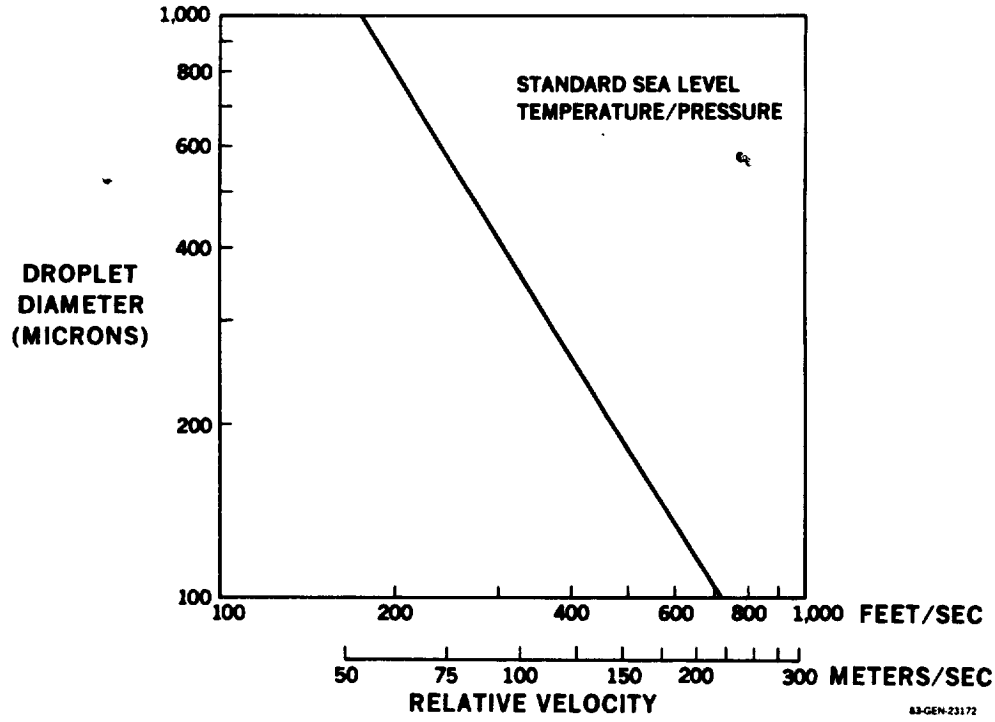

FIGURE 11-46. MAXIMUM DROPLET DIAMETER (WITHOUT SHATTERING)

11.7.1.4 Preliminary Shield Spray Design - A shield spray system similar to that shown previously in Figure 11-37 would be supplied with liquid by a system similar to that shown in Figure 11-39. The amount of contamination avoidance and ice protection required to supplement the shield will be determined during the flight test program. Conservatively, 254kg (560 pounds) of liquid can be used to provide contamination avoidance for the entire wing during two complete flights (take-off, climb, descent and landing). An additional 91kg (201 pounds) of liquid will provide three de-icing cycles for each of two clights. The total weight of the portion of the system located in the fuselage chargeable to the shield spray is about 466kg (1028 pounds) including shield ice protection. This includes the liquid, tankage, pump, motor, filter and regulator.

A less conservative estimate of the liquid requirement can be based on the assumption that the spray system is required only for the portion of the wing inboard of the aerodynamic break. To provide insect protection for the flight envelope as described above, the amount of liquid could be reduced to about 216kg (476 pounds) and the total system weight (in the fuselage) would be about 243kg (535 pounds).

11.7.1.5 Shield Spray System Evaluation - Many of the features of the spray system are identical to those of the liquid-film system discussed in Section 11.3.2.1. Therefore, to simplify the evaluation, this section will stress differences between the two systems.

The most important difference between the shield spray and liquid-film is in the area of design. The spray system uses fully developed components and greatly simplifies the design of the surface suction panels in the wing leading edge area because integration of LFC suction and liquid systems is not required.

A second major difference is that the shield spray can only operate when the shield is extended. This poses an operational constraint in that the shield must be extended during or after icing encounters. Flight testing will be required to determine the frequency of occurrence and, hence, the operational impact of this consideration.

The final differences involve spray efficiency and nozzle characteristics. The inefficiencies of the spray system, including any effects of drop shattering, will result in higher system weights for a spray system when compared with a liquid-film system. Also, limitations on nozzle size may require pulsing. This is felt to be a minor penalty against the shield spray system.

In summary, the shield spray system is a low risk method of providing supplemental contamination-avoidance and ice protection. Flight testing is required to fully evaluate the fluid requirements, de-icing capability, and suitability of operational procedures.

11.7.2 Wing Spray System Evaluation

The evaluation of the wing spray system is similar to the shield spray study and includes:

(a) The effect of the high velocity airstream on the droplet trajectory.

(b) The selection of a nozzle and operating conditions that will provide the desired distribution of droplets both in size and space.

(c) Droplet breakup due to high relative air-to-droplet velocities.

11.7.2.1 Liquid Droplet Trajectory - The trajectory analysis for the wing spray system is similar to that described in Section 11.7.1.1 with several exceptions. The shield is in the retracted position and the droplet is directed forward and upward into the airstream from below the wing leading edge. Typical cruise flight conditions were used for the analysis. The parameters that were found to have the greatest influence on droplet trajectory were the angle of attack (α), the angle at which the droplet was initially directed (ϕ), and the initial droplet velocity (Vd).

Early studies showed that if a value of ϕ were less than 25^{o}, the range of drop sizes that would impinge on the wing leading edge became infinitesimally small at certain initial drop velocities. The studies also showed that if ϕ were increased to 35^{o} or more, the range of drop sizes that would impinge on the wing leading edge decreased. This decrease is a result of the sensitivity of the droplet trajectory to α when the initial velocity vector has a large vertical component. A value of $\phi = 30^{o}$ was therefore chosen for the analysis.

A series of computer runs was conducted to determine the range of drop sizes that will impinge on the wing leading edge as a function of initial droplet velocity for various angles of attack. Figures 11-48 through 11-52 show the trajectories of various drops at $\alpha = 0^{o}$ with initial droplet velocities of 45.7m.s (150 fps) and 18.3 m.s (60 fps). The droplet starts at the lower surface aft of the leading edge, travels forward and upward into the airstream, and is finally blown back. The largest drops tend to travel over the wing and the smallest droplets are blown back under the wing.

Figure 11-53 through 11-56 show comparative trajectories for $\alpha = -1^{o}$ and $\alpha = +1^{o}$ and initial droplet velocities of 45.7 m.s (150 fps). The distance that the droplet travels in front of the wing increases as the angle of attack decreases. The results of these and similar trajectory analyses are summarized in Figure 11-57 through 11-59. It can be seen that the band of drop sizes that impinge on the wing increases as angle of attack decreases.

11.7.2.2 Droplet Shattering - When the spray is discharged into the airstream, the relative velocity between the liquid and air is very high. The initial relative velocity is mainly a function of the location of the spray nozzle along the airfoil and is secondarily dependent on nozzle pressure. Data regarding the drop size distribution of nozzles are generally based on tests in still air. In the airstream, however, the larger droplets will shatter so that the mean drop size will be less than that based on available literature.

High relative velocities may also be encountered as the droplet approaches the body. Figure 11-60 shows the relative velocity of the droplet for the trajectory shown in Figure 11-51. Droplets that impinge lower on the leading edge will not encounter the high velocity region near impingement.

Figure 11-61 presents the maximum droplet diameter to avoid shattering versus relative velocity for a cruise condition. It can be seen that droplets in the range of 400 to 600 microns may shatter at the relative velocities shown in Figure 11-60.

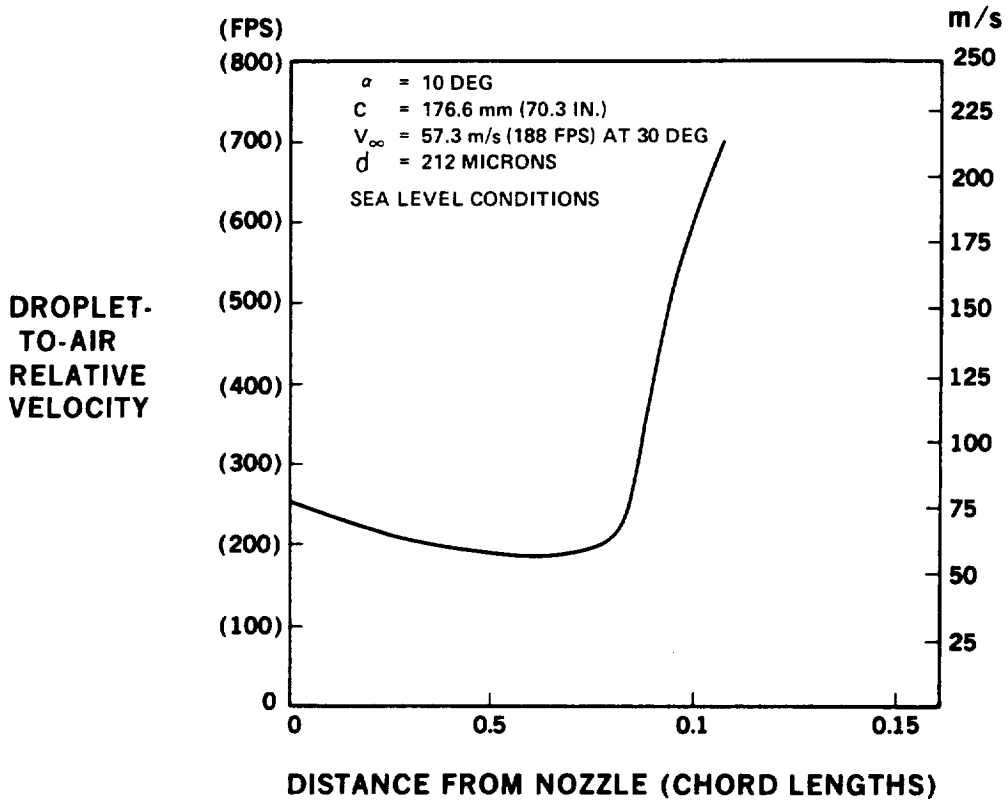

FIGURE 11-47. DROPLET-TO-AIR RELATIVE VELOCITY (SHIELD SPRAY SYSTEM)

ANGLE OF ATTACK	**= 0.0 DEGREES**	**AMB PRESS**	**= 24.1 kPa (3.5 PSI)**
CHORD LENGTH	**= 1.78 m (70.3 IN.)**	**AMB TEMP**	**= 420°R**
AIRSPEED	**= 140 m/s (272 KIAS)**	**DROP VELOCITY**	**= 45.7 m/s (150 FPS)**

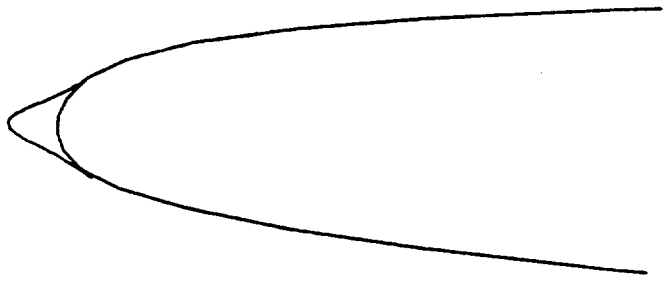

83-GEN-23174

FIGURE 11-48. DROPLET TRAJECTORIES FOR SPRAY NOZZLE - DC-9 ICING TUNNEL AIRFOIL – DROP SIZE 279. MICRONS

ANGLE OF ATTACK	=	0.0 DEGREES	CHORD LENGTH	=	1.78 m (70.3 IN.)
DROP VELOCITY	=	45.7 m/s (150 FPS)	AIRSPEED	=	140 m/s (272 KIAS)
AMB PRESS	=	24.1 kPa (3.5 PSI)	AMB TEMP	=	420° R

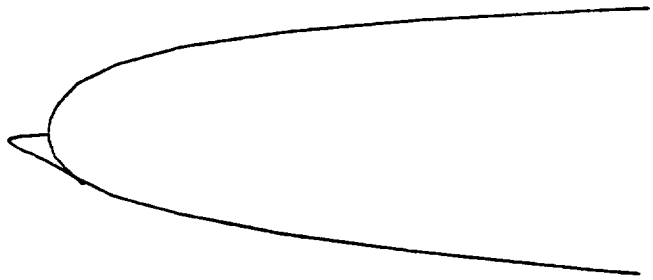

83-GEN:23135
uc583 m1895a2

FIGURE 11-49. DROPLET TRAJECTORIES FOR SPRAY NOZZLE - DC-9 ICING TUNNEL AIRFOIL – DROP SIZE 260. MICRONS

ANGLE OF ATTACK	= 0.0 DEGREES	AMB PRESS	= 24.1 kPa (3.5 PSI)
CHORD LENGTH	= 1.78 m (70.3 IN.)	AMB TEMP	= 420°R
AIRSPEED	= 140 m/s (272 KIAS)	DROP VELOCITY	= 45.7 m/s (150 FPS)

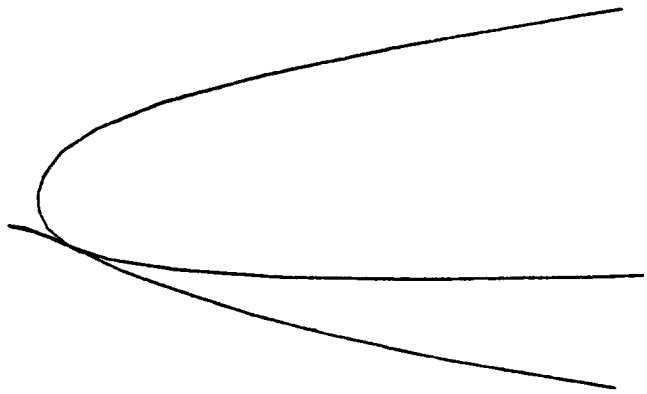

83-GEN:23175

FIGURE 11-50. DROPLET TRAJECTORIES FOR SPRAY NOZZLE - DC-9 ICING TUNNEL AIRFOIL – DROP SIZE 245. MICRONS

ANGLE OF ATTACK	=	0.0 DEGREES	AMB PRESS	=	24.1 kPa (3.5 PSI)
CHORD LENGTH	=	1.78 m (70.3 IN.)	AMB TEMP	=	420° R
AIRSPEED	=	140 m/s (272 KIAS)	DROP VELOCITY	=	45.7 m/s (150 FPS)

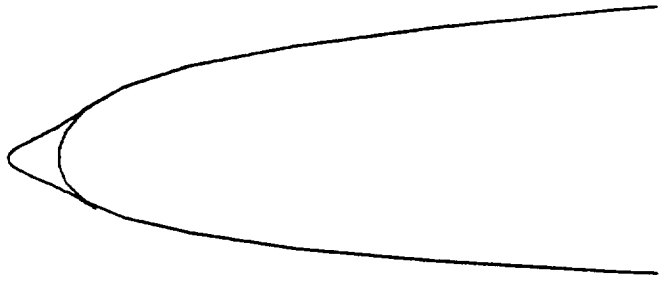

83-GEN-23176
uc583 m1895a1

FIGURE 11-51. DROPLET TRAJECTORIES FOR SPRAY NOZZLE - DC-9 ICING TUNNEL AIRFOIL – DROP SIZE 1,160. MICRONS

ANGLE OF ATTACK	=	0.0 DEGREES	AMB PRESS	=	24.1 kPa (3.5 PSI)
CHORD LENGTH	=	1.78 m (70.3 IN.)	AMB TEMP	=	420° R
AIRSPEED	=	140 m/s (272 KIAS)	DROP VELOCITY	=	45.7 m/s (150 FPS)

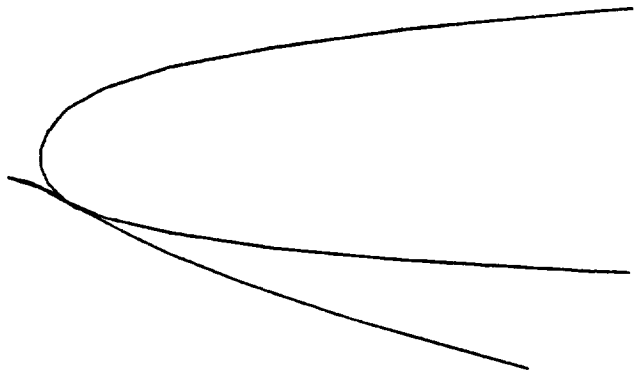

83-GEN-23177

FIGURE 11-52. DROPLET TRAJECTORIES, FOR SPRAY NOZZLE - DC-9 ICING TUNNEL AIRFOIL – DROP SIZE 1,025. MICRONS

ANGLE OF ATTACK	=	1.00 DEGREES	AMB PRESS.	=	24.1 kPa (3.5 PSI)
CHORD LENGTH	=	1.78 m (70.3 IN.)	AMB TEMP	=	420°R
AIRSPEED	=	140 m/s (272 KIAS)	DROP VELOCITY	=	45.7 m/s (150 FPS)

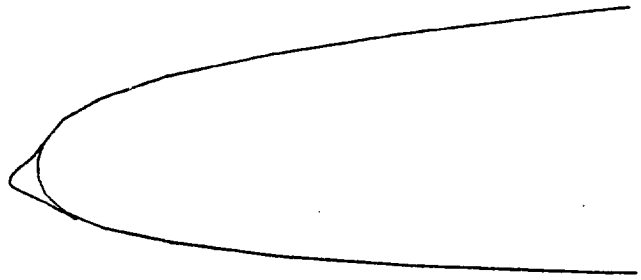

83-GEN-23240
uc583 m1895a

FIGURE 11-53. DROPLET TRAJECTORIES FOR SPRAY NOZZLE - DC-9 ICING TUNNEL AIRFOIL – DROP SIZE 187 MICRONS

ANGLE OF ATTACK	=	1.00 DEGREES	AMB PRESS.	=	24.1 kPa (3.5 PSI)
CHORD LENGTH	=	1.78 m (70.3 IN.)	AMB TEMP	=	420°R
AIRSPEED	=	140 m/s (272 KIAS)	DROP VELOCITY	=	45.7 m/s (150 FPS)

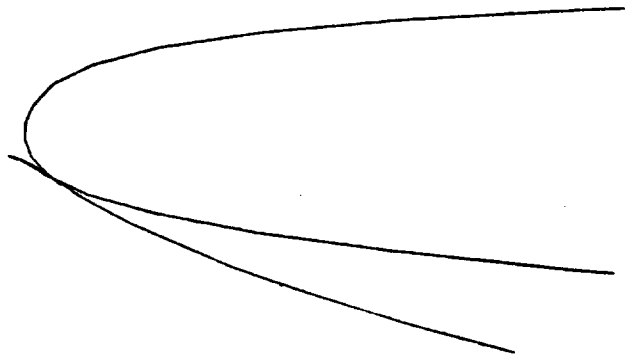

83-GEN-23239
uc583 m1895a

FIGURE 11-54. DROPLET TRAJECTORIES FOR SPRAY NOZZLE - DC-9 ICING TUNNEL AIRFOIL – DROP SIZE 170 MICRONS

ANGLE OF ATTACK	=	−1.00 DEGREES	AMB PRESS.	=	24.1 kPa (3.5 PSI)
CHORD LENGTH	=	1.78 m (70.3 IN.)	AMB TEMP	=	420°R
AIRSPEED	=	140 m/s (272 KIAS)	DROP VELOCITY	=	45.7 m/s (150 FPS)

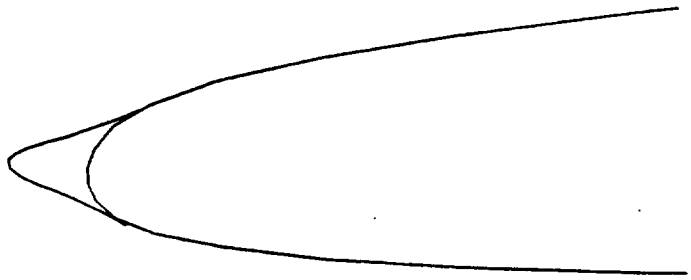

83-GEN-23236
uc583 m1895

FIGURE 11-55. DROPLET TRAJECTORIES FOR SPRAY NOZZLE - DC-9 ICING TUNNEL AIRFOIL – DROP SIZE 410 MICRONS

ANGLE OF ATTACK	=	−1.00 DEGREES	AMB PRESS.	=	24.1 kPa (3.5 PSI)
CHORD LENGTH	=	1.78 m (70.3 IN.)	AMB TEMP	=	420°R
AIRSPEED	=	140 m/s (272 KIAS)	DROP VELOCITY	=	45.7 m/s (150 FPS)

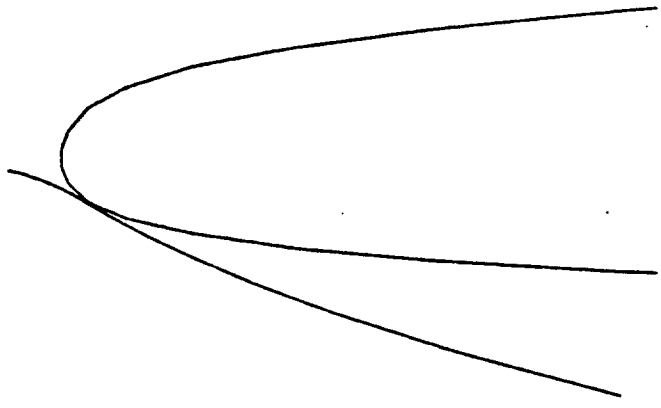

83-GEN-23237
uc583 m1895

FIGURE 11-56. DROPLET TRAJECTORIES FOR SPRAY NOZZLE - DC-9 ICING TUNNEL AIRFOIL – DROP SIZE 348 MICRONS

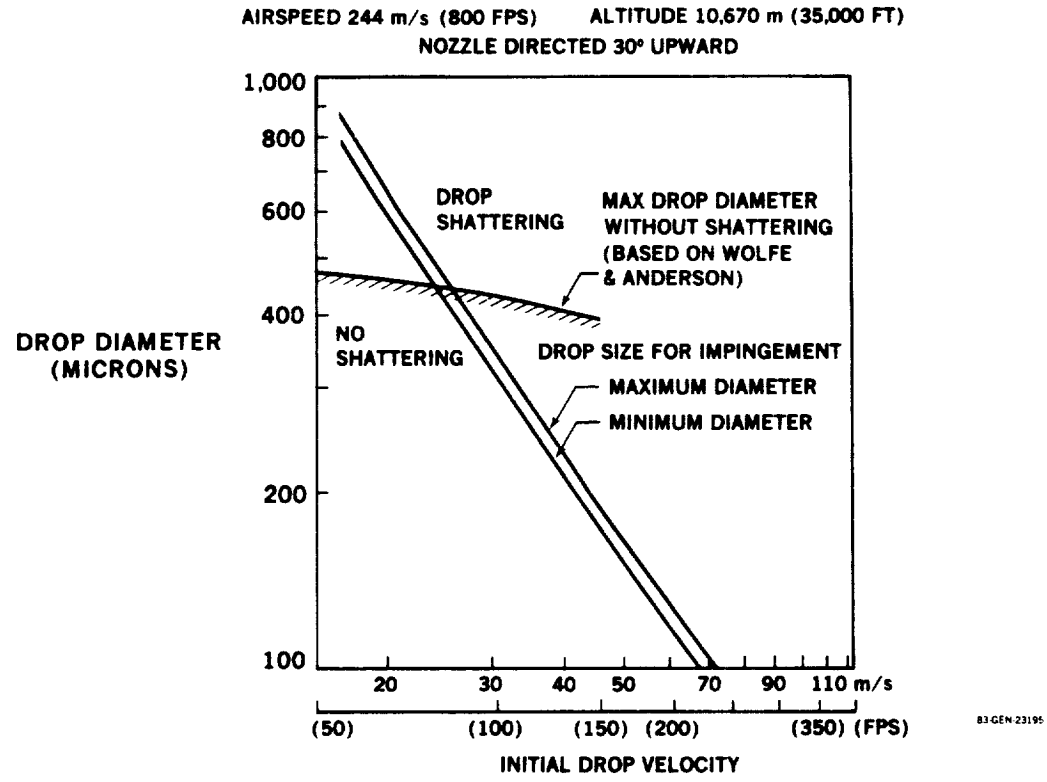

FIGURE 11-57. RANGE OF DROP SIZE FOR IMPINGEMENT – DC-9 ICING TUNNEL WING ANGLE OF ATTACK (α) = +1°

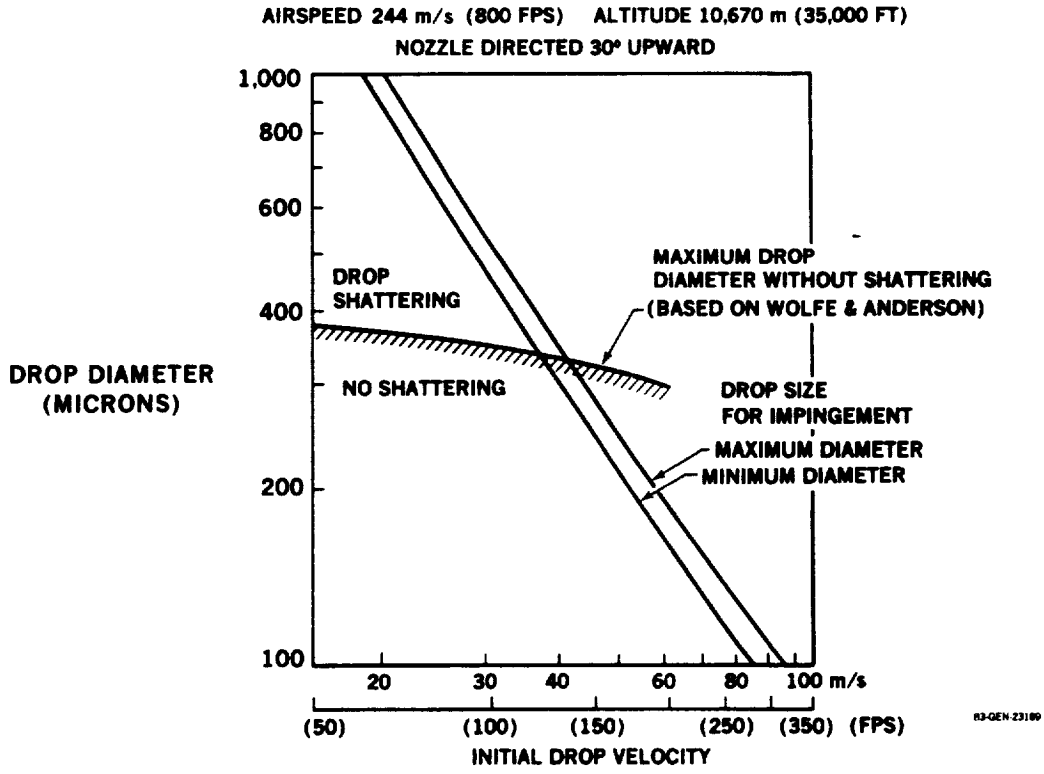

FIGURE 11-58. RANGE OF DROP SIZE FOR IMPINGEMENT – DC-9 ICING TUNNEL WING ANGLE OF ATTACK (α) = 0°

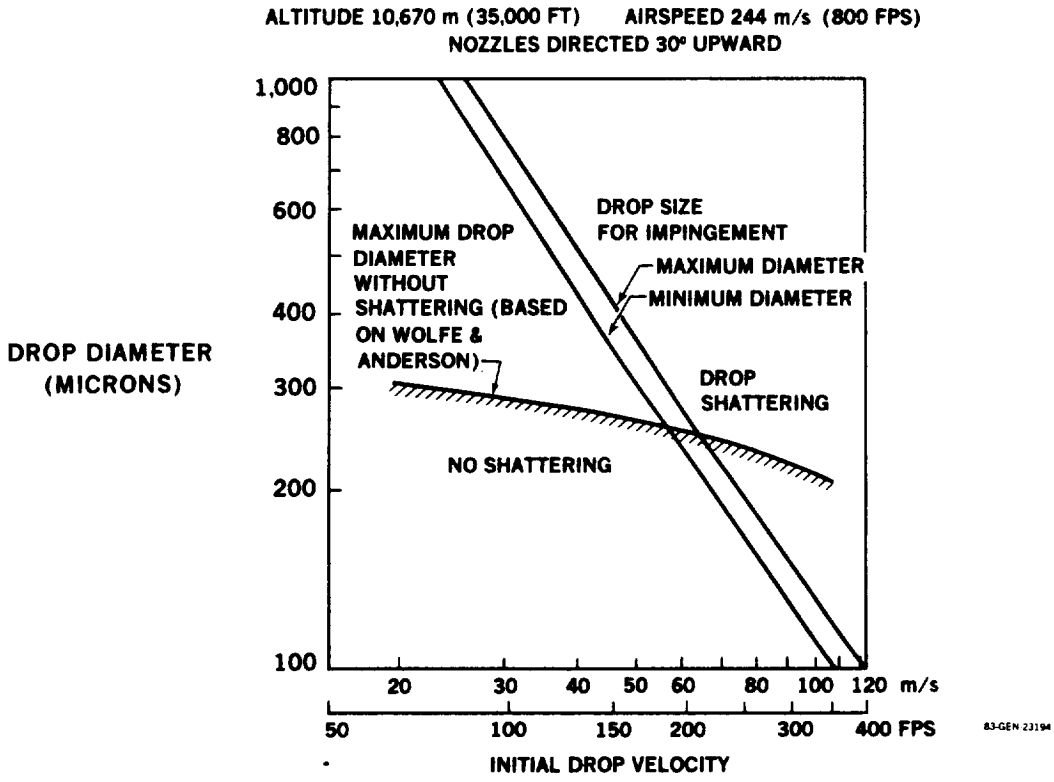

FIGURE 11-59. RANGE OF DROP SIZE FOR IMPINGEMENT – DC-9 ICING TUNNEL WING ANGLE OF ATTACK (α) = -1°

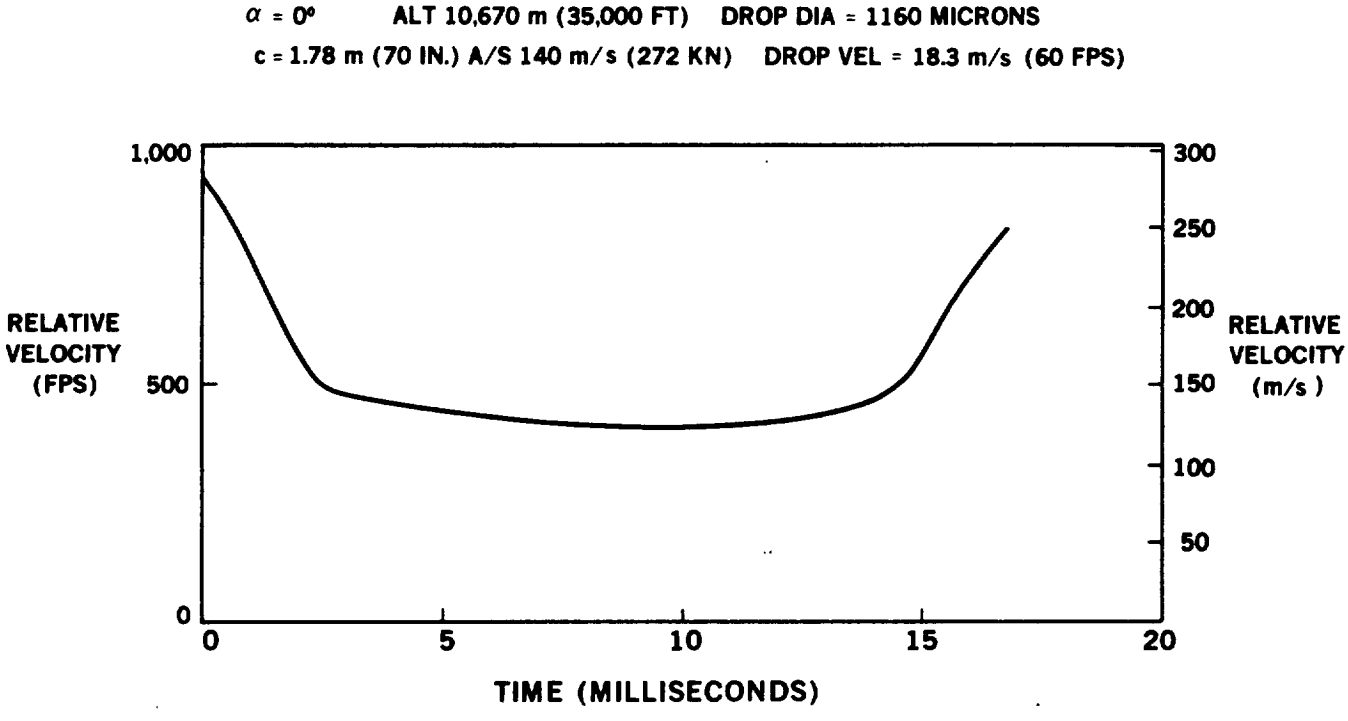

FIGURE 11-60. DROPLET-TO-AIR RELATIVE VELOCITY (WING SPRAY SYSTEM)

The region in which drop shattering affects the design of the wing spray system is shown in Figures 11-57 through 11-59. On each curve, the limiting value of diameter to avoid shattering is indicated.

11.7.2.3 Nozzle Selection and Performance - The design and method of analysis of the wing spray nozzles is similar to that described in Section 11.7.1 for the shield spray system. Flat spray nozzles with an angle of 95^{o} are spaced in a spanwise direction under the wing leading edge and are directed upward at an angle of about 30^{o}. Two types of systems were evaluated: a constant pressure system and a system in which pressure varies with the angle of attack.

From Figures 11-57 through 11-59, it is seen that the minimum initial droplet velocity that will impinge on the surface and avoid shattering is about 61m/s (200 fps) and is set by the -1^{o} angle of attack condition. The nozzle pressure required to achieve an initial droplet velocity of 61 m/s (200 fps) is about 2.0 MPa (290 psig). Figure 11-62 shows the percent of liquid that will impinge on the wing leading edge as a function of angle of attack for the two smallest off-the-shelf nozzle sizes. For a constant pressure system, it is seen that the efficiency at an angle of attack of $+1^{o}$ is less than 4%. Figure 11-63 presents the drop size distribution at the design conditions with the band of drop diameters required for impingement superimposed. The reason for the low efficiency is a combination of the narrow band of drop sizes that will impinge at $\alpha = 1^{o}$ (114 to 126 microns) and the low frequency of drops in this size range using a 0.66mm (0.026") diameter nozzle. The smaller nozzle results in an increase in the number of drops in this band and a resulting increase in efficiency (see Figure 11-62).

The efficiency of impingement can be increased by varying the nozzle pressure as a function of angle of attack. The minimum initial droplet velocity that will avoid shattering and the required pressure is tabulated below as a function of angle of attack.

Angle of Attack (α) degrees	Minimum Initial Droplet Velocity m/s	(fps)	Nozzle Pressure KPa	(psig)
+1	25.3	(83)	352	(51)
0	39.6	(130)	841	(122)
-1	60.35	(198)	2000	(290)

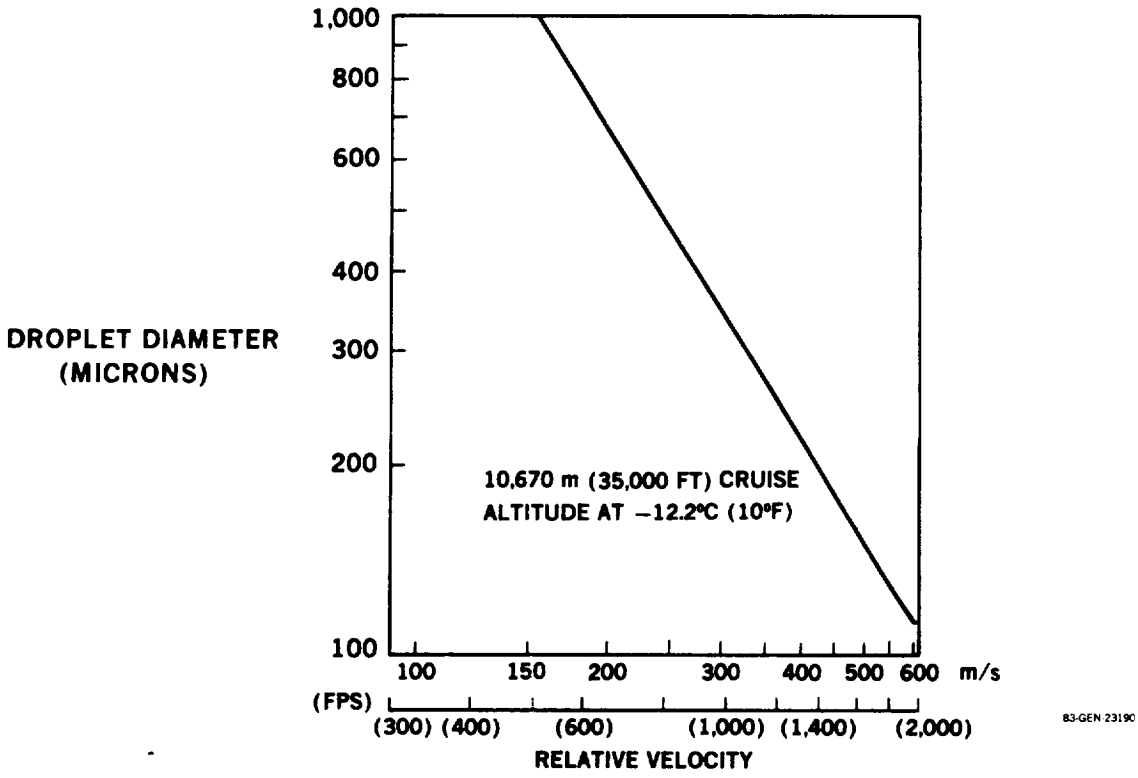

FIGURE 11-61. MAXIMUM DROPLET DIAMETER (WITHOUT SHATTERING)

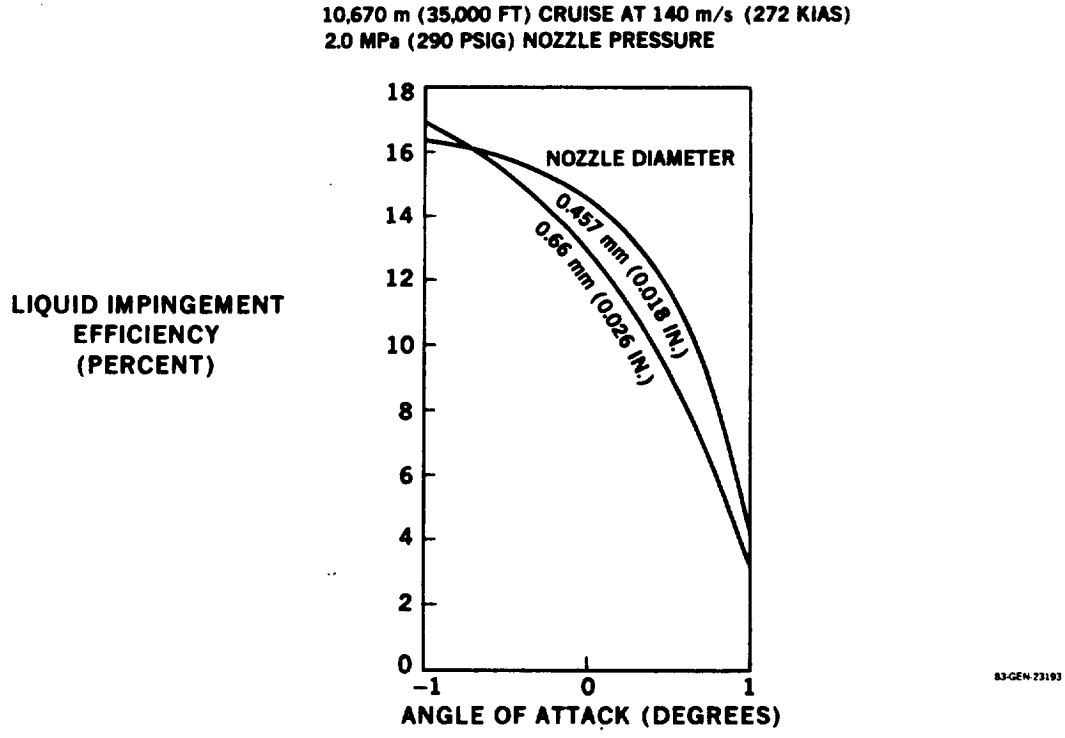

FIGURE 11-62. LIQUID IMPINGEMENT EFFICIENCY VERSUS ANGLE OF ATTACK

Figure 11-64 shows the percent of liquid that will impinge on the wing leading edge as a function of angle of attack for two nozzle sizes that are near optimum. Figure 11-65 shows the corresponding drop size distribution for the 1.3mm (0.052") diameter nozzle with the band of drop diameters required for impingement superimposed. The band is seen to occur near the peak of the drop size distribution and the band width has increased as a result of the lower nozzle pressure and initial droplet velocity. The combined effect is an increase in impingement efficiency from less than 4% to about 11%.

The significant improvement in impingement efficiency justifies the added complexity of the variable pressure system. A nozzle such as Spraying Systems nozzle 9504 spaced from 15.24cm to 30.48cm (6" to 12") in the spanwise direction will provide the required drop size distribution. The pressure will be varied as a function of angle of attack to achieve a minimum efficiency of about 11%.

11.7.2.4 Preliminary Wing Spray System Design - A wing spray system similar to that shown previously in Figure 11-39 would be supplied with liquid from the same system as the shield spray (Section 11.7.1). Approximately 107kg (236 pounds) of liquid would be required for a single de-icing cycle of the entire wing during cruise. Liquid capacity for a single application is adequate considering the infrequent number of icing encounters during normal cruise conditions.

11.7.2.5 Wing Spray System Evaluation - A wing spray system is a feasible method of providing wing ice protection when the shield is retracted. The system could be used in conjunction with a shield spray system to eliminate any operational restrictions imposed by shield deployment.

Although the pop-out nozzle would need to be designed, it does not appear to be a high risk item. The major disadvantages of the wing spray is the low impingement efficiency and high sensitivity to angle of attack, However, the infrequency of use anticipated for this system mitigates the actual performance penalty. If a wing spray system is used, the nozzle pressure should be varied with angle of attack to achieve reasonable efficiencies. Flight testing is required to evaluate the effect of sweep and drop shattering. As with the shield spray, flight testing is required to evaluate the fluid requirements and de-icing capability. The use of the wing spray system in an anti-icing mode would require unreasonably high quantities of fluid.

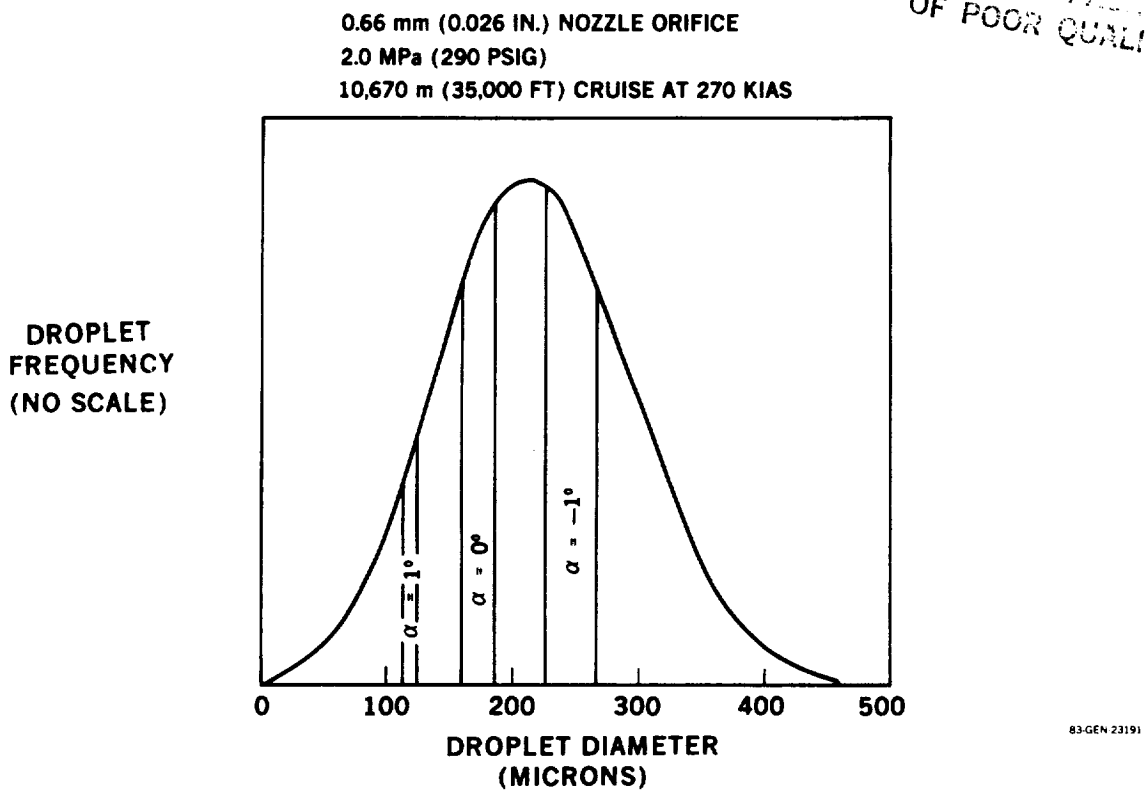

FIGURE 11-63. WING SPRAY DROPLET SIZE DISTRIBUTION (WITH RANGE OF IMPINGEMENT LIMITS SUPERIMPOSED)

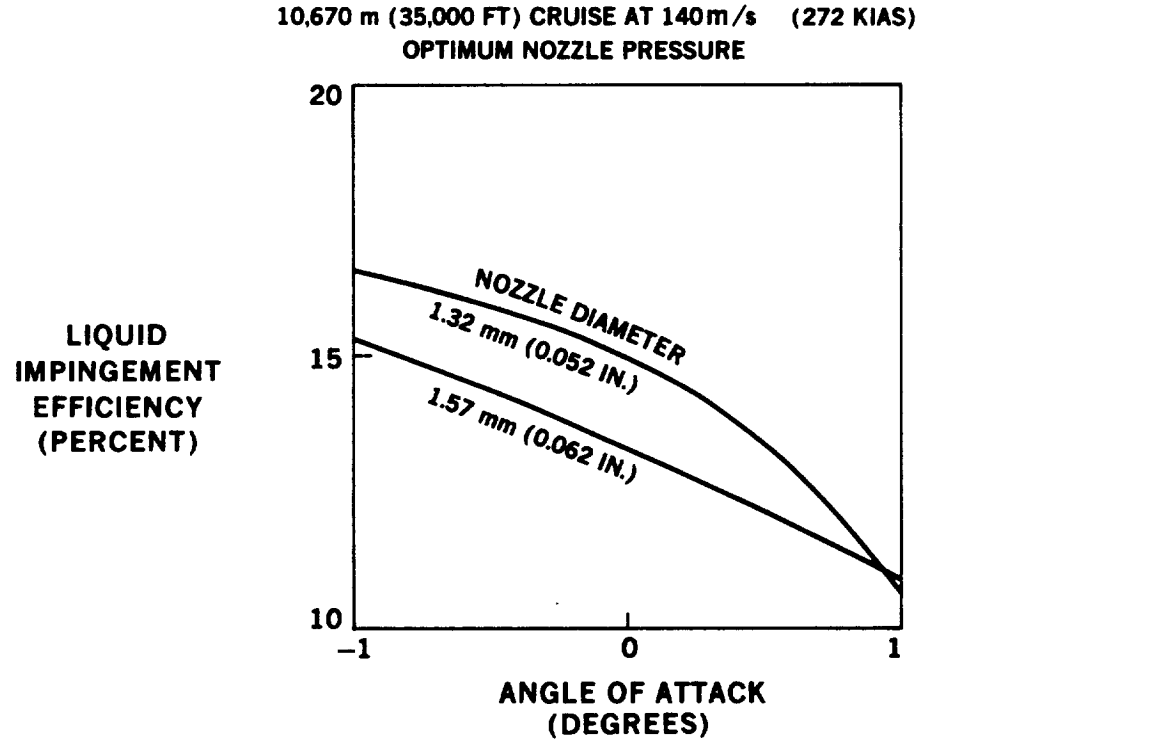

FIGURE 11-64. LIQUID IMPINGEMENT EFFICIENCY VERSUS ANGLE OF ATTACK

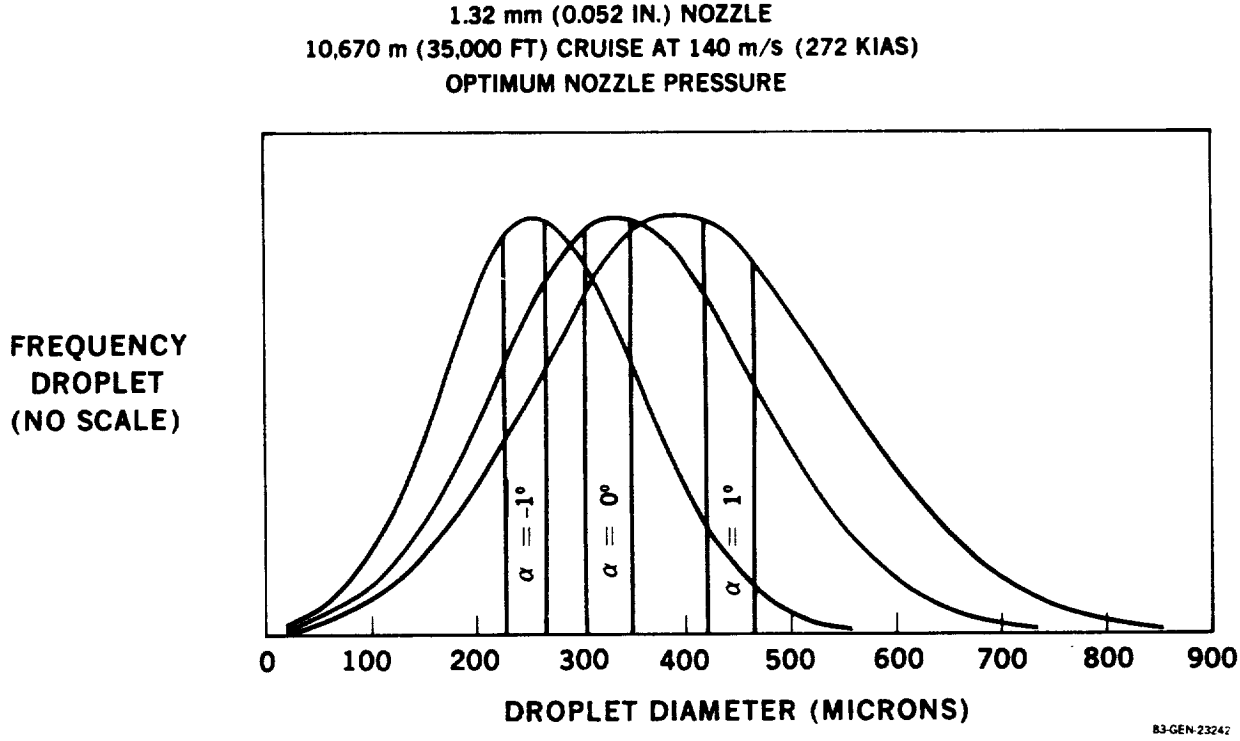

FIGURE 11-65. WING SPRAY DROPLET SIZE DISTRIBUTION (WITH RANGE OF IMPINGEMENT LIMITS SUPERIMPOSED)

11.8 EFFECT OF ATMOSPHERIC ICE CRYSTALS

Concern regarding the frequency at which ice crystals will be encountered during normal LFC cruise operation was generated as a result of material presented in Reference 11-27 by Gordon Hall. To explain loss of laminar flow during X-21 flights in high altitude clouds and in clear air, Hall postulated a mechanism for transition resulting from the passage of particles through the boundary layer. Figures 11-66 and 11-67 reproduced from Reference 11-27 illustrate the severity of the problem in which laminar flow can be disrupted at an altitude of 7,620m (25,000') by particles of diameter $\pm$ 17 microns, and at 12,190 m (40,000') by particles of diameter $\pm$ 32 microns.

Figures 11-66 and 11-67 indicate that Hall's criteria for disruption of laminar flow can occur in "typical" cirrus cloud conditions and under conditions of good visibility (clear air).

Assuming Hall's theory to be correct, the question pertinent to the LFC feasibility study is: "During what percentage of typical commercial airline cruise flight operation will ice crystals of sufficient mass and flux density be encountered such that laminar flow will be disrupted?" In spite of the abundance of literature in cloud physics, little data are available to answer this question. Most previous studies were interested in ice accretion, visability, meteorology, communications, or other technological fields.

Reference 11-28 presents the results of a brief investigation of cloud physics and frequency of occurrence pertaining to the impact of ice crystals on LFC aircraft design. Three tables are included which present "High Cloud Frequency" over various localities in the United States. The probability of encountering high altitude clouds at specific flight altitudes is presented in Table 11-9. These results are the yearly averages calculated from the data presented in Reference 11-28.

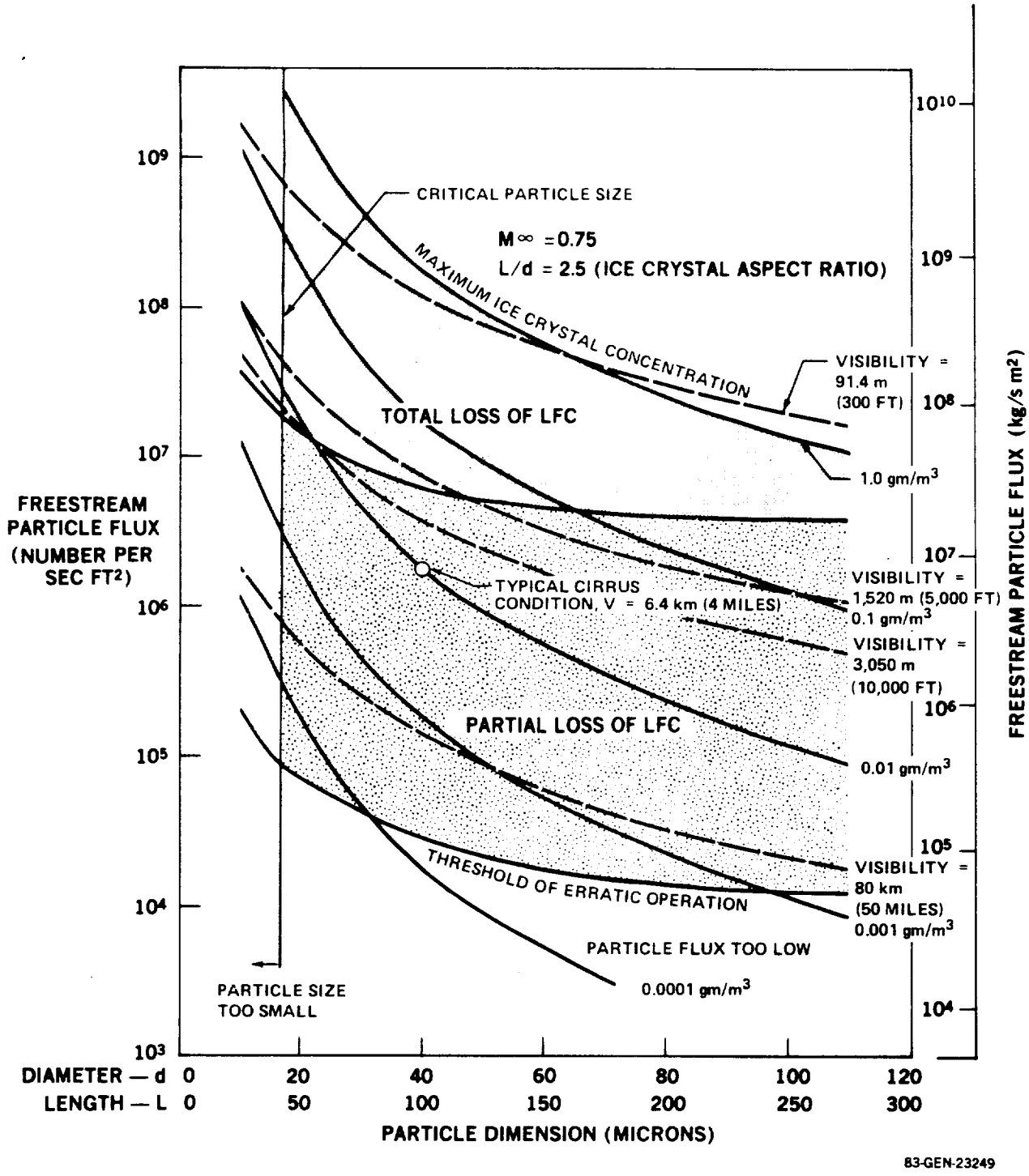

FIGURE 11-66. ESTIMATED LFC PERFORMANCE IN CLOUDS AND LIGHT HAZE ALTITUDE = 7,620 m (25,000 FT)

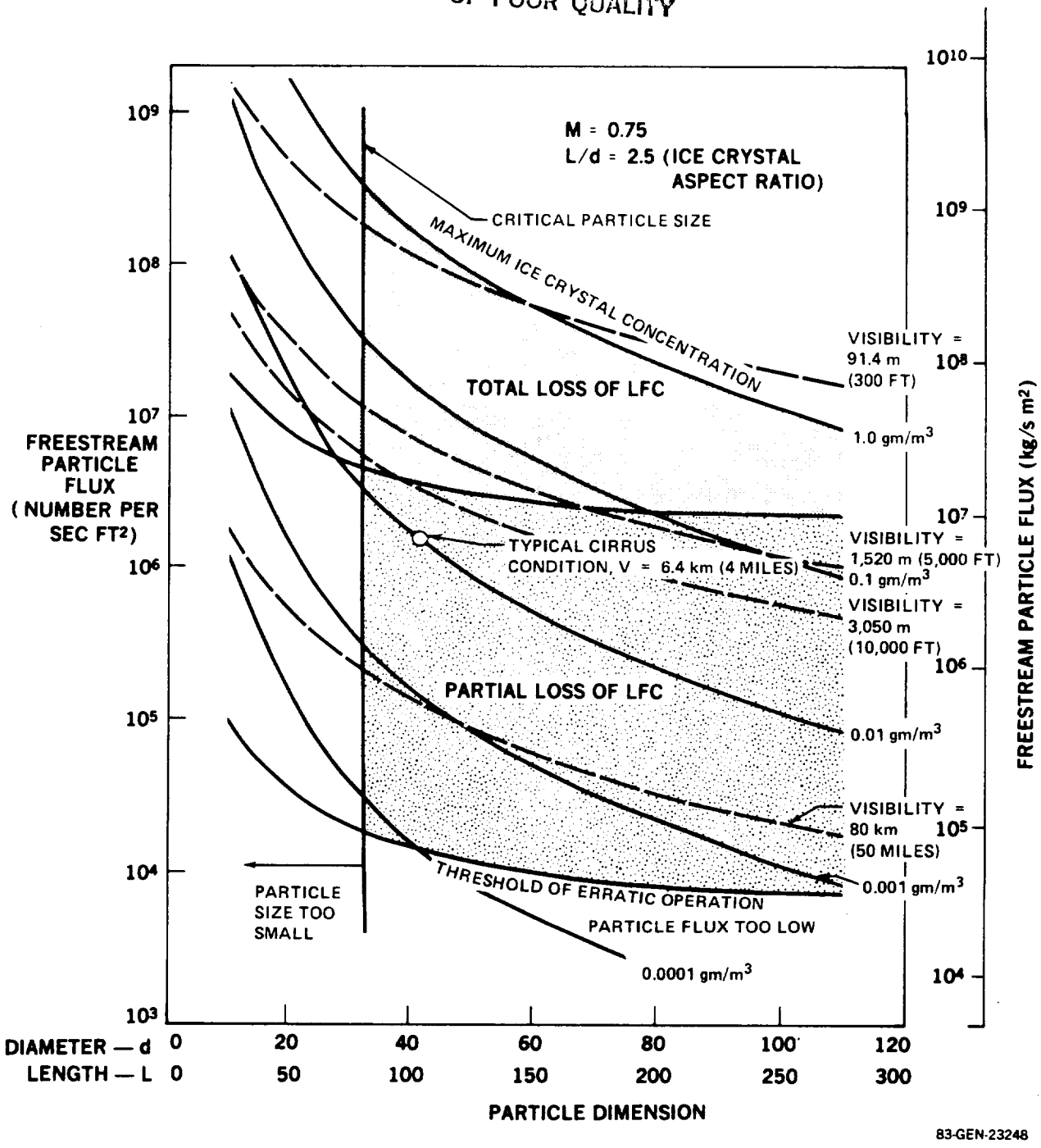

FIGURE 11-67. ESTIMATED LFC PERFORMANCE IN CLOUDS AND LIGHT HAZE – ALTITUDE = 12,190 m (40,000 FT)

TABLE 11-9

PROBABILITY OF ENCOUNTERING CIRRUS CLOUDS

(From Reference 11-28)

ALTITUDE		LOCATION IN UNITED STATES		
		NORTHEAST	NORTHWEST	SOUTHWEST
9,450m	(31,000FT)	13.33%	12.58%	7.93%
10,670m	(35,000FT)	12.43%	11.38%	6.58%
11,890m	(39,000FT)	7.08%	4.53%	3.43%
13,110m	(43,000FT)	3.98%	1.60%	1.25%

In the tropics, cirrus clouds extend for hundreds of miles in the horizontal plane and have frequently been encountered for over a 2,570km (1600 mile) flight route. Clouds in the temperate and polar zones are not as extensive. Most cirrus clouds are layered with the most frequent thickness of individual strata being 180 to 300m (600 to 1000 feet). For an LFC aircraft of intercontineltal range it is assumed that laminar flows will be lost for 20% of any flight in which clouds are encountered. A further reduction in the probability of encountering ice crystals of 50% is assumed by providing the aircraft with the ability to avoid cirrus clouds, with the initial cruise altitude capability 1,220m (4,000 feet) greater than required for mission performance. Based on these considerations, the estimated time that laminar flow will be lost in the cruise regime is less than 1.5%.

The actual probability of ice crystal encounter will be highly variable and will not necessarily correlate with the incidence of visual cirrus clouds. The frequency of cirrus clouds varies as a function of meterological conditions, altitude, the time of year, and location. There are also variations due to time of day and from year-to-year. The average yearly data presented should not be considered as representative of world-wide conditions.

Based on Hall's analysis, a specific ice crystal size and particle flux must be exceeded to destroy laminar flow. Since particles in the range of 0.2 to 2.0 microns have a disproportionately large impact on visibility, the fact that visibility is obscured does not necessarily imply the presence of ice crystals of the size or flux density necessary to destroy laminar flow.

Conversely, because of the good visability in the presence of a significant quantity of large particles-visibility 1600m with 212,000 particles per m^3 (1 mile with 6,000 particles per cubic foot), the absence of visible clouds does not imply the absence of ice crystals. Therefore, data based on visibility considerations is not a dependable guide to the probability of loss of laminar flow due to ice crystals.

Efforts have been made to estimate the probability of cloud encounter based on visability data from sources such as Reference 11-29. The original data present contours of altitudes above which there is a given probability of having less than 0.1 sky cover at a stated time of the year. An estimate is then made of the flight altitude required to provide 0% and 30% probability of cloud encounter. This approach suffers from the inability to correlate visibility and ice crystal size and flux as discussed previously.

A review of available data on cloud physics, ice crystals in the atmosphere, and measurement techniques indicates that virtually all of the data are taken at low altitudes (below 8000m) and during investigations of weather phenomena. Data below 8,000m is not pertinent to the LFC program since cruise altitude is expected to be in the 9140m (30,000 feet) to 12,190m (40,000 feet) range. Data associated with storms are generally of short extent compared to the 8,050 km (5,000 mile) LFC range and can be neglected. The most pertinent cloud data is that associated with cirrus class clouds of large horizontal extent in the cruise altitude regime. Such clouds are expected to have very weak vertical air currents and, therefore, the size of the ice crystals will be predominantly small. This is in contrast with data gathered in adverse weather conditions where the vertical air currents cause droplet and ice crystal growth.

A large quantity of data has been gathered in the GASP program by NASA Lewis Research Center including measurement of particle flux. Douglas has requested that this data be reduced and made available for the LFC program. In view of the expected variability of the data, it is felt that only data of a comprehensive nature and taken along realistic routes can provide a valid indication of the severity of the ice crystal problem. Final verification will be required by an LFC test aircraft.

11.9 EFFECT OF ENVIRONMENTAL CONDITIONS ON FLOW THROUGH POROUS SURFACES

One concern regarding the use of perforated or porous materials for the suction surface of a wing laminar control system is the possibility of clogging by atmospheric particulate contamination. Although the suction system normally operates only at cruise altitudes where the air is clean, clogging can occur by (1) sucking in contaminated air during ground check-out, (2) as a result of deposition or particulate atmospheric comtaminats while the aircraft is parked, and (3) while flying through the lower atmosphere. The results of tests to evaluate the susceptibility of various surface materials to environmental contamination and the effectiveness of various cleaning methods are presented in Section 11.9.1.

To develop surface suction materials with the proper flow resistance, it is necessary to translate operational pressure drop characteristics into laboratory requirements. Two variables are expected to have a significant influence: density and viscosity. The results of tests to evaluate the influence of these parameters are presented in Section 11.9.2.

11.9.1 Environmental Contamination

Environmental contamination tests were conducted on thirteen surface material specimens. Each specimen consisted of a 152mm (6") square flat panel of the surface material attached to a typical substructure. Table 11-10 describes the construction of the test samples and includes a parameter to indicate the overall airflow characteristics of the specimen.

A series of contamination/cleaning cycles was used to evaluate the porous materials. Each cycle consisted of up to five steps:

(1) Baseline Pressure Loss: The sample was subjected to an initial pressure drop versus air flow test.

(2) Contamination Exposure: Up to eight samples were clamped in a test fixture and placed on the roof of a building (Building 36 at Douglas adjacent to the Long Beach airport and on the roof of the Continental Airlines building adjacent to the Los Angeles International Airport).

(3) Retest: After each exposure period, the sample materials were retested to determine any change in the pressure drop.

(4) Cleaning: After repeated exposures, the samples were cleaned using either steam or tap water.

(5) Retest: The pressure drop versus air flow characteristic of each sample was checked after each cleaning operation to determine the effectiveness of the cleaning technique. Data from this test were also used as the baseline for the succeeding contamination/cleaning cycle.

Four test cycles were conducted; the first three at Douglas, Long Beach and the fourth at Los Angeles Airport.

From the results, it appears that the effect of environmental contamination is dependent primarily on the surface porosity.

Microperforated Plate #21: Figure 11-68A is a typical result of the effect of contamination on porosity for microperforated plate with high porosity (samples 229 and 243). During the early February exposure period, the panels were subjected to a severe storm. High winds blew rain as well as dirt and gravel from the roof onto the samples. In spite of the severity of the contamination, the pressure drop increased only 10% during this test cycle. Steam cleaning restored the original porosity. Variations in pressure drop during all other contamination cycles was within the measuring accuracy of the test equipment. In general, microperforated plate #21 demonstrated excellent tolerance to environmental contamination.

High Porosity Surface: The next most tolerant set of samples was 164M-194-1, 300S-120-1, 300M-1 20-3, and 300M-120-1. All of these samples used a high porosity surface material 0.8 to 1.5$m^3/s/m^2$ @ 670Pa (164 to 300 $SCFM/FT^2$ @ 14PSF). A typical effect of contamination on porosity is presented in Figure 11-68B. A 13% increase in pressure drop resulted from the 62 day contamination period. Steam cleaning restored the original porosity.

TABLE 11-10

ENVIRONMENTAL CONTAMINATION

TEST SAMPLE DESCRIPTIONS

SAMPLE IDENTIFICATION	COMPOSITION	AIRFLOW @ 670Pa (14psf) $m^3/s/m^2$	SCFM/SEC/FT^2
229	$[0/90]_5$ E719/DW 42% + MMP #21	1.14	225
243	" " "	1.14	225
244	24 x 110 Dynapore (114)	0.58	114
245	50 x 250 Dynapore (75)	0.38	75
246	80 x 700 Dynapore (2.8)	0.014	2.8
247	80 x 700 Dynapore (15)	0.076	15
258	$[0/90]_4$ 5143/120 + 50 x 250 Dynapore (75)	0.28	55
267	50 x 250 Dyna plated .0006 with Nickel	0.006	1.1
C1	$[0/90]_1$ 7251/120 + impact layer + $[0/90]_1$ 7251/120 + 80 x 700 Dynapore (28)	0.004	0.8
164M-194-1	$[0/90]_5$ 7251/120 + 80 x 700/80x80 Dynapore (164) sintered & callendered	0.60	118
300S-120-1	$[0/90]_1$ 7251/120 + impact layer + 80 x 700 Dynapore (300)	0.41	80
300M-120-3	$[0/90]_4$ $7251/120_1$ + $7251/194_3$ + impact layer + 80 x 700 Dynapore (300)	0.17	34
300M-120-1	$[0.90]_2$ 7251/120 + impact layer + 80 x 700 Dynapore (300)	0.05	10

Notation

$0/90_n$	Two sheets oriented at 90 degrees to each other, repeated n times
E719, 5143 7251	Resin designation
/120	Sheets in $[0/90]_n$ are 120 weave fiber glass cloth
/DW	Sheets in $[0/90]_n$ are Doweave
42%	Percent resin in fabric before laminating
MMP #21	Microperforated plate, 30.7% open. Square weave cloth made from 316L stainless steel wire in a 120 weave. Bonded by sintering and callendered to obtain desired resistance to airflow.
24/110	Dutch weave cloth made of 316L stainless steel wire with 24 wires per inch warp and 110 wires in the fill direction. Bonded by sintering and callendered to obtain desired resistance to airflow as indicated by the flow rate in parenthesis (114) measured in SCFM at 14 psf.

Moderate to High Porosity Dynapore: Table 11-11 summarizes the results of contamination and cleaning on samples of a single layer of Dynapore of moderate to high porosity in the range from 0.08 to 0.58$m^3/s/m^2$ @ 670Pa (15 to 114 $SCMF/FT^2$ @ 14 PSF). During the first contamination cycle, the four samples were exposed to the strom previously described. The pressure drop increased between 49% and 60% of the original pressure drop following exposure.

The results with sample #247 showed that the original pressure drop characteristics may not be restored by steam cleaning for very low porosity samples; the pressure drop was 10% higher than before contamination and steam cleaning. The 16% increase in pressure drop following the first cycle on sample #258 is believed to be due to inadequate cleaning. Following removal of backing material, sample #258 was exposed to an additional three cycles of contamination and cleaning. The pressure drop increased between 26% and 77% for these tests and seemed to vary with both the length of exposure and the severity of contamination. Steam cleaning after cycles 2, 3 and 4 restored the pressure drop to 6% below that measured after cycle 1 showing that the effect of clogging and cleaning was not cumulative.

During contamination/ cleaning cycle #2, an attempt was made to clean sample #258 using tap water instead of steam. The result shows that tap water is ineffective in removing contamination.

Low Porosity Samples: The remaining samples (#246, #267 and C1) had porosities below a level presently anticipated for use on the LFC aircraft. The results obtained were more erratic than previously reported findings. This probably due to the sensitivity of the data to small leaks in the test facility when testing high pressure drop specimens.

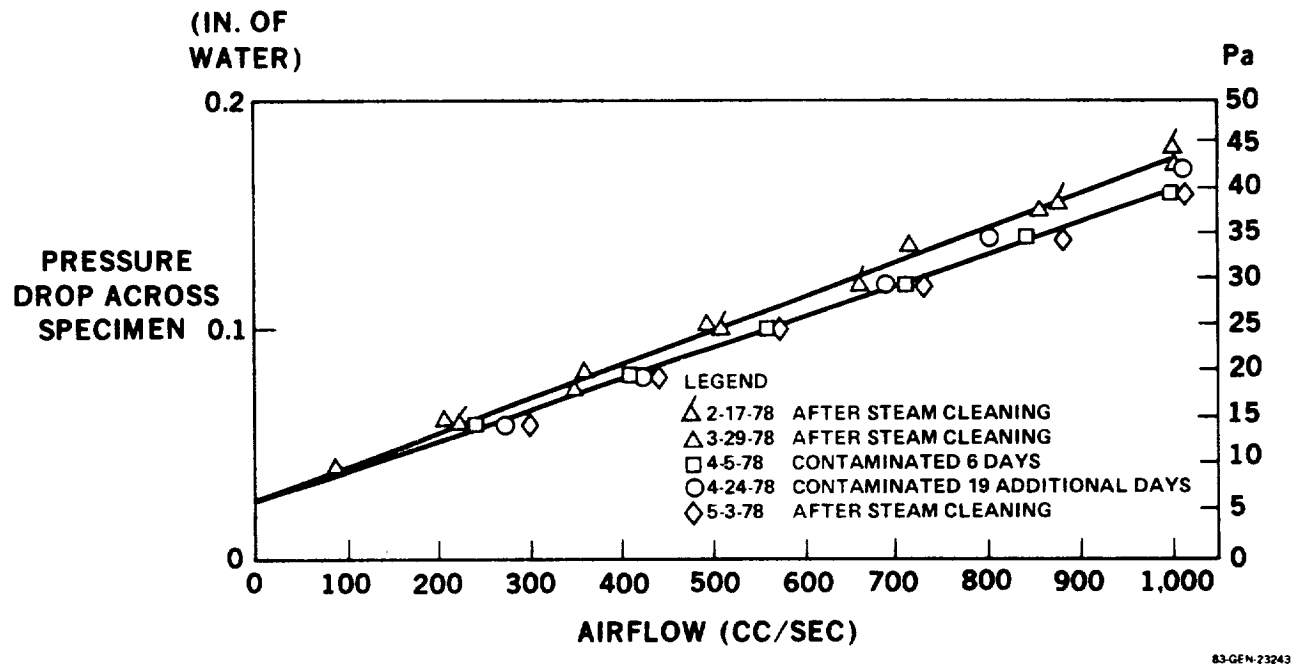

FIGURE 11-68a. EFFECT OF ENVIRONMENTAL CONTAMINATION (SAMPLE NO. 229 – MPP NO. 21 + [0/90] 5)

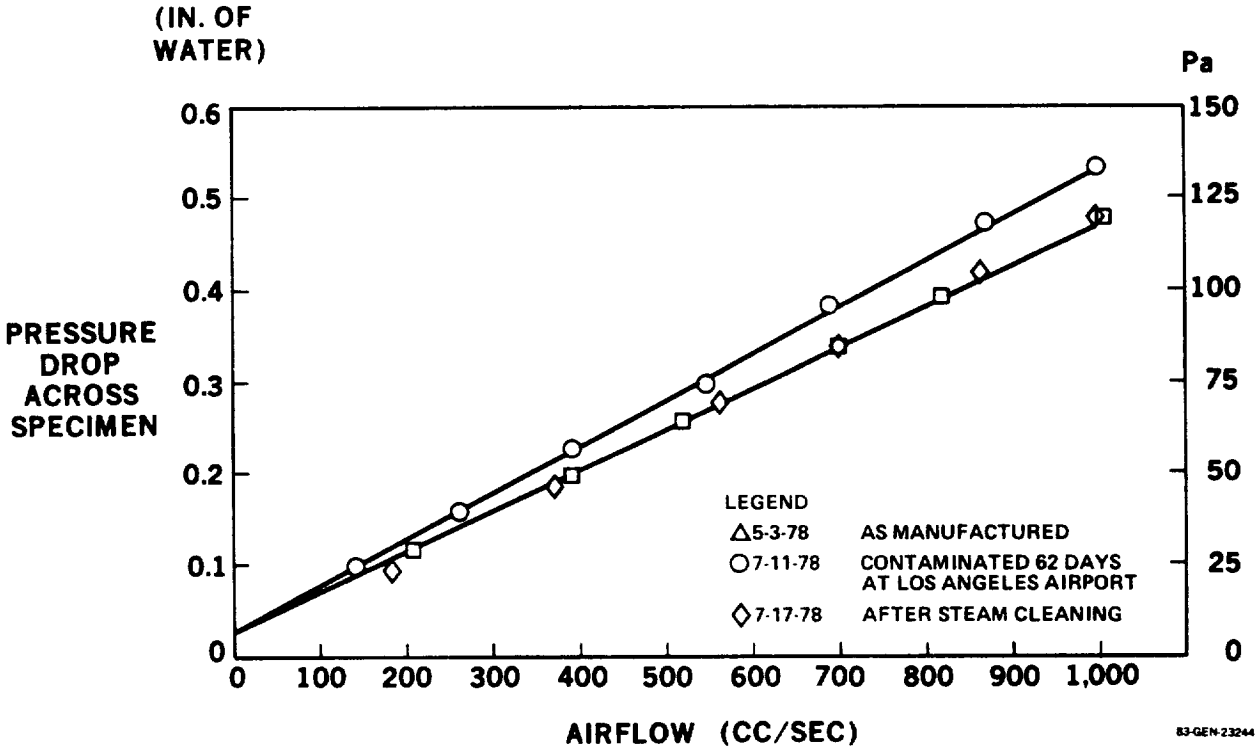

FIGURE 11-68b. EFFECT OF ENVIRONMENTAL CONTAMINATION (SAMPLE 164 M – 194-1 – 80 BY 700/80 BY 80 DYNAPORE) WITHOUT INPACT LAYER

TABLE 11-11

EFFECT OF CONTAMINATION/CLEANING ON PRESSURE DROP

OF MODERATE POROSITY SAMPLES

SAMPLE	CONTAMINATION CYCLE	ORIGINAL AIRFLOW @ 670Pa (14 psf)		PERCENT CHANGE IN AIRFLOW @ 670 Pa (14 psf)		
		$m^3/s/m^2$	$SCFM/FT^2$	CONTAMINATED	STEAM CLEANED	TAP WATER CLEANED
242	1	0.58	114	-49	-2	--
245	1	0.38	75	-60	+4	--
258	1	0.28	55	-58	-16	--
258	2	0.38*	75*	-26	+6	-17
258	3	0.38*	75*	-77	+6	--
258	4	0.38*	75*	-72	+6	--
247	1	0.76	15	-51	-10	--

*Overall flow resistance decreased as indicated after glass cloth backing material was removed.

-- = Not Tested.

In general, the results indicate that (1) environmental contamination can cause a substantial increase in the pressure drop characteristics of the samples, (2) tap water is ineffective in cleaning contaminated materials, and (3) steam cleaning is effective in restoring the original airflow characteristics other than for one low porosity Dynapore specimen.

Electron Beam Perforated Titanium: Figure 11-69 shows the reduction of porosity of an E.B. perforated titanium sheet after exposure to a contaminating environment on the roof of the Douglas engineering building adjacent to Long Beach Airport. The original porosity was completely restored by steam cleaning by directing steam against the surface from a typical hand held steam cleaning wand.

11.9.2 Effect of Ambient Pressure and Temperature on Flow Through Porous Surfaces

During operation of the suction system in flight, the ambient conditions will be significantly different from the laboratory test conditions. Both pressure and temperature will be lower. To permit extrapolation of the porosity requirements to laboratory conditions or extrapolation of test data to operational conditions requires validation that the pressure drop of porous panels follows generally accepted theory such as Darcy's equation.

Pressure drop testing was conducted at both sea level and altitude conditions for specimens having pressure drop characteristics in both the laminar and turbulent internal flow ranges. The results presented in Figures 11-70 and 11-71. The data were correlated by expressing the relationship $\sigma\Delta P$ versus mass flow rate (σ is the ratio of the air density at operating conditions to that at standard temperature and pressure at sea level).

Low temperature testing was conducted on two test specimens down to $-40^{o}C$. The results are shown in Figure 11-72 and 11-73. The data are correlated by means of a viscosity correction to the pressure drop term. The changing slope indicates a change from laminar to turbulent internal flow characteristics.

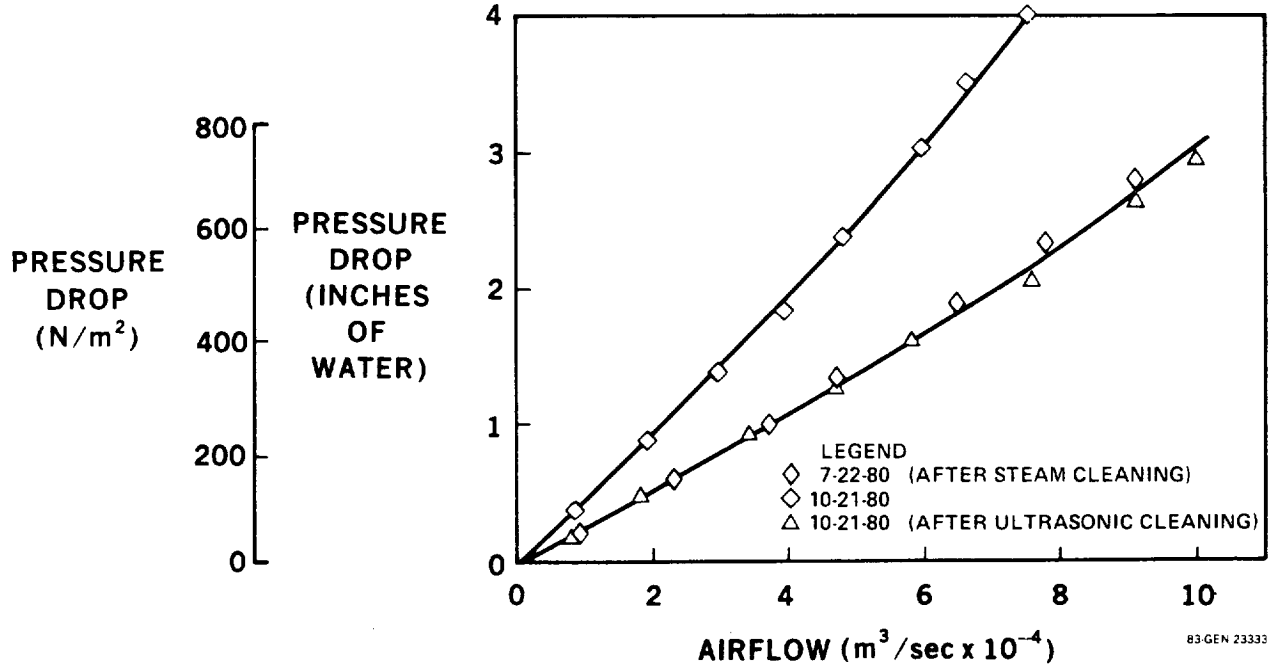

FIGURE 11-69. EFFECT OF ENVIRONMENTAL CONTAMINATION AND CLEANING (0.0026-INCH-DIAMETER EB PERFORATED HOLES IN IN 0.025-INCH TITANIUM SHEET)

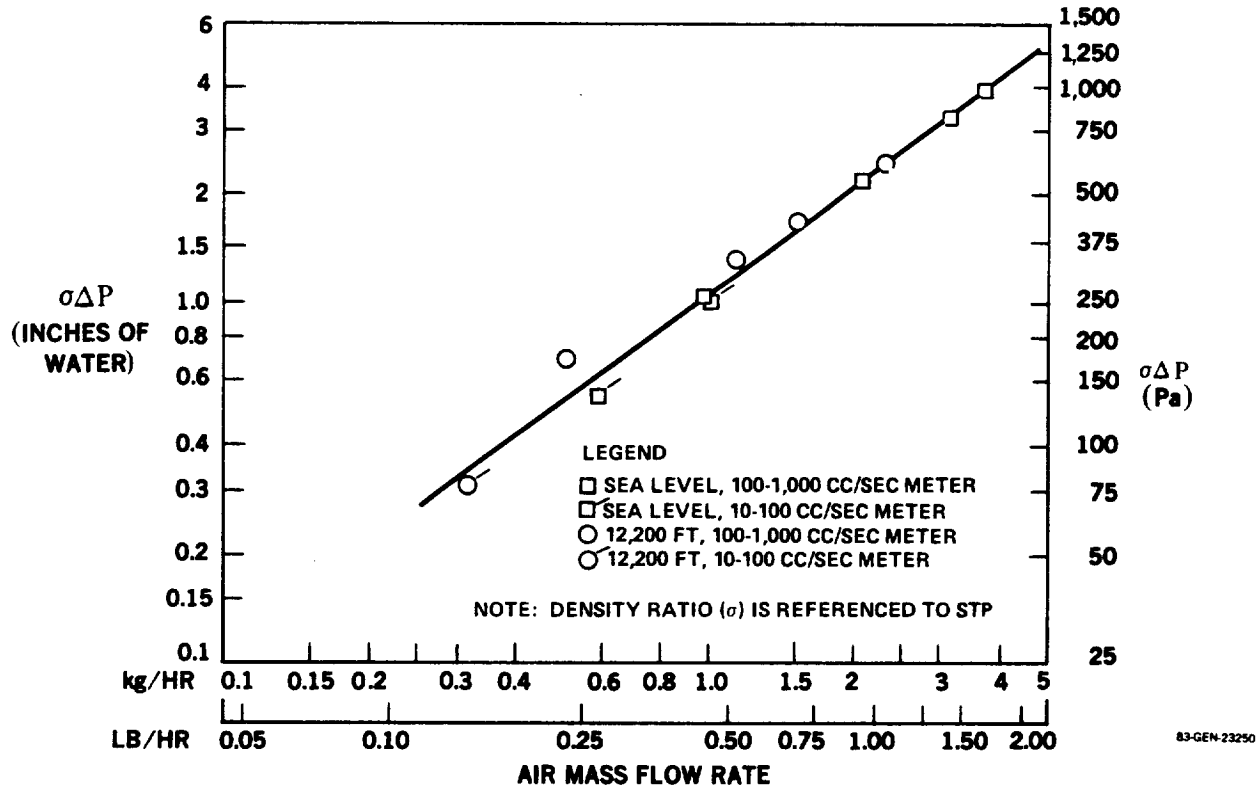

FIGURE 11-70. EFFECT OF AMBIENT PRESSURE ON PRESSURE DROP CHARACTERISTICS WITH INTERNAL LAMINAR FLOW CHARACTERISTICS (SAMPLE NO. 247 – 80 BY 700 DYNAPORE)

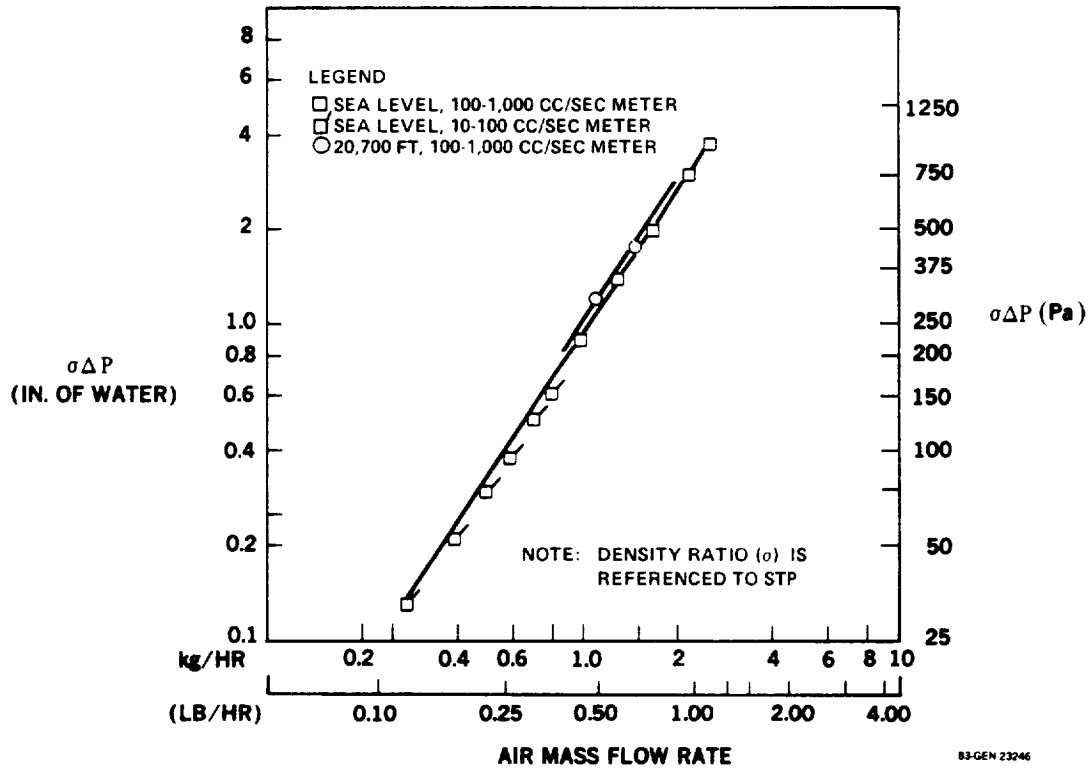

FIGURE 11-71. EFFECT OF AMBIENT PRESSURE ON PRESSURE DROP CHARACTERISTICS WITH INTERNAL TURBULENT FLOW CHARACTERISTICS (SAMPLE NO. 201 – DOWEAVE)

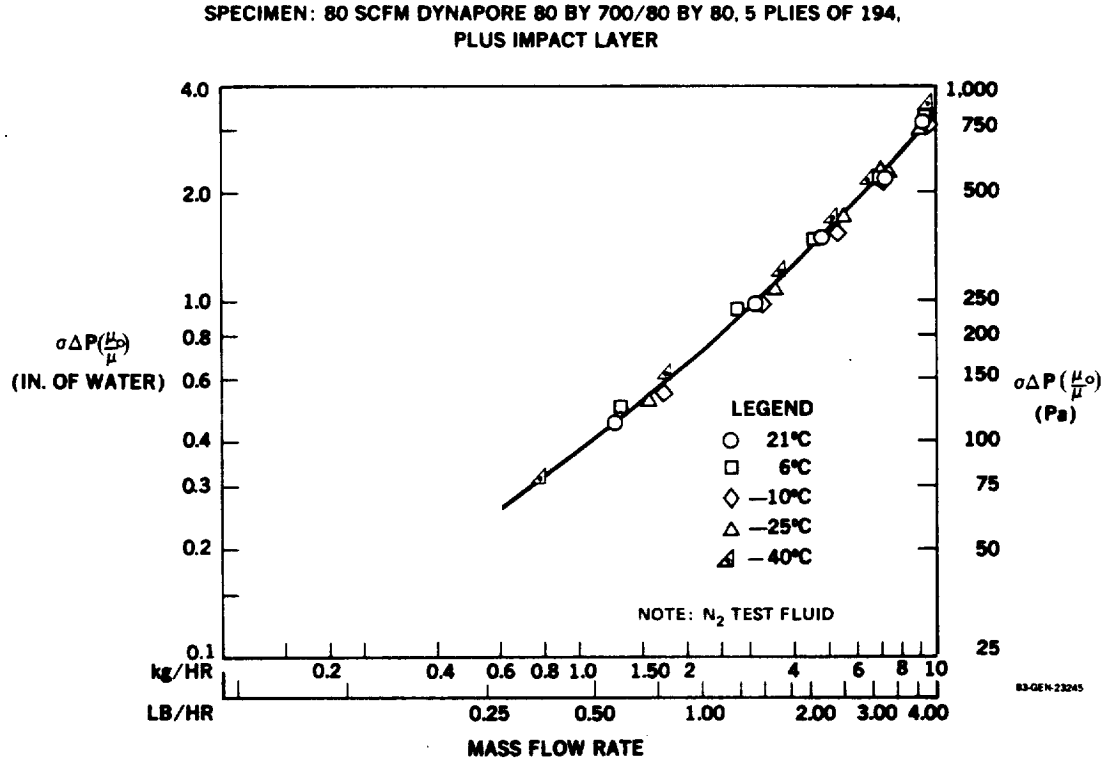

FIGURE 11-72. POROUS SURFACE PRESSURE DROP AT VARIOUS FLUID TEMPERATURES

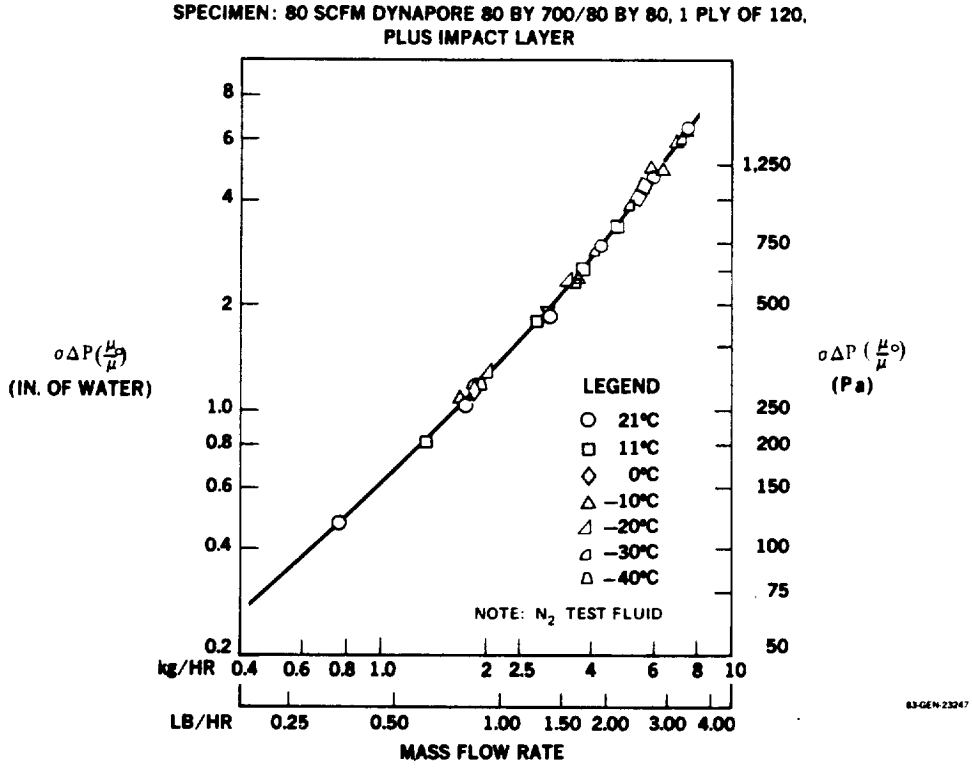

FIGURE 11-73. POROUS SURFACE PRESSURE DROP AT VARIOUS FLUID TEMPERATURES

It is recommended that laboratory pressure drop data for the type of porous materials currently being considered for the LFC suction surface be presented in the form $\sigma\Delta P \frac{\mu o}{\mu}$ versus airflow, where $\sigma\Delta P$ is the pressure differential corrected to standard density conditions and $\mu o / \mu$ is the ratio of viscosities at standard conditions to actual operating conditions.

11.10 CONCLUSIONS - ENVIRONMENTAL

Based on the results of analyses and tests conducted during the LFC Phase I feasibility study, the following conclusions have been drawn:

1. A retractable shield is a practical method of providing primary protection of the wing leading edge against ice and airborne contaminants.

    a. Studies have shown that a shield of reasonable size can be housed in the leading edge box, compatible with the space envelope and structural design of the LFC aircraft.
    b. Analyses have shown that the shield is highly effective in avoiding contamination of the wing leading edge but that a supplemental system may be required for a thick inboard wing section and possibly for the upper surface near the wing tip.
    c. The shield should be extended during all low altitude operations when airborne contaminants are present. This includes takeoff roll, rotation, climbout, descent, landing, and hold operations. The shield may also be extended when operating in icing conditions.
    d. Shield ice protection can be provided by a "liquid-film" system in which a freezing-point=depressant is distributed in the attachment line region through a porous surface. To provide ice protection for two flights, a typical 300 passenger LFC aircraft would require about 82kg (180 pounds) of liquid based on three de-icing cycles per flight.

2. Supplemental contamination avoidance and ice protection can be provided effectively by a "shield spray" system in which a series of flat pattern spray nozzles are mounted on the aft face of the shield and direct a liquid spray onto the wing leading edge. Aerodynamic forces distribute the liquid over the surface. The liquid-film prevents adhesion of the contaminats that impinge directly on the wing and transports the contaminants aft off the trailing edge.

    a. An impingement efficiency of 90% can be achieved by optimum nozzle selection and system design.
    b. Flat spray nozzles with a 0.91mm (0.036 inch) equivalent orifice diameter operated at 1.76MPa (255 psig) with a 22% duty cycle will provide the liquid coverage of the wing required for contamination avoidance.
    c. Droplets that impinge above the leading edge encounter relative velocities that could result in shattering of the droplet. Since the time required for the droplet to travel across the high velocity region is of the same order as the time to shatter, it is unclear whether the drops will actually shatter. Flight tests will be required to determine the influence of drop shattering.
    d. About 254kg (560 pound) of liquid is sufficient to provide contamination avoidance for the entire wing during take-off and landing for two flights. An additional 91kg (201 pound) of liquid could provide three de-icing cycles for each of two flights.
    e. To provide ice protection during operation above 1524m (5,000 feet), the shield can be extended and the spray system used in the de-icing mode.

3. An alternative method of providing supplemental contamination avoidance and ice protection is the use of "liquid-film" system in the wing leading edge.

    a. Tests have demonstrated that a porous dispensing system is capable of distributing a liquid such as aqueous propylene glycol methyl ether across the surface.

b. About 230kg (504 pound) of liquid is sufficient to provide contamination avoidance for the entire wing during takeoff and landing for two flights. An additional 82 kg (181 pound) of liquid could provide three de-icing cycles for each of two flights.

4. To avoid the necessity of extending the shield and using the shield spray system to de-ice the wing leading edge, a wing spray system may be used. The wing spray system comprises a series of flat nozzles located under the wing leading edge and directed forward and upward. Aerodynamic forces blow the droplets back onto the wing leading edge.

   a. The use of pop-out nozzles appears to be a feasible method of implementing this concept.
   b. Flat spray nozzles with a 1.32mm (0.052") equivalent orifice diameter will provide at least 10% impingement efficiency when operated at the optimum pressure as a function of angle of attack.
   c. The droplets may encounter airflow velocities that would result in drop shattering. Judicious selection of nozzle design, pressure, and location can minimize this possibility. Flight tests will be required to determine the actual extent of drop shattering.
   d. The system is uneconomical in the use of liquid. Approximately 107kg (236 pound) of de-icing fluid is required to provide one de-icing cycle during cruise with the shield retracted compared with 30kg (67 pound) or 27kg (60 pound) for the shield/spray or liquid-film systems respectively.

5. If integration of the liquid and air suction systems can be accomplished satisfactorily, a liquid-film system would be preferable to the wing spray system because of the high efficiency and insensitivity to angle of attack of the liquid-film system.

6. When applying the liquid to the surface, care is required to ensure complete, uniform coverage.

    a. During application of the liquid, the pressure in the suction plenums must be at least equal to the local ambient pressure to prevent the liquid from being forced through the porous surface.
    b. An economical means of maintaining a completely wet surface is the use of a high initial flow of about 10cm^3/s/m(11 cu in/min/ft) of span to completely wet the surface followed by a low sustaining flow of about 2cm^3/s/m 92.3 cu in/min per foot) of span.
    c. The liquid flow over the surface tends to neck in at the end of the dispenser plenum. The design must therefore include a means of avoiding resulting discontinuities in the spanwise flow (such as the spanwise overlapping of dispenser plenums or sprays).
    d. At the lower sustaining flow rates, the fluid did not break up into rivulets on the porous material over the full 254mm (10 inch) chord length of the porous specimen tested.
    e. To ensure uniform spanwise distribution, the pressure drop in the dispenser plenum should be small compared to the pressure drop across the dispensing surface.
    f. The surface was found to stay wet for 20 seconds to one minute after glycol application and this time decreases as water is added to the glycol.
    g. The maximum viscosity of a liquid that will permit transport of contaminants off the training edge of the wing lies between that of water and 100% ethylene glycol.
    h. Evidence to date indicates that the film left on the porous surface after the glycol evaporates will not significantly affect transition of the boundary layer.

7. Aerodynamic forces will not blow small contaminants off of either a dry or damp wing.

8. A means is required to expel the liquid from the porous or perforated surface material.

    a. The porosity of the material directly at the surface has a strong influence on the pressure required to expel liquid lodged in the porous structure. An increase in the required pressure is especially noticeable when the surface porosity is reduced below .762$m^3/s/m^2$ @ 670Pa (150 SCFM per sq. ft. at 14 psf).
    b. The overall porosity of the surface bore no apparent relation to the clearing pressure required.*
    c. Clearing pressure was strongly influenced by the surface tension of the liquid.
    d. A liquid with a surface tension of about 0.35MN/m can be cleared by applying about 6.9kPa (1 psi) for one minute.

9. A freezing-point-depressant liquid having low surface tension, low viscosity, and a high flash point is required for the contamination avoidance/ice protection system.

    a. A number of glycols and glycol methyl ethers are suitable for use as contamination avoidance/ice protection fluid for the LFC aircraft. A solution of 60% propylene glycol methyl ether/40% water meets the requirements and was the best of the liquids tested.
    b. Further work is desireable to develop a formulation with a higher flash point.

10. Airborne contaminants that settle on the suction surfaces or are drawn into the pores during ground checkout may degrade suction system performance unless periodically removed.

    a. Materials having a porosity greater than approximately 0.76$m^3/s/m^2$ @ 670 Pa (150 SCFM per sq. ft. at 14 psf) are not significantly degraded by exposure to atmospheric contaminants for time periods up to two months.

* The required overall porosity ranges from 0.07 to 0.15 $m^3/s/m^2$.

b. Steam cleaning restores the original airflow characteristic to previously contaminated surfaces with porosities greater than approximately $0.05 m^3/s/m^2$ @ 670 Pa (10 SCFM per square feet at 14 psf).

11. Pressure drop characteristics of porous surface materials can be expressed as $\sigma\Delta P(\mu o/\mu)$ versus weight flow rate (where σ is the density ratio and $\mu o / \mu$ is the viscosity ratio of the air) to account for variations in environmental conditions between laboratory and inflight operation.

12. Available information indicates that ice cyrstals of sufficient size and particle flux to destroy laminar flow could be encountered during cruising flight. Insufficient data are available to determine whether occasional loss of laminar flow due to ice crystals will be significant economically.

11.11 RECOMMENDATIONS - ENVIRONMENTAL

Based on the results of analyses and tests conducted during this study, the following recommendations are made:

1. Early experimental flight evaluation of LFC, the aircraft should utilize a Krueger-type shield as the primary contamination avoidance/ ice protection mechanism, supplemented by a shield spray system. The shield should incorporate a liquid-film system for ice protection of the shield.

    a. The shield should be extended during all low altitude operation in the presence of airborne contamination or icing conditions.
    b. The following areas should be explored during flight testing:

        - Possible need for a supplemental system for (1) contamination avoidance, (2) low altitude icing or (3) icing during cruise.
        - De-icing capability of a liquid spray

- The effect of drop shattering and sweep on the nozzle flow, pressure and spacing requirements.
- The ability of the liquid spray system to perform satisfactorily at low ambient temperatures.

2. Development of the liquid-film concept should be continued as a back-up to the shield spray and because of its potential for higher efficiency.

3. Work on the wing spray system with retractable nozzles should be discontinued if flight testing indicates no need for de-icing during cruise operations.

4. A mixture of 60% propylene glycol methyl ether/40% water should be used for the contamination avoidance/ice protection system. Care should be exercised in the test aircraft design and operation to provide adequate ventilation and isolation from ignition sources.

5. A positive pressure purge system should be used to clear liquids from the porous materials. The system should provide one psig across the surface material for one minute. The purge system should also be used to pressurize the suction plenums slightly during liquid application.

6. To avoid excessively high purge system pressure requirements and to minimize the sensitivity of the surface material to environmental contamination, the surface material porosity should be greater than about $0.76 m^3/s/m^2$ @ 670 Pa (150 SCFM per square feet at 14 psf) if Dynapore is used for the suction surface.

7. Further research is needed to adequately define the ice crystal environment and its effect on an LFC aircraft.

    a. GASP data should be analyzed to determine the size and flux of particles in the cruise altitude regime. If necessary, additional GASP testing and instrument modification should be requested.

b. Flight testing of an LFC aircraft with instrumentation to measure ice crystal size and flux should be conducted to verify Hall's theory.

c. It is recommended that a minimum initial cruise altitude not less than 10,670m (35,000 feet) should be considered, in order to provide a choice of altitude for ice crystal avoidance, even though this may result in an economic penalty on the airplane.

11.12 REFERENCES - ENVIRONMENTAL

11-1 Coleman, W. S.: Roughness Due to Insects, Boundary Layer and Flow Control, Volume 2 by G. V. Lachman, 1961.

11-2 Hardy, A. C. and Milne, P. S.: Studies in the Distribution of Insects by Aerial Currents, Journal of Animal Ecology, Volume 7, November 1938.

11-3 Glick, P. A.: The Distribution of Insects, Spiders, and Mites in the Air, USDA Technical Bulletin No. 673, May 1939.

11-4 Freeman, J. A.: Studies in the Distribution of Insects by Aerial Currents, Journal of Animal Ecology, Volume 14, 1945.

11-5 Johnson, C. G.: The Distribution of Insects in the Air and the Empirical Relation of Density to Height, Journal of Animal Econogy, Volume 26, 1957.

11-6 Johnson, C. G.: The Study of Wind-Borne Insect Populations in Relation to Terrestrial Ecology, Flight Periodicity and the Estimation of Aerial Populations, Science Progress, No. 153, 1951.

11-7 Coleman, W. S.: The Characteristics of Roughness from Insects as Observed for Two-Dimensional, Incompressible Flow Past Airfoils, Journal of Aero-Space Science, Volume 26, May 1959.

11-8 Lachmann, G. V.: Aspects of Insect Contamination in Relation to Laminar Flow Aircraft, A.R.C. Technical Report C.P. No. 484, 1960.

11-9 Lachmann, G. V.: Boundary Layer Control for Low Drag, Aircraft Engineering, April 1962.

11.12 REFERENCES - ENVIRONMENTAL (Continued)

11-10 Eichelkraut, W. L.: Ice Protection System, LFC Airplane Design Data Report NOR-61-141, March 1964.

11-11 Coleman, W. S.: Roughness Due to Insects, Boundary Layer and Flow Control, Volume 2, by G. V. Lachmann, 1961.

11-12 Nichols, G. L.: TKS Fluid De-icing System Preparation, presented to the Air Conditioning Forum, June 12, 1969.

11-13 Meyer, H. J.: Performance of a Freezing Point Depressant Ice Protection System in an Icing Tunnel, Douglas Aircraft Company Report MDC 50859, December 1971.

11-14 Wahl, N. E.: Investigation of the Phenomena of Rain Erosion at Subsonic and Supersonic Speeds, AFML-TR-65-330, October 1965.

11-15 Engel, O. G.: Mechanism of Rain Erosion - Impact Pressure in Solid-Liquid Sphere Collisions, WADC TR-53-192, Part 1, July 1953.

11-16 Levin, I. A.: USSR Electric Impulse De-icing System Design, Aircraft Engineering, July 1972.

11-17 Shoh, A.: Industrial Applications of Ultrasound - A Review, IEEE Transactions of Sonics and Ultrasonics, March 1975.

11-18 Coleman, W. S.: Wind Tunnel Experiments on the Prevention of Insect Contamination by Means of Soluble Films and by Liquids Discharged Over the Surface, July 1952.

11-19 Hay, G. C.: Experiments with Icephobic Surfaces, presented to the FAA Symposium on Aircraft Ice Protection, April 30, 1969.

11-20 Merkle, E. L.: Icing Tunnel Tests of Icephobic Coatings (Douglas Paper 5102), Proceedings of the 8th Annual National Conference on Environmental Effects on Aircraft and Propulsion Systems, Bordentown, N. J., October 1958.

11-21 Wortmann, F. X.: A Method for Avoiding Insect Roughness on Aircraft, NASA TTF-15,454, April 1974.

11-22 Langmuir, I., and Blodgett, K. B.: A Mathematical Investigation of Water Droplet Trajectories, AAF Technical Report 5418, 1946.

11-23 Dorsch, R. G., and Brun, R. J.: A Method for Determining Cloud Droplet Impingement on Swept Wings, NACA Technical Note 2931, 1953.

11-24 Dodson, E. D., Manual for Ice Protection, Douglas Aircraft Company Report SM-23978, January 1961.

11-25 Coleman, W. S.: Roughness Due to Insects, Boundary Layer and Flow Control, Volume 2, by G. V. Lachmann, 1961.

11-26 Peterson, J. B. and Fischer, D. F.: Flight Investigation of Insect Contamination and Alleviation, presented at the CTOL Transport Technology Conference, NASA Langley Research Center, February 28-March 3, 1978.

11-27 Hall, G. R.: On the Mechanism of Transition Produced by Particles Passing Through an Initially Laminar Boundary Layer and the Estimated Effect on the LFC Performance of the X-21 Aircraft, Northrop Norair Internal Report No. 3711-64-62, October 1964.

11.12 REFERENCES - ENVIRONMENTAL (Continued)

11-28 Mee, T. R.: An Investigation of Atmospheric Factors That May Affect Laminar Flow Control, Meteorology Research Report MR164 R-212a, 1 Cecember 1964.

11-29 Handbook of Military Infrared Technology, edited by W. L. Wolfe, 1965.

Appendix A Wolfe, H. E. and Anderson, W. H.: Kinetics, Mechanism, and Resultant Droplet Sizes of the Aerodynamic Break-up of Liquid Drops, Aerojet General Corporation Report No. 0395-04 (18) SP, April 1964.

12.0 CONCLUSIONS AND RECOMMENDATIONS

12.1 LFC SURFACE

Test results with a wide variety of possible LFC suction surfaces indicate that electron beam (E.B.) perforated titanium has the greatest potential for achieving LFC under practical aircraft operating conditions. It provides a tough, corrosion resistant, effectively smooth LFC surface that can be worked satisfactorily to strain levels corresponding to those of an advanced technology wing structure. (Section 9.3.4.5 and Figures 9-52, 9-54 and 9-79.)

Low speed wind tunnel testing showed that the .0635 mm (.0025 in) diameter perforations through the surface are small enough to not cause transition or to attract particles onto the surface that would trip the flow. On the other hand, the perforations are large enough to allow purging in flight of any trapped liquids and to allow cleaning to be accomplished satisfactorily using simple steam cleaning equipment without removing the LFC panel. (Figures 8-46, 11-35 and 11-69.)

LFC panels having woven stainless steel "Dynapore" surfaces were also thoroughly investigated. Their LFC characteristics were very good but structural and damage resistance properties were inferior to the EB perforated titanium selected.

In support of porous surfaces in general, there were indications that due to inherent noise damping characteristics, they would be less sensitive to the effects of noise interference. It is also anticipated that any shock waves at the surface would have less adverse effects.

12.2 LFC AIRCRAFT CONFIGURATION

The final LFC aircraft configuration proposal by Douglas, Figure 12-1, utilizes suction to 85 percent chord on the wing upper surface only. This was shown to be more than competitive with a configuration having suction on both wing surfaces to 70 percent chord, Figure 12.2. By comparison, the

	WING	HORIZ	VERT
AREA-m^2 (FT^2)	288 (3100)	80.3 (864)	52.7 (567)
ASPECT RATIO	10	5	1.1
TAPER RATIO	0.25	0.4	0.7
SWEEP	30 DEG	30 DEG	40 DEG
THICKNESS RATIO	0.108 AVG	0.11	0.11
TAIL VOLUME COEF	—	1.24	0.068

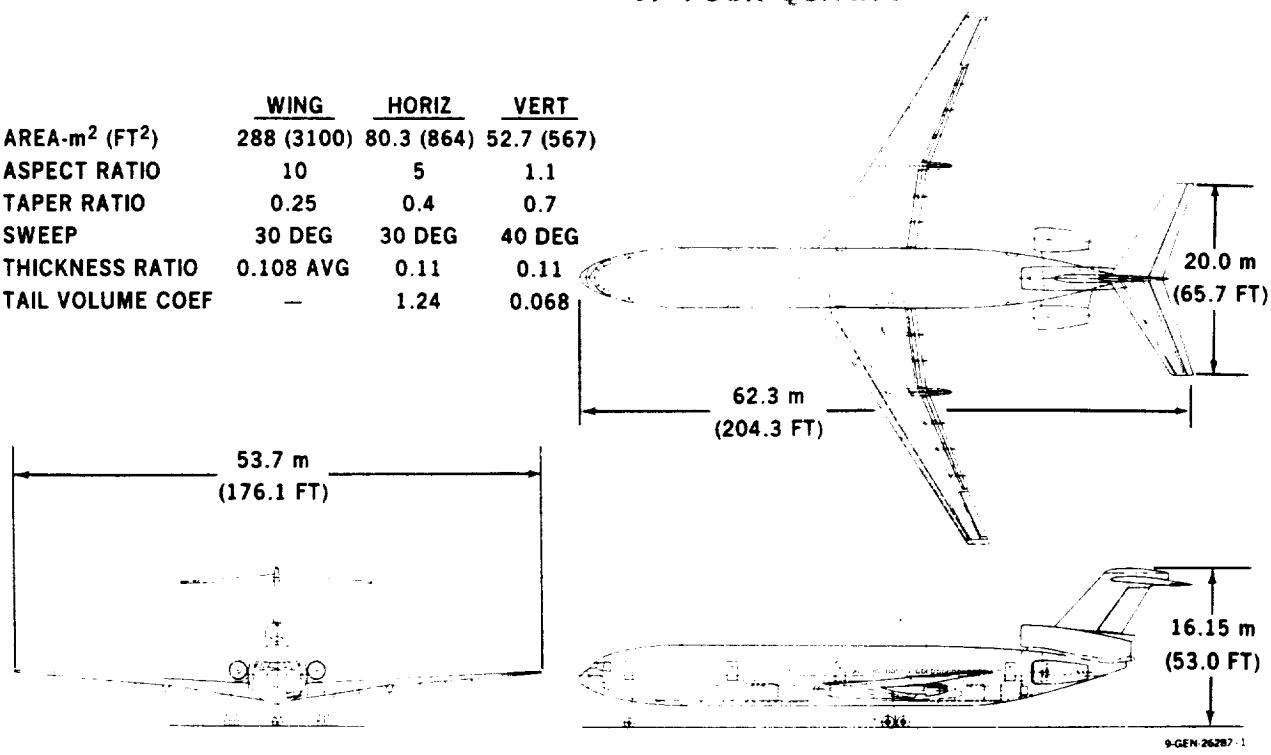

FIGURE 12-1. LFC AIRCRAFT – WING UPPER SURFACE LAMINARIZED TO 85 PERCENT CHORD

	WING	HORIZ	VERT
AREA m^2 (FT^2)	331 (3560)	98.8 (1064)	62.0 (667)
ASPECT RATIO	10	5	1.1
TAPER RATIO	0.25	0.4	0.7
SWEEP	30 DEG	30 DEG	40 DEG
THICKNESS RATIO	0.117 AVG	0.11	0.11
TAIL VOLUME	—	1.23	0.0646

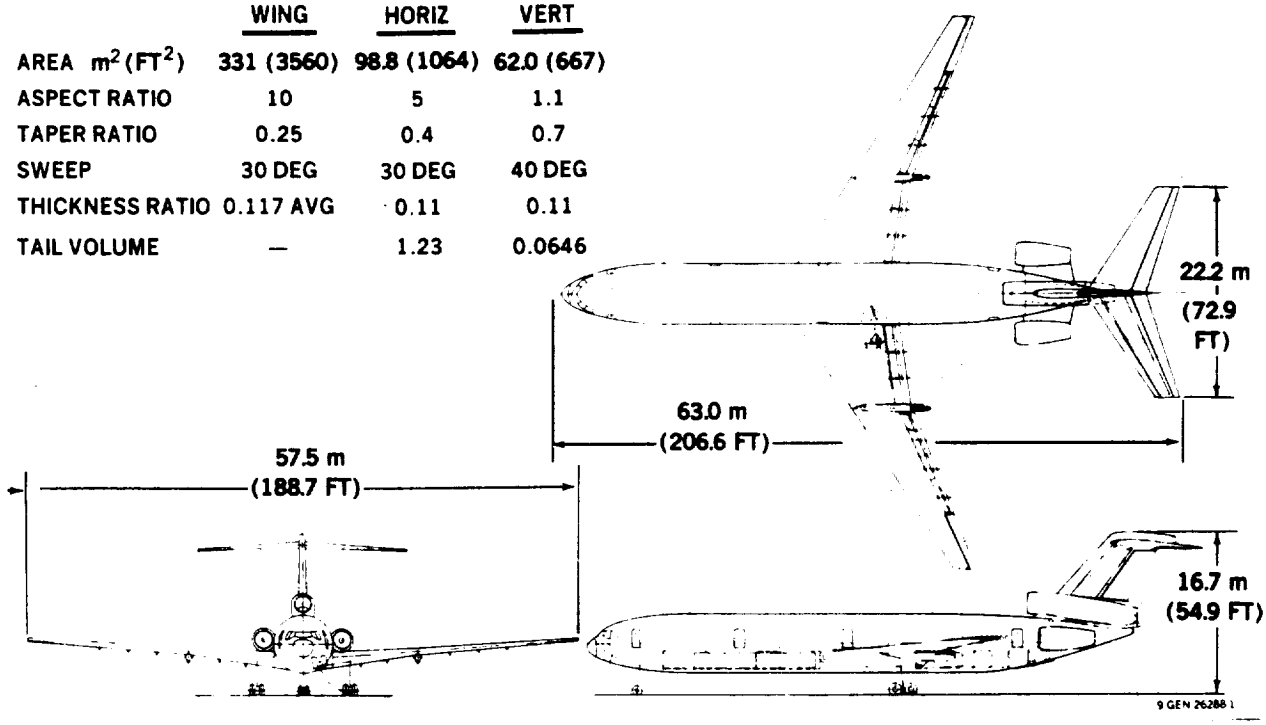

FIGURE 12-2. LFC AIRCRAFT – UPPER AND LOWER WING SURFACE LAMINARIZED TO 70 PERCENT CHORD

configuration with LFC on the upper wing surface only, had lower weights, lower initial cost, lower operating cost and lower fuel consumption for the same mission. Some other advantages are listed below:

(1) Simplification of the LFC system.

(2) Vulnerability of the lower LFC surface to damage from foreign objects thrown up from the runway (FOD) is avoided.

(3) The possibility of fuel leakage into the LFC panels and integral ducts is reduced.

(4) Conventional access panels to wing leading and trailing edge systems and fuel tanks can be provided for inspection and maintenance without affecting any LFC surface.

(5) Maintenance costs are reduced.

(6) A shield for contamination avoidance can be deployed forward of the wing leading edge and be retracted into the lower surface when not required.

(7) The shield can be designed geometrically to function as a high lift device. Wing area can then be reduced and wing loadings become more competitive with those of advanced turbulent aircraft.

(8) The use of a retractable high lift device allows the safe use of a sharper leading edge on the basic wing. This results in a reduction or possible elimination of suction requirements along the attachment line.

12.3 COMPARISON WITH AN ADVANCED TURBULENT AIRCRAFT

The study indicates that the proposed LFC configuration should result in a practical LFC transport aircraft providing substantial fuel saving of at least 18 percent compared with the equivalent advanced turbulent aircraft shown in Figure 12-3. With LFC, although the manufactured empty weight is higher by 2,300 kg (5,000 lb), the takeoff gross weight is lower by 8,500 kg (18,600 lb) and the Direct Operating Cost (DOC) would be reduced by more than 8 percent.

12.4 RECOMMENDATIONS

Considerable progress has been made under this contract on the evaluation of laminar flow control system concepts for subsonic commercial transport

aircraft. The use of porous suction surfaces has been demonstrated as a practical approach to achieving LFC. The configuration selected was shown as having very large fuel saving potential and to be economically advantageous compared with an equally advanced turbulent configuration. With a shielded leading edge and LFC on the upper wing panels only, the LFC surface is well protected from environmental contamination and damage. Normal access for inspection and maintenance is provided through the lower wing surface. The progress achieved justifies a continuation of the design, development and testing that will be necessary before an LFC system is ready for immediate application to production commercial transport aircraft.

The follow-on programs already sponsored by NASA, Contracts NAS1-16234 and NAS1-16220, on LFC structural surface development and testing, and flight testing of an LFC leading edge system on a "Jetstar" aircraft respectively, are logical and necessary steps towards the practical application of LFC to transport aircraft. The NASA LFC high speed wind tunnel program at Langley, for which Douglas is supplying perforated LFC glove panels for the upper surface of the swept wing model, under Contract NAS1-16892, will test performance at high Mach numbers. Wind tunnel testing at Douglas, Long Beach has already demonstrated that porous and perforated surfaces can be used to achieve LFC satisfactorily on a 30-degree swept wing at Reynold's numbers per unit length approaching those of high altitude cruising conditions.

The structural program is needed to further develop an efficient LFC suction panel that is compatible with strain levels in the primary wing structure. It should include design and testing of small test specimens and panels large enough to check Euler buckling between fasteners attaching the panel to the primary structure. An overall LFC wing structure design program is unnecessary, assuming that a composite wing is to be developed under a separate structural development program. Panel joints also require further development. They must be designed to minimize local blockage of porosity and to retain a sufficiently smooth and wave-free surface during cruising flight; both design work and testing are necessary.

The JetStar flight test should demonstrate the feasibility of achieving LFC under realistic operating conditions. The leading edge test specimen will be subjected to the environmental effects of rain, ice and insect impingement. The LFC system will also be tested on a swept wing with regions of cross flow and possible attach line instabilities.

12.4.1 Full Chord LFC Glove

Following the JetStar flight tests, it will be necessary to flight test a full chord glove to test LFC back to 85 percent chord, where the combined effects of cross flow and Tollmein Schlichting instabilities can be evaluated at larger chord Reynolds Numbers. It is suggested that this testing should be done on a larger aircraft such as the DC-9 which offers the advantage of a clean wing and aft located engines. A study of full chord LFC glove configurations has shown that the DC-9 would be practical for this purpose. Figure 12-4 shows how the LFC glove could be superimposed on the existing DC-9 wing box structure. To obtain the maximum benefit from a full chord glove flight test, Douglas proposed and presented the configuration shown in Figure 12-5 following a design study completed in 1979. The splitting of the suction surfaces into separate regions, one on each side offers two advantages. Firstly, the size of the suction ducting that must be accommodated within the glove envelope is halved and secondly, the inboard region with its own peculiar LFC problems can be investigated separately.

The glove region outboard of the inboard LFC panel could be used to compare natural laminar flow and the region inboard of the mid span LFC suction surface could be used to investigate the use of discrete suction applied only in the leading edge region. With the attachment line and cross-flow problems caused by sweep being controlled by suction, extensive regions of laminar flow may be possible further aft, where the Tollmein-Schlichting instabilities can be controlled by the pressure gradients induced by the airfoil shape. This opens up the possibility of modifying existing wings to achieve significant LFC benefits at relatively low cost.

	WING	HORIZ	VERT
AREA — m^2 (FT^2)	260 (2800)	89.6 (964)	47.2 (508)
ASPECT RATIO	10.85	3.95	1.60
TAPER RATIO	0.25	0.35	0.35
SWEEP	30 DEG	35 DEG	40 DEG
THICKNESS RATIO	0.127 AVG	10	10.5
TAIL VOLUME COEF	—	1.38	0.079

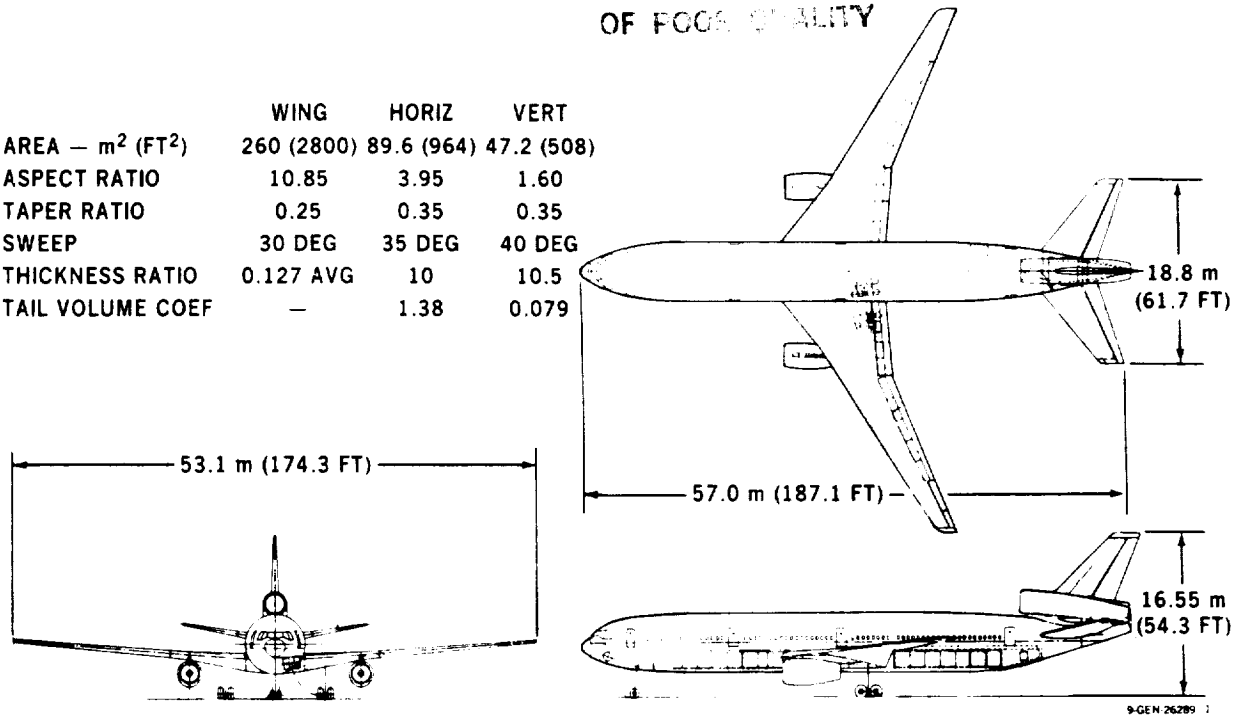

FIGURE 12-3. ADVANCED TURBULENT AIRCRAFT

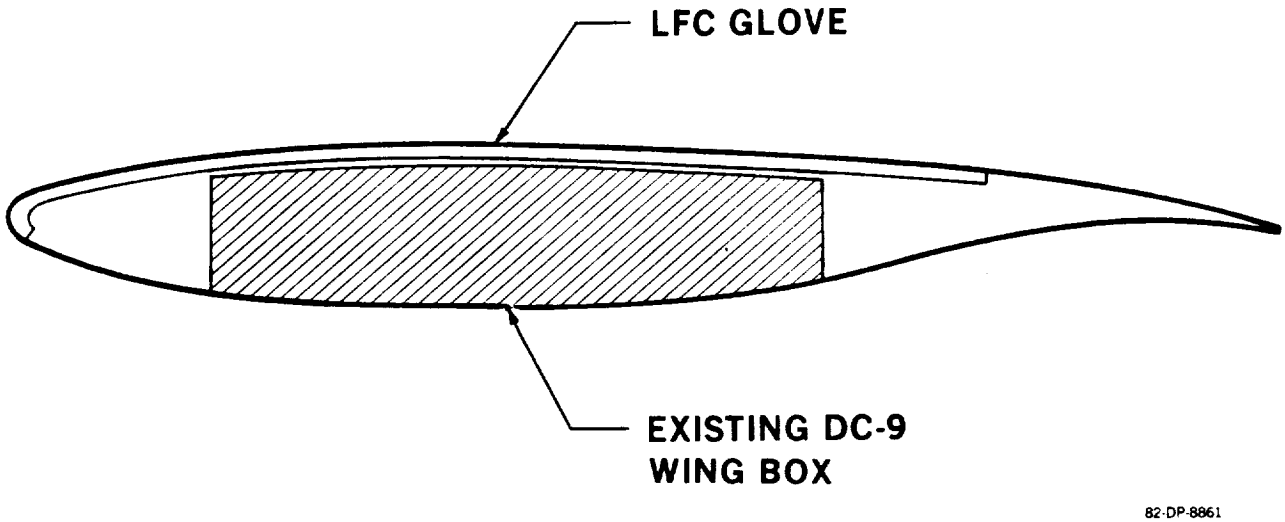

FIGURE 12-4. PROPOSED LFC GLOVE ON DC-9 WING BOX

12.4.2 Supporting LFC Programs

Before proceeding with the next phase of LFC development a complete aerodynamic LFC wing design study is advisable. This should consider wing sweep effects including the possibility of forward sweep. This is particularly advantageous with LFC because it results in reduced sweep at the leading edge for the same effective wing sweep.

Other items that need further investigation include:

(1) Flow checks and pressure drop measurements on simulated suction ducting and glove panels.

(2) Further development of perforating, welding, cutting and forming techniques with perforated titanium sheet material.

(3) Further development and testing of environmental protection systems to either improve the liquid dispensing system or preferably to eliminate it altogether.

(4) Further investigation and development of the possibility of using a superplastic formed diffusion bonded all titanium porous glove panel.

(5) The base case LFC aircraft configuration needs to be recycled to update the design and determine the cumulative effect of recent design improvements.

12.4.3 LFC Demonstration Aircraft

With the selected LFC design, it will finally be necessary to demonstrate the practical achievement of LFC over the complete wing of a sufficiently representative commercial transport aircraft. Otherwise, airlines and aircraft manufacturers would be unwilling to risk the level of expenditure necessary to launch an LFC aircraft program. An in-depth study at Douglas, funded by NASA, showed that the DC-9 would be suitable for this purpose. The configuration is shown in Figure 12-6. It would require only the addition of the LFC system and the installation of an LFC wing outboard of the center section. The existing center wing including the main gear could be retained. As a further cost saving, the same aircraft used previously for the glove testing could be modified to incorporate the complete LFC wing.

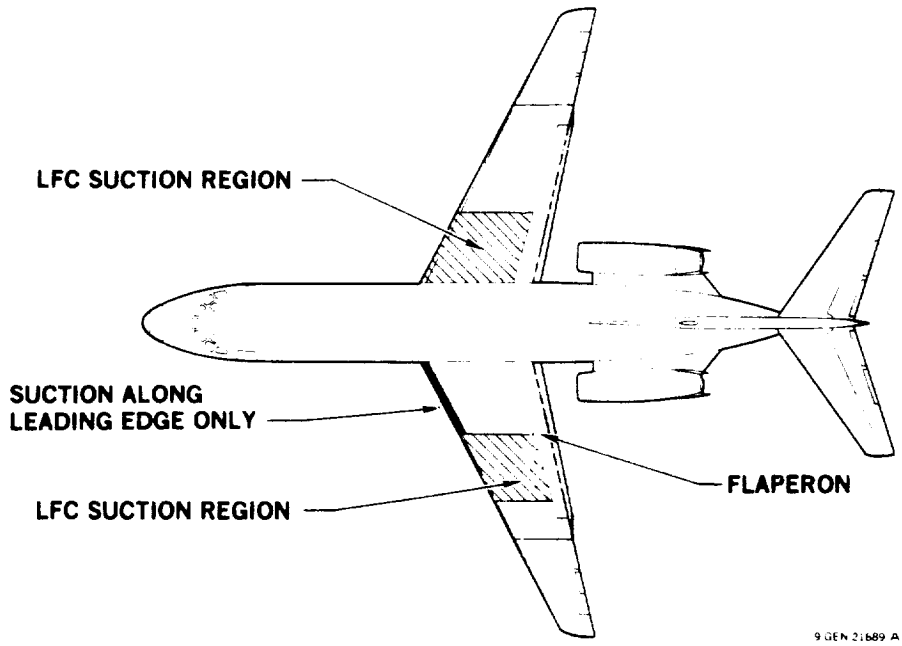

FIGURE 12-5. LFC WING GLOVE ON DC-9

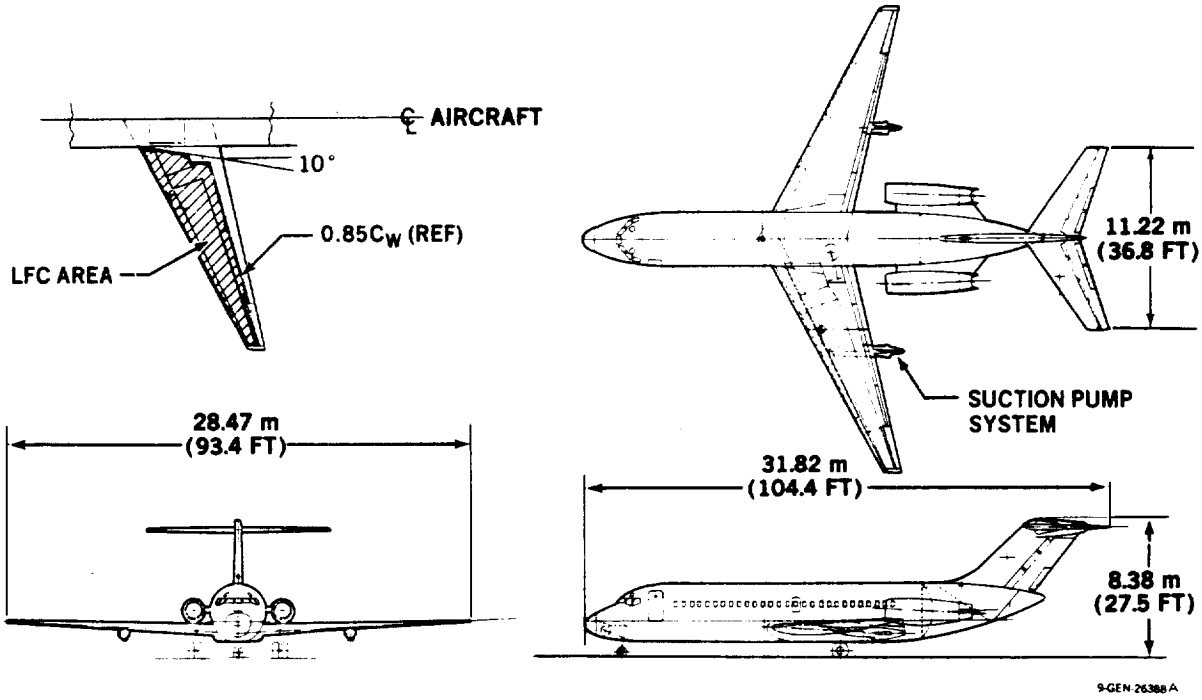

FIGURE 12-6. DC-9 WITH LFC WING

1. Report No.	2. Government Accession No.	3. Recipient's Catalog No.
NASA CR-159251		

4. Title and Subtitle	5. Report Date
Evaluation of Laminar Flow Control Systems Concepts for Subsonic Commercial Transport Aircraft - Final Report	June 1983
	6. Performing Organization Code
7. Author(s)	8. Performing Organization Report No.
W. E. PEARCE et Al.	ACEE-01-FR-3132
	10. Work Unit No.
9. Performing Organization Name and Address	11. Contract or Grant No.
Douglas Aircraft Company 3855 Lakewood Boulevard Long Beach, California 90846	NAS1-14632
	13. Type of Report and Period Covered
12. Sponsoring Agency Name and Address	Contractor Report
National Aeronautics and Space Administration Washington, D.C. 20546	14. Sponsoring Agency Code

15. Supplementary Notes

NASA Langley Research Center
Langley Technical Monitor: J. Cheely

16. Abstract

@ N83 5 An evaluation was made of laminar flow control (LFC) system concepts for subsonic commercial transport aircraft. Configuration design studies, performance analyses, fabrication development, structural testing, wind tunnel testing, and contamination-avoidance techniques were included. As a result of trade studies, a configuration with LFC on the upper wing surface only, utilizing an electron beam-perforated suction surface, and employing a retractable high-lift shield for contamination avoidance, was selected as the most practical LFC system. The LFC aircraft was then compared with an advanced turbulent aircraft designed for the same mission. This comparison indicated significant fuel savings and reduced direct operating cost benefits would result from using LFC.

@ N83 X

17. Key Words (Suggested by Author(s))	18. Distribution Statement
Laminar Flow Transport Aircraft Fuel Economy ACEE LFC	[redacted]

19. Security Classif. (of this report)	20. Security Classif. (of this page)	21. No. of Pages	22. Price
[redacted]	Unclassified	509	

[redacted]